Report No. UMTA-IL-06-0043-78-3

ANALYSIS OF GROUND-LINER INTERACTION FOR TUNNELS

OCTOBER 1978

FINAL REPORT

Prepared for

U.S. Department of Transportation
OFFICE OF THE SECRETARY
AND
URBAN MASS TRANSPORTATION ADMINISTRATION
Washington, D.C. 20590

NOTICE

Technical Report Documentation Page

1. Report No.	2. Government Accession No.	3. Recipient's Catalog No.
UMTA-IL-06-0043-78-3		PB 294 [illegible]

4. Title and Subtitle	5. Report Date
ANALYSIS OF GROUND-LINER INTERACTION FOR TUNNELS	OCTOBER, 1978
	6. Performing Organization Code
7. Author(s)	8. Performing Organization Report No.
R. E. RANKEN, J. GHABOUSSI, A. J. HENDRON, JR.	UILU-ENG-78-2021
9. Performing Organization Name and Address	10. Work Unit No. (TRAIS)
Department of Civil Engineering University of Illinois at Urbana-Champaign Urbana, Illinois 61801	11. Contract or Grant No. DOT-OS-70024 (DOT-UT-80039)
	13. Type of Report and Period Covered
12. Sponsoring Agency Name and Address	Final Report Oct. 1976 - Oct. 1978
U.S. Department of Transportation Office of the Secretary Washington, D. C. 20590	14. Sponsoring Agency Code

15. Supplementary Notes: This project also sponsored by --
Urban Mass Transportation Administration
Office of Rail and Construction Technology
Washington, D. C. 20590

16. Abstract

Both analytical and numerical solution techniques are used to investigate ground-liner interaction for various loading conditions and construction sequences.

The relationship between ground and liner material properties and the distributions of liner forces, stresses and displacements resulting from interaction is illustrated for a circular liner inserted in a stressed (in situ stress) ground mass. This is accomplished through the use of an analytical solution derived for tunnels located at great depth. To illustrate the influence of the ground surface boundary on liner behavior the finite element method is used to analyze tunnels located at shallow depths.

The finite element method is used to simulate the actual advancement of a tunnel through the ground mass. The axisymmetric finite element analyses performed for this part of the investigation yielded information as to the longitudinal distribution of ground stresses and displacements and liner forces and displacements for tunnels in which the liner was installed right at the advancing face, a short distance behind the face, and far behind the face.

The problem of two adjacent and parallel tunnels is also considered. The influence of pillar width and construction sequence is examined.

The finite element method is also used to examine the ground-liner interaction resulting from what is called the localized gravity loading condition. This loading condition occurs when portions of the surrounding ground mass fall onto or against the liner such that an active pressure is applied to only a portion of the liner circumference.

17. Key Words	18. Distribution Statement
Tunnel Liners; Ground-Liner Interaction; Finite Element Analysis	Document is available to the public through the National Technical Information Service, Springfield, Va. 22151

19. Security Classif. (of this report)	20. Security Classif. (of this page)	21. No. of Pages	22. Price
Unclassified	Unclassified	441	

PREFACE

Research described in this report was performed by the Department of Civil Engineering at the University of Illinois at Urbana-Champaign, Urbana, Illinois from October 1976 to October 1978.

The report is the thesis submitted by Dr. Ranken to the faculty in partial fulfillment of the requirements for the degree of Doctor of Philosophy in Civil Engineering in the Graduate College of the University of Illinois at Urbana-Champaign. The work was accomplished under the direct supervision of Professor Ghaboussi and Hendron of the Department of Civil Engineering.

The project was sponsored by the U. S. Department of Transporation, through contract No. DOT-OS-70024 (Office of the Secretary) and DOT-UT-80039 (Urban Mass Transportation Administration). The sponsor's technical representatives were Mr. Russell K. McFarland of the Office of the Secretary and Mr. Gilbert Butler of the Urban Mass Transportation Administration.

TABLE OF CONTENTS

Page

Page

LIST OF TABLES

LIST OF FIGURES

FIGURE Page

FIGURE Page

FIGURE Page

CHAPTER 1

INTRODUCTION

In designing tunnel supports it is necessary to evaluate the forces expected to develop in the support system as a result of the interaction that occurs between the support and the surrounding ground. The magnitude and distribution of forces in the support system can be evaluated by an analysis of the ground-support interaction. Such analyses can also provide information about the stresses and deformations in the surrounding ground mass and, with certain analysis methods, the displacements of the ground surface.

All these quantities are strongly dependent on the stress-strain-time properties and geologic nature of the ground mass, the dimensions and properties of the support, the initial stresses existing in the ground, the method of excavation, and the type and manner of placement of the liner or permanent support system.

The capability to perform analyses of ground-liner interaction has increased steadily in recent years through the development of new analytical solutions and modern numerical techniques such as the finite element method. However, a great deal still needs to be done to explore the full potential of such solution methods and to obtain results which can be used in design of tunnel support systems.

Reported herein are the results of a study of ground-liner interaction for tunnels. The main factors considered in this study were the material properties of the ground and liner, tunnel depth, interaction between two parallel tunnels, position of liner installation relative to the

tunnel face, and the type of loading to which the liner is subjected.

The various methods available for the analysis of ground-liner interaction are described in Chapter 2. A brief description of the types of loading considered in this study is also given in this chapter.

Interaction due to excavation loading is considered in Chapters 3 through 6. Chapter 3 describes the results that can be obtained from an analytical solution for deep tunnels. Shallow tunnels are considered in Chapter 4, wherein the results obtained from a series of finite element analyses of tunnels at various depths below the ground surface are presented. Chapter 5 gives the results of a study in which the actual advancement of the tunnel through the ground mass was simulated. The axisymmetric finite element analyses performed for this investigation yielded information as to the longitudinal distribution of ground stresses and displacements and liner forces and displacements for tunnels in which the liner was installed right at the advancing face, a short distance behind the face, and far behind the face. Chapter 6 consists of a study of interaction for the case of two parallel tunnels. The main parameters considered in this investigation were the width of the pillar separating the tunnels and the sequence of excavation and liner installation for the two tunnels.

The results obtained from finite element analyses of ground-liner interaction due to localized gravity loading are presented and discussed in Chapter 7. The main parameters considered in this series of analyses were the material properties of the ground and liner and the distribution of the load acting on the liner.

Chapter 8 contains a summary of the work performed and the conclusions derived from the results obtained.

CHAPTER 2

REVIEW OF AVAILABLE METHODS FOR ANALYSIS OF GROUND-LINER INTERACTION

2.1 GENERAL REMARKS

There are numerious analytical solutions and numerical techniques available that can be, and have been, applied to the analysis of ground-liner interaction. Each of these methods of analysis attempts to simulate mathematically the response of the ground-liner system for a range of possible conditions. Unfortunately, there is no one method that can faithfully simulate all relevant details of the problem. All methods are based on assumptions that are designed to reduce the complexity of the problem to a sufficient degree so as to allow a solution to be obtained. Some methods make more simplifying assumptions than others and, in general, the more assumptions made the less accurately the procedure simulates the real problem.

The majority of the analytical solutions have the advantage of being straight forward and easy to use. They can usually be performed by hand and seldom require the use of, and thus access to, large computer installations. The major disadvantage to these solution methods is that they are necessarily highly idealized. The results they yield must be carefully examined and applied with caution.

Numerical solution techniques, such as the finite element method, have become quite popular in recent years, and for good reason. With the finite element method almost any degree of simulation detail desired can be

achieved. At least, this is theoretically possible. However, as the degree of simulation detail is increased, the complexity of the analysis also increases. At one extreme are the highly detailed analyses which are quite complex and thus difficult to perform and interpret. Such analyses can be performed only with the most sophisticated finite element computer programs, programs which require large and equally sophisticated computer facilities. At the other extreme are the analyses which provide solutions to a much more idealized form of the problem. Although these simplified analyses can be inexpensive and easy to perform, they may provide no more useful information than would be available from the analytical solutions. As with the analytical methods, the results obtained from finite element analyses can not be applied to the design of a tunnel system without first being carefully evaluated with respect to the relationship between the ground-liner system as simulated and as it exists in reality.

Indiscriminate use of any of the available methods of analysis can lead to unfortunate consequences. It is important that the method selected be applicable to the problem at hand. It is also important that the results obtained from the analysis be interpreted properly. This requires knowledge of both the anticipated tunneling conditions and the adequacy of the analysis to simulate these conditions.

2.2 LOADING CONDITIONS CONSIDERED

Ground-liner interaction is a consequence of the liner's resistance to the movement of the surrounding ground mass, or portions thereof, into the tunnel opening. These ground movements, or displacements, can be initiated by events associated with the excavation and construction processes

or by events external to the ground-liner system.

The external loading to which a tunnel liner is subjected as a result of its resistance to ground displacements depends on the nature and source of these displacements. Three different loading conditions are considered in this investigation. These are called excavation loading, localized gravity loading, and overpressure loading. The expressions, or names, for these loading conditions are intended to be descriptive of the causative factor that results in the inward ground displacement in each case.

Excavation of the tunnel opening alters the state of stress in the ground mass surrounding the opening. As it adjusts to this new state of stress the surrounding ground moves into the tunnel opening. If the ground mass around the opening remains intact as this displacement occurs, and if the tunnel liner is installed in time to resist this displacement, the excavation loading condition will result. This loading condition is illustrated in Fig. 2.1 which shows the longitudinal distribution of the instantaneous radial ground displacements that occur in response to the excavation of the opening for an hypothetical case. In this figure, the solid curve represents the displacements that have occurred as the tunnel face was advanced to point A. Similarily, the dashed curve represents the distribution of displacements that will exist after the face is advanced to point AA. If the liner is installed, in contact with the ground, at point B just prior to advancement of the face from point A to point AA, the liner will resist the additional ground displacement δu and ground-liner interaction will result.

For the excavation loading condition the magnitude of the external load that initially acts on the liner is related to the ratio u_p/u_t,

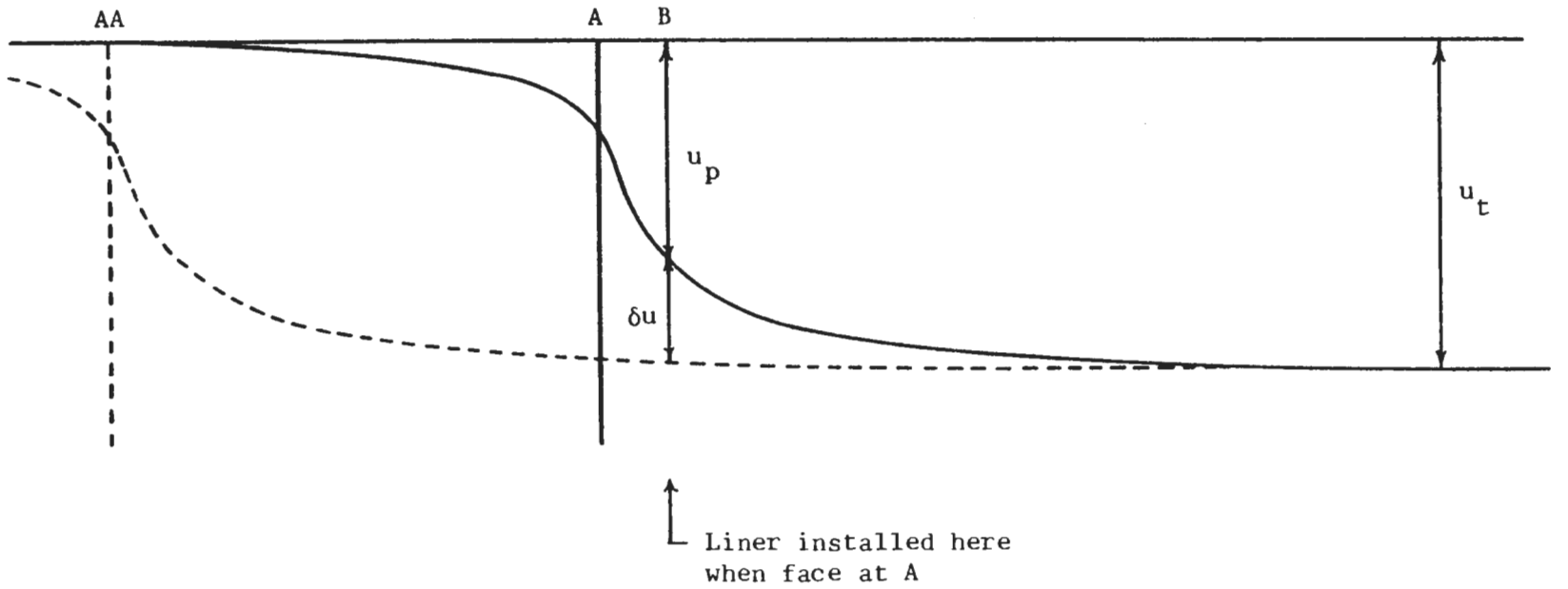

FIGURE 2.1 GROUND DISPLACEMENTS RELEVANT TO THE EXCAVATION LOADING CONDITION

where u_p is the ground displacement that occurs prior to ground-liner contact and u_t is the total ground displacement that would have occurred if no liner had been installed. If a liner could be installed prior to any displacement of the surrounding ground mass ($u_p = 0$) the initial external load would exert a pressure on the liner equal to the in situ ground stress. At the other extreme, if the surrounding ground mass achieved its new equilibrium state without coming into contact with the liner ($u_p = u_t$) there would be no load applied to the liner and, thus, no ground-liner interaction.

It is clear that, for the excavation loading condition, ground-liner interaction is a function of the position of liner installation with respect to the face. Additionally, if the construction procedures are such that an open gap (radial) is left between the liner and the ground mass, the thickness of this gap will also influence the extent of interaction. If the ground mass exhibits time-dependent (viscous) behavior the displacement u_t will consist of both instantaneous and time-dependent components and, the magnitude of u_p will depend on such additional factors as time of ground-liner contact and rate of tunnel advance.

Following excavation the distribution of stresses in the ground mass around the tunnel opening can be such that the shear strength of the soil or rock is exceeded to the extent that the earth's gravitational attraction is sufficient to cause portions of the material around the tunnel to dislodge from the surrounding ground mass and displace, or fall, into the opening. If this occurs after the tunnel liner is installed this material will come to rest on or against the liner. The weight of this material, which usually acts over only a portion of the liner circumference, constitutes what is called herein the localized gravity load. In some soils

and fractured rock masses, raveling of material from around the opening perimeter can gradually build up a large dead load on the liner. On a larger scale, zones of high shear stress may develop above each side of the opening (Hansmire, 1975) such that within these zones the shear strength of the soil is exceeded, allowing the mass of soil between these zones to displace downward onto the liner. In discontinuous rock masses the possibility exists for the displacement of rock blocks into the opening and on to the liner. In such materials the shear strength and orientation, with respect to the tunnel opening, of the discontinuities are often of more significance than the intact rock strength.

The overpressure loading condition is a result of the application of an externally applied pressure (e.g., that due to the weight of new surface structures or the pressure applied at the ground surface by a nuclear blast) that mobilizes a system of vertical and horizontal stresses in the ground mass surrounding the lined tunnel. Ground-liner interaction results from the liner's resistance to the displacements the ground mass undergoes in adjusting to these new stresses. This loading condition is applicable only to existing tunnels and does not account for ground-liner interaction resulting from the construction of the tunnel. The overpressure and excavation loading conditions are similar in that the ground mass stress fields, and thus the forms of the inward ground displacements, causing the two types of loading are similar. However, the magnitudes of the liner forces and displacements resulting from ground-liner interaction in the two cases are quite different because other aspects of the two loading conditions are fundamentally different. These differences are discussed in the following sections of this chapter.

2.3 ANALYTICAL SOLUTIONS

2.3.1 EXCAVATION LOADING

SOLUTIONS BASED ON THE GROUND REACTION CURVE CONCEPT

The ground reaction curve (also called "ground unloading curve" and "characteristic line") concept is one approach to the analysis of ground-liner interaction. The ground reaction curve is the pressure vs. displacement curve for a tunnel opening in a given ground mass and for a given in situ stress field. Only a two-dimensional section normal to the tunnel axis and at a location far behind the tunnel face is considered. When such a curve is used in combination with the pressure vs. displacement curve of the tunnel liner, it allows the equilibrium value of ground pressure acting on the liner to be determined. The early work that led to the development of the ground reaction curve concept was performed by Labasse (1949), Kastner (1962), and Pacher (1964). In recent years Rabcewicz (1969), Lombardi (1970, 1973), Ladanyi (1974), and Daemen (1975) have refined and extended the method to encompass a wide range of material behavior models for the ground mass. Daemen (1975) presents a comphrehensive summary of the development of the concept. The majority of this work has been concerned with tunnels in rock and the influence of the broken rock zone around the tunnel on liner loading. However, in most cases the solutions can also be applied to tunnels in soils where, instead of broken rock zones, zones of plastic yielding form around the tunnels.

Analytical solutions which account for inelastic behavior of the surrounding ground have, to date, been obtained only for the special case

of an isotropic, or axisymmetric, in situ stress field, $K_o = 1$. If applied to a ground-liner system in which the in situ stress state is not axisymmetric, $K_o \neq 1$, only the average stresses can be considered and the equilibrium state obtained is expressed in terms of the average ground and liner response. For example, if the in situ stress state is given by $\sigma_V = \gamma H$ and $\sigma_H = K_o \gamma H$ ($K_o \neq 1$), the solution only indicates that the average pressure acting on the liner is some fraction of the quantity $\frac{1}{2}(1 + K_o)\gamma H$.

The inability to consider conditions resulting in flexure of, and thus the mobilization of bending moments in, the liner is the primary shortcoming or disadvantage to this approach.

Solutions based on the ground reaction curve concept consist of two sets of equations. These equations are derived for a unit thickness cross section of the three-dimensional ground-liner system. These two-dimensional sections are oriented normal to the longitudinal centerline of the tunnel and are located at a point far behind the tunnel face. The condition of plane strain is normally assumed. One set of equations defines the displacement response of the tunnel support or liner to the application of external pressure. The second set of equations defines the displacement response of the tunnel opening to unloading. For a specific liner and ground mass combination the ground reaction curve and the liner reaction curve, obtained from the solution equations, are plotted together. The point of intersection of these two curves defines the equilibrium state for the conditions assumed and gives the magnitude of the ground pressure acting on the liner and the displacement of the liner due to interaction. Hypothetical ground reaction and liner reaction curves are illustrated in Fig. 2.2.

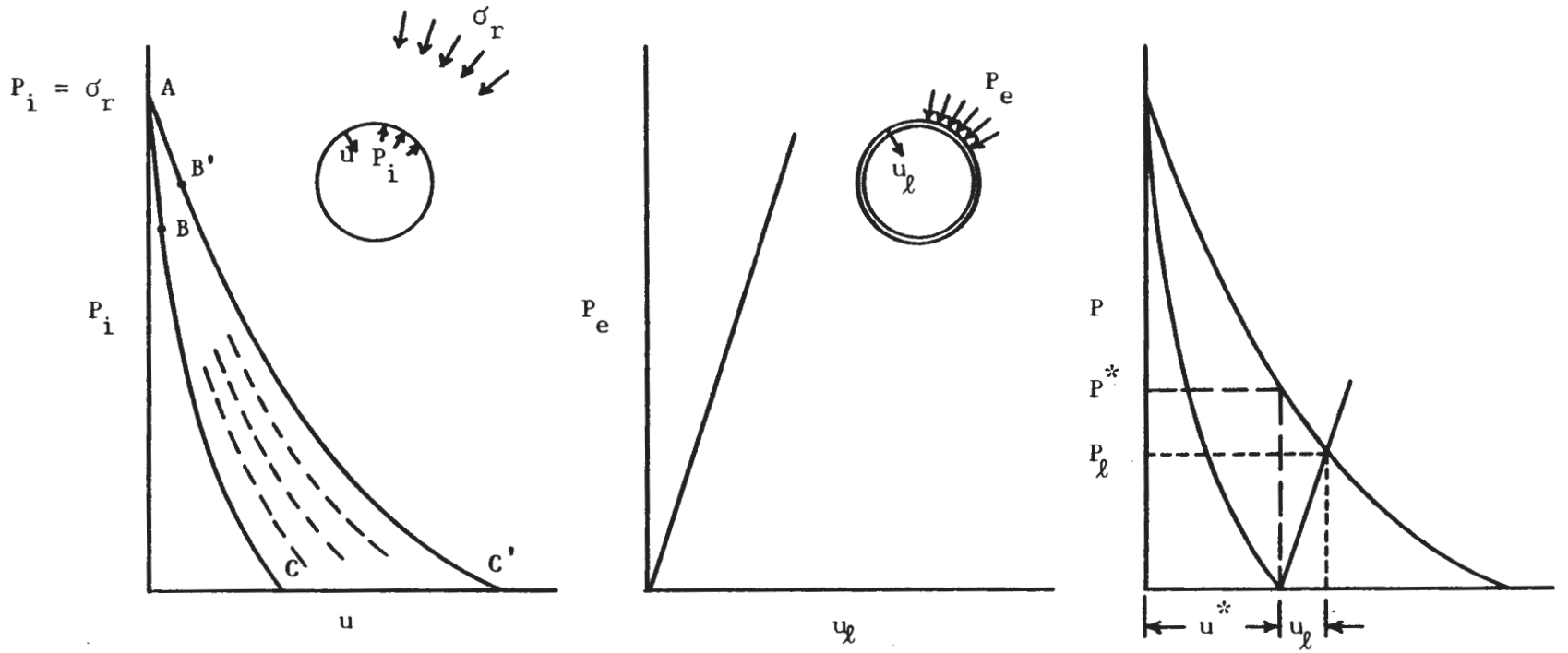

a) Ground reaction curve + b) Liner reaction curve = c) Equilibrium state of the lined tunnel opening

FIGURE 2.2 CONCEPTUAL LINER AND GROUND REACTION CURVES

The ground reaction curves ABC and AB'C', Fig. 2.2a, represent the relationship between the magnitude of an internal pressure applied to the perimeter of the tunnel opening and the resulting radial displacement of the opening. The curve ABC represents the instantaneous response of the opening, while AB'C' gives the long term response. The difference between these two curves reflects the loss of strength with time experienced by the surrounding ground mass. The dashed lines indicate that similar curves exist for conditions intermediate to those of the short term and long term. the shape of the ground reaction curve is a function of the stress-strain-time and shear strength properties of the ground mass. For example, portions AB and AB' of the curves represent linear elastic response of the ground mass, while portions BC and B'C' represent elasto-plastic response. The curves intersect the horizontal axis (points C and C'), indicating that the opening would be stable without internal support. In order for stability to be achieved the ground mass surrounding the opening must retain sufficient shear strength in the form of cohesion. For an unstable opening the decreasing pressure-displacement curve would never reach the horizontal axis, indicating that the opening would eventually close without some form of internal support being provided. Ladanyi (1974) presented a solution that allows consideration of either a linear or non-linear elastic-plastic yield criterion, volume dilation in the zone of broken rock around the opening, and rock strength decrease with time. The strength loss with time is not accounted for directly in the equations. Rather, the ground reaction curves for later times are obtained by inserting in the equations reduced or residual values for the rock stress-strain and shear strength parameters. A set of curves, such as those in Fig. 2.2a, is obtained. Daemen (1975) pre-

sented a solution that allows consideration of the influence of a progressive, strain dependent strength decrease during rock failure. His model assumes an exponential strength decrease beyond the peak shear strength value. The resulting equations are quite lengthy and complex.

The liner reaction curve, Fig. 2.2b, represents the relationship between the magnitude of the external pressure applied to the tunnel liner and the radial displacement of the liner. The shape and slope of this curve are functions of the stress-strain properties and dimensions of the liner. For an incompressible liner the curve is a vertical straight line. Daemen (1975) presents liner reaction curve equations for continuous concrete or shotcrete liners, blocked steel sets, and rock bolt support systems.

In fig. 2.2c the ground reaction and liner reaction curves have been combined to obtain the equilibrium state of the lined tunnel opening. For this example it is assumed that the liner is installed in contact with the surrounding ground immediately after all instantaneous displacement, u^*, has occurred (Note: The instantaneous displacement u^* occurs within a short distance behind the tunnel face. Because the solution considers only cross sections far behind the face, the displacement occurring before liner installation cannot be less than u^*). With commencement of the time-dependent ground displacements, pressure is gradually built up on the liner. This pressure increases, following the liner reaction curve, until it equals the magnitude of the internal opening pressure required to halt further displacement of the surrounding ground. The resulting state of equilibrium between ground and liner is given by the intersection of the two curves. Had the liner been incompressible (vertical broken line) there would have been no additional displacement of either the ground or liner, and thus

there would have been no interaction. The equilibrium pressure acting on such a liner, P^*, represents the maximum possible pressure on a liner installed when $u = u^*$. Figure 2.2c shows that, for a compressible liner, ground-liner interaction does occur and results in the additional ground-liner displacement u_ℓ and the reduction of the pressure from the potential maximum value P^* down to the lesser value P_ℓ.

From the equilibrium pressure value the magnitude of the circumferential compressive force, i.e., thrust, in the liner can easily be calculated ($T = P_\ell a$, where a = liner radius). Because the magnitude of the pressure is assumed to be constant around the liner, there are no bending moments or shear forces.

GROUND-LINER INTERACTION FOR THE CIRCULAR TUNNEL IN ELASTIC GROUND

Despite the fact that the ground surrounding a tunnel usually does not behave as an elastic material, several analytical solutions for ground-liner interaction based on the assumption of elastic ground behavior have been proposed. Justification for this assumption is usually based on the argument that the details of the true ground conditions are usually not sufficiently well known to warrent the use of the more complex analytical models for ground behavior, which are themselves no more than idealizations of actual ground behavior. In addition, the point is made that solutions based on elasticity theory can be derived so as to take into consideration in situ stress states other than $K_o = 1$. Thus, these solutions allow determination of the complete response of the liner, i.e., the distributions of thrust, bending moments, shear forces, and displacements around the liner, for $K_o \neq 1$.

Like the ground reaction curve solutions the elastic solutions are two-dimensional, plane strain solutions that can be applied only to tunnels located at great depth where the influence of the ground surface boundary and the increase of insitu stress with depth from crown to invert is negligible. Because it is assumed that the ground behaves elastically and since the problem is reduced to two dimensions, it is necessary to assume that the liner is installed in contact with the surrounding ground mass prior to any displacement of the ground mass. Therefore, it is necessary to assume that the liner is installed before excavation of the tunnel. Such a construction sequence is certainly not common, but it is also not impossible. Large diameter tunnels to be located in poor ground could be constructed by mining, and backfilling with concrete, a series of small diameter drifts around the perimeter of the tunnel to form the liner. This would then be followed by excavation of the soil from within the completed liner. Small diameter conduits installed through high fills by the pipe-jacking method also follow a similar type of construction sequence. Liners as large as 10 ft (3 m) in diameter have been installed by the jacking method. Since the ground displacements occurring ahead of the tunnel face are usually small relative to the potential total displacements, these solutions approximate the case of a liner installed right at the face (or slightly behind the face if measures are taken to limit ground displacements).

The elastic ground-liner interaction solutions for $K_o \neq 1$ can be conveniently separated into two catagories on the basis of the types of interaction problems to which they apply. Work by Morgan (1961), Muir Wood (1975), and Curtis (1976) resulted in the solution to the problem of a lined tunnel constructed in a stressed ground mass (excavation loading condition).

Solutions by Burns and Richard (1964) and Dar and Bates (1974) are applicable to the problem of a lined tunnel located in a ground mass that is subjected to an externally applied pressure at the ground surface (overpressure loading condition). This pressure is applied after the tunnel is constructed and in situ stresses are not considered. The Burns and Richard and the Dar and Bates solutions, while for the same problem, yield slightly different results for certain ground-liner combinations. These differences arise because Burns and Richard used extensional shell theory to model the liner while Dar and Bates used elasticity theory to model both the ground and the liner. In the autumn of 1975 the writer modified both the Burns and Richard and the Dar and Bates derivations to obtain solutions for the excavation loading condition. Upon publication of the Curtis paper early in 1976, it was found that the equations of the modified solutions were quite similar to, and yielded essentially the same results as, the Curtis solution equations.

Figure 2.3 illustrates the distribution of in situ radial and shear stresses around an imaginary circle representing the location of the tunnel in the undisturbed ground mass. The corresponding distributions of stresses that act on the liner, prior to removal of the ground inside the liner, are not necessarily the same as those shown because these "initial" stresses are influenced by the shear strength at the ground-liner interface. The ground-liner interaction solutions normally consider only the two extreme interface conditions. These are:

1. The No Slippage Condition - If the interface shear strength everywhere exceeds the in situ shear stress, there is no slippage at the interface.

Distributions shown for $K_o = \frac{1}{2}$

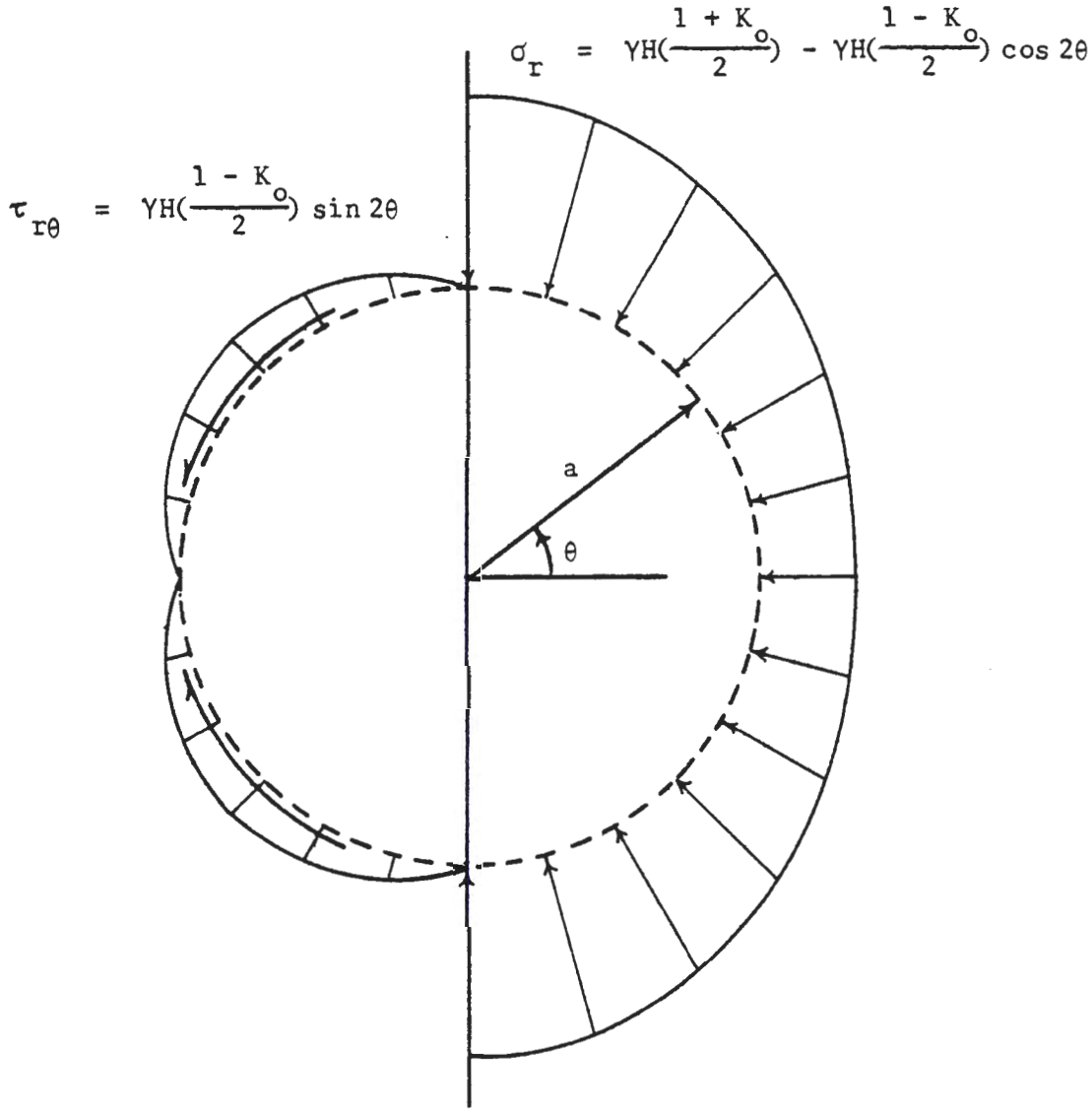

FIGURE 2.3 DISTRIBUTION OF IN SITU RADIAL AND SHEAR STRESSES FOR $K_o \neq 1$

2. The Full Slippage Condition - If the interface shear strength is zero the liner offers no resistance to tangential displacement of the ground at the interface and full slippage occurs.

The "initial" radial and shear stresses acting on the liner are the same as those shown in Fig. 2.3 only if the no slippage condition is satisfied. If this condition is not satisfied, i.e., if any amount of slippage occurs, the "initial" stress distribution will be different from that shown. For the full slippage condition the shear stresses go to zero and the radial stresses increase around the crown and invert and decrease around the springlines.

The initial work in the derivation of the solution for a lined tunnel constructed in a stressed ground mass was done by Morgan (1961). Morgan assumed the full slippage condition and considered only the interaction due to the distortional component of an assumed radial stress distribution. Thereafter several commentators observed that Morgan's derivation contained a basic error related to the required stress-strain relations for the case of plane strain. Muir Wood (1975) presented a paper in which this error was corrected and the solution was extended to include the uniform component of the radial stress distribution (solutions for the distortional and uniform components were derived separately as allowed by the principle of superposition).

The Morgan and Muir Wood derivations for distortional loading proceed from an assumed distortion of the shape of a circular, incompressible liner and an assumed initial pressure distribution. Unfortunately, the resulting solution equations are not correct because the assumed initial pressure distribution is not correct for the slippage condition at the ground-liner interface considered. Both Morgan and Muir Wood assumed that

for the full slippage condition the initial distribution of radial pressures acting on the liner is the same as shown in Fig. 2.3 for the in situ stresses. However, as previously discussed, this is not the case. For full slippage the distortional component of the radial pressure is greater, by some unknown amount, than that shown in Fig. 2.3. Thus, the Muir Wood solution for distortional loading underestimates the magnitude of liner bending moments. However, his solution for the uniform component of loading is correct since interaction due to this type of loading is independent of the slippage condition.

In a discussion of Muir Wood's paper, Curtis (1976) pointed out the above mentioned error and proposed an alternate derivation that yielded the correct equations. Considering only the distortional components of loading, Curtis derived solutions for both the full slippage and no slippage conditions. Thus, the complete solutions for both interface conditions can be obtained by combining the Curtis equations for distortional loading and the Muir Wood equations for uniform loading.

Both Muir Wood (1975) and Curtis (1976) presented equations for interface conditions intermediate to the full slippage and no slippage conditions. To obtain these solutions the expression for the "initial" shear stresses acting on the liner for the no slippage condition, $\mathcal{T}_{r\theta} = \tau_{r\theta} = \frac{1}{2}\gamma H(1 - K_o)\sin 2\theta$, was replaced by $\mathcal{T}_{r\theta} \leq S \sin 2\theta$, where S is the interface shear strength. While this approach provides a means of obtaining a solution, it does not accurately reflect the complex redistribution of stress that would occur with partial slippage. It seems reasonable to expect that only those shear stresses in excess of the shear strength would be reduced in magnitude and that the reduction of these stresses would lead to increases

of the adjacent shear stresses which were initially less than the shear strength. Thus, it is not likely that the new distribution of shear stress could be expressed in terms of as simple a function of θ as $\sin 2\theta$.

The Burns and Richard (1964) and Dar and Bates (1974) ground-liner interaction solutions are similar in that both were derived for the problem of a deep circular tunnel in an unstressed medium which is subsequently loaded by a ground surface overpressure (one-dimensional loading for which the lateral stress ratio is a function of Poisson's ratio of the medium, $K = \nu_m/(1 - \nu_m)$). They differ in that Burns and Richard used elasticity theory to model the ground mass and extensional shell theory to model the liner, while Dar and Bates used elasticity theory to model both the ground mass and the liner. The Burns and Richard equations yield the liner response at equilibrium in terms of thrusts and bending moments, whereas the Dar and Bates equations give the radial and circumferential stresses in the liner. Because of assumptions made in the derivation with respect to the liner, the Burns and Richard solution is applicable only to liners of small thickness relative to their radius. The two solutions yield essentially the same results for thin liners, but for thick liners the results can be quite different.

Höeg (1968) presented a set of equations for the ground mass stresses and displacements that accounts for ground-liner interaction under conditions of overpressure loading. This solution corresponds to that given by Burns and Richard (1964). However, it must be noted that while the Höeg solution, as given, is correct for the no slippage condition, it is incorrect for the full slippage condition. Höeg maintains that the full slippage and no slippage solutions differ only in the expressions for three constants

that appear in the one set of equations given for ground mass stresses and displacements. Actually, the stress and displacement equations for no slippage are not identical to those for the full slippage condition. The stress and displacement equations given by Höeg are correct for the no slippage condition, but they cannot be used for the full slippage condition.

As previously mentioned, the writer has modified the Burns and Richard (1964) and Dar and Bates (1974) solutions to obtain the equivalent solutions for the problem of a lined tunnel inserted in an already stressed ground mass. With the exception of only a few significant changes the derivations of the modified solutions are identical to those for the original solutions. The derivations for a total of eight different ground-liner interaction solutions are given in Appendix A. The final equations of each of these solutions are presented in Appendix B. The solutions derived consist of the following: solutions for thin liners subjected to overpressure loading under conditions of no slippage and full slippage (these solutions correspond to those given by Burns and Richard, 1964); solutions for thin liners subjected to excavation loading under conditions of no slippage and full slippage (these solutions are similar to those obtained by combining the work of Muir Wood, 1975, and Curtis, 1976); solutions for thick liners subjected to overpressure loading under conditions of no slippage and full slippage (the solution for no slippage corresponds to that which can be obtained from the work of Dar and Bates, 1974); and solutions for thick liners subjected to excavation loading under conditions of no slippage and full slippage.

LINER INSTALLED CLOSE TO THE TUNNEL FACE

The longitudinal distribution of radial ground displacements, at the radial distance a, for an unsupported tunnel in an elastic medium is illustrated for a hypothetical case in Fig. 2.4. In this figure it can be seen that at points more than about one tunnel diameter ahead of the face no displacements have occurred, while at a distance of approximately two diameters behind the face full displacement, u_t, has occurred. At any point between -D and 2D, $u_d = u_t - u_p$, where u_p is the displacement that has already occurred at that point and u_d is the remaining displacement that will occur when the tunnel face is advanced far beyond its present location. The pressure that will act on the liner section installed near the face position shown, after the face has been advanced at least 2D beyond the point of liner installation, is directly proportional to the ratio u_d/u_t. In terms of the displacement u_p, the pressure is proportional to the quantity $(1 - u_p/u_t)$.

The ground reaction curve solutions and the elastic, $K_o \neq 1$ solutions just described are all two-dimensional, plane strain solutions that are not applicable within the zone of three-dimensional stress and longitudinal variation of instantaneous displacement that exist around the tunnel face. If applied to liners installed near the tunnel face the elastic solutions overestimate the pressures acting on the liner because they assume no prior displacements (liner installed before excavation) and therefore cannot account for the relaxation of the ground that would occur ahead of the point of liner installation. It would appear that the ground reaction curve solutions would necessarily underestimate the pressure on the liner because they assume that all of the instantaneous ground displacements occur

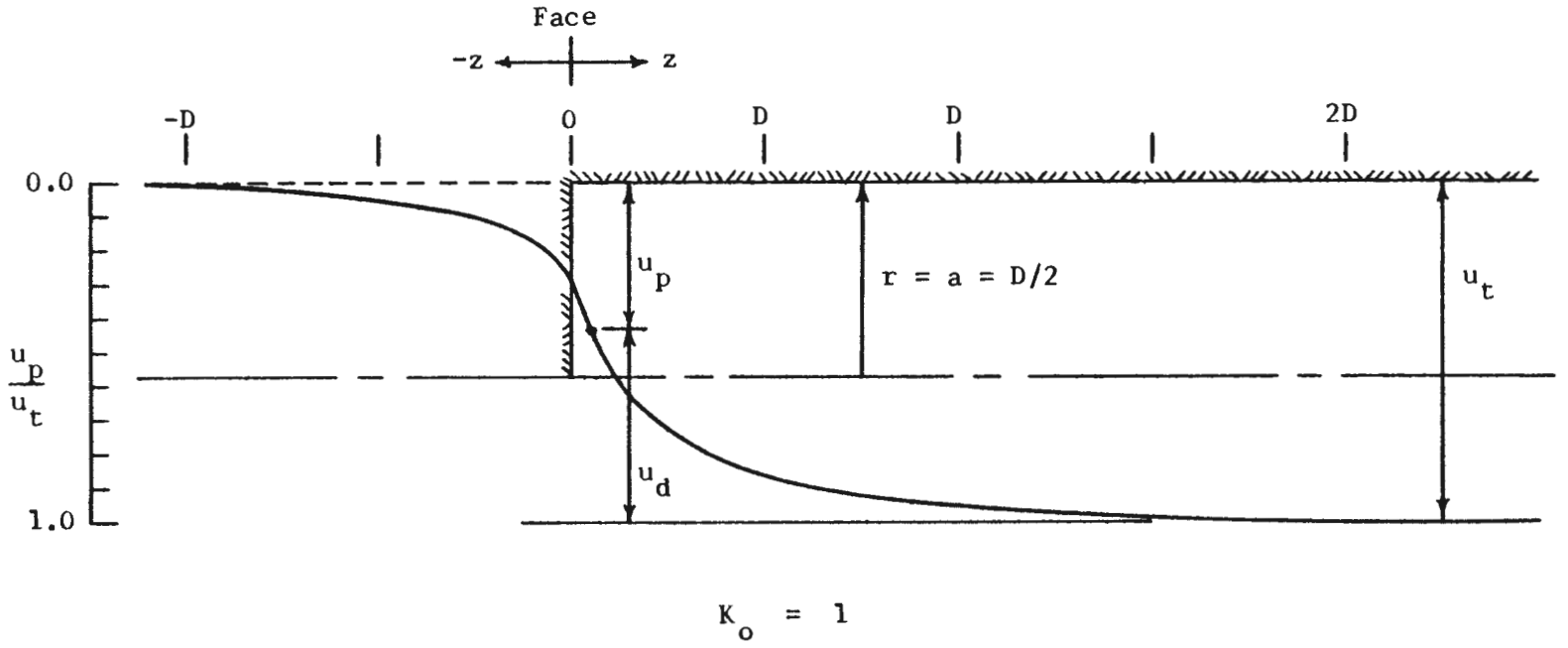

FIGURE 2.4 LONGITUDINAL DISTRIBUTION OF RADIAL DISPLACEMENTS NEAR THE TUNNEL FACE

before the liner is installed and this would not be the case if the liner were installed within the three-dimensional zone.

However, both approaches to the interaction problem could be applied to liners installed close to the tunnel face if a relationship between 1) liner location relative to the face and 2) the ground displacement u_p at that location could be established. For the ground reaction curve approach this relationship would be needed to determine the correct position of the liner reaction curve relative to the instantaneous ground reaction curve (the P = 0 position of the liner reaction curve between the origin and point C in Fig. 2.2).

The relationship between potential liner pressure and the prior displacement of the tunnel opening, u_p, plots as a straight line for elastic behavior, as shown in Fig. 2.5 (line AC). This curve corresponds to the ground reaction curve for the instantaneous displacements of an opening in an elastic medium, and can be used, in combination with a liner reaction curve, in a similar manner. For the case illustrated in Fig. 2.5 the line DB is the liner reaction curve. (Note: If point D is located at the origin of axes, the case corresponds to liner installed far ahead of face - 2-D elastic $K_o \neq 1$ solutions; if point D is located at or to the right of point C, corresponds to liner installed far behind face - ground reaction curve solutions). Here it is assumed that the liner is installed right at the tunnel face. Thus, the displacement that has already occurred is $u_p = u_f$. As the tunnel is advanced beyond this point the liner resists the additional displacement u_d, allowing only the displacement u_ℓ to occur before a condition of equilibrium is achieved. Because the displacement $u_p = u_f$ occured before the liner was installed, the maximum pressure that could have acted

Points on curve A - C represent maximum potential pressure, $P_{\ell p}$, that can act on liner installed after displacement u_p has occurred.

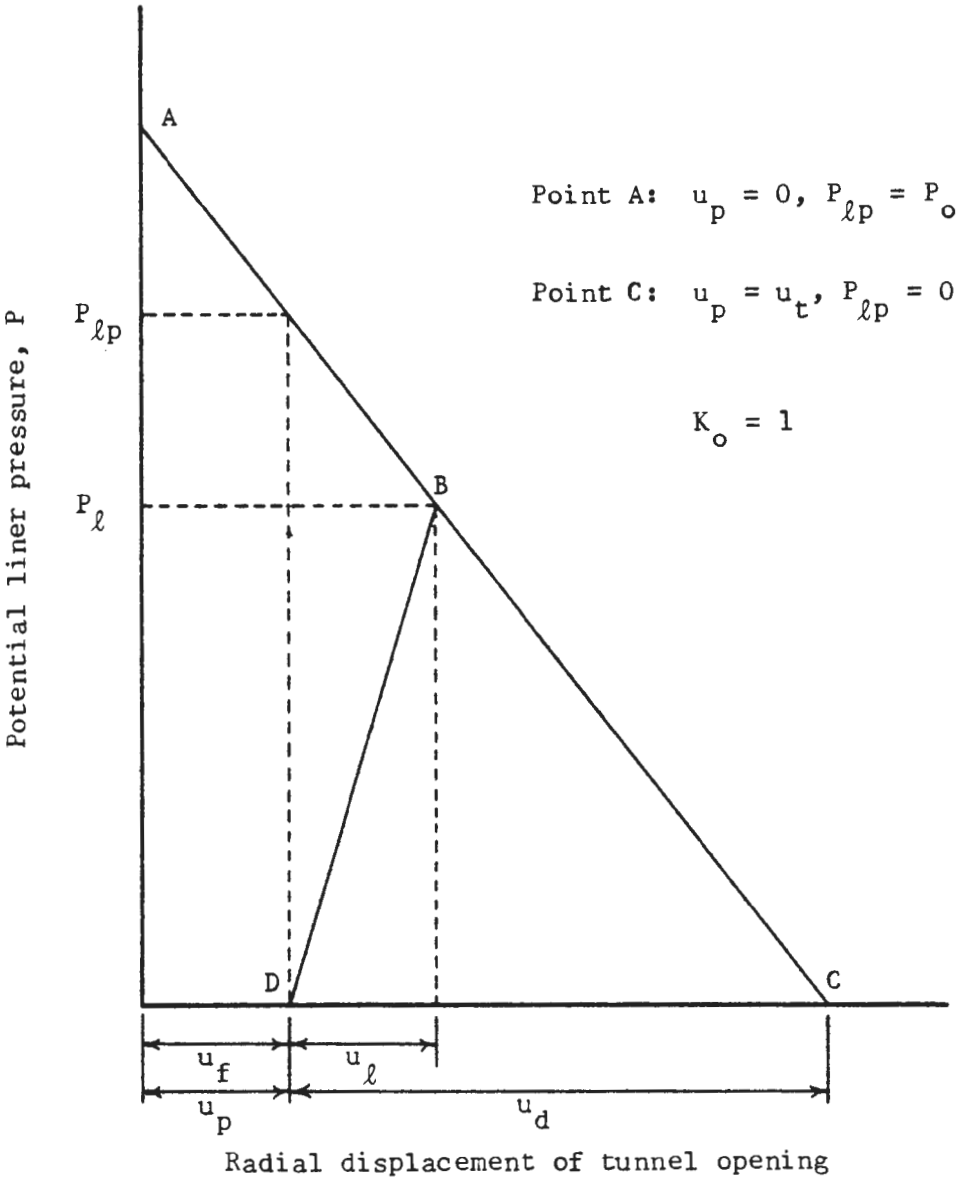

FIGURE 2.5 TYPICAL CURVE FOR POTENTIAL LINER PRESSURE VERSUS PRIOR DISPLACEMENT — ELASTIC GROUND

on the liner was only $P_{\ell p}$, not the full insitu pressure P_o. Interaction between the ground and the compressible liner led to the further reduction of pressure to P_ℓ at equilibrium.

The relationship between P_ℓ and u_p, illustrated in Fig. 2.5 for a specific case ($u_p = u_f$), can be generalized in equation form. Using the Lamé equations for an elastic thick-wall cylinder, Daemen (1975) derived the following expression:

$$\frac{P_\ell}{P_o} = \left(1 - \frac{u_p}{u_t}\right) \cdot \frac{1}{1 + \frac{1+\nu_\ell}{1+\nu_m} \cdot \frac{E_m}{E_\ell} \cdot \frac{(1-2\nu_\ell) + (1-t/a)^2}{\frac{t}{a}(2 - t/a)}} \qquad (2.1)$$

To obtain this equation two thick-wall cylinders are considered. One cylinder, representing the liner, has an outer radius of a and an inner radius of (a - t). The second cylinder, representing the ground mass, has an inner radius of a and an outer radius of b such that $b \gg a$. If the liner is installed at the point indicated in Fig. 2.4 it will resist the displacement u_d when the face is advanced. At equilibrium the ground-liner interface pressure is P_ℓ. The displacement of the liner, u_ℓ, is obtained from consideration of the first cylinder, which is subjected to an external pressure of $P_e = P_\ell$ and an internal pressure of $P_i = 0$. The displacement of the ground mass that the liner has prevented, u_{pr}, is obtained from consideration of the second cylinder, which is subjected to an internal

pressure of $P_i = P_\ell$. Equation 2.1 is obtained by substituting the expressions for these displacements into the relation $u_d = u_\ell + u_{pr}$. In this relation u_d is some fraction $(1 - u_p/u_t)$ of the total displacement u_t; the expression for u_t being obtained from consideration of the second of the above cylinders when it is subjected to an external pressure of $P_e = P_o$ and an internal pressure of $P_i = 0$.

Equation 2.1 can also be obtained by modifying the derivation of the thick liner solution for excavation loading to account for the prior displacement u_p. The corresponding equation for a thin liner, obtained by similarly modifying the derivation of the thin liner solution for excavation loading, is:

$$\frac{P_\ell}{P_o} = \left(1 - \frac{u_p}{u_t}\right) \cdot \frac{1}{1 + \frac{1 + \nu_\ell}{1 + \nu_m} \cdot \frac{E_m}{E_\ell} \cdot (1 - \nu_\ell) \cdot \frac{a}{t}} \qquad (2.2)$$

The in situ ground pressure is denoted by P_o (for $K_o = 1$). Typical curves of P_ℓ/P_o vs. u_p/u_t obtained from these equations are illustrated in Fig. 2.6. The liner pressure for a given prior displacement is indicated by the intersection of the vertical line located at u_p/u_t and the P_ℓ/P_o vs. u_p/u_t line. The equations, and thus Fig. 2.6, do not give the liner displacement, u_ℓ, resulting from interaction.

If the relationship between position of liner installation and prior displacement is available, Fig. 2.5 or Eqns. 2.1 or 2.2 can be used to determine the equilibrium liner pressure for a given position of liner

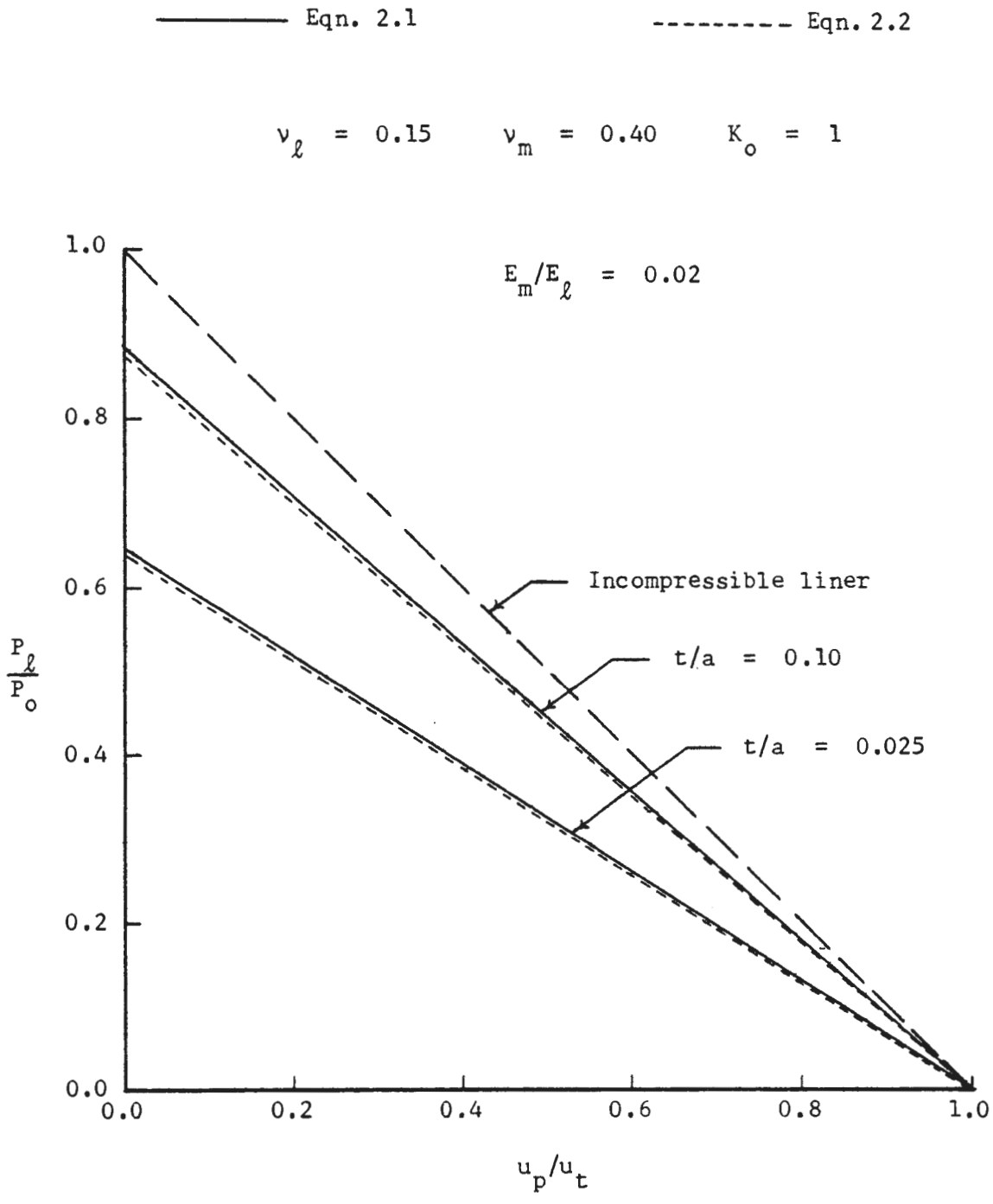

FIGURE 2.6 EQUILIBRIUM LINER PRESSURE VERSUS PRIOR GROUND DISPLACEMENT - ELASTIC GROUND

installation. Figure 2.7 gives the liner pressure for liner sections installed at various distances, z_ℓ, from the tunnel face. The curves can also be interpreted as the longitudinal distribution of pressure on a continuous liner that extended all the way to the tunnel face before excavation was resumed. The u_p/u_t vs. z curve was obtained from Fig. 2.4.

Although Fig. 2.5 and Eqns. 2.1 and 2.2 are useful as a means of illustrating the nature of the relationship between the position, relative to the tunnel face, at which a liner is installed, z_ℓ, and the resulting ground pressure that acts on the liner, such methods are useless without prior knowledge of the relationship between u_p and z. For the examples just considered the u_p - z relationship was obtained from Fig. 2.4 which, however, is not applicable to the general case of an advancing lined tunnel. The problem is that the u_p - z relationship is a function of z_ℓ.

The displacement distribution of Fig. 2.4 is valid for a lined tunnel only if liner installation always occurs at a distance greater than 2D behind the advancing face. As far as ground-liner interaction (with respect to instantaneous ground displacement) is concerned, this is a trivial case because at this distance behind the face all of the ground displacements have occurred (Fig. 2.4) and there can be no interaction. The u_p - z relationship for an unlined tunnel, Fig. 2.4, can be applied only to the following special case. If face advance was halted while liner installation continued until the tunnel was lined up to the face, the u_p - z relationship from Fig. 2.4 could be used to determine the longitudinal distribution of pressure that would act on the length of liner $0 \leq z \leq 2D$ (as shown in Fig. 2.7) after the face had been advanced a distance of at least 2D beyond the end of the liner. For the general problem of the advancing

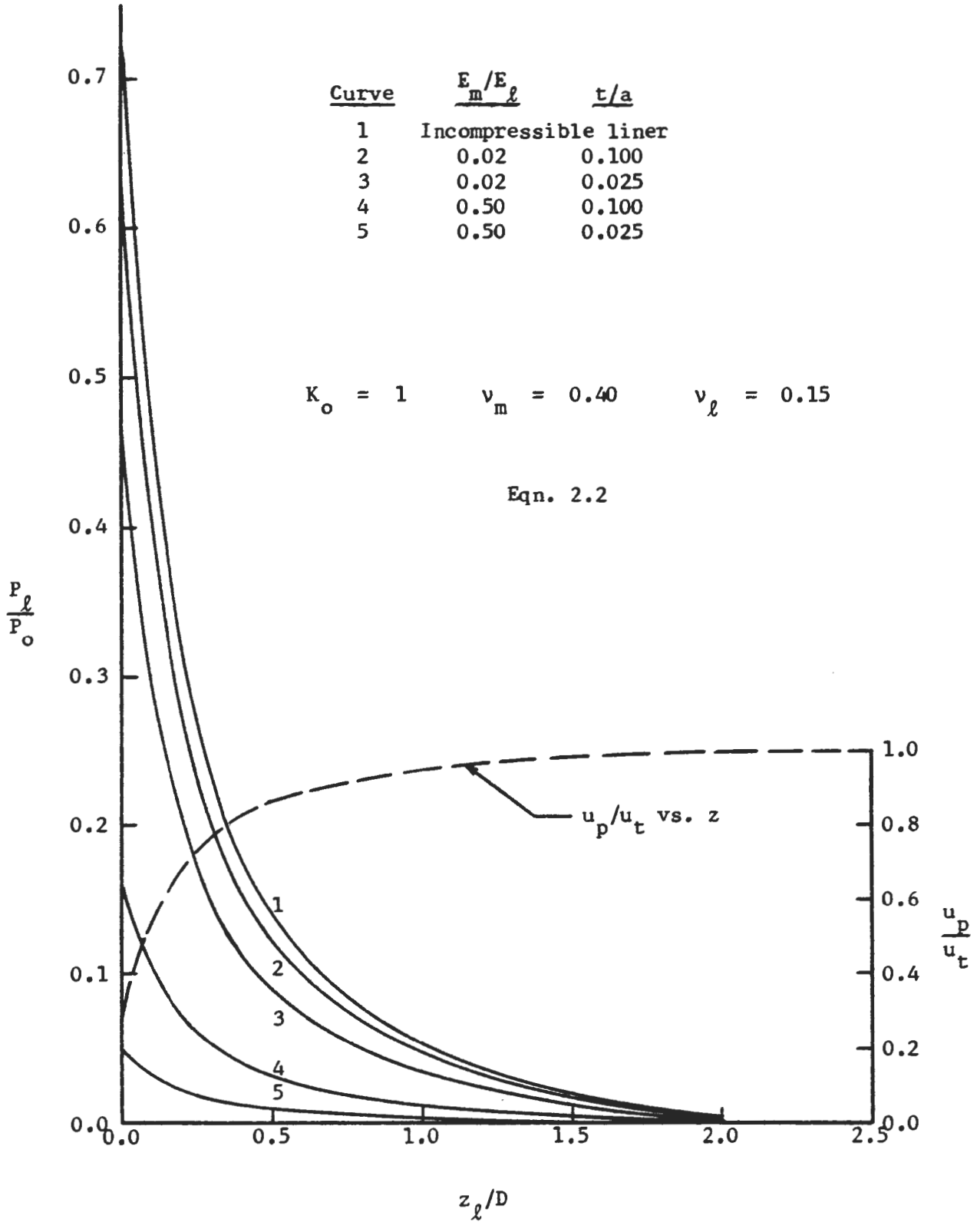

FIGURE 2.7 PRESSURE ACTING ON SECTION OF LINER VERSUS DISTANCE, z_ℓ, BEHIND FACE AT WHICH LINER SECTION INSTALLED

tunnel interaction will occur only if, as the face is advanced, new sections of liner are continually installed at a distance of less than 2D behind the face. However, the resulting interaction inhibits the ground displacement (u_p) ahead of the liner, causing the longitudinal displacement distribution (the u_p - z relationship) to be different from that shown in Fig. 2.4 for an unsupported tunnel.

It would seem reasonable to expect that any method employed to determine the correct u_p - z relationship for use in Fig. 2.5 of Eqns. 2.1 or 2.2 would also yield the P_ℓ - z_ℓ relationship, thereby eliminating the need for Fig. 2.5 or Eqns. 2.1 and 2.2 as a means of determining P_ℓ vs. z_ℓ.

2.3.2 LOCALIZED GRAVITY LOADING

As described in Section 2.2, localized gravity loading occurs when portions of the surrounding ground mass dislodge and come to rest on or against the tunnel liner. Most of the literature on the subject of this type of loading is devoted to empirical methods for correlating ground (rock) mass characteristics and support requirements. Terzaghi (1946), Barton, et al.(1974) and Wickham, et al. (1974) have presented ground mass classification systems for use in estimating the magnitude of the support pressure required to stabilize openings in the various types of ground. As these methods have developed over the years they have come to include more and more of the details of the rock mass characteristics. As an example, Barton, et al. (1974) give the following empirically derived expression for the required roof support pressure:

$$P_{roof} = (2/J_r)\ Q^{-1/3} \qquad (2.3)$$

where Q, the rock mass quality factor, is a function of six parameters. These parameters are: the RQD index value, the number of joint sets, the roughness of the weakest joints (J_r), the degree of alteration or filling along the weakest joints, and two additional parameters which account for the source of the rock load and for water inflow.

Analytical solutions for consideration of interaction between the gravity loaded liner and the surrounding ground mass are few in number. The graphical-analytical solution technique given by Procter and White (1946) and the three solutions (Bodrov-Gorelik, Polygonal Method, Bougayera) described by Széchy (1966) are probably the best known and most widely used. Each of these solution methods requires prior knowledge of the distribution and magnitude of the pressure that the gravity load imposes on the liner. Thus, in order to analyze ground-liner interaction for a given ground-liner system, empirical methods such as those mentioned above must first be used to estimate the active pressure on the liner.

2.4 NUMERICAL TECHNIQUES - THE FINITE ELEMENT METHOD

Among the many numerical techniques available, the finite element method is emerging as the most likely candidate for analysis of ground-liner interaction and underground construction problems in general. There are numerous finite element programs available that can be used to analyze this type of problem. Some of the significant aspects of the various procedures that have been used are described in the following discussion of finite element simulation of ground-liner interaction.

2.4.1 EXCAVATION LOADING

The task of accurately simulating the ground-liner interaction

problem is an extremely complex one and the state of the art of the finite element method does not permit consideration of all the relevant details of the problem. However, most of the important aspects can be considered with many of the available programs. A finite element mesh of the region which contains the tunnel can be developed and analyzed for simulation of the excavation and construction process. Nonlinear and time-dependent ground behavior as well as many additional degrees of analytical refinement can be introduced in the analysis to the extent allowed by practical limitations imposed by the computer capabilities, and the theoretical limitations imposed by insufficient knowledge of material behavior or how to model such behavior.

In the finite element simulation of underground structures three phases of analysis can be differentiated, each representing a distinct stage under significantly different conditions.

a. Initial Phase. The aim of this phase of analysis is to duplicate, as closely as possible, in the finite element mesh the initial state of stress existing in the ground prior to construction.

b. Construction Phase. This phase of analysis starts with the initial state of stress present in the mesh and proceeds to simulate the actual sequence of excavation and construction.

c. Operation Phase. The purpose of this phase is the analysis of the completed structure subjected to the various loading conditions that may arise during the life of the structure.

The first step in the analysis of an underground structure is the development of an appropriate mathematical model of the system to be analyzed.

The finite element model necessarily covers a finite region while modeling what in reality can be assumed to be a half space. Only a limited number of boundary conditions are available which can be imposed on the outer boundaries of such a finite region. The most important considerations are the choice of an adequate region for modeling and the type of boundary conditions to use so as to minimize the effect of the artificial boundaries on the quantities of interest. For a deep opening a region extending to a distance of a few opening widths in each direction seems sufficient. If the source of action is within the region, then fixed boundary conditions can be used, whereas the force boundary condition is the obvious choice for analysis of the effect of in situ stresses. In the case of near surface openings the region of analysis should extend to the ground surface. In situations where surface displacements are of interest, the lateral extent of the region is determined by the depth of the opening as well as the opening width.

Material behavior of the medium also becomes a factor in determination of the region of analysis in certain cases. When the medium is modeled as a nonlinear or elasto-plastic material, and the zone of plastic yield or nonlinear behavior reaches or closely approaches an artificial boundary, the results should be regarded with suspicion, because the artificial boundary will most likely have influenced the response of the system.

Prior to simulation of construction the insitu stress conditions should be represented in the mathematical model as closely as possible. This is a difficult task and in some cases it is impossible to model the true in situ stress condition even if it can be determined in the field. In

such cases it becomes necessary to compromise and use approximate values for the initial stress conditions. Generally, the in situ stress condition is achieved by applying the weight of the medium as a body force to the pre-excavation configuration of the region of the ground mass to be analyzed. Additional types of loading may be present, such as that due to the weight of adjacent surface structures and/or the presence of tectonic forces, and these can be included through the use of boundary forces.

For deep openings the weight of the medium contained within the bounded finite element mesh may be negligible compared to the stresses due to the total overburden. In such cases the full overburden stress can be applied as a force boundary condition and the self-weight of the medium encompassed by the finite element mesh can be neglected.

The coefficient of lateral stress, K_o, arising from the self-weight of a linear medium, becomes a function of Poisson's ratio, ν, when the lateral boundaries are constrained against horizontal movement. Under these conditions the value of K_o will vary from one for $\nu = 0.5$ to zero for $\nu = 0$. To simulate values of K_o independent of ν a force boundary condition must be applied to reflect the appropriate values of the lateral stresses. When the material properties of the medium vary with depth, such as in a layered system, a lateral force boundary condition appears to be the only way to obtain a uniform value of K_o. The boundary conditions used in the first step of analysis to simulate the insitu stress conditions may have to be modified in subsequent steps for simulation of construction, in order to reflect the restraining effects of the medium outside the boundaries.

The technique for the simulation of construction using the finite element method was initially developed by Clough and Woodward (1967) in an

analysis of the construction of earth dams. The technique has been used for the analysis of numerous geotechnical problems involving the simulation of excavation as well as construction. The simulation technique has been used in the analysis of the incremental construction of earth dams (Kulawy, et al., 1969), large open excavations (Duncan and Dunlop, 1968), and braced excavations (Christian and Ing, 1973, and O'Rourke, 1975).

The purpose of the analysis of the excavation process is to determine the change of state (displacements, strains, stresses) resulting from the removal of a stressed portion of the system. Before excavation (pre-excavation stage) certain stresses act on the surface which is to form the boundary of the excavated region. These stresses vanish upon the completion of excavation (post-excavation stage) if no internal support or pressure is immediately applied. Using the finite element method, some researchers (e.g., Christian and Ing, 1973) have simulated the process of excavation by computing the forces acting on the excavation surface at the pre-excavation stage and subsequently applying the opposite of these forces to the model of the post-excavation stage which is formed by the removal of the excavated portion. However, such techniques can be used only in linear analyses and involve awkward and lengthy multistage computer analyses of the different stages of excavation and construction.

A more general approach to the simulation of excavation and construction is to treat the problem as a nonlinear one. The source of nonlinearity in this case is the change of the geometry of the system. Therefore, a general solution scheme for nonlinear problems can be used. Using such a procedure nonlinear material behavior can be considered along with the change of geometry resulting from excavation and construction in a

unified manner. For the portions of the system to be excavated or constructed, elements are assigned initially and the analysis is carried out in steps similar to incremental nonlinear analysis. The elements in the portions to be excavated are active originally and at a designated step when excavation is to take place these elements are deactivated, i.e., they are not assembled in the remainder of the analysis. The construction of support systems is simulated using a reverse process; the elements are initially inactive and they are activated at a designated step when the installation of the support structure is to take place. The activated elements may already be stressed to simulate prestressing, such as is the case with pretensioned rock bolts. The installation and removal of a temporary support system can be simulated be activating elements at one step and subsequently deactivating them at a later designated step to simulate the removal of the temporary structures.

In the analysis of tunnels the simplest and least expensive model is that which considers a two-dimensional, plane strain section of the tunnel in the plane which is perpendicular to the axis of the tunnel. A simulation analysis can be performed on this model. However, if the tunnel is to be excavated full face the analysis consists of just two steps. At the first step the in situ stress condition is simulated and at the next step the elements within the tunnel are deactivated to simulate excavation and the liner elements are activated to simulate liner installation. The ground-liner interaction takes place at the second step. If excavation and liner placement are performed at two separate steps, no ground-liner interaction will occur.

Although this type of two-dimensional analysis may provide some

useful information and have the additional attraction of simplicity, it does not correspond to the true development of deformations and stress changes during the process of tunnel construction. At a cross section on the tunnel line, as the tunnel face approaches and passes, the stress changes and deformations develop gradually. When the liner is installed behind the face at this cross section, some displacement of the ground mass has already occurred prior to the start of interaction. This effect cannot easily be taken into account in a two-dimensional analysis. Another important effect which cannot be modeled in two-dimensional analyses is the fact that as the tunnel face advances, the excavation is done in a zone ahead of the face in which the stress condition has already been modified by the approach of the face.

In order to consider such effects, it is necessary to perform a three-dimensional simulation of tunnel construction. In such an analysis the ground mass is modeled as a three-dimensional body and the actual excavation of the tunnel, and liner installation with the advancement of the tunnel face, is simulated.

However, even with the present state of the finite element method and computer technology three-dimensional analyses for simulation of tunnel construction can be quite expensive due to the size of the mesh required and the large number of construction steps required in the analysis. While this approach may be feasible for study of underground structures on a case by case basis, parametric studies, requiring numerous analyses, of the general problem appear to be impractical at this time.

A compromise can be made by assuming the coefficient of lateral stress, K_o, to be equal to one. For this special case the problem reduces

to a manageable axisymmetric form with the axis of symmetry coinciding with the tunnel centerline. The cost of such an analysis is comparable to that of two-dimensional, plane strain analyses. This is, of course, a reasonable approximation for moderately deep tunnels where the ground surface effects are negligible.

The response of the ground-liner system as obtained from the finite element analysis of ground-liner interaction is strongly influenced by the sequence of events simulated in the analysis. This is illustrated in the following discussion of two such simulation sequences.

One approach to the finite element analysis of ground-liner interaction that has been used frequently in the past does not include simulation of excavation and construction. In this type of analysis the finite element mesh is generated with the tunnel and liner already in place. Interaction occurs when the boundary forces are applied. The sequence of events as simulated in this type of analysis is illustrated in Fig. 2.8a. This type of analysis is only appropriate if the overpressure loading condition is being considered. Analyses of this type cannot be used to investigate interaction resulting from excavation loading.

If the excavation loading condition is to be considered the finite element analysis must include the simulation of excavation and construction as previously described in the discussion of the three phases of analysis. The sequence of events as simulated in this type of analysis is illustrated in Fig. 2.8b.

The liner thrusts resulting from these two types of analysis (with and without simulation of construction) are shown in Fig. 2.9 as functions of the compressibility ratio, C, and for various values of Poisson's ratio

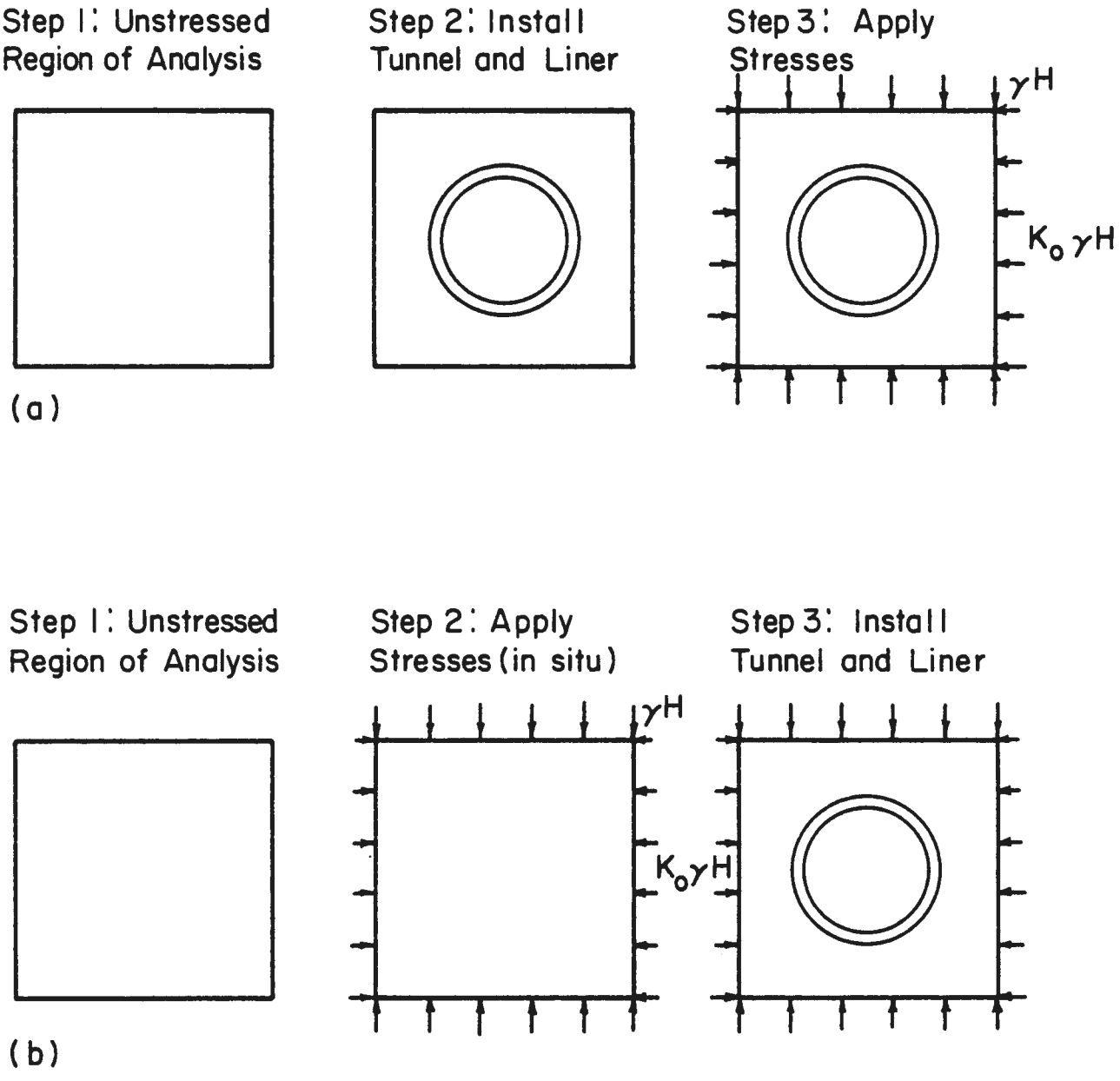

FIGURE 2.8 SEQUENCE OF ANALYSIS FOR, (a) WITHOUT SIMULATION OF CONSTRUCTION, (b) WITH SIMULATION OF CONSTRUCTION

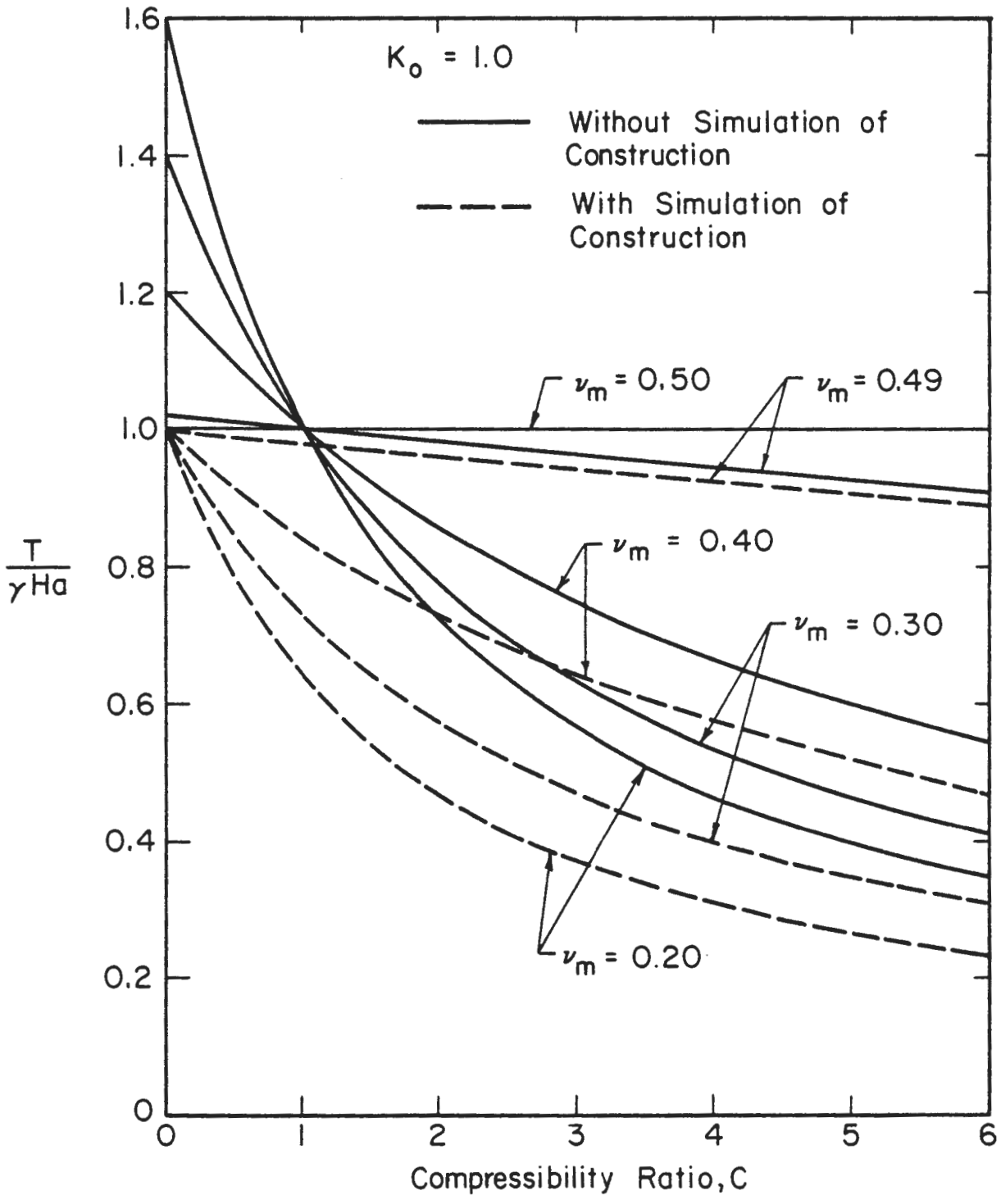

FIGURE 2.9 VALUES OF THRUST COEFFICIENT FROM ANALYSES WITH AND WITHOUT SIMULATION OF CONSTRUCTION

of the medium. The compressibility ratio is a measure of the relative stiffness of the medium and the liner (Peck, et al., 1972) given by the following equation.

$$C = \frac{E_m}{(1 + \nu_m)(1 - 2\nu_m)} \Big/ \frac{E_\ell}{(1 - \nu_\ell^2)} \cdot \frac{t}{a} \qquad (2.4)$$

The radial displacements resulting from these two types of analysis are summarized in Fig. 2.10.

It can be seen from these figures that without simulation of construction the liner thrusts and radial displacements are consistently higher, especially for low values of the compressibility ratio which correspond to a stiff liner in soft ground. It is also interesting to note that the Poisson's ratio of the medium has significant effect on the results. It is only for an incompressible medium ($\nu_m = 0.5$) that the two analyses give the same radial displacement and liner thrust.

The differences in the results obtained from the two types of analysis can be attributed to the differences in the ground displacements the liner must resist in each. Considering an unlined opening, Fig. 2.11 shows that the analysis sequence for simulation of excavation yields the total displacement u_t in going from the imaginary circle in step 1 to the stable opening at the end of step 3. This displacement is composed of two components, $u_t = u_i + u_o$, where u_i is the displacement of the imaginary circle caused by the application of the in situ stresses in step 2, and u_o

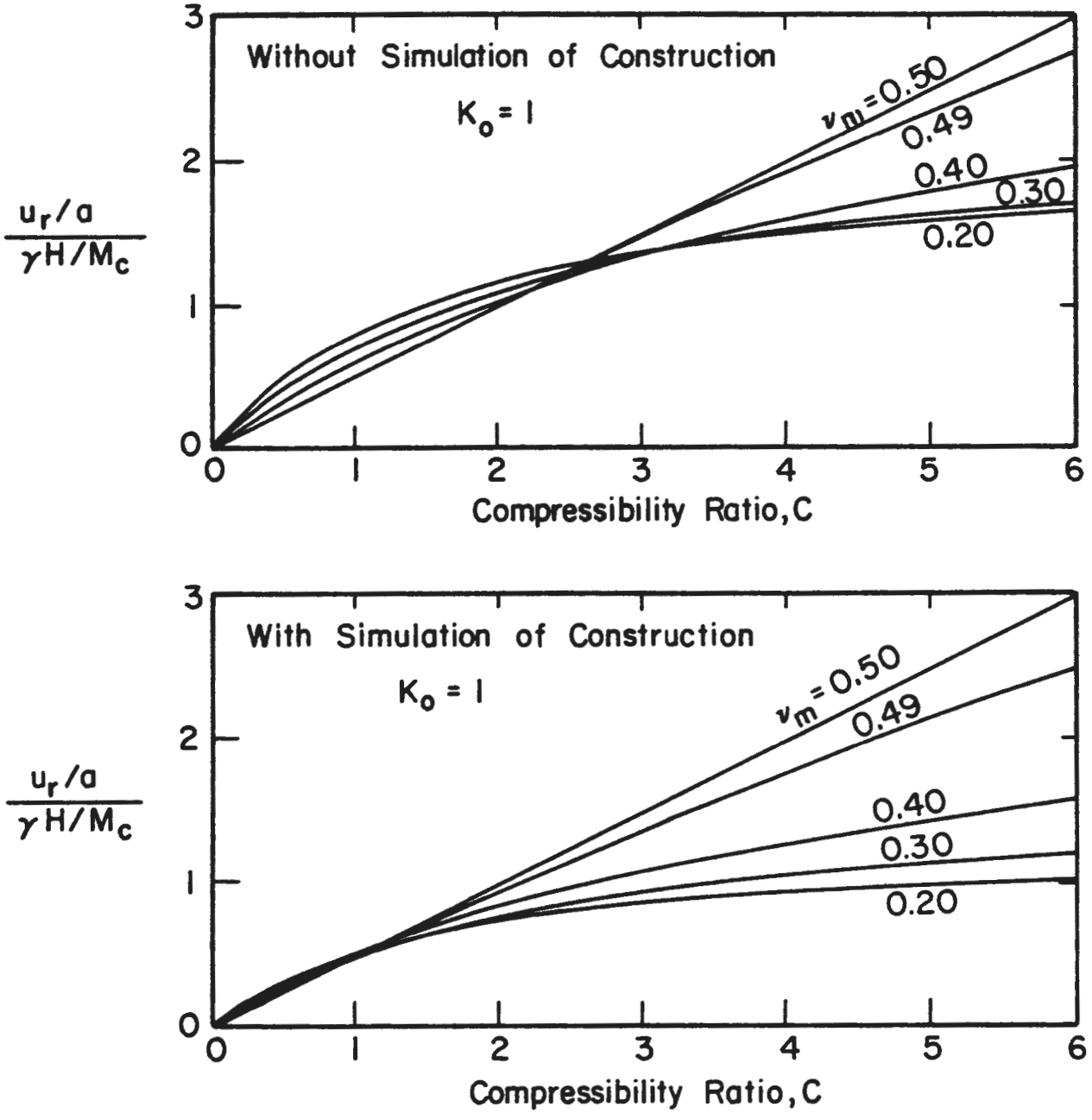

FIGURE 2.10 VALUES OF RADIAL DISPLACEMENT COEFFICIENT FROM ANALYSES WITH AND WITHOUT SIMULATION OF CONSTRUCTION

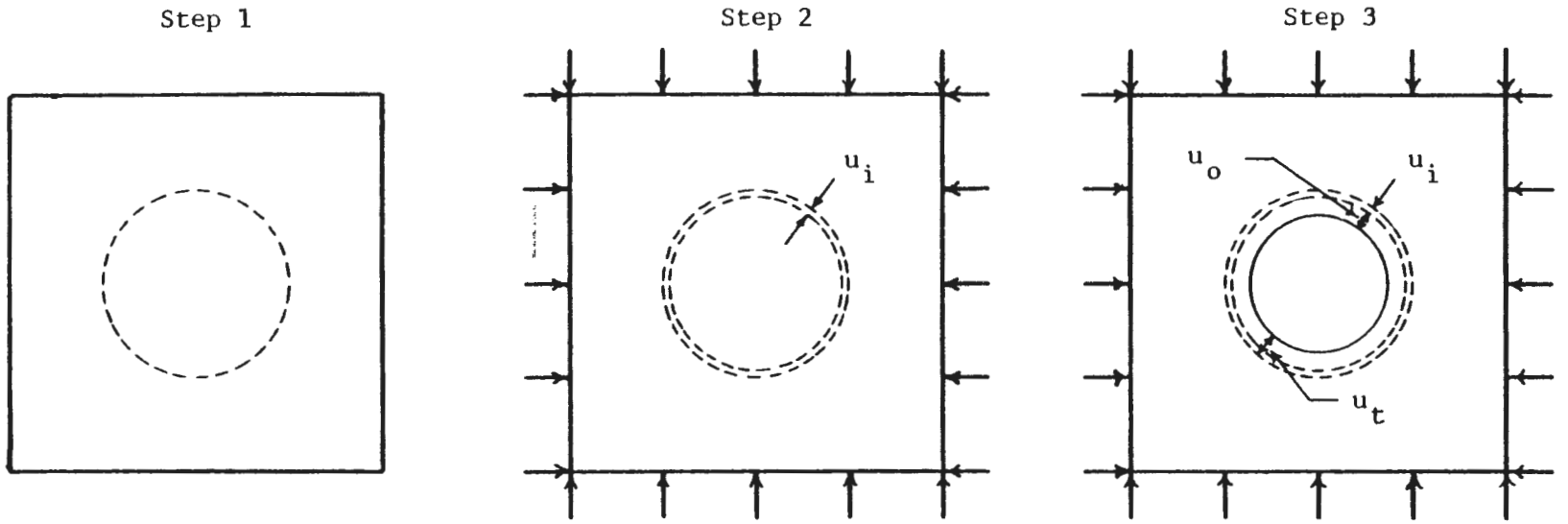

Step 1 : Unstressed region of analysis - finite element mesh composed entirely of "ground" elements

Step 2 : Apply boundary forces (or body forces) to mobilize in situ stress field in mesh

Step 3 : "Excavate" opening

FIGURE 2.11 GROUND DISPLACEMENTS FOR ANALYSIS OF UNLINED OPENING WITH SIMULATION OF CONSTRUCTION

is the displacement caused by the creation of the opening in step 3. When simulation of construction is not included in the analysis of a lined opening, the liner must resist the full displacement u_t. When simulation of construction is analyzed, the displacement u_i occurs before the the tunnel is created, and thus the liner must resist only the displacement u_o. The displacement u_i is, of course, a function of Poisson's ratio of the ground mass, ν_m, and for $\nu_m = 0.5$, $u_i = 0$.

Figures 2.8, 2.9, and 2.10 and the above discussion apply to two-dimensional, plane strain finite element analyses. However, these comments also apply to the differences between the original and modified Burns and Richard (1964) and Dar and Bates (1974) closed form analytical solutions previously described. The original solutions (overpressure loading) correspond to the finite element analyses that do not simulate construction. The modified solutions (excavation loading) correspond to the finite element analyses that do simulate construction.

The influence of the simulation of the longitudinal excavation and construction of tunnels on the results of analysis is shown in Fig. 2.12. One curve in this figure shows the liner thrust obtained when no excavation was simulated; the insitu stresses were applied to the mesh which already contained the tunnel with the liner extended to within one tunnel radius of the face. The final (far behind the face) thrust value for this case is equal to the two-dimensional analysis result with no excavation simulation. The second curve in this figure is the result of an analysis in which excavation and construction of the support was simulated in one step; i.e., in one step all the elements within the tunnel were deactivated and all liner elements were activated. The final value of the thrust in this case is

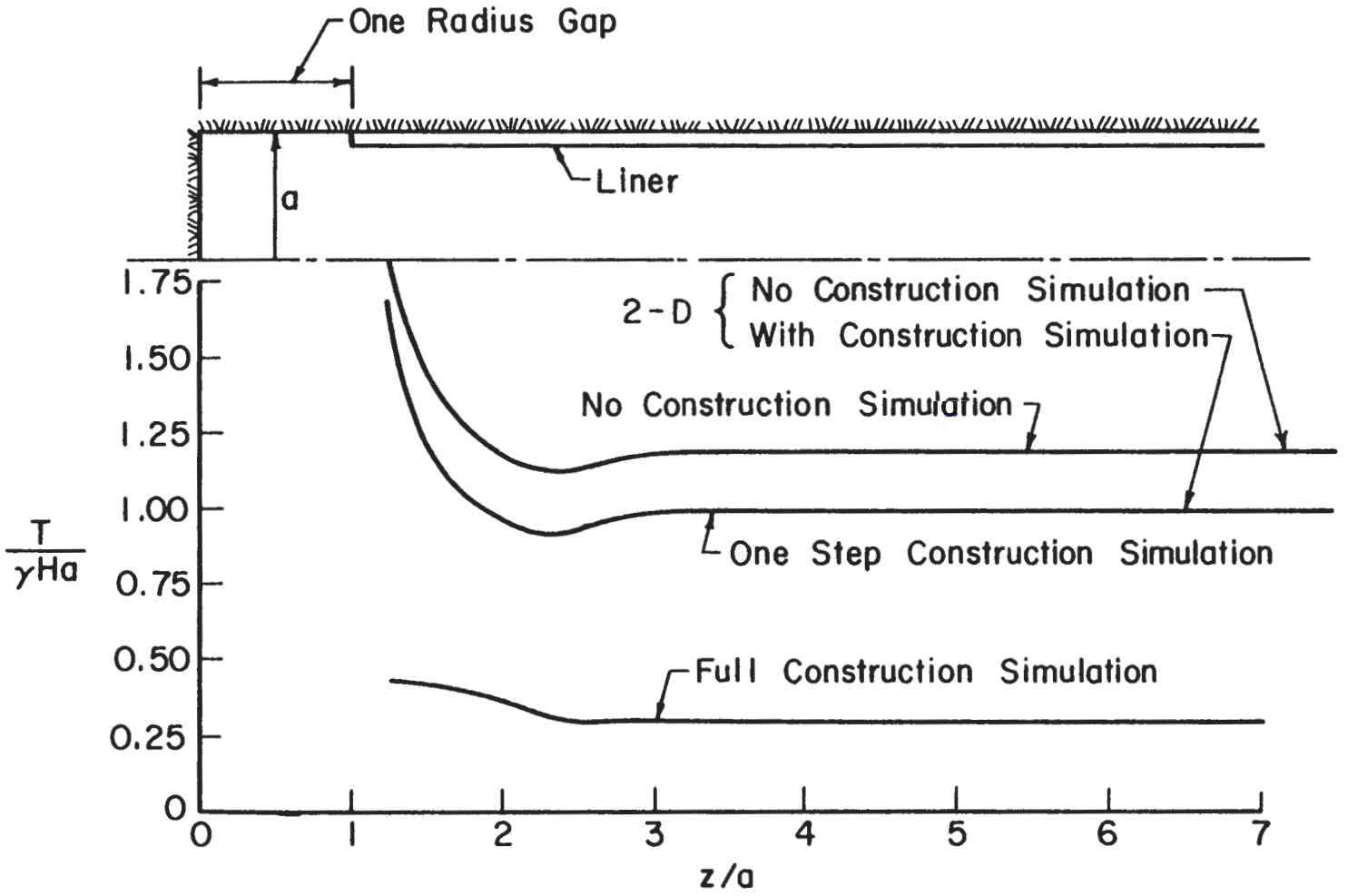

FIGURE 2.12 LONGITUDINAL VARIATION OF LINER THRUST FOR DIFFERENT FORMS OF CONSTRUCTION SIMULATION

equal to the value given by the two-dimensional analysis with simulation of excavation. The last curve in Fig. 2.12 is the result of an analysis in which excavation of the tunnel and placement of the liner were simulated as occurring in small steps to reflect the true process of tunnel construction with gradual advancement of the tunnel face. Each step of the analysis consisted of advancing the tunnel face and the leading edge of the liner along the centerline by a distance equal to one half of the tunnel radius. The dramatic reduction of the thrust in this case as compared to the thrust values obtained in the other cases is the result of the displacements taking place ahead of the liner.

These examples clearly demonstrate the strong influence of construction process simulation on the results obtained from analyses of ground-liner interaction. A true measure of the ground-liner response for excavation loading can only be determined if the construction process is simulated as closely as possible in the analysis.

It is a well established fact that when soil is modeled as a linearly elastic material, the results of the analysis are approximate in that they do not reflect the true material behavior of soils which exhibit strong nonlinearity. To discuss the effects of nonlinear soil behavior on the results of numerical simulation of ground-liner interaction, results are presented from analyses in which the soil was assigned elasto-plastic material properties with a Drucker-Prager (1952) yield condition. This yield condition is given by the following equation:

$$\sqrt{J_2} + \alpha J_1 - k = 0 \qquad (2.5)$$

in which J_1 and J_2 are the first invarient of the stresses and the second invarient of the deviatoric stresses, respectively, and α and k are material constants.

Shown in Fig. 2.13a, for two-dimensional, plane strain analyses, are typical plastic yield zones that form around an unlined and a lined tunnel when the excavation and liner installation are simulated. For the unlined tunnel, when the excavation is simulated by deactivating the elements within the tunnel, a large plastic zone develops due to lack of internal support. This large plastic zone strongly influences the stress distribution around the tunnel and gives much larger displacement of the tunnel perimeter than the elastic analysis. When a lined tunnel is simulated, excavation and liner installation occur simultaneously; in one step the elements within the tunnel are deactivated and the liner elements are activated. As a result the zone of plastic yield is very small and has very little effect on the tunnel behavior. In this type of analysis the stiffness of the liner is an additional parameter influencing the extent of plastic yield. A relatively stiff liner may prevent yielding entirely, in which case the elasto-plastic analysis would give results identical to those of a linear elastic analysis.

The plastic yield zones, around an unlined and a partially lined tunnel, resulting from the simulation of longitudinal excavation and liner placement are shown in Fig. 2.13b. As can be seen, in both the unlined and lined cases the plastic yield zones develop gradually as the tunnel face advances, and continue to expand within some distance behind the face, consistent with the material properties assigned to the soil and with support conditions. Nonlinear soil behavior can a significant effect on the results

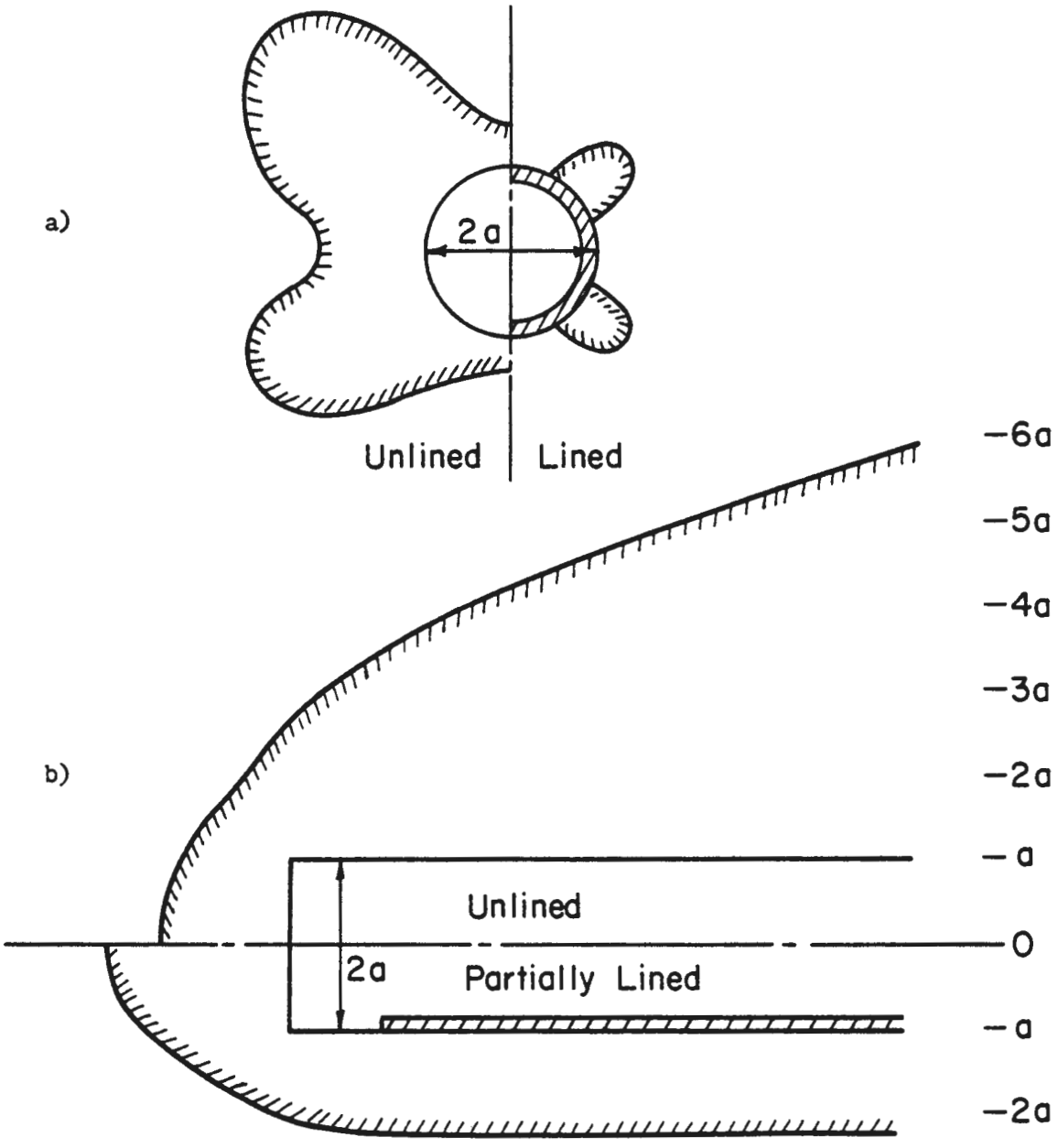

FIGURE 2.13 TYPICAL PLASTIC YIELD ZONES AROUND TUNNELS

of simulation analyses and this effect is more drastic, but rational, when the longitudinal process of tunnel construction is simulated.

The above examples illustrate the inadequacy of the standard two-dimensional finite element analysis as a tool for simulation of tunnel construction and the resulting ground-liner interaction. The ground around real tunnels almost always undergoes some displacement and stress change prior to coming into contact with the liner. This prior ground disturbance results in the formation of a plastic zone around the tunnel ahead of ground-liner contact. Figure 2.13 shows that the two-dimensional analysis, because it assumes no prior ground disturbance, severly underestimates the extent of plastic yielding around the lined tunnel. Because of this, the two-dimensional analysis does not adequately account for the influence of non-linear ground behavior on liner response. This indicates that attempts to increase the utility of the two-dimensional analysis (of lined tunnels) by introducing the additional refinement of nonlinear ground mass behavior will not be successful. In order to fully exploit the available nonlinear ground behavior models in the analysis of this type of problem the longitudinal effects must be taken into consideration.

2.4.2 LOCALIZED GRAVITY LOADING

The ground-liner interaction problem for localized gravity loading is usually reduced to a highly idealized form for numerical analysis. At the present state of the art of numerical analysis methods it is not normally practical to include in an interaction analysis simulation of the details of the rock mass characteristics and the mechanical processes that result in separation of soil or rock from the surrounding ground mass.

Figure 2.14a illustrates a cross section through an hypothetical rock mass which contains three intersecting joint sets; one parallel to the plane of the cross section and two normal to the cross section. Figure 2.14b shows that upon excavation and construction of a tunnel through this rock mass a number of rock blocks have loosened and come to rest on the liner. This load has forced the crown inward, away from the surrounding rock, and the invert and springlines outward, against the surrounding rock. The result is a complex distribution of active (rock load) and passive, or interaction, pressures acting on the liner. The magnitude and distribution of the active pressure are functions of the rock jointing (spacing, orientation, conitinuity, and shear strength of the joints), the in situ stress field, and the methods and details of the construction procedure. The distribution and magnitude of the passive pressures are functions of the active pressures, the rigidity and stiffness of the liner, the shear strength of the rock-liner contact, and the pressure-deformation response of the surrounding rock mass.

Figure 2.14c illustrates the problem as commonly analyzed. The simulated ground-liner system consists of a two-dimensional, plane strain section normal to the tunnel axis containing a liner embedded in a homogeneous, elastic ground mass. The factors important to the formation of the loosened rock mass and the physical presence of this material on the liner are usually not simulated in the numerical analysis. These factors must, of course, be considered prior to analysis in order to estimate the extent of active pressure on the liner, and those factors that affect the deformational response of the surrounding rock can be indirectly accounted for when the deformation modulus and Poisson's ratio values are assigned to

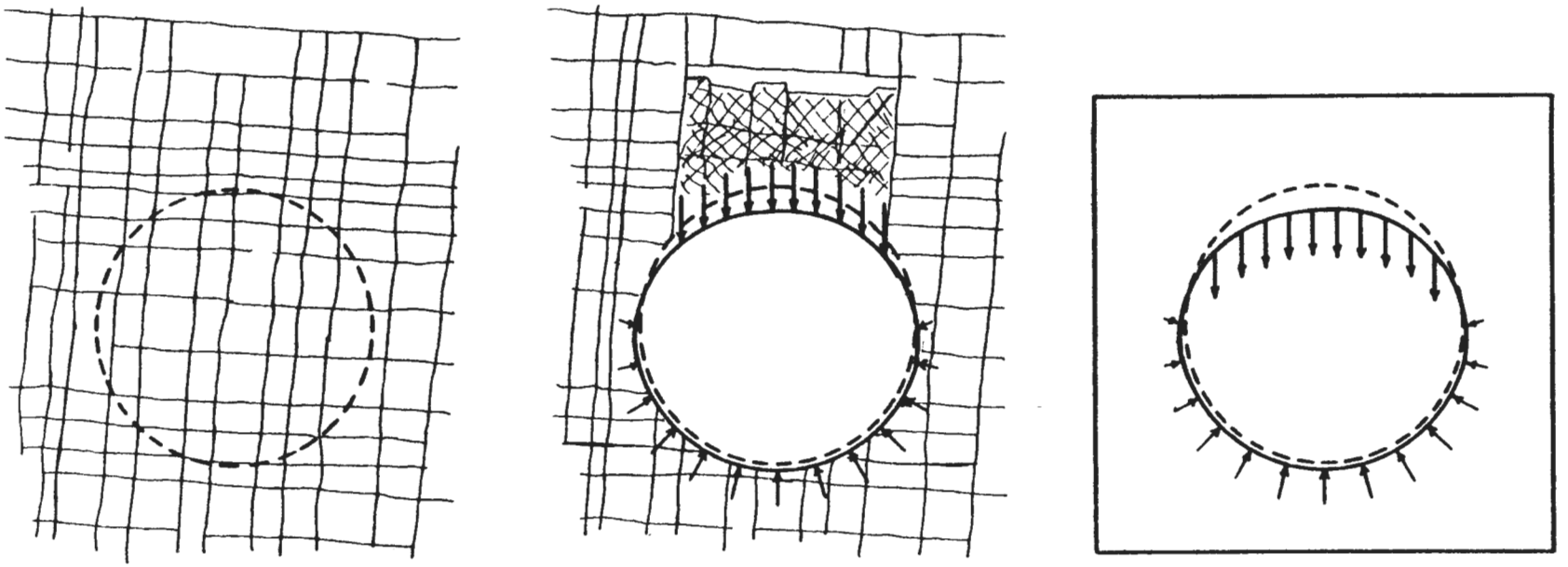

a.

b.

c.

a and b : Problem to be simulated

c : Problem as simulated

FIGURE 2.14 IDEALIZATION OF THE LOCALIZED GRAVITY LOADING GROUND-LINER INTERACTION PROBLEM

the simulated ground mass. The surrounding rock mass can be modeled by an assemblage of finite elements (Dixon, 1973, Mohraz, et al., 1975) or by a system of elastic springs (Dixon, 1971, Bawa and Bumanis, 1972, Brierly, 1975). This second model is similar to the Winkler-type foundation used for the analysis of beams on elastic foundations. The mass of rock resting on, and thereby applying the active pressure to, the liner is simulated by a system of forces applied to the nodal points of the liner, The liner usually consisting of an assemblage of beam elements.

It is important that the analysis provide for separation of the liner from the surrounding medium in the region of loading. If separation is not allowed a portion of the applied load will be transmitted by tension across the ground-liner contact. If this occurs the active load will be shared by the ground and the liner instead of being carried entirely by the liner. If the rock mass is modeled by a system of springs, separation can be insured by solving the problem in a series of two or more analyses. After each analysis the springs are checked to determine if they are in compression or tension. All springs found to be in tension are removed and the analysis is repeated with the new configuration. The problem is solved when all remaining springs are in compression. If the rock mass is modeled by finite elements a third type of element must be inserted between the liner and rock elements to allow separation. Dixon (1973) used stiff one-dimensional bar (spring) elements. With this type of element the procedure for obtaining a solution is the same as that just described; two or more separate analyses are required. The interaction analyses for localized gravity loading described in Chapter 7 utilized a special "joint" element (Goodman, 1968) that has zero tensile strength and which offers no resistance to separation of

liner elements from the rock elements. The advantage gained by using this type of element is that the analysis can be performed in just one computer run instead of several as is required for the spring models.

CHAPTER 3

TUNNELS IN ELASTIC GROUND: ANALYTICAL SOLUTION FOR EXCAVATION LOADING

3.1 GENERAL REMARKS

Peck (1969) provides an excellent description of the basic concepts of ground-liner interaction. The analytical solutions derived in Appendix A constitute generalizations of the two special case solutions (i.e., for perfectly flexible and perfectly rigid liners) discussed by Peck in that they allow consideration of liners of intermediate flexibilities and stiffnesses.

The analytical solutions for excavation loading assume a lined tunnel is to be constructed in a ground mass subjected to a system of in situ stresses as illustrated in Fig. 3.1a. In the rectangular coordinate system one of the principal stresses is assumed to act in the vertical direction and the remaining two principal stresses act in horizontal directions, one being perpendicular and the other parallel to the longitudinal axis of the tunnel. The magnitude of the vertical stress is equal to the weight of the overburden, γH, where H is the depth from the ground surface to the tunnel axis. The magnitude of the horizontal stress is equal to the coefficient of earth pressure at rest, K_o, times the vertical stress. The increase of stress from the tunnel crown to the invert is not considered. Thus, the solutions apply only to deep tunnels. The in situ stress state in terms of the polar coordinate system is also given in Fig. 3.1a. The dashed circle of radius r = a in the figure represents the future location of the lined tunnel.

a) In situ stress state

In polar coordinates:

$$\sigma_r = \tfrac{1}{2}\gamma H\left[(1 + K_o) - (1 - K_o)\cos 2\theta\right]$$

$$\sigma_\theta = \tfrac{1}{2}\gamma H\left[(1 + K_o) + (1 - K_o)\cos 2\theta\right]$$

$$\tau_{r\theta} = \tfrac{1}{2}\gamma H(1 - K_o)\sin 2\theta$$

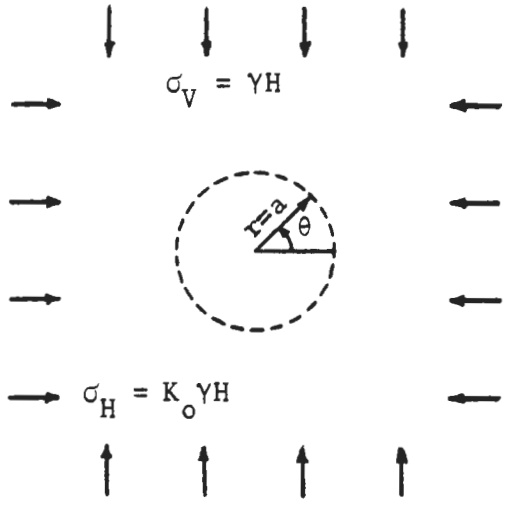

b) Distribution of pressures acting on cylinder of ground to be replaced by liner

$K_o = 0.5$

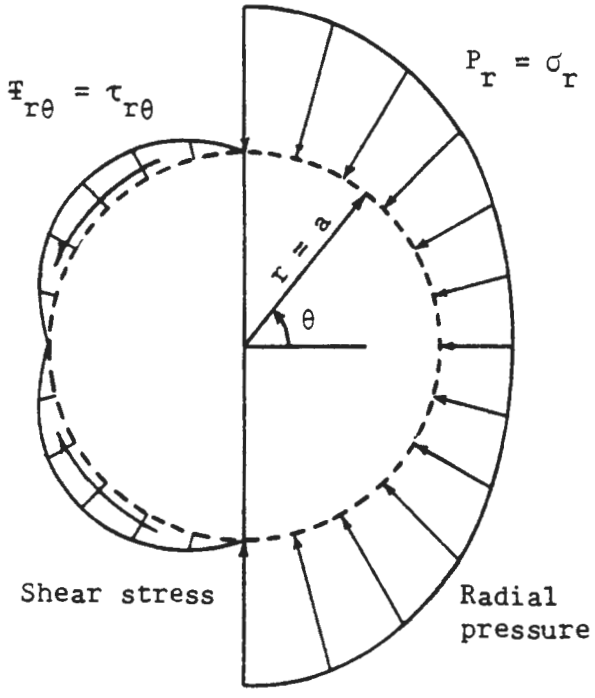

FIGURE 3.1 THE IN SITU STRESS STATE

These solutions further assume that excavation and liner installation occur instantaneously and simultaneously so that no ground displacement or relaxation occurs prior to ground-liner contact and interaction. An alternate assumption is that given by Peck (1969), i.e., the liner is installed first, without disturbing the ground outside or inside the liner, and the ground inside is removed. This approach can be approximated in reality for large diameter tunnels by constructing the liner in a series of small diameter drifts around the circumference of the tunnel and then excavating the soil core.

In this chapter ground-liner interaction is examined on the basis of the information obtained from the analytical solutions derived in Appendix A for thin liners subjected to excavation loading (equations of solutions 3 and 4 in Appendix B).

3.2 EXTERNAL PRESSURES ACTING ON THE LINER

3.2.1 IN SITU STRESSES AND THE GROUND-LINER INTERFACE CONDITION

Figure 3.1b illustrates the distributions of tangential shear and radial normal stresses that, in the undisturbed ground mass, act on the cylinder of ground to be excavated and replaced by the liner. Except for one special case, when the liner is installed the surrounding ground mass will no longer be in equilibrium and ground displacements will occur. These displacements lead to distributions of external pressures acting on the liner that are different from those shown in Fig. 3.1b.

The distributions of external pressures acting on the liner are determined by the extent of the liner's resistance of ground displacements (i.e., interaction between ground and liner). Thus, the external pressure

distributions are functions of the relative stiffnesses of the liner and the ground mass (expressed in terms of the compressibility ratio, C, and flexibility ratio, F; see Appendix A) and the magnitude of the ground-liner interface shear strength (S_i), in addition to the nature of the in situ stress state (K_o). As Peck (1969) points out, the cross sectional shape of the tunnel and liner can also be a factor, but this is not considered herein because the analytical solutions are limited to liners of circular shape.

In regard to the ground-liner interface shear strength, the analytical solution considers only the two extreme conditions. The no slippage condition assumes, in effect, infinite shear strength at the interface. This condition is applicable, however, whenever the finite shear strength exceeds the greatest mobilized shear stress ($S_i > \tau_{max}$). The full slippage condition assumes zero shear strength ($S_i = 0$) and approximates the condition of very low shear strength relative to the potential shear stresses ($S_i << \tau$).

In general, the two interfacial shear strength conditions yield decidedly different external liner pressure distributions. There are, however, certain special cases for which the value of S_i is of no consequence. The first of these is the case in which the shape of the tunnel opening and liner is matched to the insitu stress state (K_o), for example, the circular shape and $K_o = 1$. The second case is that of the liner which is perfectly flexible and perfectly compressible ($F = C = \infty$). Such a liner offers no resistance to the deformation of the surrounding ground mass and, thus, no external pressures can be mobilized.

Discussion of the external pressure distributions is facilitated by comparing these distributions with the distributions of insitu stresses acting, in the undisturbed ground mass, on the cylinder of ground to be

replaced by the liner.

3.2.2 LINER PRESSURES FOR THE FULL SLIPPAGE CONDITION

Because the shear strength at the ground-liner interface is zero for the full slippage condition there are no external shear stresses acting on the liner. This leaves only the radial pressures to be considered, and all of the theoretically possible radial pressure distributions can be separated into six distinct classes, three of which are special cases. These six classes are:

1. The pressure distribution for the special case of a perfectly rigid and incompressible liner ($F = C = 0$).
2. Those pressure distributions that are intermediate to the $F = C = 0$ distribution and the in situ radial stress distribution.
3. The pressure distribution that is identical to the in situ radial stress distribution.
4. Those pressure distributions characterized by crown and invert pressures less than the in situ magnitude and springline pressures greater than in situ (for $K_o < 1$; if $K_o > 1$ relationships are reversed).
5. Those distributions of radial pressures which at every location are less than the corresponding in situ pressure.
6. The zero magnitude pressure distribution for the special case of a perfectly flexible and compressible liner ($F = C = \infty$). This is a special case of the class 5 distributions.

Figure 3.2 illustrates, for $K_o < 1$, the radial pressure distributions

of classes one and four.

Part a of Fig. 3.2 shows the distribution of radial pressures acting on a perfectly rigid and incompressible liner. It can be seen that the radial pressures around the crown and invert of the liner are greater than the corresponding in situ stresses, while the radial pressures in the vicinity of the springlines are less than the corresponding in situ stresses. In order for the pressure distribution acting on the liner to be different from the in situ stress distribution, ground displacements must occur after the liner is installed. Because it is not possible for this liner to deform it is somewhat surprising to find a pressure distribution different from the in situ distribution. However, the fact that there is a difference, as well as the nature of the difference, is explained by the effects of the full slippage condition assumed.

For this special case the difference between the in situ and liner pressure distributions is entirely the result of the ground displacements that occurred because slippage was allowed at the ground-liner interface. As a result of this slippage, the ground mass has moved inward toward the top and bottom of the liner, tangentially from the crown and invert toward the springlines, and outward away from the liner in the vicinity of the springlines. Note that while both radial and tangential displacements occur in the surrounding ground mass, right at the ground-liner interface only tangential displacements are allowed. Relative to the in situ radial stresses, the liner pressures are of greater magnitude around the crown and invert because of the inward ground displacement there; and the liner pressures are of lesser magnitude around the springlines because of the outward ground movement there.

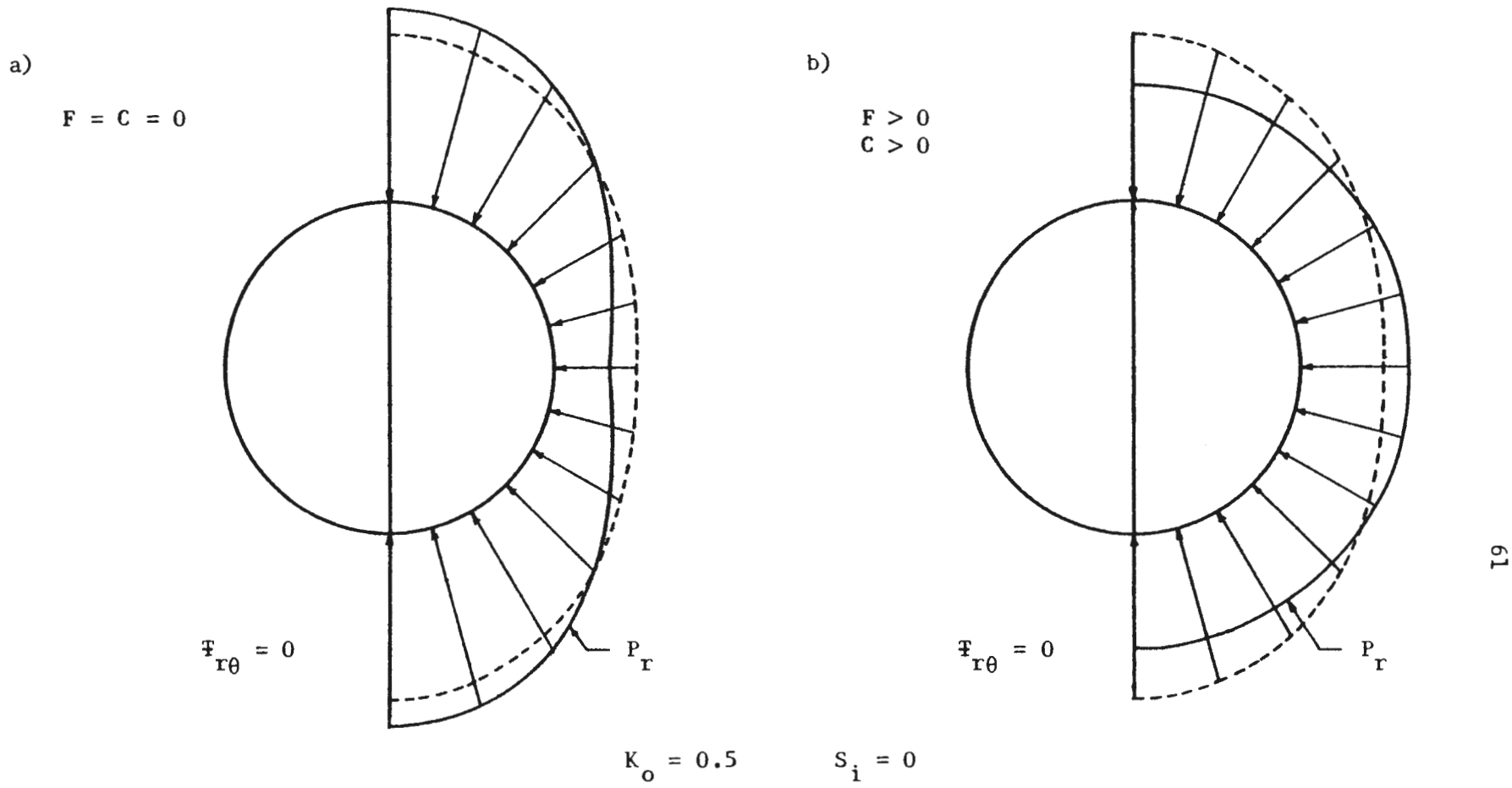

FIGURE 3.2 DISTRIBUTIONS OF EXTERNAL PRESSURES ACTING ON LINER FOR THE FULL SLIPPAGE CONDITION

The class 2 liner radial pressure distributions are characterized by crown and invert pressures less than those for F = C = 0, but greater than the corresponding in situ stresses and by springline pressures greater than those for F = C = 0, but less than the corresponding in situ stresses. Examination of the analytical solution equations for the full slippage condition reveals that such distributions can result if, and only if, $0 < F < (2 - 3\nu_m)$. Liners with flexibility ratio values in this range would be relatively inflexible and incompressible. Most realistic liner and ground mass combinations will not satidfy this condition.

The class 3 pressure distributions, which are identical to the in situ radial stress distributions ($P_r = \sigma_r$), can occur if, and only if, F = 0.5 and $\nu_m = 0.5$.

A typical example of the class 4 liner pressure distribution is illustrated in Fig. 3.2b. For $K_o < 1$ the radial pressure exerted by the ground mass causes the crown and invert of the liner to displace inward. In addition, the compressional and flexural stiffnesses of the liner are such that this movement of the crown and invert forces the springlines to displace outward against the adjacent ground. Inward displacement of the crown and invert allows dissipation of some of the potential ground displacements at these locations and thus, the external pressure there decreases in magnitude. Outward displacement of the springlines mobilizes passive pressures against these portions of the liner. Deformation of the liner continues, with decreasing crown and invert pressures and increasing springline pressures, until an equilibrium state is achieved between the distribution of external pressures and the distribution of internal liner forces and bending moments. The analytical solution equations have not

revealed specific ranges of C and F values that must be satisfied in order to obtain the pressure distributions of class 4 other than that $F > (2 - 3\nu_m)$ is required. It would seem however that the liner must be fairly flexible and yet relatively incompressible.

The class 5 external pressure distributions include all those distributions for which the pressure magnitudes are everywhere less than the corresponding in situ radial stress magnitudes. In order for a distribution of this type to occur, the liner springlines as well as the crown and invert must displace inward. This displacement pattern indicates that the liner must be highly compressible.

3.2.3 LINER PRESSURES FOR THE NO SLIPPAGE CONDITION

Figure 3.3 illustrates a typical distribution of external radial and shear pressures acting on a liner for the no slippage condition.

It was mentioned previously that there is only one special case for which no ground displacements occur after liner installation and, consequently, for which the distribution of pressures acting on the liner are identical to the in situ stress distributions. It is the no slippage requirement that makes this special case possible. This case can occur only if the liner is perfectly rigid and incompressible ($F = C = 0$) and only if the shear strength at the ground-liner interface everywhere exceeds the shear stress existing at that location in the undisturbed ground mass (the analytical solution's no slippage condition). Metaphorically speaking, when such a liner is installed (under the conditions assumed herein) the surrounding ground mass is unaware that a core of soil has been removed and replaced by the liner. The equilibrium of the ground mass remains undisturbed and the

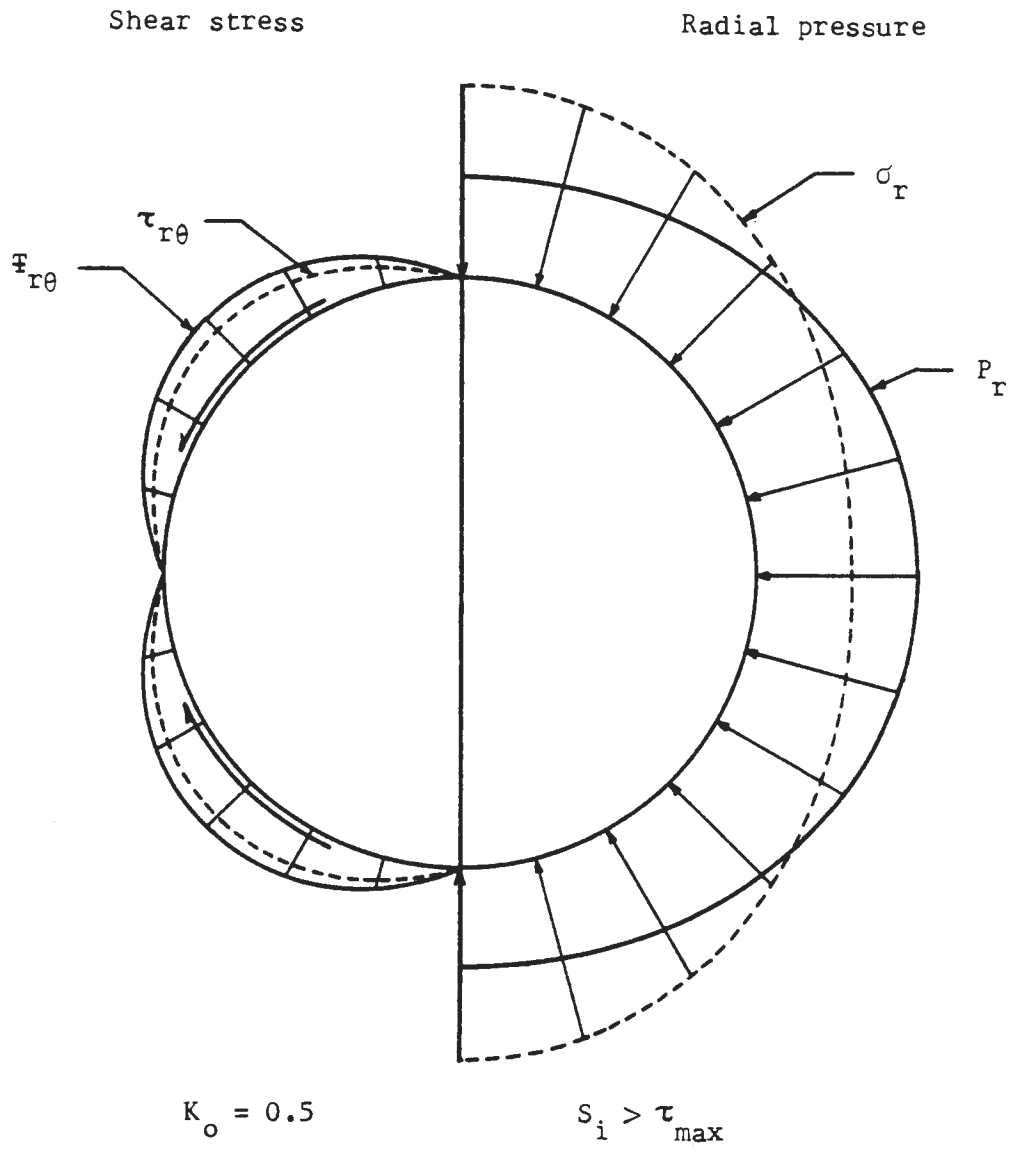

--------- Distribution of in situ stresses; and liner pressures for F = C = 0

———— Typical distributions of liner pressures for F > 0 and C > 0

FIGURE 3.3 DISTRIBUTIONS OF EXTERNAL PRESSURES ACTING ON LINER FOR THE NO SLIPPAGE CONDITION

external pressures that act on the liner are identical to those that acted on the core of soil the liner replaced (Fig. 3.1b and dashed curves in Fig. 3.3).

A liner that is not perfectly rigid and incompressible ($F \neq 0$, $C \neq 0$) will be forced to deform by the surrounding ground mass. Because of the no slippage condition the liner will resist tangential as well as radial displacements and, as a result, the liner will be subjected to both external shear stresses and radial normal stresses. The distribution of these external pressures will be different from the distribution of the insitu stresses (Fig. 3.3).

Figure 3.3 illustrates two interesting points concerning the external pressure distributions for the no slippage condition. First, it is possible for the external shear stresses acting on the liner to be greater in magnitude than the in situ shear stresses. Second, it is possible to begin with an in situ stress state characterized by $K_o < 1$ and yet end up with radial pressures acting on the liner that are smaller at the crown and invert than at the springlines.

Examination of the analytical solution equations for the no slippage condition reveals that the relationship between the magnitude of the shear stresses acting on the liner, $\mathfrak{T}_{r\theta}$, and the magnitude of the in situ shear stress, $\tau_{r\theta}$, is a function of the relative stiffnesses of the ground and liner (expressed in terms of C and F). In order for any one of the three possible relationships ($\mathfrak{T}_{r\theta} >$, $=$, or $< \tau_{r\theta}$) to hold, the C and F values must satisfy a certain condition. The relationships and the corresponding conditions are:

$$\text{For} \quad \mathfrak{T}_{r\theta} \begin{Bmatrix} > \\ = \\ < \end{Bmatrix} \tau_{r\theta}, \quad \text{must have} \quad C \begin{Bmatrix} < \\ = \\ > \end{Bmatrix} \left[\frac{6F}{2F + 5 - 6\nu_m}\right]$$

For large values of F the required value of C is approximately three. The F and C values for most ground-liner combinations are such that $\mathcal{T}_{r\theta} > \tau_{r\theta}$ results. Note that while it is possible to have $\mathcal{T}_{r\theta} = \tau_{r\theta}$ for certain combinations of C and F values other than F = C =0, the corresponding liner-in situ radial stress relationship for these nonzero C and F values will be of the form $P_r \neq \sigma_r$. It is possible to have both $\mathcal{T}_{r\theta} = \tau_{r\theta}$ and $P_r = \sigma_r$ only when F = C = 0.

It is difficult to visualize the process by which the external shear stresses acting on the liner attain magnitudes in excess of the in situ shear stress magnitudes because both potential and actual radial and tangential displacements of the ground and liner are involved. It is somewhat easier to see how it is possible to obtain radial liner pressures at the crown and invert that are smaller than the radial pressures at the springlines (for $K_o < 1$). Prior to liner deformation the radial pressure acting on the liner is the same as the in situ radial stress that acted on the soil core that was removed. Inward displacement of the crown and invert reduces the radial pressures at these locations, while outward displacements of the springlines increases the radial pressures around the springlines. Simultaneously, however, the ground mass at the ground-liner interface is attempting to displace tangentially -- for $K_o < 1$, from crown and invert toward the springlines. However, because of the no slippage condition only a portion of this displacement (that equal to the tangential displacement of the liner) is allowed to occur. Aside from the mobilization of the external shear stresses, $\mathcal{T}_{r\theta}$, the prevention of the remaining portion of the potential ground mass tangential displacement has the effect of reducing the tendency for inward ground displacement at the crown and invert and outward ground

displacement at the springlines. The reduced tendency for inward ground displacement at the crown and invert (equivalent to starting with smaller potential ground displacements for the liner to resist) results in smaller external radial normal pressures at these locations than would be the case for the full slippage condition. Similarly, the reduced tendency for outward ground displacement at the springlines results in larger radial pressures at these locations than would exist for the full slippage condition.

As shown in Fig. 3.3 the no slippage requirement can result in radial pressures at the crown and invert, $P_r(C\text{-}I)$, that are less than the springline pressures, $P_r(SL)$, when $K_o < 1$. It appears that this will generally be the case since all that is required for $P_r(C\text{-}I) < P_r(SL)$ is that $\left[F - 1.5(1 - 2\nu_m)C\right] > 2$. Most of the possible C and F combinations can easily satisfy this requirement. On the other hand, in order for $P_r(C\text{-}I) > P_r(SL)$ it is necessary that $\left[F - 1.5(1 - 2\nu_m)C\right] < 2$. This is a very restrictive requirement that can be satisfied only by a relatively rigid liner, a liner with a flexibility ratio in the range $0 \leq F < (\approx 2)$.

3.3 LINER FORCES, BENDING MOMENTS, AND DISPLACEMENTS

3.3.1 DISTRIBUTION AROUND THE LINER

The external pressures acting on the liner must, of course, be balanced by the forces and bending moments within the liner. Figure 3.4 illustrates the nature of the liner thrust and bending moment distributions, as well as the distributions of radial displacement, for two different in situ stress conditions and for both the no slippage and full slippage conditions.

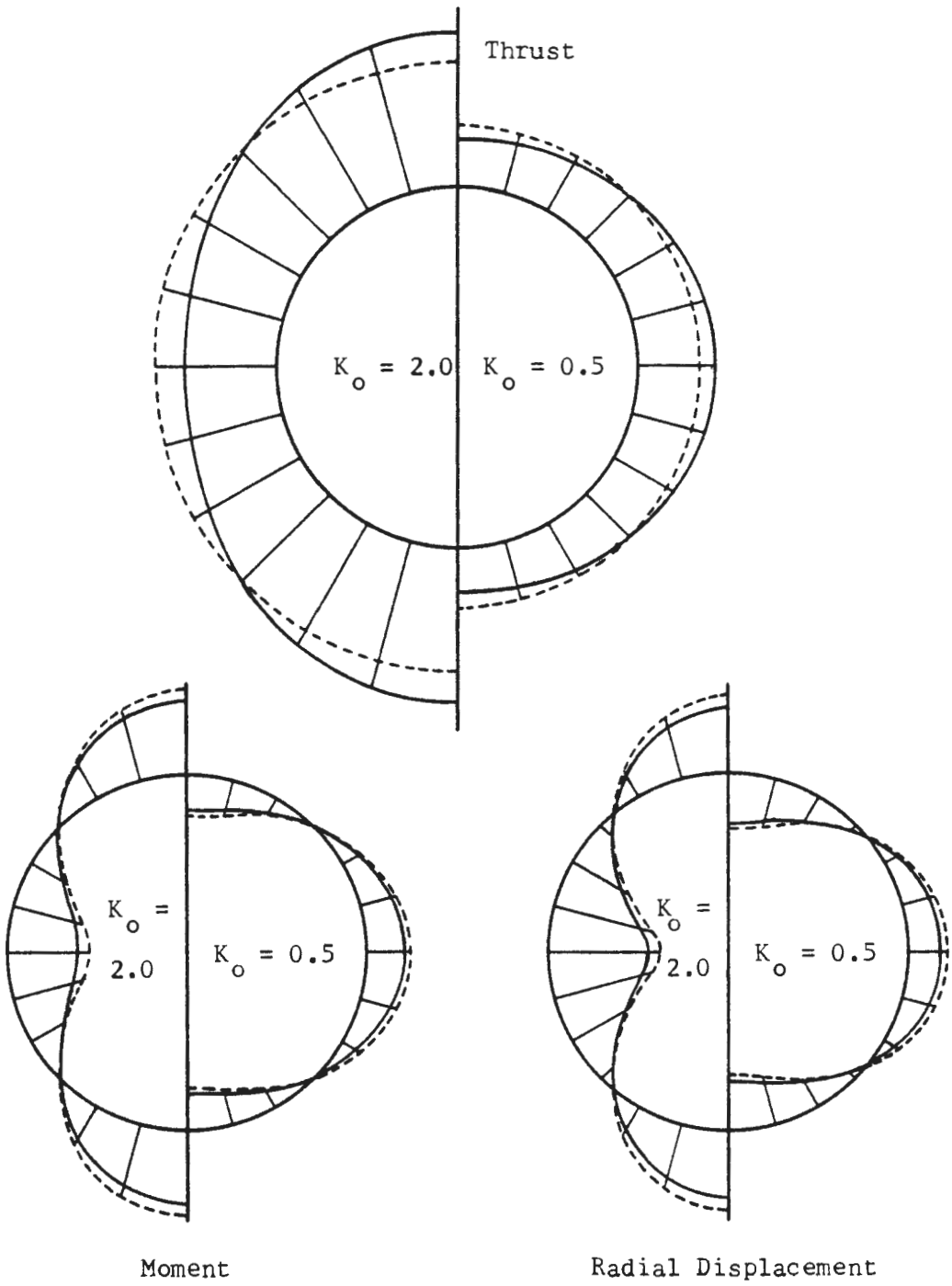

FIGURE 3.4 DISTRIBUTIONS OF LINER THRUSTS, MOMENTS AND RADIAL DISPLACEMENTS

As in Figs. 3.1 through 3.3, the distributions shown in Fig. 3.4 are symmetrical about a vertical plane through the tunnel centerline. In addition, because the analytical solution assumes the tunnel to be located at great depth, i.e., assumes the variation of in situ stress with depth from crown to invert to be negligible, the distributions are also symmetrical about a horizontal plane through the tunnel centerline.

The effect of the K_o value on the distributions of liner thrusts, moments and displacements, as illustrated in Fig. 3.4, is straight forward and self explanatory. The differences between corresponding distributions for the no slippage and full slippage conditions illustrates the effect of external shear stresses on liner response.

The external pressure distributions shown in Figs. 3.2b and 3.3 are for $K_o = 0.5$ and the same combination of liner and ground mass material properties as the distributions of Fig. 3.4. The no slippage condition radial pressure distribution of Fig. 3.3 indicates that the radial pressures at the crown and invert are less than those at the springlines. Thus, the radial pressures alone mobilize thrusts in the liner that are greater at the crown and invert than at the springlines. However, the external shear stresses, which are also acting on the liner, mobilize negative thrusts (tension) at the crown and invert and positive thrusts (compression) at the springlines. The total thrust distribution ($K_o = 0.5$) in Fig. 3.4 shows that when the thrust contributions of the exteranl shear stresses and radial pressures are combined the resulting total thrust at the crown and invert is smaller than that at the springlines, as would be expected for $K_o < 1$. Figure 3.4 also shows that the effect of the external shear stresses is great enough so that the crown and invert thrusts for no slippage are smaller than

those for the full slippage condition, while at the springlines the relationship is reversed. This result is not immediately obvious from examination of Fig. 3.3.

Liner bending moments are related to liner distortion. Thus, the distributions of liner radial displacements and bending moments, given in Fig. 3.4, are of similar form. This figure shows that the distortion of the liner is greater for the full slippage condition than it is for the no slippage condition. This result is obtained because for full slippage the crown and invert of the liner must resist greater ground displacements than for the no slippage condition; while at the same time at the springlines the ground provides less resistance to the outward movement of the liner than it does for the no slippage condition.

The distributions of liner thrusts, bending moments, and radial displacements given in Fig. 3.4 were obtained for a specific combination of parameter values describing the properties of the liner and surrounding ground mass. Had a different combination of material properties been selected, a different set of curves would have been obtained. However, this second set of curves would have differed from that shown only in magnitude. The general shapes of the curves of Fig. 3.4 apply to all material property combinations.

3.3.2 VARIATION WITH THE GROUND-LINER COMPRESSIBILITY AND FLEXIBILITY RATIOS

Peck, et al., (1972) and Mohraz, et al., (1975) have illustrated the effect of material properties of the liner and ground mass on the magnitude of liner thrusts, moments, and radial displacements for the full slippage and no slippage conditions, respectively. In the figures presented

in these papers the liner and ground mass properties were conveniently combined in the form of the compressibility, C, and flexibility, F, ratios. However, the analytical solution used by the above authors was essentially that of Burns and Richard (1964) (the overpressure loading solution altered to remove the restriction to only one-dimensional loading) which does not apply to the case of a tunnel being constructed in an initially stressed medium (excavation loading). Presented here, in Figs. 3.5 through 3.8, are the corresponding figures (liner moments, thrust, and radial displacements versus the flexibility and compressibility ratios) obtained from the analytical solutions for a thin liner subjected to excavation loading derived in Appendix A.

The curves shown here are similar in form to those given by Peck, et al., (1972) and Mohraz, et al., (1975). However, the overpressure and excavation loading solutions yield results that differ in magnitude by an amount that varies with the value of ν_m. In general, the overpressure loading solution overestimates the magnitudes of liner forces, moments, and displacements when applied to the problem considered herein (see Figs. 2.9 and 2.10).

Curves of maximum moment coefficient ($M/\gamma Ha^2$) versus flexibility ratio (F) for K_o = 0.5 and 2.0 and for the full slippage and no slippage conditions are given in Fig. 3.5. The maximum moments occur at the crown, invert, and springlines. The curves shown represent absolute values of the moment coefficient. According to the sign convention adopted herein (Fig. A.4), for $K_o < 1$ moments at the springlines are positive while those at the crown and invert are negative. The positive-negative signs for $K_o > 1$ are the opposite of those for $K_o < 1$.

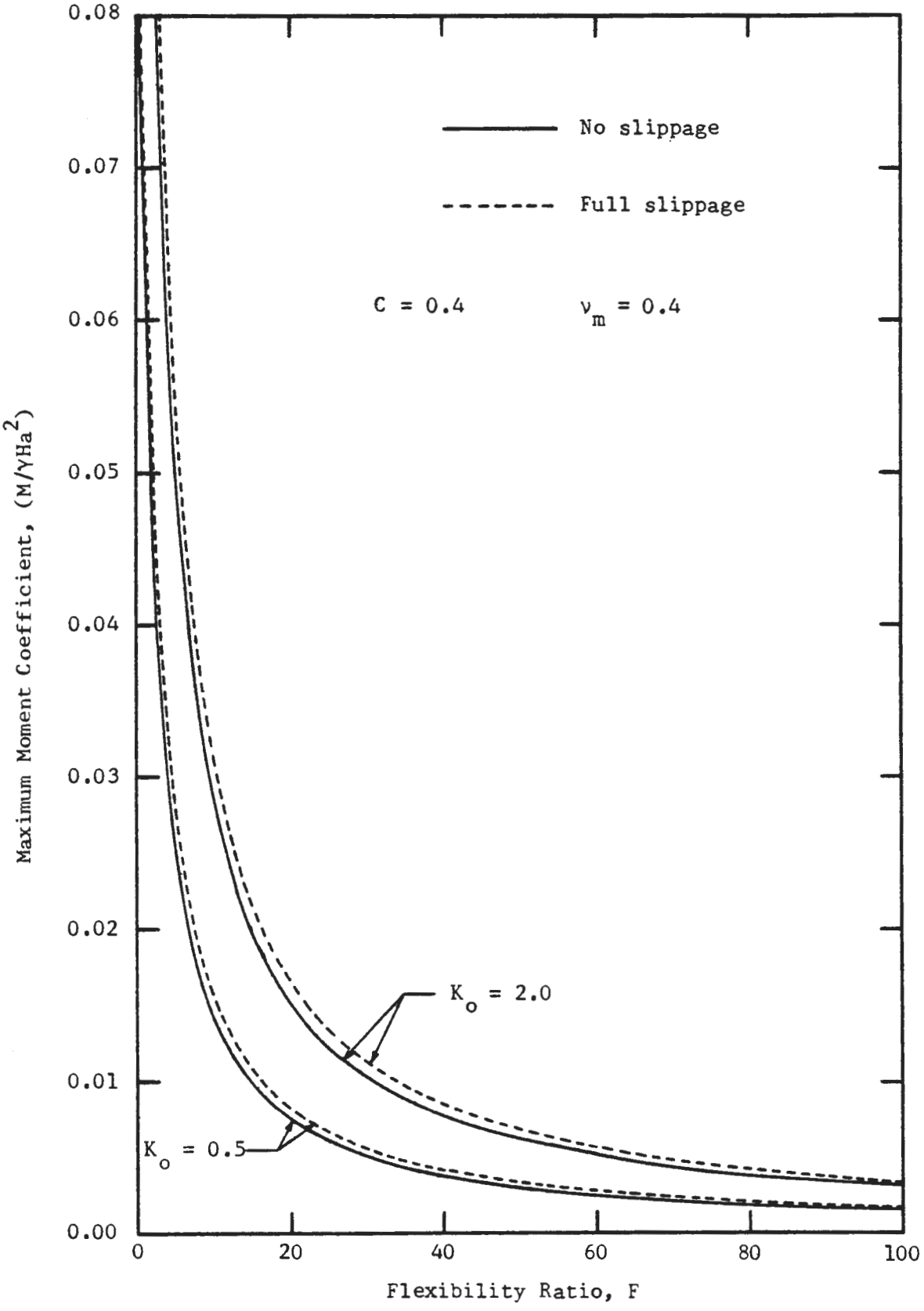

FIGURE 3.5 VARIATION OF MOMENT COEFFICIENT WITH FLEXIBILITY RATIO

Figure 3.5 shows that the moment coefficient decreases rapidly as the flexibility ratio increases from zero to about 20. Thereafter there is a further, but much more gradual, reduction of the moment coefficient with increasing F; however, this is of little consequence since for $F > 20$ the moment coefficients are very small. For $K_o = 0.5$ and $F \geq 17.5$ the maximum bending moment in the liner is less than one percent of γHa .

The curves in Fig. 3.5 provide further illustration of the statement made previously, in discussion of Fig. 3.4, that the no slippage condition yields slightly smaller bending moments than the full slippage condition. For $F = 0$ (perfectly rigid liner) the no slippage moment coefficient is eight percent less than the full slippage value. For $F = 100$ the difference has increased only to nine percent, but for $F = 100$ the moment coefficient values are so small that the difference is of little consequence. For $F = \infty$ (perfectly flexible liner), of course, both the no slippage and full slippage conditions yield the same moment coefficient value, that being zero.

As noted in Fig. 3.5 the curves shown apply only for one value of the compressibility ratio ($C = 0.4$) and one value of Poisson's ratio of the ground mass ($\nu_m = 0.4$). Fortunately, however, neither of these parameters has that great of an effect on the moment coefficient and the curves shown give a good approximation of the curves that would be obtained for any other possible C and ν_m values.

Variation of the liner thrust coefficient ($T/\gamma Ha$) with the flexibility ratio is illustrated in Fig. 3.6 for $K_o = 0.5$ and 2.0 and for the full and no slippage conditions. The figure shows this variation for both the maximum and minimum thrust coefficients. For $K_o < 1$ the maximum thrust

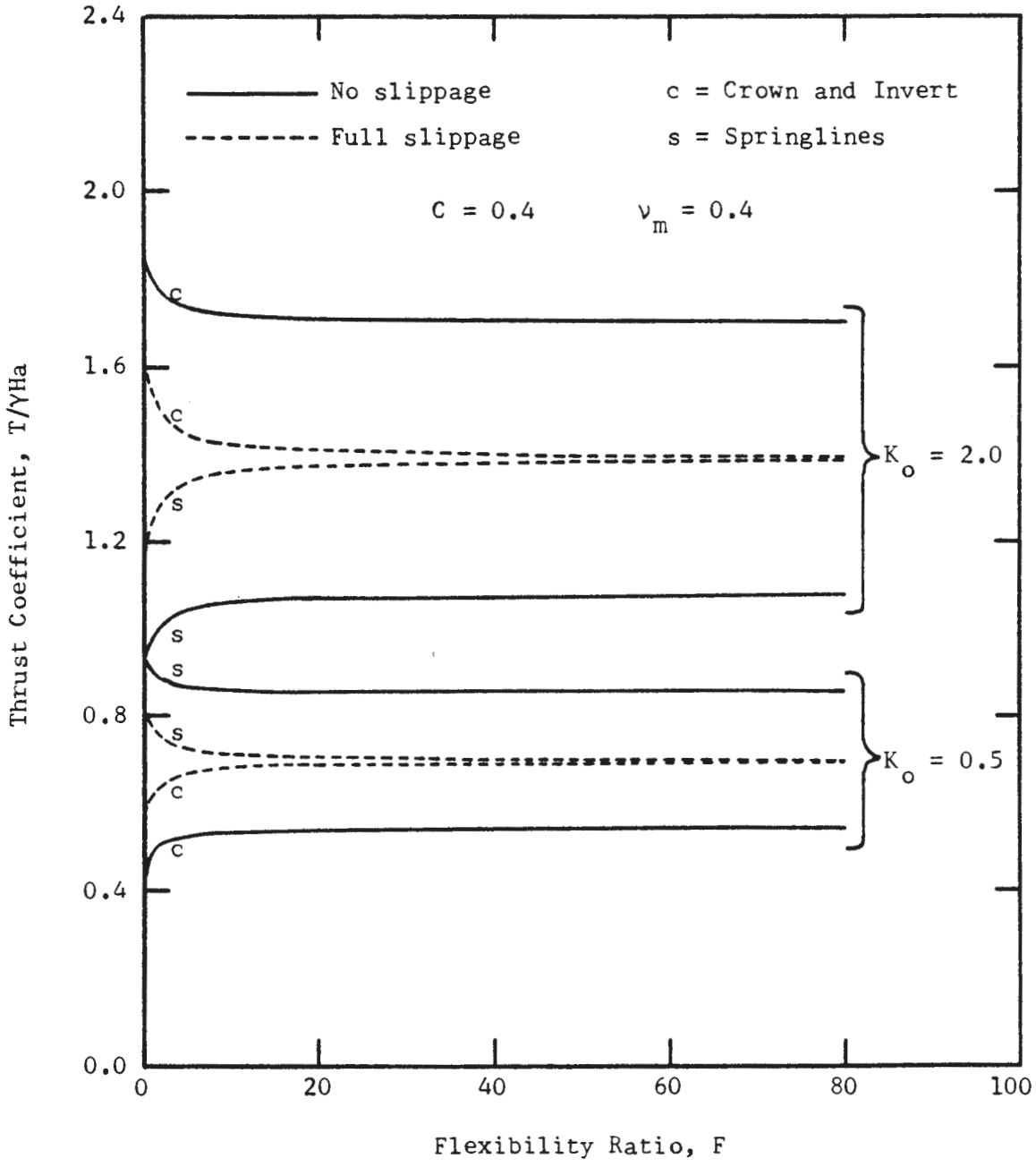

FIGURE 3.6 VARIATION OF THRUST COEFFICIENT WITH FLEXIBILITY RATIO

occurs at the springlines (s) and the minimum thrust occurs at the crown and invert (c). For $K_o > 1$ the locations of the extreme values are reversed.

Examination of the analytical solution equations for the thrust coefficient (See Sections B.3.3 and B.4.3) reveals several interesting facts that help to explain the curves in Fig. 3.6. These equations consist of two terms. The first term is independent of θ (circumferential location) and represents the average liner thrust. The second term is a function of θ and gives the variation of thrust magnitude with circumferential location. Because the average thrust is also independent of the flexibility ratio, in Fig. 3.6 the average thrusts would plot as horizontal lines (not shown) located at $(T/\gamma Ha) = 1.4$ for $K_o = 2.0$ and at $(T/\gamma Ha) = 0.7$ for $K_o = 0.5$. What Fig. 3.6 really shows then is the variation of the second of the thrust equation terms with flexibility ratio.

With increasing F the second term in the full slippage thrust equation rapidly approaches zero (i.e., no variation of thrust magnitude with location around the liner circumference). Likewise, the second term in the no slippage thrust equation rapidly approaches a constant value (>0) with increasing F. For F greater than 10 or 20 the second term of the thrust coefficient, thus the total thrust coefficient, is essentially independent of the value of the flexibility ratio. Thus, for large F values liner thrust can be approximated by the following simplified expressions for the thrust coefficient:

Full Slippage Condition:

$$\left(\frac{T}{\gamma Ha}\right) = \frac{\frac{1}{2}(1 + K_o)}{1 + (1 - 2\nu_m)C} \qquad (3.1)$$

No Slippage Condition:

$$\left(\frac{T}{\gamma Ha}\right) = \frac{\frac{1}{2}(1 + K_o)}{1 + (1 - 2\nu_m)C} + \frac{\frac{1}{2}(1 - K_o)(3 - 4\nu_m)}{3 - 2\nu_m + (1 - 2\nu_m)C} \cdot \cos 2\theta \qquad (3.2)$$

The curves in Fig. 3.6 apply only for one value of the compressibility ratio (C = 0.4). Unlike the moment coefficient, the thrust coefficient can be significantly affected by changes in the value of C. Figure 3.7 illustrates the variation of the thrust coefficient with compressibility ratio.

The average thrust term, which is a function of C but not F, is the term most strongly influenced by the compressibility ratio. The second term of the full slippage condition thrust equation is independent of C. While the second term of the no slippage condition equation is a function of both F and C, it is influenced only slightly by the compressibility ratio. Thus, the variation of $(T/\gamma Ha)$ with C shown in Fig. 3.7 is primarily the variation of the average thrust term.

Only curves for two different flexibility ratio values (F = 2 and 10) are given in Fig. 3.7. Because the thrust coefficient rapidly approaches a constant value with increasing F, all full slippage curves for F > 10 fall between the two dashed F = 10 curves. Similarly, all no slippage curves for F > 10 plot just slightly inside the two continuous F = 10 curves.

Note that, in effect, the K_o value magnifies the variation with C and, the differences between the full and no slippage conditions. The variation is a minimum for $K_o = 1$ and increases as the value of K_o is increased or decreased.

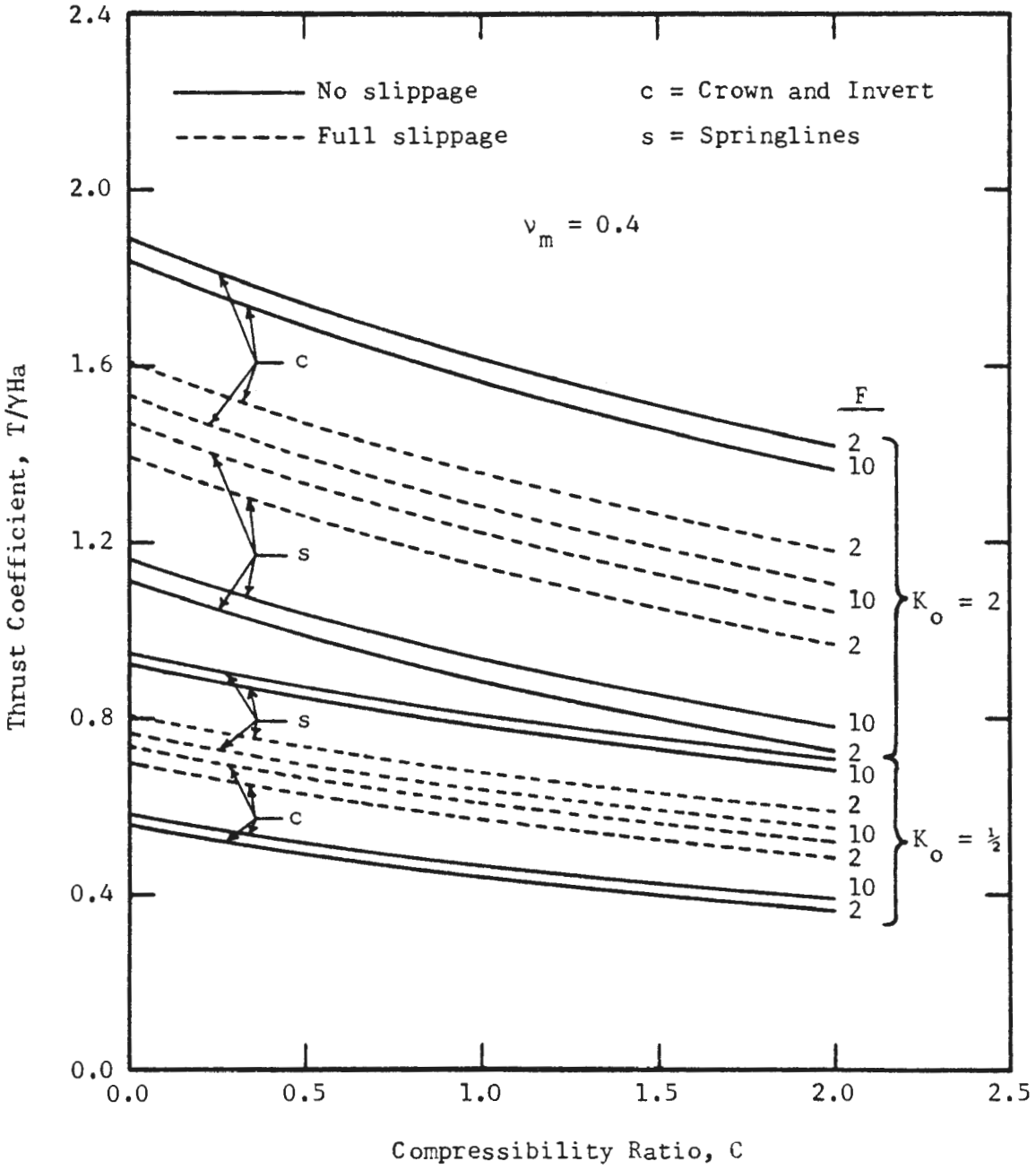

FIGURE 3.7 VARIATION OF THRUST COEFFICIENT WITH COMPRESSIBILITY RATIO

Although not shown, the thrust coefficient also exhibits a significant variation with Poisson's ratio of the ground mass, ν_m. The curves of Fig. 3.6 should be shifted upward (higher thrusts) for $\nu_m > 0.4$ and downward (lower thrusts) for $\nu_m < 0.4$. The evident curvature and slope of the curves in Fig. 3.7 would be increased (C of greater influence) for $\nu_m < 0.4$ and decreased for $\nu_m > 0.4$. All of the curves in Fig. 3.7 revert to horizontal lines (thrust coefficient independent of C) for $\nu_m = 0.5$. This occurs because all of the C terms in the thrust coefficient equations are multiplied by the expression $(1 - 2\nu_m)$. Inclusion of the $(1 - 2\nu_m)$ expression is the analytical solution's method of providing a solution for the special case of an incompressible ($\nu_m = 0.5$) medium.

The variation of the vertical and horizontal diameter change coefficients $(\Delta D/D)/(\gamma H/E_m)$ with flexibility ratio is shown in Fig. 3.8 for $K_o = 0.5$ and 2.0 and for both the full slippage and no slippage conditions. Positive coefficient values indicate a diameter increase and negative values indicate a diameter decrease or shortening.

Like the moment coefficient (Fig. 3.5), the diameter change coefficient is relatively insensitive to the degree of slippage that occurs at the ground-liner interface. Like the thrust coefficient (Fig. 3.6), the diameter change coefficient is essentially independent of the flexibility ratio for $F > 10$ or 20.

The average diameter change coefficients for the two K_o values are indicated by the horizontal broken lines. These average values are given by the first term of the full and no slippage condition equations (both equations have the same first term) which is independent of the flexibility ratio. The average diameter change coefficient values are negative because

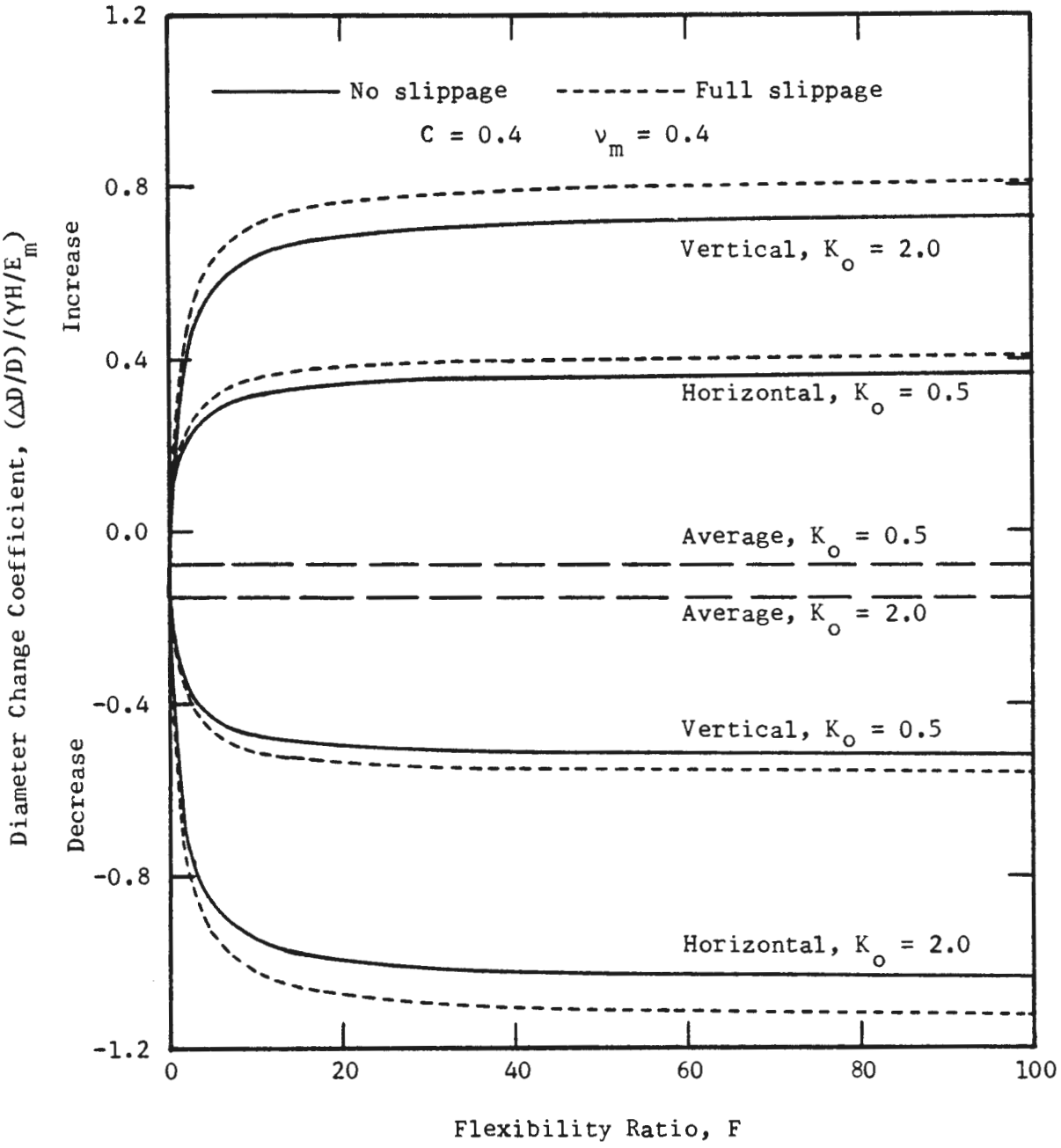

FIGURE 3.8 VARIATION OF DIAMETER CHANGE COEFFICIENT WITH FLEXIBILITY RATIO

the liners are compressible ($C > 0$).

The horizontal and vertical diameter change coefficient curves are symmetrical about the average value lines. The difference between the average value and either the horizontal or vertical diameter value is the magnitude of the second term in the diameter change coefficient equations. Thus, Fig. 3.8 illustrates the variation with F of these second terms. Unlike the second term of the full slippage thrust equation which rapidly approached a value of zero with increasing F, the second terms of both the full and no slippage condition diameter change equations approach a constant value other than zero.

Note that the diameter parallel to the maximum insitu stress direction shortens more than the diameter parallel to the minimum insitu stress direction lengthens. Here, this is a direct result of the compressibility of the liner. If either the liner or the ground mass were incompressible ($C = 0$ or $\nu_m = 0.5$, respectively; average diameter change = 0) one diameter would increase by the same amount the other decreased.

The diameter change coefficient is more sensitive than the moment coefficient, but less sensitive than the thrust coefficient, to variation of the compressibility ratio and Poisson's ratio of the ground mass. Of these two parameters, ν_m is probably the more significant because it affects the sensitivity of the diameter change coefficient to both the compressibility ratio and, to a lesser degree, the flexibility ratio.

Radial displacements of the crown, invert and springlines can be obtained from Fig. 3.8 by replacing $\Delta D/D$ in the diameter change coefficient by u_r/a and thereby obtaining the radial displacement coefficient. Positive values indicate outward displacement while negative values indicate inward

displacement.

The variation of the liner transverse shear forces (V) with the flexibility or compressibility ratios has not been plotted. However, the maximum transverse shear coefficient's variation with flexibility ratio can be obtained from Fig. 3.5 by noting that $V = (1/a)(\partial M/\partial\theta)$ which gives $(V/\gamma Ha) = (2a)(M/\gamma Ha)$. All comments in the discussion of Fig. 3.5 apply to the maximum transverse shear coefficient also.

3.3.3 VARIATION WITH THE LINER RADIUS-TO-THICKNESS RATIO AND THE GROUND-LINER MODULUS RATIO

Figures 3.5 through 3.8 are of interest because they provide an indication of how liner flexibility and compressibility affect liner behavior. However, by grouping the ground mass and liner parameters together in the form of the flexibility and compressibility ratios the influence of each of the individual parameters has been obscured. In addition, these figures tend to give the impression that the C and F values can be selected or determined independently of each other when in reality they are interrelated. Normally, changing one ratio value (by changing liner thickness, for example) results in a change in the other ratio value. While it is possible to alter the value of F while keeping C constant (or vice versa), this requires careful adjustment of two or more ground and/or liner parameter values. Manipulations of this nature can yield C and F combinations that are theoretically possible but totally unrealistic in terms of real ground-liner systems.

The figures that follow avoid these difficulties. These figures give the variation of the various components of liner response with the liner

radius-to-thickness ratio (a/t) and the ground-liner modulus ratio (E_m/E_ℓ), where,

$$C = \frac{E_m}{E_\ell} \cdot \frac{a}{t} \cdot \frac{(1 - \nu_\ell^2)}{(1 + \nu_m)(1 - 2\nu_m)} \tag{3.3}$$

$$F = \frac{E_m}{E_\ell} \cdot \left(\frac{a}{t}\right)^3 \cdot \frac{2(1 - \nu_\ell^2)}{(1 - \nu_m)} \tag{3.4}$$

Plotting the variations in this way allows direct assesment of the influence of the individual parameters. Also, since the (a/t) and (E_m/E_ℓ) ratios consist of familiar parameters the figures cannot easily be misinterpreted.

Figure 3.9 gives the variation of the liner thrust coefficient with (a/t) and (E_m/E_ℓ). For the purpose of illustration the total thrust has been separated into its two components. The average thrust, given by the first term in the thrust equation, is represented by T_1 in the top chart of Fig 3.9. This thrust component is independent of liner flexibility. The curves in the chart for T_1 apply to both the full slippage and no slippage conditions. The lower chart in Fig. 3.9 is for T_2, the second term in the thrust equation and the term that, when multiplied by $\cos 2\theta$, gives the variation of thrust with location around the liner circumference. There are two sets of curves in this chart. The continuous curves apply for the no slippage condition and the dashed curves apply for the condition of full slippage at the ground-liner interface.

The average thrust component, T_1, exhibits significant variation

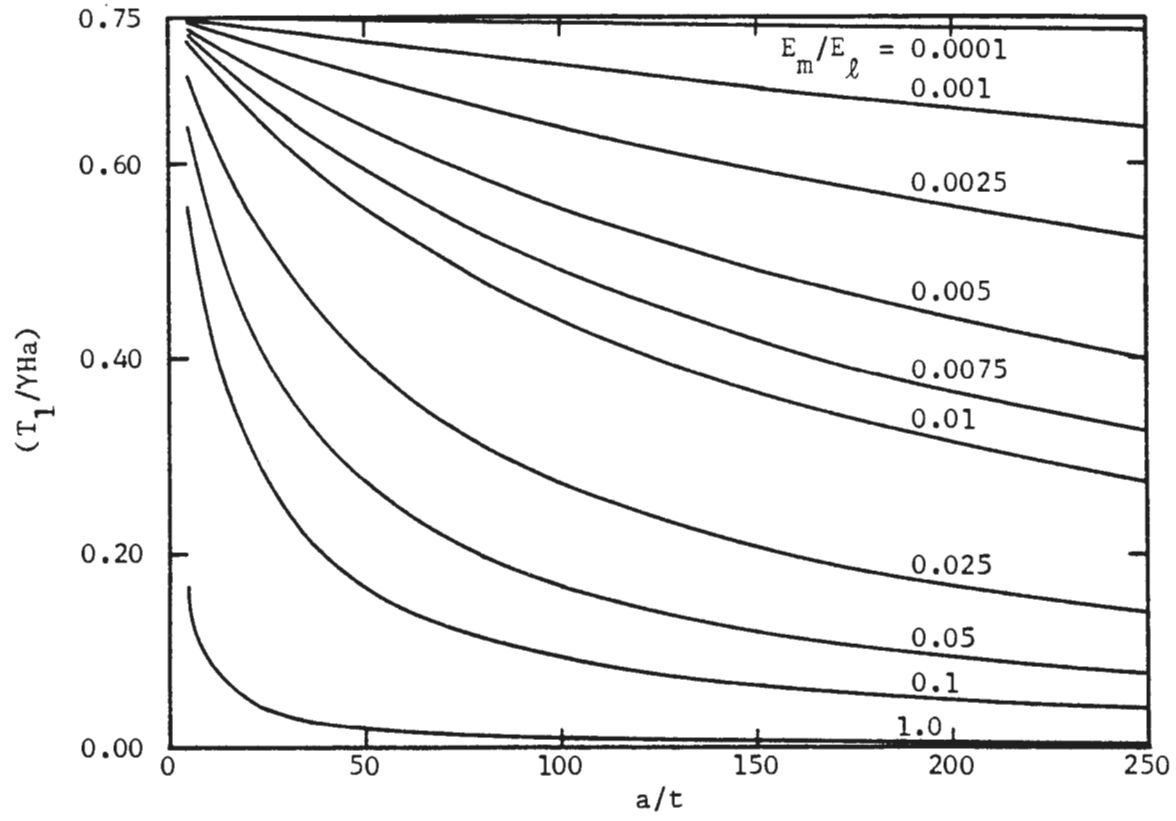

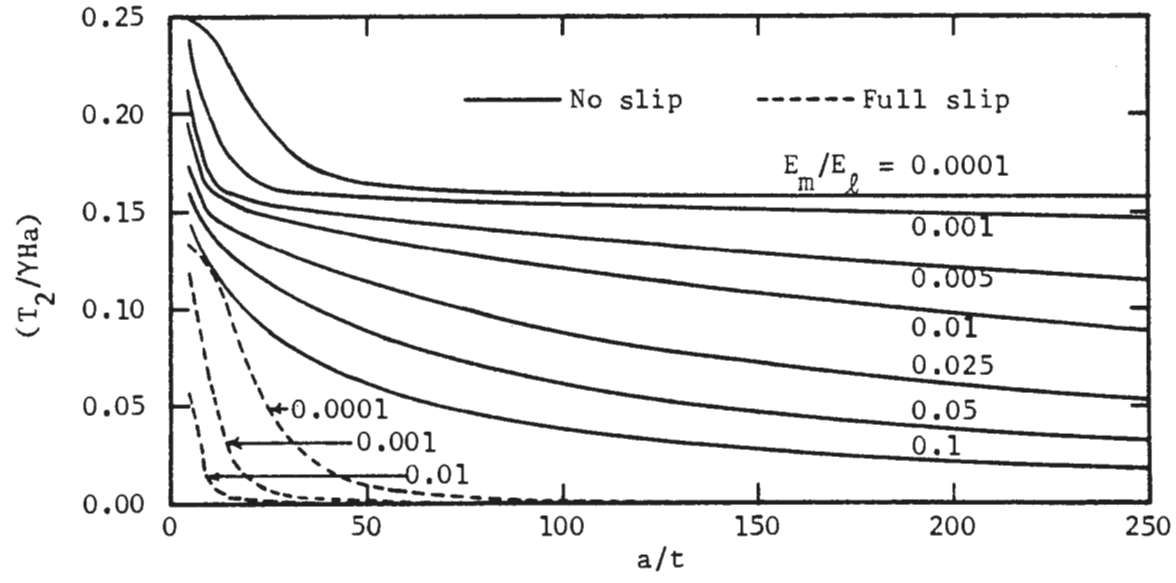

$K_o = 0.5$ $\quad \nu_m = 0.40$ $\quad \nu_\ell = 0.15$

$$T_{total} = T_1 + T_2 \cos 2\theta$$

FIGURE 3.9 VARIATION OF THRUST COEFFICIENT WITH (a/t) AND (E_m/E_ℓ)

with the liner radius-to-thickness ratio (within the range of a/t considered) only if the modulus ratio is greater than 0.0001. If $(E_m/E_\ell) \leq 0.0001$ the average thrust component is essentially, $T_1 = 0.75\ \gamma Ha$ for all (a/t). This is a reflection of the fact that for $(E_m/E_\ell) \leq 0.0001$ (and for a/t < 250, at least) the liner is essentially incompressible relative to the ground mass. At the other extreme, if $(E_m/E_\ell) \geq 1.0$ and (a/t) > 50 the liner is so compressible, relative to the ground mass, that $T_1 \approx 0$.

The bottom chart in Fig. 3.9 shows that the range of (E_m/E_ℓ) and (a/t) values within which these ratios significantly influence the magnitude of the variable thrust component, T_2, depends on the slippage condition at the ground-liner interface. This range is relatively small for the full slippage condition. For all $(E_m/E_\ell) \geq 0.1$ the liner is so flexible, relative to the surrounding ground, that, regardless of the liner's thickness, $T_2 \approx 0$. If the modulus ratio is reduced to 0.0001, (a/t) values up to about 50 will yield T_2 magnitudes significantly greater than zero. The variable thrust component exhibits greater variation with (a/t) and (E_m/E_ℓ) if the no slippage condition applies. Like the average thrust component, the variable thrust component for the no slippage condition is essentially zero for all $(E_m/E_\ell) \geq 1.0$ and (a/t) > 50 (curve for $E_m/E_\ell = 1.0$ not shown). If (E_m/E_ℓ) equals 0.0001, T_2 is essentially a constant for all values of (a/t) > 50. Curves for $(E_m/E_\ell) < 0.0001$ -- for both the full and no slippage conditions -- are similar in form to those of $(E_m/E_\ell) = 0.0001$, but shifted to the right. The amount of shift increases as the modulus ratio approaches zero. For the limiting case of $(E_m/E_\ell) = 0$, T_2 is independent of (a/t) and $(T_2/\gamma Ha) = 0.250$ and 0.135 for the no slippage and full slippage conditions, respectively.

Given a specific ground mass (E_m) and tunnel radius (a), Fig. 3.9 shows that by reducing the liner thickness and/or the liner modulus the compressibility of the liner can be increased with a resulting reduction of liner thrusts. Such attempts at thrust reduction can be counterproductive, however. Figure 3.10 shows that, while reducing the liner thickness reduces liner thrusts, it increases the circumferential stress in the liner (Fig. 3.10 assumes a continuous liner of uniform cross section). This occurs because the cross sectional area of the liner decreases faster than the thrust as the liner thickness is reduced. Too great of a reduction can yield compressive stresses in excess of the compressive strength of the liner. Another possible approach would be to keep the liner thickness constant and reduce the modulus of the liner in order to increase the modulus ratio and thereby reduce the liner thrust. Because the liner thickness remains constant the liner stresses (due to thrust) also would be reduced. However, reduction of E_ℓ would undoubtedly cause a reduction of the liner's compressive strength also. Thus, care would have to be taken to insure that liner strength was not reduced to a magnitude less than that of the reduced stresses.

Variation of the maximum bending moment coefficient (and maximum transverse shear force coefficient) with (a/t) and (E_m/E_ℓ) for the full slippage and no slippage conditions is illustrated in Fig. 3.11. The plotted curves show that by reducing either liner thickness or modulus, and thereby increasing liner flexibility, the liner bending moments (and shear forces) can be significantly reduced. It can be seen that the full and no slippage conditions give nearly the same bending moment and shear force values. Throughout the range of (a/t) and (E_m/E_ℓ) considered in Fig. 3.11, the no

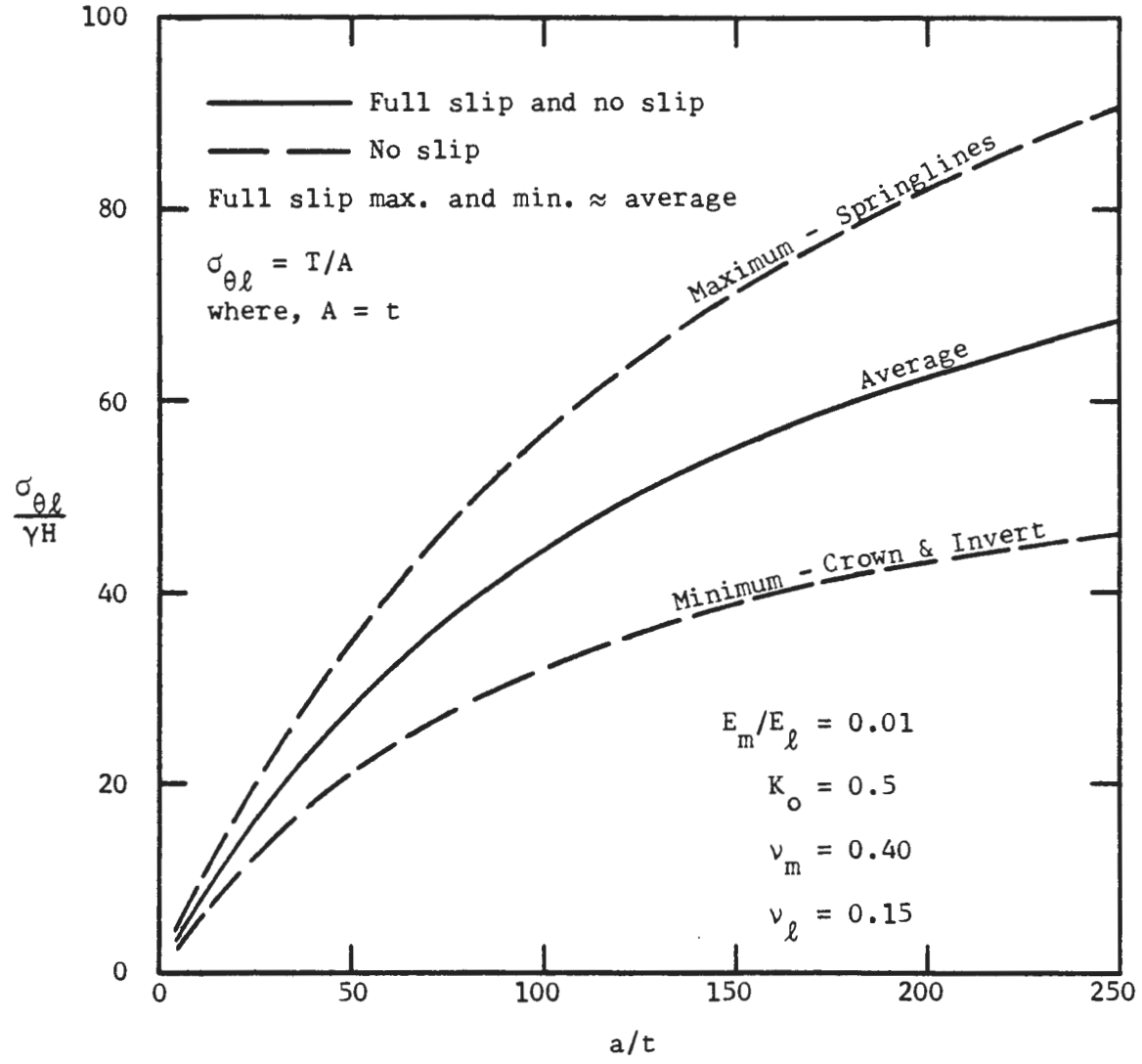

FIGURE 3.10 THRUST COMPONENT OF LINER CIRCUMFERENTIAL STRESS VERSUS (a/t)

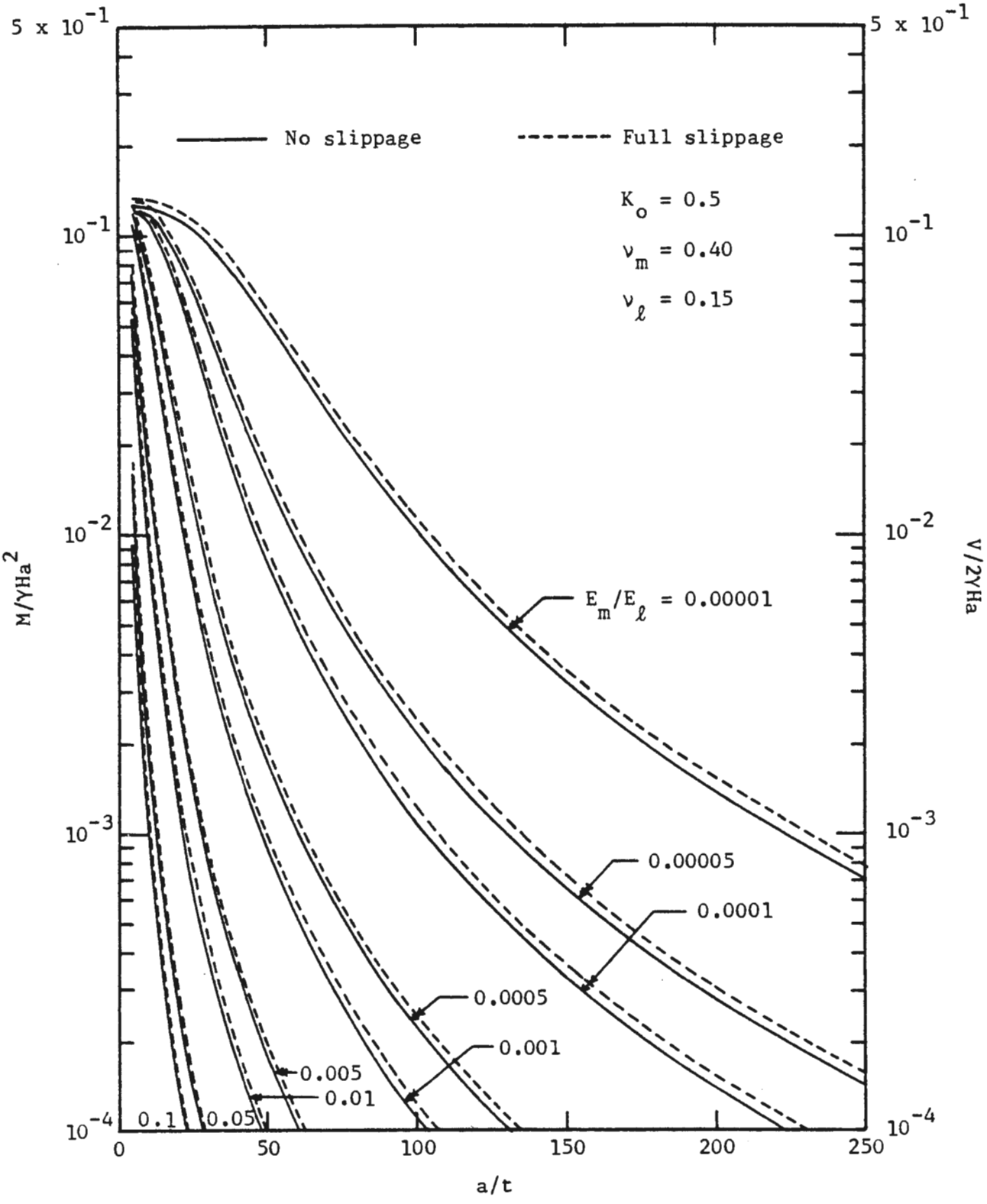

FIGURE 3.11 VARIATION OF MAXIMUM BENDING MOMENT AND SHEAR FORCE COEFFICIENTS WITH (a/t) AND (E_m/E_ℓ)

slippage values are, on average, approximately five percent less than the full slippage values. The maximum difference occurs for $(E_m/E_\ell) = 10^{-5}$ and (a/t) = 250, and amounts to approximately nine percent.

Figure 3.12 illustrates the variation of liner stresses due to bending with (a/t) for several values of the modulus ratio. It can be seen that reduction of liner modulus always leads to smaller bending stresses. For (E_m/E_ℓ) greater than approximately 0.005, reducing liner thickness also always leads to smaller bending stresses, but for (a/t) > 50 the stress reductions, and the stresses themselves, are very small. For (E_m/E_ℓ) values less than approximately 0.005, the curves indicate an initial stress increase up to a peak value and then a stress decrease as (a/t) is increased from initially very small values. For a continuous liner of uniform cross section the bending stresses are given by $\sigma = Mc/I = 6M/t^2$. Thus, the initial bending stress increase with increasing (a/t) can be explained by the fact that as the liner thickness is reduced the t^2 term initially decreases faster than the bending moment.

In Fig. 3.13 the liner stresses (full slippage condition) due to thrust and bending have been combined to give the maximum and minimum liner stresses. The curves show the variation of these stresses with liner radius-to-thickness ratio for several values of the modulus ratio. For $K_o < 1$ the maximum stresses occur at the inner surface of the liner springlines and the minimum stresses occur at the inner surfaces of the crown and invert. In the lower range of (a/t) values the bending stresses predominate and the total stress curves exhibit initial peaks followed by stress decreases. As (a/t) is increased further stress decrease is halted (minimum stresses become positive) and the stresses begin to increase in magnitude again. At

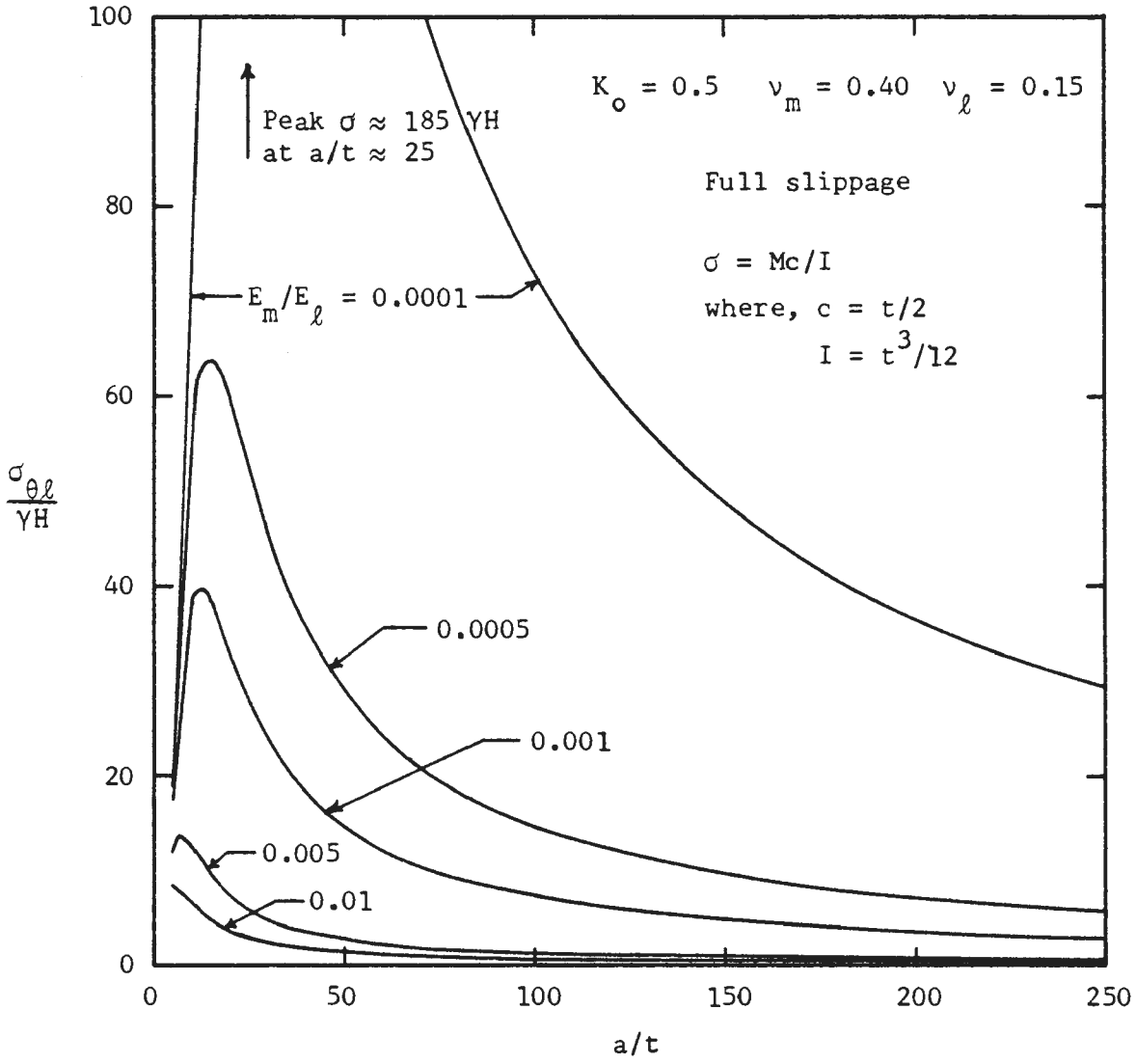

FIGURE 3.12 BENDING MOMENT COMPONENT OF LINER CIRCUMFERENTIAL STRESS (OUTER FIBER STRESSES) VERSUS (a/t)

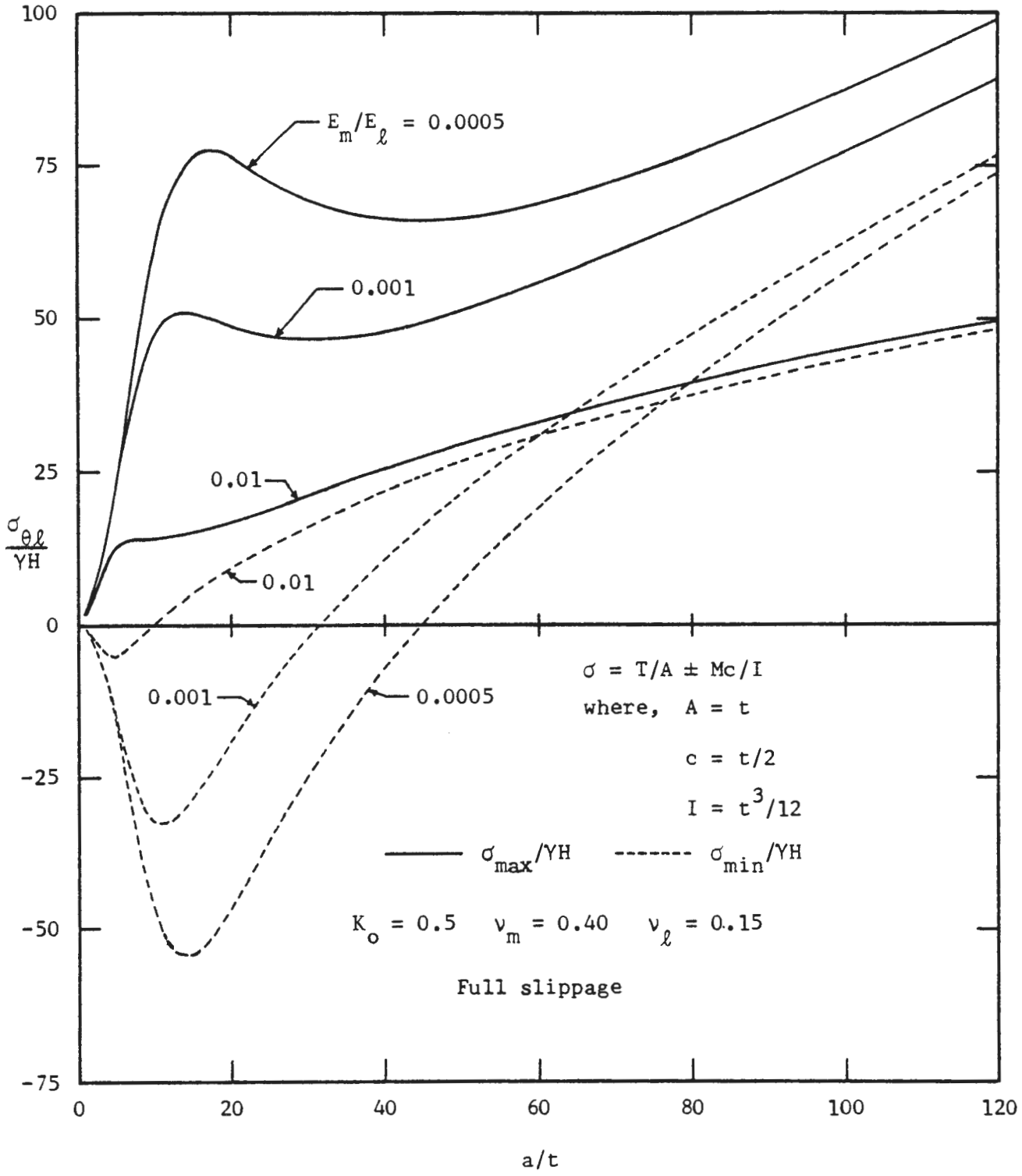

FIGURE 3.13 MAXIMUM AND MINIMUM TOTAL CIRCUMFERENTIAL LINER STRESSES VERSUS (a/t)

these higher (a/t) values the bending stresses have been reduced to such an extent that the compressive stresses due to thrust now predominate. The dashed curves for the minimum liner stresses show that as (E_m/E_ℓ) is decreased the range of (a/t) values which yield tensile stresses in the crown and invert increases.

Given the compressive and tensile strengths of a liner material, the appropriate maximum and minimum stress curves can be used to estimate the range of acceptable liner thicknesses.

The variation of the diameter change coefficient, $(\Delta D/D)(YH/E_m)$, with the liner radius-to-thickness ratio,(a/t), and the ground-liner modulus ratio, (E_m/E_ℓ), is shown in Fig. 3.14. As was done with the thrust coefficient, the diameter change coefficient has been separated into its two components. The average diameter change, given by the first term in the radial displacement equation, is given in the top chart of Fig. 3.14 and is denoted by the subscript 1. This component is independent of liner flexibility and the slippage condition at the ground-liner interface. The second term in the radial displacement equation is denoted by the subscript 2. This is the term that, when multiplied by $\cos 2\theta$, gives the variation of radial displacement with the location around the liner circumference. This component of the total diameter change coefficient is considered in the lower chart of Fig 3.14. The dashed curves apply for the full slippage condition and the continuous curves apply for the no slippage condition.

The top chart in Fig. 3.14 shows that if $(E_m/E_\ell) \leq 0.0001$ the liner is essentially incompressible ($\Delta D_1 \approx 0$) and thus the (a/t) ratio has little effect on the average displacement. As the modulus ratio is increased the liner (regardless of its a/t value) becomes more compressible and the value

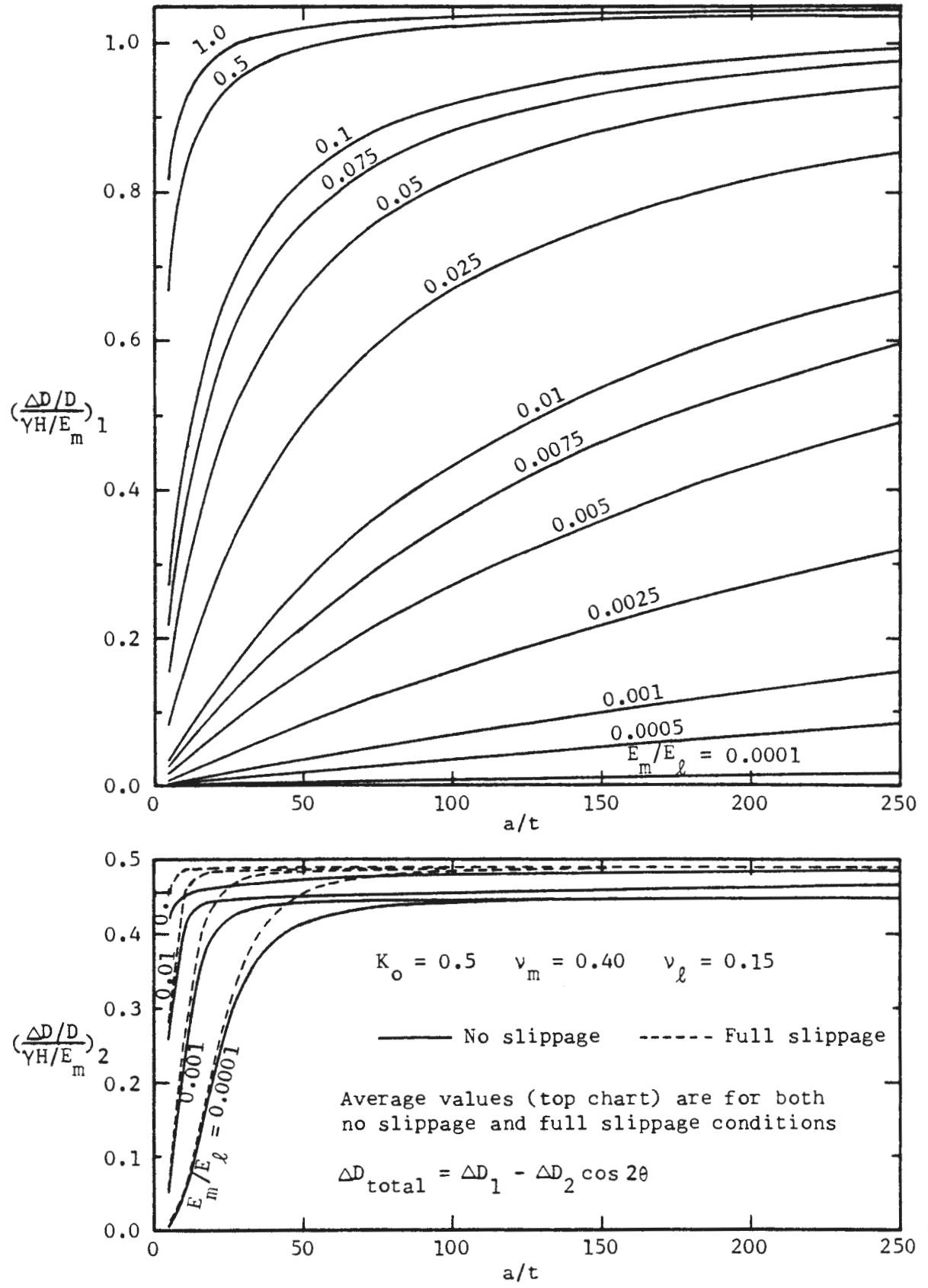

FIGURE 3.14 VARIATION OF DIAMETER CHANGE COEFFICIENT WITH (a/t) AND (E_m/E_ℓ)

of (a/t) becomes more significant. Further increase of (E_m/E_ℓ) eventually causes the liner compressibility to become so great that the (a/t) ratio value is again of little significance. For $(E_m/E_\ell) = 1$ alteration of the (a/t) value has essentially no effect on the average displacement unless it is reduced to (a/t) < 50.

The lower chart in Fig. 3.14 shows that if (a/t) > 50 the liner is very flexible regardless of the modulus ratio value (down to 0.0001, at least). For a given modulus ratio value, (a/t) must be reduced below 50 (how far below depends on the E_m/E_ℓ value) before a significant reduction can be made in the magnitude of the variable component of displacement.

The curves in Figs. 3.9 through 3.14 were obtained for $K_o = 0.5$, $\nu_m = 0.4$ and $\nu_\ell = 0.15$, and, strictly speaking, are not applicable for other values of these parameters. However, the value of ν_ℓ has little influence on the results obtained from the analytical solution equations, and for any ν_ℓ value within the range encompassing the usual liner materials the figures presented can be used without adverse effect. Additionaly, the figures can easily be extended to apply for other K_o values by multiplying the values taken from the figures by one of two simple correction factors. If the magnitude of the term considered does not vary with θ, the correction factor is $(1 + K_o)/1.5$. For example,

$$\left\{\frac{T_1}{\gamma Ha}\right\}_{(\text{for any } K_o)} = \left(\frac{1 + K_o}{1.5}\right)\left\{\frac{T_1}{\gamma Ha}\right\}_{(\text{from Fig. 3.9})} \qquad (3.5)$$

If the magnitude of the term considered varies with θ, the correction factor is $2(1 - K_o)$. For example,

$$\left\{\frac{M}{\gamma Ha^2}\right\}_{(\text{for any } K_o)} = 2(1 - K_o)\left\{\frac{M}{\gamma Ha^2}\right\}_{(\text{from Fig. 3.11})} \tag{3.6}$$

The use of the curves presented in Figs. 3.9 through 3.14 is not advisable for ν_m values significantly different from $\nu_m = 0.4$. For ν_m values outside the range $0.35 \leq \nu_m \leq 0.45$ the values taken from these figures should be adjusted by means of the appropriate ν_m correction factor.

Considering the complexity of the ground-liner interaction problem the analytical solution is remarkably uncomplicated and simple to use. Unfortunately, because of the many simplifying assumptions that were necessary in order to obtain the solution, it is directly applicable to few real tunneling situations. On the positive side, however, it does seem to have some potential for use as a means of quickly and easily obtaining numerical values for the important parameters describing liner response. If these values are then conscientiously evaluated with the method's limitations in mind they can yield useful estimates of probable liner behavior for a given set of conditions.

CHAPTER 4

FINITE ELEMENT ANALYSIS OF SHALLOW TUNNELS

4.1 GENERAL REMARKS

Application of the analytical solutions for ground-liner interaction is restricted to tunnels located at great depth below the ground surface. This restriction is imposed because these solutions do not take into consideration two factors that can have significant influence on the behavior of shallow lined tunnels. These factors are:

1. The proximity of the ground surface free boundary.
2. The variation of stress magnitude with depth from the tunnel crown to the invert. Assuming a horizontal ground surface and stresses due to the weight of the overburden in a homogeneous ground mass, the stresses exhibit a linear increase with depth and no horizontal variation.

The Kirsch and Lamé solutions, which have been applied to the unlined tunnel problem (Obert and Duvall, 1967) are also restricted to deep tunnels for these same reasons. However, the analytical solutions applicable to the shallow unlined tunnel case (circular opening near a horizontal boundary in an elastic half-space) that are available (Savin, 1968, and Mindlin, 1940) indicate that for depths greater than one or two tunnel diameters the influence of the above factors is negligible. There are no analytical solutions of the ground-liner interaction problem for shallow tunnels to give an indication of the variation of liner behavior with tunnel depth. Therefore, the finite element method was used to investigate this problem.

4.2 METHOD OF ANALYSIS

Figure 4.1 illustrates the finite element mesh used to simulate the ground mass in this study (liner elements not shown). The two-dimensional, plane strain analyses assumed linear elastic stress-strain behavior for both the liner and the ground mass. Additionally, the ground mass was assumed to be isotropic and homogeneous. Values of the relevant in situ stress state, material property and dimensional parameters are given in the figures that summarize the results of the analyses.

Because the problem is symmetrical about a vertical plane through the tunnel axis, only half of the region was analyzed. The mesh shown was generated with the tunnel opening and liner in place so that each analysis could be performed in just one solution step. The in situ stress state was introduced into the mesh by applying, at the perimeter of the tunnel opening, a distribution of pressures corresponding to that in the undisturbed ground mass.

Both the no slippage and full slippage conditions were considered. To simulate the full slippage condition the mesh was generated with a small gap between the ground elements and the liner elements. Ground and liner were connected by means of one-dimensional bar elements. These elements allowed radial pressures, but not shear stresses, to be transmitted from ground to liner and vice versa. The cross sectional areas of the bars were selected such that the bars "filled" the gap between ground liner. However, it was found that with these dimensions the bar element stiffnesses had to be selected carefully in order to avoid distorting the analysis results. Initial analyses (later discarded) indicated that assigning liner stress-strain properties to the bar elements was equivalent to increasing the

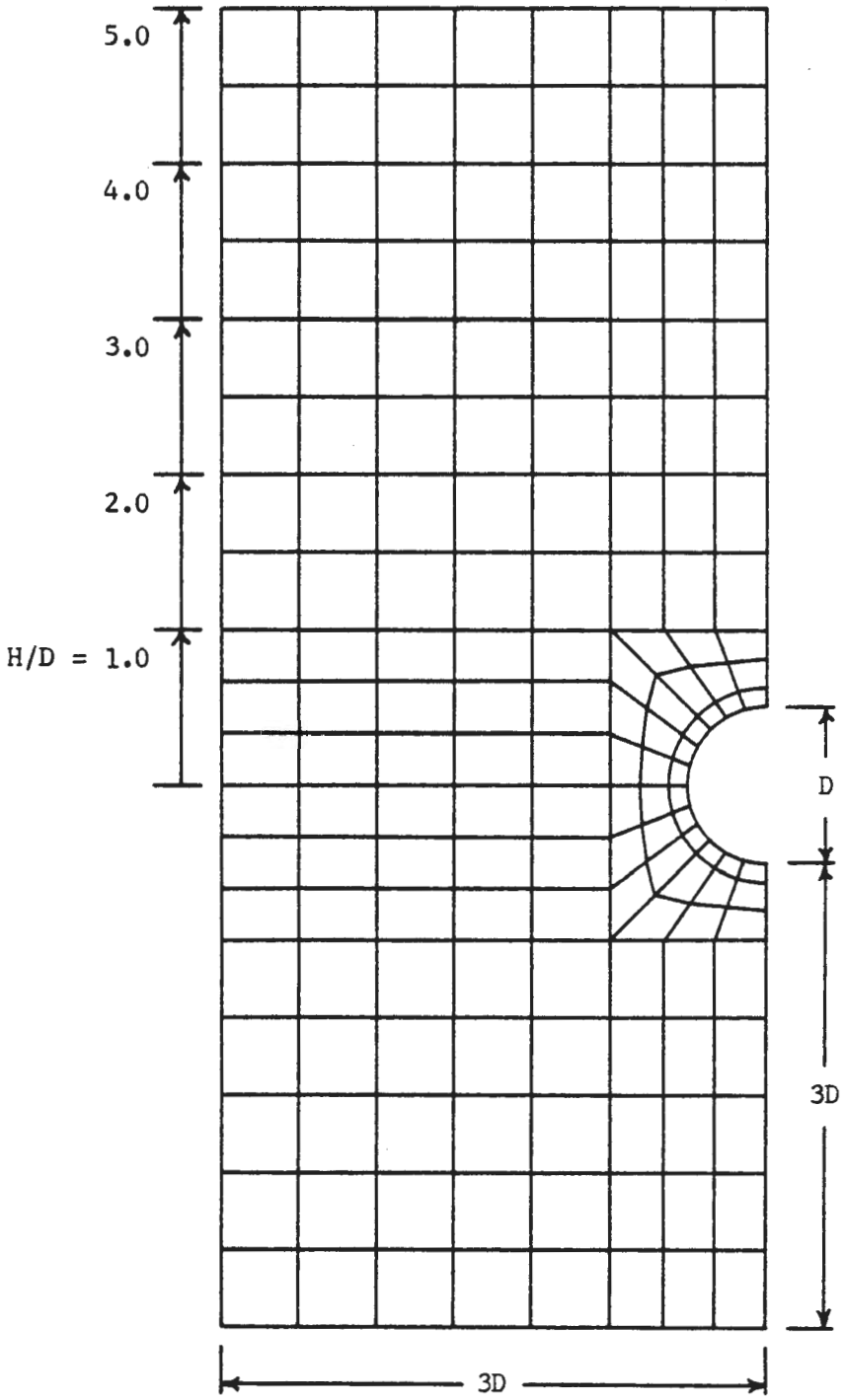

FIGURE 4.1 FINITE ELEMENT MESH FOR THE ANALYSIS OF SHALLOW TUNNELS

thickness of the liner by an amount equal to the thickness of the gap. Correct results were obtained by assigning to the bar elements the same elastic properties as those of the surrounding rock mass.

A total of six analyses were performed for each of the full slippage and no slippage conditions. Tunnel depth-to-diameter ratios of $H/D = 5.0$, 4.0, 3.0, 2.0, and 1.0 were analyzed. Analyses for $H/D \gg 5.0$ were also performed. The depth, H, is measured from the ground surface to the tunnel centerline. Thus, for $H/D = 1.0$ the depth of cover over the tunnel crown is equal to one tunnel radius.

The displacement boundary conditions imposed on the finite element mesh were such that the left and bottom boundaries were completely fixed, while the top boundary (ground surface) was free and the right boundary (plane of synmetry) was allowed only vertical displacements. As generated the finite element mesh was set up for $H/D = 5.0$. To analyze the case of a very deep tunnel ($H/D \gg 5.0$) the top boundary (not the ground surface in this case) was completely fixed against displacement and the distribution of pressures applied around the tunnel opening was specified so that there was no variation of pressure with depth. For the H/D values of 5.0 through 1.0 the pressure distribution was adjusted to reflect the appropriate tunnel depth. In addition, for $H/D < 5.0$ elements in the top part of the mesh were assigned activity numbers such that the correct number of element layers were turned off during each analysis to yield the correct depth of cover for that analysis.

4.3 INFLUENCE OF TUNNEL DEPTH ON LINER RESPONSE

4.3.1 LINER THRUSTS

Variation of the liner thrust coefficient with tunnel depth is illustrated in Fig. 4.2 for several locations around the liner and for both the no slippage and full slippage conditions. The continuous curves for the no slippage condition show that as H/D is reduced from very large values the springline thrust coefficient remains essentially constant until a value of H/D = 3.5 is reached. Thereafter, the magnitude of this coefficient gradually decreases. At H/D = 2.0 the coefficient value is just two percent less than the deep tunnel value, while at H/D = 1.0 it is 12 percent less.

For deep tunnels the maximum liner thrust occurs at the springlines (for $K_o < 1$). This was found to be the case for H/D > 3.5 also. However, as H/D is reduced further the stress increase from crown to invert causes the location of maximum thrust to shift. As noted in Fig. 4.2 the angular distance from the springlines to the location of maximum thrust is given by α. For H/D = 3.0, 2.0, and 1.0 the maximum thrust was found to be located at $\alpha \approx 5$, 10, and 25 degrees, respectively. As can be seen in Fig. 4.2 the magnitude of the maximum thrust coefficient exhibits even less variation with depth than does the springline coefficient.

The no slippage condition curves for the crown and invert thrust coefficients show the greatest variation with depth. As H/D is reduced the invert thrust coefficient increases. This should be expected since the pressures acting on the liner are greatest at the invert and smallest at the crown. These pressure differences increase as tunnel depth is reduced. It is also apparent that the crown and invert thrust coefficients approach the deep tunnel value only gradually as H/D is increased.

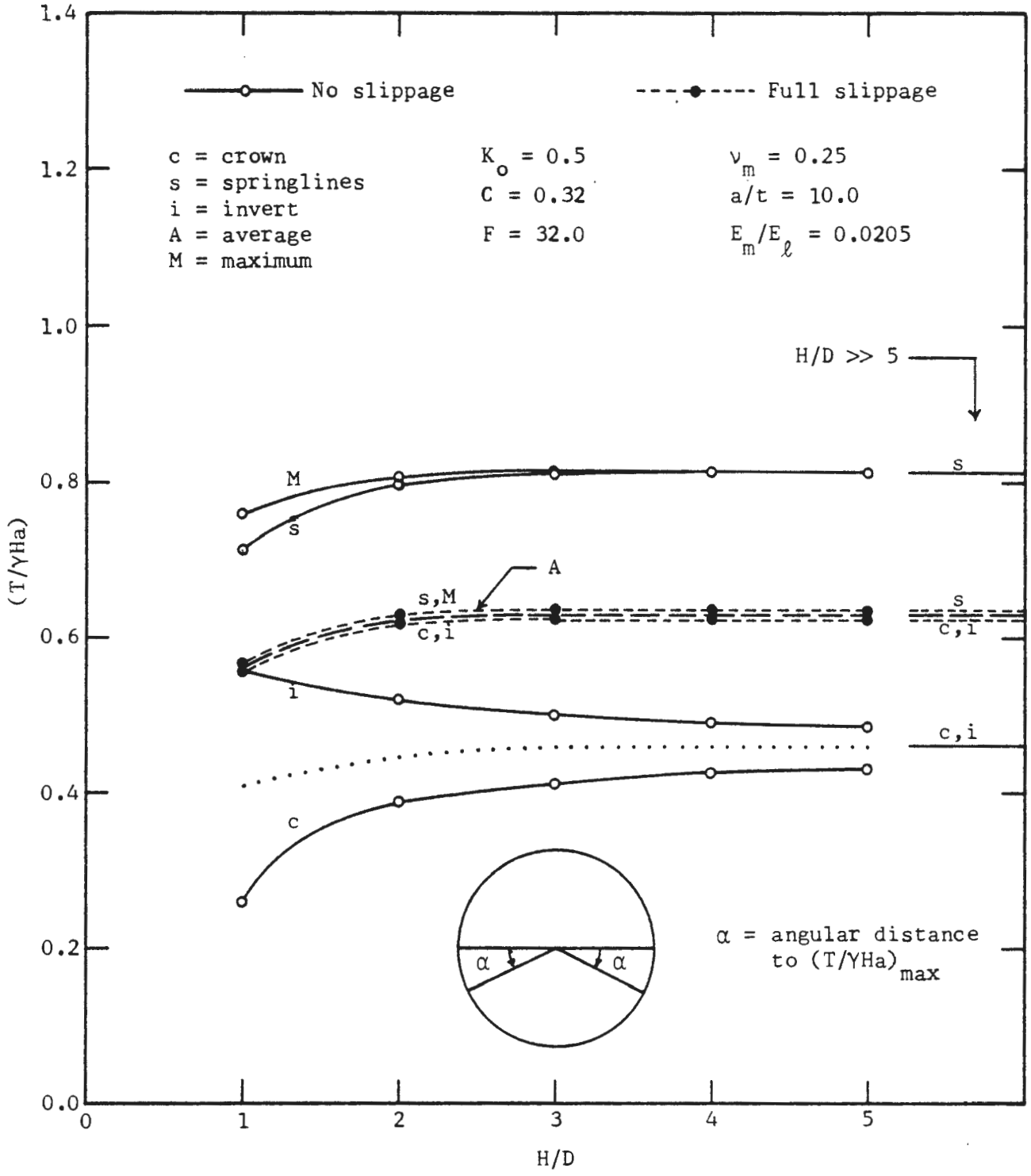

FIGURE 4.2 VARIATION OF THRUST COEFFICIENT WITH TUNNEL DEPTH

The broken curve labeled A in Fig. 4.2 gives the variation with H/D of the average liner thrust coefficient. This curve applies for both the no slippage and the full slippage conditions.

The dashed curves in Fig. 4.2 give the variation of the liner thrust coefficients with tunnel depth for the full slippage case. There is essentially no variation of liner thrust coefficient magnitude for H/D > 2. It would appear that slippage occurring at the ground-liner interface transforms the unsymmetrical insitu stress distribution into a distribution of external pressures that is symmetrical about a horizontal plane through the tunnel centerline. This would account for the fact that at all depths the maximum thrusts occur at the springlines, and also for the fact that at all depths the crown and invert thrusts are equal. The significance of the dotted curve in Fig. 4.2 is discussed in Section 4.4.

4.3.2 LINER BENDING MOMENTS

Figure 4.3 shows the variation with tunnel depth of the crown, springline and invert bending moment coefficients. While the slippage condition at the ground-liner interface influences the magnitude of the moment coefficients, it has little effect on the variation of the moment coefficient magnitude with depth.

For shallow tunnels the largest bending moment occurs at the invert and the smallest moment occurs at the crown. As H/D is increased the differences between the maximum and minimum moments and the intermediate springline value is gradually reduced. It appears that the deep tunnel case is attained at a shallower depth for the full slippage condition than it is for the no slippage condition. However, it is clear that this depth is greater

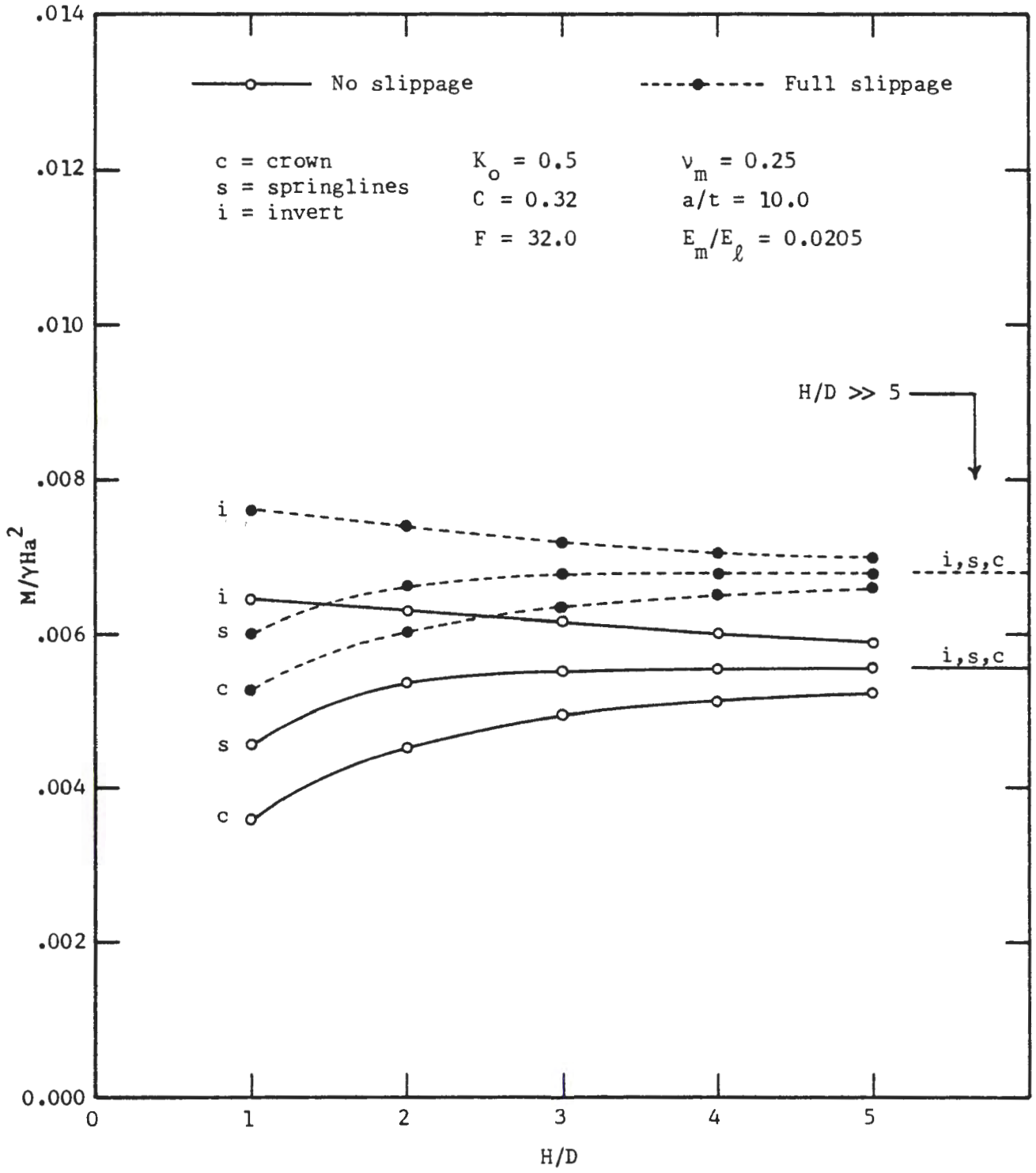

FIGURE 4.3 VARIATION OF MOMENT COEFFICIENT WITH TUNNEL DEPTH

than H/D = 5.0 for both interface conditions. The springline moment coefficient, on the other hand, exhibits relatively little variation with tunnel depth and rapidly approaches the deep tunnel value. For all H/D > 2.0 this coefficient is essentially constant and equal to the deep tunnel case value.

4.3.3 LINER STRESSES

In Fig. 4.4 the thrust coefficients of Fig. 4.2 and the moment coefficients of Fig. 4.3 have been combined to give the liner stress coefficients. The curves illustrate the variation with tunnel depth of the maximum and minimum circumferential liner stresses at the crown, springlines, and invert for the full slippage and no slippage conditions. At the crown and invert the maximum and minimum stresses occur at the outer and inner liner surfaces, respectively. At the springlines the maximum stresses occur at the inner surfaces of the liner and the minimum stresses occur at the outer surfaces. For this particular ground-liner combination (C = 0.32 and F = 32.0) both maximum and minimum stresses are compressive.

For the full slippage condition both the maximum and minimum (least compressive) liner stresses occur at the invert. This is understandable, because at all tunnel depths the maximum bending moment is located at the invert, and while the invert thrust is the minimum liner thrust it is only slightly less than the other thrust values.

Figure 4.4 also shows that for the no slippage condition the maximum and minimum liner stresses are located at the springlines and crown, respectively. Actually, for H/D < 3.5 the true maximum stress is slightly larger than the springline stress and is located slightly below the spring-

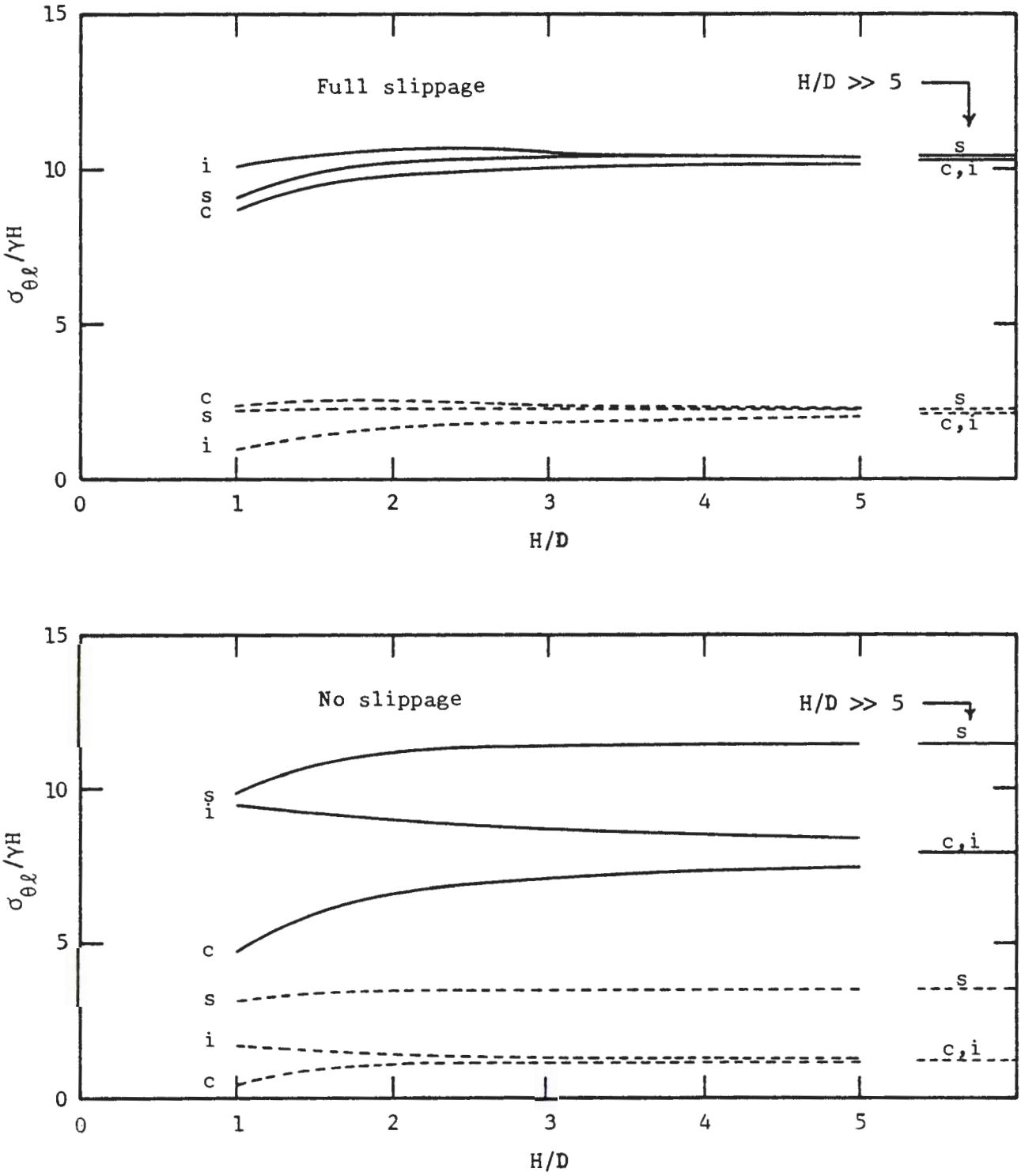

FIGURE 4.4 VARIATION WITH TUNNEL DEPTH OF MAXIMUM AND MINIMUM CIRCUMFERENTIAL LINER STRESS COEFFICIENTS AT CROWN, SPRINGLINES AND INVERT

lines (same location as maximum thrust, Fig. 4.2). For H/D = 1.0 the maximum stress is approximately six percent greater than the springline stress and is located approximately α = 25 degrees below the springlines.

The curves of Fig. 4.4 show that if the deep tunnel analysis (either finite element or analytical solutions) were to be applied to a shallow tunnel it would yield a conservative estimate of the maximum liner stress, but an unconservative estimate of the minimum stress.

4.3.4 LINER DISPLACEMENTS

Figure 4.5 illustrates the variation of the horizontal and vertical diameter change coefficient with tunnel depth. As in the case of the bending moments, the slippage condition at the ground-liner interface influences the magnitude of the diameter change coefficients, but not their variation with depth. For all H/D > 2.0 both horizontal and vertical diameter change coefficients are essentially constant and equal to the deep tunnel case values. The vertical diameter change coefficient represents an average of the crown and invert displacements and therefore does not give a true indication of the variation of these displacements with tunnel depth. To illustrate this variation Fig. 4.6 has been provided.

Figure 4.6 shows that the variation with tunnel depth of the crown and invert displacement coefficients is quite pronounced, relative to the variation of the vertical diameter change coefficient. For a very deep tunnel the active pressures acting downward on the top of the liner are equal to the active pressures acting upward on the bottom of the liner, and, as a result, the crown and invert are both forced inward the same amount. At shallow depths the active pressures acting downward on the top of the

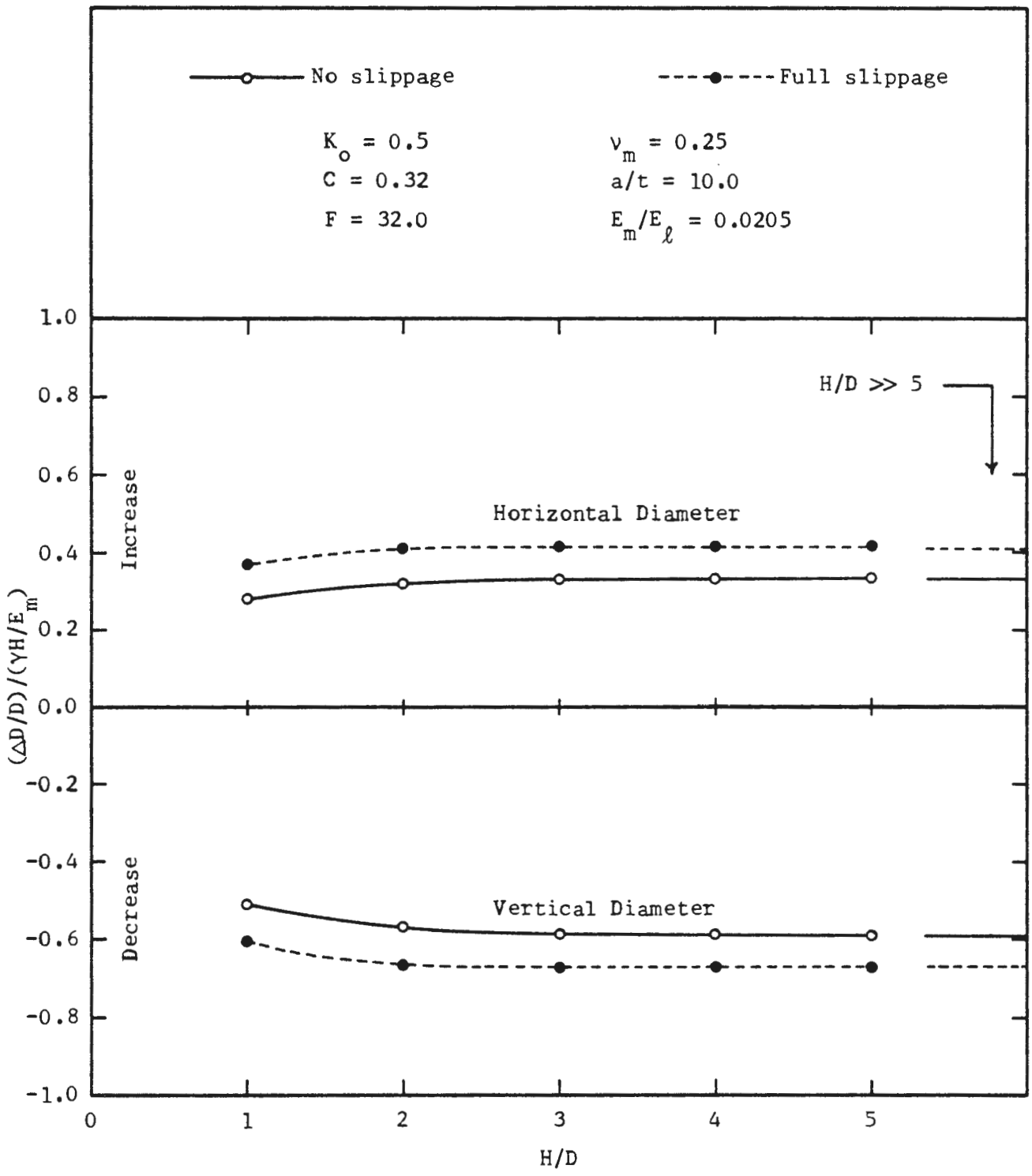

FIGURE 4.5 VARIATION OF HORIZONTAL AND VERTICAL DIAMETER CHANGE COEFFICIENTS WITH TUNNEL DEPTH

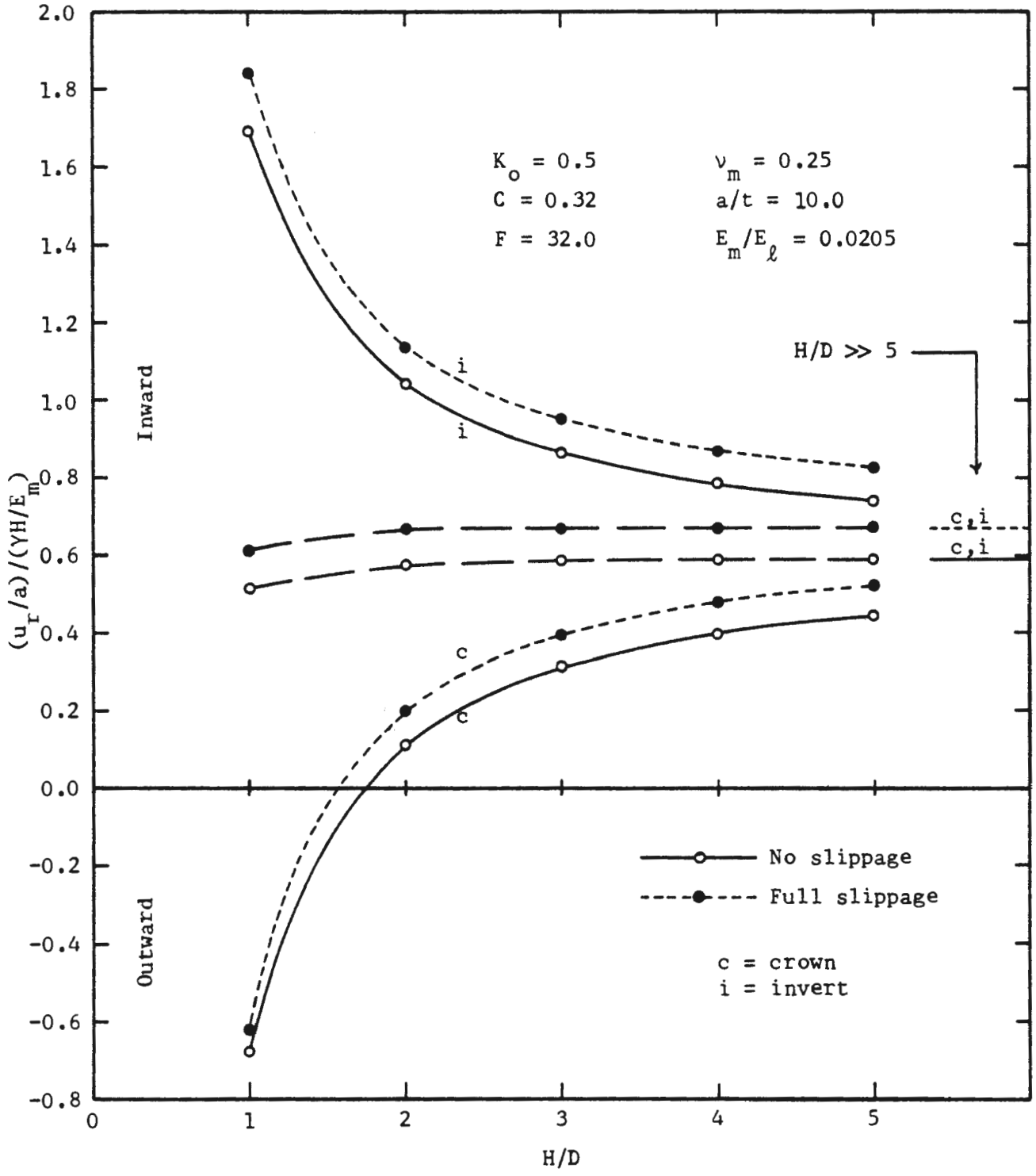

FIGURE 4.6 VARIATION OF CROWN AND INVERT DISPLACEMENT COEFFICIENTS WITH TUNNEL DEPTH

liner are less than the active pressures acting upward on the bottom of the liner. In the interaction process required to eliminate this imbalance the invert displaces upward more than the crown displaces downward. In the terms of Fig. 4.6 the inward displacement of the invert exceeds the inward displacement of the crown. At very shallow depths (here, $H/D < 1.5 - 1.75$) the downward active pressure is so small, relative to the upward active pressure, that the entire liner is shifted upward. At these depths, not only is the upward (inward) displacement of the invert quite large, but the crown is also forced upward (outward). Of course, the magnitudes of these liner displacements would be reduced if some ground displacements were allowed to occur prior to installation of the liner. The significance of the broken line curves in Fig. 4.6 is discussed in Section 4.4.

4.4 DISCUSSION OF RESULTS

The various curves in Figs. 4.2, 4.3, 4.5, and 4.6 provide an indication of the relative influence of the two previously mentioned factors (proximity of the ground surface boundary and stress increase with depth) that affect shallow, but not deep, tunnels. In these figures the normalized curves for liner response at the springlines would be independent of the increase of stress with depth from crown to invert. In addition, the average thrust coefficient curve in Fig. 4.2 should also be independent of this factor. Thus, these curves give the average influence of the ground surface boundary on liner response. They indicate only the average because the influence of the surface boundary should change slightly from crown to invert, being greatest at the crown and least at the invert. All curves for liner response (thrust, moment, displacement) at the crown and invert

reflect the combined influence of both factors. To isolate the effect of the stress increase with depth, the effect of the ground surface boundary must be subtracted out of these curves (Note: Because only the springline or average influence of the ground surface boundary is available, its subtraction from the combined total at crown and invert removes most, but not all, of the ground surface boundary influence at these locations). For the no slippage thrust coefficient curves of Fig. 4.2 the ground surface boundary effects can be removed by first drawing in an additional curve that exhibits the same variation with H/D as the springline and average thrust coefficient curves (dotted curve in Fig. 4.2). Points on this additional curve are obtained by multiplying the values of points on the average thrust coefficient curve by 0.73 (for the very deep tunnel, crown and invert thrust are 73 percent of the average thrust magnitude). The curves can also be obtained by multiplying values of points on the springline curve by 0.57. Differences between the crown and invert curves and this curve are due to the influence of the increase of stress with depth. The dashed curves in Fig. 4.2 for the full slippage condition indicate that for this slippage condition and this particular ground-liner combination the liner thrust coefficient is essentially independent of the stress increase with depth from crown to invert.

The variation of springline bending moment coefficient with tunnel depth, as shown in Fig. 4.3, is due almost entirely to the effect of the ground surface boundary. The variation of the crown and invert bending moments with tunnel depth is due to the combined effects of both the ground surface boundary and the stress increase with depth. Thus, an estimate of the stress increase with depth effect on crown and invert moment coefficients

can be obtained by noting the difference between corresponding points on the crown and springline curves and the invert and springline curves.

In Fig. 4.5 the variation with H/D exhibited by both the horizontal and vertical diameter change coefficient curves is due solely to the influence of the ground surface boundary. Points on the vertical diameter change coefficient curves represent averages of the crown and invert displacement coefficients and thus the effect due to stress increase with depth has been eliminated.

In Fig. 4.6 the curves for crown and invert displacement coefficients reflect the influence of both the ground surface boundary and the stress increase with depth. Differences between these curves and an additional curve (broken line curves shown), obtained by transfering the vertical diameter change coefficient curve of Fig. 4.5 to this figure, represent the effect of the stress increase with depth on the crown and invert displacement coefficients.

In summary, examination of the curves presented suggests the following:

1. The influence of the ground surface boundary on liner response is small for all H/D > 1.0 and negligible for all H/D > 2.0, and
2. the influence of the stress increase with depth from crown to invert is greater than the influence of the ground surface boundary and remains at a significant level to a much greater depth.

CHAPTER 5

FINITE ELEMENT ANALYSIS OF ADVANCING TUNNELS

5.1 GENERAL REMARKS

At every stage of the advancement of a tunnel three distinct zones of stresses and displacements in the ground can be distinguished. Far ahead of the tunnel face the ground mass remains undisturbed; the state of stress is in situ and no displacements have taken place. Far behind the face all the possible displacements have occurred and the state of stress in the ground and the liner has approached a final equilibrium, independent of the position of the tunnel face. In a zone around the tunnel face, extending to several radial distances ahead and behind the face, the state of stress is essentially three-dimensional and there is a longitudinal variation of ground displacements. As the tunnel face advances, assuming the ground conditions do not change, the spatial extent of this three-dimensional stress zone remains unaltered and its longitudinal position advances.

The initial loading to which any tunnel liner is subjected is strongly influenced by the amount of ground displacement that occurs before the liner and the ground mass come into contact and begin to interact. Since these displacements change with time and position along the axis of the advancing tunnel, the time and position of liner installation are important considerations in any analysis undertaken to estimate support loading. One of the major deficiencies that the majority of the two-dimensional methods of analysis (analytical and numerical) have in common is the inability to properly take into consideration the position of liner installation.

Behavior of the ground-liner system within the three-dimensional

zone around the tunnel face, of course, can not be considered by two-dimensional analyses, because these analyses, by definition, are applicable only for cross sections far from the tunnel face. However, the greatest difficulty that must be faced in using the two-dimensional approach is the determination of the relationship between position of liner installation and the amount of ground displacement occurring ahead of the liner. Two-dimensional analyses (e.g., those obtained with the analytical solution as in Chapter 3 and the finite element analyses of Chapter 4) which avoid this problem by assuming that no prior displacements occur overestimate the magnitude of the ground pressures that act on the liner. In addition, finite element analyses in which inelastic ground behavior is to be considered will yield misleading results if the correct magnitude of prior displacement is not considered, because the extent of plastic yielding is related to the amount of ground disturbance (prior displacement) allowed.

In regard to the extent of prior displacements, the general case corresponds to that of a liner of intermediate flexibility and compressibility installed some distance behind the tunnel face such that a small gap (e.g., thickness of a tunneling shield's tailskin) is left between the liner and the ground. The total radial displacement that occurs before ground-liner equilibrium is reached is then $u_f + u_u + u_g + u_\ell$, where

u_f = radial displacement occurring ahead of the face

u_u = radial displacement occurring between the face and the point of installation

u_g = radial displacement occurring at the point of installation before the gap is filled

$u_f + u_u + u_g$ = prior displacements

u_ℓ = radial displacement of the liner under load.

The equilibrium ground pressure decreases as the ratio $(u_f + u_u + u_g + u_\ell)/u_{po}$ increases from zero to one. The displacement u_{po} is the total potential ground displacement. Assuming the tunnel opening remains stable, the initial (end of construction) liner load is zero if $u_f + u_u + u_g = u_{po}$ (i.e., if all ground displacements occur before ground-liner contact). However, if the ground mass exhibits time-dependent behavior the pressures acting on the liner may increase in the months and years following construction. For some soils the ground pressure may increase to a magnitude corresponding to the full overburden pressure.

Figure 5.1 illustrates the relationship between prior displacements and the resulting ground pressure acting on the liner for three different cases. The curve ABC illustrates the relationship between potential ground pressure and prior radial ground displacement. The shape of this curve is a function of the stress-strain-strength properties of the ground mass. Here, the ground (assumed to be an elasto-plastic material) remains elastic if displacements in excess of those required to reach point B are not allowed. If internal support is not provided to halt displacement beyond point B a plastic zone forms around the tunnel and the additional plastic displacements change the ground reaction curve from a straight line to a curve with decreasing negative slope. In this case the curve intersects the horizontal axis indicating that the opening would be stable without internal support (since time-dependent behavior is not considered this curve says nothing about the long term stability of the opening). The solid, straight line curve rising from the horizontal axis to intersect the ground reaction curve represents the reaction of the liner to load. The liner

$K_o = 1$

P = Potential ground pressure

$P_{max} = \gamma H$

$K_o \neq 1$

P = potential average ground pressure

$P_{max} = \frac{1}{2}(1 + K_o)\gamma H$

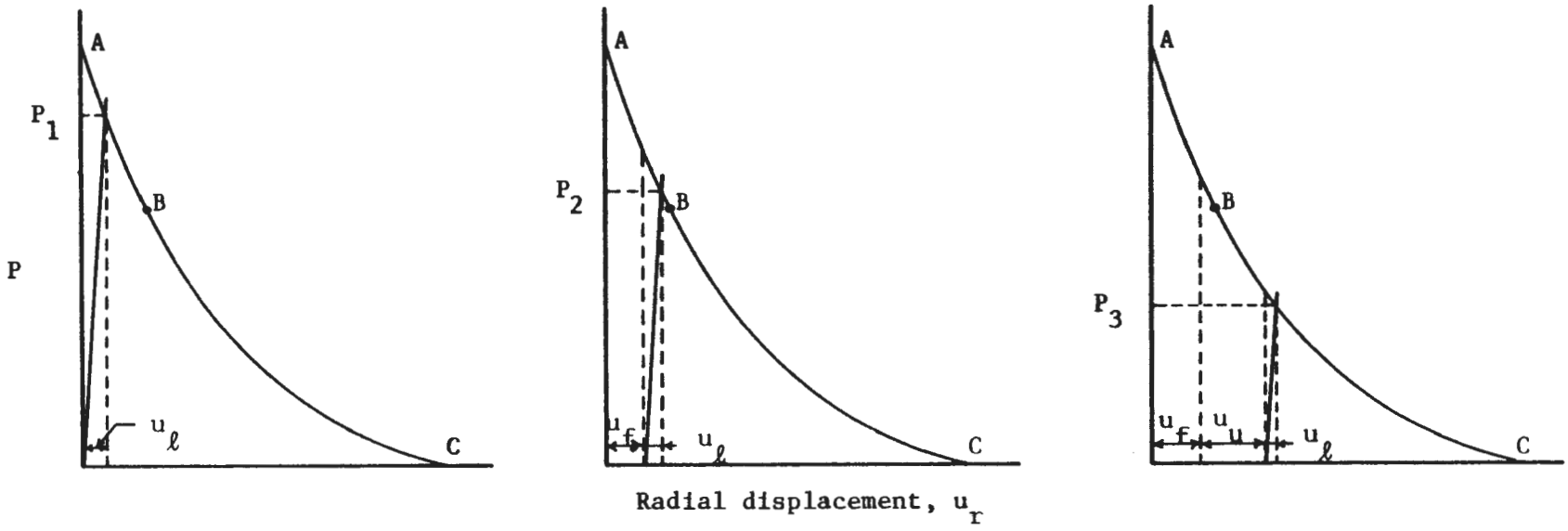

a) No prior displacements

b) Liner installed at face

c) Liner installed some distance behind face

FIGURE 5.1 HYPOTHETICAL GROUND PRESSURE ACTING ON LINER FOR VARIOUS AMOUNTS OF PRIOR GROUND DISPLACEMENT

reaction curve shown is for a liner of intermediate compressibility and thus it has a finite, nonzero slope. If the liner was perfectly incompressible (C = 0) its reaction curve would be vertical. At the other extreme, a perfectly compressible (C = ∞) liner would be represented by a horizontal line along the horizontal axis (no resistance to ground displacements).

Part a of Fig. 5.1 illustrates the case in which no prior displacements are allowed. The pressure acting on the liner at equilibrium, P_1, is determined solely by the interaction (indicated by the displacement u_ℓ) that occurs between the liner and ground mass. This is the case considered in Chapter 3 with the modified analytical solution and in Chapter 4 with the two-dimensional, plane strain finite element analyses. The condition of no prior displacement is rarely satisfied because there is almost always some ground displacement ahead of the tunnel face. In Fig. 5.1b this displacement has been designated u_f. In this case it is assumed that the liner is installed right at the tunnel face such that the tunnel is kept fully lined as it is advanced. Because some displacement has occurred before the liner was installed, the equilibrium pressure, P_2, is less than P_1. If the liner is installed some distance behind the face additional ground displacement, u_u, will occur before interaction between ground and liner can begin. Fig. 5.1c shows that this additional displacement leads to the even smaller equilibrium pressure, P_3.

Figure 5.1 illustrates the misleading results that can be obtained when prior displacements are ignored in the analysis of a tunneling situation in which the liner is installed some distance behind the face. Note also, in Fig. 5.1a, that despite the fact that the ground mass exhibits elasto-

plastic behavior which could easily be modeled with the finite element method, a finite element analysis that did not consider prior displacements would yield the same results for both elastic and elasto-plastic ground behavior.

It should be emphasized that the difficulty with most analyses that reduce the tunnel problem to two dimensions is not that they cannot account for prior displacements, but that they cannot account for the relationship between prior displacements and the position of liner installation that determines the magnitude of the prior displacements. As Fig. 5.1 implies, analytical solutions based on the ground reaction curve can account for prior displacements through the use of displacement terms such as u_f and u_u. The analytical solutions for excavation loading can be modified to account for prior displacements (but only for the elastic case, of course). It is conceivable that two-dimensional, plane strain finite element analyses could also be modified to allow given amounts of ground displacement before insertion of the liner. However, in each of these approaches it is not possible to determine the correct amount of prior displacements to allow without considering the longitudinal effects of the three-dimensional problem which control the ground stresses and displacements ahead of the tunnel liner.

To investigate the influence of the behavior of the ground mass ahead of the tunnel liner on liner response, a finite element study was performed in which the actual advancement of the tunnel through the ground mass was simulated. Summarized in Table 5.1 are the various cases analyzed and the material properties used in each analysis.

With respect to liner installation, three conditions were simulated. In a third of the analyses it was assumed that the liner was continually installed right at the advancing tunnel face; in the remainder of this chapter

TABLE 5.1

MATERIAL PROPERTIES

Case	ν_m	c		ϕ	$\frac{\ell_u}{a}$
		psi	kPa	degrees	
A	0.40	--	--	--	0
B	0.40	--	--	--	1
C	0.40	--	--	--	>>1
D	0.49	14	96.5	0	0
E	0.49	14	96.5	0	1
F	0.49	14	96.5	0	>>1
G	0.40	14	96.5	30	0
H	0.40	14	96.5	30	1
I	0.40	14	96.5	30	>>1

Initial stress state: $\sigma_r = \sigma_\theta = \sigma_z = \gamma H = 83.33$ psi (575 kPa), $\tau_{rz} = 0$

Soil modulus: $E_m = 5000$ psi (34.5 MPa)

Liner properties: $E_\ell = 2 \times 10^6$ psi (1380 MPa), $\nu_\ell = 0.15$

Liner thickness: t = 1 ft (0.305 m)

Tunnel diameter: D = 20 ft (6.1 m)

this is referred to as a "fully lined" tunnel. An additional third of the analyses assumed that the liner extended to a distance of one tunnel radius behind the face; this is referred to as a "partially lined" tunnel. In the remaining analyses it was assumed that the liner was installed at a point far behind the face; this is referred to as an "unlined" tunnel because all ground displacements occur before the liner is installed. The last column in Table 5.1 indicates these three conditions; ℓ_u/a being zero, one, or much greater than one, where ℓ_u is the distance between the leading edge of the liner and the tunnel face and a is the tunnel radius.

Two types of stress-strain behavior were considered for the surrounding ground mass; linear elastic and elastic-perfectly plastic. In the elasto-plastic analyses a modified Drucker-Prager yield condition (see Section 5.2.3) was used, with the additional material parameters being the cohesion, c, and the angle of internal friction, ϕ. Two values for the friction angle were considered; $\phi = 0$ and $\phi = 30$ degrees. The liner, assumed to be concrete, was assigned linearly elastic material properties which were not varied.

In order to avoid the considerable difficulty and expense involved in the performance of a large number of fully three-dimensional finite element analyses, only the special case of axially symmetric loading was considered. The ground mass within which the tunnel was to be constructed was modeled by an appropriate axisymmetric finite element mesh with the axis of symmetry coinciding with the centerline of the circular tunnel. The in situ stress state was assumed to be isotropic ($K_o = 1$).

Because of the restrictions on geometry and loading the axisymmetric analysis cannot be applied to shallow tunnels. It is not possible to

simulate the boundary effects imposed by the ground surface nor the increase of stress with depth from crown to invert that become significant at shallow depth. Thus, these analyses correspond to the special case of a deep tunnel (depth > several diameters).

5.2 METHOD OF ANALYSIS

5.2.1 THE FINITE ELEMENT MESH

The quadrilateral, isoparameteric axisymmetric finite elements (Zienkiewicz, 1971) used in this study are circular rings, called toroidal elements (Fig. 5.2a). Although an assemblage (mesh) of these elements can be constructed in a wide variety of forms, here a simple solid cylindrical shape (Fig. 5.2b) was considered the most suitable for the problem at hand. The position of any point within such a mesh is defined by the cylindrical coordinates; r, θ and z. When such a mesh is subjected to axially symmetric loading the problem becomes mathematically two-dimensional. Because of symmetry, the stress components are independent of the angular (θ) coordinate and, thus, all derivatives with respect to θ vanish and the components v, $\gamma_{r\theta}$, $\gamma_{\theta z}$, $\tau_{r\theta}$, and $\tau_{\theta z}$ are zero. The nonzero stress components are σ_r, σ_θ, σ_z, and τ_{rz} (see Fig. 5.2c).

Figure 5.3 represents the upper half of a longitudinal cross section through a typical finite element mesh used in this investigation. Boundary stresses were applied so as to achieve an initial uniform isotropic stress state throughout the mesh, $\sigma_r = \sigma_\theta = \sigma_z = \gamma H$, where γ is the unit weight of the ground mass and H is the depth of the tunnel axis below the ground surface. At the beginning of each analysis all elements were assigned soil properties. The shaded elements in Fig. 5.3 are the soil elements which

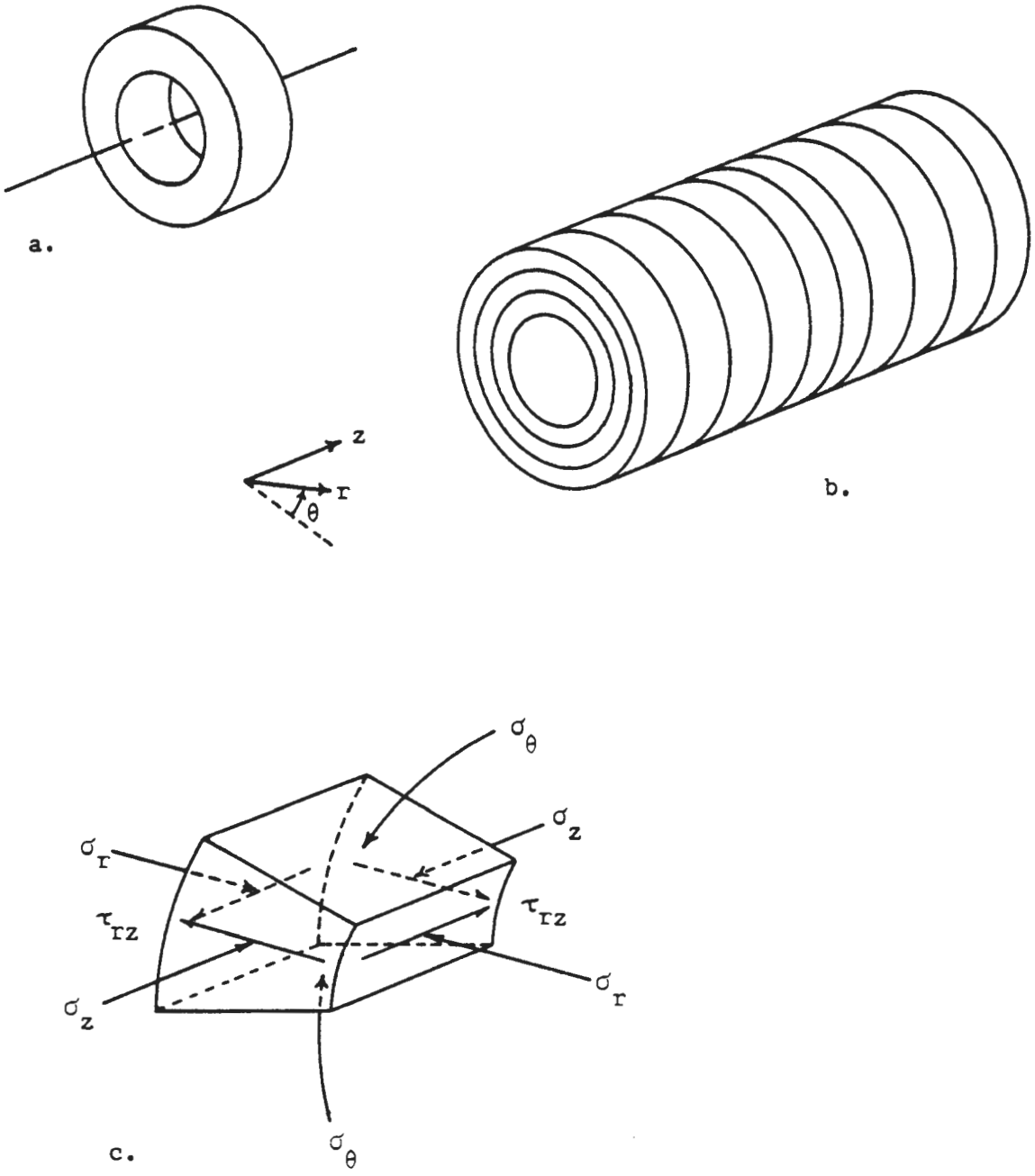

FIGURE 5.2 AXISYMMETRIC FINITE ELEMENT (a), CONCEPTUAL AXISYMMETRIC FINITE ELEMENT MESH AS USED HERE (b), AND NON-ZERO STRESS COMPONENTS (c)

FIGURE 5.3 TYPICAL FINITE ELEMENT MESH

were "excavated" to form the tunnel. The elements with diagonals indicate the positions where liner elements were "installed" after excavation.

5.2.2 EXCAVATION AND LINER INSTALLATION SEQUENCE

Each analysis consisted of a series of solution steps in which the mesh and/or its boundary conditions were modified so as to simulate advancement of the tunnel through the soil. In step one the boundary forces were applied to the mesh, all elements of which were assigned soil properties. At the end of this step the mesh represented a fully stressed, undisturbed ground mass. The first excavation into this ground mass occurred in step two when the first set of soil elements was removed. Also in this step the force boundary condition along the right boundary was replaced by a displacement boundary condition to prevent longitudinal displacements there and to maintain the stress field in the mesh. If the tunnel was to be lined a liner element was inserted at this step (fully lined case) or the following step (partially lined case). In each of the remaining steps the tunnel was advanced a distance equal to the length of the next ring of soil elements. These steps, which constitute an incremental analysis of the geometrically nonlinear problem, are carried out internally by the computer program GEOSYS (Ghaboussi and Ranken, 1974).

The excavation and construction sequence is achieved through the deactivation or activation of the elements involved. When the mesh is generated all elements (soil and liner) are assigned to the positions that they are to occupy at one time or another throughout the analysis. An activity number is assigned to each element that will be removed from or added to the mesh. The activity number indicates the step at which the element will be

removed or added. In the case of excavation, the soil elements involved have the appropriate material properties and contribute to the global stiffness of the system up to the indicated step, beyond which the contribution of these elements to the global stiffness of the system is zero. The reverse of this procedure is applied to those elements (liner) to be added to the mesh.

5.2.3 MATERIAL BEHAVIOR MODELS

Linear elastic and elastic-perfectly plastic (elasto-plastic) material behavior models were considered in this investigation. The elasto-plastic model utilized by the finite element program GEOSYS is a modified form of the Drucker-Prager (1952) model which is, in turn, a three-dimensional generalization of the Mohr-Coulomb failure criterion. The modified Drucker-Prager failure criterion is given as follows (compressive stresses taken as positive here):

$$\text{For } J_1 \leq m, \quad \ell\left(1 - \left|1 - \frac{J_1}{m}\right|^2\right) + k - \sqrt{J_2'} = 0 \tag{5.1}$$

$$\text{For } J_1 \geq m, \quad \ell + k - \sqrt{J_2'} = 0 \tag{5.2}$$

The quantity J_1 is the first invarient of the stress tensor. The quantity J_2' is the second invarient of the deviatoric stress tensor. For small values of J_1 tne yield surface corresponds closely to that of the Drucker-Prager model wherein the failure envelope varies linearly with confining pressure, J_1. As J_1 increases in magnitude, the modified yield function diverges from the Drucker-Prager line and gradually approaches the Mises yield function

at m. For $J_1 \geq m$ the shear strength is a constant, S_{max}, independent of confining pressure. For the majority of soils whose shear strength is a function of the angle of internal friction, ϕ, this latter condition is achieved only at exceedingly high confining pressures, much higher than those encountered in most underground construction projects.

The yield surface is defined within the finite element program by specifying values for the three parameters k, ℓ, and m. These material constants are functions of the shear strength parameters ϕ and c and the maximum shear strength, S_{max}, as shown in the following equations:

$$k = \frac{3c}{\sqrt{9 + 12 \tan^2\phi}} \tag{5.3}$$

$$\ell = S_{max} - k \tag{5.4}$$

$$m = \frac{2\ell}{\alpha} \tag{5.5}$$

$$\alpha = \frac{\tan\phi}{\sqrt{9 + 12 \tan^2\phi}} \tag{5.6}$$

In the $\phi \neq 0$ analyses performed for this study the J_1 values were quite small relative to m and thus the relevant portion of the yield surface closely approximated that of Drucker-Prager. For the $\phi = 0$ analyses, $S_{max} = k = c$ = cohesion and the yield function corresponded to that of Mises.

The $\phi = 0$ assumption is valid only for saturated soils and only for as long as the moisture content of the soil remains unchanged. Any change

in moisture content would be accompanied by a change in effective stresses and would introduce an effective frictional component of shear strength. Thus, the results from an analysis that assumes $\phi = 0$ apply only to the short term behavior of a tunnel. Theoretically, the $\phi = 0$ analysis could be used for any saturated soil. However, this type of analysis becomes practical only if the permeability of the soil is low enough so that the condition of no change in moisture content is satisfied for a reasonable length of time. A soil composed of particles larger than silt size would experience a change of water content almost immediately upon excavation. Thus, the $\phi = 0$ analysis would not be justified for such a soil. However, most clays and some silts possess sufficiently small permeabilities so that the no drainage condition can be satisfied for a time (days or weeks) after excavation. It is to these soils that this type of analysis can be applied.

5.3 RESULTS OF ANALYSIS

5.3.1 GENERAL

The results obtained from the finite element analyses performed in this investigation are presented in this section. The following data are provided:

- -- configuration of the plastic zone (elasto-plastic analyses)
- -- distribution of soil stresses
- -- distribution of soil displacements
- -- radial displacements of the actual and projected tunnel wall
- -- longitudinal displacements of a reference cross section as the tunnel approaches
- -- liner thrust

It should be pointed out here that minor distortions of the data due to boundary and other procedural effects have been removed in order to isolate and clarify the information related solely to the behavior of an advancing tunnel.

5.3.2 PLASTIC YIELD ZONES

The plastic yield zones obtained for the fully lined, partially lined, and unlined tunnels are illustrated in Fig. 5.4.

The plastic zone for the fully lined tunnel is confined to a relatively small region just ahead of the face. Behind the face the liner provides enough support to the soil so that the stresses do not change very much from their free field values. The changes that do occur are not great enough for the resulting stress difference or shear stress to exceed the shear strength of the soil.

A considerably larger plastic zone is obtained for the partially lined tunnel. For this case the unsupported length of tunnel just behind the face allows sufficient redistribution of stresses in the soil to cause yielding out beyond the tunnel perimeter. The effect of the liner in this case is to halt further yielding beyond that which has already taken place ahead of it. Very little, if any, yielding occurs behind the liner.

The plastic zones shown in Fig. 5.4b and 5.4c, to the extent they exist, are similar in shape to those obtained for the unlined tunnels shown in Fig. 5.4a. The effect of the liner is to reduce the size of the plastic zone that forms behind its leading end and to increase the longitudinal extent of the plastic zone ahead of the face.

The effect of the liner, once it is installed, on the extent of

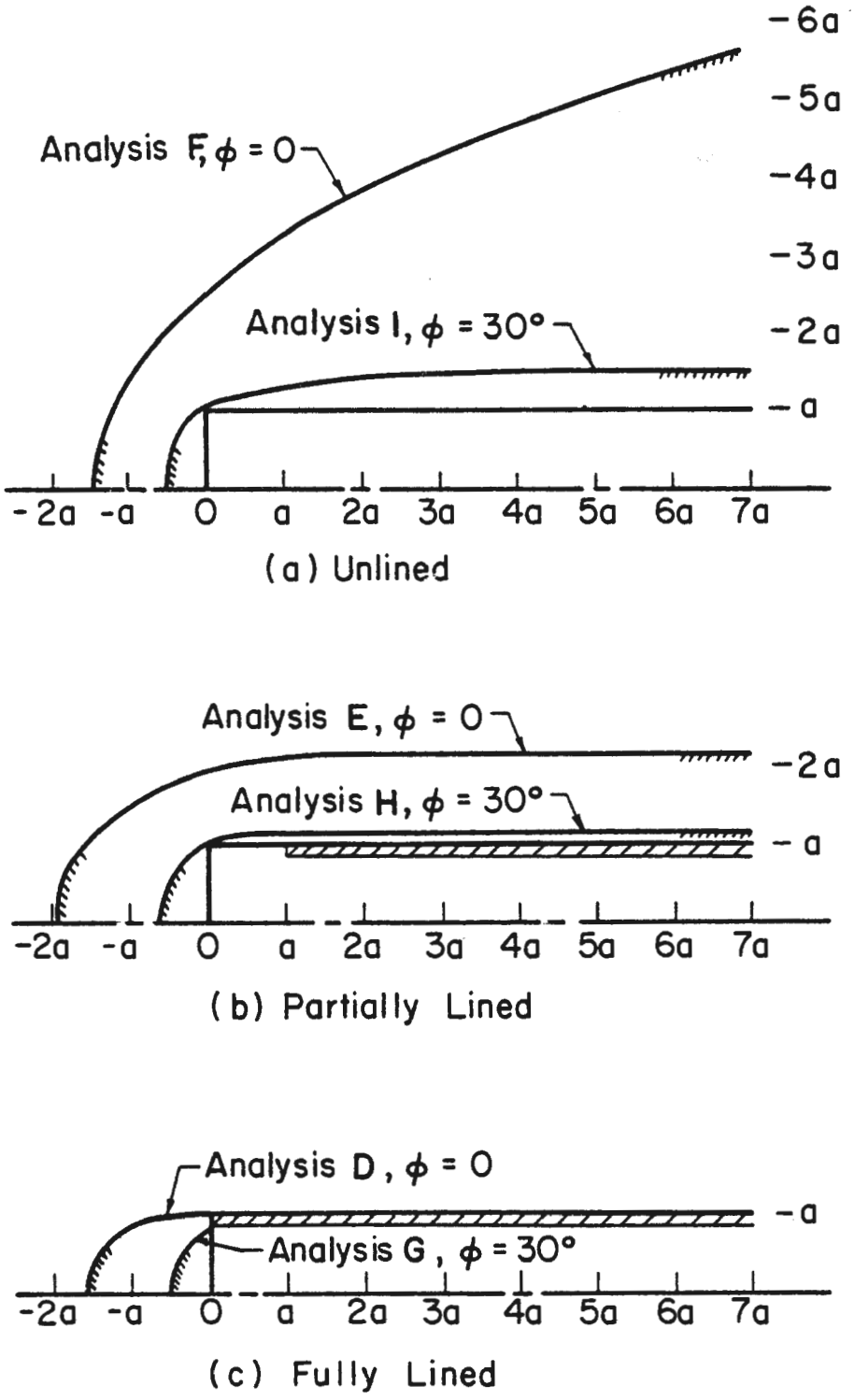

FIGURE 5.4 PLASTIC YIELD ZONE AROUND ADVANCING TUNNEL

plastic yielding (and ground displacements and stresses) depends, of course, on the compressibility of the liner (flexibility also if $K_o \neq 1$). In these analyses the ground-liner compressibility ratio was quite small, indicating a nearly incompressible liner. For larger compressibility ratios the extent of yielding behind the leading edge of the liner would be greater. However, over the range of realistic compressibility ratio values the influence of liner compressibility is of minor significance compared to the effect that position of liner installation has on the extent of the plastic zone.

5.3.3 SOIL STRESSES

The distributions of stresses in the soil surrounding the tunnel are shown in Figs. 5.5 and 5.6 for the cases of fully lined and partially lined tunnels, respectively. These are results from analyses D and E of Table 5.1 in which the soil was assigned values of c = 14 psi (96.5 kPa) and $\phi = 0$.

Stresses in the soil change from their undisturbed, free field values when displacements toward the tunnel are allowed. For the fully lined case the liner permitted only a small amount of radial displacement to occur after the liner was installed. Thus, this type of deformation contributed little to the stress redistributions shown in Fig. 5.5. The relatively large displacements, both radial and longitudinal, that occurred ahead of the face and liner were the major causes of the stress changes observed both ahead and behind the tunnel face (the tunnel is advanced through a zone of altered stresses).

One effect of the liner is to reduce the magnitude of stresses in a zone immediately ahead of the face from their free field values to an extent

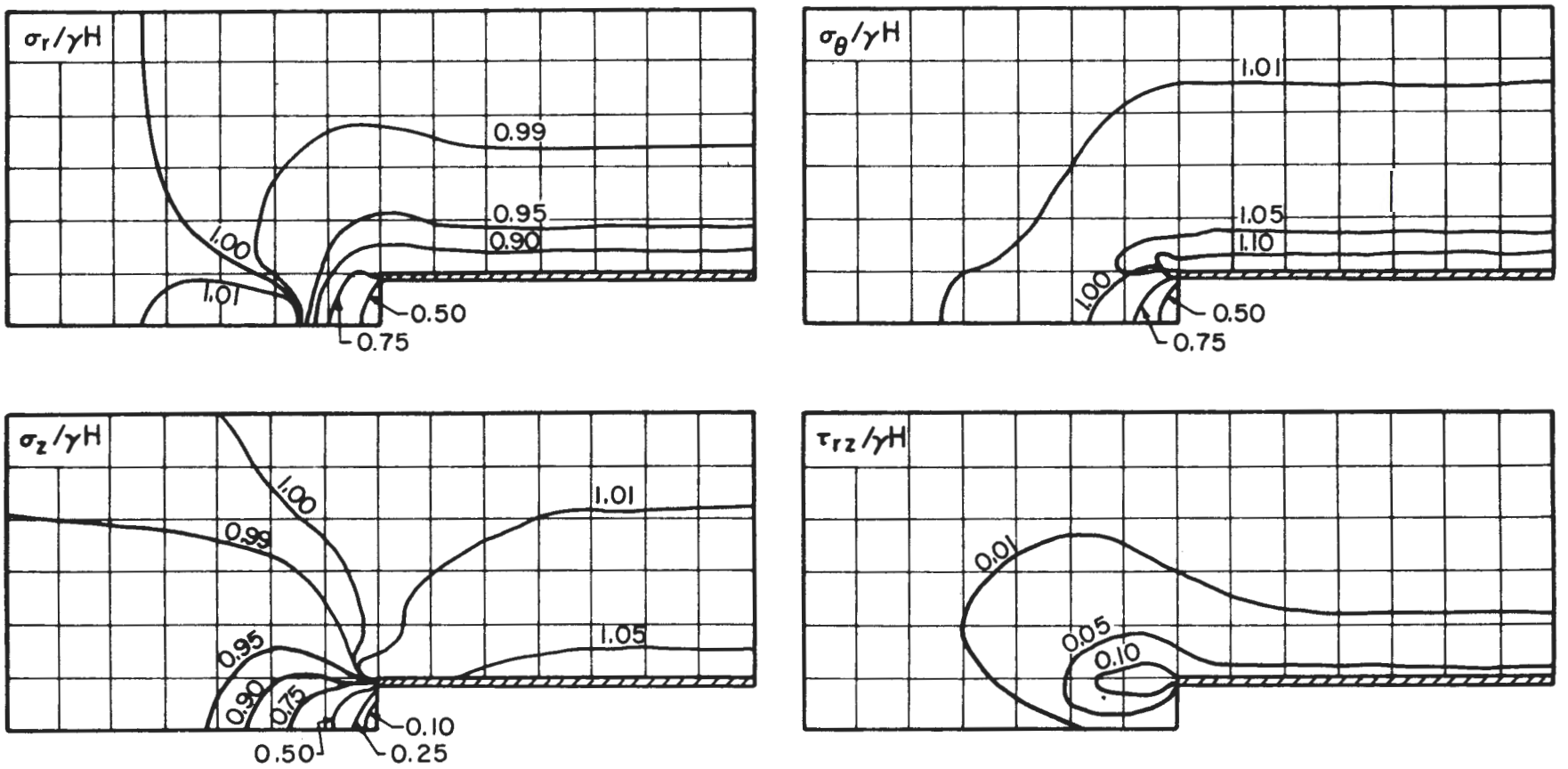

FIGURE 5.5 DISTRIBUTION OF STRESSES AROUND A FULLY LINED TUNNEL IN ELASTO-PLASTIC MEDIUM, ϕ = 0 (ANALYSIS D)

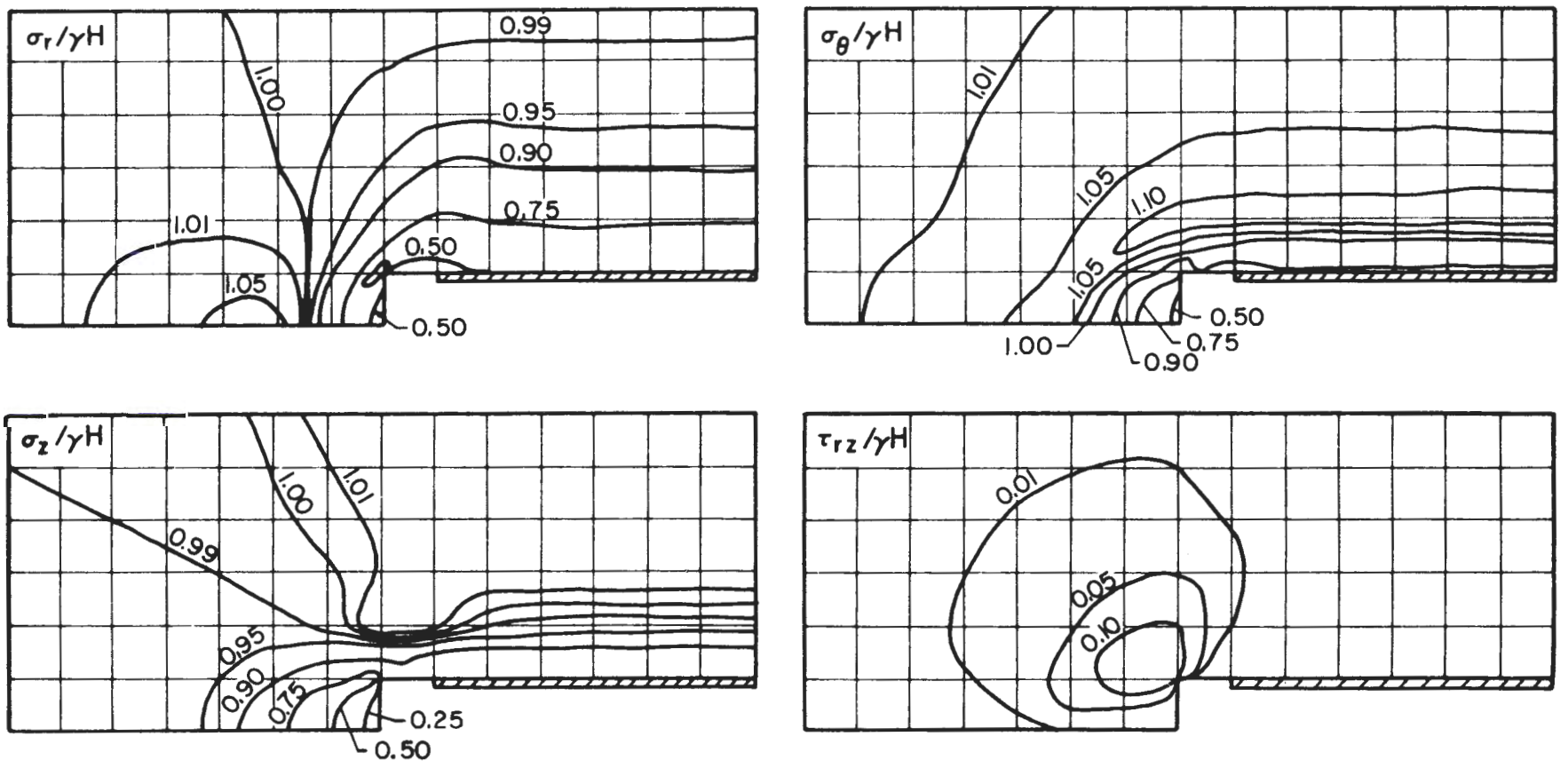

FIGURE 5.6 DISTRIBUTION OF STRESSES AROUND A PARTIALLY LINED TUNNEL IN ELASTO-PLASTIC MEDIUM, $\phi = 0$ (ANALYSIS E)

greater than that observed for an unlined tunnel. This is especially true for the radial (σ_r) and circumferential (σ_θ) stresses. It was observed that the stresses in this zone are further reduced when plastic yielding is concentrated in a zone just ahead of the face, as in the case D shown in Fig. 5.5.

For the fully lined case, the stresses in the soil surrounding the tunnel behind the face are controlled primarily by the magnitude of the stresses ahead of the face. It is assumed in these analyses that the tunnel and liner are advanced simultaneously and that this advancement takes place in a series of steps, each of which occurs instantaneously. When the tunnel is advanced a portion of the soil in the altered stress zone ahead of the face is removed and an additional length of liner is installed. Since these operations occur instantaneously, no stress changes can occur in the soil around the newly excavated volume of soil until after the liner is in place. Then, since the liner is relatively stiff it deforms only a small amount, resulting in only a slight change in the stresses. Thus, the stresses behind the face are only slightly different from those immediately ahead of the face.

The stress distributions for the partially lined tunnel are given in Fig. 5.6. If the tunnel is left unlined for a distance of only one tunnel radius behind the face, as in this figure, the disruption of the initially undisturbed stress state that results due to the presence of the tunnel closely approximates that found for an unlined tunnel. This is expected, since the results for the unlined tunnel cases indicate that most of the radial displacements occur within a zone immediately behind the face (note the steep slopes of the dashed curves in Fig. 5.9). When the radial extent of plastic

yield is small this zone extends only one to two tunnel radii behind the face. Up to 80 percent of the total displacements occur within this zone. Since, in the partially lined tunnel case, the majority of the displacements have occurred before the liner is installed, the amount of soil-liner interaction is small and the liner has little effect on the stresses in the soil. Thus, there is little difference between the stress distributions obtained for this partially lined tunnel case (liner installed one tunnel radius behind face) and the unlined tunnel case.

As expected, plastic yielding reduces stress magnitude, relative to the stresses obtained from elastic analyses, in the immediate vicinity of the tunnel opening -- in both radial and longitudinal (ahead of face) directions.

5.3.4 DISPLACEMENTS

Displacements of the surrounding soil due to the advancement of a fully lined tunnel (analysis D) are given in Fig. 5.7. The displacements that the soil mass experiences when the tunnel is advanced through only a short distance are given in part b of this figure. These incremental displacements are very small at most points throughout the medium. It is only in one small region, just ahead of the tunnel face, that these movements attain significant magnitudes. The directions of the arrows in Fig. 5.7b indicate that movement is toward the tunnel face, the only unsupported portion of the tunnel opening. Additional radial displacements behind the face are prevented by the liner in this case.

Although the majority of the incremental displacements are so small that they do not show up in Fig. 5.7b, they cannot be ignored. A tunnel is

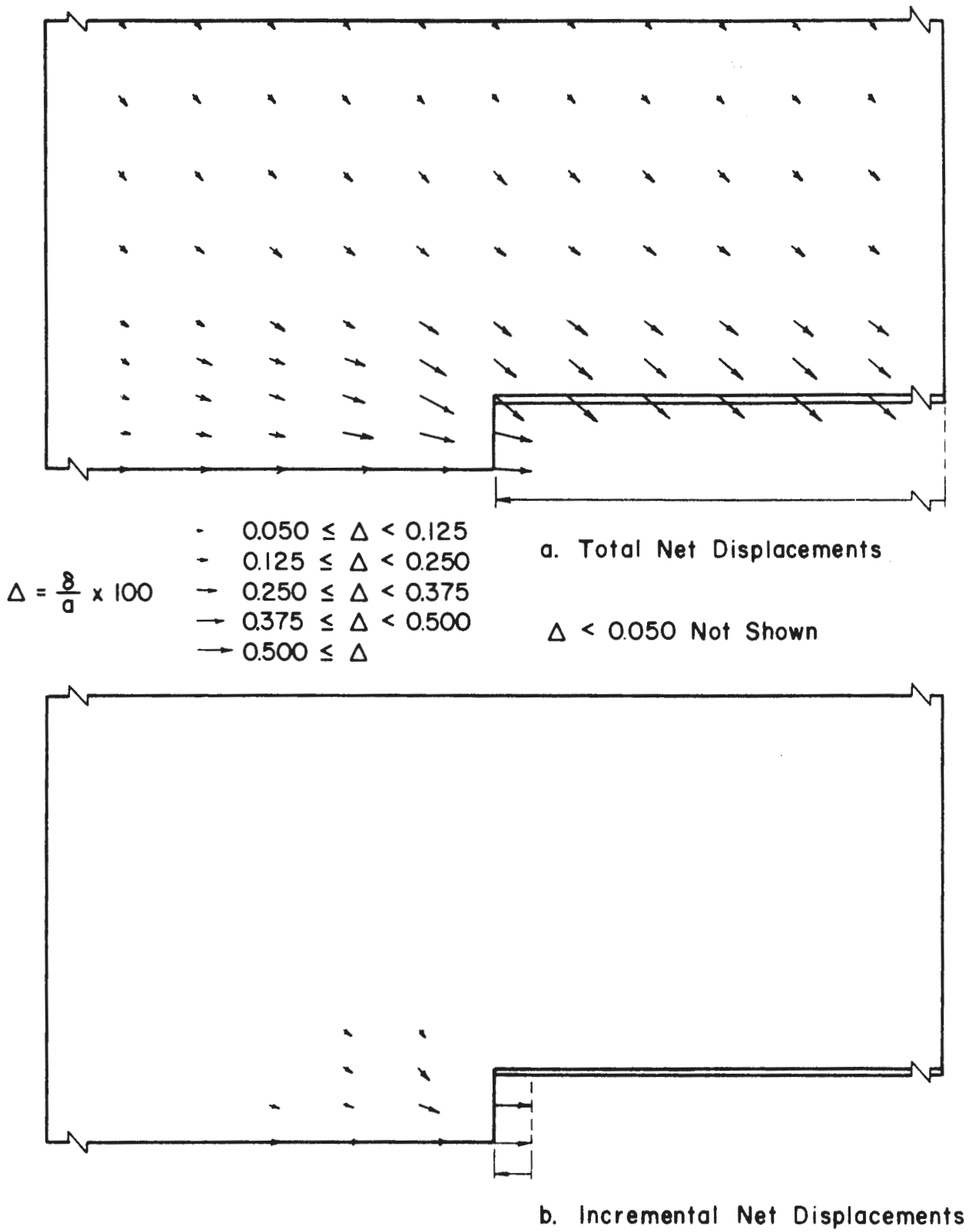

FIGURE 5.7 DISTRIBUTION OF DISPLACEMENTS AROUND A FULLY LINED TUNNEL IN ELASTO-PLASTIC MEDIUM, $\phi = 0$ (ANALYSIS D)

driven in a series of short advances, and it is the small displacements from each advance that are superimposed such that they combine to give the displacements shown in Fig. 5.7a.

Two significant features of the total displacement patterns can be seen in Fig. 5.7a. First is the fairly large displacements that occur ahead of the tunnel face. Appreciable displacements occur up to about three tunnel diameters of the face. It appears that the displacements are concentrated along the path of least resistance, which in this case is towards the unsupported tunnel face. This soil movement towards the face in a zone ahead of the face results in unusually large components of longitudinal displacements behind the face, which is the second significant feature of the soil displacement pattern. In fact, almost no appreciable displacement variations occur behind the leading edge of the liner; when a stiff liner is installed up to the face, it acts to "freeze" soil displacements at the values they had just before the face passed.

The distributions of total and incremental displacements for the partially lined tunnel (analysis E) are given in Fig. 5.8. Because the amount of unsupported tunnel surface area is greater, the soil displacements in the vicinity of this tuneel are larger than those obtained for the fully lined tunnel. This is true for both the incremental and total displacements.

Part a of Fig. 5.8 shows again that the stiff liner halts further displacements of the soil behind its leading edge. In this case, however, because of the unsupported tunnel wall more radial displacement occurs ahead of the liner than occurred in the fully lined tunnel case. Thus, the radial components of the displacements at locations far behind the face for this case are intermediate between those for the completely lined and unlined

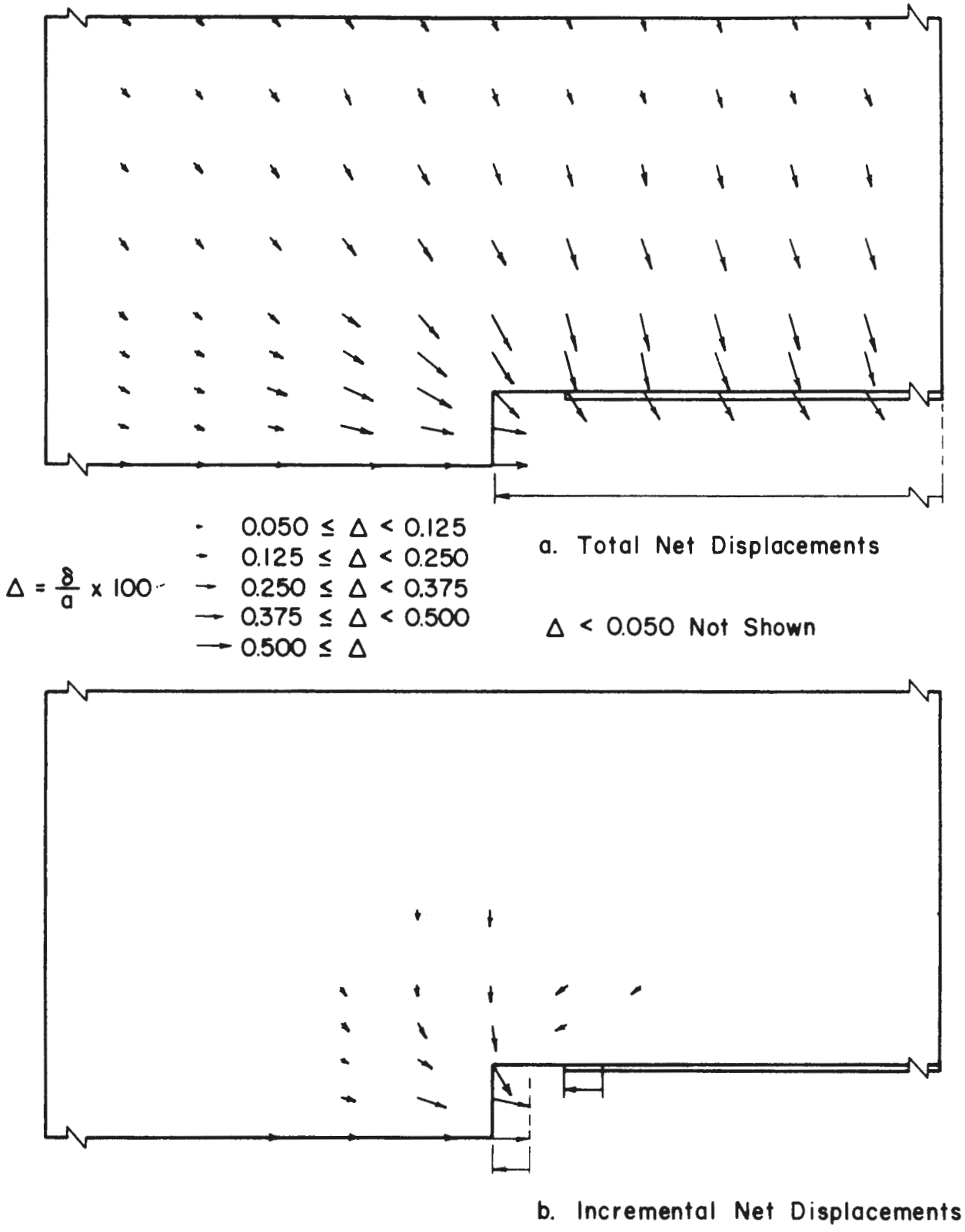

FIGURE 5.8 DISTRIBUTION OF DISPLACEMENTS AROUND A PARTIALLY LINED TUNNEL IN ELASTO-PLASTIC MEDIUM, $\phi = 0$ (ANALYSIS E)

tunnels.

The radial displacements of the fully and partially lined tunnel openings are shown in Fig. 5.9. The dashed curves represent the displacements of the corresponding unlined tunnels. The two sets of solid curves give the total displacement of the soil and liner.

Figure 5.9 shows that the radial displacements of the fully lined tunnels are considerably smaller than the displacements of the unlined tunnels. Also, it is clear that most of the displacements occur ahead of the leading edge of the liner. The actual displacement of the liner is very small and there is little variation with position along the tunnel axis. This is primarily due to the stiffness of the liner.

The corresponding displacements for the partially lined tunnel are also given in Fig. 5.9. Here the radial displacements are much larger, indicating that an unlined gap of only one radius length can significantly affect these displacements. Again, almost all of the displacements occur ahead of the liner. In front of the tunnel face there is very little difference between the displacement for the partially lined tunnel and the unlined tunnel.

The longitudinal displacements of a reference cross section as the tunnel approaches are given in Fig. 5.10 for the fully and partially lined tunnels in an elasto-plastic medium. Also shown are the displacements associated with the unlined tunnel in the same medium.

Longitudinal displacements for the lined tunnels generally exceed those of the unlined tunnel, with one exception. Longitudinal displacements of the tunnel face ($z^* = 0$) for the fully lined tunnel are less than those of the unlined tunnel. This indicates that the liner can have a restraining

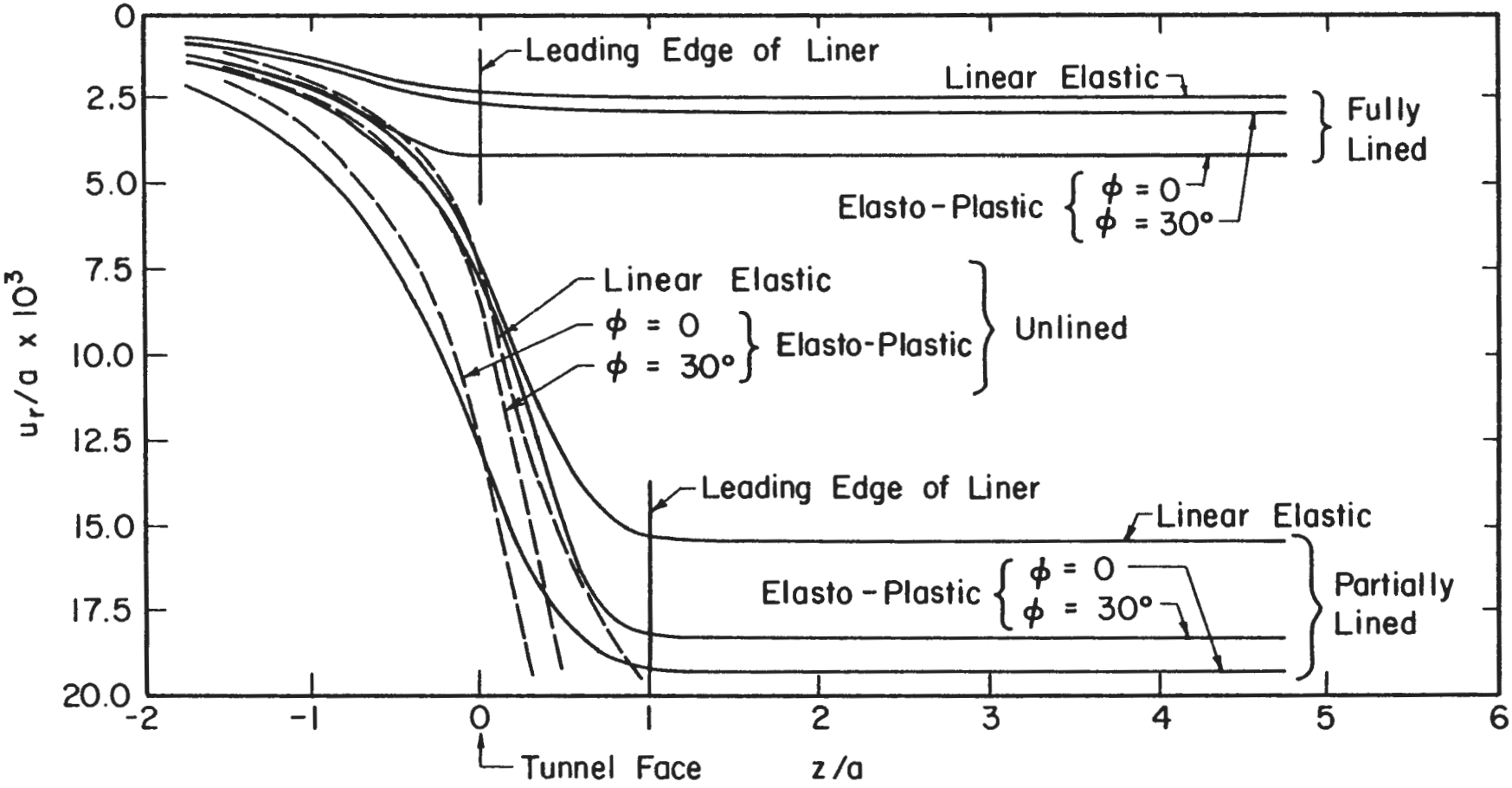

FIGURE 5.9 RADIAL DISPLACEMENTS

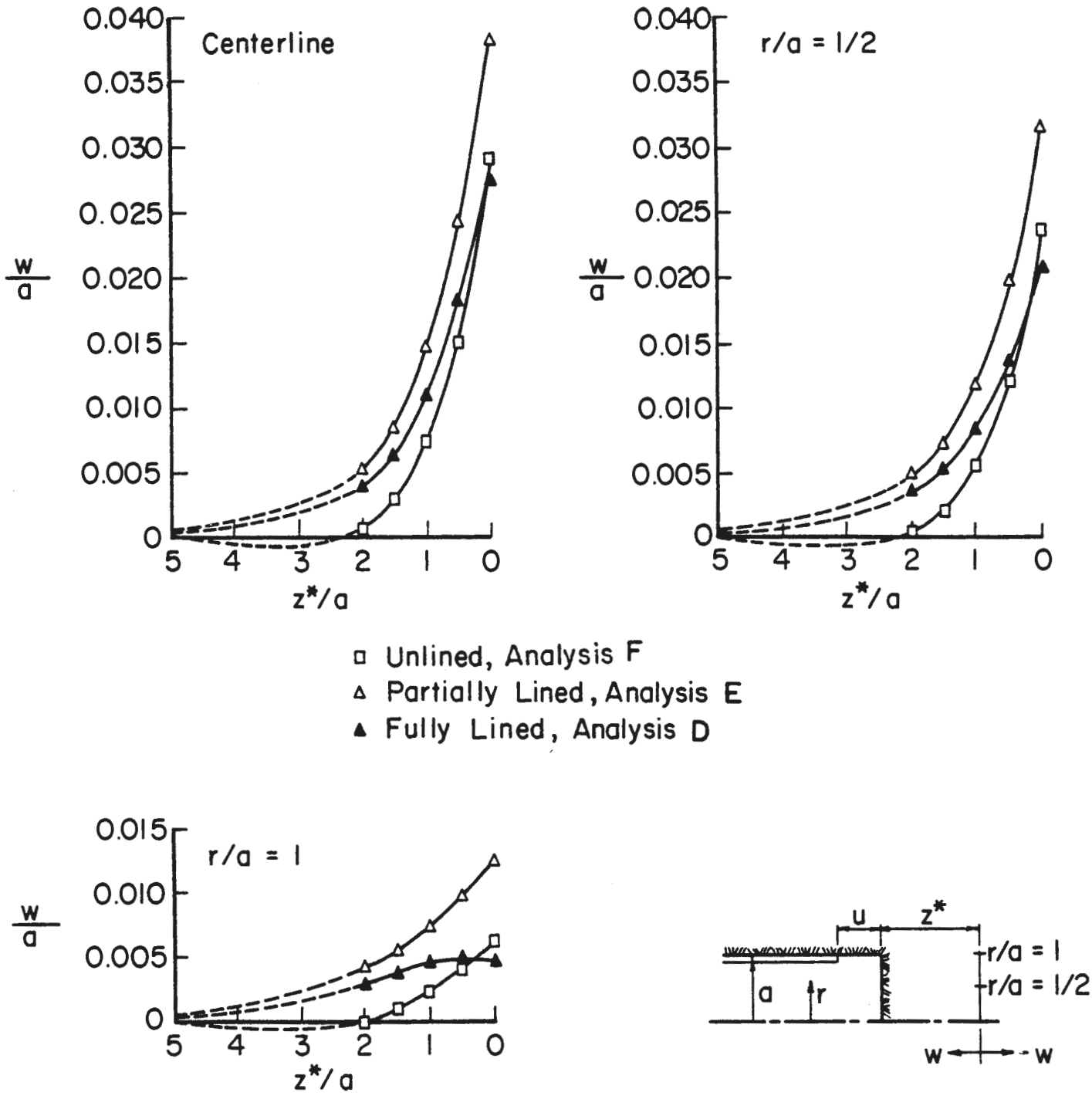

FIGURE 5.10 LONGITUDINAL DISPLACEMENTS AS TUNNEL FACE APPROACHES FOR FULLY AND PARTIALLY LINED TUNNELS IN ELASTO-PLASTIC MEDIUM, $\phi = 0$

effect on longitudinal as well as radial displacements.

The maximum displacement occurred at the centerline of the partially lined tunnel and was approximately four percent of the tunnel radius. This compares to a maximum of two percent of the radius obtained in the linear elastic analysis.

When the longitudinal displacement curves for the three fully lined tunnel analyses (linear elastic, elasto-plastic - $\phi = 0$, elasto-plastic - $\phi \neq 0$) are considered together in Fig. 5.11a, it is clear that as the size of the plastic zone ahead of the tunnel increases the displacements at all z^* increase. The longitudinal displacements for analysis G ($\phi \neq 0$) are everywhere greater than those for analysis A (no plastic zone) and the displacements for analysis D ($\phi = 0$) are everywhere greater than those for analysis G. For the partially lined tunnels a similar relationship holds only within the plastic zones (see $z^*/a = 0$, Fig. 5.11b). In the elastic regions beyond the plastic zones the longitudinal displacements from the elasto-plastic analyses are smaller than the corresponding displacements from the linear elastic analyses.

5.3.5 LINER THRUST

The longitudinal distributions of liner thrust for both the fully and partially lined tunnels are given in Fig. 5.12. In addition, the thrusts predicted by two two-dimensional, plane strain solutions are shown at the far right in this figure.

In the fully lined case, support provided by the soil ahead of the tunnel face reduces the external load and thus the thrust in the liner near the face. The effect of this natural support rapidly decreases with distance

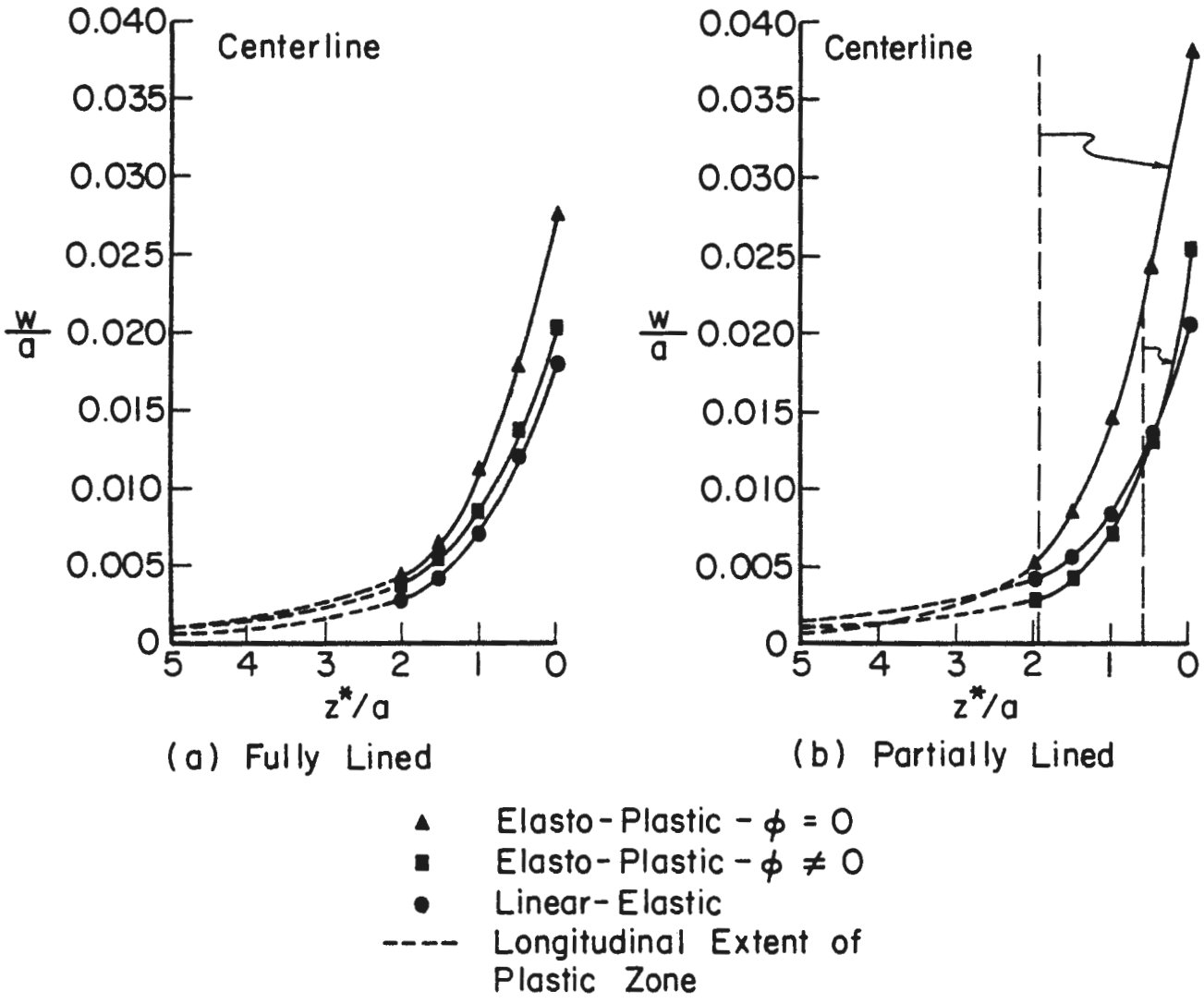

FIGURE 5.11 RELATIONSHIP BETWEEN LONGITUDINAL DISPLACEMENTS FROM LINEAR-ELASTIC, ELASTO-PLASTIC - $\phi = 0$, AND ELASTO-PLASTIC - $\phi \neq 0$ ANALYSES

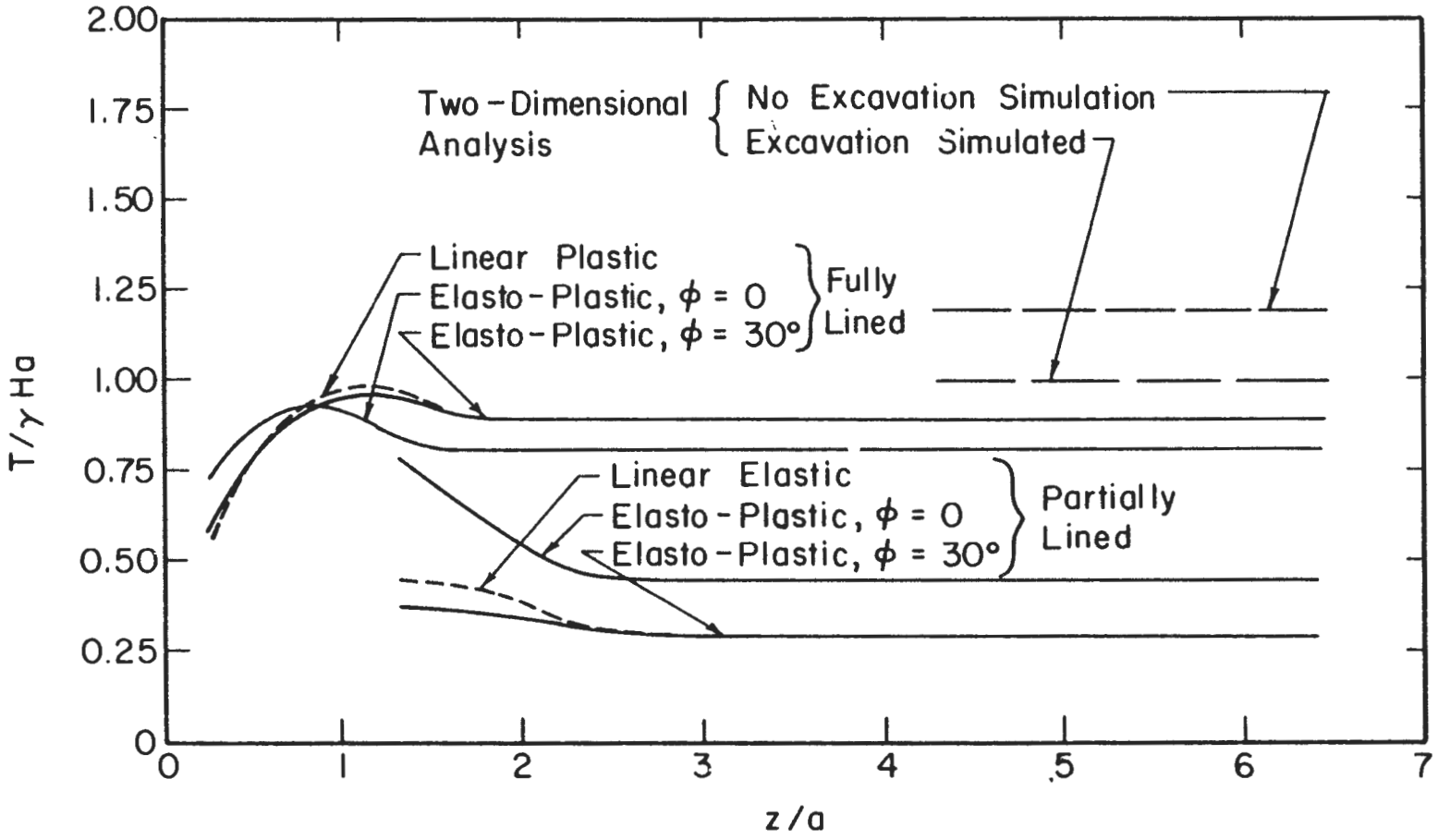

FIGURE 5.12 TUNNEL LINER THRUST VALUES

behind the face resulting in an increase of liner thrust. At distances greater than approximately one tunnel diameter behind the face liner thrust is independent of longitudinal position.

For the partially lined tunnel the weight of the unsupported soil is transmitted by arching to both the ground ahead of the face and the forward end of the liner. Thus, that portion of the liner installed last carries the greatest load. With increasing distance behind the end of the liner, the thrust decreases to a minimum value.

Figure 5.12 shows that after the face and liner have advanced one or two diameters beyond a given point the liner thrust at that point has stabilized and is no longer influenced by what takes place ahead of the liner.

The magnitude of the thrust that remains in the liner is a function of the amount of radial displacement that has occurred both before and after the liner was installed. If no displacements whatsoever are allowed, the liner thrust should correspond to that due to the full overburden pressure, $T = \gamma Ha$.

As shown in Fig. 5.12, the two-dimensional, plane strain solution with simulation of excavation (finite element analysis or analytical solution for excavation loading) yields higher values of liner thrust than the fully lined tunnel analysis. This is because the two-dimensional analyses do not consider the ground displacements occurring ahead of the tunnel face. The two-dimensional analysis that does not simulate excavation (finite element analysis in which overburden stress is applied to boundary of mesh with tunnel and liner already in place, or analytical solution for overpressure loading) yields an even more unrealistic value for liner thrust.

The values of liner thrust for various analyses are summarized in Table 5.2.

5.4 ADDITIONAL COMMENTS ON RESULTS OBTAINED

5.4.1 LONGITUDINAL EXTENT OF TRANSITION ZONE OF THREE-DIMENSIONAL RESPONSE AROUND THE TUNNEL FACE

TUNNEL LINED FAR BEHIND FACE OR UNLINED

An attempt was made to estimate the longitudinal extent of the zone around the heading of a circular tunnel (for $K_o = 1$) within which the ground mass stress and radial displacement magnitudes are functions of the longitudinal position relative to the position of the tunnel face. It is difficult to delineate precise boundaries that separate this transition zone from the undisturbed ground ahead of the tunnel and the final equilibrium state behind the face, because these boundaries are not indicated by abrupt changes in medium behavior. The change from one state or type of behavior to the next is very gradual. Nevertheless, the picture obtained from the available data is that of a transition zone of three-dimensional response extending over a total distance of approximately six times the maximum radius of the plastic zone, R, that forms around the unlined tunnel. If no plastic yielding occurs this distance is approximately 6a, where a is the radius of the tunnel. Figure 5.13 illustrates the longitudinal extent of the zone and its relationship to the position of the advancing tunnel lace.

To arrive at the indicated transition zone boundaries the distances from the tunnel face to 1) the point where the ground mass was first disturbed from its original equilibrium and 2) the point at which final equilibrium was attained were estimated from the stress and displacement data.

TABLE 5.2

VALUES OF THE LINER THRUST COEFFICIENT, T/γHa

Stress-strain Behavior	Fully Lined			Partially Lined			2-D Solutions	
	Leading End	Max.	Final	Leading End	Max.	Final	A*	B+
Linear-elastic	.570	.950	.875	.425	.425	.290	.983	1.179
Elasto-plastic $\phi = 0$	.725	.925	.800	.780	.780	.450	.984	1.004
Elasto-plastic $\phi \neq 0$	.590	.930	.875	.350	.350	.300	.983	1.179

* Excavation simulated

\+ No excavation simulation

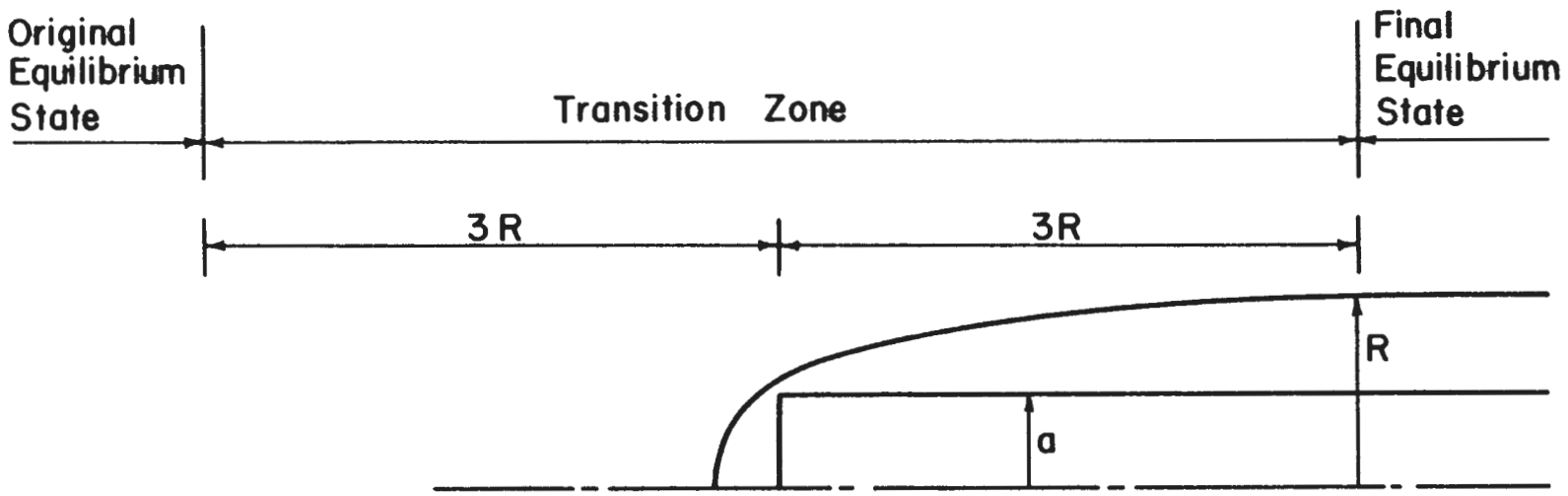

FIGURE 5.13 TRANSITION ZONE OF THREE-DIMENSIONAL VARIATION OF STRESS AND DISPLACEMENT - TUNNEL LINED FAR BEHIND THE FACE

This data was obtained from analyses F and I previously described, and from four additional analyses of unlined tunnels (F1, F2, F3, and I1) the matrial properties for which are summarized in Table 5.3. The distances obtained are given in Table 5.4. For analyses F, F1 and I1 the length of the finite element mesh was not sufficient to encompass the entire transition zone (e.g., the radius of the plastic zone was still increasing at the mesh boundary, seven tunnel radii behind the face). It was possible to estimate most of the values of the indicated distances for analyses F1 and I1, but for analysis F the length of tunnel considered was much too short to make any reasonable estimates.

The quantities Z_i and Z_f (i.e., distance ahead of face to first stress change, and distance behind face to point where stresses become independent of face position, respectively) were obtained from the distributions of ground mass stresses. All of the stresses (σ_r, σ_θ, σ_z, τ_{rz}) for a given analysis did not always indicate precisely the same values for Z_i and Z_f. Therefore, these quantities are given as ranges of values in Table 5.4.

For each analysis the radial distribution of ground mass stresses, size of the plastic zone, and magnitude of tunnel wall displacements were examined for points far behind the tunnel face beyond the transition zone. It is in this region, previously described as the zone of final equilibrium, that the available analytical solutions for elasto-plastic stress-strain behavior, such as those given by Deere, et al. (1969) and Ladanyi (1974) are supposedly applicable.

Normalized values for the maximum plastic zone radius, R, and maximum radial displacement of the tunnel wall, u, obtained from the finite element analyses are compared to values calculated from the analytical solutions

TABLE 5.3

MATERIAL PROPERTIES FOR THE UNLINED TUNNEL ANALYSES

Case	ν_m	c		ϕ
		psi	kPa	degrees
F	0.49	14	96.5	0
F1	0.49	28	193	0
F2	0.49	31.5	217	0
F3	0.49	37	255	0
I1	0.40	14	96.5	15
I	0.40	14	96.5	30

Additional data same as given in Table 5.1

TABLE 5.4

DATA DEFINING EXTENT OF THREE-DIMENSIONAL ZONE - TUNNEL UNLINED OR LINED FAR BEHIND FACE

Analysis	$\frac{R}{a}$	$3(\frac{R}{a})$	$\frac{Z_i}{a}$	$\frac{Z_u}{a}$	$\frac{Z_r}{a}$	$\frac{Z_f}{a}$
F	Length of tunnel considered much too short to make an estimate					
F1*	2.55	7.65	8	8.0	8.0	8
F2	2.25	6.75	6-7	---	6.5	6-7
F3	1.75	5.25	4-5	5.5	5.5	4-5
I1*	2.6	7.8	8-9	---	8.0	7-8
I	1.5	4.5	4-5	4.5	4.5	4-5

* Estimated values

Z_i = distance ahead of face to first stress change

Z_u = distance behind face to maximum radial displacement

Z_r = distance behind face to maximum radius of plastic zone

Z_f = distance behind face to point where ground stresses become independent of face position

in Table 5.5. As in Table 5.4, values for finite element analyses F, F1, and I1 are estimates. The "greater than" symbols in front of the values from finite element analyses F and I1 indicate that these quantities had not, within the length of tunnel considered, sufficiently approached a maximum value for an estimate to be made.

In general, the finite element results are in good agreement with those given by the analytical solutions for unlined openings. It is felt that this lends credibility to both solution techniques and, at the same time, provides an indication that the finite element results for the transition zone are reasonable.

TUNNEL LINED CLOSE TO THE FACE

Similar observations for the tunnel lined near the face indicate that the liner significantly influences the longitudinal extent of the transition zone. It is estimated that this zone extends out ahead of the tunnel face to a distance of approximately three times the radius of the plastic zone that forms around the lined tunnel. Thus, this distance is a function of the position of liner installation, relative to the face, and the stiffness of the liner as well as the magnitudes of the in situ stresses and the shear strength of the ground mass. Behind the tunnel face the transition zone seems to extend only to a distance of one tunnel radius behind the leading edge of the liner. However, this estimate is based on the analysis of a relatively stiff liner and it may be that for a more compressible liner this distance would be larger.

TABLE 5.5

COMPARISON OF RESULTS FROM FINITE ELEMENT AND ANALYTICAL SOLUTIONS FOR A TUNNEL LINED FAR BEHIND THE FACE

	R/a		u/a	
Analysis	F.E.	C.F.	F.E.	C.F.
F	>6.0	12.0	>.125	.325
F1	2.55	2.7	.053	.055
F2	2.25	2.25	----	.045
F3	1.75	1.88	.034	.036
I1	2.6	2.55	>.088	.103
I	1.5	1.5	.043	.050

F.E. = Axisymmetric finite element analysis, points far behind face

C.F. = Two-dimensional closed form analytical solutions (e.g., Deere, et al, 1969, and Ladanyi, 1974)

5.4.2 GROUND LOSS INTO TUNNEL

Longitudinal displacements of the ground into the tunnel face and radial displacements occurring ahead of the face result in overexcavation, i.e., removal of a volume of ground greater than the undisturbed tunnel volume (area of face times length of advance). The volume of overexcavation plus the volume of ground that displaces radially into the tunnel behind the face constitute the volume of lost ground which contributes to settlements of the ground surface above the tunnel.

Table 5.6 gives the overexcavation volumes obtained from the partially and fully lined tunnel analyses, along with those from the corresponding unlined tunnel analyses. The volumes per unit length of tunnel have been expressed as percentages of the full tunnel volume per unit length. As shown in Table 5.6 the total volume of overexcavation has been divided into two components; one resulting from longitudinal displacement toward the tunnel face (column heading "Long.") and another resulting from radial displacements ahead of the face (column heading "Rad.").

The data indicate that the volume of overexcavation increases as the shear strength of the ground mass decreases. There is little difference between the total volumes obtained from the unlined and partially lined tunnel analyses, but when the tunnel is fully lined the total volume of overexcavation is sharply reduced. Note also that for the fully lined tunnel analyses approximately 65 percent of the total volume resulted from longitudinal displacements ahead of the face.

Hansmire (1975) gives values of lost ground volumes calculated from field measurements of displacements around tunnels in various types of

TABLE 5.6

VOLUME OF OVEREXCAVATION*

Stress-Strain Behavior	Unlined			Partially Lined			Fully lined		
	Long.	Rad.	Total	Long.	Rad.	Total	Long.	Rad.	Total
Linear Elastic	1.2	1.4	2.6	1.3	1.4	2.7	0.9	0.5	1.4
Elasto-plastic $\phi = 0$	2.1	2.4	4.5	2.2	2.5	4.7	1.2	0.8	2.0
Elasto-plastic $\phi = 30$	2.2	1.6	3.8	1.9	1.5	3.4	1.1	0.5	1.6

* Expressed as a percentage of tunnel volume/unit length

ground, and discusses in detail the various sources of lost ground (one of which is overexcavation) and the relationship between ground lost into the tunnel and settlement of the ground surface.

5.4.3 GROUND-LINER INTERACTION

It is clear from the discussion in Section 2.3.1 and the results presented in this chapter that the methods and details of construction, principally the position of liner installation relative to the face, can strongly influence the magnitude of the initial excavation loading ground pressure on the liner (initial = just after construction). One of the primary advantages to be gained by using the three-dimensional or axisymmetric finite element analyses with simulation of construction is the direct consideration of these factors.

Two-dimensional solutions (analytical and finite element with construction simulation) yield results that compare favorably with the fully lined tunnel case because the displacement these solutions ignore, that which occurs ahead of the face, is quite small when the liner is kept up to the face. However, the same two-dimensional solutions considerably overestimate liner thrust and displacement for the partially lined tunnel cases because the displacements they do not account for are quite large in these cases.

Two-dimensional solutions modified to account for prior displacements (Section 2.3.1) tend to underestimate the pressure on the liner, and thus liner thrust and displacement, if based on the longitudinal displacement distribution of the unlined tunnel. This can be illustrated by examining the results from analyses of cases A, B, and C. From the longitudinal

distribution of displacements obtained from case C it was found that at the face and at a point one radius behind the face, u_p/u_t = 0.32 and 0.85, respectively. Substituting these values into Eqn. 2.2 it is found that the liner thrust coefficients ($P_\ell a/P_o a = T/\gamma Ha$) for the fully lined and partially lined tunnels should be 0.668 and 0.147, respectively. Thus, this approach significantly underestimates the values, 0.875 and 0.290, found when actual advancement of the tunnel was simulated. Figure 5.9 shows the longitudinal displacement distributions that should have been used instead of the displacements for the unlined tunnel. As was mentioned in Section 2.3.1 the analyses that give these displacements also give the liner response, eliminating the need for solution methods such as Eqn. 2.2.

Three-dimensional finite element analyses, of which the axisymmetric is a special case, allow a more complete treatment of the advancing tunnel problem than is possible with two-dimensional methods. However, as was learned during the course of this investigation, simply expanding the analysis to three dimensions is not sufficient. Also important are such factors as simulation of the advancement of the tunnel (as was illustrated in Fig. 2.12) and, in certain cases, the details of excavation and liner installation.

Most soft ground tunnels are constructed with the aid of a tunneling shield behind or within which the liner is assembled and then installed. The shield and the method of liner installation, in the way that they affect radial ground displacements, are important to liner performance.

The importance of the construction details in analysis of soil-liner interaction is demonstrated here through the consideration of two case studies where field data were available. This is accomplished by comparison

of the results from analyses of advancing tunnels with displacement data reported by Ward (1969) and Muir Wood (1969) for two tunnels in London Clay. The radial displacements obtained from the finite element analyses were, of course, a function of the elastic modulus assigned to the simulated ground mass. The modulus values assumed in these analyses are within the range of values given by Ward (1971) for London Clay. The object of these comparisons is a qualitative study of the shield-liner-ground behavior interrelationship, rather than an attempt at analytical reproduction of field data.

The comparison with Ward's data (1969) is shown in Fig. 5.14. None of the displacement distributions from the lined tunnel analyses would fit the measured data unless an unreasonably low modulus was assumed for the clay. Instead, it was found that the best agreement was obtained with the displacements from the unlined tunnel analyses (broken and dashed curves). This is not too suprising when the stiff nature of the London Clay, the details of the shield, and the method of liner installation are considered. The shield was fabricated with a bead 9 in. long by 0.5 in. thick (23 cm x 1.3 cm) around the upper 300 degrees of its cutting edge. In addition, the cast iron liner was normally assembled within the shield, leaving a 1.5 in. (3.8 cm) gap between the liner and the clay when the shield advanced. This void was filled with cement grout soon after the shield advanced.

The measured displacements given in Fig. 5.14 are for a point 1.6 ft (49 cm) outside the tunnel springline, but they clearly show the effects of these construction details. The first radial displacements occur about one tunnel diameter ahead of the face, but they remain small (u_f) until the bead on the shield passes, whereupon they almost double as the clay moves into the void behind the bead. The restraining effect of the shield

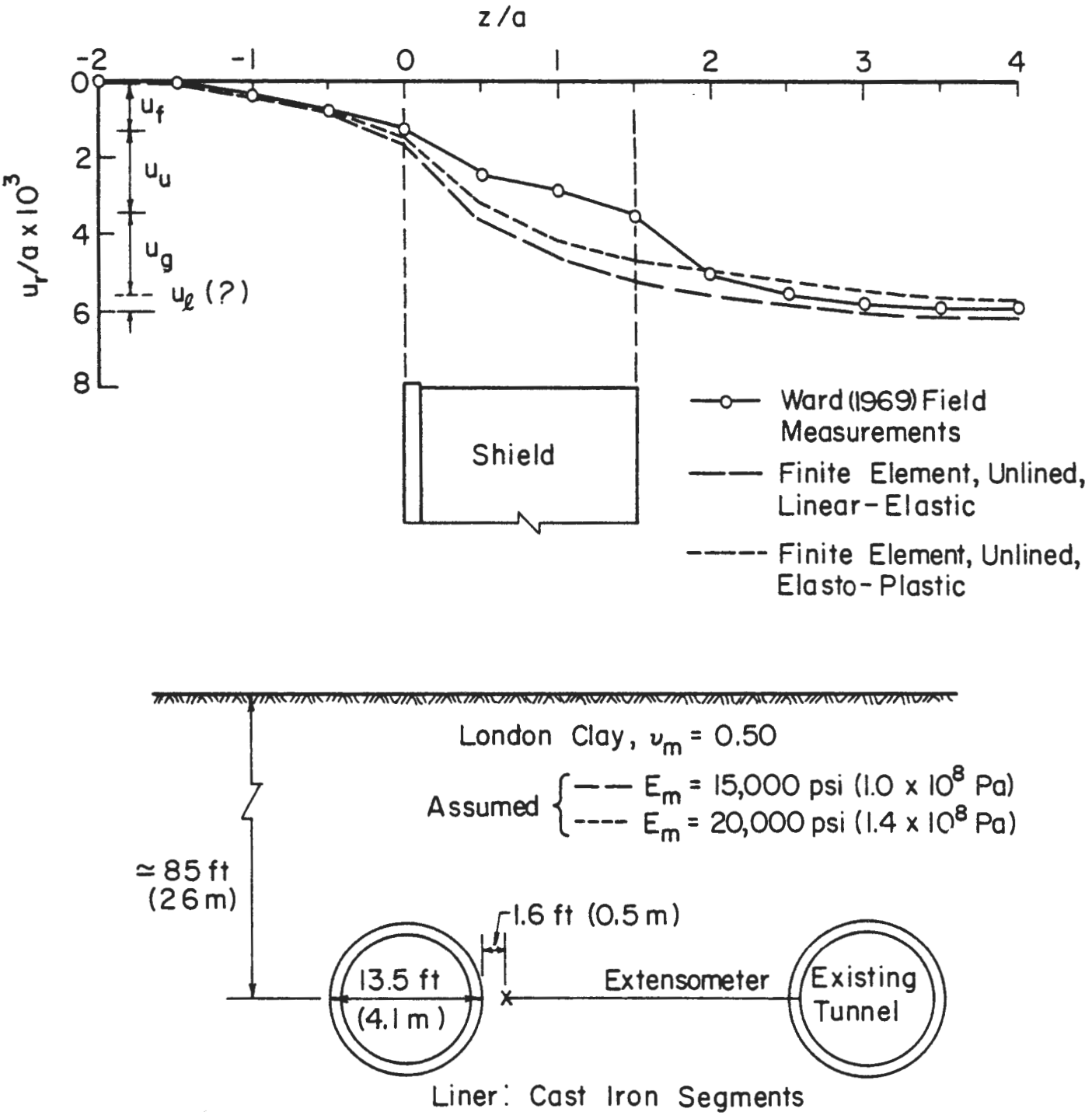

FIGURE - RADIAL GROUND DISPLACEMENTS: FIELD MEASUREMENTS (WARD, 1969) AND FINITE ELEMENT RESULTS COMPARED

on the displacements is clearly indicated, but it is also apparent that the shield only delays and does not prevent further displacement (u_u). Figure 5.14 shows that as the tail of the shield passes, the clay begins to move again, this time into the gap left by the skin of the shield (u_g). It appears that these additional displacements occur either before the grout is injected or before it has had time to set. Once the grout does set the liner becomes effective and begins to take on load. The additional displacement, u_ℓ, of the liner then occurs. It is not clear from the data at what point the liner becomes effective, so it is difficult to estimate u_ℓ from the displacement curve.

The comparison with Muir Wood's data (1969) is shown in Fig. 5.15. Here it was found that the best agreement was obtained with the displacements from the partially lined tunnel analyses (liner one radius behind face). Typical displacements for an unlined tunnel analysis are shown in Fig. 5.15. It can be seen that it significantly overestimates the displacements behind the tunnel face.

Relative to the maximum measured value, the displacements occurring ahead of the tunnel are quite large. However, as the shield's cutting edge passes the soil is pushed outward again. This suggests the presence of a bead or similar protrusion on the forward end of the shield. In terms of the ground displacement-ground pressure relationship, the reduced radial displacement at the face was taken as u_f rather than the maximum displacement occurring ahead of the face. The subsequent rapid inward displacement over the length of the shield indicates that the clay moved into a void space there. This displacement corresponds to u_u. For this tunnel each ring of precast concrete segments was expanded against the soil after leaving

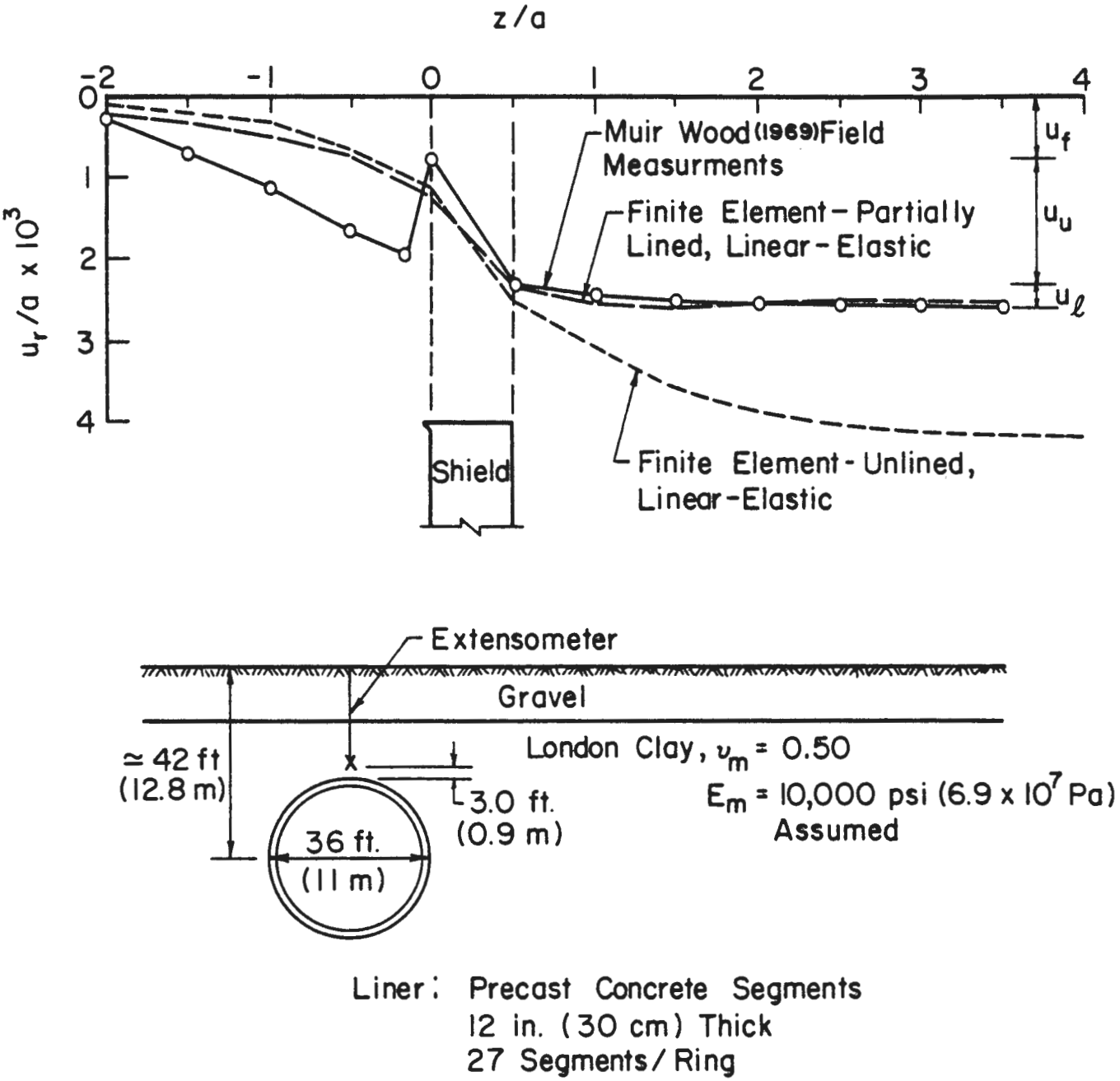

FIGURE 5.15 RADIAL GROUND DISPLACEMENTS: FIELD MEASUREMENTS (MUIR WOOD, 1969) AND FINITE ELEMENT RESULTS COMPARED

leaving the shield. Thus, the liner becomes effective almost immediately and the potential displacement u_g is essentially eliminated. Almost all displacements occurring behind the shield correspond to u_ℓ.

It appears that analyses based on the assumption that the shield acts as an extension of the liner (tunnel lined to face) would have underestimated the ground displacements and thus overestimated the initial ground pressures acting on the liner in these two cases.

In general, however, the importance of the above construction details also depends on the behavior of the ground mass. In the above examples the soil was very stiff and possessed a relatively high shear strength. Thus, at the depths considered little or no plastic yielding occurred and the potential total displacement, u_{po}, was small. The void spaces between the soil and shield-liner were large compared to u_{po} and thus the shield and liner did little to prevent displacement before a major portion of u_{po} had occurred. A shield with given bead and tailskin thicknesses (t_b, t_s) will not hold the potential displacements u_u and u_g to less than their maximum values (function of soil properties) unless $(t_b + t_s) < (u_u + u_g)_{max}$. In the first example above, $(t_b + t_s) \geq (u_u + u_g)_{max}$ and thus the shield and liner had almost no effect on the ground displacements. In the second example t_s, and thus u_g, was effectively zero, but $t_b \geq u_u$ and so the shield did little to prevent the displacement u_u.

In summary, the following can be stated. In order to correctly model a given tunneling problem with the finite element method the ground conditions, shield configuration, and method of liner installation must be considered. One way of doing this, of course, is to directly model these factors. However, it is a considerable task to effectively model the shield

and details of liner installation, and so a reasonable approach is to adjust the position of the simulated liner with respect to the face to correspond to the anticipated behavior of the real tunnel. The length of unlined tunnel that should be left between the face and the liner depends on the relative magnitudes of the two quantities $(t_b + t_s)$ and $(u_u + u_g)_{max}$. It is only when the above factors combine to yield $(t_b + t_s) \ll (u_u + u_g)_{max}$ that the assumption of the shield acting as an extension of the liner is valid.

If there is no gap between the liner and the soil ($u_g = 0$) the liner becomes effective immediately after leaving the shield. Thus, if the shield does nothing at all to prevent radial displacements this system could be modeled by assuming the liner extends to within a shield's length of the tunnel face. At the other extreme, if there are no voids around the shield, or a void is present but $t_b \ll u_u$, it could be assumed that the shield acts as an extension of the liner and the system could be modeled by extending the simulated liner up to the face.

CHAPTER 6

FINITE ELEMENT ANALYSIS OF TWO PARALLEL TUNNELS - EXCAVATION LOADING

6.1 GENERAL REMARKS

The construction of a tunnel modifies the state of stress and displacement in a zone around the tunnel. The size of this zone depends on: ground conditions -- type of soil or rock, in situ stresses, and properties of the medium; geometric parameters -- depth and radius of the tunnel; and characteristics of the support system. If two parallel tunnels are constructed far apart such that their zones of influence do not overlap, then the individual tunnels can be considered separately and analyzed as such. However, if the zones of influence of the two tunnels overlap, the behavior of each of the tunnels will be different from that of a single tunnel, as some degree of interaction between the two tunnels will take place. Interaction of the tunnels will affect the state of stress and displacement around the tunnels, ground surface displacements, and support loads. It can generally be expected that the surface settlements resulting from the construction of two tunnels will be greater than the sum of the settlements resulting from each tunnel alone. The stress distribution around two tunnels and support loads are too complex to lend themselves to a general statement and they require a comphehensive study.

There are two distinct problems related to the design and construction of two parallel tunnels in soft ground: a) additional loads and distortions are imposed on the lining of the first tunnel due to passage of the second tunnel, and b) the ground settlements due to excavation of the second tunnel may be appreciably greater than those that occurred during

excavation of the first tunnel, and may result in damage to structures and utilities at the ground surface.

In the design and construction of two parallel tunnels, designers must determine whether or not the distortions and load increases on the lining of the first tunnel due to passage of the second tunnel will be great enough to cause unacceptable damage to the lining. In many cases, the installation of the permanent lining for the first tunnel is delayed until after the second tunnel has passed. Finite element analyses provide a means of evaluating the influence of the excavation of the second tunnel on the loads and distortions of the first.

Ground settlements due to excavation of a second tunnel are usually greater than the settlements due to excavation of the first tunnel for two reasons: a) the first tunnel may disturb the soil around and above the second tunnel so that the soil will be weaker and have a greater tendency to displace into the second tunnel as it is mined, or the soil will have increased in volume during passage of the first tunnel and will undergo volume decreases during passage of the second tunnel, and b) the pillar between the two tunnels will be more highly stressed and less confined than the abutments adjacent to single tunnels. The pillar will therefore undergo greater vertical compression than the abutments of a single tunnel.

Linear elastic finite element analyses do not model the disturbance of the soil and volume changes in the soil as they occur around tunnels in real soils. However, the results from this type of analysis can be used to investigate the compression of the pillar and abutments around two parallel tunnels and its influence on ground movement. Linear analyses will therefore be of use in evaluating field measurements and determining if the

additional ground movements due to the excavation of two parallel tunnels are related to pillar compression or to other causes.

An important factor that will affect the distribution of stresses and displacements around the two tunnels is the sequence of excavation and liner installation in each tunnel. Regarding the sequence of construction, the following situations are considered herein:

1. Two tunnels constructed simultaneously - In this case, the conditions encountered by each tunnel will be similar barring some possible cross variation of the ground or surface conditions. Ideally this case will be symmetric about a vertical plane passing through the mid-distance between the two tunnels. The tunnels will be advancing through stressed media with the stress and displacement conditions ahead of the tunnels altered by the approach of both the tunnels.
2. Second tunnel constructed adjacent to an existing tunnel - In this case, the second tunnel is constructed within a medium which has higher stresses than encountered at the same location if the first tunnel was not present. Also, the material properties of the medium may have been modified by the first tunnel. The construction of the second tunnel will change the support load on the first tunnel.

In the case of two tunnels being driven simultaneously, the faces of the two tunnels need not necessarily be at the same longitudinal position; the face of one tunnel can be ahead of the face of the second tunnel by a certain distance. This may well be the rule rather than the exception, as two tunnels cannot be expected to advance at the same rate.

The results of Chapter 5 have shown that a transition zone of three-dimensional stress exists immediately ahead and behind the face of an advancing tunnel. The size of this zone depends on the type of medium and the support condition. The zone of significant stress and displacement changes can be considered to be approximately three tunnel radii ahead of, and also behind, the face when the ground remains elastic and the tunnel is unlined. Based on this information, the following cases can be considered regarding the distance between the faces of two tunnels. If the distance along the tunnel line between the faces of two tunnels is less than three tunnel diameters, the zones of influence around the tunnel faces overlap and interaction between the tunnels is taking place at the tunnel faces, Fig. 6.1a. The state of stress near the face of each tunnel is clearly a function of longitudinal position and any two-dimensional analysis of this case will suffer from drastic approximations. When the distance between the faces of the two tunnels is about one tunnel diameter or less, the stress condition around the tunnels can be reasonably considered to be the same, as in case 1 discussed above, and a two-dimensional analysis may be a good approximation.

For the case of the distance between the tunnel faces being greater than three tunnel diameters, the zones of influence around the tunnel faces are separated, Fig. 6.1b. This case is similar to case 2 discussed above and which is illustrated in Fig. 6.1c. The first tunnel encounters stress conditions, and produces distributions of stresses and displacements in its zone of influence, identical to that of a single tunnel. The second tunnel encounters a stress field which has been modified by the passage of the first tunnel and it is subjected to support loads which are basically different

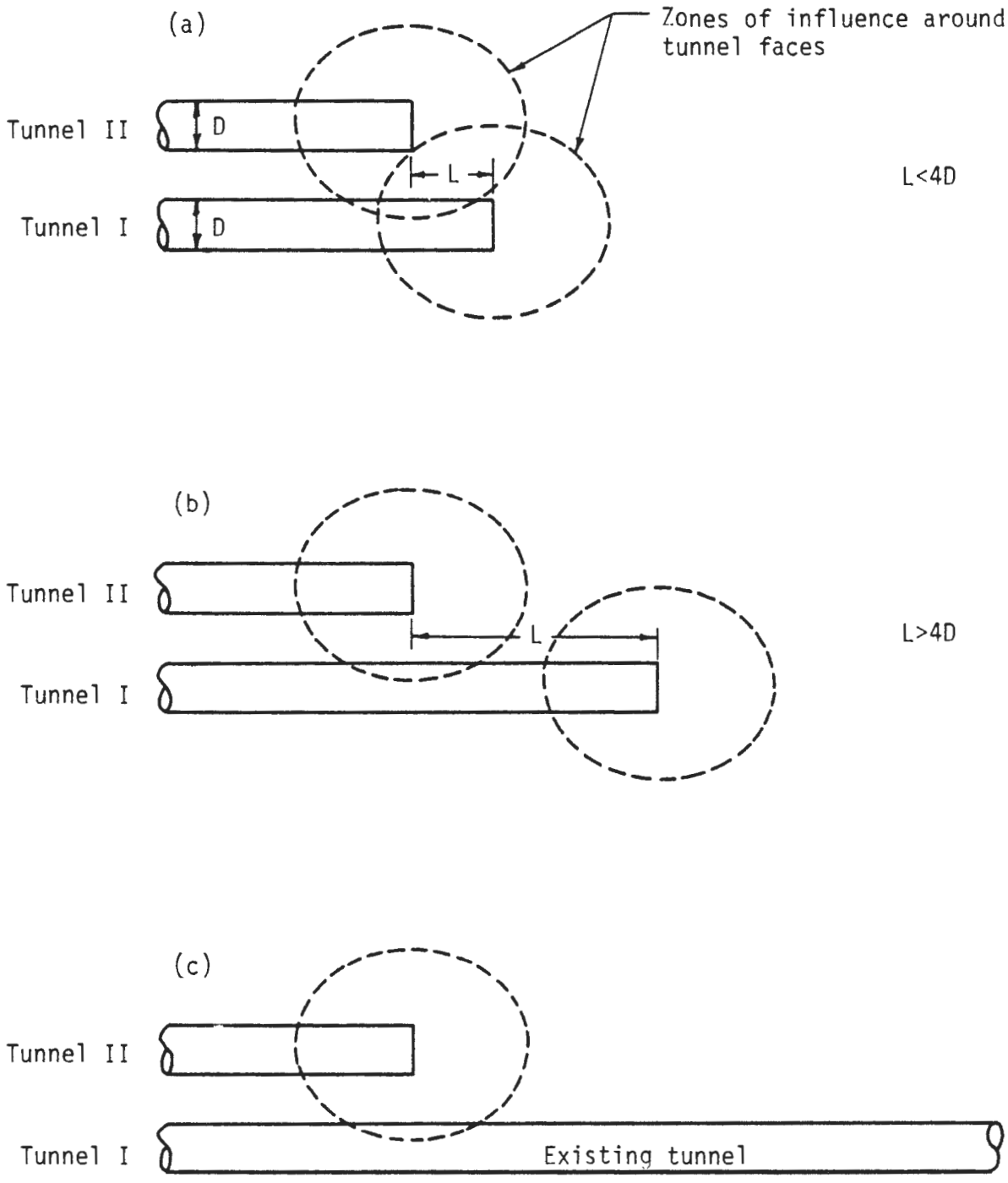

FIGURE 6.1 RELATIVE POSITION OF TWO TUNNEL FACES

than those of the first tunnel. The passing of the second tunnel itself also alters the stress condition and modifies the support load in the first tunnel. The tendency is for increase in the support loads due to the passing of an adjacent tunnel.

The subject of interaction between parallel tunnels has been studied by several authors who have reported the results of field measurements or analytical studies of the problem. This brief discussion of some of the literature on the subject is not intended as a comprehensive review and must be considered incomplete.

Barla and Ottoviani (1974) have used the finite element method to study the case of two parallel unlined tunnels excavated simultaneously. They used linear elastic and nonlinear variable moduli material properties in their analyses. They reported results of a parametric study which covered a range of geometric parameters of: depth to diameter ratios of 0.75 to 3.0; pillar width to diameter ratios of 0.25 to 1.0; and two tunnel diameter values of 19.7 and 39.4 ft (6 and 12 m). Their results seem to indicate that the interaction between two tunnels becomes negligible for values of the pillar width to tunnel diameter ratio of $W/D = 1.0$ or greater. They report large stresses in the zone between the two tunnels for small values of pillar width ratios, $W/D \leq 0.5$. Zones of tensile stresses develop around the tunnels at shallow depths, $H/D \leq 1.0$.

Peck, et al., (1969) have discussed the problem of two parallel or intersecting tunnels of different diameters at adjacent or stacked relative positions. They have given some general guidelines for liner design for two tunnel systems.

Fotieva and Sheinin (1966) have developed a method for analysis

of a tunnel driven adjacent to an existing lined tunnel. They have applied this method of analysis to an example problem of a lined tunnel of 19.7 ft (6 m) diameter at a depth of 118 ft (36 m). The medium and the liner were assigned elastic material properties of rock and concrete, respectively. A second tunnel of the same diameter was excavated adjacent to this existing tunnel at a central distance of 26 ft (8 m) which gave a pillar width to tunnel diameter ratio of W/D = 0.33. The driving of the second tunnel caused additional stresses in the liner of the existing tunnel equivalent to a maximum thrust coefficient of $T/\gamma Ha = 0.24$ and a maximum moment coefficient of $M/\gamma Ha^2 = 0.0053$. These are significant additional liner forces which occur on the pillar springline of the first tunnel.

Several researchers have reported the results of displacement measurements made during and following construction of two or more parallel tunnels. Deere, et al., (1969) gave an excellent summary of the data available prior to 1969. In most cases measurements were made as a second tunnel was driven past a test section set up in an existing tunnel or in one whose heading was a considerable distance ahead of the test section.

Ward and Thomas (1965) reported on two parallel tunnels constructed in London Clay. These particular tunnels were lined with precast concrete segments which had a thickness of 9 in. (23 cm). The tunnels were approximately 13 ft (4 m) in diameter and were separated by a pillar of 8 ft (2.4 m) minimum thickness (W/D = 0.6). Passage of the second tunnel caused an additional maximum distortion of the first tunnel of $\Delta D/D = 0.12$ percent. In addition, the average radial pressure acting on the first tunnel was increased by 8.33 psi (57 kPa). After 40 months the total maximum distortion of the first tunnel was 0.32 percent and the total average radial pressure

was estimated to be approximately 48 psi (331 kPa).

Terzaghi (1942) reported measurements taken on tunnels constructed in Chicago Clay. These tunnels had a horseshoe shaped cross section and were lined with steel ribs and liner plates. The tunnels were 20 ft (6.1 m) in diameter and were constructed at a distance of 28.5 ft (8.7 m) center-to-center, giving a pillar width of 8.5 ft (2.6 m) and W/D = 0.425. As the second tunnel was mined past, the springline nearest the second tunnel displaced outward 0.2 in. (5 mm) while the opposite springline moved outward only 0.04 in. (1 mm). This yielded a distortion of the first tunnel of $\Delta D/D = 0.10$ percent.

Contact pressures between the soil and the concrete invert of the first tunnel were measured using Carlson cell slabs. As the second tunnel passed on the north side, the contact pressure under the north rib of the first tunnel increased and thereafter remained greater than that under the south rib which was farthest from the second tunnel.

Settlements of the street surface were also recorded as the two tunnels were advanced. Different settlement profiles were obtained for different spacings between the two tunnels. When the tunnels were constructed so that there was no pillar between them (W/D = 0), settlements due to the first tunnel were consistently greater than those due to the second tunnel. Ground displacements around the second tunnel were restricted by the presence of the first tunnel's liner. When the tunnels were mined leaving a pillar between them (W/D = 0.425) support provided by the first tunnel's liner was not available. Instead the clay above the second tunnel had to be supported by the relatively weak clay pillar. As a result, settlements due to the second tunnel were everywhere greater than

those due to the first tunnel.

Recently, Sauer and Jonuscheit (1976) have reported stress measurements in the pillar separating two parallel tunnels in rock. The two tunnels were driven simultaneously and the stresses were measured as the tunnel headings approached the test section. Some of these stress measurements are compared with the results of the present study in later sections of this chapter.

Presented in this chapter are the results of a study on the behavior and interaction of two parallel circular tunnels. The objectives of this research are:

1. The study of the interaction of two parallel tunnels and the effect of such interaction on stresses and displacements around the tunnels and on support loads.
2. The parametric study of two tunnel systems to determine the effect of various parameters such as distance between the centers of the tunnels, depth, and construction sequence.

This is accomplished by performing a series of finite element analyses of the two tunnel system for ranges of various parameters and using the construction simulation technique. The results are presented in two sections. In the first section the main parameter under study is the width of the pillar between the two tunnels. In the second section the influence of the sequence of construction of the two tunnels is discussed. In both sections the effects of the tunnel depth and support conditions are also considered.

6.2 METHOD OF ANALYSIS

6.2.1 THE FINITE ELEMENT MESH

It is known that the stress condition around the face of a tunnel

is three-dimensional, and only a three-dimensional analysis can directly give an accurate picture of tunnel behavior. Unfortunately, at present such analyses are very costly and difficult to perform. For some problems, such as that of a single tunnel of circular cross section, the difficulties can be greatly reduced by considering the axisymmetric case. However, this approach is obviously not available for the study of two tunnel systems. For the type of study performed here, for which a large number of analyses are required, it is not economically feasible to conduct three-dimensional analyses. Therefore, this investigation was restricted to two-dimensional, plane strain analyses. Fortunately, information obtained from two-dimensional analyses can be useful when evaluated in combination with the knowledge of the effects that can occur at the tunnel face.

A schematic representation of the problem along with the symbols used for various dimensions in this study are given in Fig. 6.2. For the study of the influence of pillar width, it was assumed that the two tunnels were constructed simultaneously, thus making the problem symmetrical about a vertical plane through the pillar centerline. This approach has the advantage of reducing the region analyzed by one half. The disadvantage is that it allows consideration of only two construction sequences. To study the influence of construction sequence it was necessary to analyze the entire region. The number of analyses of this type were held to a minimum by considering only one pillar width.

Finite element meshes, composed of two-dimensional, plane strain, quadrilateral finite elements with four corner nodes, were developed for an appropriate region of the ground mass containing the two tunnels. Typical plots of the automatically generated finite element meshes for half the

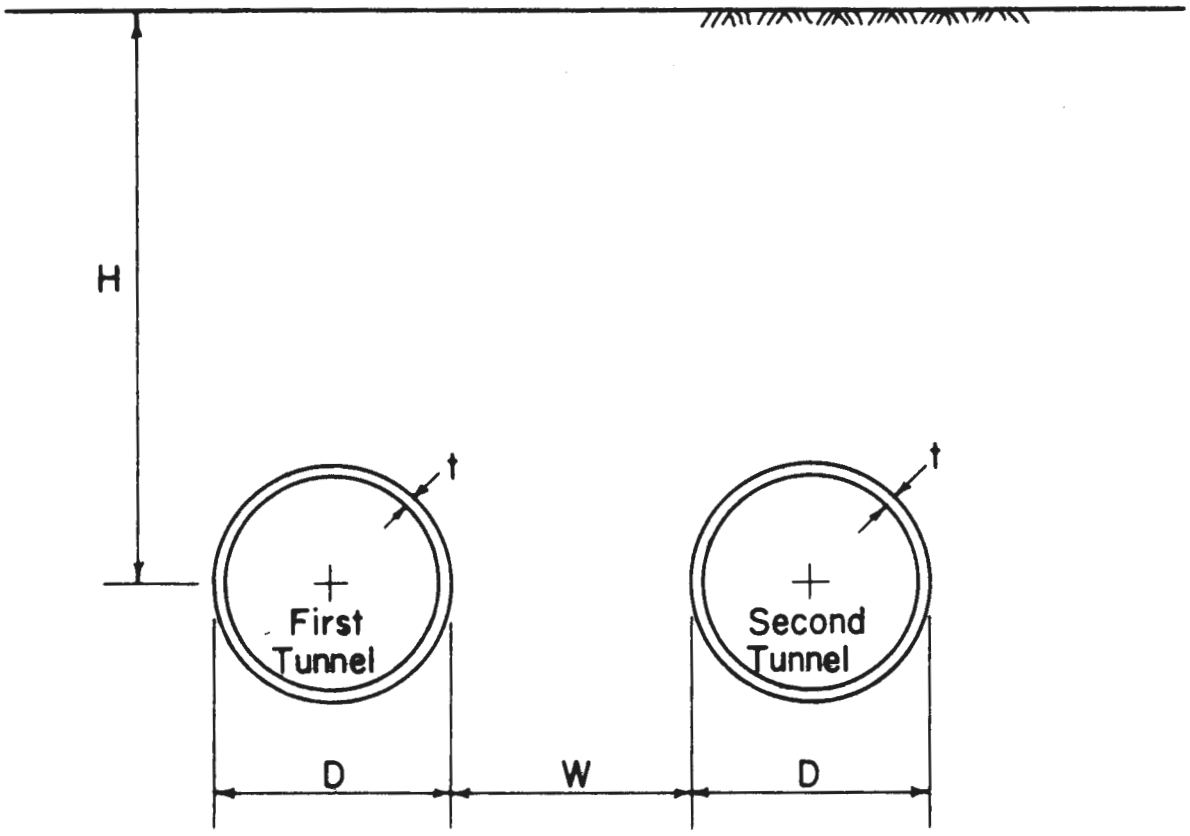

FIGURE 6.2 GEOMETRICAL CONFIGURATION OF THE PROBLEM AND DIMENSIONAL SYMBOLS

region and the whole region are shown in Figs. 6.3 and 6.4, respectively.

Initially the finite element model is subjected to the self weight of the medium to simulate the in situ stress condition. At this stage the base of the finite element model has a displacement boundary condition allowing horizontal movement but restricting vertical displacement, and the sides have a force boundary condition, consisting of a triangular force distribution corresponding to the lateral stresses resulting from the weight of the medium. By varying the rate of increase of this boundary lateral force with depth different K_o conditions can be simulated. A value of $K_o = 0.5$ was used throughout this study.

The excavation of the tunnel(s) is achieved at subsequent steps of the analysis. At the excavation step the base and sides of the finite element mesh are fixed and no further movements are allowed. The only exception is when just half of the region is analyzed. Then the vertical boundary representing the plane of symmetry is allowed vertical movements.

Using a two-dimensional, plane strain model, the excavation of a tunnel is simulated by deactivating the elements within the tunnel perimeter. This way a full face excavation is simulated. Regarding the liner placement in a two-dimensional model, the options are limited to two extreme conditions: either the elements comprising the tunnel liner are activated at the same step as the excavation is simulated; or, they are activated at a subsequent step of the analysis. In the first case it is assumed that no displacements take place prior to the liner coming into contact with the surrounding medium. This case approximates the installation of the tunnel liner right at the tunnel face in a manner such that ground displacements are held to a minimum. In the second case it is assumed that all of the

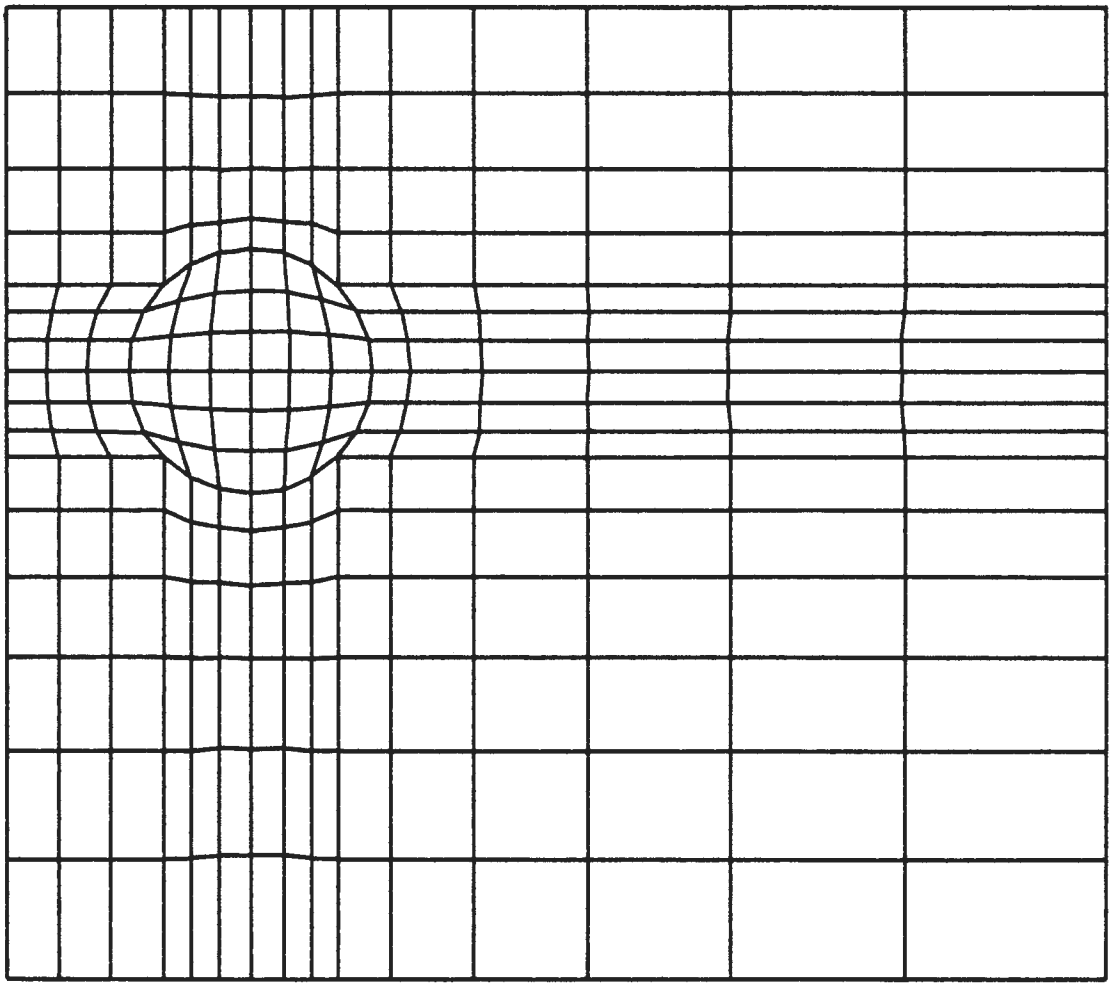

FIGURE 6.3 TYPICAL FINITE ELEMENT MESH FOR STUDY OF THE INFLUENCE OF PILLAR WIDTH

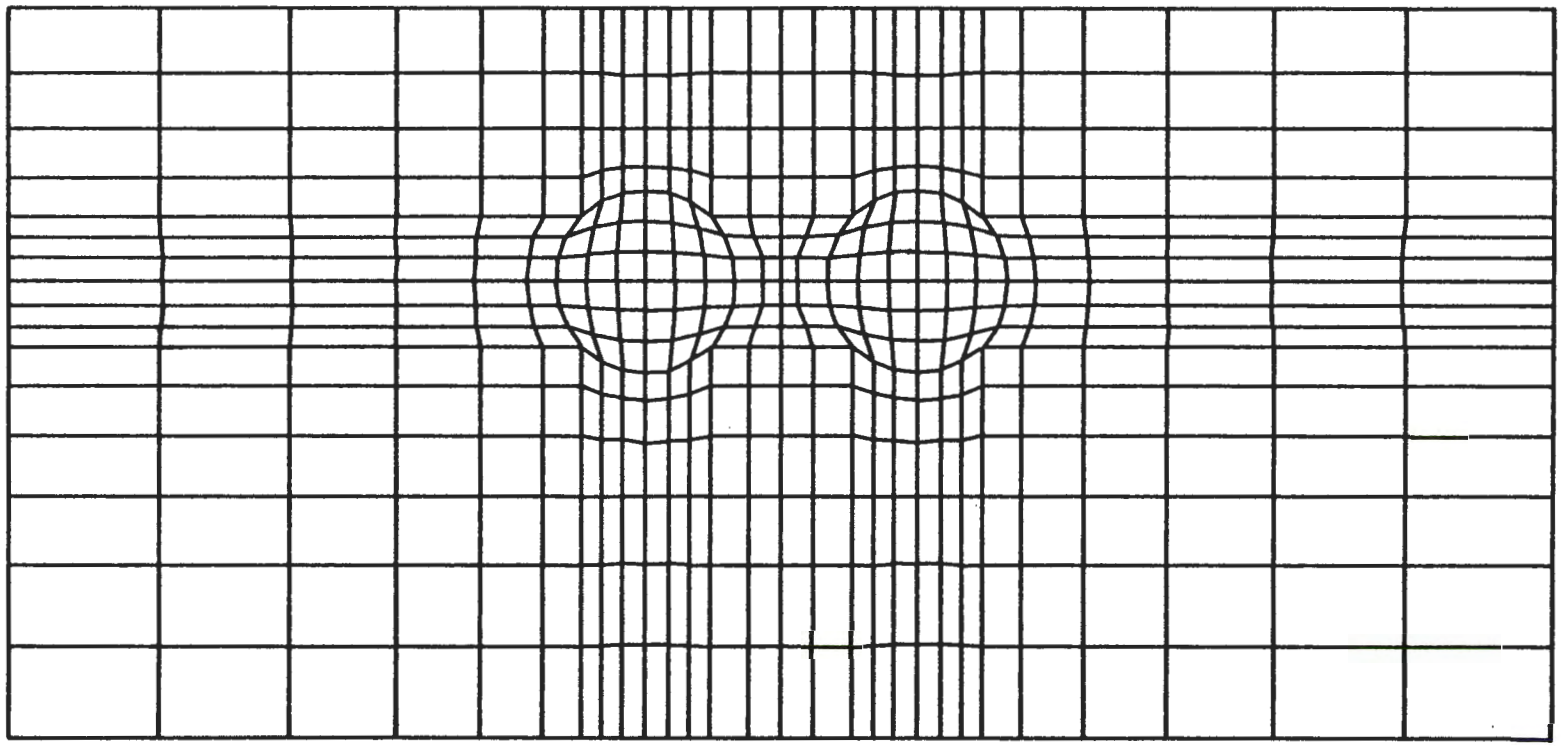

FIGURE 6.4 TYPICAL FINITE ELEMENT MESH FOR STUDY OF THE INFLUENCE OF CONSTRUCTION SEQUENCE

potential instantaneous displacements of the medium occur prior to the liner coming into contact with the surrounding medium. This case can be considered to simulate either, the installation of the liner far behind the tunnel face, outside the zone of instantaneous displacements; or, the installation of the liner near the face but such that no measures are taken to prevent occurrance of the instantaneous ground displacements before ground-liner contact. For the first case the tunnel is referred to as being fully lined. For the second case the tunnel can be referred to as being unlined, because these analyses consider only the instantaneous displacements of the medium and with respect to these displacements the simulated tunnels of this case are effectively unlined.

6.2.2 MATERIAL BEHAVIOR MODELS

For the majority of the analyses performed the ground mass was assumed to be linear elastic. Some selected cases were also analyzed with elasto-plastic properties for the ground mass. For these analyses the modified Drucker-Prager yield condition, as described in Section 5.2.3, was utilized.

6.2.3 CONSTRUCTION SEQUENCE

Basically, two types of sequence of excavation and liner placement are considered. For the case of simultaneous excavation of two tunnels only half of the region is analyzed and only two cases are considered: both tunnels are lined far behind the face; or both tunnels are lined right at the face (the liners are placed instantaneously upon excavation). In the case of two tunnels being excavated at different stages, the whole region

containing the two tunnels is used in the analysis and the number of possible construction sequence combinations is greater. The sequences of excavation and liner placement considered in this study are given in Table 6.1. It is important to note that in the case of the liner being installed at the heading, the two-dimensional analyses do not account for the ground displacements that occur ahead of the tunnel heading and therefore can only be considered approximations.

6.3 RESULTS OF ANALYSIS

6.3.1 INFLUENCE OF PILLAR WIDTH

In the first part of this study it is assumed that the two tunnels are being advanced together at or near the same rate, such that the two headings are adjacent or separated by only a small longitudinal distance (< 1D). For this condition it is reasonable to consider the problem to be one of simultaneous excavation of the two tunnels. For simultaneous excavation the problem is symmetrical about a vertical plane through the pillar centerline and only half the region needs to be analyzed. Both tunnels were assumed to be either lined right at the face (lined tunnel analyses) or far behind the face (unlined tunnel analyses).

Two tunnel depth, H, to diameter, D, ratios were considered: H/D = 1.5 for a shallow tunnel with depth of cover equivalent to one tunnel diameter, and H/D = 5.5 for a moderately deep tunnel with a depth of cover equivalent to five tunnel diameters. Tunnel depth, H, is measured from the ground surface to the tunnel axis. Three values of pillar width, W, were considered: W/D = 1.0, 0.5, and 0.25.

TABLE 6.1

SEQUENCES OF CONSTRUCTION

Case	Simulation Step 1 Excavation of First Tunnel	Simulation Step 2 Excavation of Second Tunnel	Conditions Modeled
A	line first tunnel	line second tunnel	Existing first tunnel with permanent lining or first tunnel heading far ahead of second tunnel heading with lining installed at the heading. Second tunnel lined at the heading.
B	line first tunnel	second tunnel unlined	Same as case A, but second tunnel lined far behind the heading.
C	first tunnel unlined	line first and second tunnels	First tunnel lined far behind the heading, but ahead of the second tunnel heading. Second tunnel lined at the heading.
D	first tunnel unlined	line first tunnel, second tunnel unlined	Same as case C, but second tunnel lined far behind the heading.

STRESSES AROUND TWO PARALLEL TUNNELS

It is assumed that the in situ stresses in the undisturbed medium (prior to tunnel excavation) are due to the self weight of the medium. Thus, at any given point the maximum principal stress is vertical and has a magnitude of $P = \sigma_V = \gamma z$, where γ is the unit weight of the medium and z is the depth of the point below the ground surface. Similarly, the minimum principal stress is horizontal and has a magnitude of $Q = \sigma_H = K_o \gamma z$, where K_o is the coefficient of earth pressure at rest. The distribution of in situ principal stresses thus consists of a set of horizontal contour lines showing a linear increase of magnitude with depth. Creation of one or more openings (tunnels) in the medium will alter these distributions in a region around the openings.

Figures 6.5 and 6.6 show the distribution of stresses around two parallel unlined tunnels and two parallel lined tunnels, respectively. The distributions of the maximum and minimum principal stresses and the maximum shear stresses in a region around the tunnels are shown by non-dimensionalized stress contours (stress at a point divided by γH, where H is the depth to the tunnel axes). Here the stress distributions are symmetrical about a vertical plane through the pillar centerline and, thus, stresses around the right tunnel only are shown.

From the unlined tunnel analysis it was found that to the right of the tunnel axis (as in Fig. 6.5) the stress distributions are very similar to those for a single tunnel. For a single unlined opening and $K_o = 0.5$ the maximum principal stress concentration at the springline is $P/\gamma H = 2.5$ and at the crown and invert $P/\gamma H = 0.5$. Figure 6.5, which is for the narrowest pillar considered, shows that the maximum principal stress concentrations

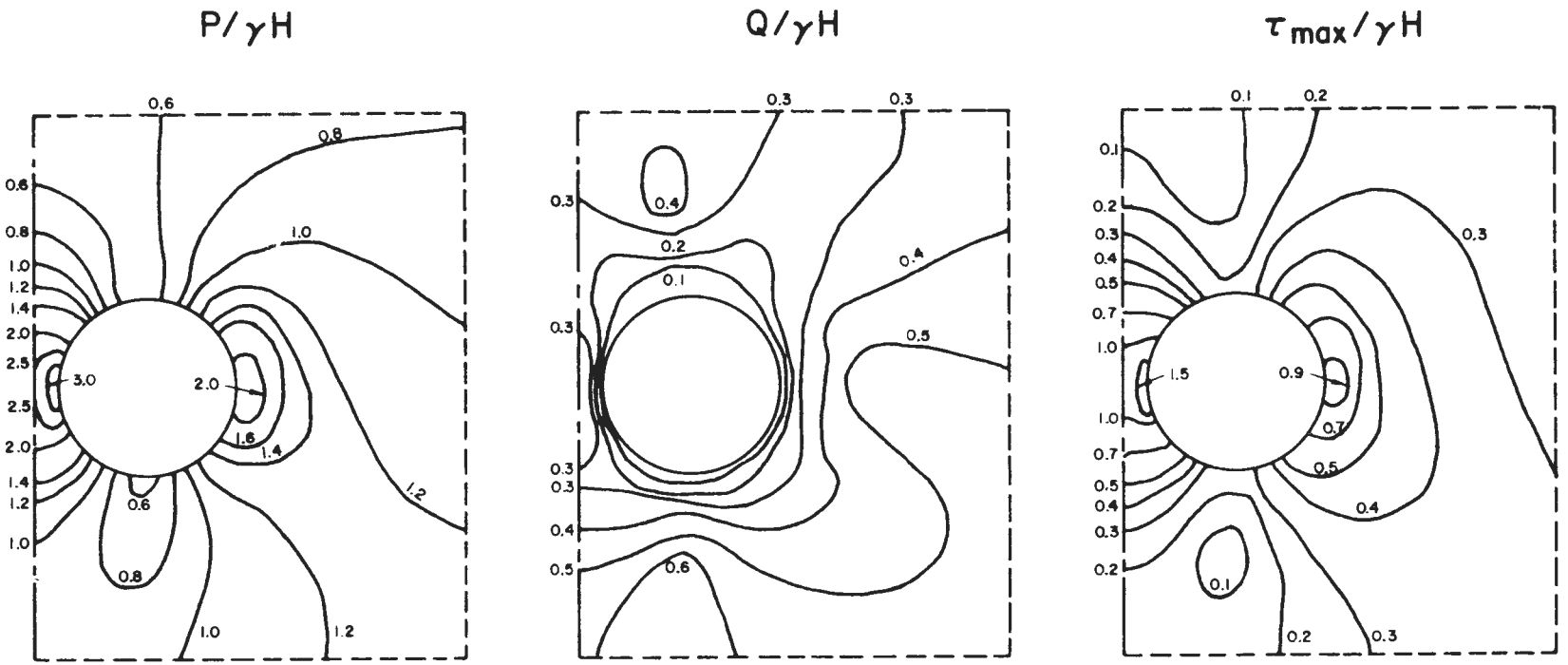

FIGURE 6.5 STRESS DISTRIBUTIONS AROUND TWO PARALLEL UNLINED TUNNELS (H/D = 5.5, W/D = 0.25)

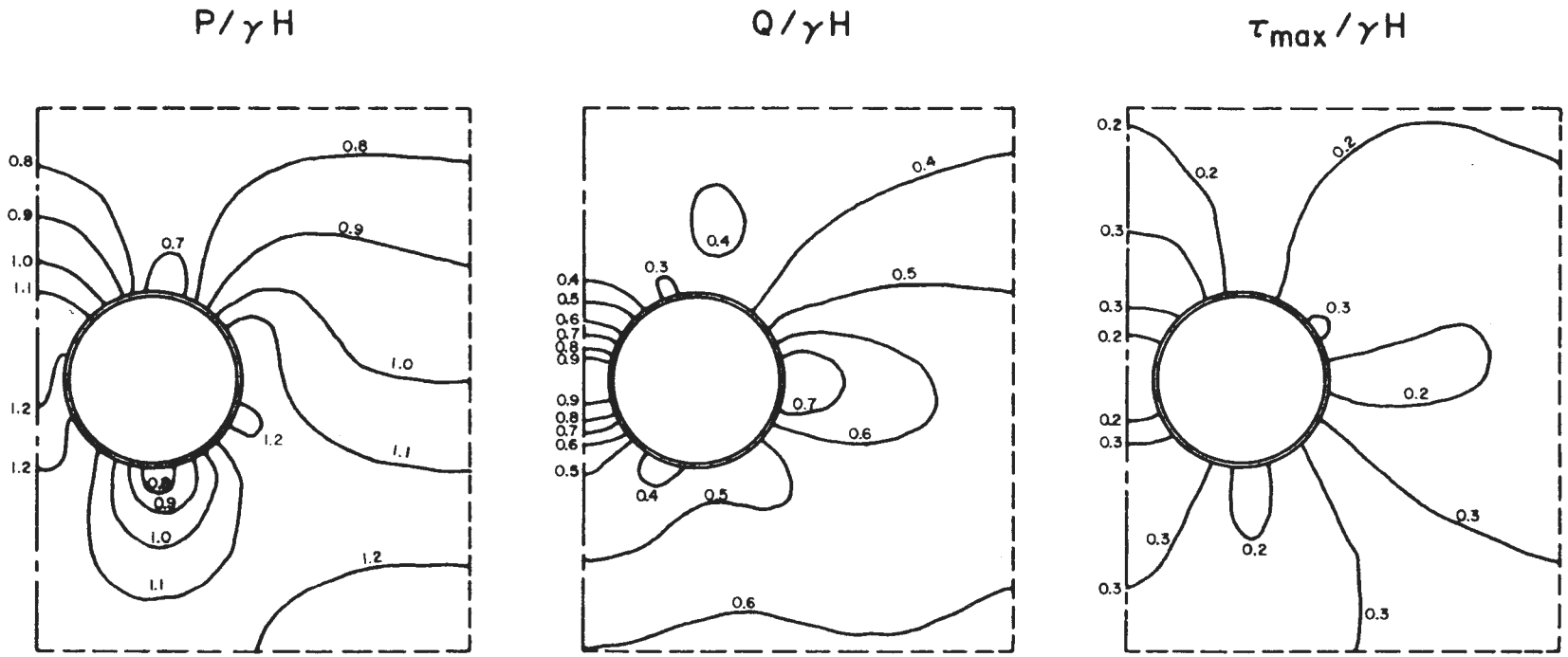

FIGURE 6.6 STRESS DISTRIBUTIONS AROUND TWO PARALLEL LINED TUNNELS (H/D = 5.5, W/D = 0.25)

at the abutment springline and the crown and invert do not differ appreciably from these values. For the wider pillars the differences are even less.

The stress distributions obtained from one of the analyses for which it was assumed that both tunnels were lined are shown in Fig. 6.6. It was assumed in the lined tunnel analyses that tunnel excavation and liner installation occur instantaneously and simultaneously. For this reason relaxation of the medium surrounding the tunnel is a minimum in these analyses. What stress redistribution that does occur is directly related to deformation of the liners. There would be no change in the stress distributions from the in situ state if the liners were perfectly rigid and incompressible (all analyses assume the no slippage condition at the ground-liner interface).

The stress distributions in Fig. 6.6 were selected for presentation because they demonstrate the greatest amount of interaction of all the lined tunnel analyses performed. However, as with the unlined tunnels the interaction that has occurred has had little effect on the distribution of stresses to the right of the tunnel axis.

As would be expected, the stress distributions for both the unlined and lined tunnel cases differ most from those for single tunnels in the vicinity of the pillar and the pillar springlines of the two tunnels. Pillar stresses from the two tunnel analyses are summarized in Fig. 6.7. In this figure horizontal and vertical stresses, σ_H and σ_V, normalized with respect to γH, are given for points at the center and edge of the pillar.

Figure 6.7 shows that for the unlined tunnels the vertical stress is maximum at point B and minimum at point A, while the horizontal stress is maximum at point A and minimum (zero) at point B. For the lined tunnels both the vertical and horizontal stresses are maximum at point B and minimum at point A.

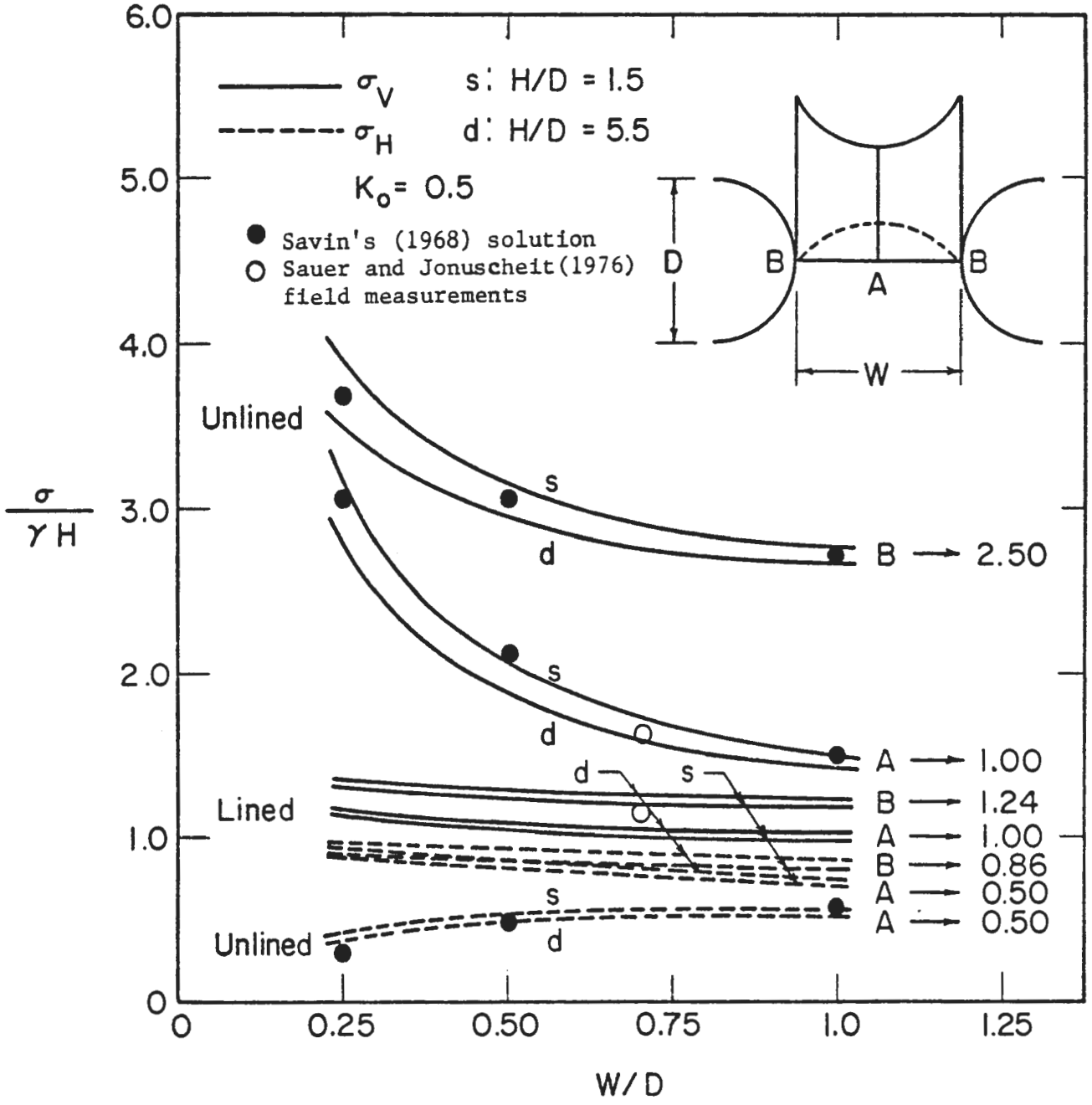

FIGURE 6.7 PILLAR STRESSES VERSUS PILLAR WIDTH

The numbers given along the right side of Fig. 6.7 represent the stress coefficient values that apply when the pillar width has been increased to such an extent that the two tunnels no longer interact. Relative to these values the curves indicate that at a pillar width ratio of one the condition of independent behavior of the two tunnels has almost been achieved. It appears, however, that a pillar width ratio of at least two would be required before all indications of interaction disappear.

Also shown in Fig. 6.7 are stress coefficient values obtained from Savin's (1968) solution for an infinite medium containing two unreinforced circular openings. Agreement between the two solution techniques is very good.

The results of field measurements of stresses at the center of the pillar, reported by Sauer and Jonuscheit (1976), are also shown in Fig. 6.7. These tunnels had a diameter of 25.25 ft (7.7 m) and were constructed in rock at a depth to diameter ratio of H/D = 2.4 with a pillar width to diameter ratio of W/D = 0.71. The in situ horizontal and vertical stresses in the rock mass were approximately equal (K_o = 1). The measured horizontal and vertical stresses at the center of the pillar appear to agree well with the finite element results (for K_o = 1 the finite element analyses, which assumed K_o = 0.5, would have given $\sigma_H/\gamma H \simeq 1.0$). Measurements of stresses near the pillar springlines were also reported by Sauer and Jonuscheit. However, the final vertical stresses were less than the in situ stress which is in contradiction to the finite element results. This reduction of stresses can be attributed to rock loosening during excavation, a phenomenon not simulated in the analyses.

Interaction between the two tunnels is most severe for the unlined tunnel case. As the spacing between two such tunnels is reduced, the vertical

stress in the pillar increases rapidly while the horizontal confining stress approaches zero. While the unconfined strength of the medium may be sufficient to withstand the stress concentrations mobilized around a single tunnel, or two widely spaced parallel tunnels, stability of the pillar, and thus of the two openings, is likely to be jeopardized by the large stress differences that result for a narrow pillar.

Interaction between two lined tunnels was also evident from the analyses performed. For this case, however, the pillar stresses were controlled by the deformation of the tunnel liners, and because the liner displacements were small, the changes in medium stresses were also small. Figure 6.7 shows that as pillar width is reduced there is a gradual increase of vertical stresses in the pillar. However, this increase is matched by a corresponding increase of horizontal stresses. Thus, the stress difference is almost unaffected by pillar width. The high horizontal stresses in the pillar result because under the $K_o = 0.5$ stress condition the pillar springlines of the two liners are forced outward, toward each other, thus causing horizontal compression of the pillar.

Figure 6.8 illustrates the extent of the plastic zones that form around the unlined and lined tunnels when the analyses consider a medium assigned elasto-plastic material properties. For the lined tunnel analyses it was assumed that excavation and liner installation occur simultaneously and therefore that no relaxation of the medium is allowed prior to liner installation. Under these conditions plastic zone formation is tied directly to liner deformation. A relatively stiff and inflexible liner may prevent yielding entirely. Here the liner was sufficiently flexible to allow a small amount of yielding to occur. Had the liner been more flexible , or

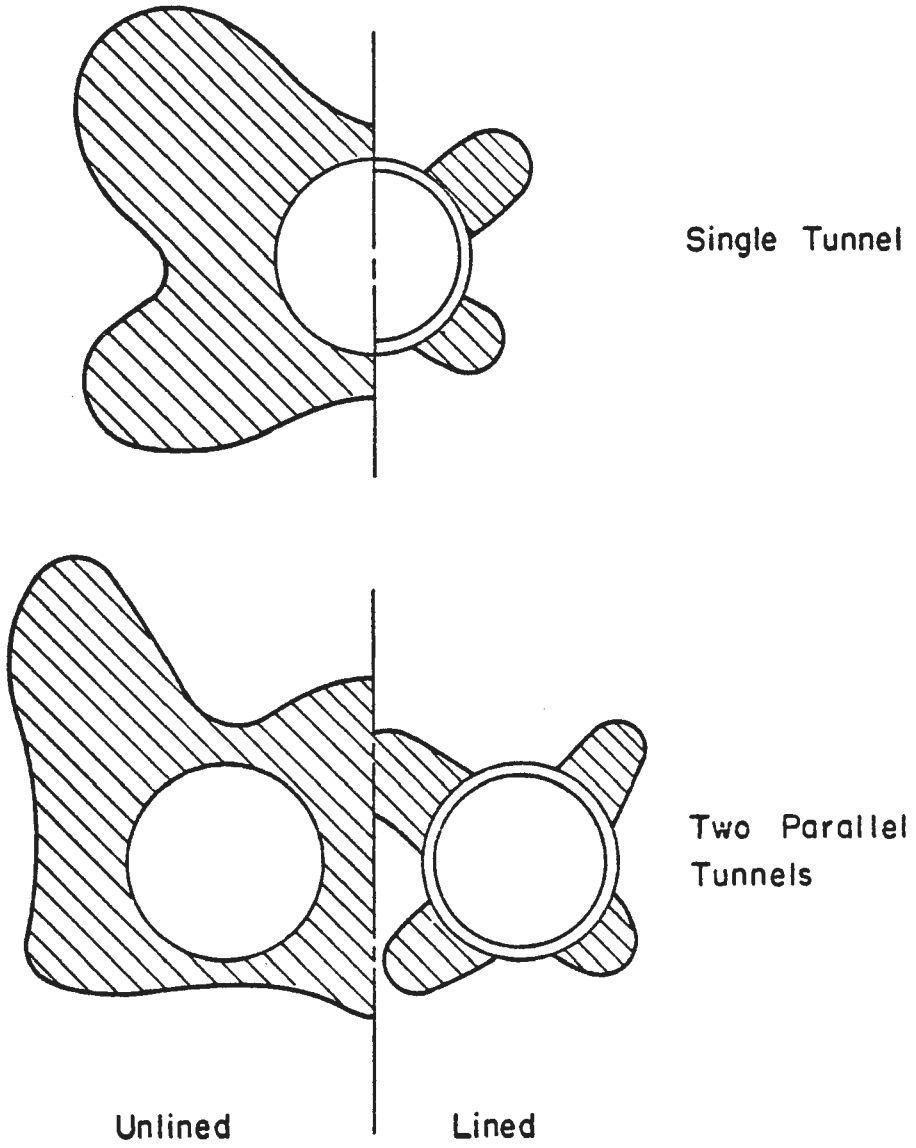

FIGURE 6.8 TYPICAL PLASTIC ZONES AROUND TUNNELS FROM FINITE ELEMENT ANALYSES

had a small amount of ground relaxation been allowed prior to liner installation, the extent of the resulting plastic zone would be somewhere between the two extremes shown in Fig. 6.8.

TUNNEL DISPLACEMENTS

Normalized displacements of the unlined and lined tunnel openings for the symmetrical case are plotted in Figs. 6.9 through 6.12 (for right hand tunnel only). Also shown in these figures are the corresponding single tunnel displacements. Note that because the displacements of the unlined tunnels were so much larger than those of the lined tunnels two different displacement scales are used.

Figures 6.9 and 6.10 show that as the pillar width between two unlined tunnels is reduced, the downward displacements of the upper half of the tunnels increase. This is a result of the vertical compression of the pillar, which is greater for a narrow pillar than for a wide pillar. Above the springlines there is little difference between the displacements for W/D = 1.0 and those for a single tunnel when the tunnels are located at a shallow depth. However, for deep tunnels this difference is more pronounced, indicating that the minimum pillar width at which the two tunnels can be said to act independently of each other increases with depth of the tunnels. Pillar width seems to have its greatest effect on the vertical displacement component. The greatest variation of horizontal displacements occurs on the pillar side of the tunnel where there is slightly less inward displacement as the pillar width is reduced. Pillar width has almost no effect on displacements in the lower right hand quadrant of the tunnels.

Figure 6.11 gives the displacements of the shallow (H/D = 1.5) lined tunnels. At this depth the weight of the overburden is not sufficient

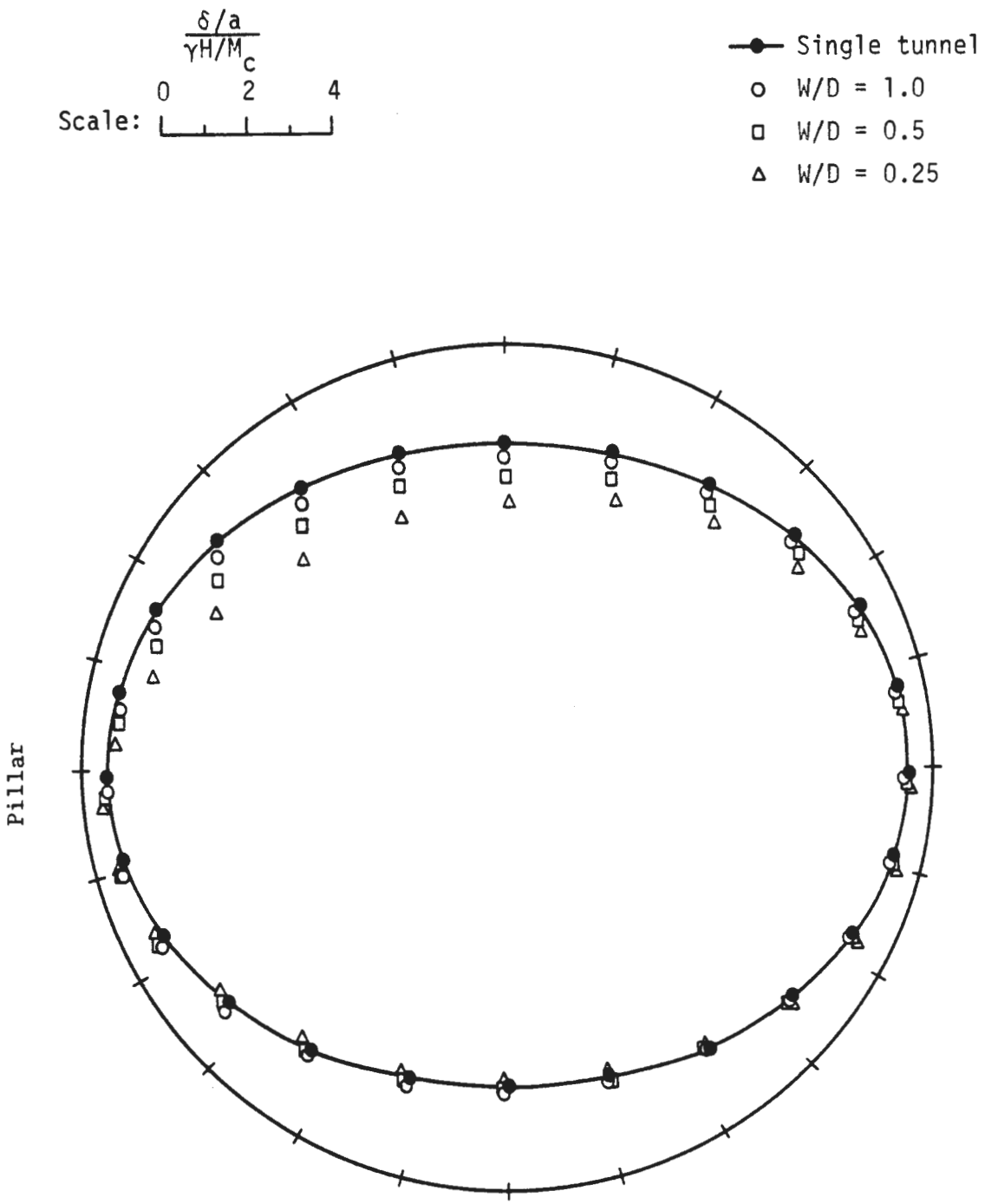

FIGURE 6.9 UNLINED TUNNEL DISPLACEMENTS FOR THE SYMMETRICAL CASE (H/D = 1.5)

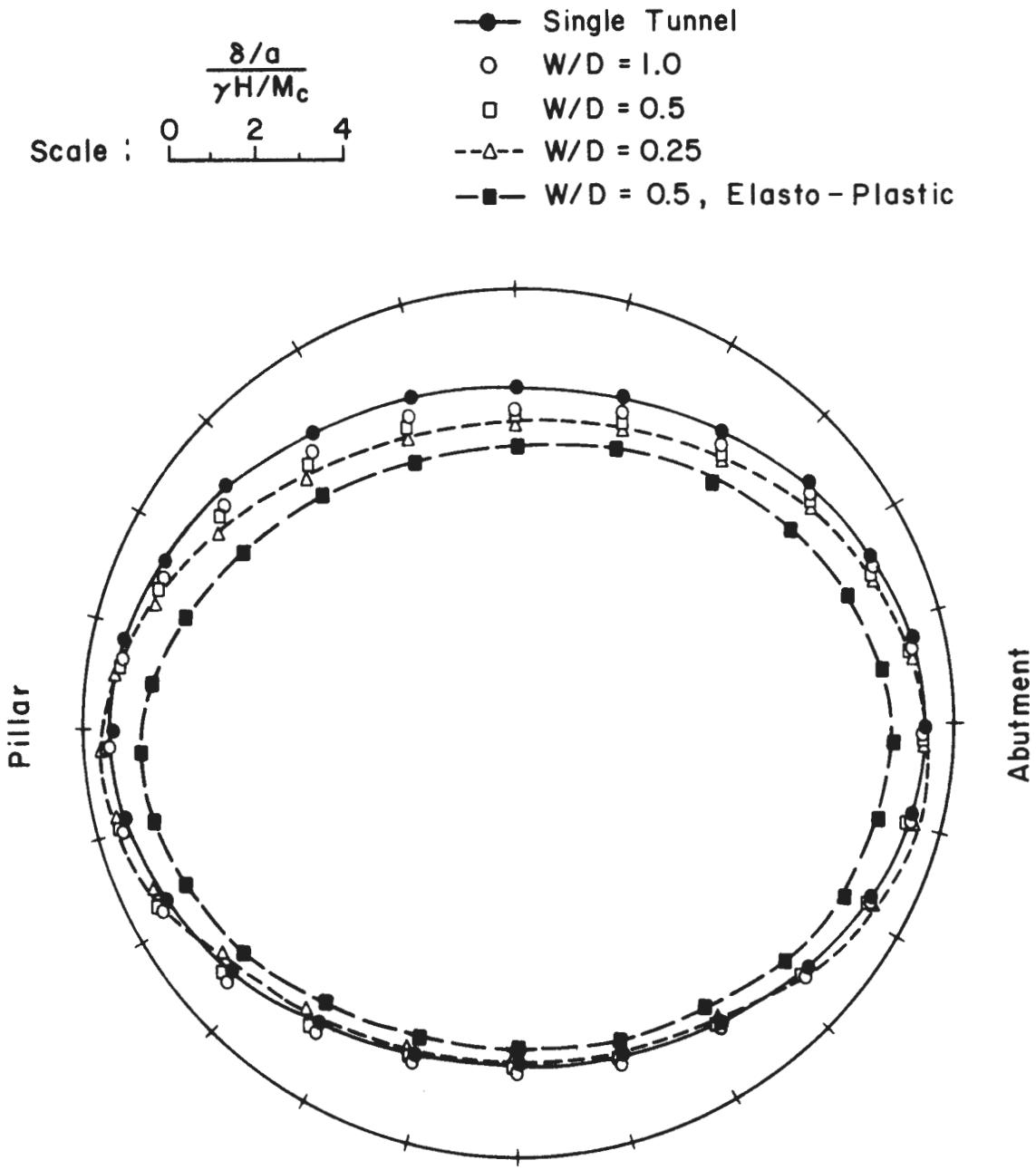

FIGURE 6.10 UNLINED TUNNEL DISPLACEMENTS FOR THE SYMMETRICAL CASE (H/D = 5.5)

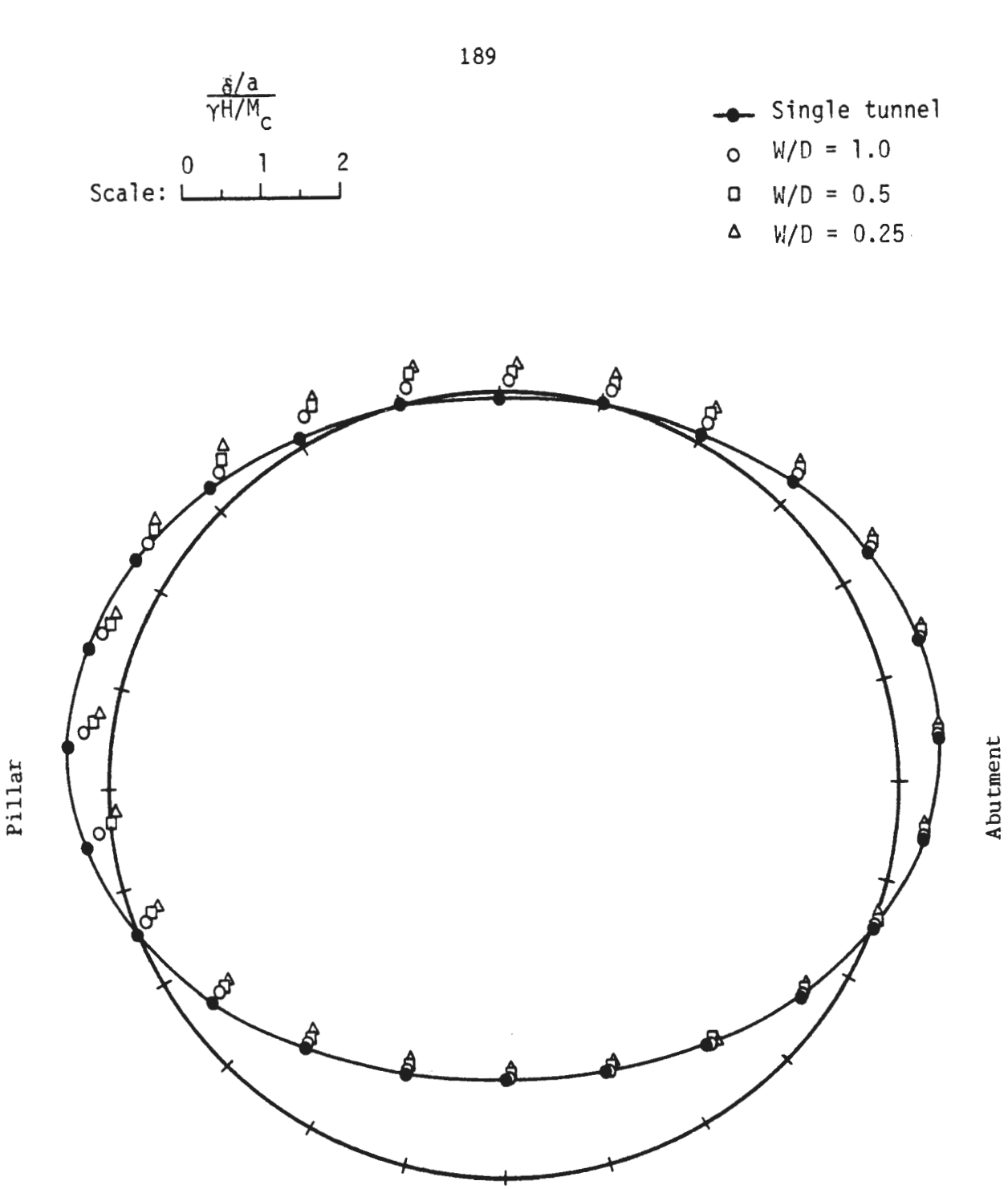

FIGURE 6.11 LINED TUNNEL DISPLACEMENTS FOR THE SYMMETRICAL CASE (H/D = 1.5)

to prevent the upward rise of the liner. This effect is more pronounced for two parallel tunnels than for a single tunnel. It is also clear that the upward displacement is greater for a narrow pillar than for a wide pillar, and that the pillar springline of the liner moves upward more than the abutment springline.

Displacements of the deep (H/D = 5.5) lined tunnels are given in Fig. 6.12. At this depth the weight of the overburden is great enough to prevent the rise of the liner and a more symmetrical deformed liner shape results. At this depth the interaction of two parallel lined tunnels is indicated primarily by the horizontal displacements of the liner next to the pillar. This effect is also observed for the shallow tunnels (Fig. 6.11). Under the K_o condition assumed, a tunnel liner will be forced outward at the springlines until sufficient passive pressure is built up to balance the vertical pressures acting at the crown and invert. This reaction is indicated by the single tunnel displacements in Figs. 6.11 and 6.12. These figures also indicate that when two parallel lined tunnels are constructed simultaneously with a pillar width of approximately one tunnel diameter or less they will interact so as to yield smaller outward displacement of the tunnels' pillar springlines than would result for a single tunnel. In addition, the necessary passive pressure at the two pillar springlines is mobilized with less displacement of each springline as the pillar width is reduced.

Tunnel displacements obtained from the corresponding elasto-plastic analyses are given in Fig. 6.10. It can be seen that the plastic yielding illustrated in Fig. 6.8 has led to increased displacements at all points around the unlined tunnel perimeter for both the single tunnel and two tunnel (W/D = 0.5) cases.

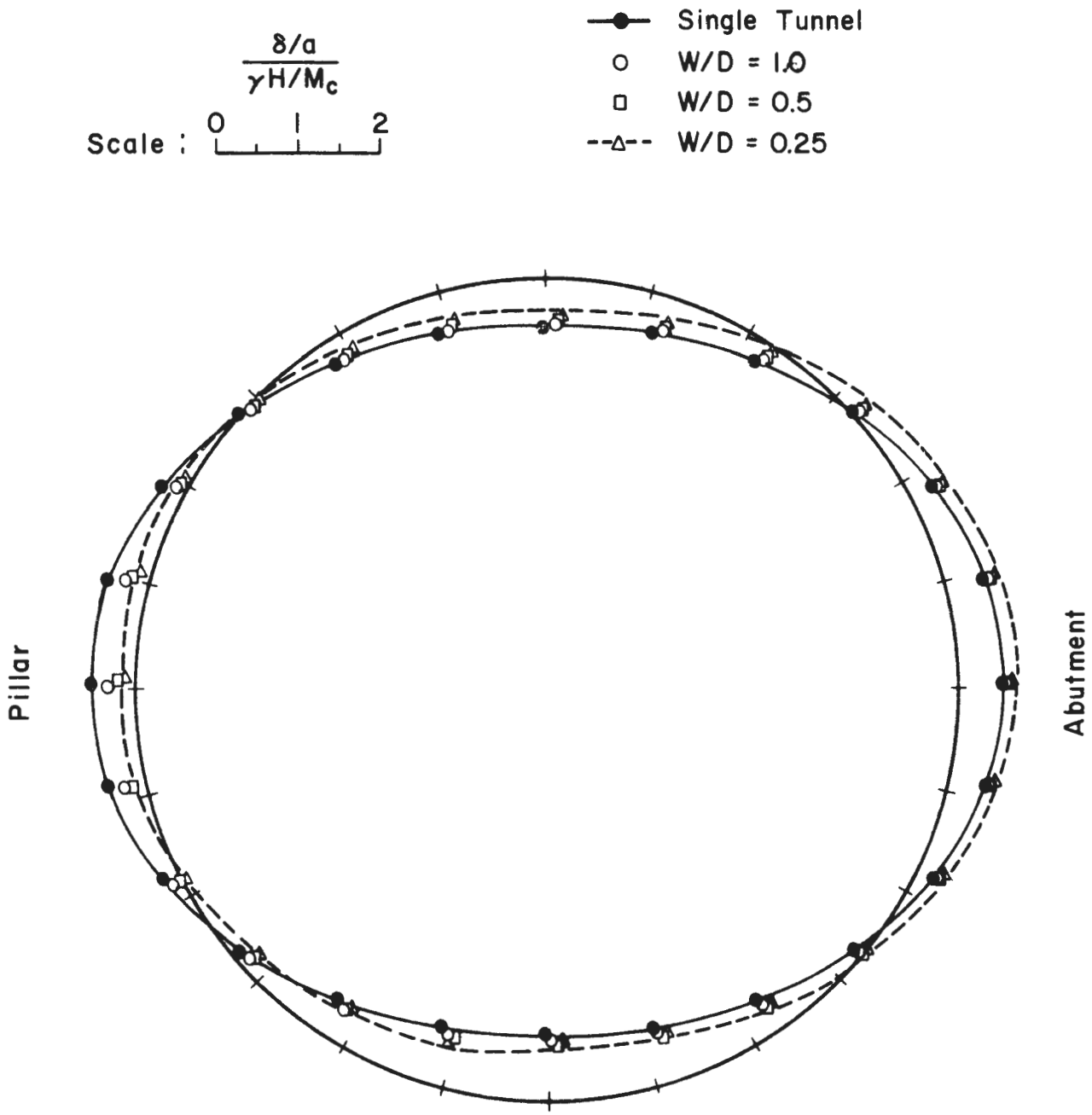

FIGURE 6.12 LINED TUNNEL DISPLACEMENTS FOR THE SYMMETRICAL CASE (H/D = 5.5)

The effect of pillar width on tunnel displacements is also illustrated in Fig. 6.13 in which the horizontal and vertical diameter change coefficients have been plotted versus W/D. The resulting curves show again that for unlined tunnels the vertical diameter change is much larger than, and is influenced to a greater degree by pillar width than, the horizontal diameter change. On the other hand, for the lined tunnels the vertical and horizontal diameter changes are approximately equal in magnitue (but of opposite sign) and equally influenced by pillar width.

Diameter change coefficients for the two elasto-plastic analyses (single tunnel and two parallel tunnels with W/D = 0.5) of unlined tunnels are also given in Fig. 6.13. It can be seen that the additional displacements due to plastic yielding are much greater around the springlines than around the crown and invert. The elasto-plastic ΔD_H is approximately 130 percent greater than the elastic value, while the elasto-plastic ΔD_V is only about 20 percent greater than the elastic value. The additional displacements around the springlines are so much greater than those around the crown and invert because, as Fig. 6.8 shows, there is much more plastic yielding around the springlines.

In each plot of Fig. 6.13 the corresponding values for a single tunnel, which is equivalent to either of two widely spaced parallel tunnels, are given along the right-hand side. Convergence of the plotted curves to these values provides an indication of the pillar width required to eliminate interaction, with respect to diameter changes at least, between two parallel tunnels. Most of the curves have almost reached the single tunnel values at W/D = 1.0. And it appears that if the curves were extrapolated beyond W/D = 1.0, they would all reach the single tunnel values at pillar

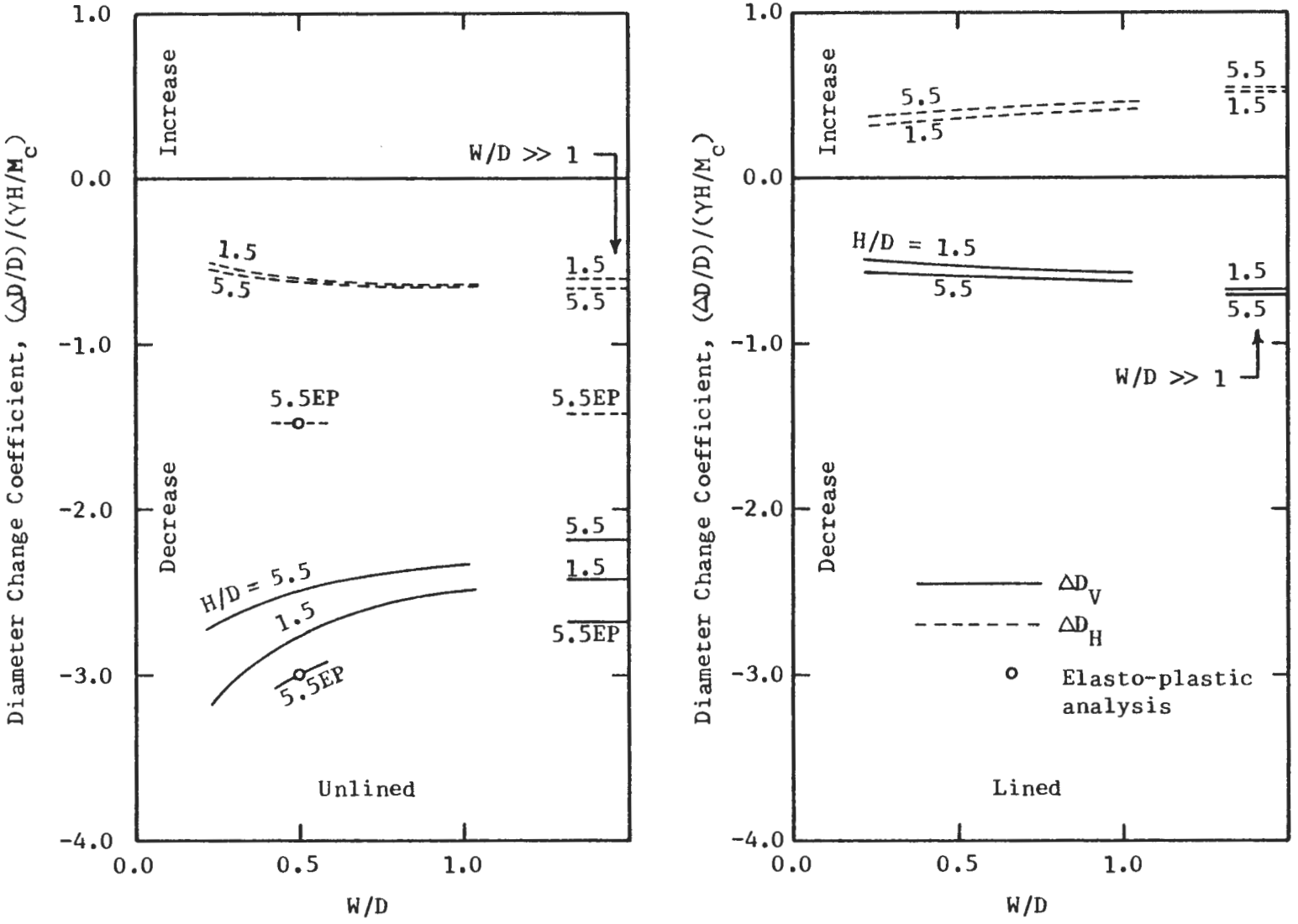

FIGURE 6.13 DIAMETER CHANGE COEFFICIENTS VERSUS PILLAR WIDTH

widths of no more than W/D = 2.0. The curves also indicate that the pillar width required to eliminate interaction is greater for deep tunnels than it is for shallow tunnels.

LINER FORCES AND MOMENTS

Under the condition of simultaneous construction assumed in this part of the study the interaction between two parallel tunnels leads to distributions of liner forces and moments that, in general, do not differ greatly from the distributions for a single tunnel. Maximum normalized liner force and moment coefficients are summarized in Table 6.2.

Interaction between the two tunnels led to only slightly larger thrust values at most points around the liners. Relative to the single tunnel case the greatest thrust increases occurred in the vicinity of the pillar side of the crown and invert. However, in all cases the maximum thrust occurred at or near the pillar springline, and here the changes were small. Table 6.2 shows that for two shallow tunnels the maximum thrust values were actually less than the single tunnel maximum, while for two deep tunnels the maximum thrust was only slightly larger than that for a single tunnel at the same depth.

The liner bending moment distributions, shown in Fig. 6.14 and Table 6.2, exhibit the greatest variation from the single tunnel case, but the general trend is toward smaller, not larger, bending moments due to interaction. The interaction effect on bending moments is greatest at the liners' pillar springlines where reduced displacements have led to a significant reduction in moments. However, at the liner invert, where the maximum bending moments are mobilized, the moments have been reduced to a lesser extent.

TABLE 6.2

MAXIMUM LINER FORCE AND MOMENT COEFFICIENTS

	$T/\gamma Ha$		$M/\gamma Ha^2$		$V/\gamma Ha$	
	Shallow	Deep	Shallow	Deep	Shallow	Deep
Single tunnel	.859	.871	-.0105	-.0099	-.0237	-.0218
W/D = 1.0	.834	.866	-.0091	-.0088	-.0220	-.0214
W/D = 0.5	.837	.881	-.0086	-.0088	-.0214	-.0205
W/D = 0.25	.853	.905	-.0083	-.0087	-.0211	-.0205

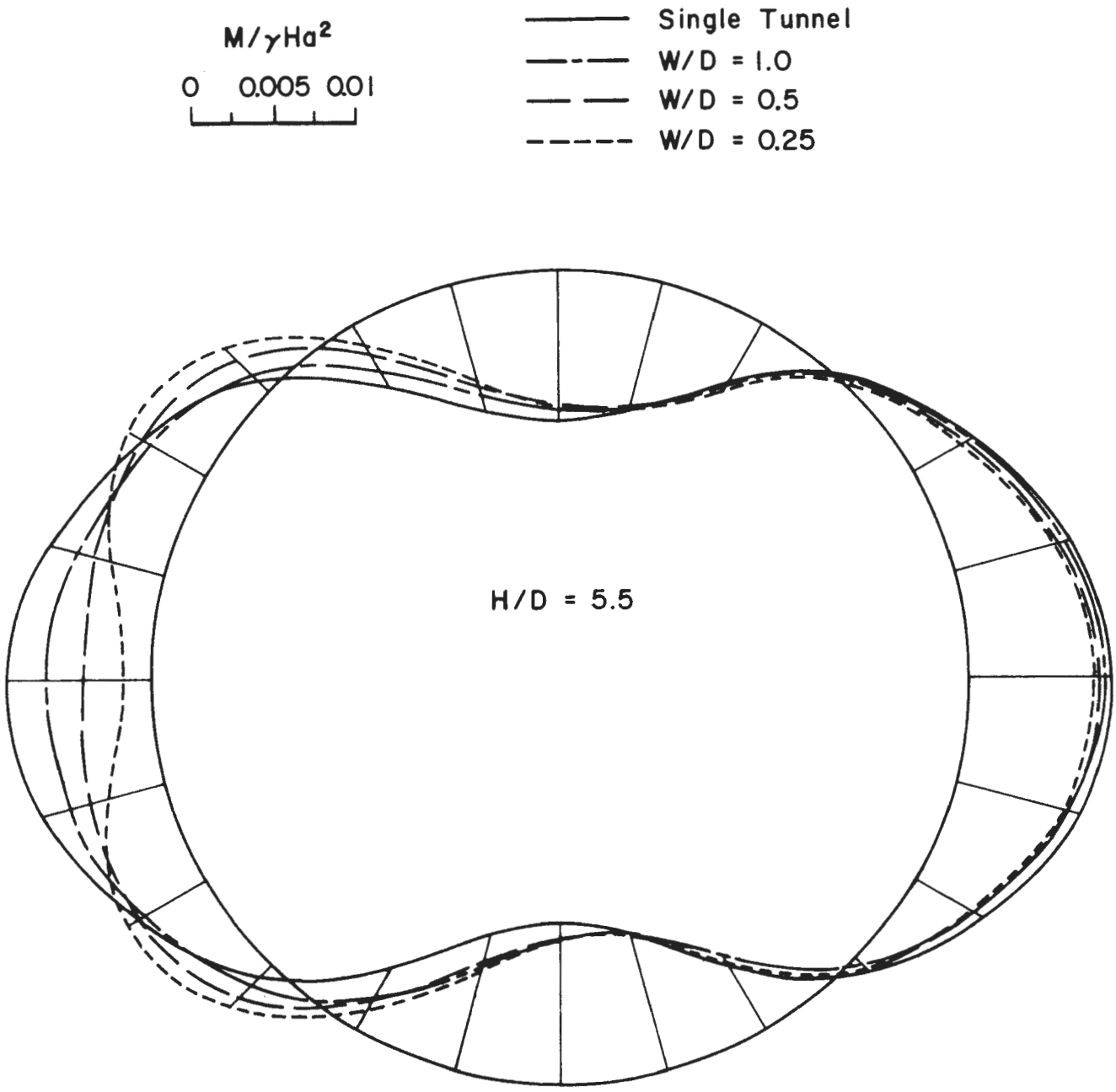

FIGURE 6.14 DISTRIBUTIONS OF LINER MOMENTS FOR THE DEEP TUNNELS

SURFACE DISPLACEMENTS

For two adjacent and parallel tunnels it seems reasonable to expect that the settlements at the ground surface would consist of two components. The first component would be equal to the settlements resulting from the superposition of the two single tunnel settlement troughs, assuming that the two tunnels are so spaced that their individual troughs overlap. The second component would consist of additional settlements resulting from interaction of the two tunnels (pillar shortening, increased crown displacements), assuming that the two tunnels are close enough together so that interaction will occur. These two components are illustrated in Fig. 6.15.

The additional settlement due to two tunnel interaction is illustrated in Figs. 6.16 and 6.17 wherein the surface displacement profiles obtained from the finite element analyses are compared to profiles obtained by superposing two single tunnel settlement curves. Settlements were normalized with respect to S_{max} which is the maximum settlement from the single tunnel analyses.

Figure 6.16 gives the comparison for the analyses of shallow, unlined tunnels at three different pillar widths. This figure indicates that the additional surface settlement due to interaction between the two tunnels is small at a pillar width ratio of W/D = 1.0, but increases as the pillar width is decreased. The pattern of increasing additional settlements over the tunnel crown (x/a = 0) corresponds to the pattern of the vertical diameter changes shown in Fig. 6.13.

The comparison for the analyses of deep, unlined tunnels is shown in Fig. 6.17. Here the additional surface settlement due to two tunnel

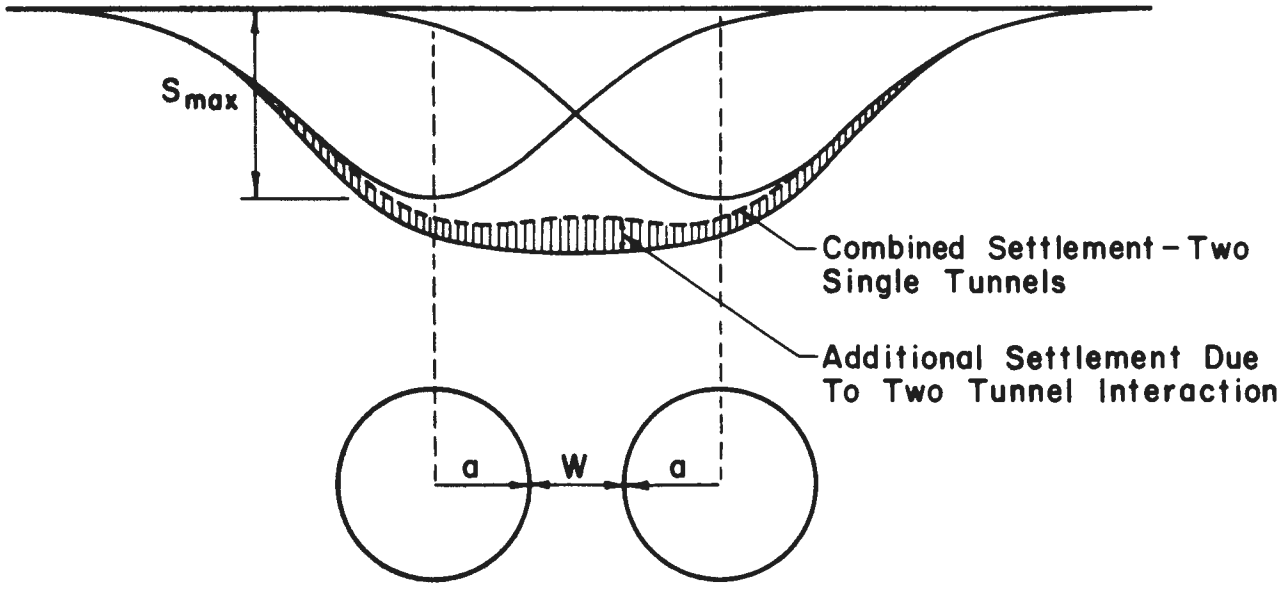

FIGURE 6.15 SCHEMATIC REPRESENTATION OF ADDITIONAL SURFACE SETTLEMENT ARISING FROM TWO-TUNNEL INTERACTION (SIMULTANEOUS EXCAVATION)

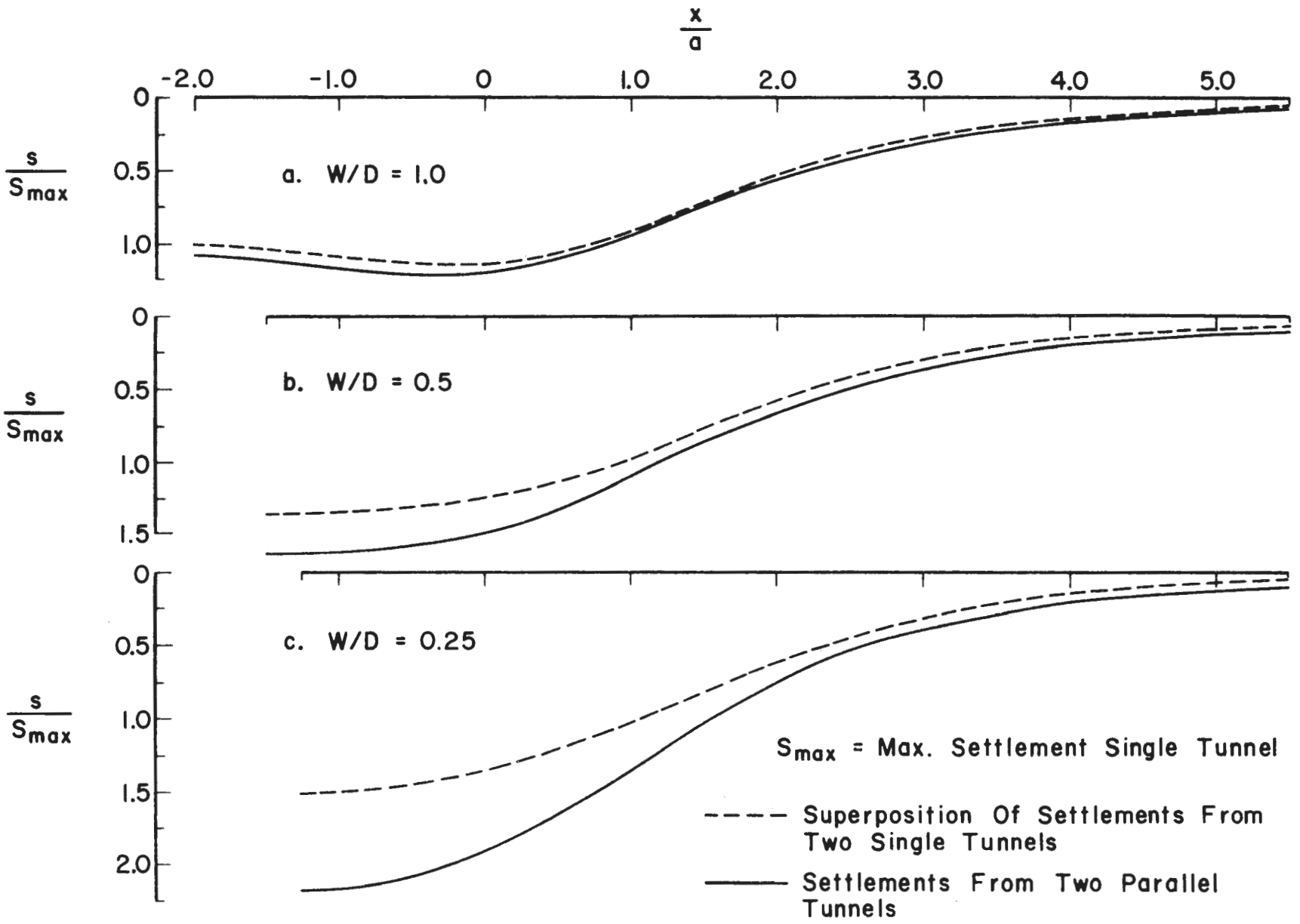

FIGURE 6.16 SETTLEMENT TROUGHS FROM TWO-TUNNEL ANALYSES AND FROM SUPERIMPOSING TWO SINGLE TUNNEL TROUGHS - H/D = 1.5

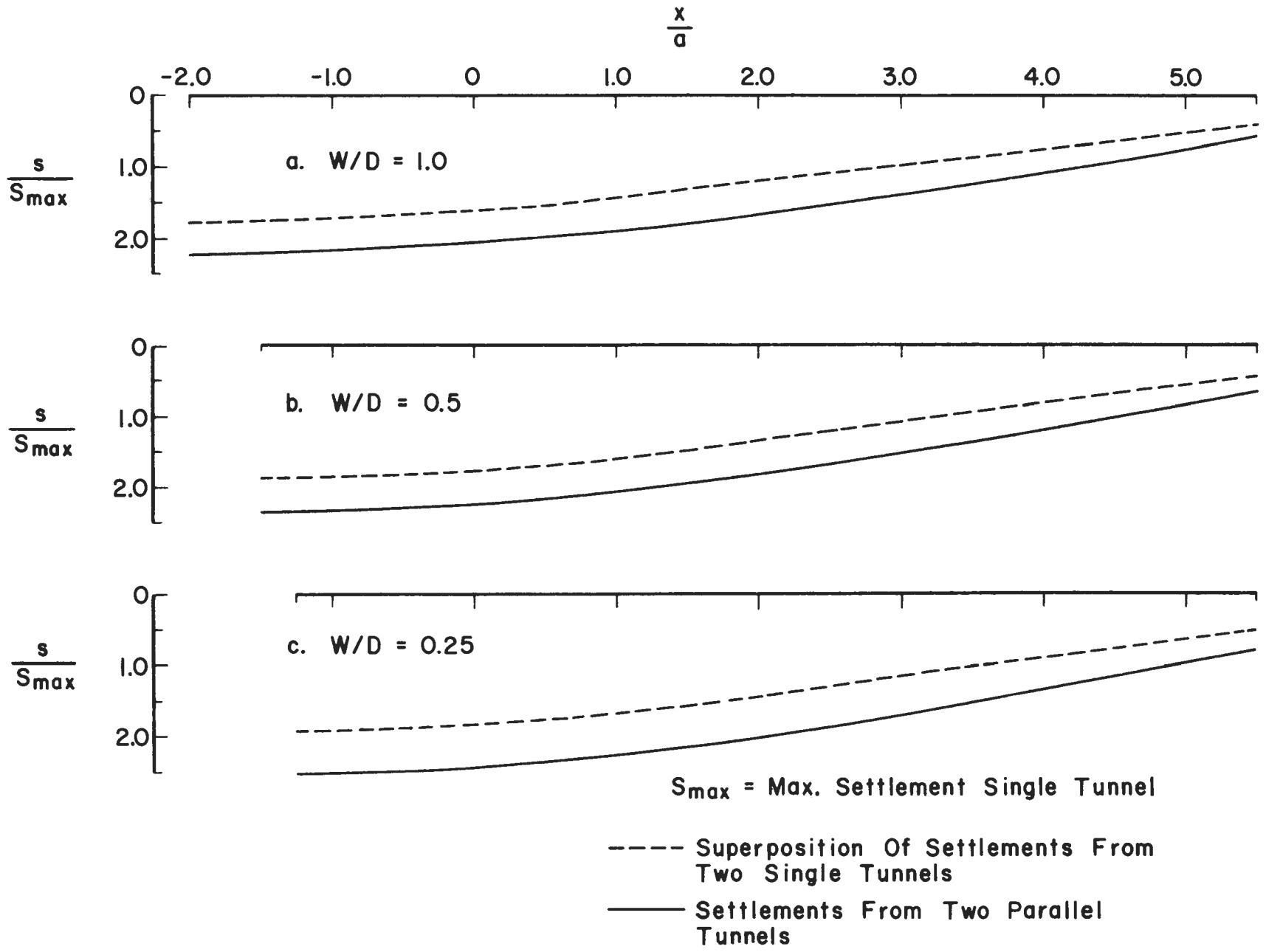

FIGURE 6.17 SETTLEMENT TROUGHS FROM TWO-TUNNEL ANALYSES AND FROM SUPERIMPOSING TWO SINGLE TUNNEL TROUGHS - H/D = 5.5

interaction also increases as the pillar width decreases. However, the amount of additional settlement for W/D = 1.0 is already quite large and there is only a slight increase as the pillar width is reduced. This pattern can be related to the relationships between displacements of the tunnel openings and pillar width in Fig. 6.10 and between vertical diameter change and pillar width in Fig. 6.13. Because of the depth of these tunnels the width of the individual ssttlement troughs is large and, for two parallel tunnels at the spacings considered, tha amount of overlap at the ground surface is extensive.

Interaction effects on ground surface displacements can also be illustrated by examining the settlement trough volumes (Hansmire, 1975). The ratio obtained by dividing the interaction settlement volume by the settlement volume for a single tunnel, $\Delta V/V_s$, was calculated for the unlined tunnel analyses. The interaction settlement volume is obtained by subtracting the settlement volume for two single tunnels from the settlement volume for the two tunnel case. These ratios are plotted versus pillar width in Fig. 6.18. The curves also show that the additional settlements due to two tunnel interaction increase as the pillar width is reduced. The data indicate that the volume ratio is greater for deep tunnels than for shallow tunnels. If this relatioship is valid it means that the deeper two tunnels are to be located the wider the the pillar between them must be if no interaction, with respect to surface displacements, is to occur. In Fig. 6.18 the absence of interaction effects on surface settlements is indicated by $\Delta V/V_s = 0$. The trend of the shallow tunnel curve suggests that this condition is satisfied at a pillar width ratio of approximately W/D = 2.0. The deep tunnel curve indicates a much

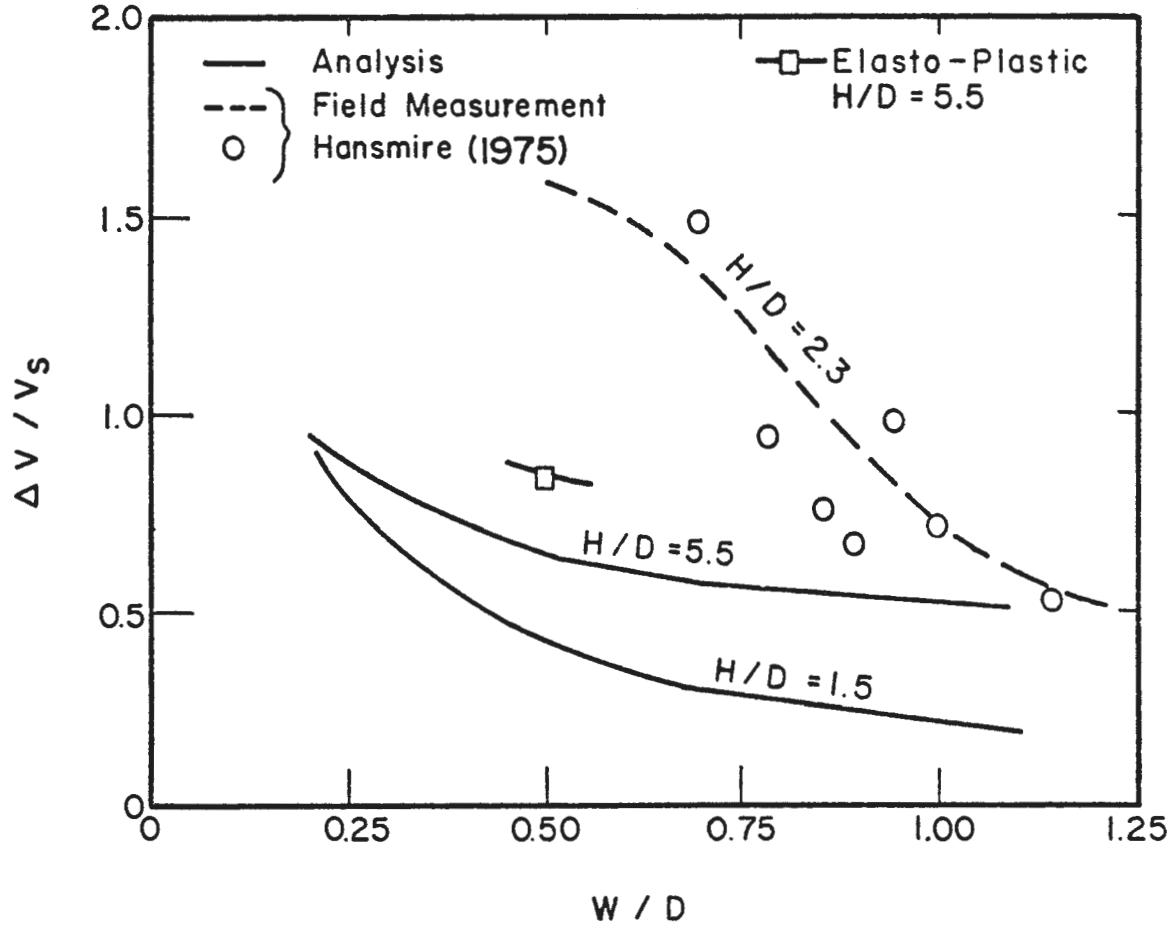

FIGURE 6.18 INTERACTION SETTLEMENT VOLUME AT GROUND SURFACE VERSUS PILLAR WIDTH

wider separation is required before interaction effects on surface displacements cease.

Also shown in Fig. 6.18 are the volume ratios calculated by Hansmire (1975) from field measurements of surface settlement over two parallel tunnels constructed in Washington, D. C. The data from the Washington Metro indicates that the interaction settlement volume ratio, $\Delta V/V_s$, for dense sands is two to three times larger than predicted from elastic theory. The difference is primarily due to soil volume decreases and disturbance that occurred in the sands and gravels but which were not modeled by the elastic analyses.

6.3.2 INFLUENCE OF CONSTRUCTION SEQUENCE

In this section the behavior of the two tunnel system is studied for various sequences of construction of the two tunnels. The emphasis here is on the case of a tunnel being constructed parallel and adjacent to an existing tunnel, or the case of two tunnels being constructed simultaneously with the heading of the first tunnel far ahead of the heading of the second tunnel. Both of these two tunnel systems behave similarily and no distinction is made between them subsequently in this study.

Each of these analyses consisted of three solution steps. In the first step the initial stress state was simulated. The initial stress state consisted of the vertical and horizontal stresses caused by the weight of the medium with the coefficient of lateral stress $K_o = 0.5$ used in all the cases. The two subsequent steps simulated the excavation of the tunnels and liner installation.

Four sequences of construction and lining of the two tunnels are

possible. These construction sequences are given in Table 6.1. In the last column of the table are given the actual conditions to which the analyzed sequences correspond.

All the cases in Table 6.1 were analyzed for a shallow tunnel with depth to diameter ratio of H/D = 1.5 and a deep tunnel with H/D = 5.5. In all the cases a central distance of 1.5 diameters was used. This is equivalent to a pillar width to diameter ratio of W/D = 0.5. While linear elastic material properties were assigned to both the medium and liner in all cases, case B was also analyzed with elasto-plastic properties assigned to the medium.

STRESSES AROUND TWO TUNNELS CONSTRUCTED SEPARATELY

It is generally expected that the stresses at the abutment side of each tunnel will differ only slightly from those of a single tunnel. However, on the pillar side of each tunnel higher stresses are expected, as the two tunnels interact. The degree of overstress in the pillar, to a varying extent, depends on a combination of factors such as depth, tunnel diameter, pillar width, and the support condition which in these analyses are equivalent to the fully lined or unlined conditions. The sequence of construction also has some influence on the stress condition in the pillar.

For cases A and D the stress distributions around the tunnels resemble closely those of two lined and two unlined tunnels, respectively, as simulated in the previous section of this chapter; being almost symmetrical about a vertical plane bisecting the pillar. In case D the first tunnel is excavated and left unlined with the resulting stress distribution of a single tunnel. At the end of this step the liner is installed but

remains stress free until the next step when the second tunnel is excavated and left unlined. The excavation of the second tunnel only slightly modifies the stresses around the first tunnel because the liner in this tunnel inhibits further displacements and stress changes. A similar situation exists in analysis case A but with both the tunnels lined at the time of excavation.

The final stress distributions around two deep tunnels for cases B and C are shown in Figs. 6.19 and 6.20, respectively.

In case B the first tunnel was excavated and lined, and subsequently the second tunnel was excavated, but left unlined. The medium stresses around the first tunnel are similar to those found when both tunnels are lined, and the stresses around the second tunnel bear some resemblance to those stresses found when both tunnels are unlined. It is evident, however, that each tunnel has had an effect on the other and that interaction between the two tunnels has taken place resulting in new stress distributions .

A similar effect is observed for the stresses in the medium surrounding the two tunnels of case C. Figure 6.20 shows that although both tunnels were lined in this analysis the stress distributions are almost mirror images of those in Fig. 6.19. This occurs because the liner of the first tunnel was not installed until after all medium displacements associated with the creation of this opening had occurred. The second tunnel was lined immediately upon excavation.

The distributions of stresses around two shallow tunnels for the case B construction sequence are given in Fig. 6.21. The influence of the ground surface can be seen be comparing Figs. 6.21 and 6.19. Although

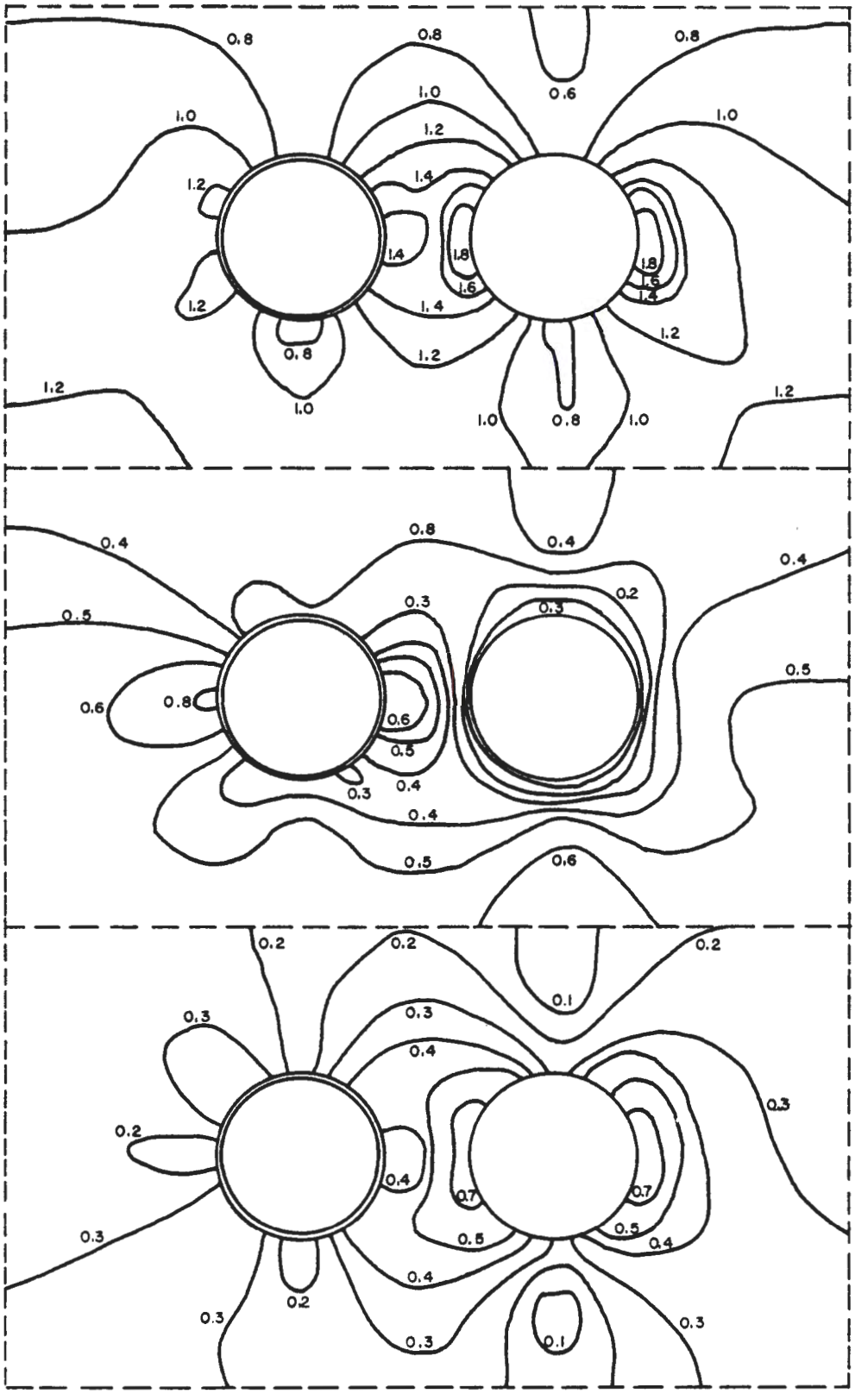

FIGURE 6.19 STRESS DISTRIBUTION FOR CASE B (SEE TABLE 6.1), H/D = 5.5

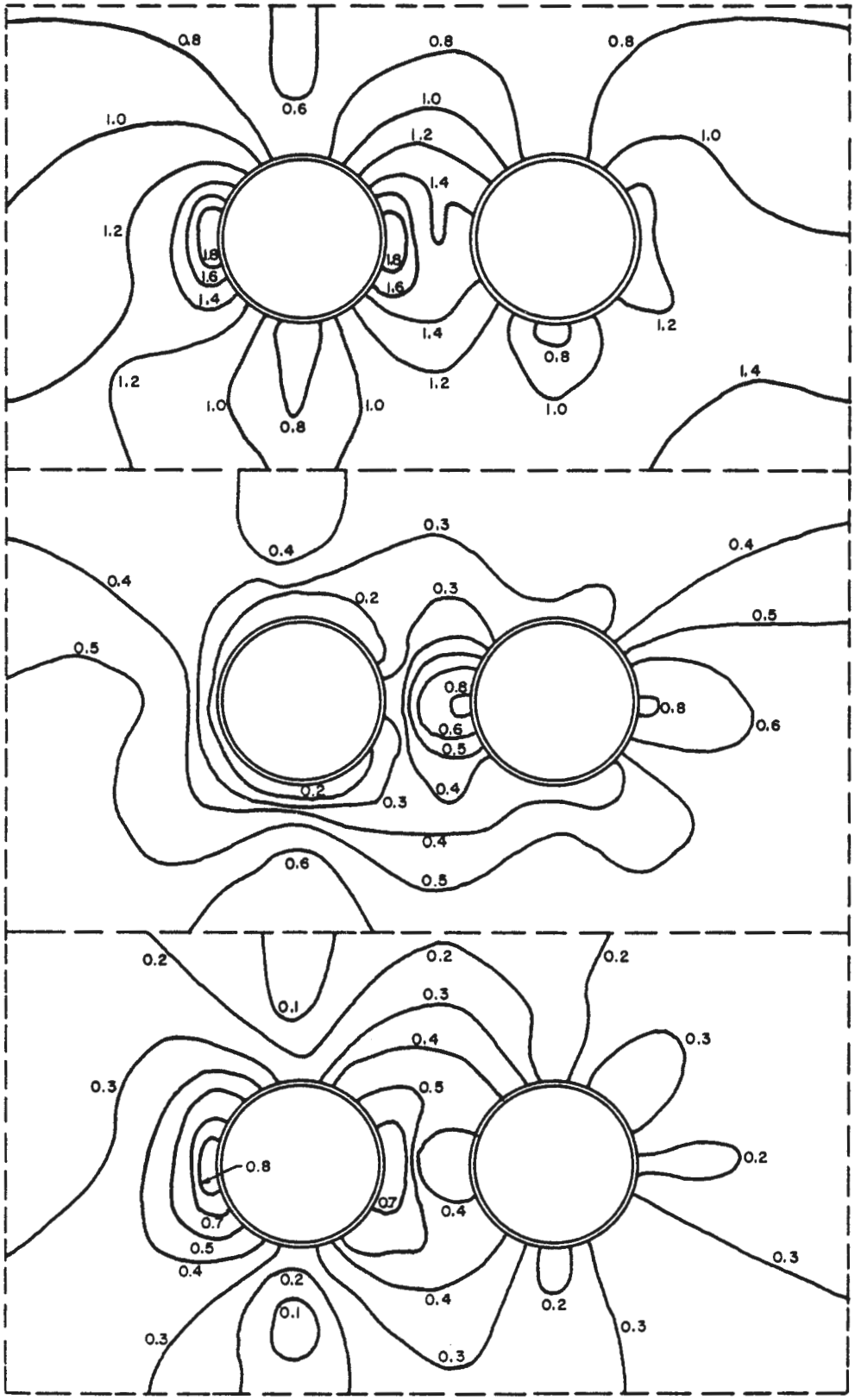

FIGURE 6.20 STRESS DISTRIBUTION FOR CASE C (SEE TABLE 6.1), H/D = 5.5

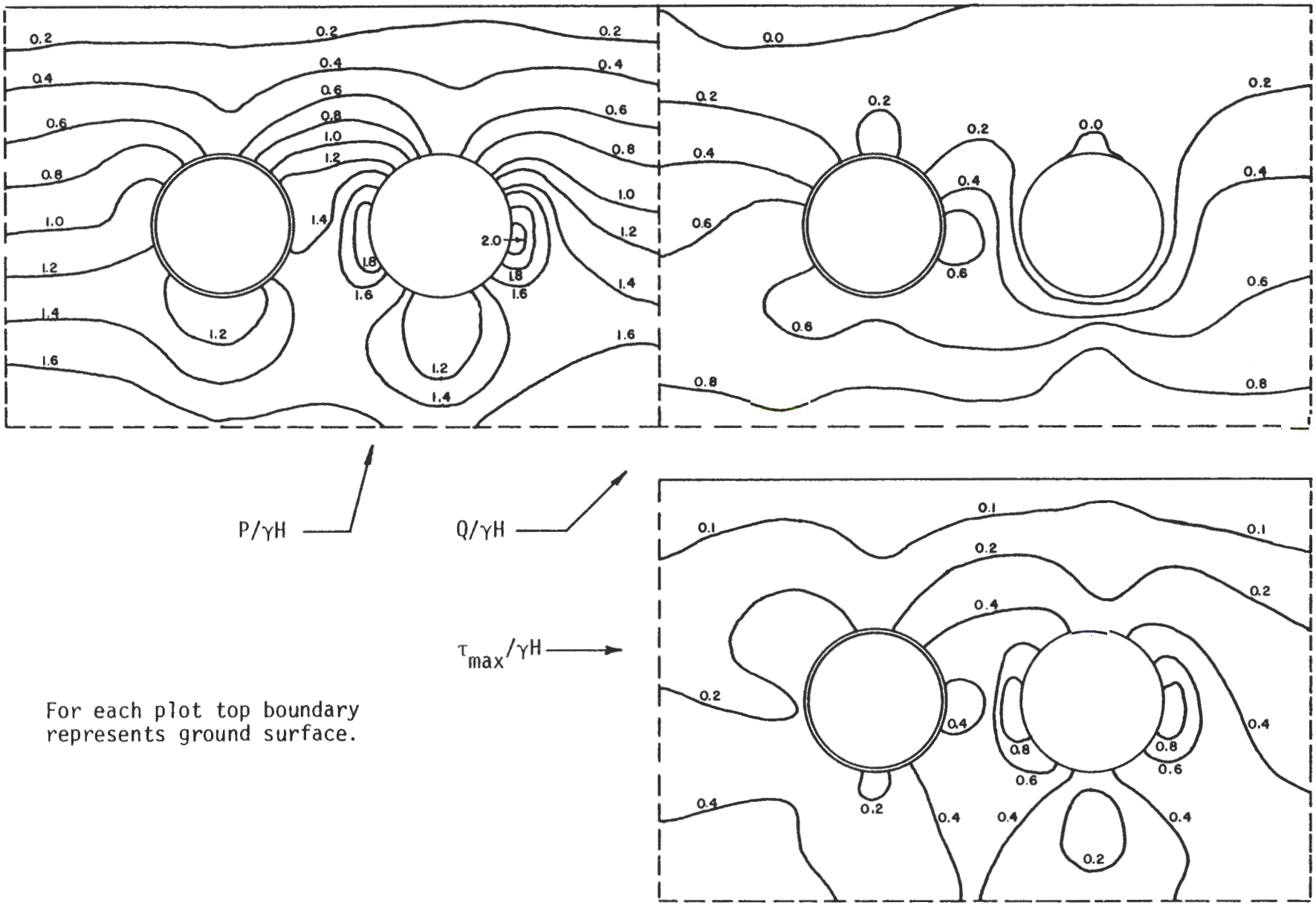

FIGURE 6.21 STRESS DISTRIBUTIONS FOR CASE B (SEE TABLE 6.1), H/D = 1.5

there are many similarities in form of the distributions for the shallow and deep cases, there is a greater range of normalized magnitudes associated with the shallow tunnels. This is because the stress increase with depth over a given vertical distance (e.g., one tunnel diameter) is more pronounced near the ground surface than at great depth. Figure 6.21 illustrates the presence of two small regions of tensile minimum principal stress, one at the ground surface and the other at the crown of the unlined tunnel. Similar tensile stress regions were observed for all shallow tunnel analyses that considered unlined tunnels. These stresses were always of very small magnitude, usually less than 1.0 psi (7 kPa) and never greater than 2.0 psi (14 kPa). The tensile stresses above the crown of the unlined tunnels are oriented in a nearly radial direction and act in combination with relatively small circumferential stresses. Figure 6.21 shows only one zone of tensile stresses at the ground surface. There were usually two such zones observed, symmetrically located to the left and right of the unlined tunnels. These tensile stresses are undoubtedly the result of the lateral (horizontal) component of the surface displacements.

The zones of plastic yielding that formed around the tunnels in the elasto-plastic analysis of case B are shown in Fig. 6.22. In this analysis the first tunnel was lined simultaneously with excavation. The liner provided sufficient support to the medium to prevent yielding initially. When the second tunnel, which was left unlined, was excavated the medium surrounding it yielded. This induced additional displacement of the liner of the first tunnel and the two small zones of yielding on the left side of this tunnel. Increased horizontal passive pressures exerted by the outward deflecting right springline of the liner helped keep the stress difference

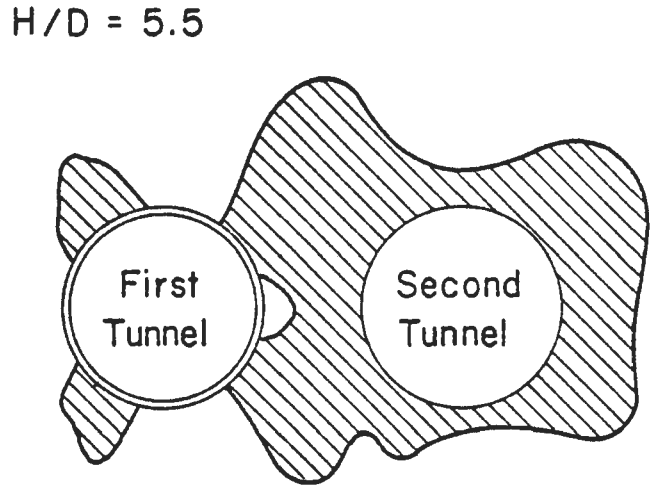

FIGURE 6.22 PLASTIC YIELD ZONE AROUND TWO TUNNELS FOR CASE B (SEE TABLE 6.1)

small in a region right next to the springline. As a result the medium did not yield at that location. The implications of the plastic yielding on the behavior of the two tunnel system will be discussed in later sections.

DISPLACEMENTS OF AN EXISTING TUNNEL DUE TO SECOND TUNNEL

The displacements of a tunnel can be separated into two components; the overall displacement of the tunnel as a rigid body; and, relative displacements or distortions of the tunnel liner shape. The overall displacement of a tunnel can be defined by the centerline shift along horizontal and vertical directions. In a single tunnel the centerline shifts upward. This upward shift is caused by an upward force resultant, due to excavation of the tunnel, which acts on the ground mass and is always present in the analysis when the weight of the medium is considered. The magnitude of this upward shift diminishes with increasing depth. The tunnel shape distortions can best be specified by two diameter change values; horizontal diameter change at springline level; and, vertical diameter change. In a single tunnel, for $K_o < 1$, the springlines tend to move outward resulting in horizontal diameter increase, but the crown and invert tend to move inward causing a vertical diameter decrease.

The passing of a second tunnel causes some additional displacement in the liner of the existing tunnel. The final displacements of the existing tunnel after the excavation of the second tunnel are given in Fig. 6.23 for two depths for the cases A and B. It can be seen from Fig. 6.23 that the excavation of the second tunnel causes some significant additional displacements in the liner of the first tunnel, especially in the region around the pillar springline of the liner. The values of the diameter change and

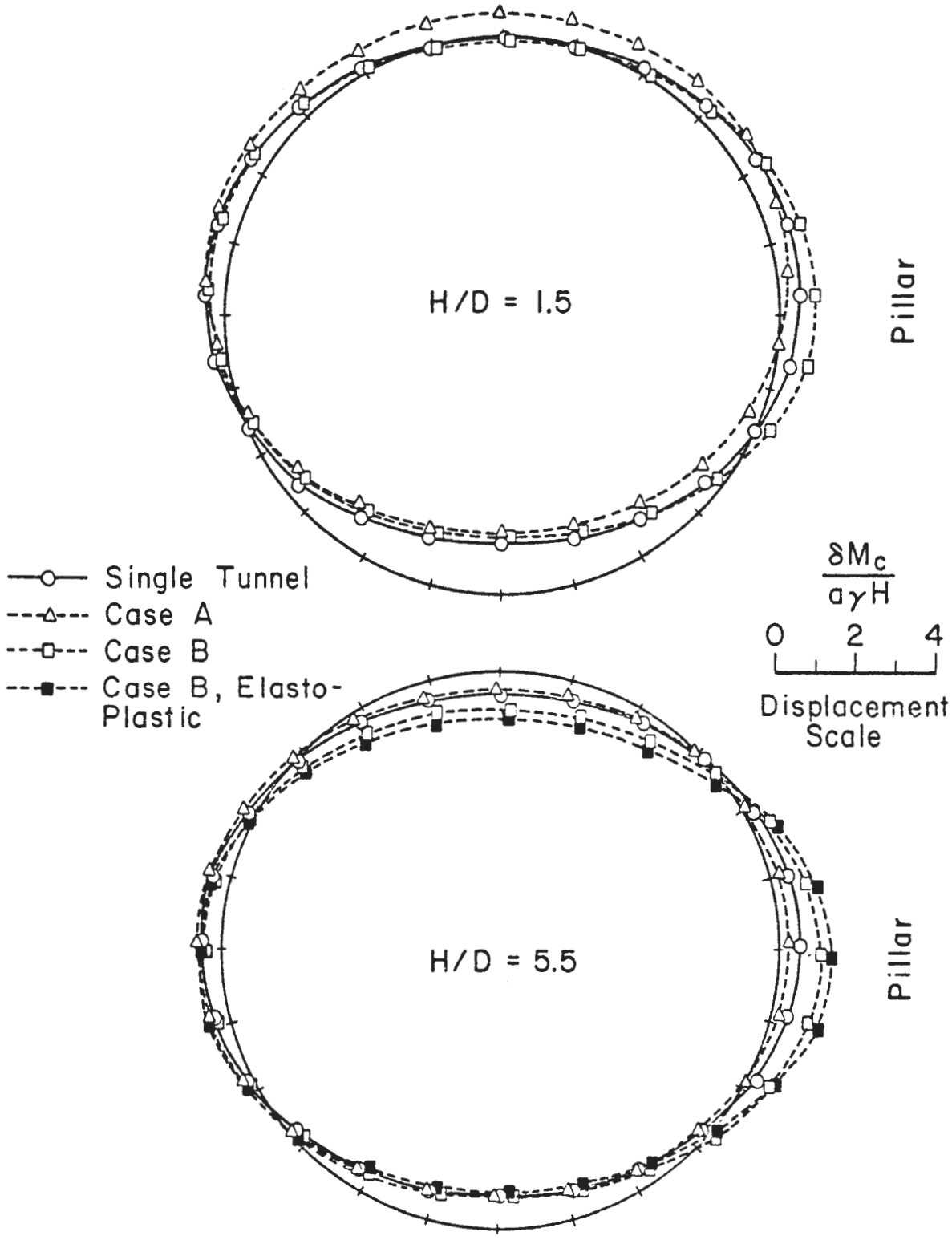

FIGURE 6.23 FINAL LINER DISPLACEMENTS OF EXISTING TUNNEL

centerline shift for the cases A and B along with the single tunnel values are given in Table 6.3. It can be seen that, relative to the single tunnel case, case B, in which the second tunnel was left unlined, produces additional displacements of opposite sign to those of case A, in which the second tunnel was lined upon excavation. Also, in case A the centerline shifts away from the pillar, but in case B the centerline shift is towards the pillar.

The additional displacements due to the second tunnel in case A tend to reduce the displacement of the existing tunnel (compare single tunnel and case A in Table 6.3) due to the fact that the second tunnel is lined upon excavation, providing lateral support to the pillar. The deformation of the pillar under the added load due to excavation of the second tunnel tends to push the existing tunnel away from the pillar and create the favorable displacement condition.

In the case B the second tunnel is left unlined after excavation, thus the pillar displaces toward the second tunnel causing additional displacements which increase the original displacements of the existing tunnel (compare case B and single tunnel in Table 6.3). This is an unfavorable displacement condition for the existing tunnel.

The displacements of the second tunnel depend on the stress increase caused by the first tunnel in the zone that the second tunnel is to be excavated in. The magnitude of these stress increases are related to the amount of medium displacements allowed during the construction of the first tunnel; the more displacements allowed in the first tunnel, the higher the stresses are in the zone through which the second tunnel is to be excavated. For this reason the second tunnel in case C shows higher displacements than the fisrt tunnel (referring to liner displacements).

TABLE 6.3

TUNNEL DISPLACEMENTS DUE TO PASSAGE OF SECOND TUNNEL

Case	H/D	Horizontal Diameter Change*	Vertical Diameter Change*	Horizontal Centerline Shift+	Vertical Centerline Shift**
Single Tunnel	1.5	1.037	-1.330	--	0.533
	5.5	1.086	-1.381	--	0.088
A	1.5	0.707	-1.015	0.112	0.979
	5.5	0.869	-1.215	0.180	0.148
B	1.5	1.344	-1.600	-0.165	0.567
	5.5	1.535	-1.803	-0.220	-0.053
	5.5#	1.910	-2.064	-0.222	-0.134

Displacements given in the form of normalized coefficients, $(\delta/a)/(\gamma H/M_c)$, where M_c = constrained modulus.

* Positive values mean diameter increase

\+ Positive values mean shift away from pillar

** Positive values mean upward shift

\# Elasto-plastic analysis

(Cases A and B are described in Table 6.1).

In summary, the magnitude and direction of the additional displacements imposed on the liner of an existing tunnel due to the excavation of an adjacent parallel tunnel strongly depend on the support conditions and the magnitude of displacements allowed in the second tunnel. The most favorable condition for the first tunnel displacements occurs in case A. However, in the analysis of this case no displacements are allowed in the second tunnel prior to ground-liner contact and this can not be expected to occur in reality. As the heading of the second tunnel advances, a certain amount of displacement does occur ahead of the heading. Any amount of additional displacements allowed during the construction of the second tunnel before the liner in this tunnel becomes effective is likely to adversely affect the liner in the existing tunnel.

CHANGES IN LINER FORCES DUE TO SECOND TUNNEL

The bending moments and thrust in the liner of the existing tunnel after excavation of the second tunnel are shown in Fig. 6.24. Also shown in this figure are the liner forces for the existing tunnel prior to excavation of the second tunnel (identical to liner forces in a single tunnel). It can be seen that the magnitudes of the bending moments and thrusts in the existing tunnel are modified by the passing of the second tunnel and that the most significant changes occur in a region around the pillar springline (PSL). Again, the magnitude of displacements in the second tunnel strongly influences the changes of liner forces in the existing tunnel. In case A, where the liner in the second tunnel restricts the medium displacements, there is a reduction of moments in the existing tunnel, whereas in case B, where the second tunnel is left unlined and no restrictions are imposed on the medium

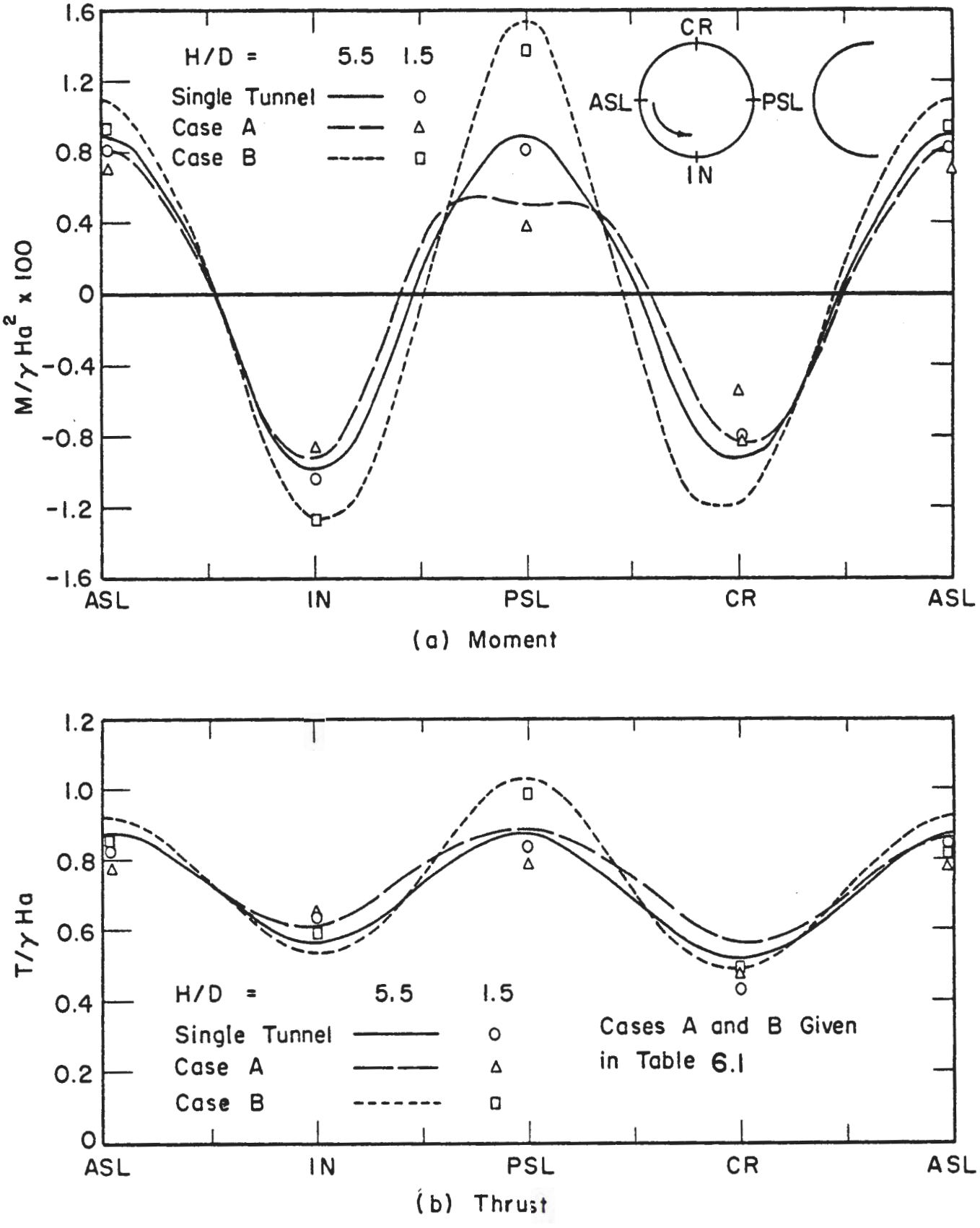

FIGURE 6.24 FINAL LINER FORCES FOR EXISTING TUNNEL

displacements, the bending moments in the pillar springline are increased by almost 70 percent and the thrust increases by 18 percent (H/D = 5.5).

The additional bending moments and thrusts in the existing tunnel due to excavation of the second tunnel are shown in Fig. 6.25 for all the cases listed in Table 6.1. For the cases C and D, the liner for the first tunnel is activated in the analysis only when the second tunnel is being excavated, therefore the only liner forces present are caused by the passage of the second tunnel and these are the values shown in Fig. 6.25. This figure clearly shows the completely opposite nature of the liner force changes in cases A and C where the second tunnel is lined as opposed to cases B and D where the second tunnel is unlined, again emphasizing the importance of the displacement control during the construction of the second tunnel.

Also shown in Fig. 6.25 are the results for case B when the medium is assigned elasto-plastic properties. This elasto-plastic analysis exhibits the same pattern of moment and thrust change as in case B with elastic properties. However, the magnitudes of the liner bending moment changes at PSL are much greater in this case; about 150 percent increase as compared with 70 percent for the elastic analysis.

The bending moments and thrusts for the second tunnel are shown in Fig. 6.26. Only in cases A and C was the second tunnel lined upon excavation. From Fig. 6.26 it can be expected that the liner forces in the second tunnel will be somewhat different than the liner forces in a single tunnel. However, the differences are small. It is also seen from this figure that the magnitude of medium displacements allowed during the excavation of the first tunnel have some influence on the expected liner forces in the second tunnel (case A as compared to case C).

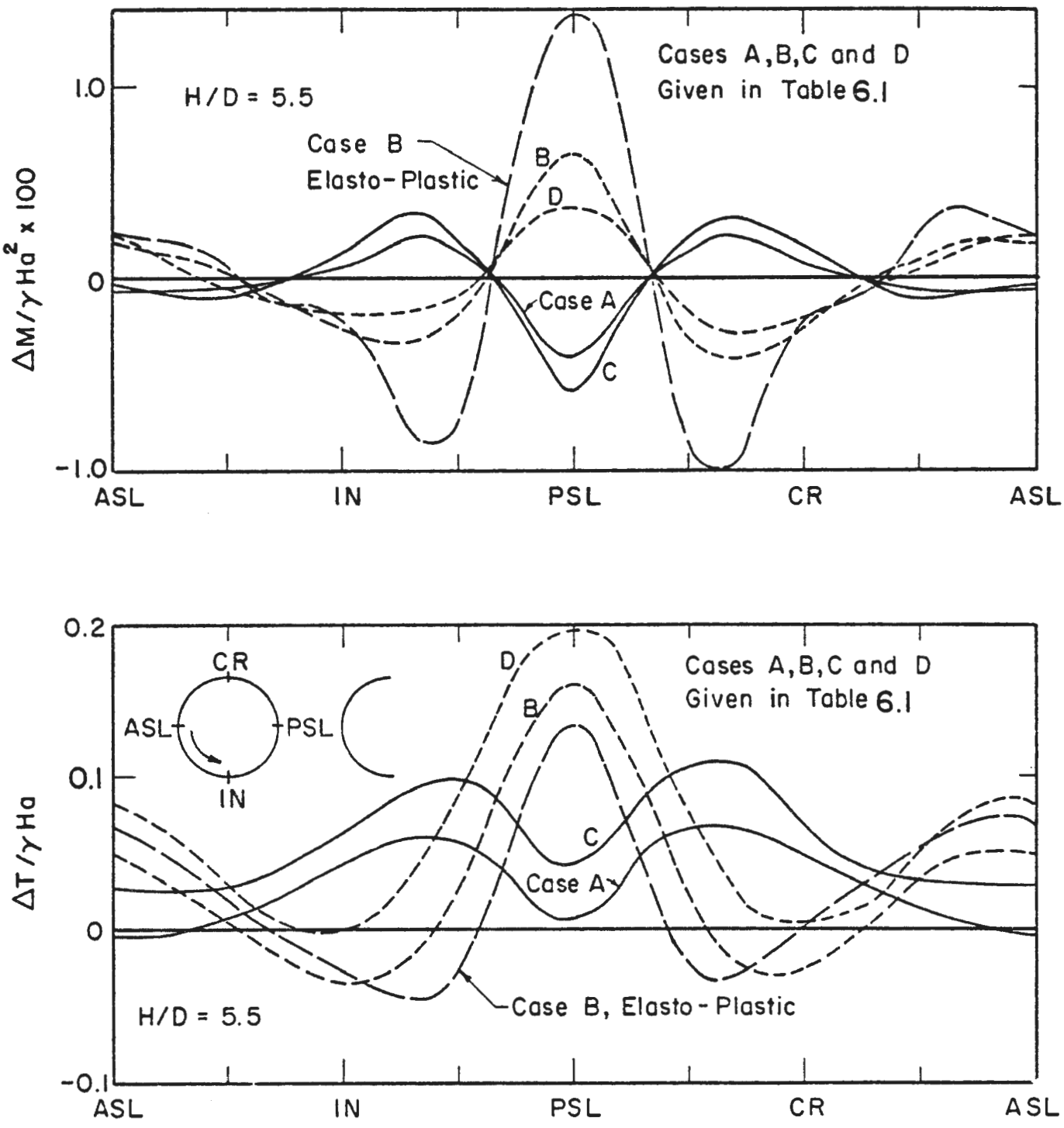

FIGURE 6.25 ADDITIONAL LINER FORCES IN EXISTING TUNNEL DUE TO EXCAVATION OF SECOND TUNNEL

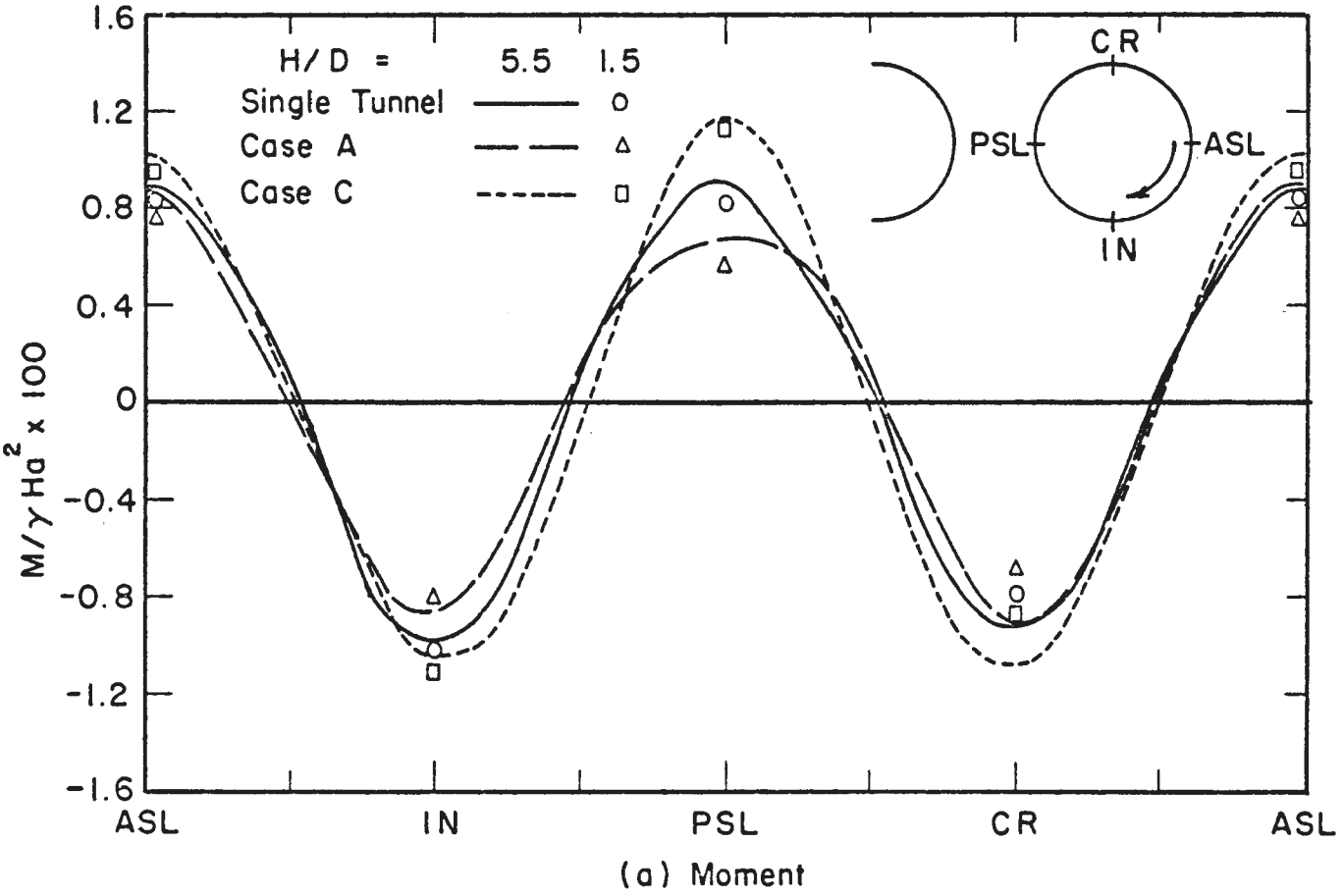

(a) Moment

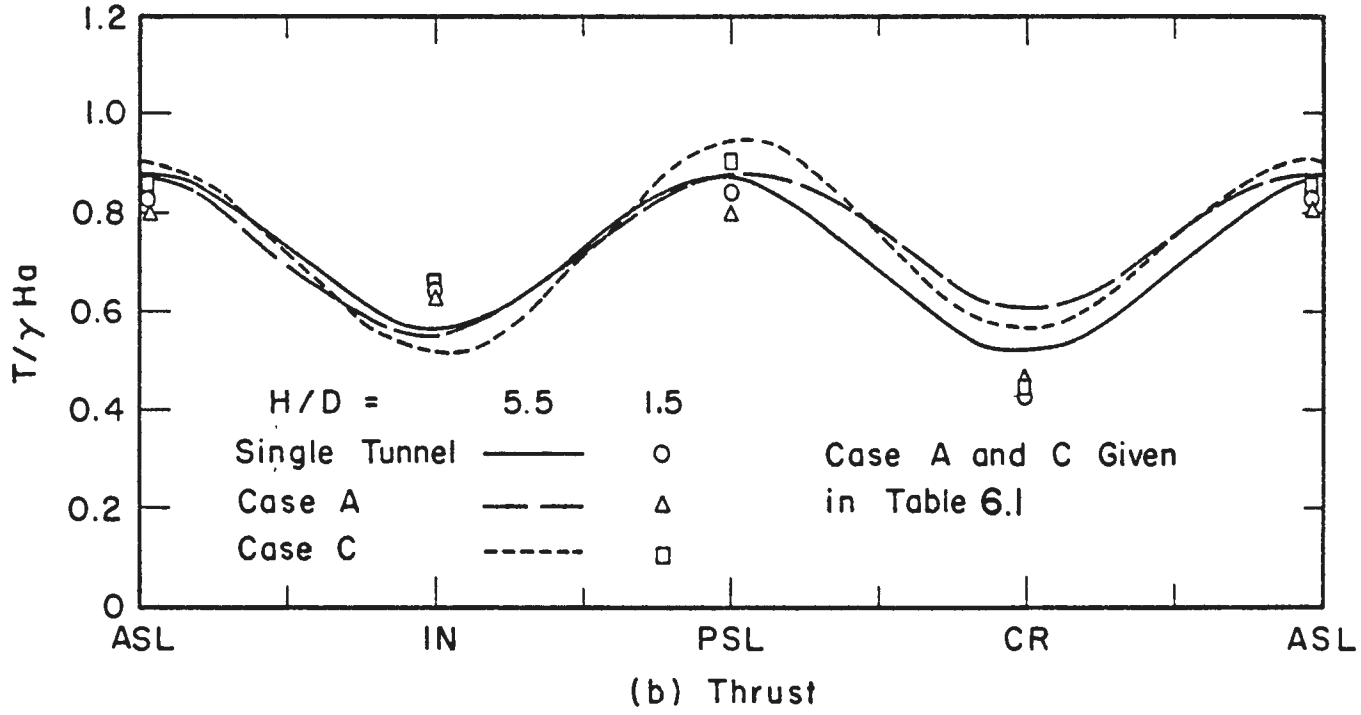

(b) Thrust

FIGURE 6.26 LINER FORCES FOR SECOND TUNNEL

SURFACE SETTLEMENTS DUE TO SECOND TUNNEL

It is generally expected that the surface displacements resulting from the excavation of the second tunnel should be somewhat greater than the surface displacements caused by a single tunnel. This can be attributed to interaction between the second tunnel and the first tunnel (primarily pillar shortening) and to the disturbance of the ground caused by excavation of the first tunnel. This disturbance takes the form of altered stresses, i.e., stress differences greater than in situ, and reduced shear strength of the ground through which the second tunnel is mined. The larger stress differences and reduced shear strength result in vertical compression of the ground on either side of the second tunnel that is greater than that for a single tunnel. Also, the displacements into the second tunnel are larger than for a single tunnel driven through undisturbed ground. The larger displacements at the tunnel level are translated into surface settlements for the second tunnel which are greater than the settlements for a single tunnel.

Most of the cases analyzed here, with the exception of case C, do not exhibit any significant amount of additional displacements of the ground surface due to excavation of the second tunnel over an equivalent single tunnel. This can be attributed to the fact that linear elastic material properties are used and, in the case of lined tunnels, the displacements that would normally occur prior to liner installation are not considered. However, when the medium is assigned elasto-plastic material properties the analysis shows that the excavation of the second tunnel causes significant additional displacements.

The surface displacements for case B with elasto-plastic material

properties are shown in Fig. 6.27. Since the first tunnel is lined, the settlement trough for this tunnel is much narrower than the settlement trough over the second tunnel, which is considered to be an unlined tunnel. The additional settlements due to the second tunnel appear to be maximum over the pillar, but fairly wide spread. The maximum settlement due to the second tunnel is 13 percent greater than the maximum settlement for a single tunnel. As the depth of the tunnels decrease the additional settlements are expected to be more concentrated over the second tunnel.

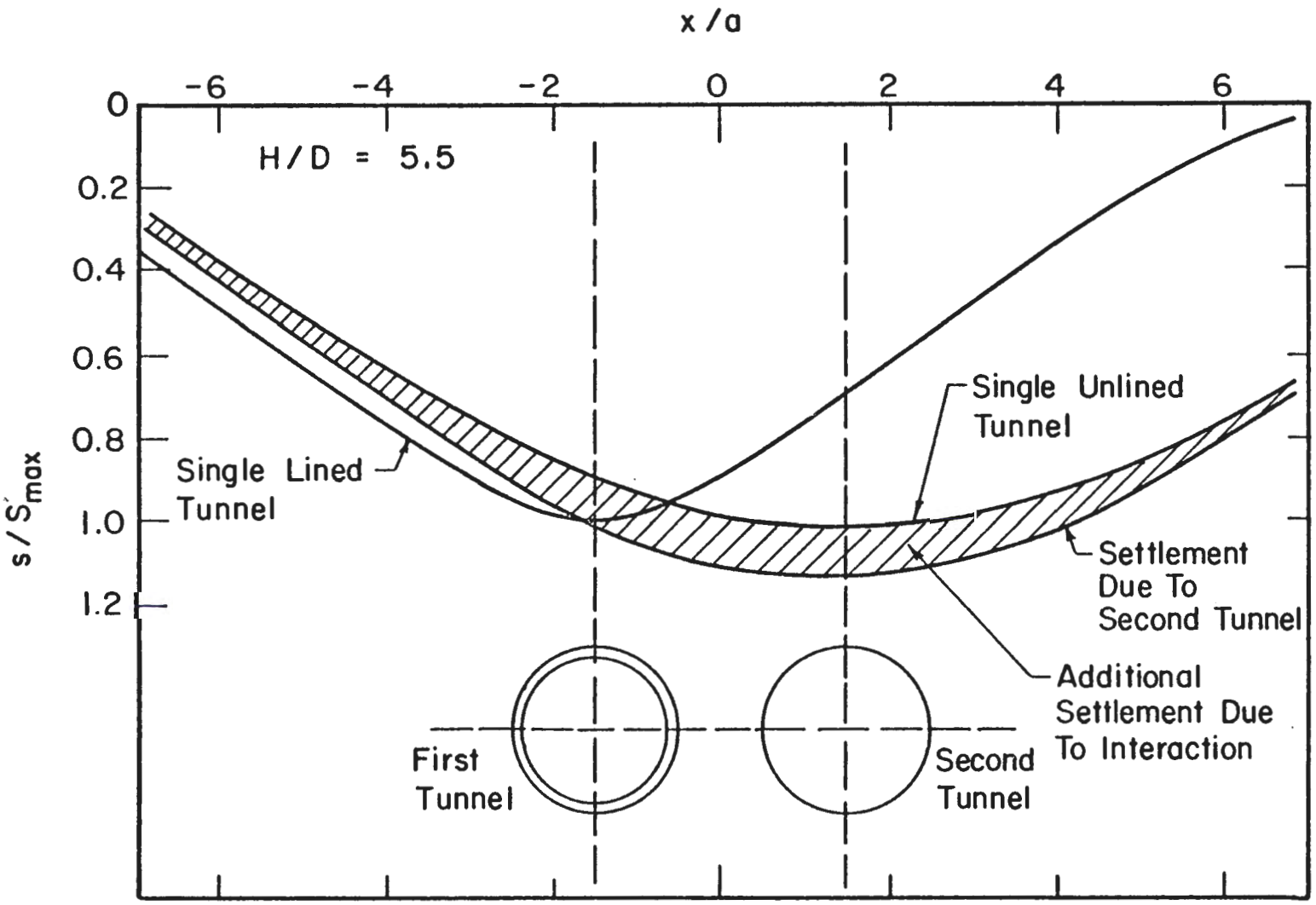

FIGURE 6.27 GROUND SURFACE SETTLEMENT TROUGHS OVER TWO TUNNELS, CASE B, ELASTO-PLASTIC (SEE TABLE 6.1)

CHAPTER 7

FINITE ELEMENT ANALYSIS OF GROUND-LINER INTERACTION FOR LOCALIZED GRAVITY LOADING

7.1 GENERAL REMARKS

If the tunnel liner does not come into contact with the surrounding ground until after all or most of the instantaneous ground displacements, of the type illustrated in Fig. 2.1 of Chapter 2, have occurred the initial pressures acting on the liner due to excavation loading will be nonexistent or very small. Such a liner can still be subjected to significant external pressures as a result of events occurring over either the short term or long term that affect the ground mass surrounding the tunnel. Such events include the passage of an adjacent parallel tunnel, additional, time-dependent inward movement of the surrounding ground mass, the application of an external pressure at the ground surface resulting in the overpressure loading condition at the tunnel level, and the development of what is called herein the localized gravity loading condition.

Following excavation the distribution of stresses in the ground mass surrounding the tunnel opening can be such that the shear strength of the soil or rock is exceeded to the extent that the force of gravity is sufficient to cause portions of the soil or rock to be dislodged and fall onto the liner. The weight of this material, which usually comes to rest on or against only a portion of the liner circumference, constitutes the localized gravity load.

The distributions and magnitudes of the external pressures applied to the liner for the localized gravity loading and excavation loading condi-

tions are quite different. Thus, it is reasonable to expect that liner responses for the two types of loading are also quite different. A liner designed for excavation loading may not be suitable for conditions that correspond more closely to those of localized gravity loading.

Presented in this chapter are the results of a finite element study of localized gravity loading induced ground-liner interaction for a circular tunnel. The objective of this research was the determination of liner response as a function of ground and liner stress-strain properties for various gravity loading distributions and a range of flexibility and compressibility ratio values. Although the results obtained are directly applicable only to the ground-liner systems and conditions analyzed, a procedure is given for estimation of liner response for other ground-liner combinations and other, more complex, loading distributions.

The results presented in the following sections of this chapter were obtained from a series of two-dimensional, plane strain, linear elastic finite element analyses of a circular tunnel. Like the analytical solutions described by Széchy (1966) and the finite element work of Dixon (1971) the analyses did not simulate the actual development of the localized gravity load on the liner. Instead, as illustrated in Fig. 2.14 of Chapter 2, the localized gravity load was modeled by applying forces to the liner elements in the finite element mesh. In this investigation of the general problem the distribution and magnitude of the load were treated as variables for study. The other variables considered were the ground-liner flexibility and compressibility ratios. Although these ratios were derived for ground and liner behavior under conditions of excavation loading and, strictly speaking, have no meaning for localized gravity loading, they provide a

convenient means for expressing the elastic stress-strain properties and dimensions of the liner and surrounding ground mass.

Initial analyses of both the full slippage and no slippage ground-liner interface conditions indicated that, in general, the full slippage condition yielded the most unfavorable distributions of liner forces and moments. Therefore, only the full slippage condition was given further consideration.

In all analyses it was assumed that the localized gravity load exerted a uniform vertical pressure over a given portion of the liner. However, it is shown that the principle of superposition can be used to obtain approximate results for nonuniform loadings. In addition, results in the form of liner thrust and bending moments are presented in chart form to allow determination of these values, by interpolation, for compressibility and flexibility ratio combinations other than those analyzed.

7.2 METHOD OF ANALYSIS

7.2.1 THE FINITE ELEMENT MESH

The finite element mesh used in this study is illustrated in Fig. 7.1. It is a circular mesh with its outer boundary completely fixed. Because the presence of the ground surface was not simulated, the influence of this boundary is not included in the results of analysis. However, due to the nature of the problem it is doubtful that the ground surface boundary would have much influence on liner response beyond that which, for shallow tunnels, affects the formation of the localized gravity load acting on the liner.

For the localized gravity loading condition, as analyzed, it is

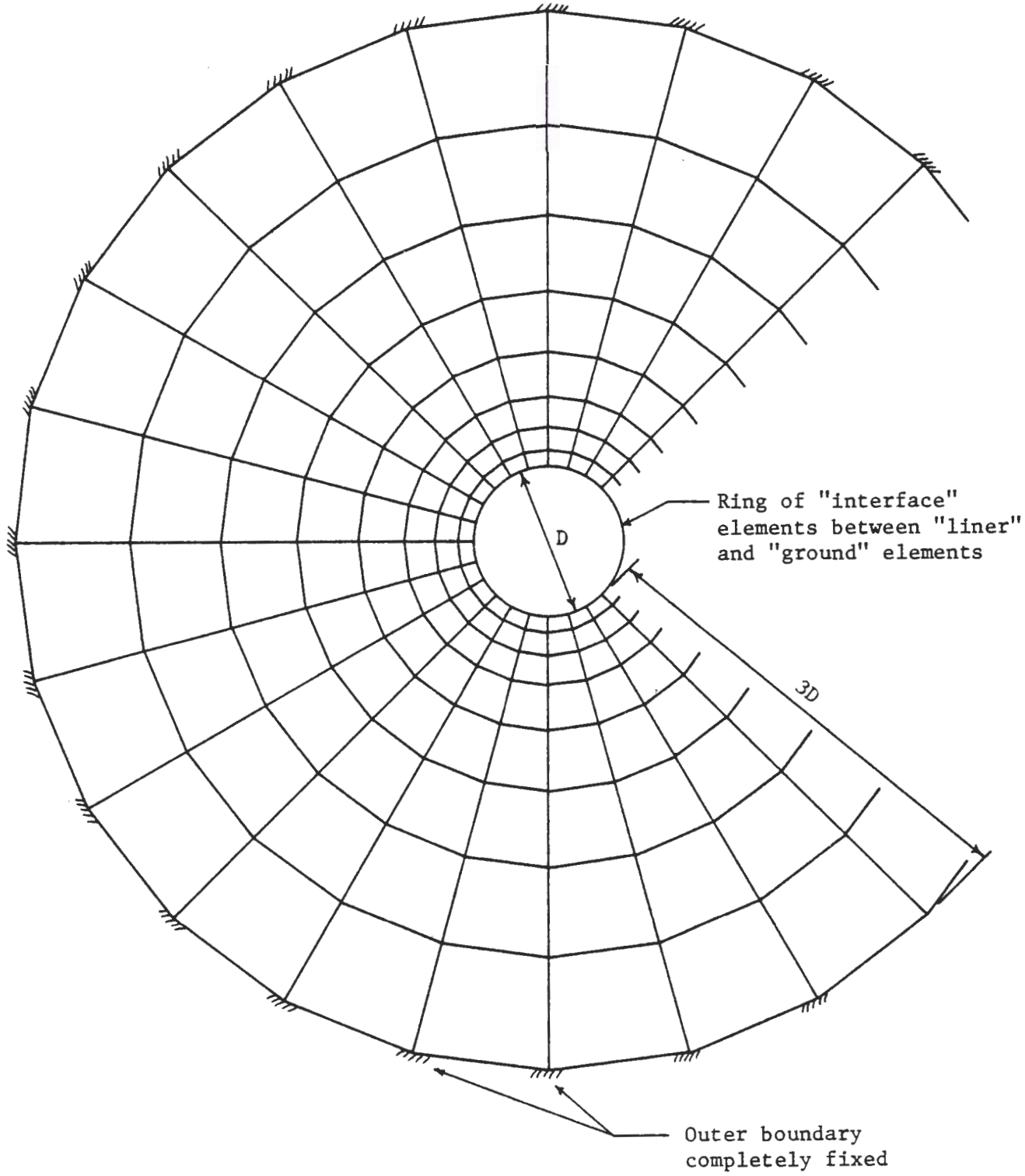

FIGURE 7.1 FINITE ELEMENT MESH FOR LOCALIZED GRAVITY LOADING ANALYSES

important that the liner be allowed to separate from the surrounding ground mass in the area of the applied load. Under actual conditions separation occurs within the ground mass above the liner. For the idealized model analyzed the mass of material resting on the liner is simulated by a distribution of forces applied to the liner elements, while the ground mass elements around the liner are left intact. Thus, separation in the model occurs at the ground-liner interface. If separation is not allowed in the analysis the applied load is carried by both the liner and the adjacent ground (in tension) instead of by the liner alone.

To insure the proper separation, and slippage condition, a special type of finite element, here called an interface element (Goodman, 1968; Ghaboussi, et al., 1973), was inserted between the liner elements and the ground elements around the perimeter of the liner. The properties of these elements can be specified so as to obtain any desired combination of normal stress-normal strain response (including zero tension) and shear stress-shear strain response (including full slippage).

7.2.2 THE GEOMETRY OF LOADING

The localized gravity load acting on a liner can be described by a set of four parameters; α, β, λ and P. The parameters α, β, and λ define the extent, position and direction of loading and P represents the magnitude of the pressure exerted on the liner by the localized gravity load. In greater detail, these parameters are defined as follows:

α = angle encompassing that portion of the liner subjected to external pressure, P

β = angle measured counter-clockwise from horizontal (right springline) to α bisector

λ = angle measured counter-clockwise from horizontal to line along which the external pressure, P, acts

P = W/A, where W is the applied force (weight) and A is the area, in plane normal to direction of loading, over which the force is applied.

These parameters are illustrated in Fig. 7.2.

In all of the finite element analyses performed it was assumed that $\beta = \lambda = 90$ degrees. That is, that the applied pressure, P, acts vertically downward and symmetrically about a vertical plane through the tunnel centerline.

Because the analyses did not consider the ground surface boundary and because it was assumed that the surrounding ground mass was homogeneous and isotropic, the results obtained from the analysis of a given loading geometry are also valid for certain other loading geometries, as illustrated in Fig. 7.3. Any number of other loading geometries (β and λ values) can be obtained from a single case analyzed by rotating the distributions of liner response obtained for that case through the appropriate angle μ. Thus, in Fig. 7.3 the liner responses at points A, A', and A", for example, are all the same. Note that rotation does not alter the value of α nor the relationship between β and λ.

7.3 RESULTS OF ANALYSIS

7.3.1 GENERAL

In this investigation of ground-liner interaction under conditions of localized gravity loading the main parameters considered were the geometry

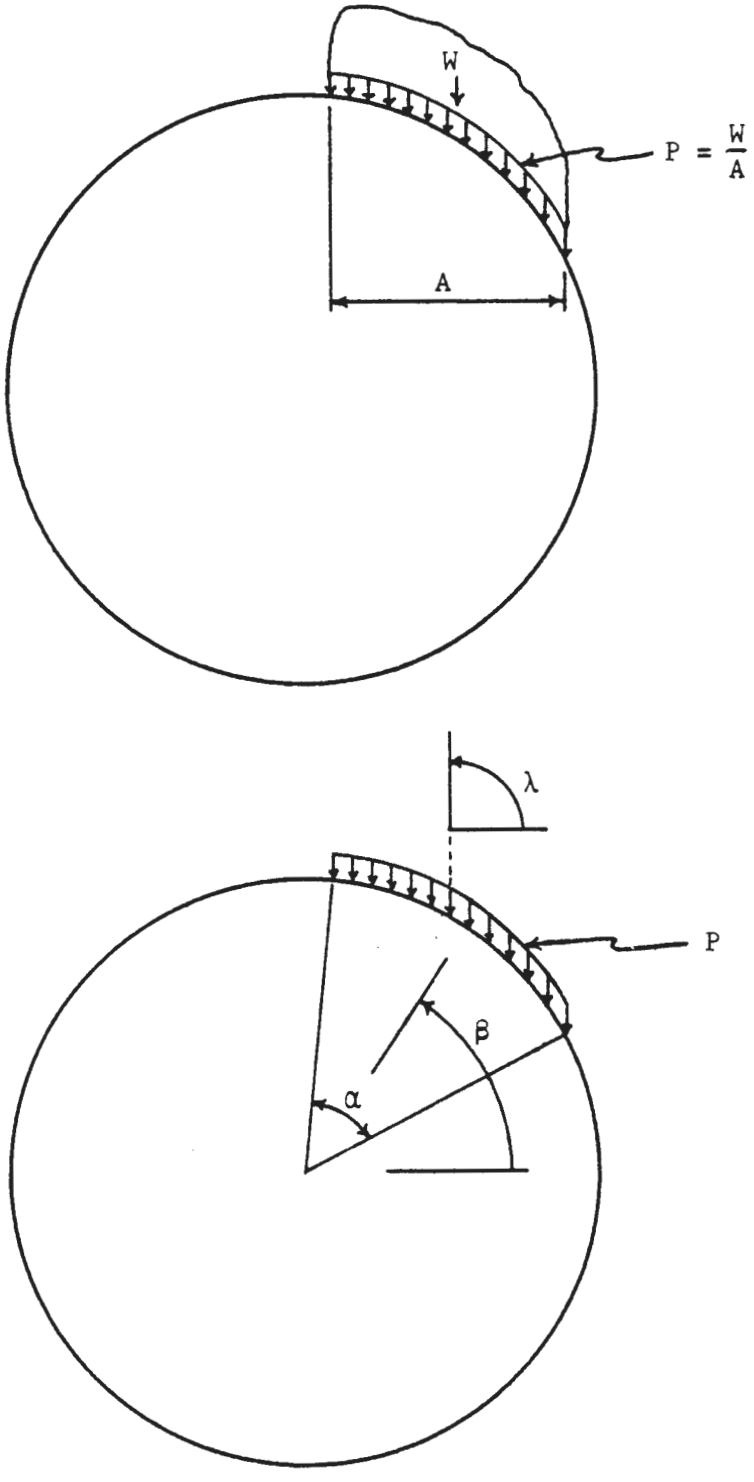

FIGURE 7.2 PARAMETERS DEFINING THE GEOMETRY OF LOADING

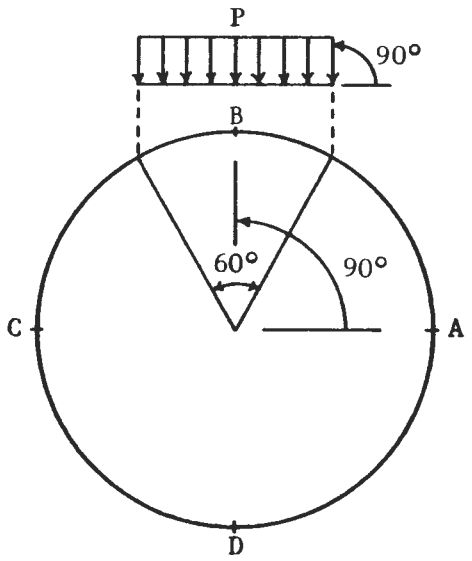

$\alpha = 60°$

$\beta = \lambda = 90°$

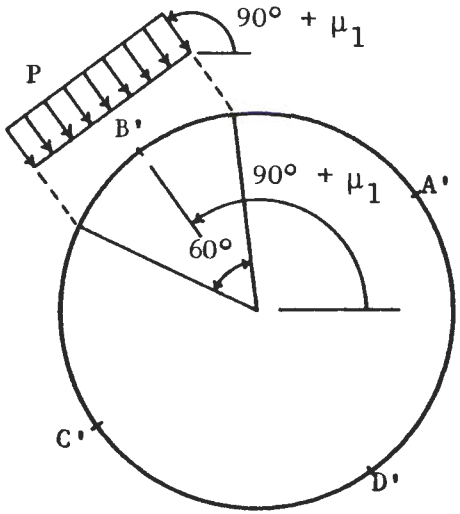

$\alpha = 60°$

$\beta = \lambda = 90° + \mu_1$

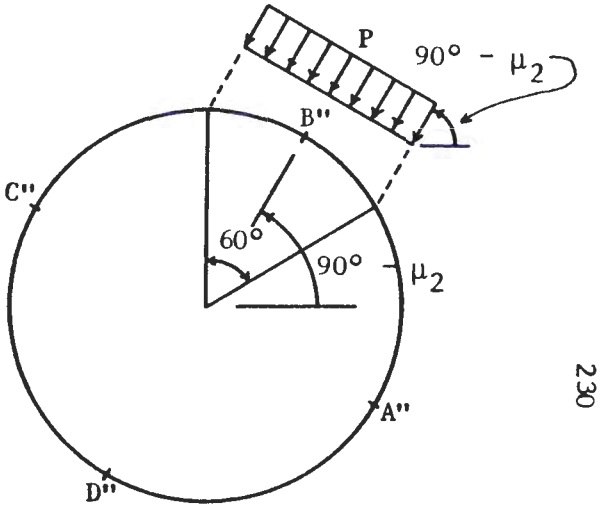

$\alpha = 60°$

$\beta = \lambda = 90° - \mu_2$

FIGURE 7.3 ILLUSTRATION OF ADDITIONAL LOADING GEOMETRIES OBTAINABLE FROM ANALYZED GEOMETRIES

of loading (principally the value of α) and the relative stiffnesses and flexibilities of the ground and liner (expressed in terms of the compressibility and flexibility ratios C and F). Four α values (α = 180, 120, 90, and 60 degrees), three C values (C = 0.04, 0.32 and 2.56), and five F values (F = 4, 16, 32, 128 and 512) were considered.

An initial series of analyses (α = 180 degrees, C = 0.32, F = 32) was performed to determine the influence of the slippage condition at the ground-liner interface on liner response; and to illustrate the diffenence between results obtained from a) analyses in which ground-liner separation in the area of loading was allowed and b) analyses in which this separation was not allowed.

Figure 7.4 illustrates the distributions of liner thrust and bending moments obtained from analyses of the full slippage and no slippage conditions. It can be seen that the full slippage condition yielded bending moments of approximately twice the magnitude of those obtained for the no slippage condition. In addition, the external shear stresses acting on the liner under the condition of no slippage resulted in liner thrusts that were greater than the full slippage values in the vicinity of the crown and less than the full slippage values everywhere else. The difference between the full and no slippage thrusts is greater at the invert than at the crown because the no slippage external shear stresses act over the entire lower half of the liner but only over a portion of the upper half due to separation of the liner from the ground mass there.

Figure 7.5 illustrates the importance of including liner separation in the analysis of localized gravity loading. In the analysis in which no separation was allowed a significant portion of the applied load was

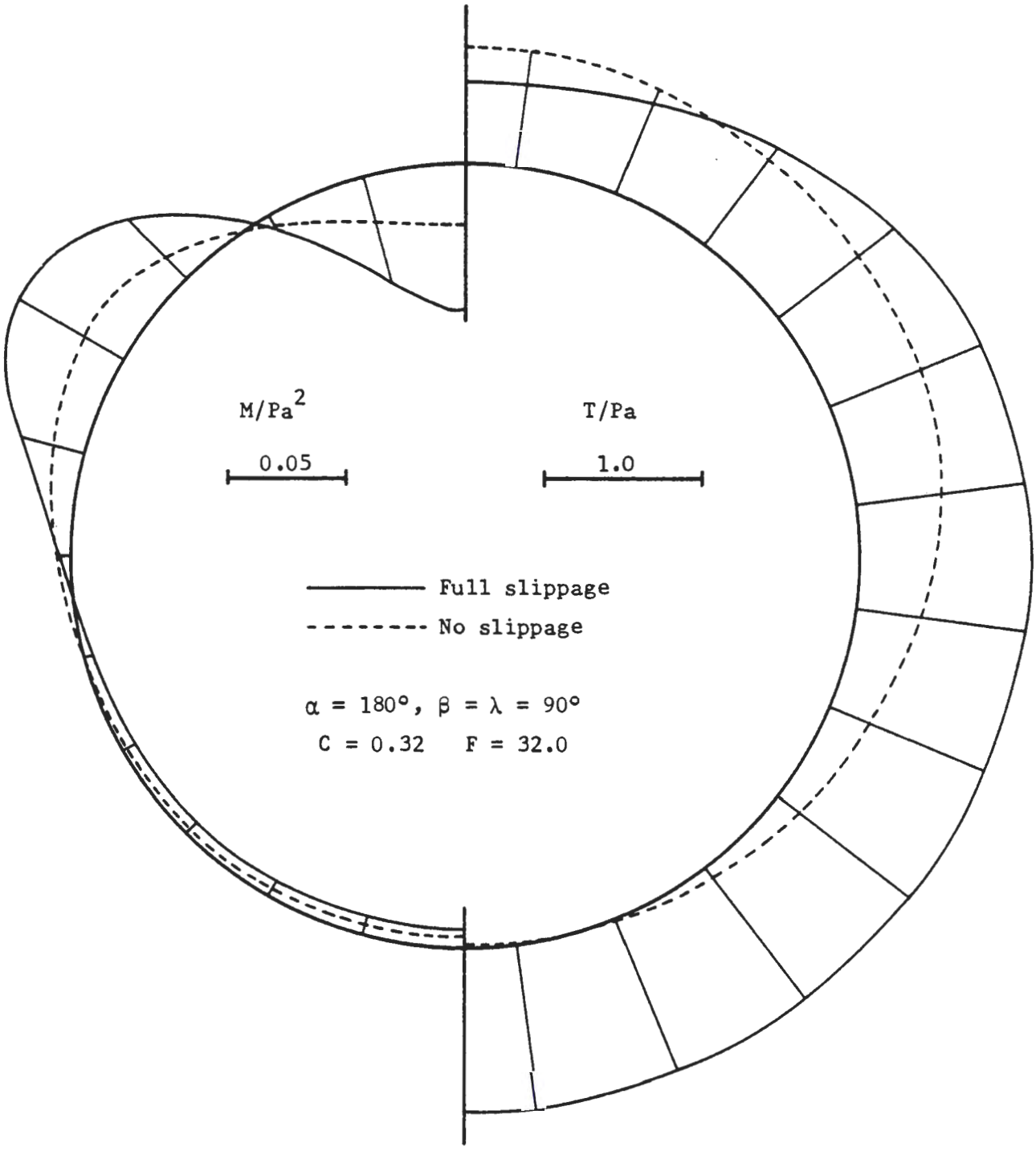

FIGURE 7.4 DISTRIBUTIONS OF LINER THRUST AND MOMENT FOR LOCALIZED GRAVITY LOADING FROM ANALYSES OF THE FULL AND NO SLIPPAGE CONDITIONS (SEPARATION ALLOWED)

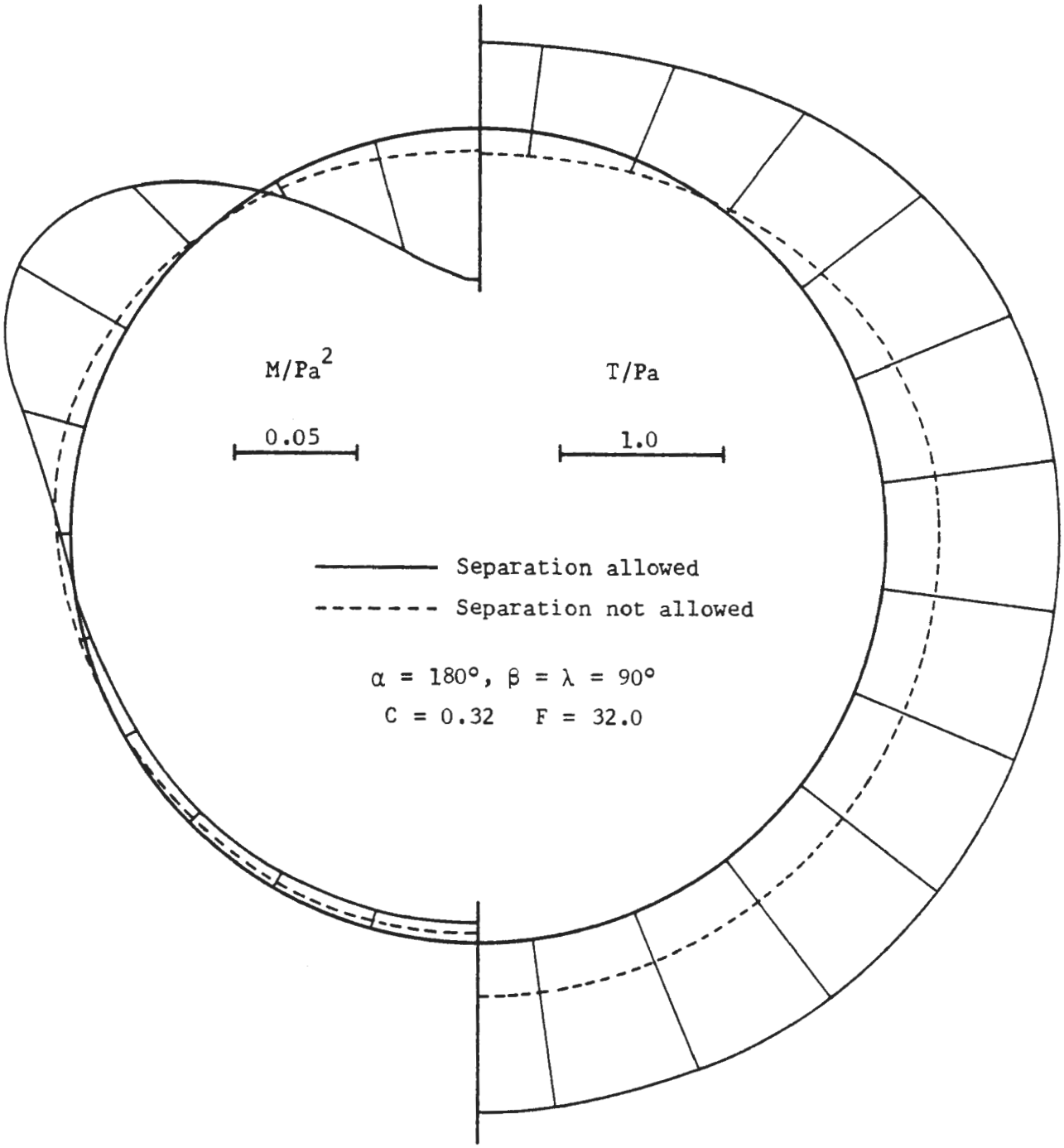

FIGURE 7.5 DISTRIBUTIONS OF LINER THRUST AND MOMENT FOR LOCALIZED GRAVITY LOADING FROM ANALYSES IN WHICH SEPARATION WAS AND WAS NOT ALLOWED (FULL SLIPPAGE)

transmitted across the ground-liner interface to the ground above the liner instead of being carried entirely by the liner, resulting in a serious underestimation of liner thrusts and bending moments.

7.3.2 VARIATION OF LINER RESPONSE WITH LOADING GEOMETRY

Distributions of liner displacements, external passive pressures (P_p), thrusts and bending moments typical of those obtained from the analyses of localized gravity loading are illustrated in Fig. 7.6.

The angular extent of liner separation from the surrounding ground mass (separation angle, Ω) is defined by that portion of the liner over which $P_p = 0$. It was found that the extent of gravity loading, i.e., the value of α, has little influence on the separation angle, which in Fig. 7.6 is approximately 2 x 60 = 120 degrees. This angular distance is much more sensitive to liner flexibility and compressibility than it is to the value of α. As liner flexibility is increased the separation angle becomes smaller. As liner compressibility is increased the separation angle becomes larger.

Because a large portion of the upper half of the liner is free of passive pressure, the smallest thrusts occur in this portion of the liner. For symmetrical loading, as considered here, the minimum thrust occurs at the crown. Because of the large displacements allowed by separation in the vicinity of the applied load, distortion of the liner shape and, thus, bending moments are quite large in this portion of the liner. The maximum bending moment occurs at the crown for symmetrical loading. Below the springlines there is little distortion of the liner shape and the distribution of passive pressure is quite uniform. Thus, in this part of the liner the bending moments are small and there is little variation of thrust magnitude.

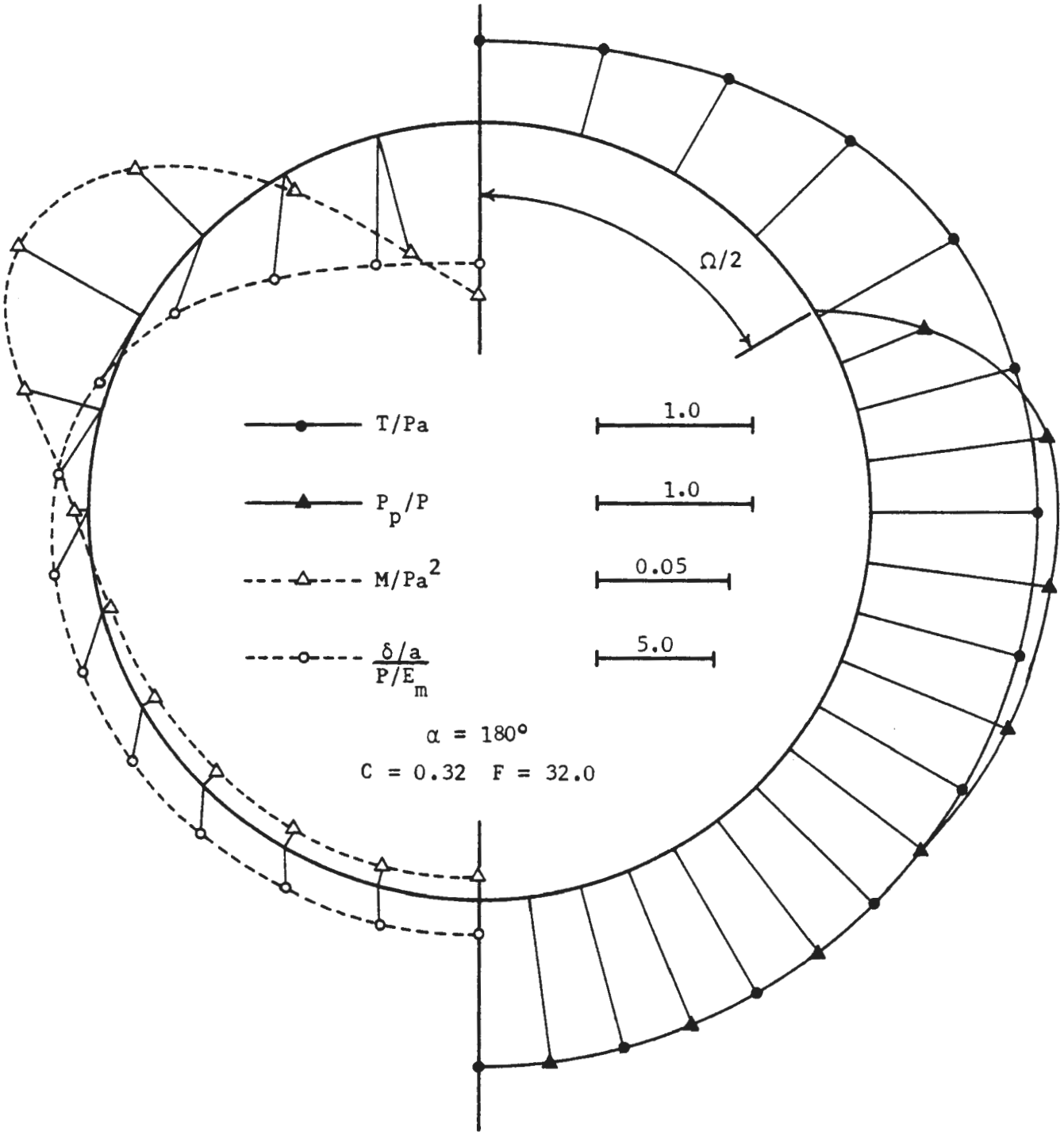

FIGURE 7.6 TYPICAL DISTRIBUTIONS OF LINER RESPONSE FOR SYMMETRICAL ($\beta = \lambda = 90°$) LOCALIZED GRAVITY LOADING

Figure 7.7 gives the thrust and bending moment distributions obtained from finite element analyses of five different α values. As shown in the figure it was found that as α was reduced from 180 degrees the maximum bending moment (located at crown) was not affected until α was reduced to less than 60 degrees. This was also found to be true for the second largest moment value. However, as α dropped below 120 degrees the location of the second largest moment (approximately 60 degrees either side of the crown for α = 180 and 120 degeees) began to shift to a position closer to the crown.

Thrust in the upper half of the liner remained essentially unchanged until α was reduced to values below 90 degrees. In contrast, in the lower half of the liner there is a much more linear relationship between the value of α (which is proportional to the total load, or weight, carried by the liner) and the thrust magnitude.

Figure 7.7 suggests that if the gravity load exerts a uniform pressure, P, over a portion of the liner, i.e., $\alpha \leq 180$ degrees, one can simply assume that α = 180 degrees and be assured the results so obtained will be conservative if, in reality, $\alpha < 180$ degrees. This approach is made especially attractive by the fact that it is often difficult to predict beforehand a true α value. However, as will be illustrated in a later section of this chapter, if the actual loading does not exert a uniform pressure on the liner, it is possible to obtain a decidedly unconservative estimate of liner response by assuming an average, uniform vertical pressure acting over 180 degrees.

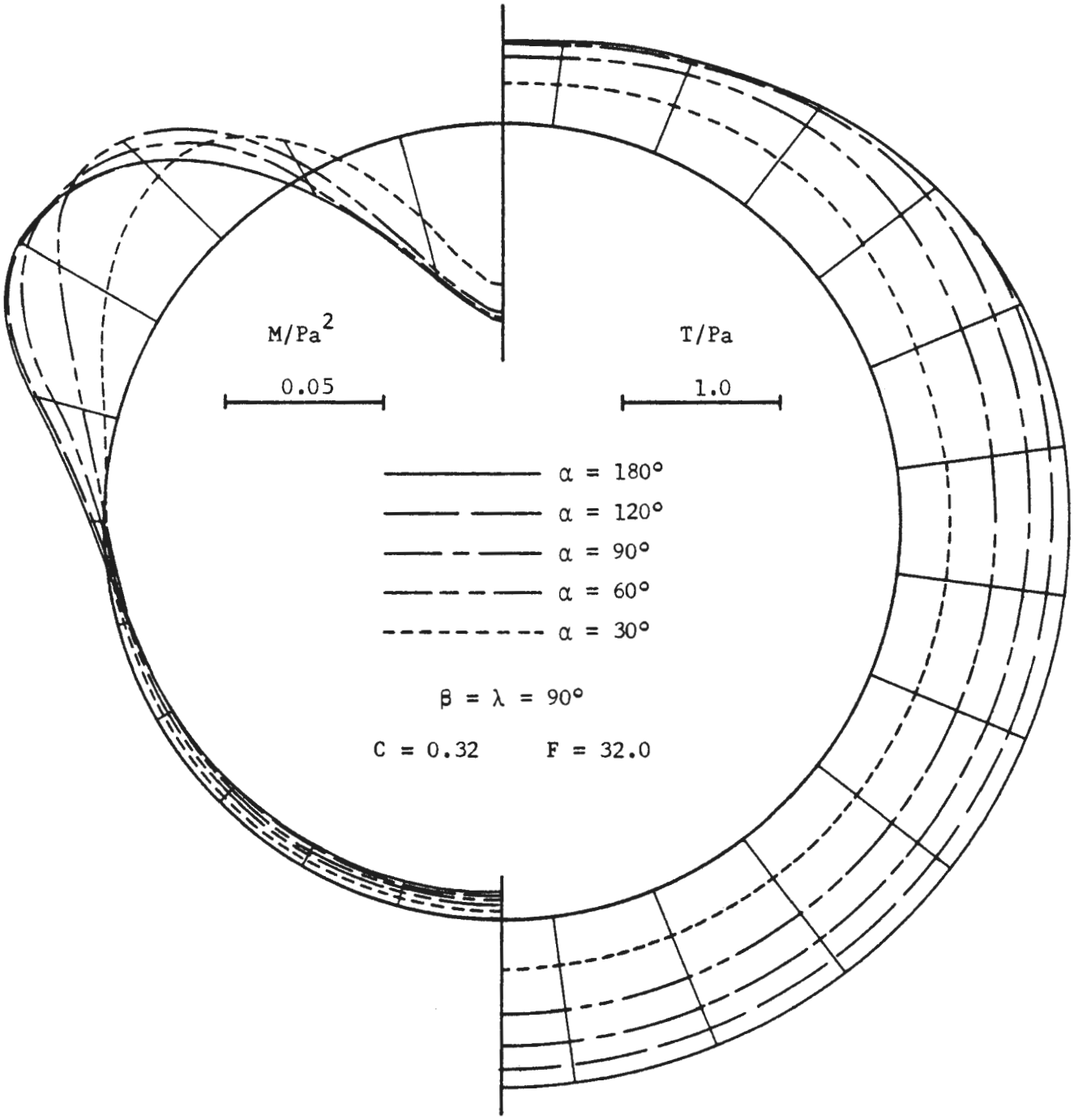

FIGURE 7.7 DISTRIBUTIONS OF LINER THRUST AND MOMENT FOR FIVE DIFFERENT α VALUES

7.3.3 VARIATION OF LINER RESPONSE WITH RELATIVE STIFFNESSES AND FLEXIBILITIES OF LINER AND GROUND

Figure 7.8 illustrates the variation of liner thrust and bending moments with flexibility ratio (for three different compressibility ratios) as determined from the finite element analyses. The curves given are for α = 180 degrees. Curves for the other α values (120, 90 and 60 degrees) are quite similar to those for α = 180 degrees and, therefore, are not shown. As indicated in the figure, the maximum thrust is located at or near the springlines, the minimum thrust is located at the crown, and the maximum bending moment occurs at the crown. The curves for C = 2.56 are not extended below F = 10 because it is highly unlikely that a ground-liner system having a compressibility ratio of 2.56 would have a flexibility ratio smaller than ten.

Figure 7.8 indicates that both crown and springline thrusts increase with increasing flexibility ratio and decrease with increasing compressibility ratio. The maximum bending moment, on the other hand, decreases with increasing flexibility ratio and increases with increasing compressibility ratio.

The variations of thrust and moment with the flexibility and compressibility ratios, F and C, are related to the variation with C and F of the passive pressures acting on the liner. If C is held constant and F is increased the separation angle, Ω, decreases. The more uniform distribution of external pressures (P_p and P) results in smaller bending moments. Also, the additional passive pressures acting above the springlines increase the crown and springline thrusts. If F is held constant and C is increased the separation angle increases. This leads to a less uniform distribution of external pressures and thus to larger bending moments. The reduction of

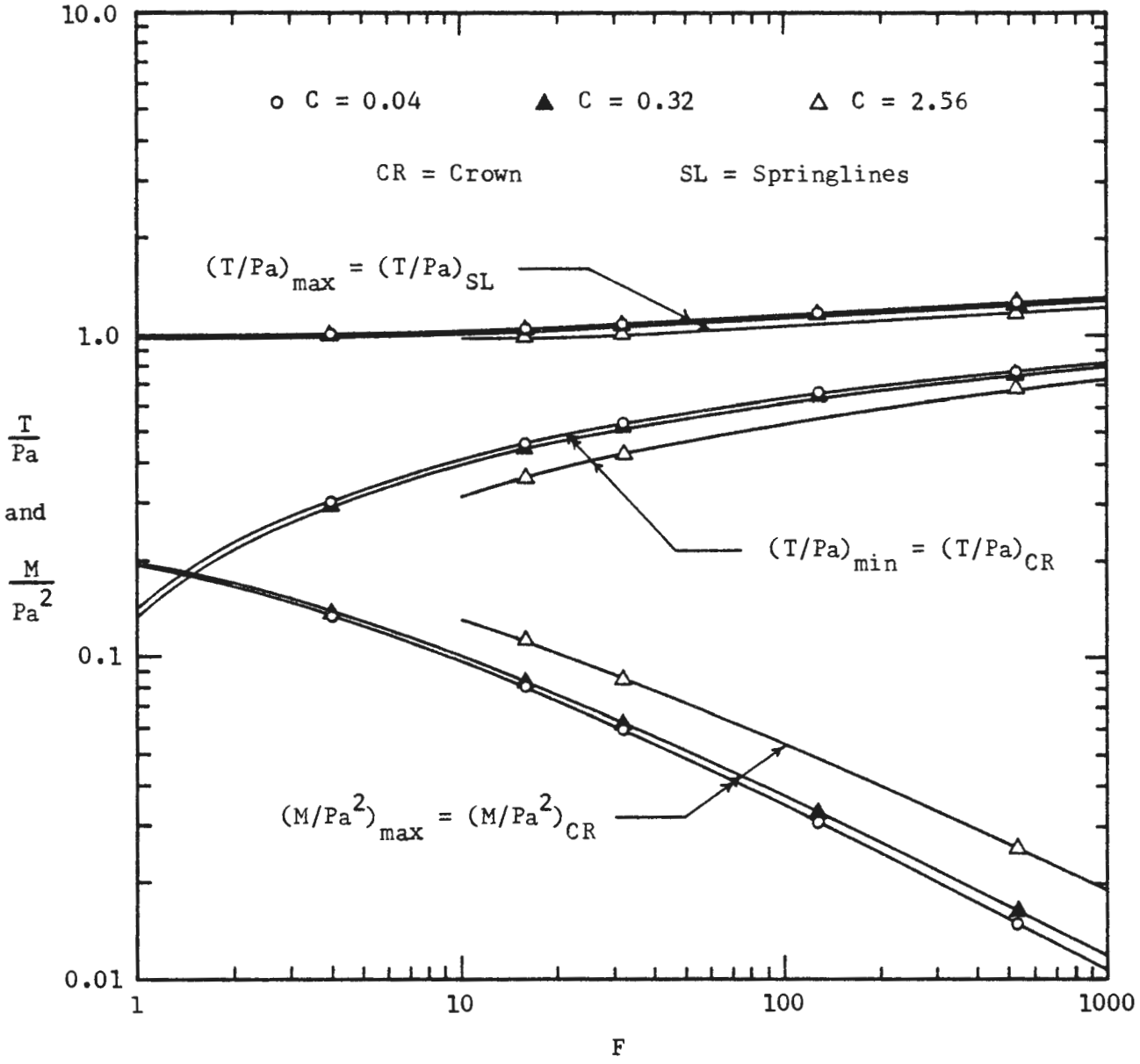

FIGURE 7.8 VARIATION OF LINER THRUST AND MOMENT WITH FLEXIBILITY AND COMPRESSIBILITY RATIOS (α = 180°)

passive pressures acting above the springlines is reflected in smaller crown and springline thrusts.

Figure 7.9 gives the variation of the vertical and horizontal diameter changes with F and C for α = 180 degrees. For relatively inflexible liners the horizontal and vertical diameter changes are nearly equal, especially if the liner is also relatively incompressible. However, for flexible liners the vertical diameter change is much larger than the horizontal.

The vertical diameter change increases with both increasing F and increasing C and is much more sensitive to the compressibility ratio than are the thrusts and moments. The horizontal diameter change increases with increasing flexibility ratio and decreases slightly with increasing compressibility ratio.

7.4 DISCUSSION OF RESULTS

7.4.1 PROCEDURE FOR ESTIMATING THRUST AND MOMENT

In the finite element study of ground-liner interaction for localized gravity loading reported herein distributions of liner thrusts and bending moments were obtained for a limited number of compressibility and flexibility ratio combinations. On the basis of this data a procedure was formulated for estimating liner thrusts and moments for any combination of C and F values within the ranges: $0.01 \leq C \leq 3.0$ and $1 \leq F \leq 1000$. With this procedure it is possible to estimate liner thrusts and moments at 24 locations (every 15 degrees) around the circumference of the liner for any of four different α values (α = 180, 120, 90 and 60 degrees). This procedure requires the use of the equations, tables, and charts given in the remaining pages of this section.

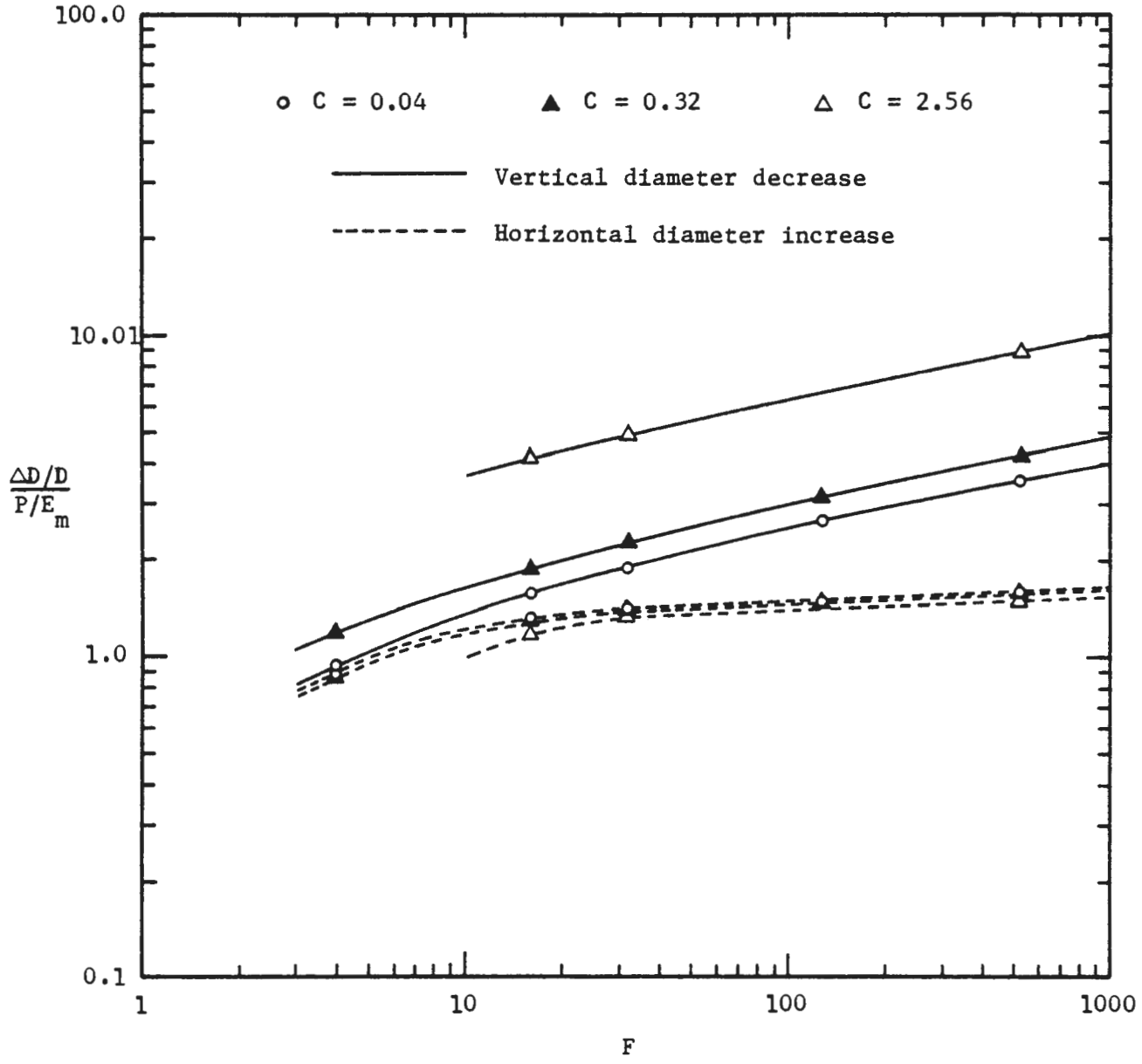

FIGURE 7.9 VARIATION OF VERTICAL AND HORIZONTAL DIAMETER CHANGES WITH FLEXIBILITY AND COMPRESSIBILITY RATIOS ($\alpha = 180^{\circ}$)

LINER THRUST

Liner thrusts are obtained from the following equation:

$$(T/Pa)_{i,j} = (B_t)_{i,j} \cdot (F'_t)_{i,j} - m_i C^{1.11} \qquad (7.1)$$

where,

T/Pa = thrust coefficient

B_t = base value of (T/Pa), given in Table 7.2

F'_t = factor required to account for liner flexibility, given in Figs. 7.10 through 7.13

C = compressibility ratio

m = factor required to account for loading geometry, given in Table 7.1

i = number from 1 to 4 specifying value being considered ($i = 1$, $\alpha = 180°$; $i = 2$, $\alpha = 120°$; $i = 3$, $\alpha = 90°$; $i = 4$, $\alpha = 60°$)

j = number from 1 to 13 specifying location of point around liner circumference being considered (points located every 15°; j = 1 = crown, j = 7 = springline, j = 13 = invert; points 14 through 24 are not necessary because the loading considered is symmetrical)

TABLE 7.1

VALUES OF m FOR USE IN EQUATION 7.1

i	α (degrees)	m
1	180	0.035
2	120	0.033
3	90	0.028
4	60	0.021

TABLE 7.2

BASE VALUES OF THE THRUST COEFFICIENT FOR USE IN EQUATION 7.1

j	$(B_t)_{1,j}$ $\alpha = 180°$	$(B_t)_{2,j}$ $\alpha = 120°$	$(B_t)_{3,j}$ $\alpha = 90°$	$(B_t)_{4,j}$ $\alpha = 60°$
1	.540	.540	.520	.440
2	.582	.582	.563	.483
3	.712	.712	.700	.621
4	.872	.872	.849	.671
5	1.015	.997	.873	.653
6	1.068	.989	.833	.653
7	1.084	.964	.817	.619
8	1.083	.960	.815	.615
9	1.080	.957	.814	.614
10	1.079	.957	.813	.613
11	1.078	.957	.812	.613
12	1.077	.957	.811	.613
13	1.076	.957	.810	.613

LINER BENDING MOMENTS

Liner bending moments are obtained from the following equation:

$$(M/Pa^2)_{i,j} = (M_f)_{i,j} + (3.53C^{1.11}) \cdot (M_{cf})_{i,j} \qquad (7.2)$$

where,

(M/Pa^2) = moment coefficient

M_f = moment coefficient as a function of flexibility ratio only, given in Figs. 7.14 through 7.17

M_{cf} = factor required to account for liner compressibility, given in Figs. 7.18 through 7.21.

Equations 7.1 and 7.2 and the associated tables and charts yield only approximate results because, 1) they are based on a limited amount of data and 2) they express the variation of thrust and moment with F and C in a somewhat simplified manner. However, as long as their use is confined to the ranges of C and F values previously given, these equations will yield thrust and moment values that fall within a few percentage points of the values obtained from finite element analyses of the type performed in this investigation.

7.4.2 LINER THRUSTS AND MOMENTS FOR NONUNIFORM LOCALIZED GRAVITY LOADING

By superposing the results from two or more loading geometries (uniform pressure) it is possible to estimate the distributions of liner thrusts and bending moments for localized gravity loads that result in nonuniform distributions of active pressure on the liner. If the pressures exerted on the liner by each of the loads to be superposed are not the same

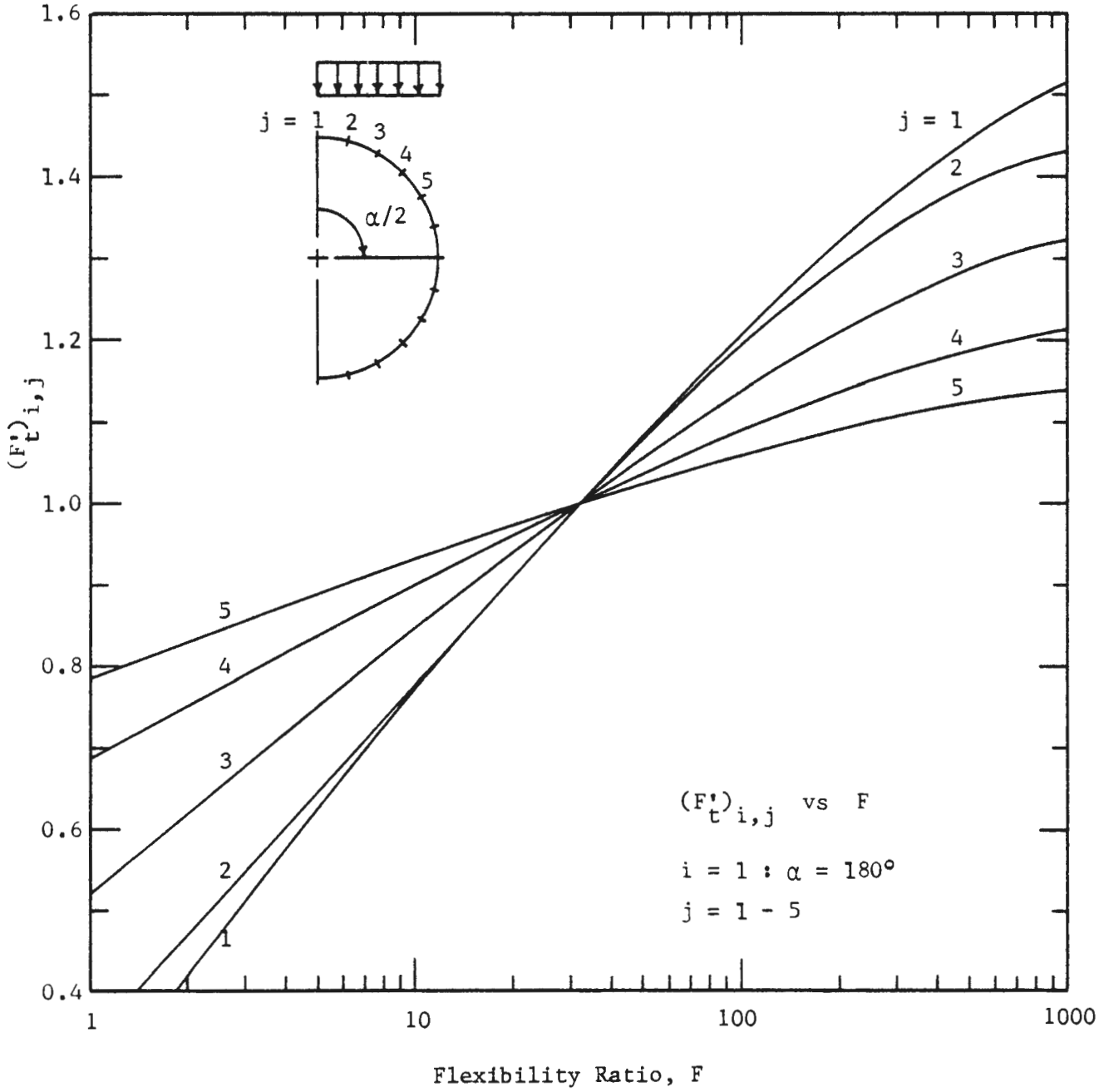

FIGURE 7.10a F'_t VERSUS FLEXIBILITY RATIO FOR $\alpha = 180°$ (j = 1 - 5)

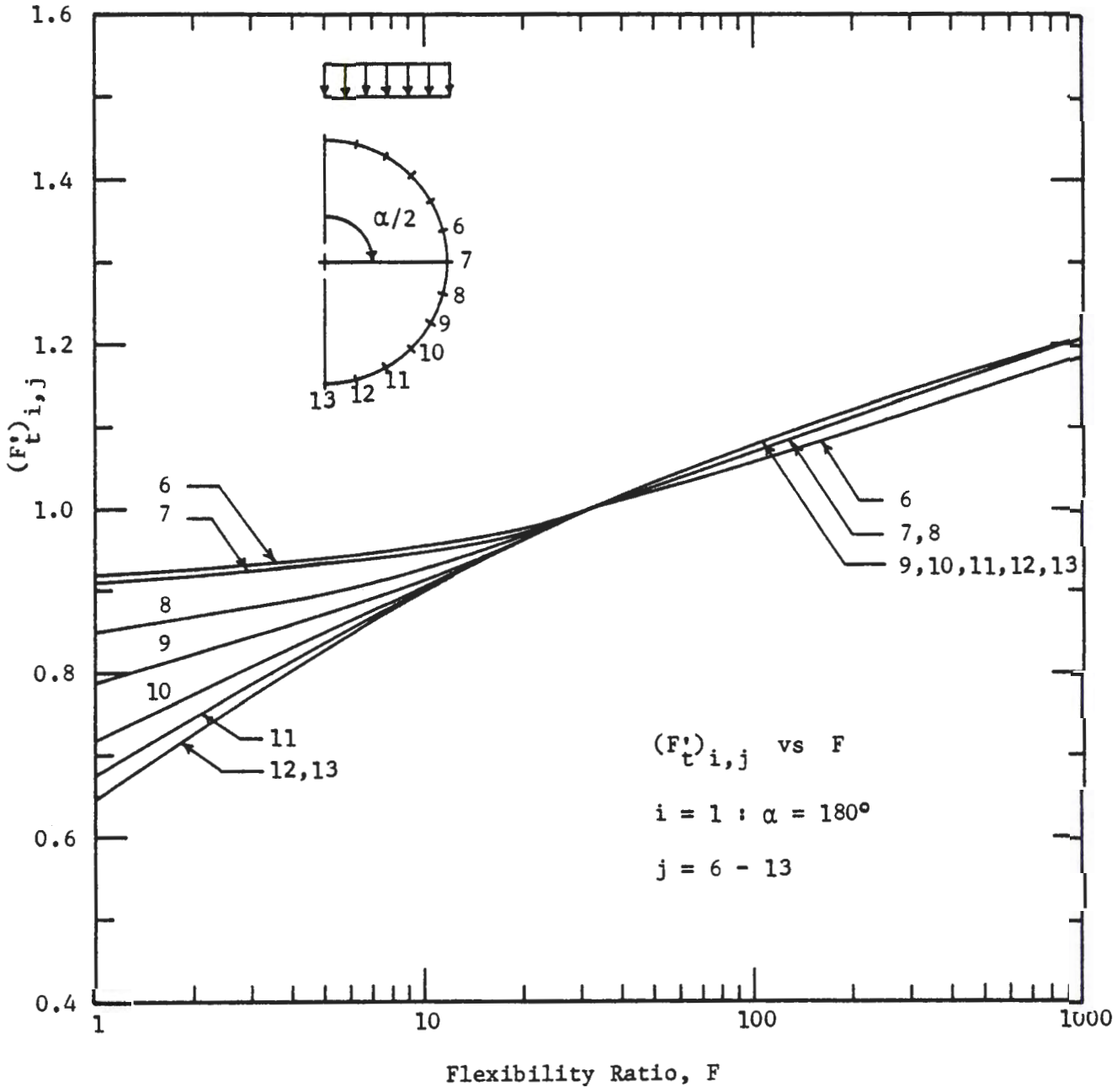

FIGURE 7.10b F'_t VERSUS FLEXIBILITY RATIO FOR α = 180° (j = 6 - 13)

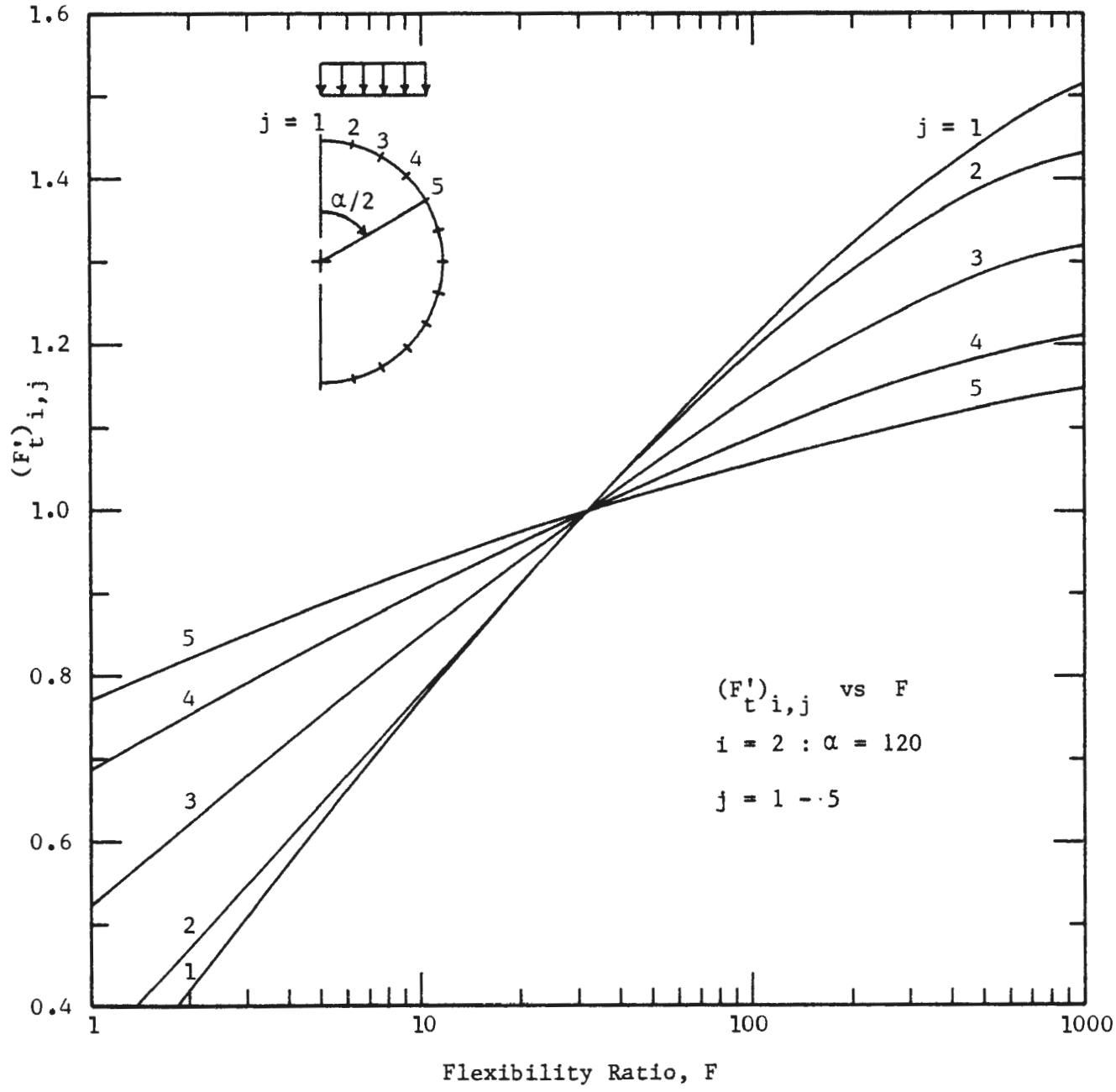

FIGURE 7.11a F'_t VERSUS FLEXIBILITY RATIO FOR $\alpha = 120°$ (j = 1 - 5)

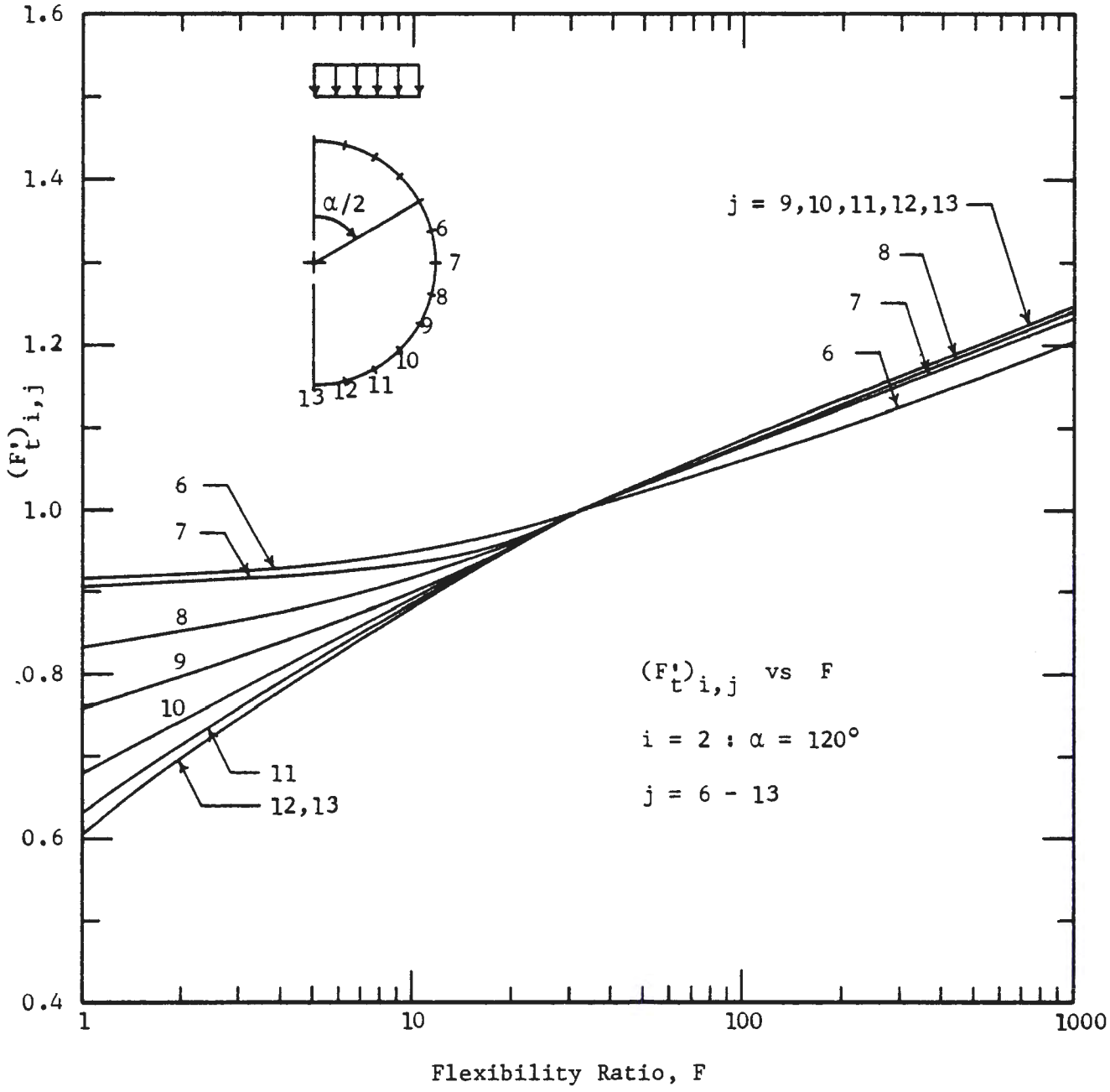

FIGURE 7.11b F'_t VERSUS FLEXIBILITY RATIO FOR $\alpha = 120°$ (j = 6 - 13)

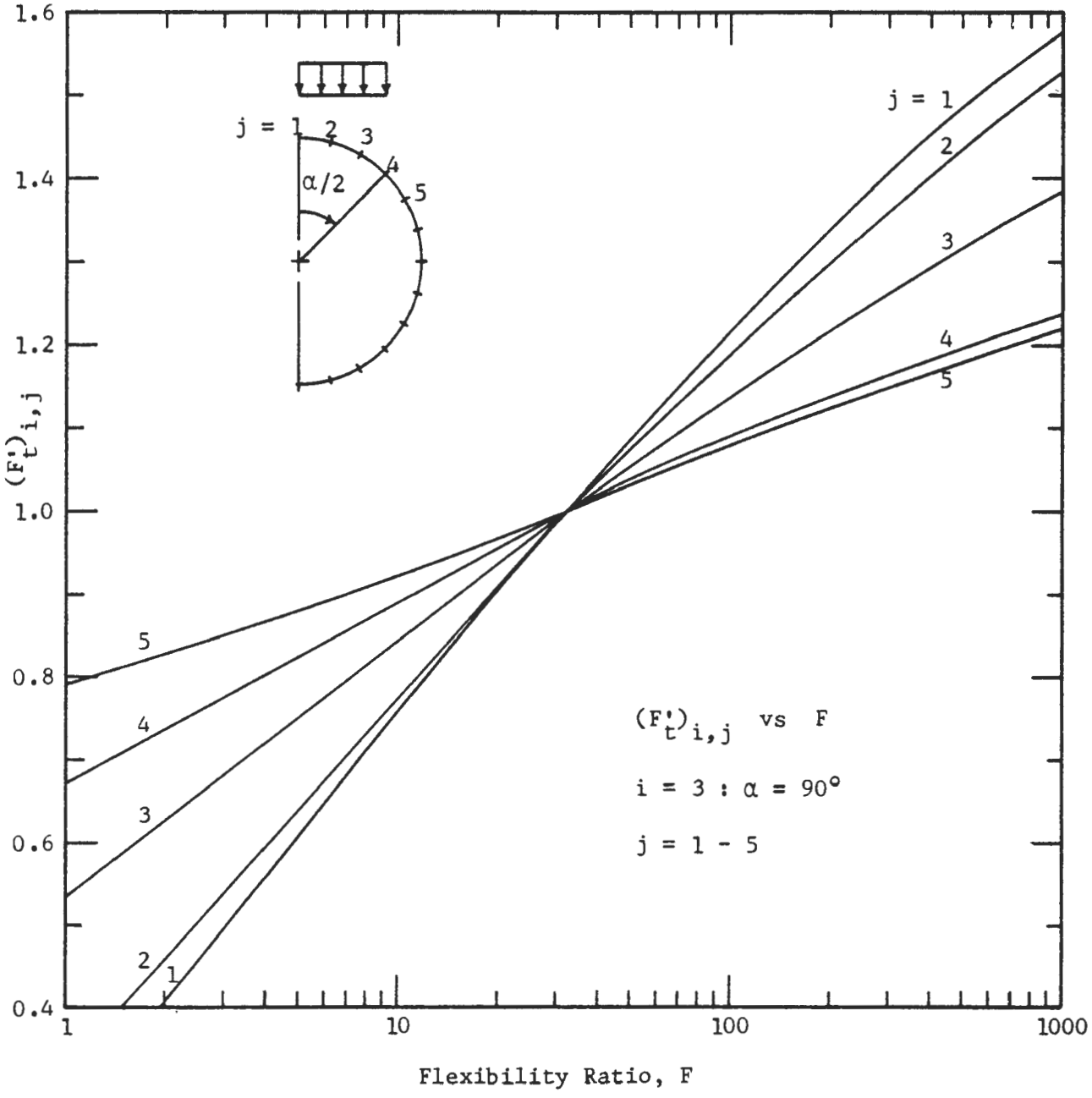

FIGURE 7.12a F'_t VERSUS FLEXIBILITY RATIO FOR $\alpha = 90°$ (j = 1 - 5)

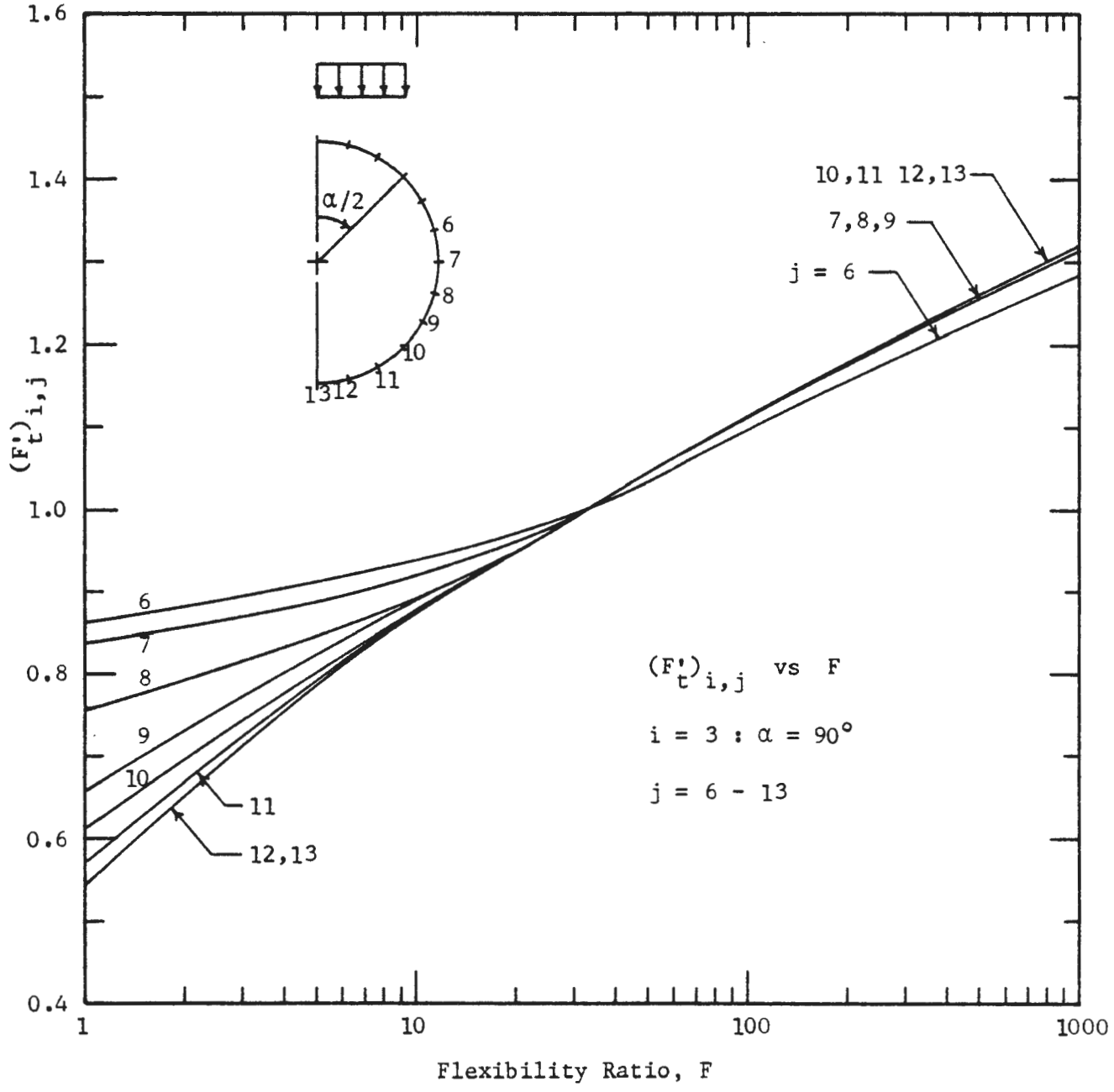

FIGURE 7.12b F'_t VERSUS FLEXIBILITY RATIO FOR $\alpha = 90°$ (j = 6 - 13)

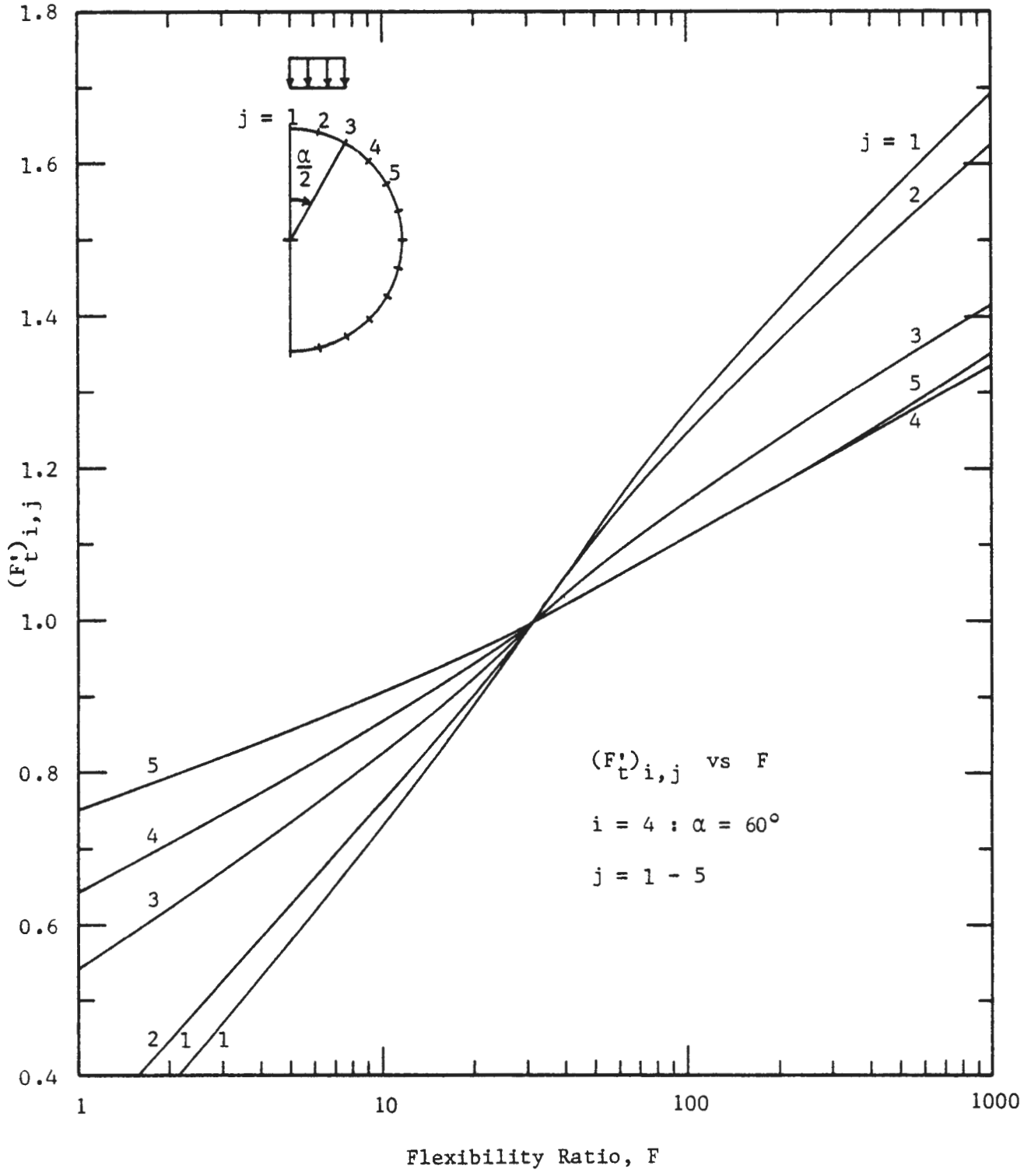

FIGURE 7.13a F'_t VERSUS FLEXIBILITY RATIO FOR $\alpha = 60°$ (j = 1 - 5)

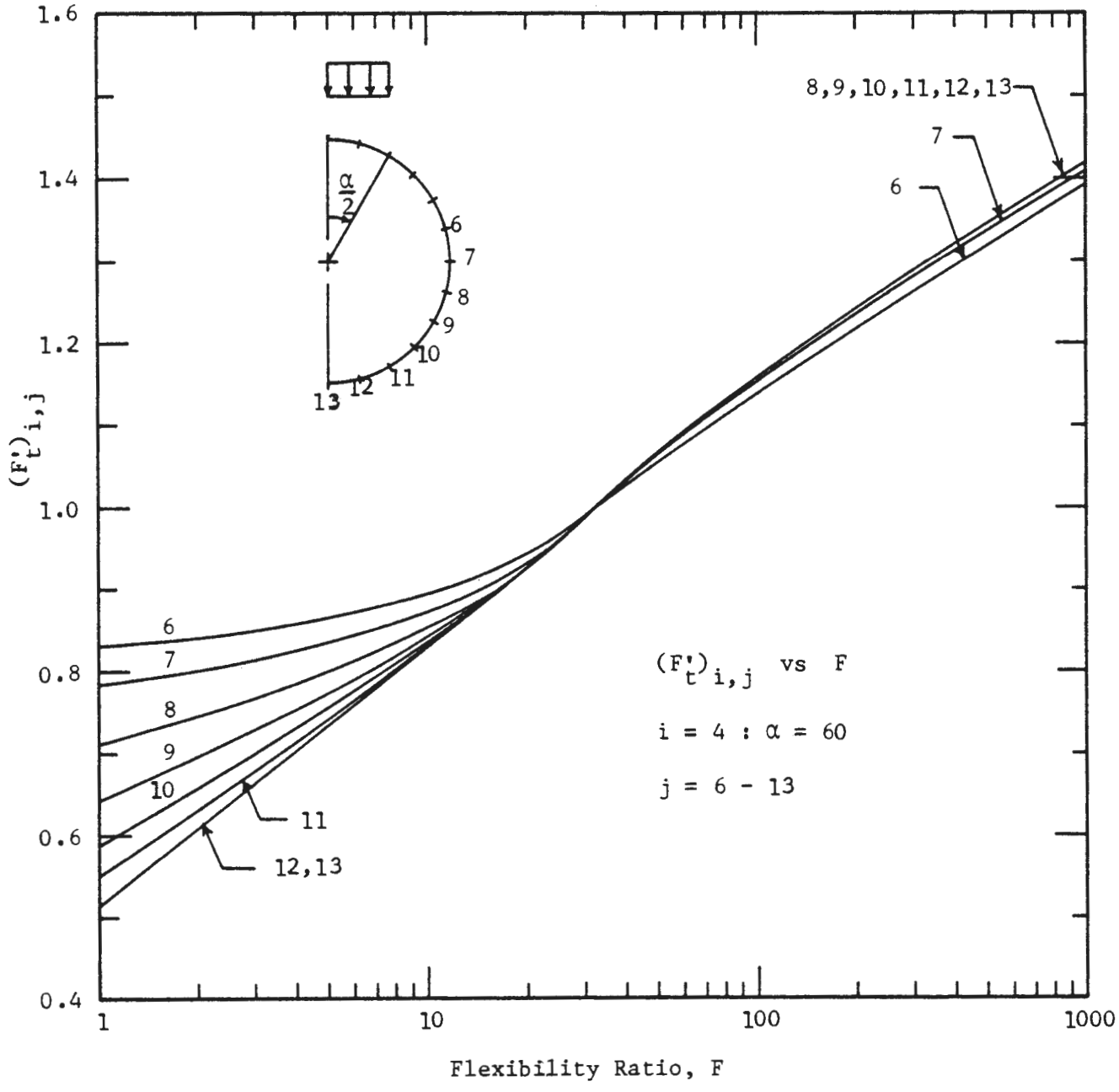

FIGURE 7.13b F'_t VERSUS FLEXIBILITY RATIO FOR $\alpha = 60°$ (j = 6 - 13)

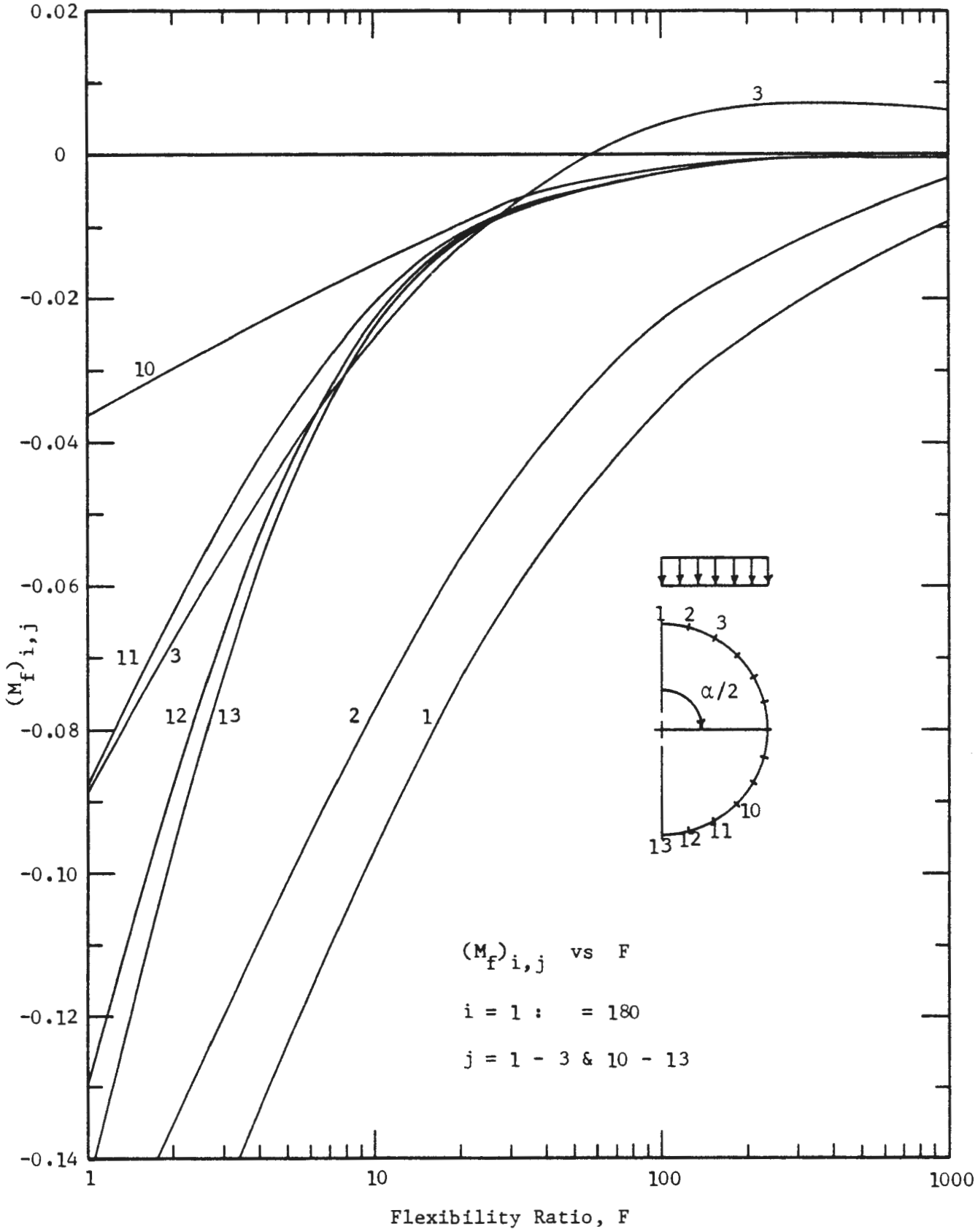

FIGURE 7.14a M_f VERSUS FLEXIBILITY RATIO FOR $\alpha = 180°$ (j = 1 - 3 AND 10 - 13)

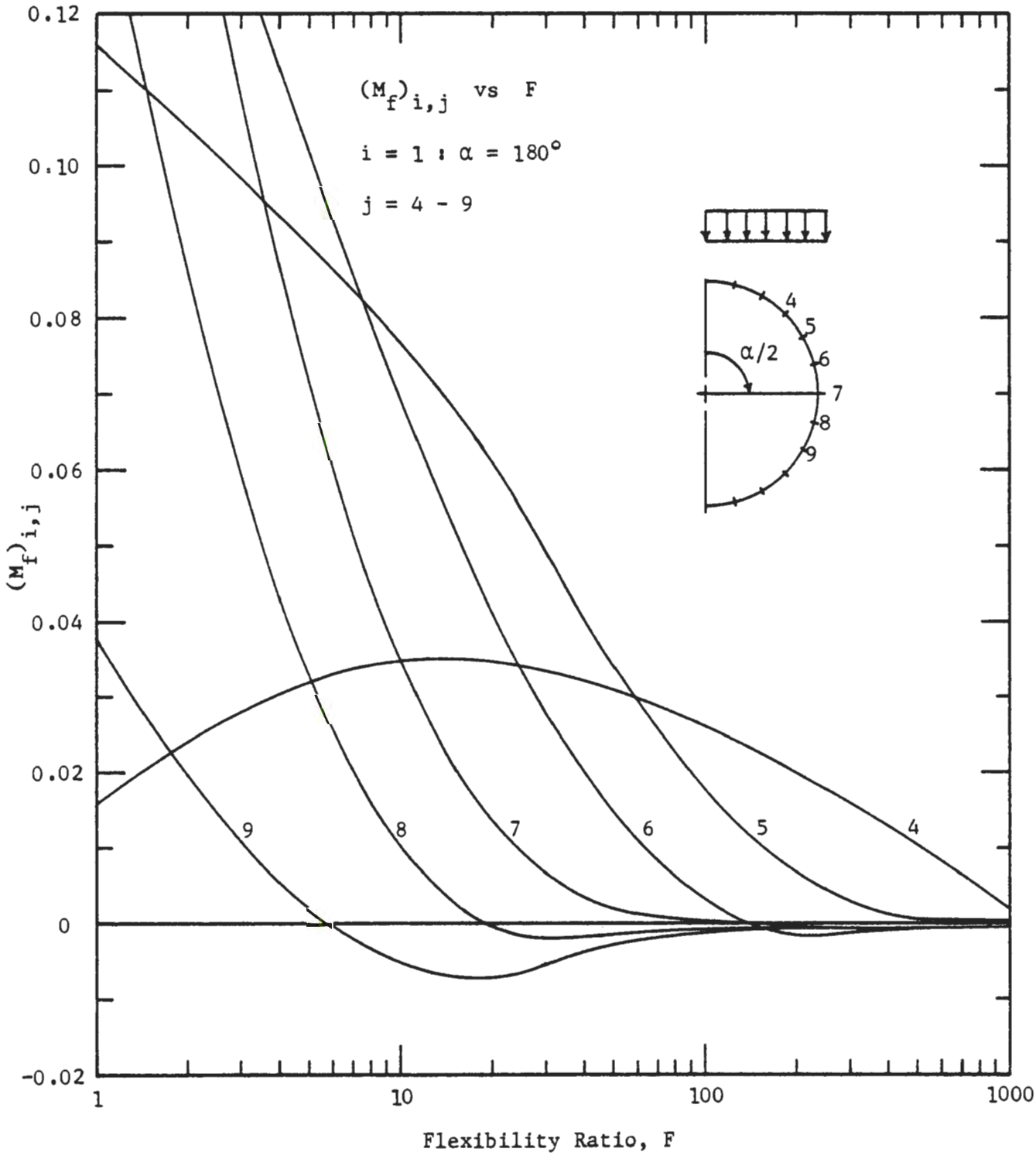

FIGURE 7.14b M_f VERSUS FLEXIBILITY RATIO FOR α = 180° (j = 4 - 9)

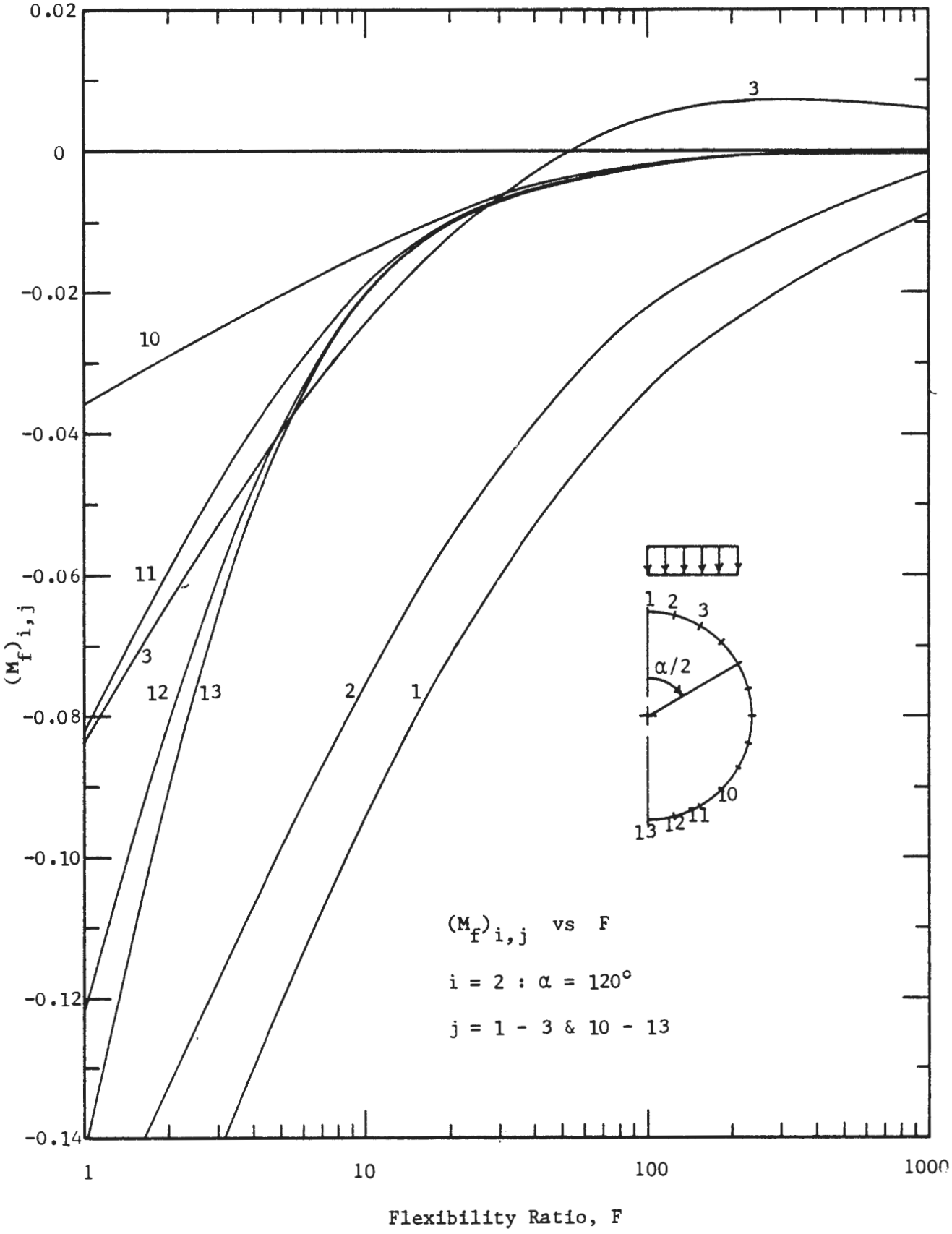

FIGURE 7.15a M_f VERSUS FLEXIBILITY RATIO FOR $\alpha = 120°$ (j = 1 - 3 AND 10 - 13)

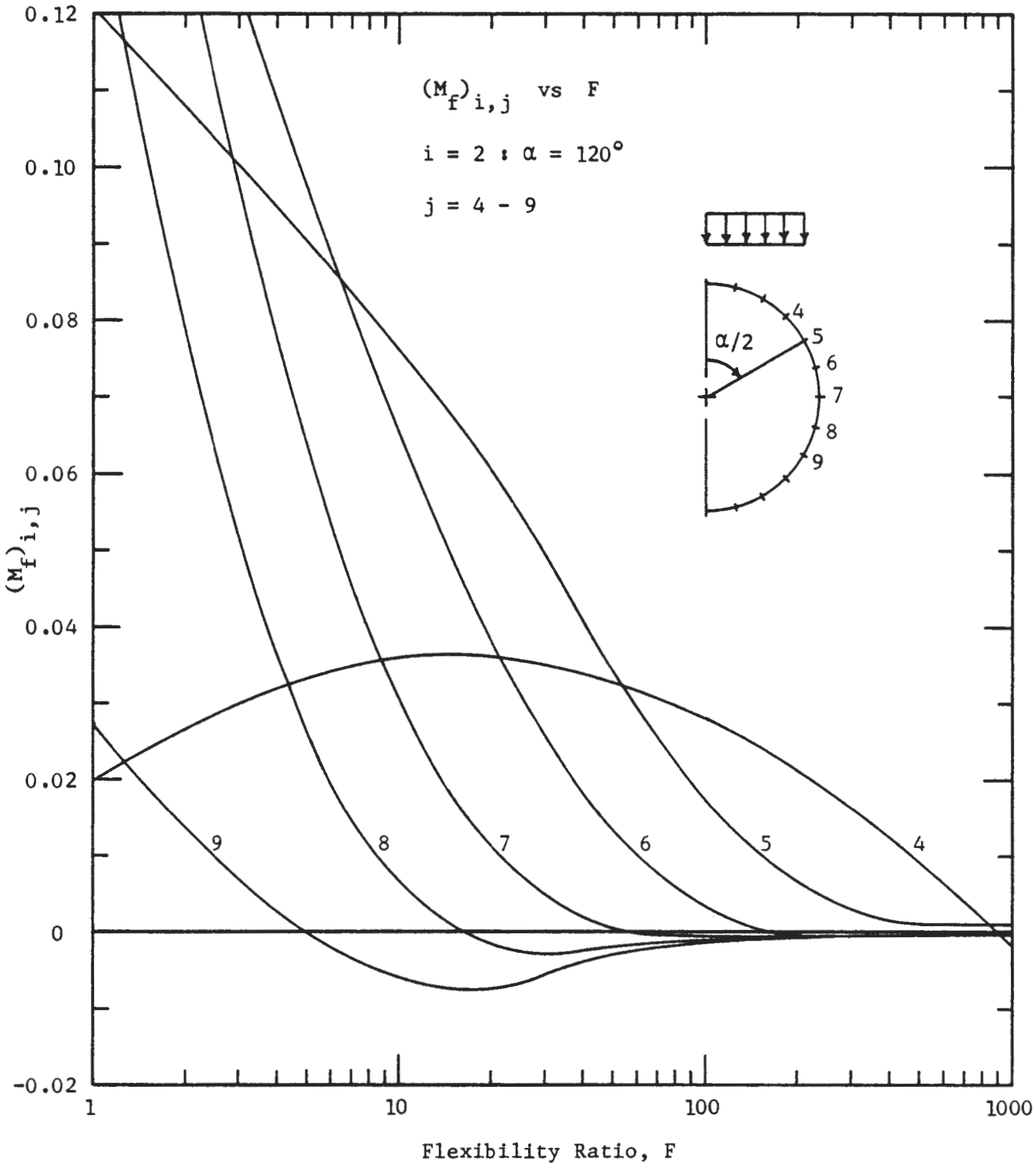

FIGURE 7.15b M_f VERSUS FLEXIBILITY RATIO FOR α = 120° (j = 4 - 9)

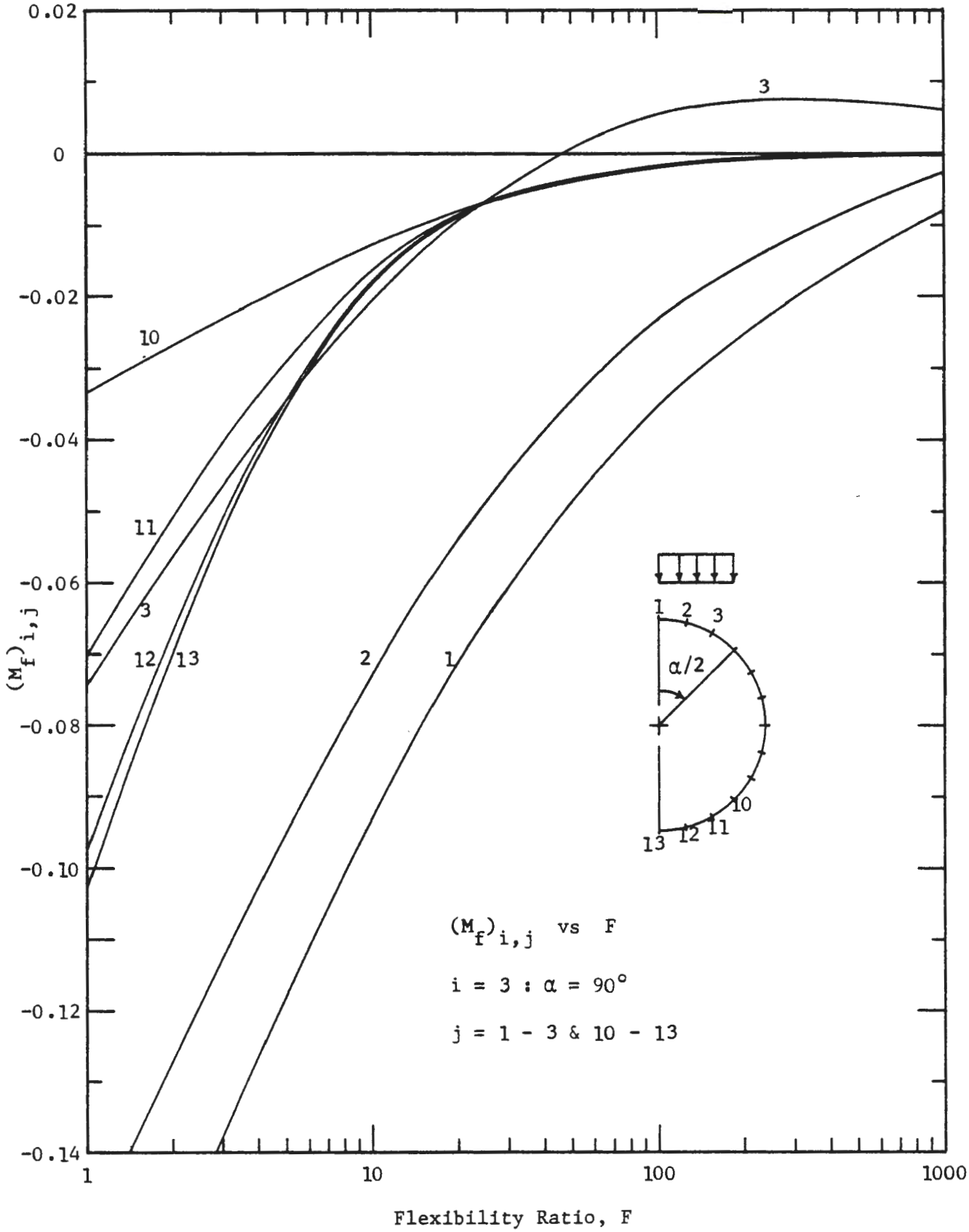

FIGURE 7.16a M_f VERSUS FLEXIBILITY RATIO FOR $\alpha = 90°$ (j = 1 - 3 AND 10 - 13)

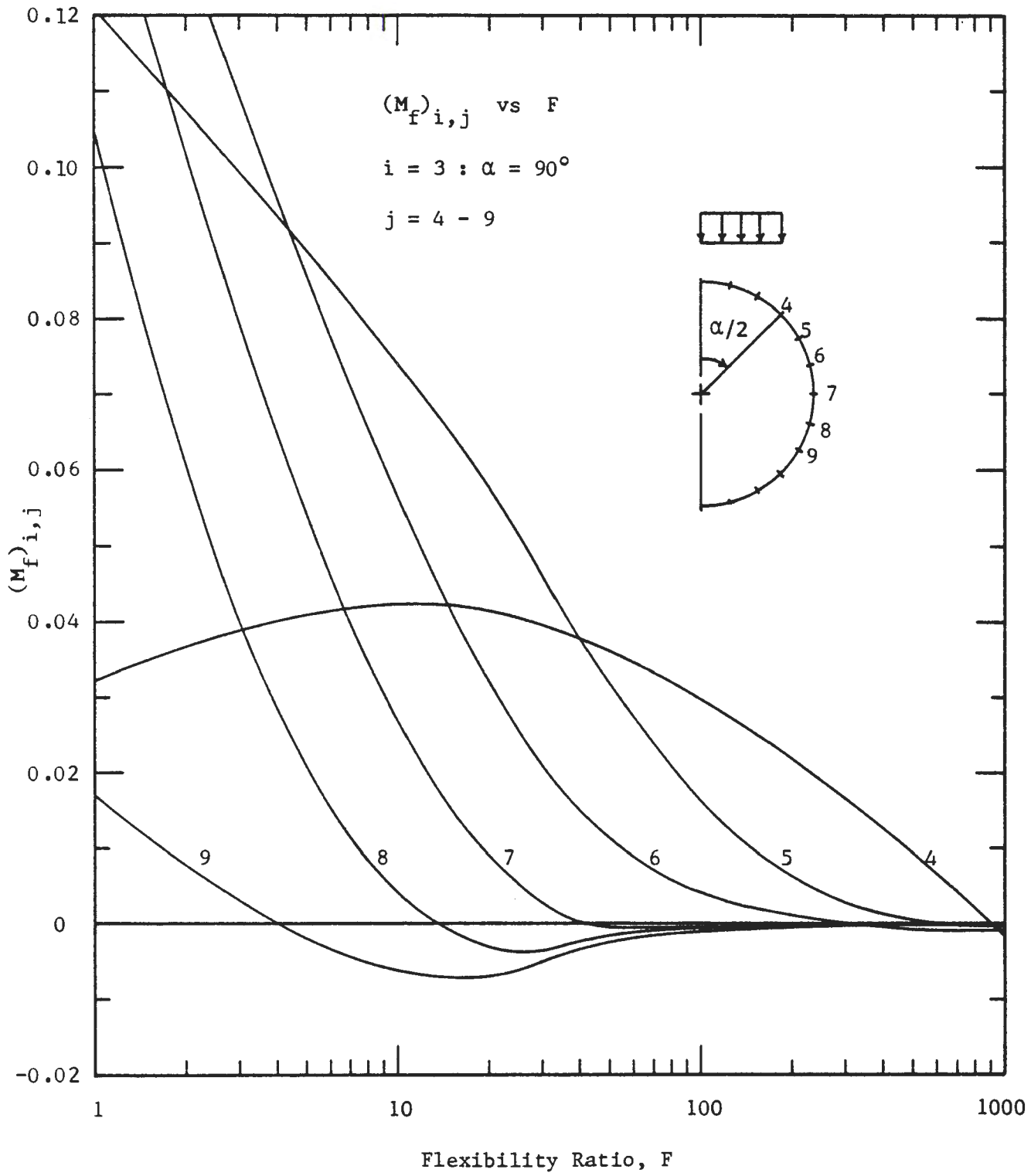

FIGURE 7.16b M_f VERSUS FLEXIBILITY RATIO FOR α = 90° (j = 4 - 9)

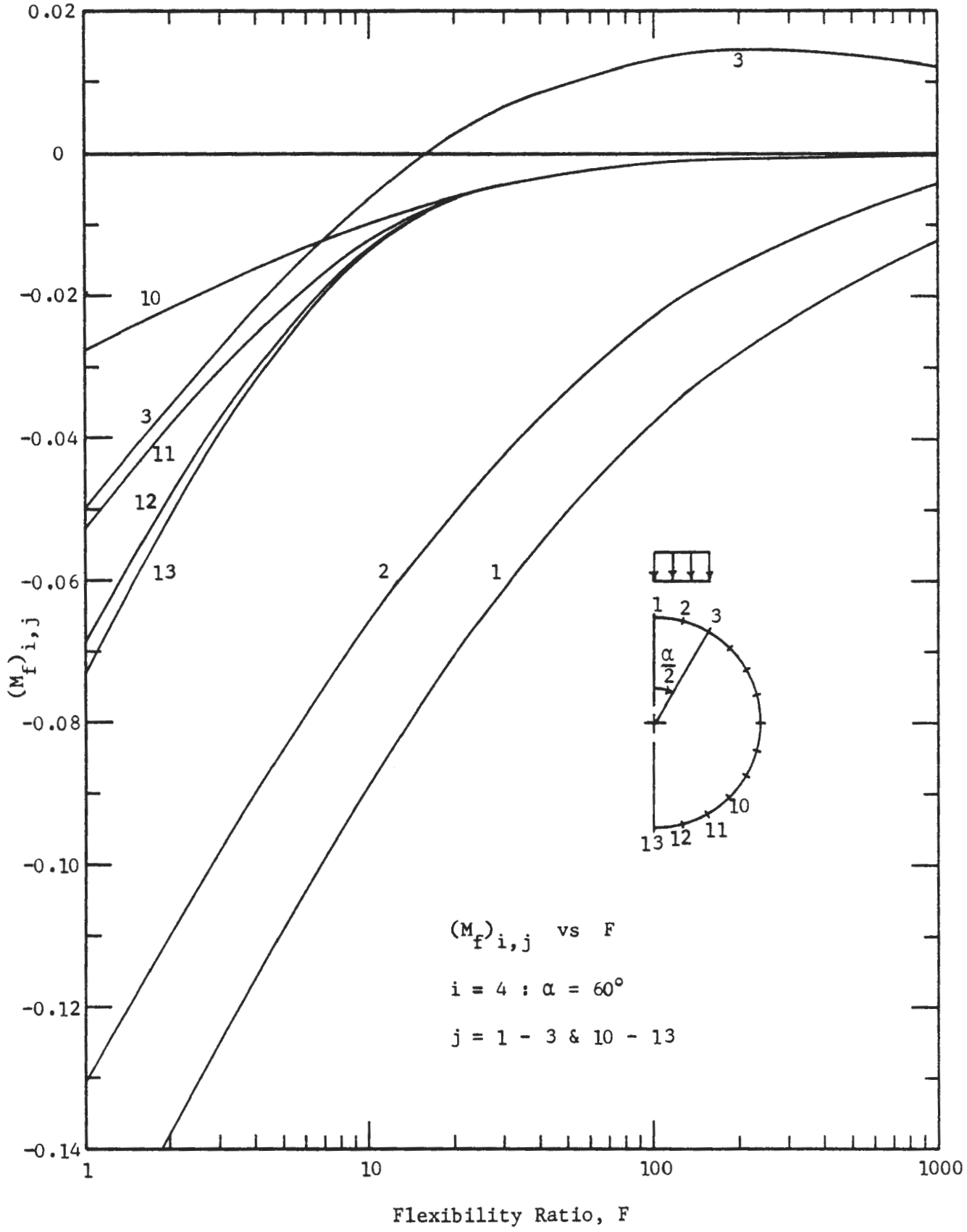

FIGURE 7.17a M_f VERSUS FLEXIBILITY RATIO FOR $\alpha = 60^\circ$ (j = 1 - 3 AND 10 - 13)

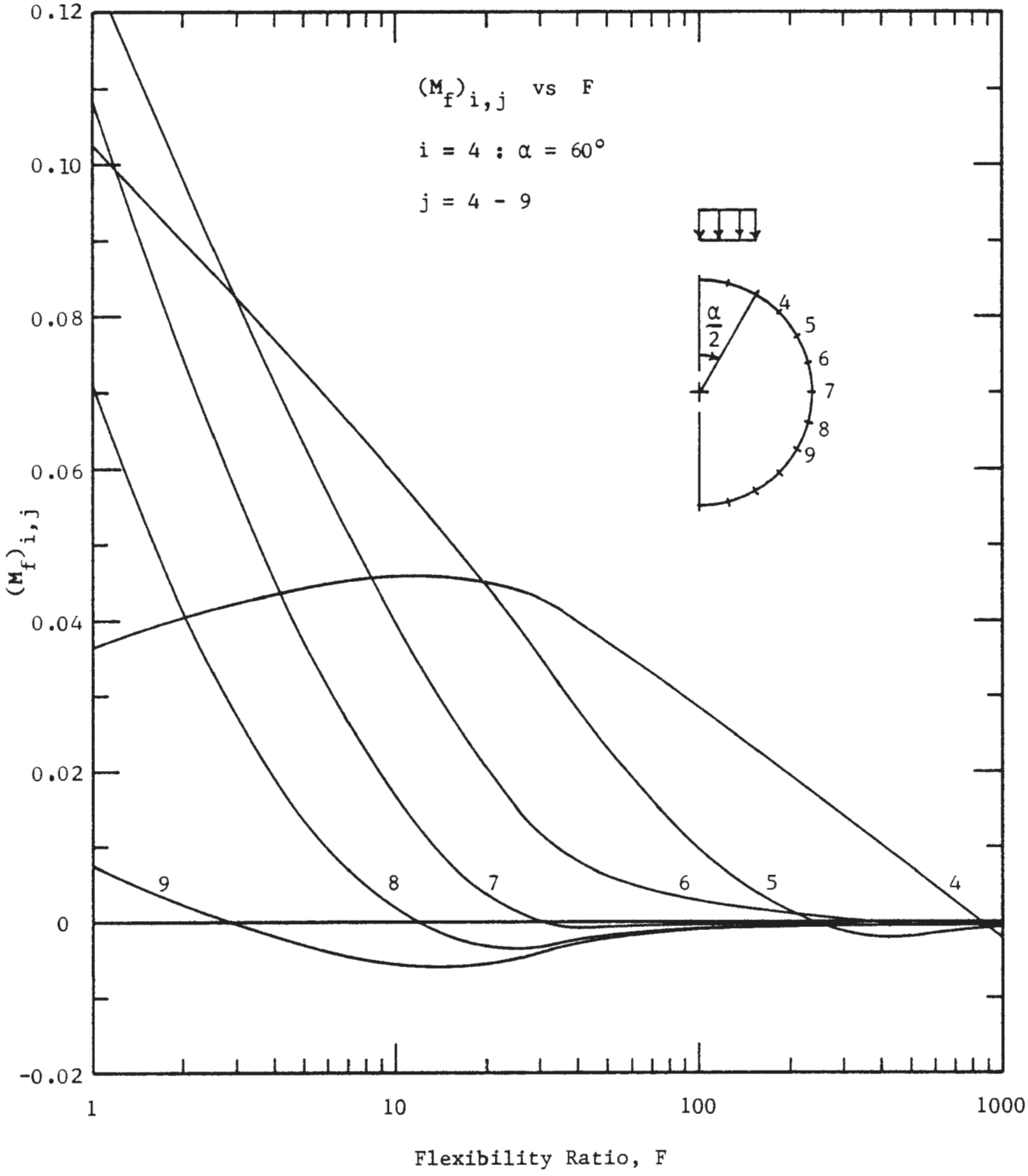

FIGURE 7.17b M_I VERSUS FLEXIBILITY RATIO FOR α = 60° (j = 4 - 9)

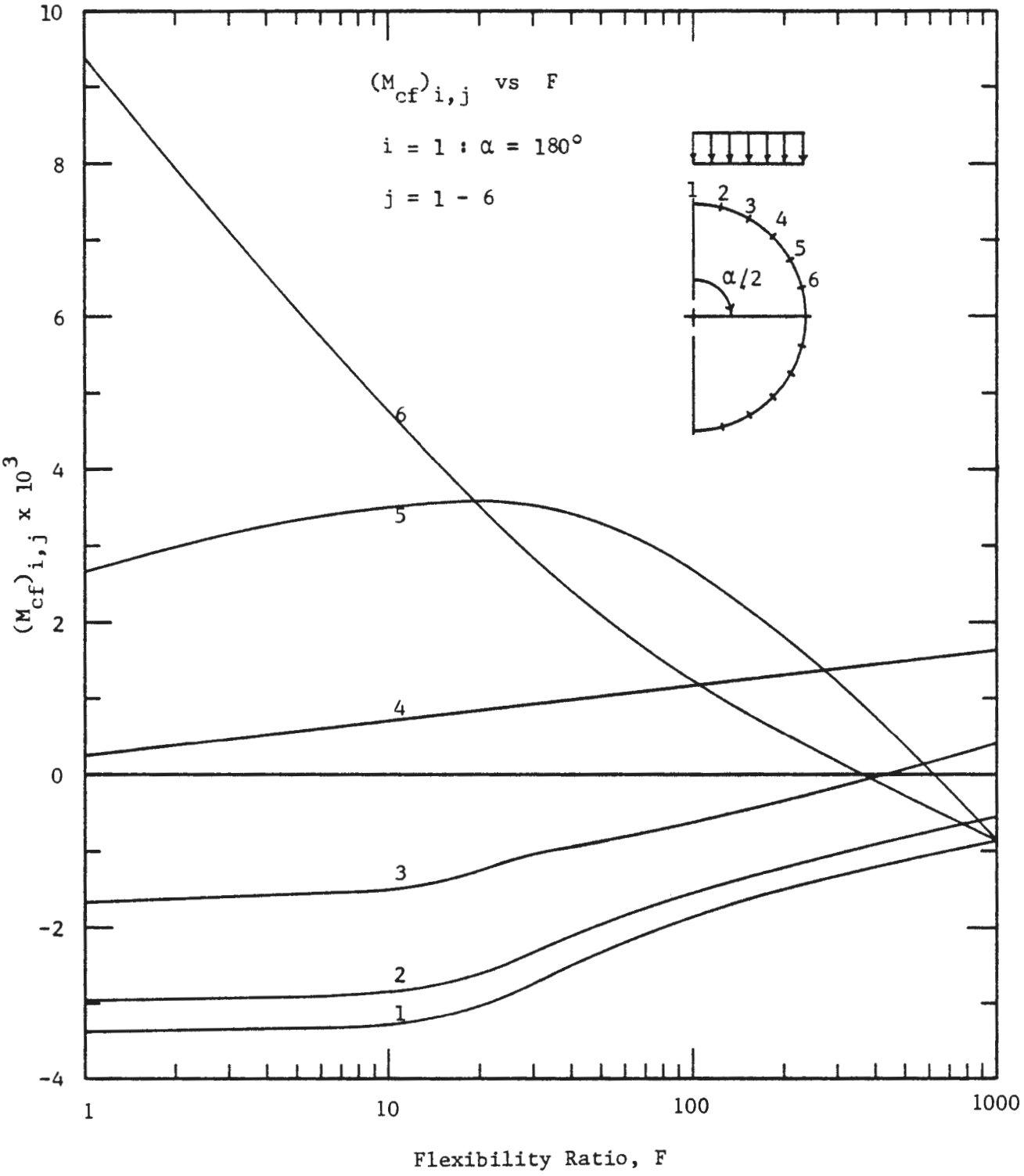

FIGURE 7.18a M_{cf} VERSUS FLEXIBILITY RATIO FOR α = 180° (j = 1 - 6)

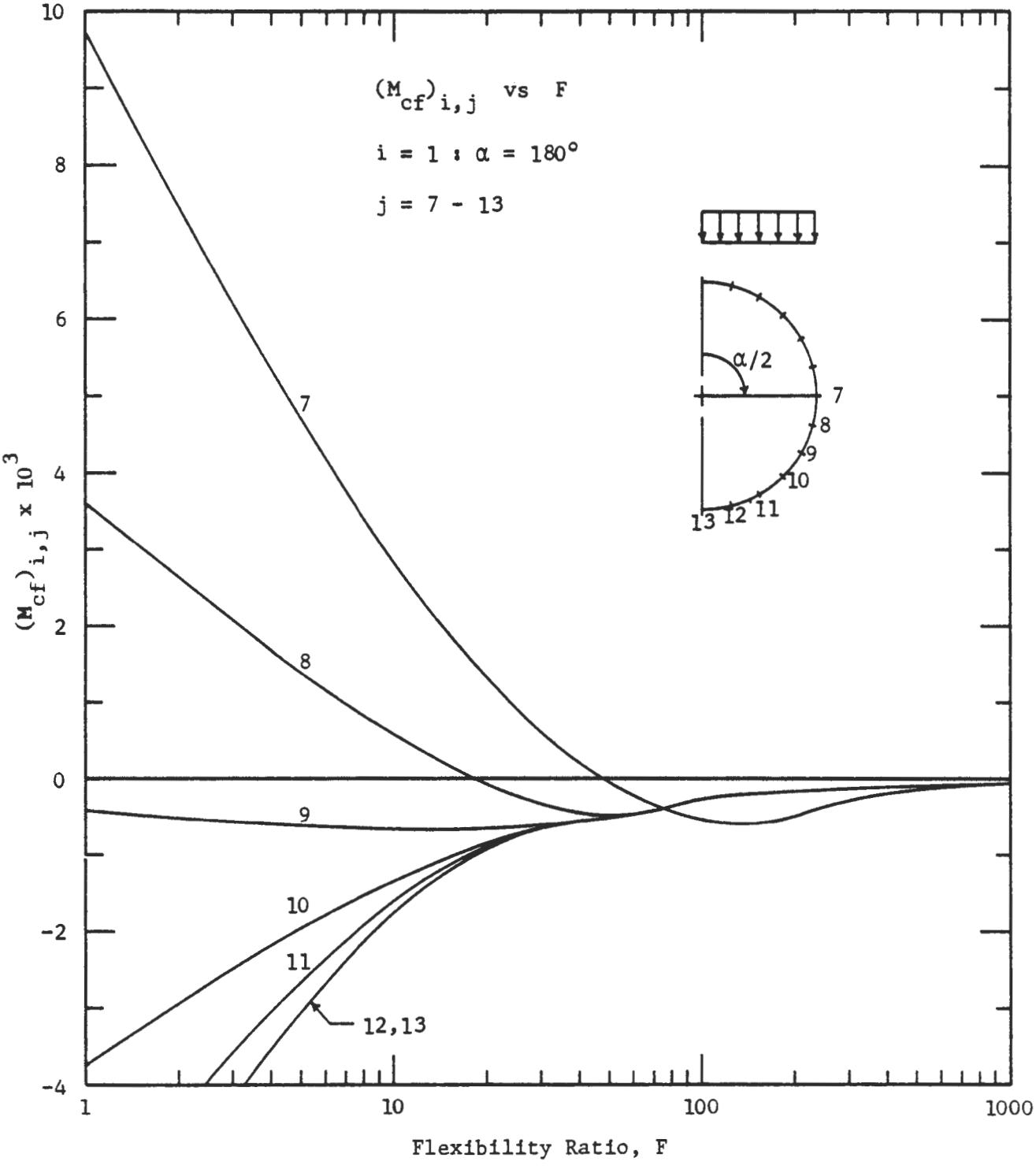

FIGURE 7.18b M_{cf} VERSUS FLEXIBILITY RATIO FOR α = 180° (j = 7 - 13)

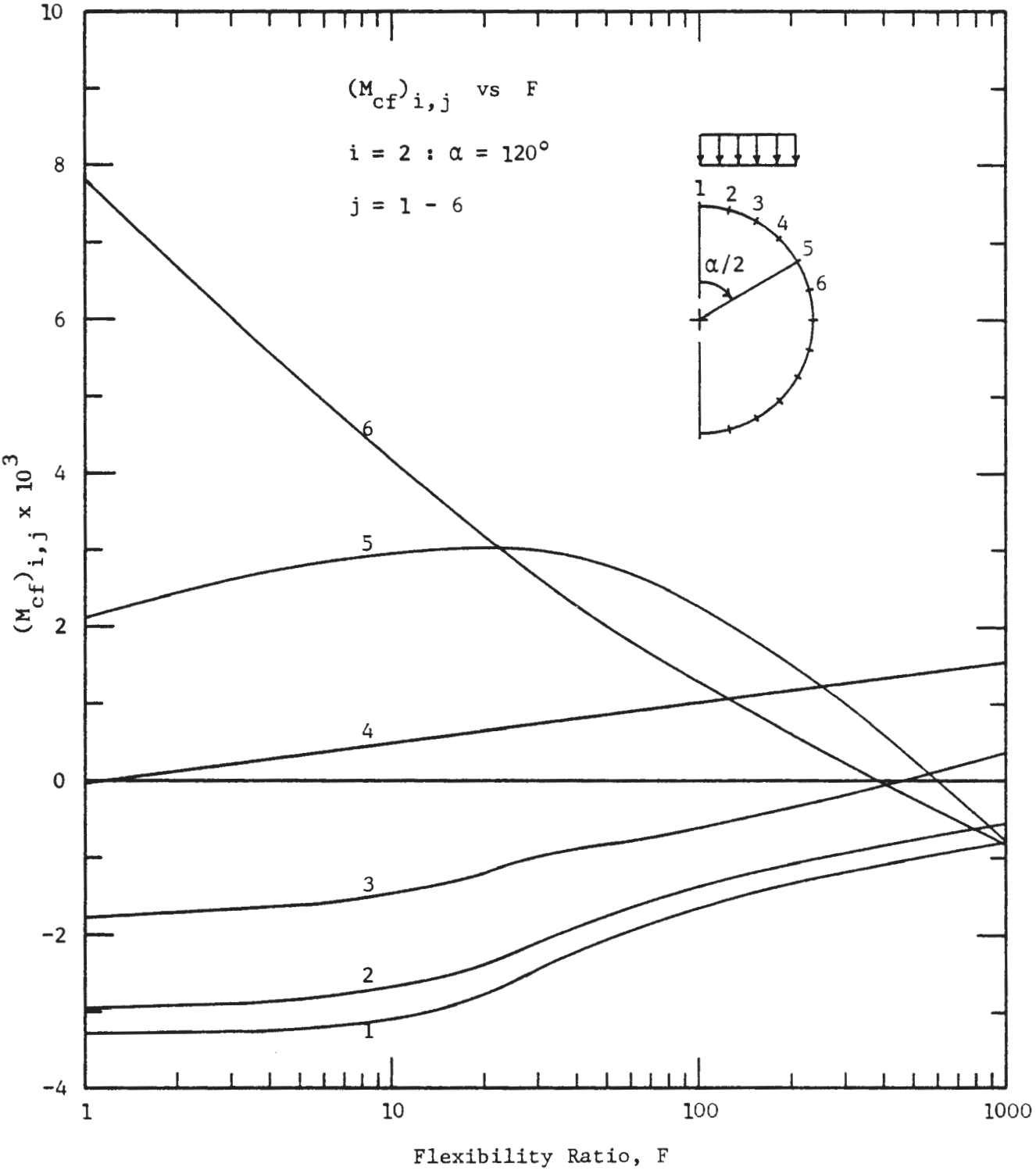

FIGURE 7.19a M_{cf} VERSUS FLEXIBILITY RATIO FOR α = 120° (j = 1 - 6)

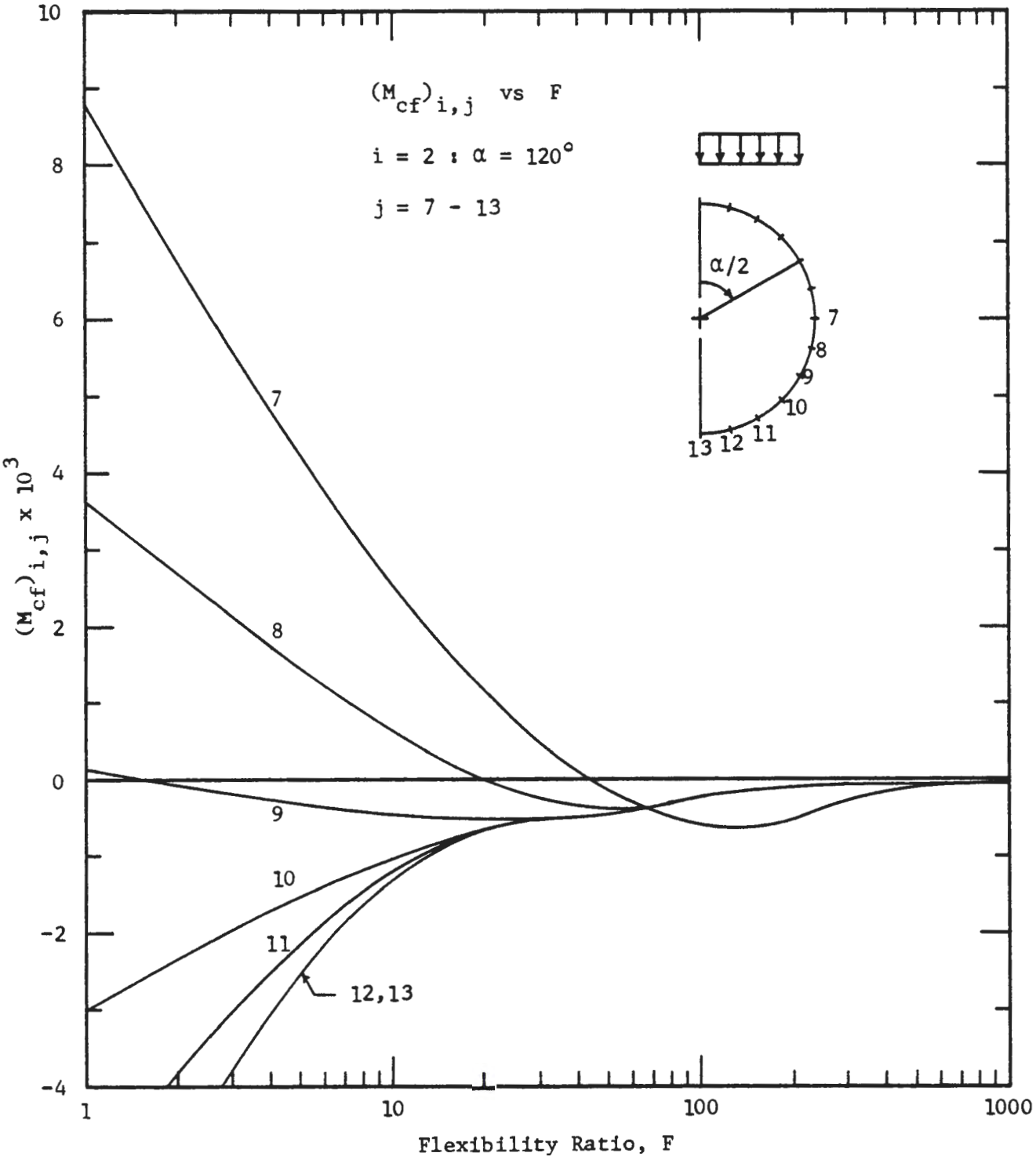

FIGURE 7.19b M_{cf} VERSUS FLEXIBILITY RATIO FOR α = 120° (j = 7 - 13)

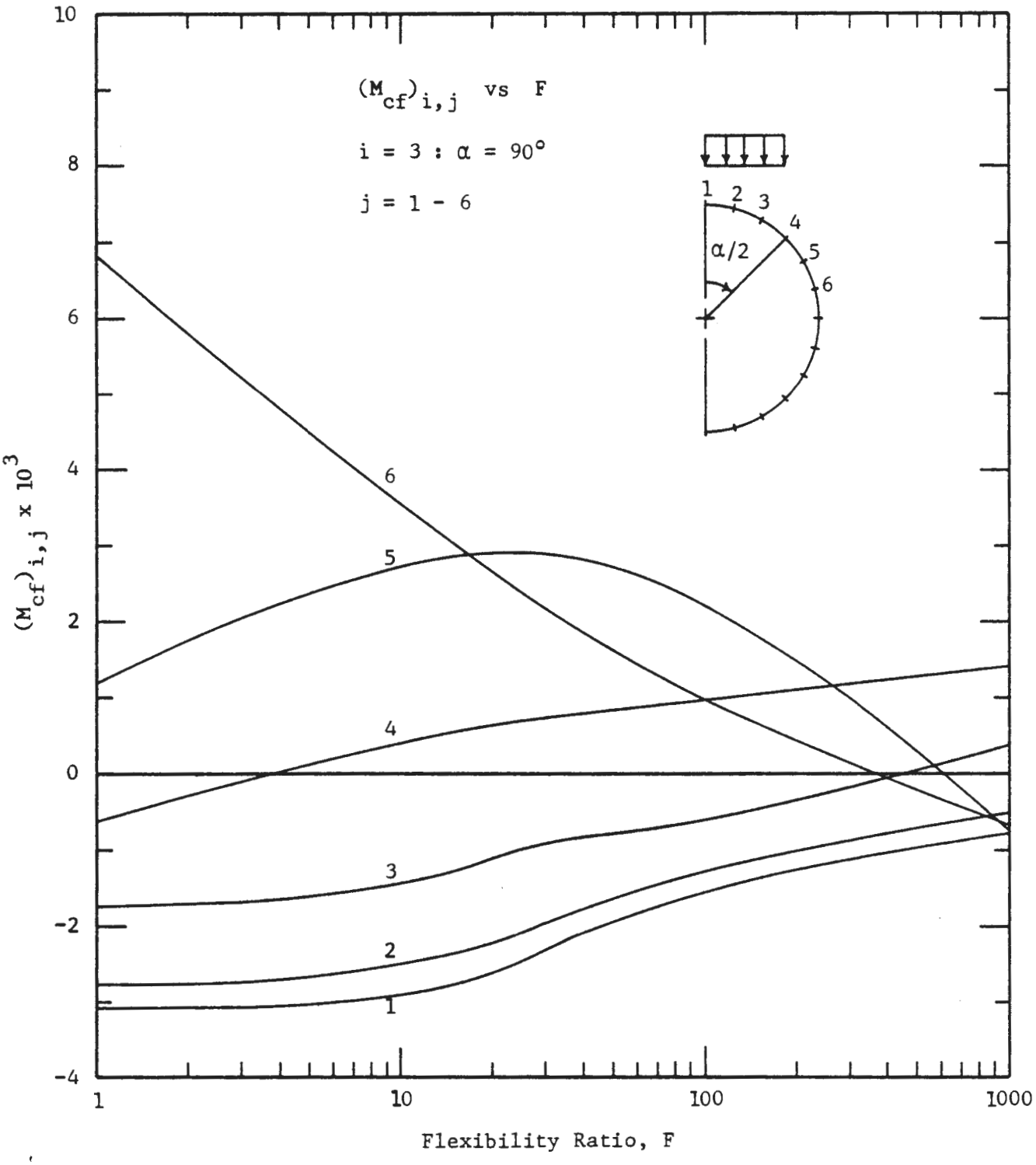

FIGURE 7.20a M_{cf} VERSUS FLEXIBILITY RATIO FOR α = 90° (j = 1 - 6)

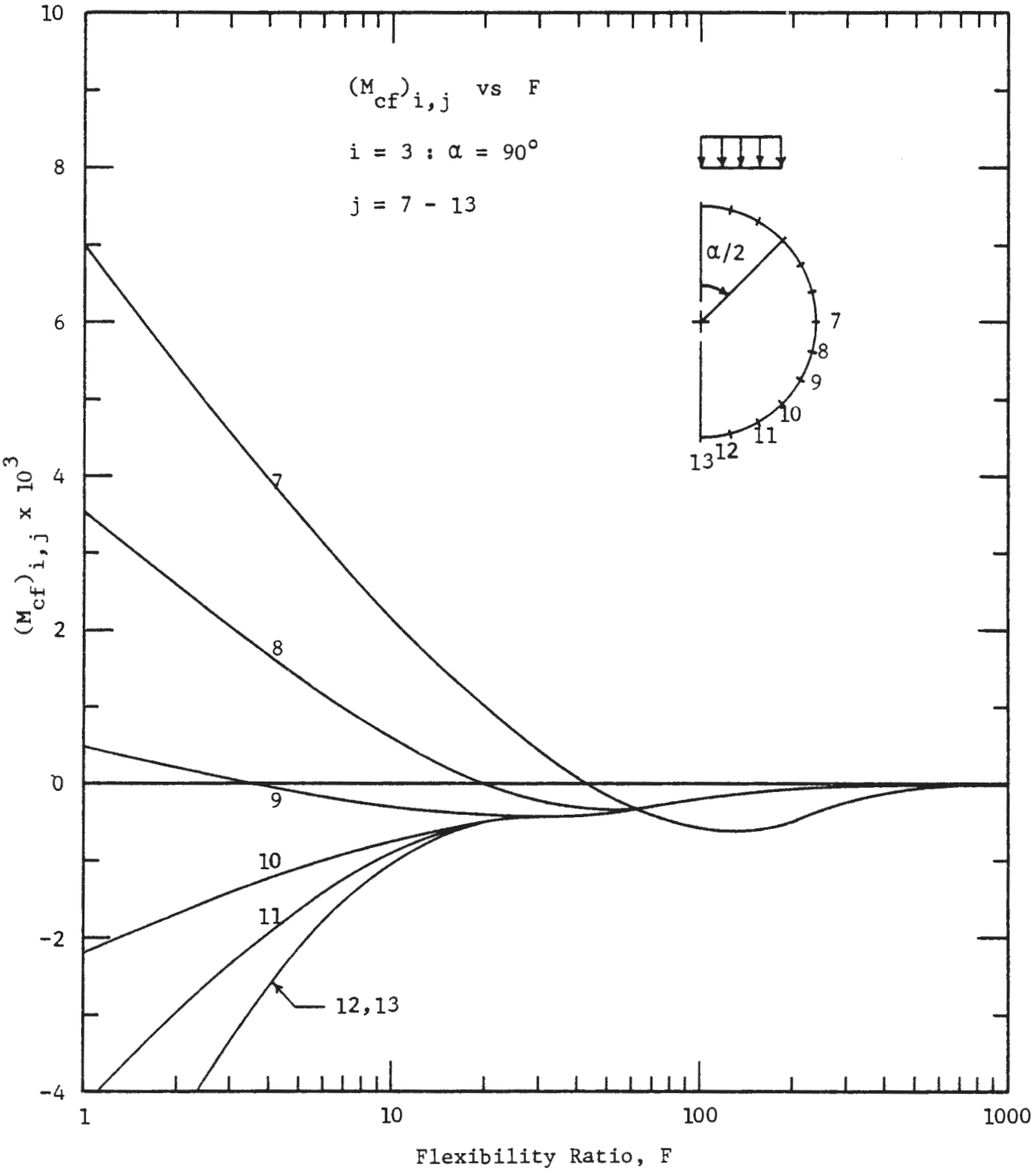

FIGURE 7.20b M_{cf} VERSUS FLEXIBILITY RATIO FOR α = 90° (j = 7 - 13)

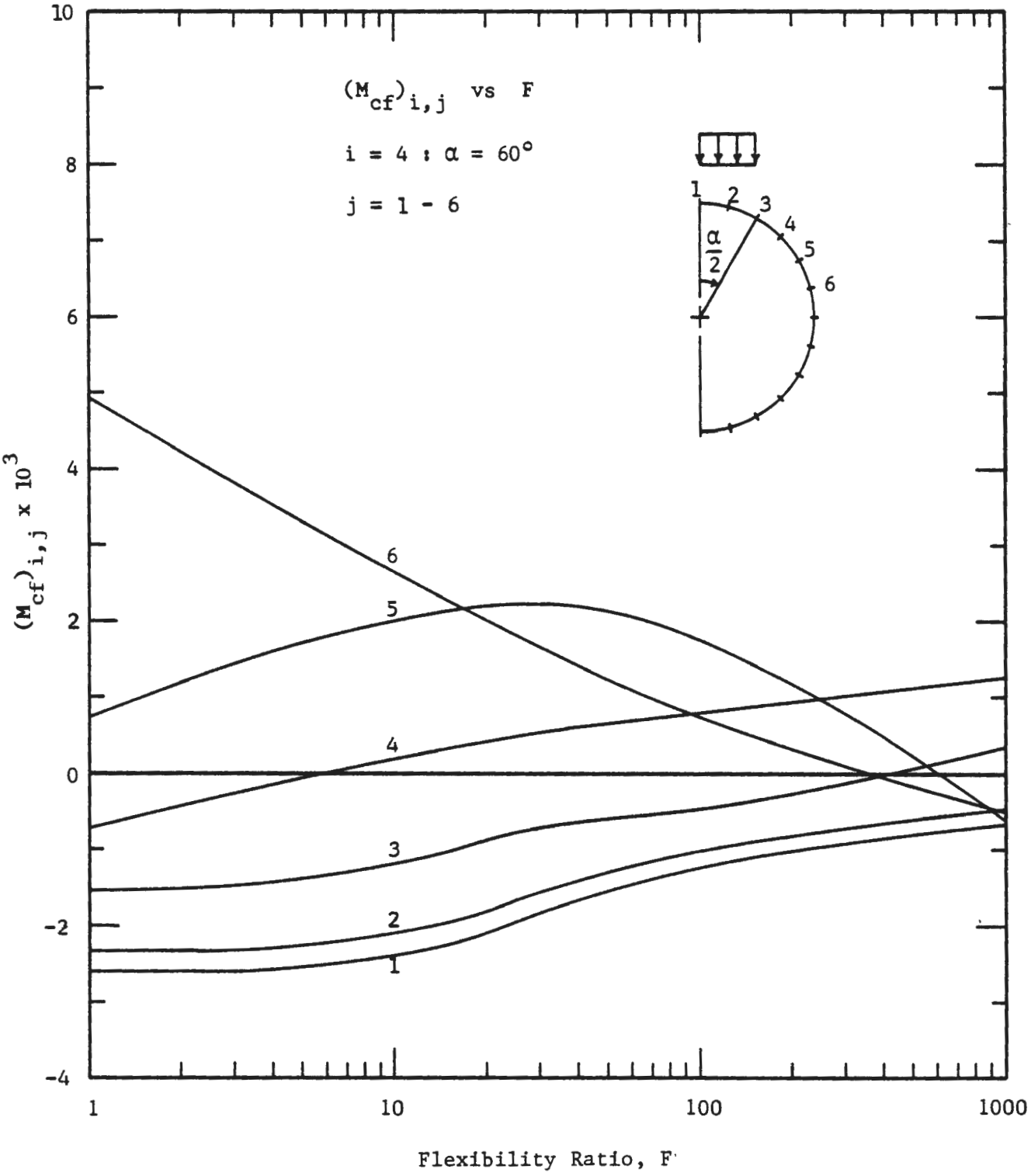

FIGURE 7.21a M_{cf} VERSUS FLEXIBILITY RATIO FOR α = 60° (j = 1 - 6)

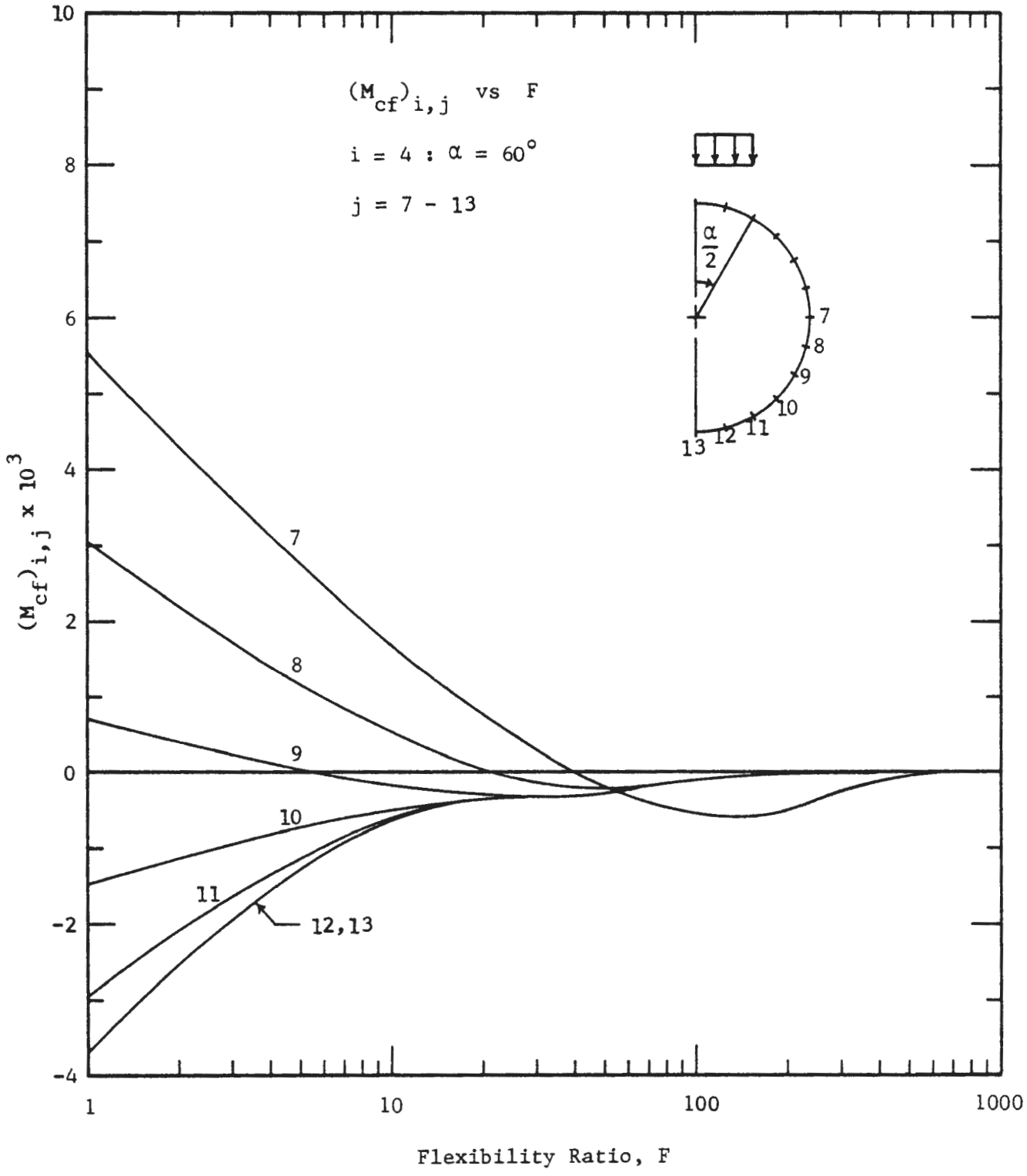

FIGURE 7.21b M_{cf} VERSUS FLEXIBILITY RATIO FOR α = 60° (j = 7 - 13)

the thrust and bending moment at a given location are obtained thusly;

$$T = P_1 a\,(T/Pa)_{\alpha 1} + P_2 a\,(T/Pa)_{\alpha 2} + \ldots\ldots\ldots \quad (7.3)$$

$$M = P_1 a^2 (M/Pa^2)_{\alpha 1} + P_2 a^2 (M/Pa^2)_{\alpha 2} + \ldots\ldots\ldots \quad (7.4)$$

where the thrust and moment coefficients for each α are obtained from Eqns. 7.1 and 7.2, respectively. However, because the localized gravity loading ground-liner interaction problem is geometrically nonlinear (i.e., nonlinear with respect to geometry of loading and the resulting extent of ground-liner separation) the superposition method can, at best, only approximate the results that would be obtained from an actual finite element analysis of the nonuniform loading. This is illustrated by the following two examples.

Example 1:

The geometry of loading considered in the first example is illustrated in Fig. 7.22. Three uniform and symmetrical pressure distributions are to be added together to give a nonuniform, but still symmetrical, pressure distribution. For this case it is assumed that ground-liner flexibility and compressibility ratios are F = 10.0 and C = 0.214, respectively. Table 7.3 gives the calculations for the thrust and moment at the crown. Figures 7.23 and 7.24 compare the thrust and moment distributions obtained from the superposition calculations to those obtained from the finite element analysis of the nonuniform loading. Because the loading is symmetrical, the distributions are given for one half of the liner only. These figures show that,

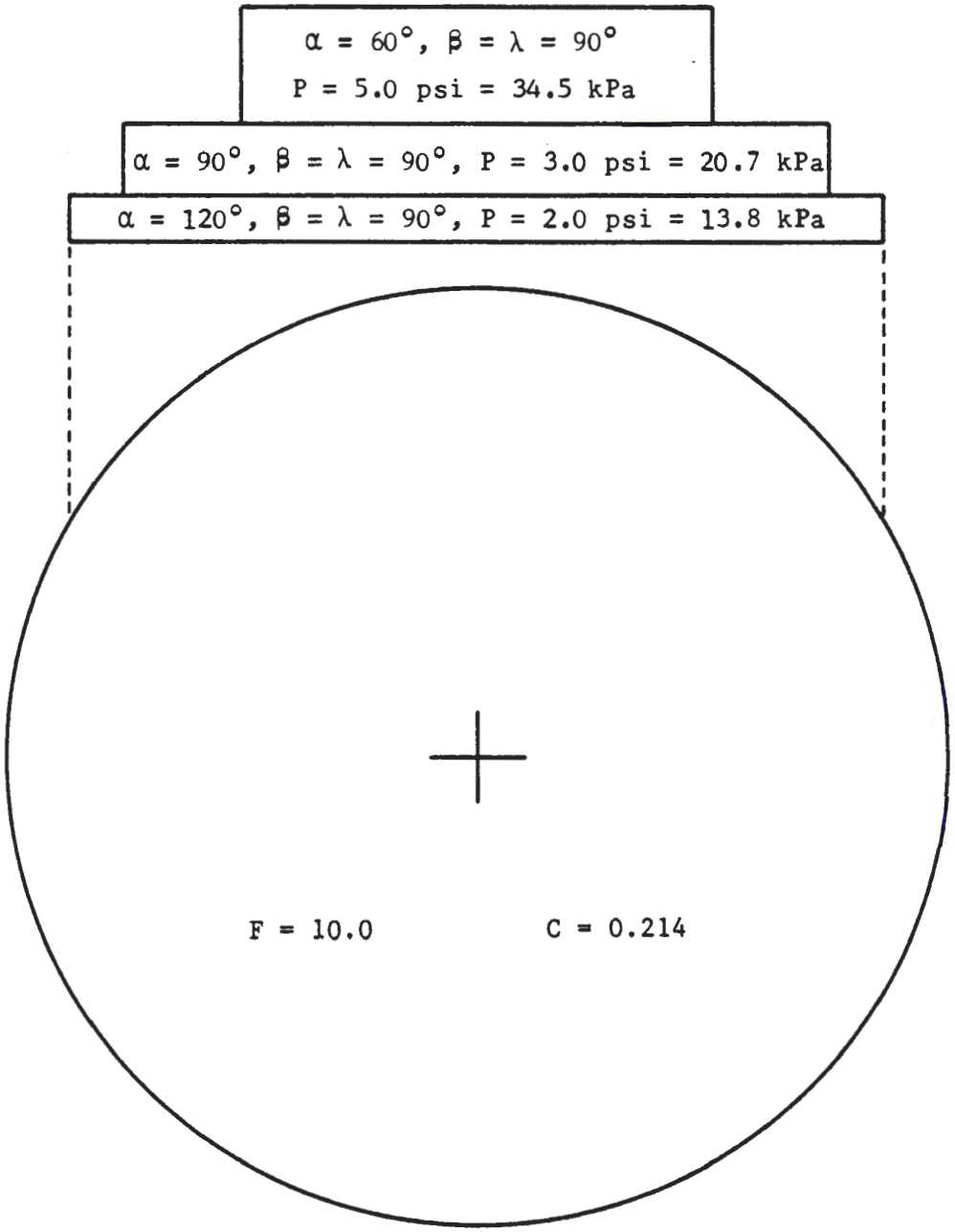

FIGURE 7.22 NONUNIFORM PRESSURE DISTRIBUTION CONSIDERED IN SUPERPOSITION EXAMPLE 1

TABLE 7.3

SUPERPOSITION CALCULATIONS FOR CROWN THRUST AND MOMENT GIVEN LOADING OF FIGURE 7.22

CROWN THRUST:

α (degrees)	P (psi)	P (kPa)	B_t	x	F_t'	-	$mC^{1.11}$	= (T/Pa)	T = Pa(T/Pa) (lb/in)	T = Pa(T/Pa) (kN/m)
120	2.0	13.8	.540		.772		.006	.411	99	17.3
90	3.0	20.7	.520		.756		.005	.388	140	24.5
60	5.0	34.5	.440		.732		.004	.318	191	33.5
								T(Crown) = Σ =	430	75.3

CROWN MOMENT:

α (degrees)	P (psi)	P (kPa)	M_f	+	$3.53C^{1.11}$	x	M_{cf}	= (M/Pa^2)	M = $Pa^2(M/Pa^2)$ (lb-in/in)	M = $Pa^2(M/Pa^2)$ (kN-m/m)
120	2.0	13.8	-.0943		.6376		-.00308	-.0963	-2773	-12.3
90	3.0	20.7	-.0929		.6376		-.00292	-.0948	-4095	-18.2
60	5.0	34.5	-.0887		.6376		-.00239	-.0902	-6494	-28.9
								M(Crown) = Σ =	-13362	-59.4

a = 120 in. = 3.05 m

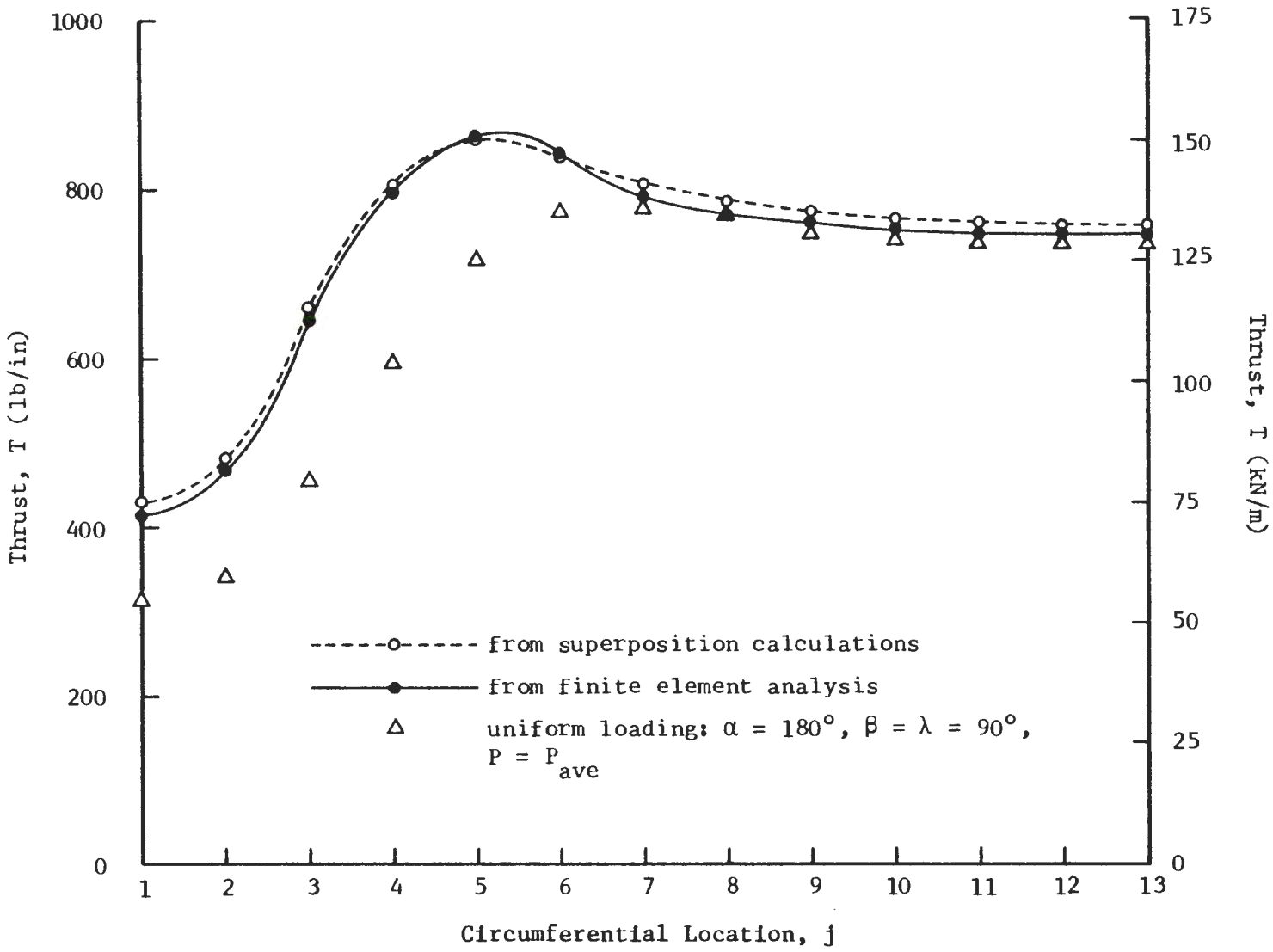

FIGURE 7.23 THRUST DISTRIBUTIONS OBTAINED FROM SUPERPOSITION CALCULATIONS AND FINITE ELEMENT ANALYSIS - EXAMPLE 1

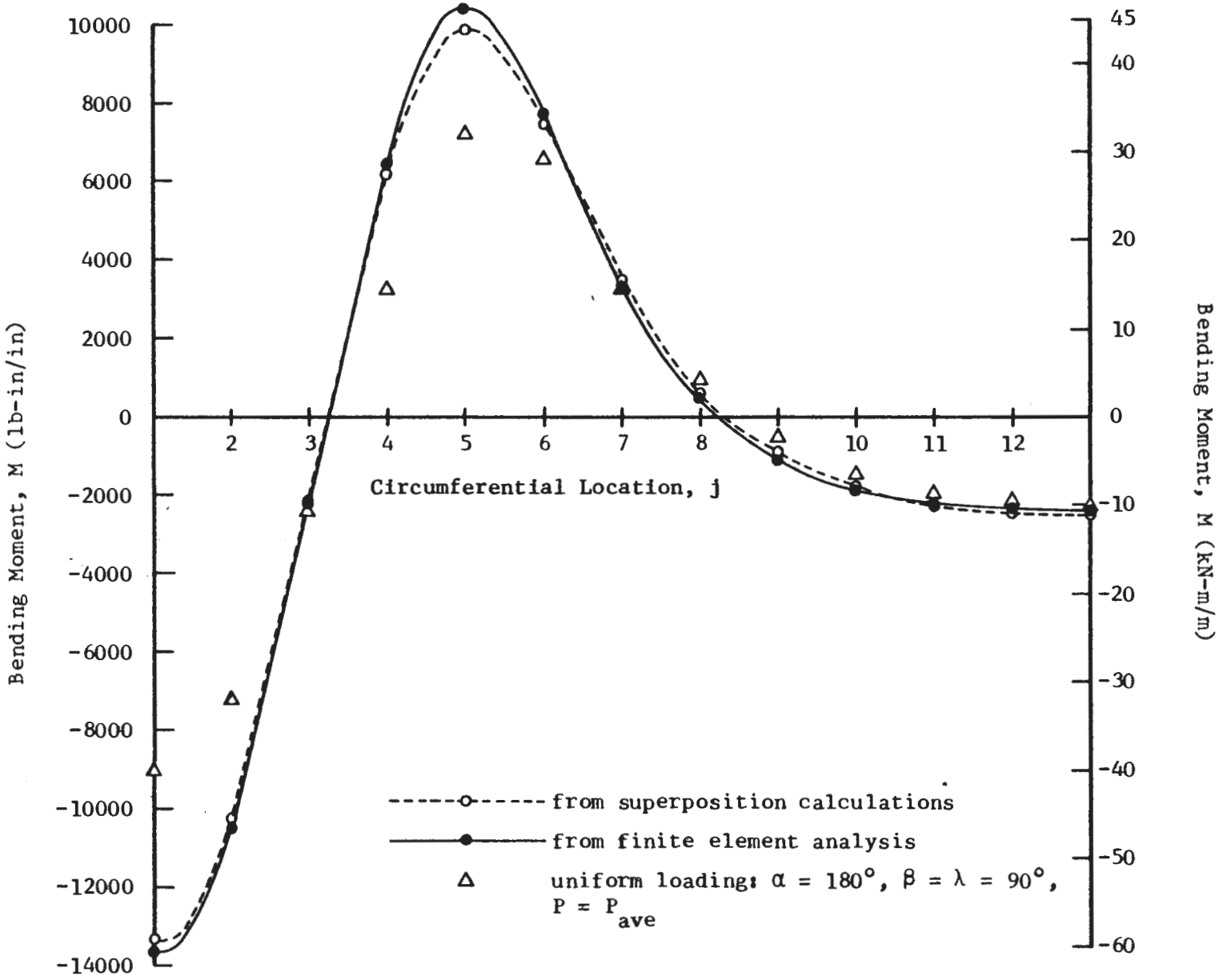

FIGURE 7.24 MOMENT DISTRIBUTIONS OBTAINED FROM SUPERPOSITION CALCULATIONS AND FINITE ELEMENT ANALYSIS - EXAMPLE 1

in this case, the superposition method yielded very good results. It is apparent, however, that the superposition method slightly overestimated the thrust magnitudes and slightly underestimated the bending moment magnitudes.

Example 2:

The loading considered for this example is shown in Fig. 7.25 and the calculations for the crown thrust and moment are given in Table 7.4. Crown thrust and moment values for the α = 60 degrees, $\beta = \lambda$ = 45 degrees loading were obtained from location j = 22 of the available α = 60 degrees, $\beta = \lambda$ = 90 degrees loading geometry (clockwise rotation through 45 degrees changes β and λ from 90 to 45 degrees and moves location j = 22 to the crown position). However, for the symmetrical α = 60 degrees loading case the liner response at location j = 22 is the same as that at location j = 4 and thus, this value of j was used in the calculations. Thrust and moment distributions obtained from the superposition calculations and from the finite element analysis of this nonuniform loading are compared in Figs. 7.26 and 7.27. It is readily apparent from these figures that, in this case, the superposition method has significantly overestimated thrust magnitudes and underestimated bending moment magnitudes.

Both nonuniform loading examples indicate that the superposition method gives a good estimate of the distribution of liner thrusts and bending moments, but, with regard to magnitudes, tends to overestimate thrusts and underestimate moments. It appears that the problem with magnitudes can be attributed to 1) the relationship between separation angle, Ω, and thrust and moment magnitudes, and 2) the difference between the separation angles given by the superposition method, Ω_s, and the actual finite element analysis, Ω_a.

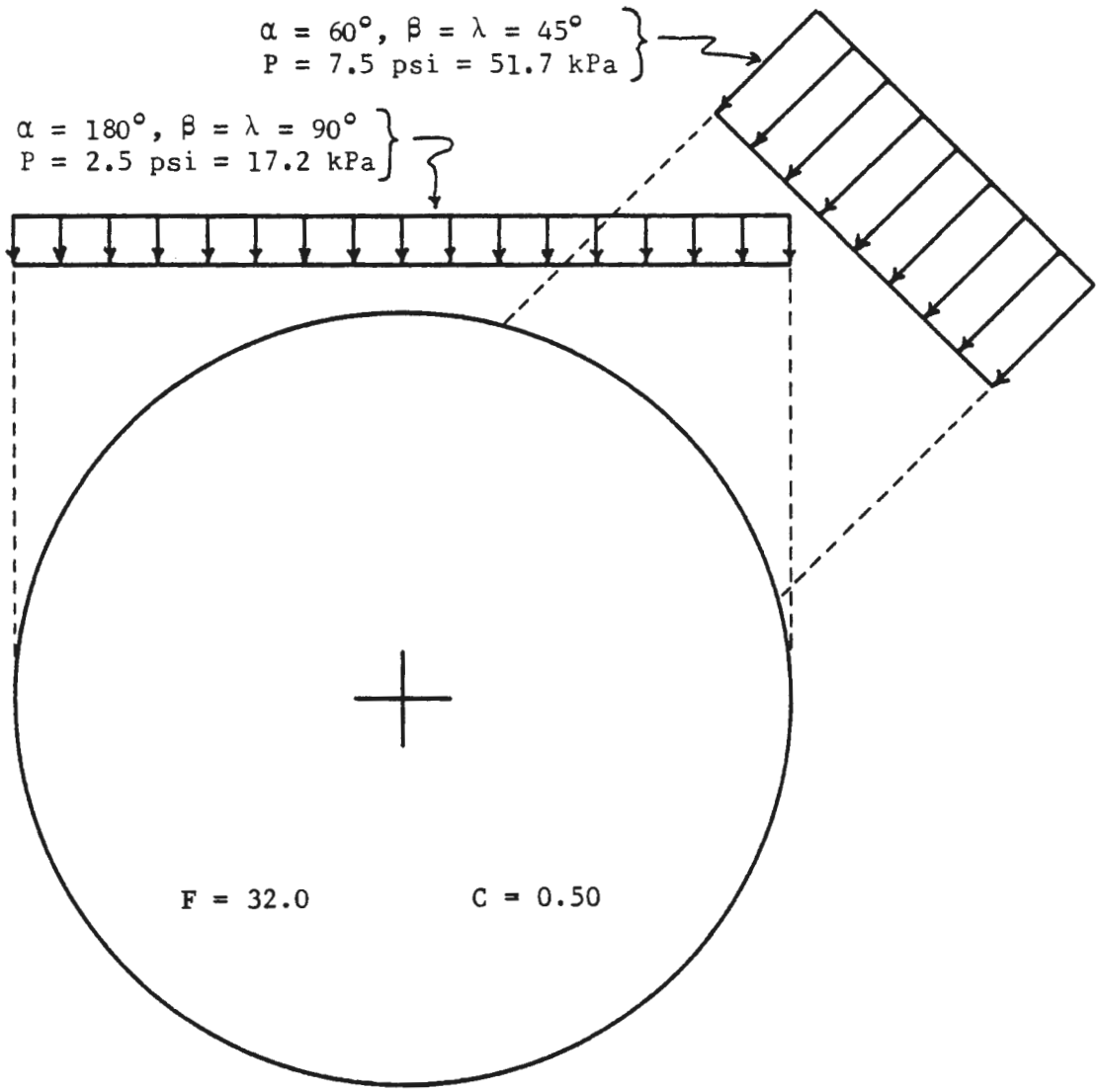

FIGURE 7.25 NONUNIFORM PRESSURE DISTRIBUTION CONSIDERED IN SUPERPOSITION EXAMPLE 2

TABLE 7.4

SUPERPOSITION CALCULATIONS FOR CROWN THRUST AND MOMENT GIVEN LOADING OF FIGURE 7.25

CROWN THRUST:

α (degrees)	P (psi)	P (kPa)	$(B_t \times F'_t) - mC^{1.11}$			= (T/Pa)	T = Pa(T/Pa) (lb/in.)	T = Pa(T/Pa) (kN/m)
180*	2.5	17.2	.540	1.0	.016	.524	157	27.5
60**	7.5	51.7	.671	1.0	.010	.661	595	104.2
						T(Crown) = Σ =	752	131.7

CROWN MOMENT:

α (degrees)	P (psi)	P (kPa)	$M_f + (3.53C^{1.11} \times M_{cf})$			= (M/Pa^2)	M = Pa^2(M/Pa^2) (lb-in./in.)	M = Pa^2(M/Pa^2) (kN-m/m)
180*	2.5	17.2	-.0596	1.635	-.00268	-.0640	-2304	-10.3
60**	7.5	51.7	.0424	1.635	.00057	.0433	4680	20.8
						M(Crown) = Σ =	2376	10.5

* j = 1

** j = 22 = 4

a = 120 in. = 3.05 m

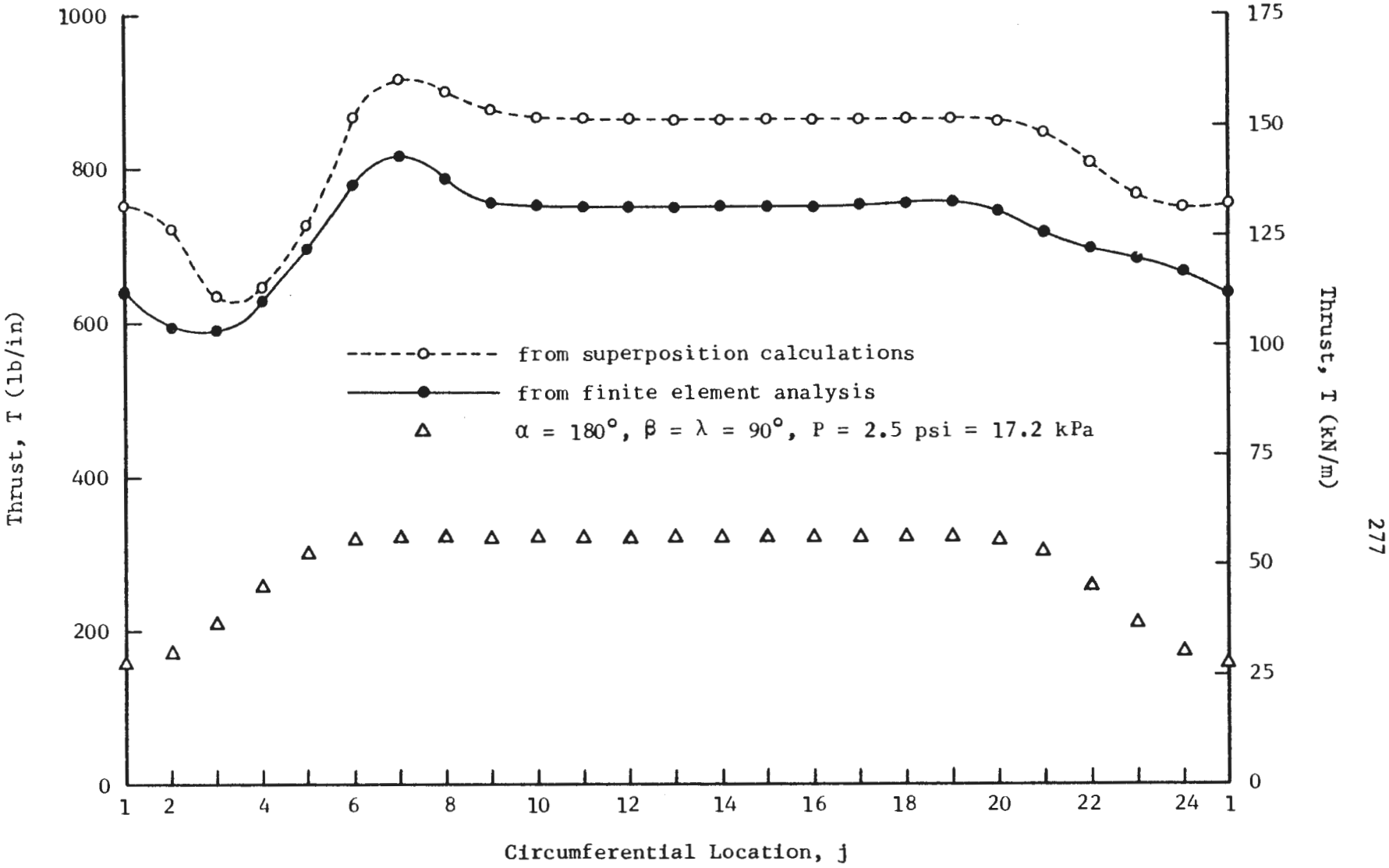

FIGURE 7.26 THRUST DISTRIBUTIONS OBTAINED FROM SUPERPOSITION CALCULATIONS AND FINITE ELEMENT ANALYSIS - EXAMPLE 2

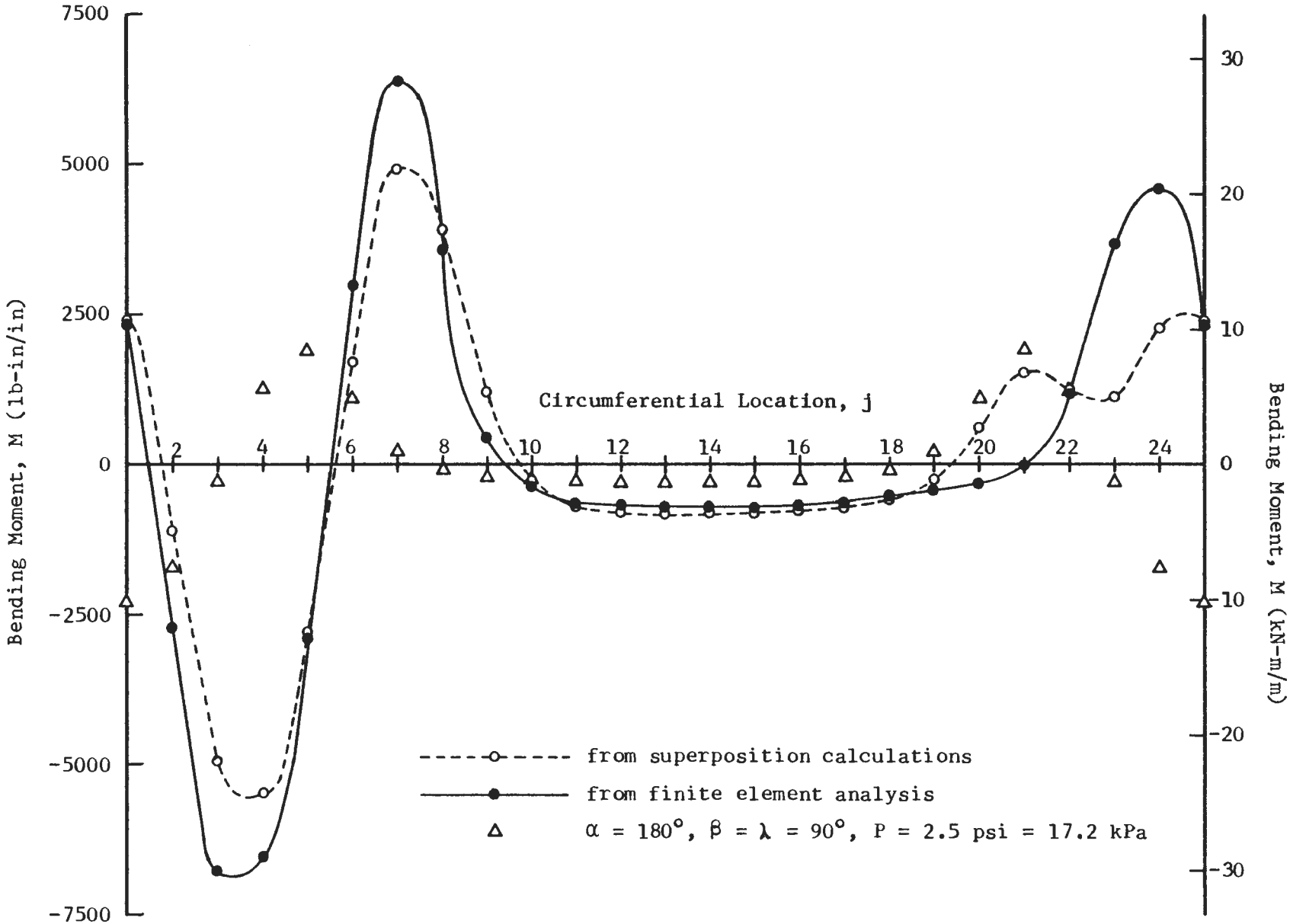

FIGURE 7.27 MOMENT DISTRIBUTIONS OBTAINED FROM SUPERPOSITION CALCULATIONS AND FINITE ELEMENT ANALYSIS - EXAMPLE 2

When two or more uniform loading geometries are superposed the resulting separation angle, Ω_s, is determined by the extent to which the various separation angles superposed overlap. This is illustrated in Fig. 7.28. The actual separation angle, Ω_a, obtained from a finite element analysis falls in the range $\Omega_s < \Omega_a < \Omega'$ as shown in Fig. 7.28. An approximate value for Ω_a is the average of Ω_s and Ω'.

From the relationship between separation angle and liner thrust and moment magnitude, as described in the discussion of Fig. 7.8, it can be expected that, because $\Omega_s < \Omega_a$ the superposition method will, as found in the above two examples, underestimate bending moment magnitudes and overestimate thrust magnitudes. The amount by which the superposition results are in error can be related to the difference between Ω_s and Ω_a, which can, in turn, be related to the difference between the β values of the various loading geometries superposed.

The analyses of the various uniform and symmetrical loading geometries considered herein (α = 180, 120, 90 and 60 degrees) indicated that for a given F and C combination the separation angle decreased only slightly as α was reduced from 180 to 60 degrees. Thus, if the β values of the various loading geometries superposed are equal their separation angles will overlap only slightly and $\Omega_s \approx \Omega_a$. This was the case for example 1 where superposition yielded very good results. As the difference in β values increases, the amount of separation angle overlap and, thus, the difference between Ω_s and Ω_a, increases. In example 2, where superposition did not yield good results, the difference between the β values of the two loading geometries superposed was 45 degrees, and it was found that $\Omega_s \approx 75$ degrees and $\Omega_a \approx 120$ degrees. On the basis of a limited amount of data it appears

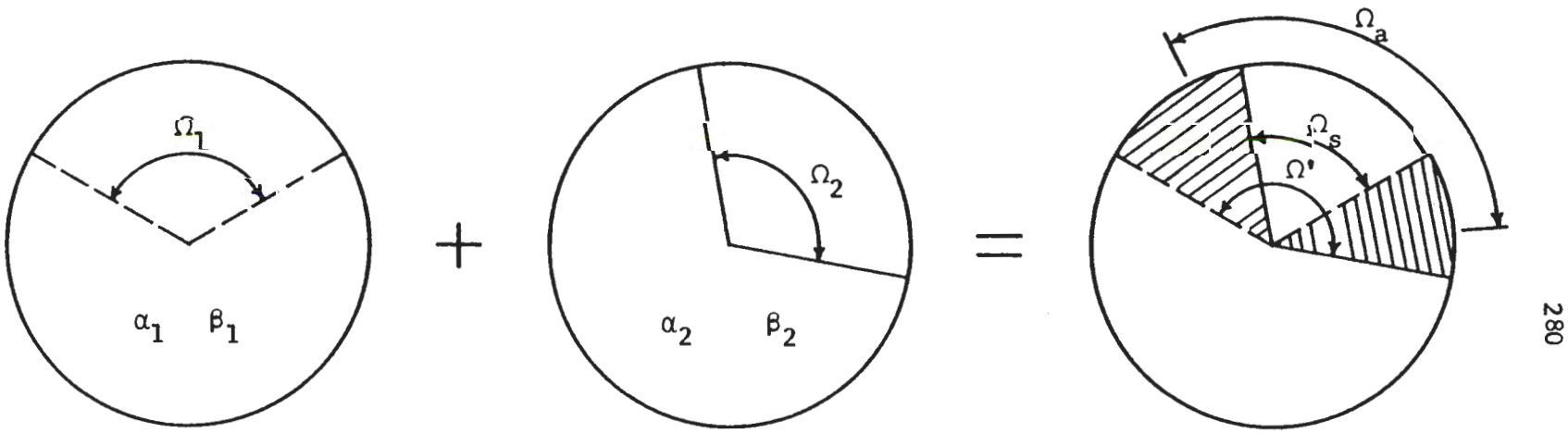

FIGURE 7.28 SEPARATION ANGLE AS OBTAINED FROM SUPERPOSITION METHOD, Ω_s, AND FINITE ELEMENT ANALYSIS, Ω_a

that the superposition method will yield good results if the β values of the various loading geometries superposed differ by no more than 30 degrees.

Most of the available methods for estimating the magnitude of the localized gravity load assume that load results in a uniform vertical pressure over the entire upper half of the liner (α = 180 degrees). This assumption can lead to erroneous estimates of liner response if the loading is actually nonuniform. In Figs. 7.23 and 7.24 thrust and moment distributions are given for a uniform average vertical pressure over the upper half of the liner. By comparing these data points (triangles) to those for the actual nonuniform loading it can be seen that the assumed uniform average loading significantly underestimates both thrusts and moments in the upper half of the liner where the critical thrust and moment combinations occur. Of course, the differences between these data depend on the magnitude of the assumed average pressure, P_{ave}.

In example 2 the α = 180 degrees loading represents the weight of rock in the loosened zone around the tunnel that may eventually have to be carried by the liner. The α = 60 degrees loading represents the load imposed on the liner by a large rock block that has dislodged and come to rest against the liner. In Figs. 7.26 and 7.27 thrust and bending moment distributions are also given for the α = 180 degrees loading only (triangles). By comparing the triangular and filled circular data points it is clear that if the effect of the rock block was not taken into consideration the liner thrusts and moments would be greatly underestimated.

7.4.3 COMPARISON OF LINER THRUSTS, MOMENTS AND STRESSES FOR LOCALIZED GRAVITY LOADING AND EXCAVATION LOADING

A tunnel liner subjected to localized gravity loading responds

quite differently than does a similar liner subjected to excavation loading. Figures 3.4 and 7.6 illustrate the differences between the circumferential distributions of liner thrusts, moments and displacements for the two types of loading.

The variation of liner thrust and moment with compressibility and flexibility ratios is also quite different for the two types of loading. The analytical solution for excavation loading under conditions of full slippage indicates that moments can be reduced with little change in thrust by making the liner more flexible (Figs. 3.5 and 3.6). If the liner is made more compressible the thrusts will be reduced (Fig. 3.7) with no change in moments. By making the liner both more flexible and more compressible the surrounding ground can be made to carry a greater proportion of the potential load (both thrusts and moments are reduced, but at the expense of increased liner displacements). This is not the case with localized gravity loading for which, once it develops, the load remains constant. Changes in liner compressibility and flexibility alter only the distribution of external passive pressures acting on the liner and thereby the proportions of the total load carried in thrust and bending moments. Figure 7.8 shows that more flexible liners have smaller moments but larger thrusts than less flexible liners. Conversely, more compressible liners have smaller thrusts but larger moments than less compressible liners.

Figures 7.29 through 7.32 illustrate the variation of liner (crown) thrusts, moments and circumferential stresses with the liner radius-to-thickness ratio (a/t) for several values of the medium-to-liner modulus ratio (E_m/E_ℓ) for both localized gravity and excavation loading. The excavation loading curves were obtained from the analytical solution discussed in

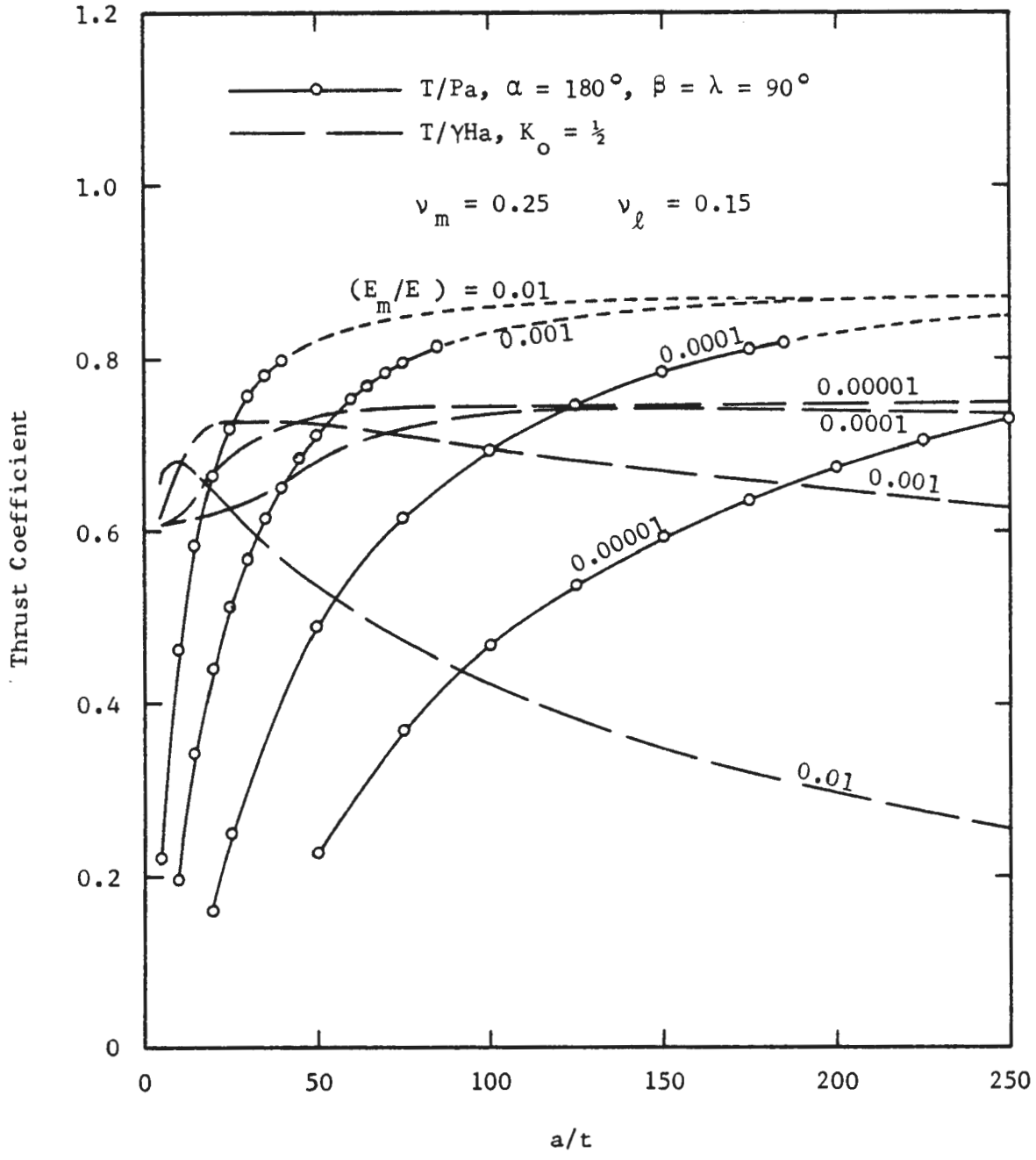

FIGURE 7.29 VARIATION OF CROWN THRUST COEFFICIENT WITH (a/t) FOR LOCALIZED GRAVITY AND EXCAVATION LOADING

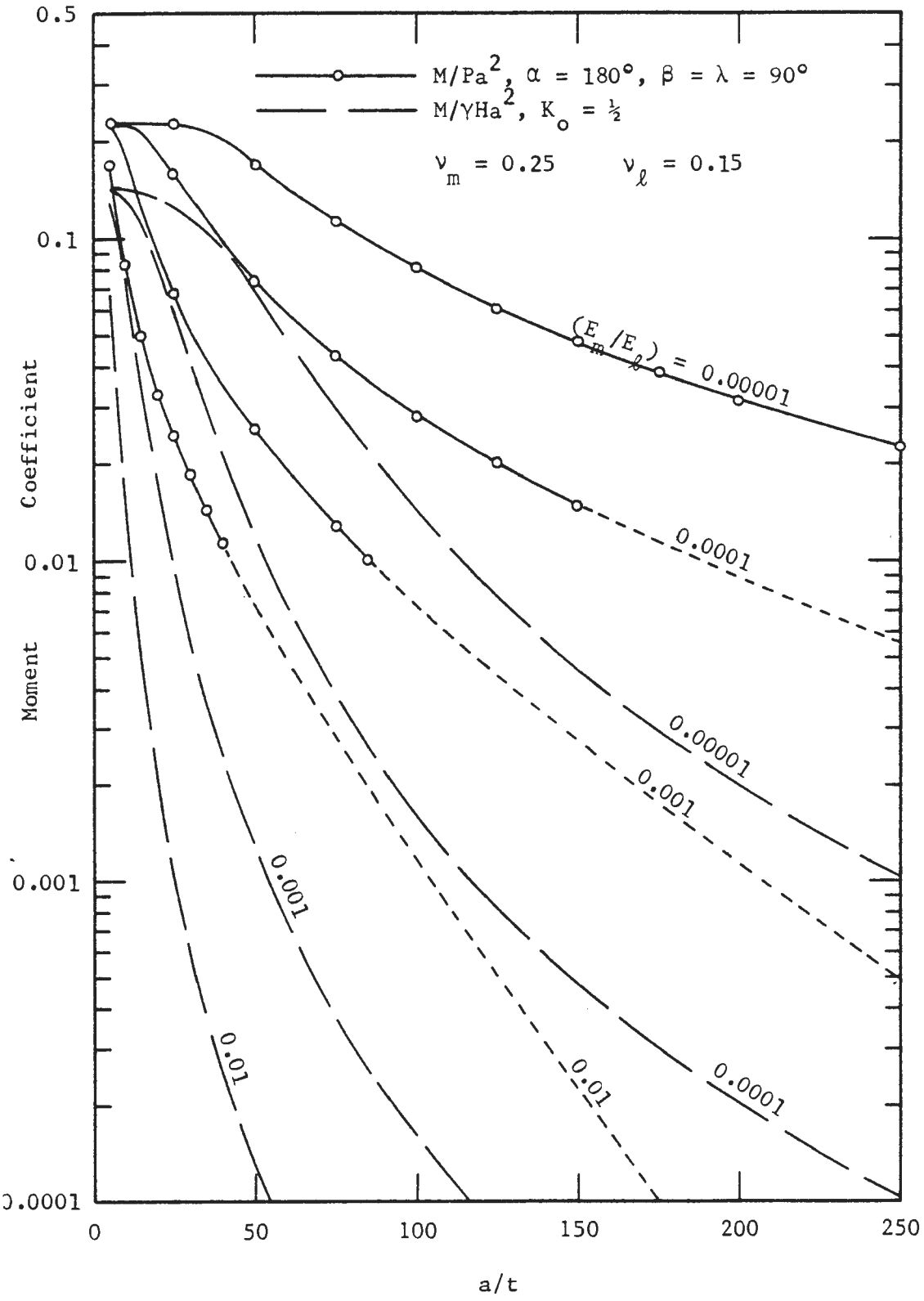

FIGURE 7.30 VARIATION OF CROWN MOMENT COEFFICIENT WITH (a/t) FOR LOCALIZED GRAVITY AND EXCAVATION LOADING

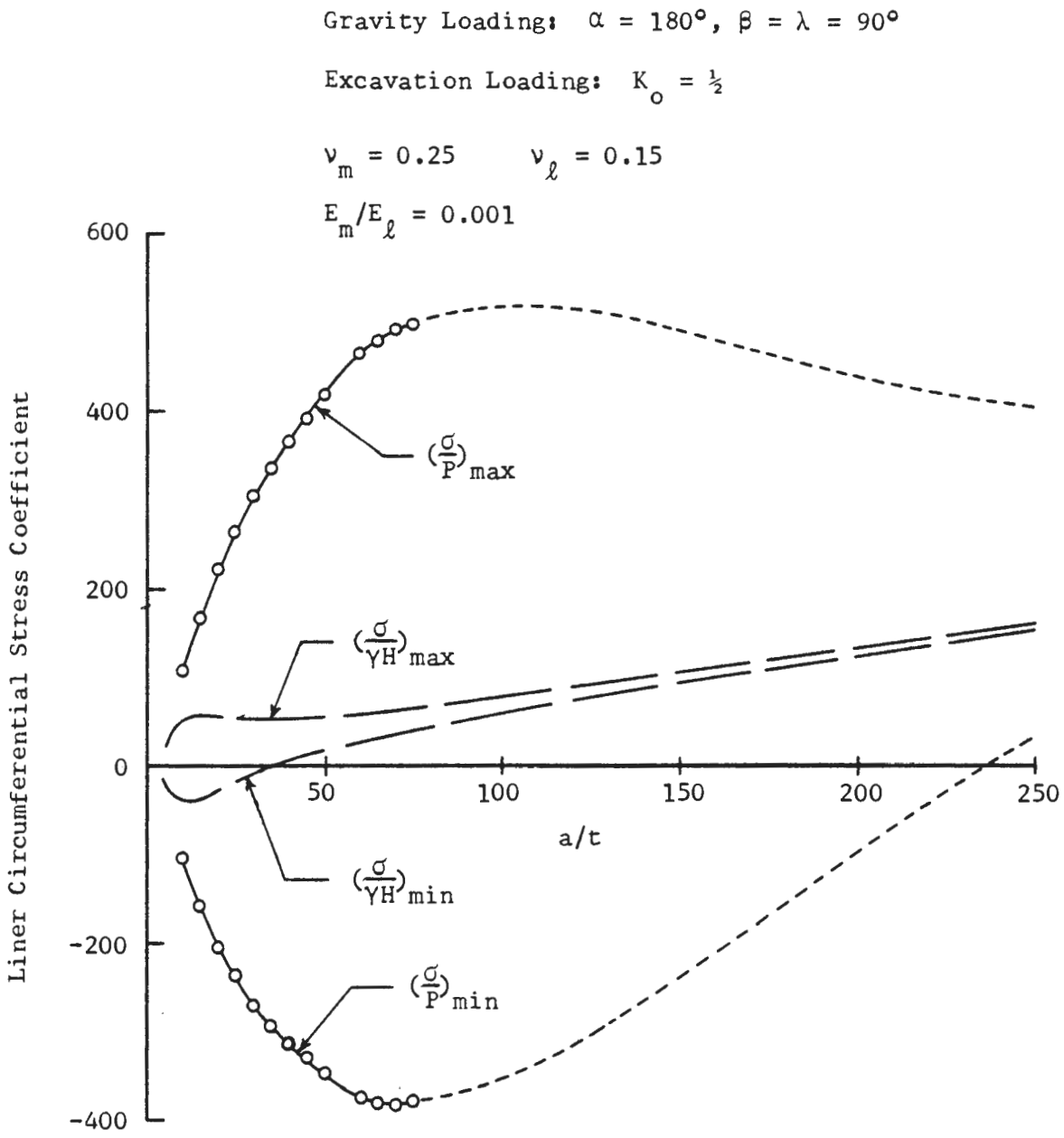

FIGURE 7.31 VARIATION OF MAXIMUM AND MINIMUM LINER CIRCUMFERENTIAL STRESSES AT CROWN FOR LOCALIZED GRAVITY AND EXCAVATION LOADING (E_m/E_ℓ = 0.001)

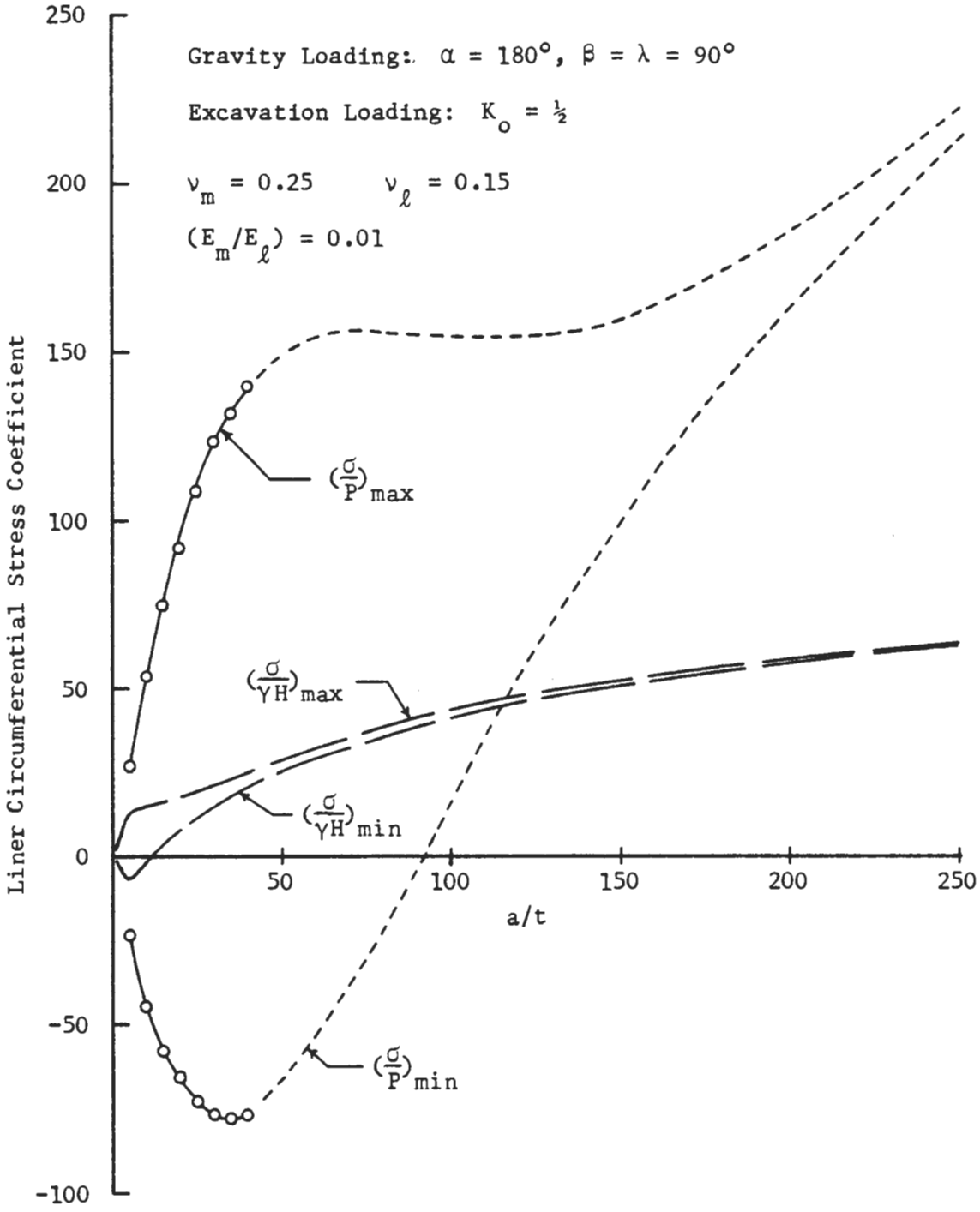

FIGURE 7.32 VARIATION OF MAXIMUM AND MINIMUM LINER CIRCUMFERENTIAL STRESSES AT CROWN FOR LOCALIZED GRAVITY AND EXCAVATION LOADING ($E_m/E_\ell = 0.01$)

Chapter 3, assuming $K_o = 0.5$. The localized gravity loading curves were obtained from Eqns. 7.1 and 7.2, assuming $\alpha = 180$ degrees. Points on these curves were obtained by first calculating the flexibility and compressibility ratios, given a/t and E_m/E_ℓ. The F and C values were then used in Eqns. 7.1 and 7.2 and the related tables and charts. Certain combinations of a/t and E_m/E_ℓ yielded F values outside the range of the charts ($1 \leq F \leq 1000$). These portions of the curves in Figs. 7.29 and 7.30 are shown as dashed lines, indicating that they consist of extrapolated and/or estimated, rather than directly calculated, points. The dashed portions of the localized gravity loading curves in Figs. 7.31 and 7.32 were obtained from calculations based on the dashed portions of the curves in Figs. 7.29 and 7.30.

Figures 7.31 and 7.32 show that the stress coefficients for localized gravity loading (σ/P) are much larger in magnitude than those for excavation loading ($\sigma/\gamma H$). However, the relative magnitudes of the stresses for the two types of loading depend on the magnitudes of P and γH. Usually, γH will be much larger than P. These same two figures show that the range of a/t values over which tensile (negative) stresses will result at the crown is much larger for localized gravity loading than it is for excavation loading.

CHAPTER 8

SUMMARY AND CONCLUSIONS

Interaction between tunnel liner and surrounding ground mass has been examined both analytically and numerically (finite element method) for various loading conditions and construction sequences.

The general class of ground-liner interaction problems can be divided into three catagories on the basis of the type of loading to which the tunnel liner is subjected. In this investigation three loading types, or conditions, were considered. These are the overpressure loading condition, the excavation loading condition, and the localized gravity loading condition.

The overpressure loading condition results when the ground-liner system is subjected to an externally applied pressure at the ground surface. In the analysis of this type of interaction problem the in situ ground stresses are neglected and the lined tunnel is assumed to be present within the ground mass before the overpressure is applied to the system. This loading condition was discussed briefly in Chapter 2. Also, derivations of analytical solutions for this loading condition were given in Appendix A.

Whereas analyses of the overpressure loading condition are applicable only to existing lined tunnels, analyses of the excavation loading condition yield the interaction response of the ground and liner resulting from construction of the tunnel. In order for ground-liner interaction due to the excavation loading condition to occur the liner must be installed such that it resists some or all of the inward displacements of the ground mass arising from excavation of the tunnel opening. Excavation loading

ground-liner interaction was considered in some detail in this investigation. Analytical solutions applicable to certain special cases of this loading condition were derived and presented in Appendicies A and B and discussed in Chapters 2 and 3. The results of finite element analyses of interaction due to excavation loading were presented in Chapter 4 for shallow tunnels and in Chapter 6 for the case of two adjacent parallel tunnels. The excavation loading condition was also considered in Chapter 5, where the results from finite element analyses that simulated the advancement of the tunnel through the ground mass were presented and discussed.

For the excavation loading condition it is assumed that the ground around the perimeter of the tunnel opening remains intact, and that the ground displaces inward, en masse, against the liner. For the localized gravity loading condition, on the other hand, it is assumed that the ground does not remain intact. Instead, it is assumed that the shear stresses mobilized in the ground mass due to excavation of the opening, relative to the ground's shear strength, are such that the force of gravity is sufficient to cause portions of this ground to dislodge and fall onto the liner. The weight of this material, which usually comes to rest on or against only a portion of the liner's circumference, constitutes the localized gravity load. The results from a number of finite element analyses of this loading condition were presented and discussed in Chapter 7.

Various solution methods available for the analysis of ground-liner interaction were briefly reviewed in Chapter 2. These include the analytical solutions based on the ground reaction curve concept, the analytical solutions for circular tunnels in elastic ground, and the finite element method.

Ground-liner interaction resulting from the overpressure loading

condition can be analyzed by both the finite element method and the analytical solutions derived for this type of loading. If inelastic stress-strain behavior of the ground mass is to be considered the finite element method must be used. However, for this type of interaction problem the surrounding ground will exhibit significant inelastic behavior only if the magnitude of the overpressure is quite high and the liner is sufficiently flexible and compressible so that large liner displacements and distortions occur. In most cases this problem can be adequately examined with the analytical solutions for elastic ground proposed by Burns and Richard (1964) and Dar and Bates (1974). The derivations of these solutions are given in Appendix A and the resulting equations are summarized in Appendix B.

Analytical solutions, such as those described by Széchy (1966) and Procter and White (1946), are available for analysis of ground-liner interaction resulting from the localized gravity loading condition. A more detailed analysis of this type of interaction problem can be achieved through the use of numerical techniques such as the finite element method. However, because of the many variables that would have to be considered in order to perform a realistic simulation of this loading condition, even the finite element method falls short of allowing a truely comprehensive treatment of all facets of this problem. Thus, in most cases, this type of problem must be reduced to an idealized form more conducive to analysis, as was done in the finite element study of this loading condition presented in Chapter 7.

As was shown in Chapters 2 and 5 the extent of ground-liner interaction resulting from the excavation loading condition is strongly dependent on the amount of ground displacement occurring prior to ground-liner contact relative to the potential total displacement. Maximum interaction occurs if

there are no prior displacements, i.e., if the liner must resist the total potential displacement. There is no interaction if all ground displacements occur before ground-liner contact is established.

Each of the three solution methods previously mentioned can be used to analyze this form of the interaction problem. Solutions based on the ground reaction curve concept allow consideration of inelastic and time-dependent material behavior models for the ground mass. However, these solutions do not allow consideration of the distortional component of loading and the resulting liner bending moments and shear forces. Conversely, the analytical solutions for a circular tunnel in elastic ground can account for both the uniform and distortional components of loading, but are restricted to elastic ground behavior. The finite element method, of course, allows consideration of both nonuniform loadings and inelastic and/or time-dependent ground behavior.

The response of a tunnel liner to interaction with the surrounding ground mass was examined in Chapter 3 for the case of excavation loading as given by the analytical solutions derived in Appendix A for thin liners. These solutions give the liner forces, moments and displacements as functions of the ground-liner compressibility and flexibility ratios. It was found that the liner bending moments are quite sensitive to the flexibility of the liner; and that, in the lower range of flexibility ratio values ($0 \leq F \leq 20$) small increases of liner flexibility result in significant reductions of bending moments. Liner thrusts are more sensitive to liner compressibility than they are to liner flexibility; and larger compressibility ratio values correspond to lower thrust magnitudes. Also illustrated in Chapter 3 were the variations of liner forces, displacements and circumferential stresses

with the liner radius-to-thickness ratio, a/t, for several values of the ground-liner modulus ratio, E_m/E_ℓ. Again, these curves were obtained from the "thin liner" analytical solutions for excavation loading derived in Appendix A. The figures presented show that liner thrusts and bending moments can be significantly reduced by reducing the liner thickness and/or modulus (thereby making the liner more flexible and compressible). However, reduction of liner thickness always leads to increased liner displacements and, except for a narrow range of a/t values, increased liner stresses. Reduction of liner modulus, as may be possible for concrete liners, results in lower stresses, but such action would also be accompanied by reduced compressive strength for this type of liner. Liner modulus reduction also always leads to increased liner displacements.

Because of the initial assumptions involved in the formulation of the analytical solutions for excavation loading ground-liner interaction, the application of these solutions is supposedly restricted to tunnels located at great depth below the ground surface. However, similar restrictions are necessarily applied to the solutions for stresses and displacements around unlined openings; and yet it is commonly held that these solutions can be applied to openings at depths as shallow as one or two opening diameters. In order to determine whether or not the depth restriction on the lined tunnel solutions could be similarily relaxed a finite element study of shallow lined tunnels was undertaken.

The results of this study, which were presented in Chapter 4, were obtained from finite element analyses of lined tunnels located at various depths of burial (H/D = 1.0 - 5.0). Except for the depth factor these analyses were equivalent to the analytical solutions for excavation loading.

It was found that there are two factors that can significantly influence the behavior of shallow lined tunnels. These factors are the proximity of the ground surface boundary and the increase of in situ stress with depth from the tunnel crown to the invert. In general, the results obtained from the analyses performed indicated that, with respect to liner thrusts, moments and displacements, the first of these factors is less significant than the second. The influence of the ground surface boundary on liner response is small for $1.0 < H/D < 2.0$ and negligible for all $H/D < 2.0$. The influence of the stress increase with depth from crown to invert is greater than the influence of the ground surface boundary, at least for $H/D > 1.0$ and remains at a significant level to a much greater depth.

For the ground-liner system considered the influence of the in situ stress increase from crown to invert was greatest for the no slippage condition. This difference between the liner responses for the full and no slippage conditions is especially evident when liner thrusts are considered. It is less evident when liner bending moments and displacements for the two interface conditions are compared.

When liner thrusts, moments and radial displacements are considered the effect of the in situ stress increase with depth is so great at shallow depths that it appears the analytical solutions should not be used for $H/D > 4$ or 5. However, when the thrusts and moments are combined to yield the liner circumferential stresses a considerably different picture is obtained, especially if only the maximum and minimum circumferential stresses are considered. It was found that, due to the nature of the depth variations of thrusts and moments, these stresses change very little with tunnel depth for $H/D > 2$. Thus, on the basis of the results obtained from the analyses

performed, it is concluded that the analytical solutions for excavation loading will yield good values of the maximum and minimum liner circumferential stresses for all $H/D > 2$ and reasonably good values of liner thrusts, moments and displacements for all $H/D > 4$ or 5.

Analytical solutions such as those derived in Appendix A for excavation loading are often criticized because they consider only a two-dimensional cross section of the ground-liner system and because they do not account for inelastic behavior of the surrounding ground mass. However, as long as these solutions are used properly this criticism is not warrented.

The analytical solutions for excavation loading were derived for the special case of a tunnel constructed such that the liner is installed first (e.g., by a series of drifts around the perimeter of the tunnel), followed by the excavation of the soil core inside the liner. For this construction sequence ground-liner interaction results because of the imbalance between the stresses on the inside (zero) and the outside (in situ stress state) of the liner. The full magnitude of the in situ stress is properly taken into account because there has been no opportunity for significant relaxation of the surrounding ground mass. At a given point along the tunnel line interaction does not commence until the excavation face approaches; and it is not complete until the face is mined a sufficient distance past this point. Within this transition zone, which exists because of the influence of the core of soil ahead of the face, there are three-dimensional (radial, circumferential and longitudinal) variations of stresses and displacements; and the analytical solutions do not apply here. However, full development of liner forces and displacements only occurs behind this zone, where interaction is complete (liner carrying entire load) and the stresses

and displacements no longer exhibit three-dimensional variations. Because the ground-liner system, at the points where interaction is complete, exhibits only two-dimensional (radial and circumferential) variations of stresses and displacements, the analytical solutions for excavation loading are directly applicable to this problem.

The inability of the analytical solutions to account for inelastic behavior of the ground mass should not, in most cases, be a serious disadvantage if these solutions are properly applied to only the special case conditions for which they were derived (i.e., liner installed before excavation of the soil core). For this special case the liner is in place before the equilibrium of the surrounding ground mass is disturbed. Once this equilibrium is disturbed, by excavation of the soil core, the liner, unless it is quite flexible and compressible, will provide sufficient restraint to prevent significant inelastic behavior from occurring.

Unfortunately, the analytical solutions for excavation loading are quite susceptible to misuse. There is a tendency for these solutions to be applied, without complete regard to their limitations with respect to construction sequence, to all problems of this type. This leads to the inappropriate use of these solutions in the consideration of tunnels constructed by more conventional means, i.e., construction sequences consisting of excavation followed by liner installation. As was illustrated by the results from axisymmetric finite element analyses presented in Chapter 5, for this type of construction sequence the behavior of a lined tunnel is strongly influenced by the ground displacements that occur before the liner comes into contact with the ground mass. When displacements of the ground mass prior to ground-liner contact are allowed to occur the interaction

problem becomes much too complex to be properly considered by solution methods that assume the problem to be two-dimensional and elastic.

The results presented in Chapter 5 indicate that the response of the liner to interaction is a function of the relative magnitudes of the ground displacements that occur ahead of the liner and the displacements that would occur if no liner was installed. In turn the magnitude of the prior displacements, and the behavior of the ground mass ahead of the liner in general, is a function of the position of liner installation relative to the position of the tunnel face; and, to a lesser extent, the flexibility and compressibility of the liner. Thus, the maximum liner thrust, as an example, results when the liner is installed right at the tunnel face (this maximum value is still less than that given by the analytical solution because of the ground displacements occurring ahead of the face). If the liner is installed far enough behind the face, beyond the point where full ground displacement has occurred, there is no interaction because the liner remains unloaded (this is assuming that the unlined portion of the tunnel remains stable and that the ground mass does not exhibit time-dependent behavior). In addition, it was shown that the extent of inelastic ground mass behavior increases as the distance between the advancing face and the point of liner installation is increased. Results obtained from the elasto-plastic analyses indicate that by installing a relatively stiff liner right at the face (or limiting displacements by some other means) the formation of plastic zones around the tunnel can be prevented. However, the results also indicate that if a length of tunnel behind the face equal to one tunnel radius is left unlined the resulting relaxation of the ground mass can be sufficient to mobilize enough plastic yielding to significantly alter liner

response relative to that obtained from elastic analyses (if the shear strength of the soil is sufficiently low relative to the shear stresses mobilized so that yielding will occur).

In the analysis of a lined tunnel constructed by conventional methods simulation of the physical advancement of the tunnel through the ground mass is just as important as consideration of three-dimensional behavior in the vicinity of the tunnel face. This point was clearly demonstrated in the discussion of Fig. 2.11, the data for which was obtained in the investigation described in Chapter 5. Simulation of tunnel advancement is especially critical if elasto-plastic behavior of the ground mass is to be considered because such simulation is required in order to obtain full development of the plastic zone around the tunnel.

On the basis of the results obtained from the investigation described in Chapter 5 it can be concluded that the behavior of a lined tunnel constructed by conventional methods cannot be accurately determined from any solution method that does not consider the three-dimensional nature of the problem and the actual advancement of the tunnel through the ground mass. This means that anything less than a fully three-dimensional finite element analysis will yield only approximate results. Because such analyses are extremely expensive and difficult to perform, especially if inelastic behavior and construction simulation are to be considered, the necessity for accepting approximate results seems inevitable in most cases.

The axisymmetric finite element analysis represents a reasonable alternative to the fully three-dimensional analysis. With this type of analysis it is possible to consider material behavior other than elastic and to simulate tunnel advancement and construction. However, shallow

tunnels cannot be considered, and if the problem being studied is not truely axially symmetric the information obtained from this type of analysis is of somewhat limited usefulness.

Two-dimensional finite element analyses allow consideration of inelastic and time-dependent material behavior. These analyses are not limited to axially symmetric conditions, but they cannot properly account for the three-dimensional effects or the advancement of the tunnel through the ground mass. Although it is possible for these analyses to be performed such that a given amount of ground displacement prior to ground-liner contact is introduced into the analysis, this can only be done by utilizing special techniques that greatly increase the difficulty of performing the analysis. In addition, without access to three-dimensional analyses the magnitude of this prior displacement can only be crudely approximated (see discussion of Figs. 2.4 - 2.6).

Two-dimensional analytical solutions such as those based on the ground reaction curve concept also allow consideration of inelastic and time-dependent behavior, but the number of available material behavior models is rather limited, and only axially symmetric conditions can be considered. While it is easier to introduce a given amount of prior displacement in these analyses than it is in the two-dimensional finite element analyses, again the magnitude of this displacement connot be determined on a rational basis.

At the very bottom of the list of solution methods suitable for the interaction analysis of tunnels constructed by conventional methods are the two-dimensional, elastic analytical solutions for excavation loading derived in Appendix A. Although these solutions can be modified to account

for prior displacements, such modification adds little to their usefulness because they are limited to consideration of elastic behavior. In addition, as was the case with the other two-dimensional methods of analysis discussed above, these modified equations, of themselves, provide no means for correctly determining the magnitudes of these prior displacements.

Despite the fact that the analytical solutions for excavation loading were not derived for, and, therefore, are theoretically not directly applicable to, the general case of a lined tunnel constructed by conventional methods, it would seem that they could serve a useful purpose for the preliminary analysis of many such cases. For example, the data presented in Fig. 5.12 suggests that, while these solutions do not account for prior displacements or inelastic behavior of the ground mass, they provide upper bound values for the initial (end of construction) liner response. Additionally, while the analytical solutions may significantly overestimate the initial liner response, the ensuing time-dependent behavior of the ground-liner system may, for some soils, result in thrust magnitudes more nearly in line with the analytical solution values. Because these solutions assume that pressures corresponding to the full overburden stress act on the liner it should only be in certain special cases (e.g., squeezing or swelling ground) that they would underestimate liner response to interaction. Thus, it would seem that, in addition to being directly applicable to the specific problem for which they were derived, the analytical solutions for excavation loading also provide a convenient means for obtaineng at least a first approximation of liner response for many of the interaction problems that consider a lined tunnel constructed by conventional methods. It must be emphasized, however, that such use of these solutions has no theoretical basis

and is, in the strictest sense, inappropriate.

As described in Chapter 6, a series of finite element analyses was performed to study the behavior of a system of two parallel tunnels. Quantities of interest in the analysis of two tunnel systems are; stresses around the two tunnels, especially in the pillar separating the two tunnels; tunnel displacements; liner forces; and the ground surface displacements. The main parameters considered in this study were; tunnel depth, width of the pillar separating the two tunnels, the tunnel support conditions, sequence of construction of the two tunnels, and, to some extent, the influence of plastic yielding in the ground mass.

The finite element analyses performed in this study indicated that interaction between two parallel tunnels influences ground stresses, tunnel displacements and liner forces in only a relatively small region around the pillar that separates the tunnels, and that these interaction effects decrease as the pillar width is increased. Response of the two tunnel system at tunnel depth, over the range of pillar widths considered herein, suggests that interaction effects are small at a pillar width to tunnel diameter ratio of one; and that at a W/D value of approximately two the two tunnels should behave independently of each other.

Interaction between the two tunnels also influences the displacements of the ground surface above the tunnels. Vertical compression (shortening) of the pillar separating the tunnels gives rise to additional settlements. Pillar compression increases as the pillar width is reduced and/or as the depth is increased. For shallow tunnels the additional interaction settlements are confined to a relatively narrow zone above the pillar and the two tunnels. However, for deep tunnels lateral spreading of vertical

ground displacements with increasing distance above the tunnels results in a very wide settlement trough with an almost uniform distribution of additional interaction settlements. The analyses performed in this study indicate that for shallow tunnels, with depth to diameter ratio of H/D = 1.5, a pillar width ratio of approximately two should be sufficient to eliminate the additional interaction settlements. The data also suggest, however, that for relatively deep tunnels (H/D = 5.5) a much greater tunnel spacing would be required to achieve this goal.

The results of the finite element analyses of various sequences of construction indicate that the construction of a tunnel parallel and adjacent to an existing tunnel causes additional displacements and liner forces in the existing tunnel. The magnitudes of these changes strongly depend on the width of the pillar separating the two tunnels and the displacements allowed in the construction of the second tunnel. Two extreme cases were considered; in one case the second tunnel was lined upon excavation, in the other case the second tunnel was left unlined. When the second tunnel was lined the changes caused by the second tunnel resulted in a more favorable condition in the existing tunnel. However, when the second tunnel was left unlined significant increases of displacements and forces in the liner of the existing tunnel occurred in the vicinity of the pillar springline. Because at least some, if not large, ground movements associated with excavation of the second tunnel can be expected to occur for real tunnels in soil, the analyses that assume the second tunnel to be unlined more closely approximate the real tunnel situation.

It was also shown that some of the analyses indicate that the excavation of the second tunnel causes greater ground surface settlement than

would a single tunnel. This is especially so when plastic yielding occurs in the medium and displacements are allowed prior to the liner becoming effective.

It should be pointed out that the analyses performed did not include simulation of the large displacements and volume changes in the soil that are often associated with excavation and construction of tunnels in soft ground. Thus, the results of these analyses represent lower bounds for the interaction effects (e.g., effect on existing tunnel due to passage of second tunnel at a given pillar width and additional surface settlements arising from interaction between two tunnels) for two parallel tunnels.

Ground-liner interaction for localized gravity loading was considered in Chapter 7. In this investigation the distribution and magnitude of the localized gravity load were treated as variables for study. The other variables considered were the ground-liner flexibility and compressibility ratios. In all analyses it was assumed that the weight of the material resting on the liner exerted a uniform pressure over a given portion of the liner. However, it was shown that the principle of superposition can be used, within limits, to consider nonuniform loadings. In addition, results in the form of liner thrust and bending moment coefficients were presented in chart form to allow determination of these values, by interpolation, for compressibility and flexibility ratio combinations other than those specifically analyzed.

Results obtained from the finite element analyses indicated that, for a uniform vertical gravity load symmetrical about the tunnel crown, the maximum bending moment and the minimum thrust both occur at the crown. Below the springlines there is little variation of thrust and bending moment

magnitudes with circumferential location; the moments here are very small whereas the thrusts are at or near their maximum magnitude. Thus, in terms of circumferential stresses the critical section is located at the crown where both the maximum and minimum liner stresses occur.

It was found that liner thrusts tend to increase with increasing flexibility ratio and decrease with increasing compressibility ratio. Liner bending moments, on the other hand, tend to decrease with increasing flexibility ratio and increase with increasing compressibility ratio.

Magnitudes of liner thrust, moments and displacements were found to increase linearly with the magnitude of the pressure exerted on the liner by the localized gravity load throughout the range of pressures considered (up to 20 psi = 138 kPa).

An initial series of symmetrical loading analyses considered a range of values for the circumferential extent or distribution of the vertical gravity load; from $\alpha = 180$ degrees to $\alpha = 30$ degrees (where $\alpha = 180$ degrees indicates that the load is distributed over the entire upper half of the liner). The results from these analyses indicate that there is little variation of liner response within the range $180 > \alpha > 60$ degrees. The variation that does occur is such that conservative results can be obtained by assuming that $\alpha = 180$ degrees.

The magnitudes and distributions of liner forces and moments, and thus stresses, resulting from the localized gravity loading condition are considerably different from those mobilized by the general form of the excavation loading condition. Thus, where conditions are such that either or both types of loading can occur, interaction analyses for both should be performed.

Each of the solution methods applicable to the analysis of ground-liner interaction discussed herein attempts to mathematically simulate the response of the ground-liner system for a range of possible conditions. However, while most solution methods include consideration of the most important aspects of the ground-liner interaction process, none of these methods can accurately simulate all of the details relevant to the problem. All solution methods are necessarily based on simplifying assumptions that are designed to reduce the complexity of the interaction problem to a sufficient degree so as to allow a solution to be obtained. Some methods require more simplifying assumptions than others and, in general, the more assumptions made the less accurately the procedure simulates the real conditions.

The majority of the available analytical solutions have the advantage of being straight forward and easy to use. The major disadvantage to these solution methods is that they only consider an highly idealized form of the real problem. Numerical solution techniques, such as the finite element method, allow much more detailed simulations. However, as the degree of simulation detail is increased, the complexity of the analysis also increases. At one extreme are the highly detailed analyses which are quite complex and thus difficult to perform and interpret. Such analyses can be performed only with the most sophisticated finite element computer programs, programs which require large and equally sophisticated computer facilities. At the other extreme are the analyses which provide solutions to a much more idealized form of the problem. Although these simplified analyses can be inexpensive and easy to perform, they may provide no more useful information than would be available from the closed form analytical solutions. As with the analytical methods, the results obtained from finite element analyses

can not be applied to the design or evaluation of a tunnel support system without first being carefully evaluated with respect to the differences between the ground-liner system as simulated and as it exists in reality.

Indiscriminate use of any of the available methods of analysis can lead to erroneous conclusions with respect to the real tunnel behavior. It is important that the method of analysis selected be applicable to the problem being considered. It is also important that the results obtained from the analysis be properly interpreted. This requires knowledge of both the anticipated tunneling conditions and the adequacy of the analysis to simulate these conditions.

REFERENCES

Barla, G. and M. Ottoviani (1974). "Stresses and Displacements Around Two Adjacent Circular Openings Near to the Ground Surface," Proceedings, Third International Congress on Rock Mechanics, Denver, Vol. II, pp. 975 - 980.

Barton, N., R. Lien and J. Lunde (1974). "Engineering Classification of Rock Masses for the Design of Tunnel Support," Rock Mechanics, Vol. 6, No. 4, pp. 189 - 236.

Bawa, K. S. and A. Bumanis (1972). "Design Considerations for Underground Structures in Rock," Proceedings, First North American Rapid Excavation and Tunneling Conference, Chicago, Vol. 1, pp. 393 - 418.

Brierley, G. (1975). The Performance During Construction of the Liner for a Large, Shallow Underground Opening in Rock, Ph. D. Thesis, University of Illinois, Urbana.

Burns, J. Q. and R. M. Richard (1964). "Attenuation of Stresses for Buried Cylinders," Proceedings, Symposium on Soil-Structure Interaction, Tucson, pp. 378 - 392.

Christian, J. T. and H. W. Ing (1973). "Errors in Simulating Excavation in Elastic Media by Finite Elements," Soils and Foundations (Japan), Vol. 13, No. 1, pp. 1 - 10.

Clough, R. W. and R. J. Woodward III (1967). "Analysis of Embankment Stresses and Deformations," Journal of the Soil Mechanics and Foundation Division, ASCE, Vol. 93, No. SM4, pp. 529 - 549.

Curtis, D. J. (1976). Discussion of: Muir Wood, A. M., "The Circular Tunnel in Elastic Ground," Geotechnique, Vol. 26, No. 2, pp. 231 - 237.

Daemen, J. J. K. (1975). Tunnel Support Loading Caused by Rock Failure, Ph. D. Thesis, University of Minnesota, Minneapolis.

Dar, S. M. and R. C. Bates (1974). "Stress Analysis of Hollow Cylindrical Inclusions," Journal of the Geotechnical Engineering Division, ASCE, Vol. 100, No. GT2, pp. 123 - 138.

Deere, D. U., R. B. Peck, J. E. Monsees and B. Schmidt (1969). Design of Tunnel Liners and Support Systems, Report for U. S. Department of Transportation, Office of High Speed Ground Transportation, Contract 3 - 0152.

Dixon, J. D. (1971). Analysis of Tunnel Support Structures with Consideration of Support-Rock Interaction, Report of Investigations 7526, U. S. Bureau of Mines.

Dixon, J. D. (1973). Structural Design Data for Concrete Drift Linings in Block Caving Stopes, Report of Investigations 7792, U. S. Bureau of Mines.

Drucker, D. C. and W. Prager (1952). "Soil Mechanics and Plastic Analysis or Limit Design," Quarterly of Applied Mathematics, Vol. 10, No. 2, pp. 157 - 165.

Duncan, J. M. and P. Dunlop (1968). Slopes in Stiff-Fissured Clays and Shales, Contract Report No. TE 68-6, U. S. Army Engineer Waterways Experiment Station, Vicksburg, Mississippi.

Flügge, W. (1973). Stresses in Shells, 2nd. Ed., Springer-Verlag, Berlin.

Fotieva, N. N. and V. I. Sheinin (1966). "Distribution of Stresses in the Lining of a Circular Tunnel when Driving a Parallel Tunnel," Soil Mechanics and Foundation Engineering (USSR), No. 6, pp. 417 - 422.

Ghaboussi, J., E. L. Wilson and J. Isenberg (1973). "Finite Element for Rock Joints and Interfaces," Journal of the Soil Mechanics and Foundation Division, ASCE, Vol. 99, No. SM10, pp. 835 - 848.

Ghaboussi, J. and R. E. Ranken (1974). Tunnel Design Considerations: Analysis of Medium-Support Interaction, Report No. FRA - ORDD 75 - 24, Federal Railroad Administration, U. S. Department of Transportation.

Goodman, R. E., R. Taylor and T. L. Brekke (1968). "A Model for the Mechanics of Jointed Rock," Journal of the Soil Mechanics and Foundation Division, ASCE, Vol. 94, No. SM3, pp. 637 - 659.

Hansmire, W. H. (1975). Field Measurements of Ground Displacements About a Tunnel in Soil, Ph. D. Thesis, University of Illinois, Urbana.

Höeg, K. (1968). "Stresses Against Underground Structural Cylinders," Journal of the Soil Mechanics and Foundation Division, ASCE, Vol. 94, No. SM4, pp. 833 - 858.

Kastner, H. (1962). Statik des Tunnel- und Stollenbaues, Springer- Verlag, Berlin.

Kreyszig, E. (1967). Advanced Engineering Mathematics, 2nd Ed., John Wiley and Sons, Inc., New York.

Kulawy, F. H., J. M. Duncan and H. B. Seed (1969). Finite Element Analysis of Stresses and Movements in Embankments During Construction, Contract Report S - 69 - 8, U. S. Army Engineers Waterways Experiment Station, Vicksburg, Mississippi.

Labasse, H. (1949). "Les Pressions de Terrains Autour des Puits," Revue Universelle des Mines, 92e Annee, S. 9, V. 5, pp. 78 - 88.

Ladanyi, B. (1974). "Use of the Long-Term Strength Concept in the Determination of Ground Pressure on Tunnel Linings," Proceedings, Third International Congress on Rock Mechanics, Denver, Vol. II, pp. 1150 - 1156.

Lombardi, G. (1970). "The Influence of Rock Characteristics on the Stability of Rock Cavities," Tunnels and Tunnelling, Vol. 2, No. 1, pp. 19 - 22, and Vol. 2, No. 2, pp. 104 - 109.

Mindlin, R. D. (1940). "Stress Distributions Around a Tunnel," Transactions, ASCE, Vol. 105, pp. 1117 - 1153.

Mohraz, B., A. J. Hendron, Jr., R. E. Ranken and M. H. Salem (1975). "Liner-Medium Interaction in Tunnels," Journal of the Construction Division, ASCE, Vol. 101, No. CO1, pp. 127 - 141.

Morgan, H. D. (1961). "A Contribution to the Analysis of Stress in a Circular Tunnel," Geotechnique, Vol. 11, No. 1, pp. 37 - 46.

Muir Wood, A. M. (1969). Discussion of: Peck, R. B., "Deep Excavations and Tunneling in Soft Ground," Proceedings, 7th International Conference on Soil Mechanics and Foundation Engineering, Mexico City, Vol. 3, pp. 363 - 365.

Muir Wood, A. M. (1975). "The Circular Tunnel in Elastic Ground," Geotechnique, Vol. 25, No. 1, pp. 115 - 127.

Obert, L. and W. I. Duvall (1967). Rock Mechanics and the Design of Structures in Rock, John Wiley and Sons, Inc., New York.

O'Rourke, T. D. (1975). A Study of Two Braced Excavations in Sands and Interbedded Stiff Clay, Ph. D. Thesis, University of Illinois, Urbana.

Pacher, F. (1964). "Deformationsmessungen im Versuchsstollen als Mittel zur Erforschung des Gebirgsverhaltens und zur Bemessung des Ausbaues," Felsmechanik und Ingenieurgeologie, Supplementum IV, pp. 149 - 161.

Peck, R. B. (1969). "Deep Excavations and Tunneling in Soft Ground," Proceedings, 7th International Conference on Soil Mechanics and Foundation Engineering, Mexico City, State of the Art Volume, pp. 225 - 290.

Peck, R. B., D. U. Deere, J. E. Monsees, H. W. Parker, and B. Schmidt (1969). Some Design Considerations in the Selection of Underground Support Systems, Report for U. S. Department of Transportation, Office of High Speed Ground Transportation and Urban Mass Transportation Administration, Contract No. 3-0152.

Peck, R. B., A. J. Hendron, Jr. and B. Mohraz (1972). "State of the Art of Soft Ground Tunneling," Proceedings, First North American Rapid Excavation and Tunneling Conference, Chicago, Vol. 1, pp. 259 -286.

1 to 2 DIAMETERS

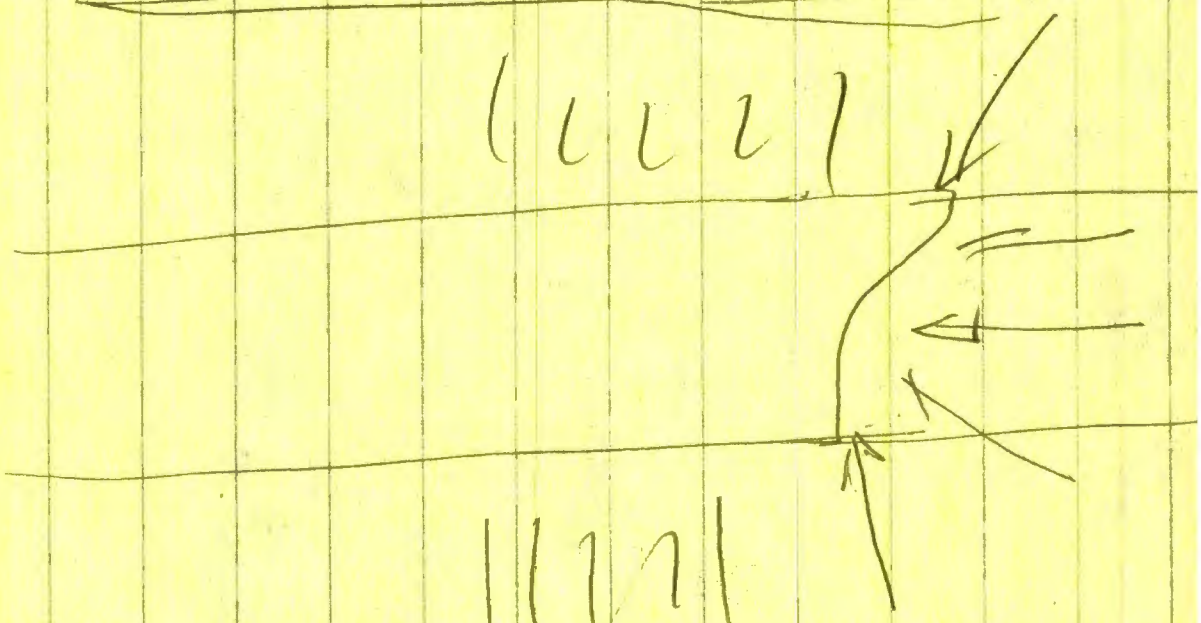

GRAVITY INCREASES DOWNWARD
COMPONENT DECREASES UPWARD COMPONENTS.

$$\frac{3800}{760} = 20\%$$

$$20\% = 760$$

$$100\% = \frac{100 \times 760}{20} = \frac{760}{.2}$$

$$100\% = 3800$$

3000
2000
1000

Proctor, R. V. and T. L. White (1946). Rock Tunneling with Steel Supports, The Commercial Shearing and Stamping Company, Youngstown, Ohio.

Rabcewicz, L. v (1969). "Stability of Tunnels under Rock Load," Water Power, June, pp. 225 - 229; July, pp. 266 - 273; August, pp. 297 - 302.

Sauer, G. and P. Jonuscheit (1976). "Krafteumlagerungen in der Zwischenwand eines Doppelrohrentunnels im Zuge eines Synchronvortriebs," Rock Mechanics, Vol. 8, No. 1, pp. 1 - 22.

Savin, G. N. (1968). Stress Distribution Around Holes, Translation of Raspredeleniye Napryazheniy Okolo Otversity, Naukova Dumka Press, Kiev. NASA Technical Translation, NASA-TT-F-607 (1970).

Selby, S. M. (1973). CRC Standard Mathematical Tables, 21st Ed., The Chemical Rubber Company, Cleveland, Ohio.

Széchy, K. (1966). The Art of Tunneling, Akademiai Kiado, Budapest.

Terzaghi, K. (1942). "Liner-Plate Tunnels on the Chicago Subway," Proceedings, ASCE, Vol. 68, No. 6, pp. 862 - 899.

Terzaghi, K. (1946). "Introduction to Tunnel Geology," in Rock Tunneling with Steel Supports by R. V. Proctor and T. L. White, The Commercial Shearing and Stamping Company, Youngstown, Ohio.

Timoshenko, S. P. and J. N. Goodier (1970). Theory of Elasticity, 3rd. Ed., McGraw-Hill Book Company, New York.

Ward, W. H. (1969). Discussion of: Peck, R. B., "Deep Excavations and Tunneling in Soft Ground," Proceedings, 7th International Conference on Soil Mechanics and Foundation Engineering, Mexico City, Vol. 3, pp. 320 - 325.

Ward, W. H. (1971). "Some Field Techniques for Improving Site Investigation and Engineering Design," Building Research Station, Current Paper No. 30/71.

Ward, W. H. and H. S. H. Thomas (1965). "The Development of Earth Loading and Deformation in Tunnel Linings in London Clay," Proceedings, 6th International Conference on Soil Mechanics and Foundation Engineering, Montreal, Vol. 2, pp. 432 - 436.

Wickham, G. E. and H. R. Tiedemann (1974). Ground Support Prediction Model (RSR Concept), Report for U. S. Bureau of Mines, Contract No. H0220075.

Zienkiewicz, O. C. (1971). The Finite Element Method in Engineering Science, McGraw-Hill Book Company, London.

APPENDIX A

DERIVATION OF ANALYTICAL SOLUTIONS FOR GROUND-LINER INTERACTION

A.1 INTRODUCTION

Analytical solutions for ground-liner interaction have been available in the literature for a number of years. Of particular interest here are the solutions derived by Burns and Richard (1964) and Dar and Bates (1974). Unfortunately, these solutions only consider overpressure loading; and, therefore, are not applicable to tunnel liners subjected to excavation loading. However, on the basis of this previous work the writer has derived the corresponding solutions for excavation loading. Presented herein, in some detail, are the derivations of these solutions for excavation loading, along with derivations that yield the solutions obtained by Burns and Richard (1964) and Dar and Bates (1974). The final equations of each of these solutions are given separately in Appendix B.

Derivations are given for a total of eight analytical solutions for ground-liner interaction. These solutions are categorized as illustrated by the chart in Fig. A.1. Note that according to this classification system Burns and Richard gave two solutions (1 and 2 in Fig. A.1) and Dar and Bates gave one solution (i.e., they briefly described the derivation of solution 5, but did not give the final equations).

Solutions obtained by combining the theory of elasticity and thin shell theory are here called "thin liner" solutions. Solutions based entirely on the theory of elasticity are called "thick liner" solutions. Although both

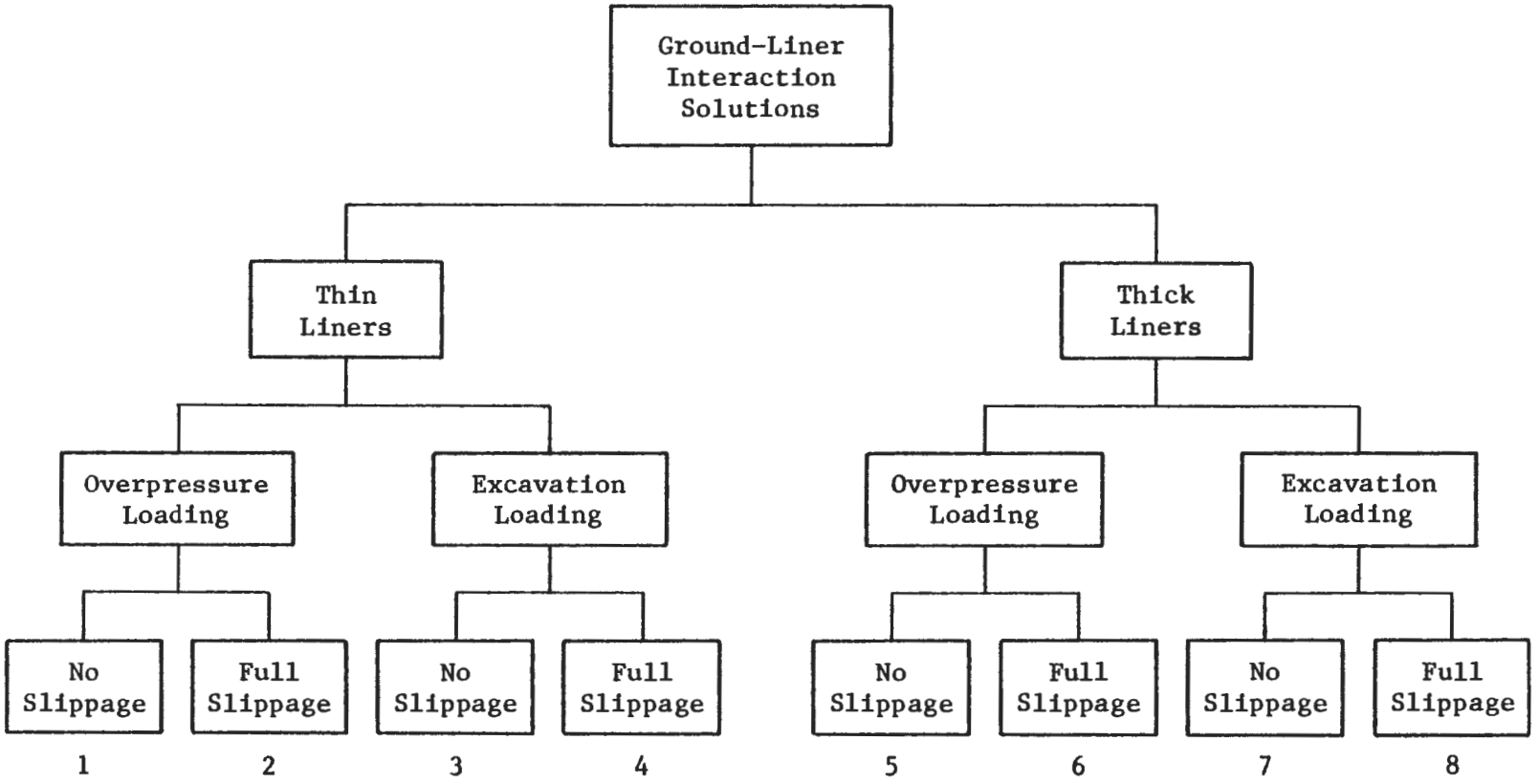

FIGURE A.1 CATEGORIZATION OF ANALYTICAL SOLUTIONS GIVEN FOR GROUND-LINER INTERACTION -- CIRCULAR TUNNEL IN ELASTIC GROUND

types of solution can be applied to liners of any thickness, only the "thick liner" solutions are theoretically correct for all liner thicknesses. However, the equations of these solutions are quite lengthy relative to the equations of the "thin liner" solutions, and if a thin liner is being considered it is much easier to use the "thin liner" solutions. In general, if $t/a < 0.10$ the two solution types will give essentially the same results. Thus, if $t/a < 0.10$ the "thin liner" solutions can be used. If $t/a > 0.10$ the "thick liner" solutions should be used.

Both "thin liner" and "thick liner" solutions give the ground mass stresses (σ_{rm}, $\sigma_{\theta m}$, $\tau_{r\theta m}$) and displacements (u_m, v_m). Liner response is given in terms of forces (T, V, M) and displacements (u_ℓ, v_ℓ) by the "thin liner" solutions, and in terms of stresses ($\sigma_{r\ell}$, $\sigma_{\theta\ell}$, $\tau_{r\theta\ell}$) and displacements (u_ℓ, v_ℓ) by the "thick liner" solutions.

The "thin liner" and "thick liner" solutions are subdivided into two groups on the basis of the type of loading considered; overpressure loading and excavation loading. For overpressure loading it is assumed that the lined tunnel is an existing structure which, along with the surrounding ground mass, is subjected to a uniform pressure, P_o, applied at the ground surface. In situ stresses present in the ground mass prior to construction of the tunnel are not considered. For excavation loading it is assumed that the lined tunnel is inserted in an already stressed (in situ stress state) ground mass. For this type of loading it is necessary to assume that either 1) the liner is installed after excavation, but in such a manner that no ground displacements occur prior to interaction, or 2) the liner is installed before excavation of the soil core and that interaction does not occur until this core is removed.

Interaction between the liner and the surrounding ground mass is

influenced by the magnitude of the shear stresses mobilized at the contact or interface between liner and ground. Unfortunately, it is not presently possible to obtain an exact solution which would account for the general case of shear stresses in excess of the shear strength over only a portion of the interface. Only the two extreme conditions will be considered here. It is possible to obtain a solution for what is called the no slippage condition by assuming that the interface shear strength everywhere exceeds the mobilized shear stress. For this condition the tangential displacements of the liner and the ground mass are everywhere equal at the interface ($v_\ell = v_m$ for all θ at $r = a$). At the other extreme, if it is assumed that the interface shear strength is everywhere zero, there will be no resistance to slippage ($v_\ell \neq v_m$ at $r = a$). The solution that can be obtained for this condition is called the full slippage condition solution.

All eight solutions assume that the ground mass extends to infinity in all directions, and therefore they are applicable only to deep tunnels. However, in effect, it is not necessary to consider the ground surface to be located at infinity. As illustrated in Chapter 4, tunnels located at depths greater than five tunnel diameters ($H/D > 5$) behave essentially like very deep tunnels. For $2 < H/D < 5$ the analytical solutions can be used if the results obtained are evaluated in accordance with the shallow depth effects.

A.2 GENERAL EQUATIONS FOR STRESSES AND DISPLACEMENTS IN A LINEAR-ELASTIC MATERIAL

A.2.1 GENERAL COMMENTS

Before the individual solutions can be derived the general equations for stresses and displacements in an elastic medium must be determined. For the "thin liner" solutions these equations are used only for the ground mass.

For the "thick liner" solutions the behavior of both the liner and the ground mass are obtained from these equations.

It is assumed that the characteristics of the ground-liner system are such that the problem can be considered to be one of plane strain. Because a circular liner is being considered the polar coordinate system will be used. Thus, the derivations that follow will yield two-dimensional, plane strain solutions given in plane polar coordinates. It is also assumed that the elastic solids considered are ideally isotropic and homogeneous. It is assumed that the ground-liner system is subjected to a uniform stress field applied far from the center of the tunnel, and that this stress distribution is symmetrical about both the horizontal and vertical axes (Fig. A.2).

The necessary and sufficient conditions which the components of stress, strain, and displacement must satisfy in order to obtain a solution of an elasticity problem are the following:

a. The strain-displacement relations

b. The stress-strain relations

c. The equilibrium conditions

d. The compatibility conditions

e. The boundary conditions at the exterior surfaces of the body.

The three strain-displacement equations in plane polar coordinates are:

$$\epsilon_r = \frac{\partial u}{\partial r} \tag{A.1a}$$

$$\epsilon_\theta = \frac{u}{r} + \frac{1}{r}\frac{\partial v}{\partial \theta} \tag{A.1b}$$

$$\gamma_{r\theta} = \frac{1}{r}\frac{\partial u}{\partial \theta} + \frac{\partial v}{\partial r} - \frac{v}{r} \tag{A.1c}$$

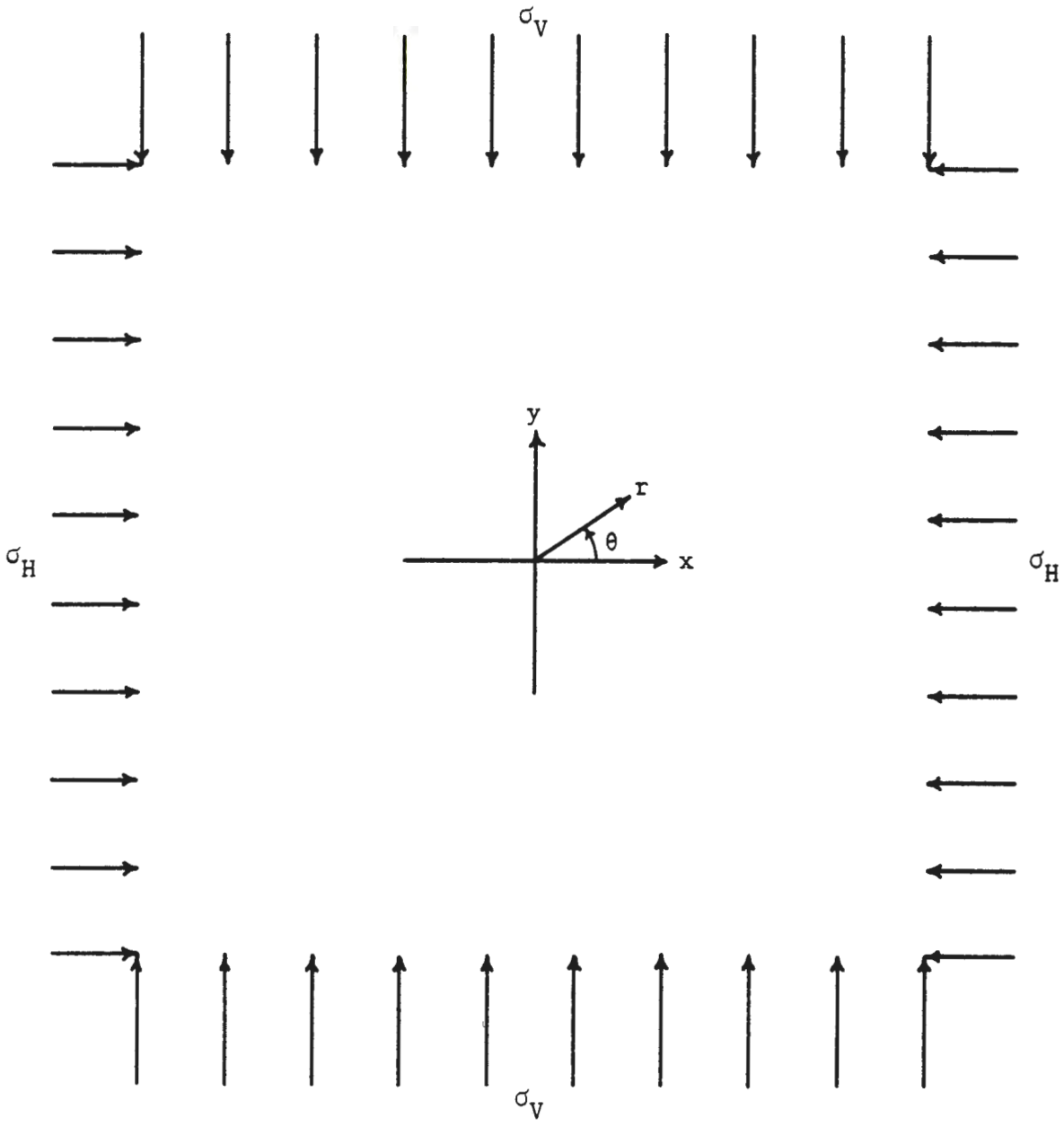

x, y : carteasian coordinates

r, θ : polar coordinates

origin of coordinate system corresponds to centerline of tunnel

FIGURE A.2 STRESS FIELD TO WHICH GROUND-LINER SYSTEM IS SUBJECTED

The three stress-strain equations in plane polar coordinates are:

$$\epsilon_r = \left(\frac{1+\nu}{E}\right)\left[(1-\nu)\sigma_r - \nu\sigma_\theta\right] \tag{A.2a}$$

$$\epsilon_\theta = \left(\frac{1+\nu}{E}\right)\left[(1-\nu)\sigma_\theta - \nu\sigma_r\right] \tag{A.2b}$$

$$\gamma_{r\theta} = 2\left(\frac{1+\nu}{E}\right)\tau_{r\theta} \tag{A.2c}$$

The equilibrium equations are obtained by considering the normal and shear stresses acting on a small element of the body. It is required that the sum of opposing forces in both the radial direction and the circumferential direction equal zero. The resulting equilibrium equations in plane polar coordinates (for zero body forces) are:

$$\frac{\partial\sigma_r}{\partial r} + \frac{\sigma_r - \sigma_\theta}{r} + \frac{1}{r}\frac{\partial\tau_{r\theta}}{\partial\theta} = 0 \tag{A.3a}$$

$$\frac{1}{r}\frac{\partial\sigma_\theta}{\partial\theta} + \frac{\partial\tau_{r\theta}}{\partial r} + \frac{2\tau_{r\theta}}{r} = 0 \tag{A.3b}$$

In plane polar coordinates the compatibility equation in terms of the strains is obtained from the strain-displacement equations (Eqns. A.1) and is

$$\frac{\partial^2 r\gamma_{r\theta}}{\partial\theta\partial r} = \frac{\partial^2\epsilon_r}{\partial\theta^2} + r\frac{\partial^2 r\epsilon_\theta}{\partial r^2} - r\frac{\partial\epsilon_r}{\partial r} \tag{A.4}$$

By substituting the stress-strain equations (Eqns. A.2) into Eqn. A.4 the

compatibility equation in terms of the stresses is obtained for plane polar coordinates. This equation is

$$\left(\frac{\partial^2}{\partial r^2} + \frac{1}{r^2}\frac{\partial^2}{\partial \theta^2} + \frac{1}{r}\frac{\partial}{\partial r}\right)(\sigma_r + \sigma_\theta) = 0 \qquad \text{(A.5)}$$

Thus, the solution of two-dimensional (plane polar coordinates) problems in elasticity theory reduces to solving the two differential equations of equilibrium (Eqns. A.3) and the differential equation of compatibility (Eqn. A.5). The resulting constants of integration are evaluated by means of the boundary conditions.

A solution is obtained by finding a set of stress components (σ_r, σ_θ, $\tau_{r\theta}$) that satisfy the boundary conditions and Eqns. A.3 and A.5. The usual procedure, assuming zero body forces, is as follows:

1. introduce a new function called the Airy stress function, $\phi(r,\theta)$,
2. express the stress components in terms of this function so that the equilibrium equations (Eqns. A.3) are satisfied,
3. use the compatibility equation (Eqn. A.5) to find the expression for ϕ in terms of r, θ, and a number of constants of integration,
4. use the boundary conditions to find expressions for the constants of integration.

Once this has been done the stress function is completely defined, and as a consequence the stresses and, by means of the stress-strain equations (Eqns. A.2) and the strain-displacement equations (Equs. A.1), the displacements are determined.

A.2.2 DERIVATION OF THE APPROPRIATE AIRY STRESS FUNCTION, $\phi(r,\theta)$

At this point it is necessary to find the Airy stress function, ϕ, that applies for each particular problem being considered. Fortunately, since the eight solutions sought here are similar (differ only with respect to "interior" boundary conditions) one stress function can be used for all eight. (Note: The same stress function can be used for the problem of an unlined circular opening.)

The stress components (σ_r, σ_θ, $\tau_{r\theta}$) expressed in terms of the Airy stress function so that the equilibrium equations (Eqns. A.3) are satisfied are:

$$\sigma_r = \frac{1}{r}\frac{\partial\phi}{\partial r} + \frac{1}{r^2}\frac{\partial^2\phi}{\partial\theta^2} \qquad \text{(A.6a)}$$

$$\sigma_\theta = \frac{\partial^2\phi}{\partial r^2} \qquad \text{(A.6b)}$$

$$\tau_{r\theta} = -\frac{\partial}{\partial r}\left(\frac{1}{r}\frac{\partial\phi}{\partial\theta}\right) \qquad \text{(A.6c)}$$

Substitution of Eqns. A.6a and 6b into the compatibility equation (Eqn. A.5) yields

$$\left(\frac{\partial^2}{\partial r^2} + \frac{1}{r^2}\frac{\partial^2}{\partial\theta^2} + \frac{1}{r}\frac{\partial}{\partial r}\right)\left(\frac{1}{r}\frac{\partial\phi}{\partial r} + \frac{1}{r^2}\frac{\partial^2\phi}{\partial\theta^2} + \frac{\partial^2\phi}{\partial r^2}\right) = 0 \qquad \text{(A.7)}$$

The expression for ϕ is obtained by solving this equation.

The solution to Eqn. A.7 can be obtained by the method of separation of variables. Let

$$\phi(r,\theta) = R(r)\,\lambda(\theta) \qquad \text{(A.8)}$$

where R(r) is a function of r only and $\lambda(\theta)$ is a function of θ only.

Substitution of Eqn. A.8 into Eqn. A.7 and expansion of the result gives

$$\lambda\left[\frac{d^4R}{dr^4} + \frac{2}{r}\frac{d^3R}{dr^3} - \frac{1}{r^2}\frac{d^2R}{dr^2} + \frac{1}{r^3}\frac{dR}{dr}\right] + \frac{d^2\lambda}{d\theta^2}\left[\frac{2}{r^2}\frac{d^2R}{dr^2} - \frac{2}{r^3}\frac{dR}{dr} + \frac{4R}{r^4}\right] + \frac{R}{r^4}\frac{d^4\lambda}{d\theta^4} = 0 \qquad (A.9)$$

Total derivative symbols are used because R = f(r) only and λ = f(θ) only.

We must now find R(r) and $\lambda(\theta)$ using Eqn. A.9 and the stress conditions at infinity. Because of the assumption of linearity the principle of superposition can be utilized and the stress system (Fig. A.2) separated into two component parts as shown in Fig. A.3.

In Figs. A.2 and A.3 the stresses at infinity are given in terms of carteasion coordinates, giving

$$\sigma_x = \sigma_H \ , \ \sigma_y = \sigma_V \ , \ \tau_{xy} = 0.$$

The following equations are used to transform these stresses to plane polar coordinates.

$$\sigma_r = \sigma_x\cos^2\theta + \sigma_y\sin^2\theta + \tau_{xy}\sin 2\theta \qquad (A.10a)$$

$$\sigma_\theta = \sigma_x\sin^2\theta + \sigma_y\cos^2\theta - \tau_{xy}\sin 2\theta \qquad (A.10b)$$

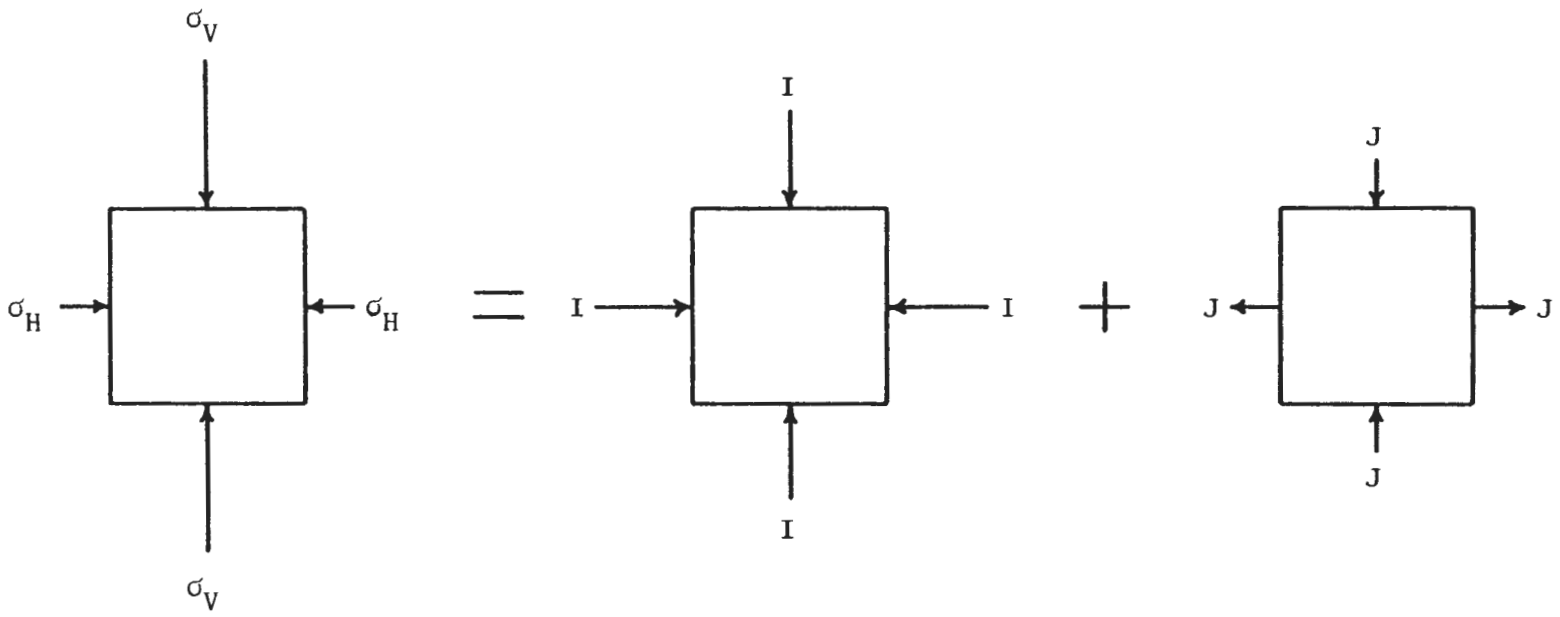

$$I = \tfrac{1}{2}(\sigma_V + \sigma_H) \qquad I + J = \sigma_V$$

$$J = \tfrac{1}{2}(\sigma_V - \sigma_H) \qquad I - J = \sigma_H$$

FIGURE A.3 STRESS FIELD DIVIDED INTO TWO COMPONENT PARTS

$$\tau_{r\theta} = \tfrac{1}{2}(\sigma_y - \sigma_x)\sin 2\theta + \tau_{xy}\cos 2\theta \qquad \text{(A.10c)}$$

Thus, we have

$$\sigma_r = \sigma_H\cos^2\theta + \sigma_V\sin^2\theta$$

$$\sigma_\theta = \sigma_H\sin^2\theta + \sigma_V\cos^2\theta$$

$$\tau_{r\theta} = \tfrac{1}{2}(\sigma_V - \sigma_H)\sin 2\theta$$

Using the trigonometric identities

$$\cos^2\theta = \tfrac{1}{2}(1 + \cos 2\theta) \quad \text{and} \quad \sin^2\theta = \tfrac{1}{2}(1 - \cos 2\theta)$$

we obtain,

$$\sigma_r = \tfrac{1}{2}(\sigma_H + \sigma_V) + \tfrac{1}{2}(\sigma_H - \sigma_V)\cos 2\theta \qquad \text{(A.11a)}$$

$$\sigma_\theta = \tfrac{1}{2}(\sigma_H + \sigma_V) + \tfrac{1}{2}(\sigma_V - \sigma_H)\cos 2\theta \qquad \text{(A.11b)}$$

$$\tau_{r\theta} = \tfrac{1}{2}(\sigma_V - \sigma_H)\sin 2\theta \qquad \text{(A.11c)}$$

Using the relations given in Fig. A.3 these equations become, for Fig. A.3a,

$$\sigma_r = I - J\cos 2\theta \qquad \text{(A.12a)}$$

$$\sigma_\theta = I + J\cos 2\theta \qquad \text{(A.12b)}$$

$$\tau_{r\theta} = J\sin 2\theta \qquad \text{(A.12c)}$$

The stress condition in Fig. A.3b is given by

$$\sigma_r = I \tag{A.13a}$$

$$\sigma_\theta = I \tag{A.13b}$$

$$\tau_{r\theta} = 0 \tag{A.13c}$$

The stress condition in Fig. A.3c is given by

$$\sigma_r = -J \cos 2\theta \tag{A.14a}$$

$$\sigma_\theta = J \cos 2\theta \tag{A.14b}$$

$$\tau_{r\theta} = J \sin 2\theta \tag{A.14c}$$

The principle of superposition also applies to the stress function, $\phi(r,\theta)$. Thus, we can find the $\phi_1(r,\theta) = R_1(r)\,\lambda_1(\theta)$ that applies for Fig. A.3b and Eqns. A.13, and the $\phi_2(r,\theta) = R_2(r)\,\lambda_2(\theta)$ that applies for Fig. A.3c and Eqns. A.14, and then add these expressions to get the $\phi(r,\theta)$ that applies for Fig. A.3a and Eqns. A.12.

$$\phi(r,\theta) = \phi_1(r,\theta) + \phi_2(r,\theta) \tag{A.15}$$

DETERMINATION OF $\phi_1(r,\theta)$

From Fig. A.3b and Eqns. A.13 we see that the stresses are independent

of θ. Thus, in Eqn. A.8 $\lambda_1(\theta)$ must be a constant, giving

$$\phi_1(r,\theta) = R_1(r)[\text{Constant}] \tag{A.16}$$

This also means that all derivatives of $\lambda_1(\theta)$ with respect to θ must be zero. As a result of this requirement Eqn. A.9 here reduces to

$$\frac{d^4R_1}{dr^4} + \frac{2}{r}\frac{d^3R_1}{dr^3} - \frac{1}{r^2}\frac{d^2R_1}{dr^2} + \frac{1}{r^3}\frac{dR_1}{dr} = 0$$

This equation can be rewritten as

$$\frac{1}{r}\frac{d}{dr}\{r\frac{d}{dr}[\frac{1}{r}\frac{d}{dr}(r\frac{dR_1}{dr})]\} = 0$$

The expression for $R_1(r)$ is obtained by successive integration of this equation. The result of such integration is

$$R_1(r) = c_1r^2\log r + c_2r^2 + c_3\log r + c_4 ,$$

where c_1 through c_4 are the constants of integration. Substituting this expression into Eqn. A.16 we get

$$\phi_1(r,\theta) = [c_1r^2\log r + c_2r^2 + c_3\log r + c_4][\text{Constant}]$$

$$\phi_1(r,\theta) = A_1r^2\log r + A_2r^2 + A_3\log r + A_4 \tag{A.17}$$

DETERMINATION OF $\phi_2(r,\theta)$

Now consider the stress state given by Fig. A.3c and Eqns. A.14. It can be shown that $\lambda_2(\theta) = \cos 2\theta$ (Timoshenko and Goodier, 1970). Thus, Eqn. A.8 is of the form

$$\phi_2(r,\theta) = R_2(r)\cos 2\theta \tag{A.18}$$

Substituting $R = R_2(r)$ and $\lambda = \cos 2\theta$ into Eqn. A.9, dividing through by $\cos 2\theta$ and collecting terms we obtain

$$\frac{d^4R_2(r)}{dr^4} + \frac{2}{r}\frac{d^3R_2(r)}{dr^3} - \frac{9}{r^2}\frac{d^2R_2(r)}{dr^2} + \frac{9}{r^3}\frac{dR_2(r)}{dr} = 0 \tag{A.19}$$

Equation A.19 is an ordinary differential equation with variable coefficients which can be reduced to a linear differential equation with constant coefficients by introducing a new variable, t, such that

$$t = \log r \quad \text{or} \quad r = e^t \quad ; \quad \frac{dt}{dr} = \frac{1}{r} \tag{A.20}$$

The chain rule for differentiation with respect to the second variable gives

$$\frac{dR_2(r)}{dr} = \frac{1}{r}\frac{dR_2(t)}{dt} \tag{A.21a}$$

$$\frac{d^2R_2(r)}{dr^2} = \frac{1}{r^2}\left[\frac{d^2R_2(t)}{dt^2} - \frac{dR_2(t)}{dt}\right] \tag{A.21b}$$

$$\frac{d^3R_2(r)}{dr^3} = \frac{1}{r^3}\left[\frac{d^3R_2(t)}{dt^3} - 3\frac{d^2R_2(t)}{dt^2} + 2\frac{dR_2(t)}{dt}\right] \tag{A.21c}$$

$$\frac{d^4R_2(r)}{dr^4} = \frac{1}{r^4}\left[\frac{d^4R_2(t)}{dt^4} - 6\frac{d^3R_2(t)}{dt^3} + 11\frac{d^2R_2(t)}{dt^2} - 6\frac{dR_2(t)}{dt}\right] \qquad (A.21d)$$

Substituting Eqns. A.21 into Eqn. A.19 and collecting terms we get,

$$\frac{d^4R_2(t)}{dt^4} - 4\frac{d^3R_2(t)}{dt^3} - 4\frac{d^2R_2(t)}{dt^2} + 16\frac{dR_2(t)}{dt} = 0 \qquad (A.22)$$

Now let

$$R_2(t) = e^{pt} \qquad (A.23)$$

and note that

$$\frac{dR_2(t)}{dt} = pe^{pt}$$

$$\frac{d^2R_2(t)}{dt^2} = p^2e^{pt}$$

$$\frac{d^3R_2(t)}{dt^3} = p^3e^{pt}$$

$$\frac{d^4R_2(t)}{dt^4} = p^4e^{pt}$$

Thus, by substituting Eqn. A.23 into Eqn. A.22 and dividing through by e^{pt} we obtain

$$p^4 - 4p^3 - 4p^2 + 16p = 0 \qquad (A.24)$$

The roots of this equation can be found by following the procedure outlined in Selby (1973). The four roots are:

$$p = 4, \quad p = 2, \quad p = 0, \quad p = -2$$

From Eqn. A.23 we find

$$R_2(t) = e^{4t} \tag{A.25a}$$

$$R_2(t) = e^{2t} \tag{A.25b}$$

$$R_2(t) = e^{-2t} \tag{A.25c}$$

$$R_2(t) = e^{0t} = 1 \tag{A.25d}$$

It can be shown that each of Eqns. A.25 satisfies Eqn. A.22. The r ght side of each of Eqns. A.25 can be multiplied by an arbitrary constant and these equations will still satisfy Eqn. A.22.

$$R_2(t) = d_1 e^{4t} \tag{A.26a}$$

$$R_2(t) = d_2 e^{2t} \tag{A.26b}$$

$$R_2(t) = d_3 e^{-2t} \tag{A.26c}$$

$$R_2(t) = d_4 \tag{A.26d}$$

Because each of Eqns. A.26 satisfies Eqn. A.22, the sum of these equations will also satisfy that equation. Thus, we can obtain

$$R_2(t) = d_1 e^{4t} + d_2 e^{2t} + d_3 e^{-2t} + d_4 \qquad (A.27)$$

Substituting Eqn. A.27 into Eqn. A.21a we obtain

$$\frac{dR_2(r)}{dr} = \frac{1}{r}\left[4d_1 e^{4t} + 2d_2 e^{2t} - 2d_3 e^{-2t}\right] \qquad (A.28)$$

From Eqn. A.20 we have that

$$e^t = r.$$

Raising each side of this equation to the appropriate power we can obtain

$$e^{4t} = r^4$$

$$e^{2t} = r^2$$

$$e^{-2t} = r^{-2}$$

Substituting these equalities into Eqn. A.28 we get

$$\frac{dR_2(r)}{dr} = 4d_1 r^3 + 2d_2 r - 2\frac{d_3}{r^3}$$

Integrating this equation with respect to r and substituting in new symbols for the constant coefficients we have (after rearragning terms)

$$R_2(r) = B_1 r^2 + \frac{B_2}{r^2} + B_3 + B_4 r^4 \qquad (A.29)$$

Substituting Eqn. A.29 into Eqn. A.18 we get

$$\phi_2(r,\theta) = (B_1 r^2 + \frac{B_2}{r^2} + B_3 + B_4 r^4) \cos 2\theta \qquad (A.30)$$

EXPRESSION FOR $\phi(r,\theta)$

Substitution of Eqns. A.17 and A.30 into Eqn. A.15 gives the general expression for the stress function.

$$\phi(r,\theta) = (A_1 r^2 \log r + A_2 r^2 + A_3 \log r + A_4) +$$
$$+ (B_1 r^2 + \frac{B_2}{r^2} + B_3 + B_4 r^4) \cos 2\theta$$

The fourth term on the right side of this equation, A_4, can be deleted since it is a function of neither r nor θ. Thus, the final expression for the Airy stress function that is appropriate for the problems to be considered is

$$\phi(r,\theta) = (A_1 r^2 \log r + A_2 r^2 + A_3 \log r) +$$
$$+ (B_1 r^2 + \frac{B_2}{r^2} + B_3 + B_4 r^4) \cos 2\theta \qquad (A.31)$$

A.2.3 GENERAL EQUATIONS FOR STRESSES AND DISPLACEMENTS

Using Eqns. A.1, A.2, A.6, and A.31 the general expressions for the

stresses and displacements can now be obtained.

Substituting Eqn. A.31 into each of Eqns. A.6 we find the stress equations.

$$\sigma_r = \left[A_1(2\log r + 1) + 2A_2 + \frac{A_3}{r^2}\right] - \left[2B_1 + \frac{6B_2}{r^4} + \frac{4B_3}{r^2}\right]\cos 2\theta \qquad (A.32a)$$

$$\sigma_\theta = \left[A_1(2\log r + 3) + 2A_2 - \frac{A_3}{r^2}\right] + \left[2B_1 + \frac{6B_2}{r^4} + 12B_4 r^2\right]\cos 2\theta \qquad (A.32b)$$

$$\tau_{r\theta} = \left[2B_1 - \frac{6B_2}{r^4} - \frac{2B_3}{r^2} + 6B_4 r^2\right]\sin 2\theta \qquad (A.32c)$$

By substituting Eqns. A.1 into Eqns. A.2 we obtain the stress-displacement relations that can be used to find the displacements. The stress-displacement relations are:

$$\frac{\partial u}{\partial r} = \left(\frac{1+\nu}{E}\right)\left[(1-\nu)\sigma_r - \nu\sigma_\theta\right] \qquad (A.33a)$$

$$\frac{1}{r}\left(u + \frac{\partial v}{\partial \theta}\right) = \left(\frac{1+\nu}{E}\right)\left[(1-\nu)\sigma_\theta - \nu\sigma_r\right] \qquad (A.33b)$$

$$\frac{1}{r}\frac{\partial u}{\partial \theta} + \frac{\partial v}{\partial r} - \frac{v}{r} = 2\left(\frac{1+\nu}{E}\right)\tau_{r\theta} \qquad (A.33c)$$

By substituting Eqns. A.32 into Eqns. A.33 and performing the necessary integrations we obtain the general expressions for the displacements, which are

$$u = \left(\frac{1+\nu}{E}\right)(r)\left\{\left[(1-2\nu)A_1(2\log r - 1) - 2\nu A_1 + 2(1-2\nu)A_2 - \frac{A_3}{r^2}\right] - \right.$$

$$\left. - \left[2B_1 - \frac{2B_2}{r^4} - \frac{4B_3}{r^2}(1-\nu) + 4\nu B_4 r^2\right]\cos 2\theta\right\} +$$

$$+ A_o \sin\theta + B_o \cos\theta \qquad \text{(A.34a)}$$

$$v = \left(\frac{1+\nu}{E}\right)(r)\left\{\left[4(1-\nu)A_1\theta\right] + \right.$$

$$\left. + \left[2B_1 + \frac{2B_2}{r^4} - \frac{2B_3}{r^2}(1-2\nu) + 2(3-2\nu)B_4 r^2\right]\sin 2\theta\right\} +$$

$$+ A_o \cos\theta - B_o \sin\theta + C_o r \qquad \text{(A.34b)}$$

where A_o, B_o, and C_o are the additional constants of integration that result.

Equations A.32 and A.34 are the generalized stress and displacement equations used in the derivations of the eight solutions considered here. For the "thin liner" solutions these equations must be combined with the equations for a thin shell. For the "thick liner" solutions these equations are sufficient. For each different solution the constants of integration in Eqns. A.32 and A.34 are evaluated on the basis of the boundary conditions that apply for that particular problem.

A.3 SOLUTIONS FOR A THIN LINER

A.3.1 GENERAL COMMENTS

The "thin liner" solutions are obtained by combining the generalized stress and displacement equations for the ground mass (Section A.3.2) with the

equations for a thin shell (Section A.3.3) in accordance with the appropriate boundary conditions.

The positive sign conventions and the relevant geometrical quantities adopted for these solutions are illustrated in Fig. A.4. As shown in this figure the radius of the tunnel is measured to the outer surface of the liner ($a = R_o$) rather than to the mid-thickness of the liner ($a = R_m$). This is an arbitrary selection based on the boundary conditions required (e.g., at $r = a$, $u_m = u_\ell$) in the derivations. As a result of this selection a descrepancy arises because the liner thrusts, shears, bending moments, and displacements should be evaluated at $a = R_m$, not at $a = R_o$. However, because the liner is thin ($t \ll a$) there is little difference between R_m and R_o and it makes little difference which value of a is used.

A.3.2 EQUATIONS FOR GROUND MASS STRESSES AND DISPLACEMENTS IN TERMS OF STRESS FUNCTION CONSTANTS

Equations A.32 and A.34 represent the generalized equations for stresses and displacements, respectively, in an elastic body. The equations for stresses and displacements in the elastic ground mass surrounding the tunnel are obtained from these equations by invoking the following two conditions:

1) at $r = \infty$,

$$\sigma_r = \sigma_{rm} = \tfrac{1}{2}(\sigma_V + \sigma_H) - \tfrac{1}{2}(\sigma_V - \sigma_H)\cos 2\theta \qquad \text{(A.11a)}$$

$$\sigma_\theta = \sigma_{\theta m} = \tfrac{1}{2}(\sigma_V + \sigma_H) + \tfrac{1}{2}(\sigma_V - \sigma_H)\cos 2\theta \qquad \text{(A.11b)}$$

$$\tau_{r\theta} = \tau_{r\theta m} = \tfrac{1}{2}(\sigma_V - \sigma_H)\sin 2\theta \qquad \text{(A.11c)}$$

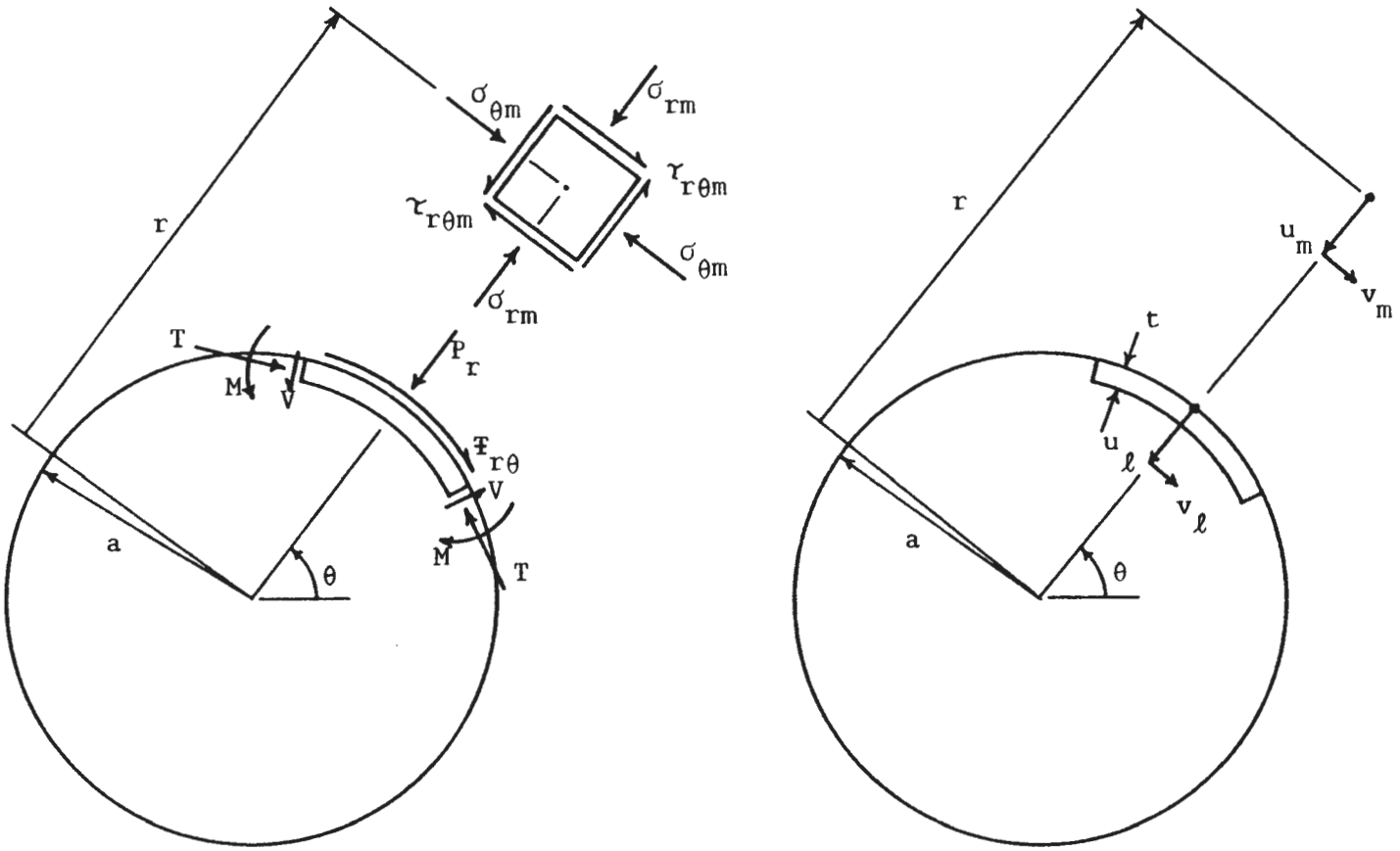

FIGURE A.4 POSITIVE SIGN CONVENTIONS - "THIN LINER" SOLUTIONS

$$2) \quad v = v_m = 0, \quad \text{for} \quad \theta = \frac{n\pi}{2} \qquad (n = 0,1,2,3,.....)$$

By substituting Eqns. A.32 into Eqns. A.11 and setting $r = \infty$; and by setting $\theta = n\pi/2$ in Eqn. A.34b and equating the result to zero for $n = 0$ and $n = 1$ we find that

$$A_1 = 0$$

$$A_2 = \tfrac{1}{2}(\sigma_V + \sigma_H)$$

$$A_3 = \text{unknown} = L$$

$$B_1 = \tfrac{1}{2}(\sigma_V - \sigma_H)$$

$$B_2 = \text{unknown} = J$$

$$B_3 = \text{unknown} = N$$

$$B_4 = 0$$

$$A_o = 0$$

$$B_o = 0$$

$$C_o = 0$$

Substituting these values for the coefficients back into Eqns. A.32 and A.34 we obtain the following:

$$\sigma_{rm} = \left[\tfrac{1}{2}(\sigma_V + \sigma_H) + \frac{L}{r^2}\right] - \left[\tfrac{1}{2}(\sigma_V - \sigma_H) + \frac{6J}{r^4} + \frac{4N}{r^2}\right]\cos 2\theta \qquad \text{(A.35a)}$$

$$\sigma_{\theta m} = \left[\tfrac{1}{2}(\sigma_V + \sigma_H) - \frac{L}{r^2}\right] + \left[\tfrac{1}{2}(\sigma_V - \sigma_H) + \frac{6J}{r^4}\right]\cos 2\theta \qquad \text{(A.35b)}$$

$$\tau_{r\theta m} = \left[\tfrac{1}{2}(\sigma_V - \sigma_H) - \frac{6J}{r^4} - \frac{2N}{r^2}\right]\sin 2\theta \qquad \text{(A.35c)}$$

$$u_m = \left(\frac{1 + \nu_m}{E_m}\right)(r)\left\{\left[\tfrac{1}{2}(\sigma_V + \sigma_H)(1 - 2\nu_m) - \frac{L}{r^2}\right] - \right.$$

$$\left. - \left[\tfrac{1}{2}(\sigma_V - \sigma_H) - \frac{2J}{r^4} - \frac{4N}{r^2}(1 - \nu_m)\right]\cos 2\theta\right\} \qquad \text{(A.35d)}$$

$$v_m = \left(\frac{1 + \nu_m}{E_m}\right)(r)\left\{\left[\tfrac{1}{2}(\sigma_V - \sigma_H) + \frac{2J}{r^4} - \frac{2N}{r^2}(1 - 2\nu_m)\right]\sin 2\theta\right\} \qquad \text{(A.35e)}$$

OVERPRESSURE LOADING

For the solutions that consider an existing tunnel such that the ground-liner system is subjected to an overpressure, P_o, applied at the ground surface we have

$$\sigma_V = P_o \qquad \text{and} \qquad \sigma_H = KP_o$$

It should be noted that, while for this type of loading the lateral displacement constraint is usually assumed, requiring

$$K = \frac{\nu_m}{1 - \nu_m},$$

the following derivations of the overpressure loading solutions yield equations that allow the selection of K and ν_m values that are independent of each other if this is deemed appropriate.

In terms of P_o and K the general equations for ground mass stresses and displacements for overpressure loading are the following:

$$\sigma_{rm} = \left[\left(\frac{P_o}{2}\right)(1 + K) + \frac{L}{r^2}\right] - \left[\left(\frac{P_o}{2}\right)(1 - K) + \frac{6J}{r^4} + \frac{4N}{r^2}\right]\cos 2\theta \qquad \text{(A.36a)}$$

$$\sigma_{\theta m} = \left[\left(\frac{P_o}{2}\right)(1 + K) - \frac{L}{r^2}\right] + \left[\left(\frac{P_o}{2}\right)(1 - K) + \frac{6J}{r^4}\right]\cos 2\theta \qquad \text{(A.36b)}$$

$$\tau_{r\theta m} = \left[\left(\frac{P_o}{2}\right)(1 - K) - \frac{6J}{r^4} - \frac{2N}{r^2}\right]\sin 2\theta \qquad \text{(A.36c)}$$

$$u_m = \left(\frac{1 + \nu_m}{E_m}\right)(r)\left\{\left[\left(\frac{P_o}{2}\right)(1 + K)(1 - 2\nu_m) - \frac{L}{r^2}\right] - \left[\left(\frac{P_o}{2}\right)(1 - K) - \frac{2J}{r^4} - \frac{4N}{r^2}(1 - \nu_m)\right]\cos 2\theta\right\} \qquad \text{(A.36d)}$$

$$v_m = \left(\frac{1 + \nu_m}{E_m}\right)(r)\left\{\left[\left(\frac{P_o}{2}\right)(1 - K) + \frac{2J}{r^4} - \frac{2N}{r^2}(1 - 2\nu_m)\right]\sin 2\theta\right\} \qquad \text{(A.36e)}$$

EXCAVATION LOADING

For solutions that consider excavation loading we have

$$\sigma_V = \gamma H \qquad \text{and} \qquad \sigma_H = K_o \gamma H$$

where,

γ = unit weight of the ground mass,

H = tunnel depth, measured from the ground surface to the tunnel centerline,

K_o = coefficient of earth pressure at rest

The generalized ground mass stress equations for excavation loading can be obtained by substituting these expressions for σ_V and σ_H into Eqns. A.36a, b and c. In order to obtain the corresponding displacement equations, Eqns.

A.36d and e require further modification. For excavation loading it is assumed that the liner is installed in an already stressed medium. Thus, some displacement of the ground mass will already have occurred prior to excavation and construction of the tunnel. These are the "in situ" displacements resulting from the application of the in situ stresses (Eqns. A.11) to the initially stress free ground mass. These displacements are obtained from Eqns. A.35d and e by assuming that the ground mass is intact (no tunnel opening) and that at $r = 0$, $u_m = v_m = 0$. By inserting these values into Eqns. A.35d and e we find

$$L = J = N = 0 ,$$

and that the "in situ" displacements are (in terms of σ_V and σ_H)

$$u_{mi} = \left(\frac{1 + \nu_m}{E_m}\right)(r)\left\{\left[\tfrac{1}{2}(\sigma_V + \sigma_H)(1 - 2\nu_m)\right] - \left[\tfrac{1}{2}(\sigma_V - \sigma_H)\right]\cos 2\theta\right\} \quad (A.37a)$$

$$v_{mi} = \left(\frac{1 + \nu_m}{E_m}\right)(r)\left\{\left[\tfrac{1}{2}(\sigma_V - \sigma_H)\right]\sin 2\theta\right\} \quad (A.37b)$$

Thus, the correct expressions for the ground mass displacements are obtained by subtracting Eqns. A.37a and b from Eqns. A.35d and e, respectively, and then substituting γH for σ_V and $K_o \gamma H$ for σ_H.

In terms of γH and K_o the general excavation loading equations for the ground mass stresses and displacements are

$$\sigma_{rm} = \left[\left(\frac{\gamma H}{2}\right)(1 + K_o) + \frac{L}{r^2}\right] - \left[\left(\frac{\gamma H}{2}\right)(1 - K_o) + \frac{6J}{r^4} + \frac{4N}{r^2}\right]\cos 2\theta \quad (A.38a)$$

$$\sigma_{\theta m} = \left[\left(\frac{\gamma H}{2}\right)(1 + K_o) - \frac{L}{r^2}\right] + \left[\left(\frac{\gamma H}{2}\right)(1 - K_o) + \frac{6J}{r^4}\right]\cos 2\theta \quad (A.38b)$$

$$\tau_{r\theta m} = \left[\left(\frac{\gamma H}{2}\right)(1 - K_o) - \frac{6J}{r^4} - \frac{2N}{r^2}\right]\sin 2\theta \quad (A.38c)$$

$$u_m = \left(\frac{1 + \nu_m}{E_m}\right)(r)\left\{\left[-\frac{L}{r^2}\right] + \left[\frac{2J}{r^4} + \frac{4N}{r^2}(1 - \nu_m)\right]\cos 2\theta\right\} \quad \text{(A.38d)}$$

$$v_m = \left(\frac{1 + \nu_m}{E_m}\right)(r)\left\{\left[\frac{2J}{r^4} - \frac{2N}{r^2}(1 - 2\nu_m)\right]\sin 2\theta\right\} \quad \text{(A.38e)}$$

A.3.3 EQUATIONS FOR A THIN SHELL (LINER)

For the "thin liner" solutions relationships between liner thrust and shear forces, bending moments, displacements, and external pressures (See Fig. A.4) are taken from thin shell theory (Flügge, 1973). These relationships are given below in terms of plane polar coordinates.

The relationships between liner thrust, shear, and moments and external pressures acting on the liner are

$$a\frac{\partial T}{\partial \theta} - \frac{\partial M}{\partial \theta} = -a^2 \mathfrak{T}_{r\theta} \quad \text{(A.39a)}$$

$$\frac{\partial^2 M}{\partial \theta^2} + aT = a^2 P_r \quad \text{(A.39b)}$$

$$V - \frac{\partial T}{\partial \theta} = a\mathfrak{T}_{r\theta} \quad \text{(A.39c)}$$

From Eqns. A.39a and c it can be shown that

$$V = \frac{1}{a}\frac{\partial M}{\partial \theta} \quad \text{(A.39d)}$$

The relationships between liner thrust, moments and displacements are

$$T = \frac{E_\ell^* A}{a}\left[\frac{\partial v_\ell}{\partial \theta} + u_\ell\right] + \frac{E_\ell^* I}{a^3}\left[u_\ell + \frac{\partial^2 u_\ell}{\partial \theta^2}\right] \quad \text{(A.40a)}$$

$$M = \frac{E_\ell^* I}{a^2}\left[u_\ell + \frac{\partial^2 u_\ell}{\partial\theta^2}\right] \qquad \text{(A.40b)}$$

The relationships between liner displacements and external pressures acting on the liner are obtained from Eqns. A.39 and A.40.

$$\frac{\partial^2 v_\ell}{\partial\theta^2} + \frac{\partial u_\ell}{\partial\theta} = -\frac{a^2}{E_\ell^* A}\mathfrak{T}_{r\theta} \qquad \text{(A.41a)}$$

$$\frac{\partial v_\ell}{\partial\theta} + u_\ell + \frac{E_\ell^* I}{E_\ell^* A a^2}\left[\frac{\partial^4 u_\ell}{\partial\theta^4} + 2\frac{\partial^2 u_\ell}{\partial\theta^2} + u_\ell\right] = \frac{a^2}{E_\ell^* A} P_r \qquad \text{(A.41b)}$$

In the above equations E_ℓ^* represents the liner modulus for plane-strain,

$$E_\ell^* = \frac{E_\ell}{(1 - \nu_\ell^2)},$$

and (assuming the liner is of rectangular cross-section of uniform thickness, t, in the radial direction and unit thickness, b = 1, in the longitudinal direction),

$$A = t = \text{cross-sectional area}$$

$$I = t^3/12 = \text{moment of inertia}$$

If the liner consists of discrete members (i.e., is not continuous in the longitudinal direction)

$$A = \frac{A_u}{L} \quad \text{and} \quad I = \frac{I_u}{L}$$

where A_u and I_u are the cross-sectional area and moment of inertia, respectively, of the member and L is the length in the longitudinal direction of that member.

A.3.4 THE LINER-GROUND MASS COMPRESSIBILITY AND FLEXIBILITY RATIOS

The mechanics of the "thin liner" solution derivations and the form of the resulting final equations are significantly simplified by the use of what are called the compressibility (C) and flexibility (F) ratios, where C is a measure of the extensional stiffness of the surrounding medium relative to that of the liner and F is a measure of the flexural stiffness of the surrounding medium relative to that of the liner. The derivation of the expressions for these ratios is given by Peck, Hendron, and Mohraz (1972).

The resulting expressions are given as

$$C = \frac{\frac{E_m}{(1+\nu_m)(1-2\nu_m)}}{\frac{E_\ell A}{(1-\nu_\ell^2)} \cdot \frac{1}{a}} = \left(\frac{E_m}{E_\ell}\right)\left(\frac{a}{t}\right)\left[\frac{(1-\nu_\ell^2)}{(1+\nu_m)(1-2\nu_m)}\right] \qquad \text{(A.42a)}$$

$$F = \frac{\frac{E_m}{(1+\nu_m)}}{\frac{6E_\ell I}{(1-\nu_\ell^2)} \cdot \frac{1}{a^3}} = \left(\frac{E_m}{E_\ell}\right)\left(\frac{a}{t}\right)^3\left[\frac{2(1-\nu_\ell^2)}{(1+\nu_m)}\right] \qquad \text{(A.42b)}$$

To express these ratios in terms of the liner radius-to-thickness ratio (a/t) it is necessary to assume that the liner is continuous in the longitudinal direction and of rectangular cross-section with uniform thickness.

By rearranging the terms in Eqns. A.42 we have that

$$\frac{a^3}{E_\ell^* I} = 6F\left(\frac{1+\nu_m}{E_m}\right) \qquad \text{(A.43a)}$$

$$\frac{a}{E_\ell^* A} = (1-2\nu_m)\, C\, \left(\frac{1+\nu_m}{E_m}\right) \qquad \text{(A.43b)}$$

A.3.5 SOLUTION NO. 1 : OVERPRESSURE LOADING - NO SLIPPAGE CONDITION

The additional boundary conditions that apply for this problem require that at $r = a$,

$$u_m = u_\ell \qquad \text{(BC1)}$$

$$v_m = v_\ell \qquad \text{(BC2)}$$

$$\sigma_{rm} = P_r \qquad \text{(BC3)}$$

$$\tau_{r\theta m} = \mathfrak{T}_{r\theta} \qquad \text{(BC4)}$$

From Eqn. A.41a we have

$$\frac{\partial^2 v_\ell}{\partial \theta^2} + \frac{\partial u_\ell}{\partial \theta} = -\frac{a^2}{E_\ell^* A}\mathfrak{T}_{r\theta} \qquad \text{(A.41a)}$$

We get the following from boundary conditions BC1, 2 and 4 and from Eqn. A.36e,

$$v_\ell = \left(\frac{1+\nu_m}{E_m}\right)(a)\left\{\left[\left(\frac{P_o}{2}\right)(1-K) + \frac{2J}{a^4} - \frac{2N}{a^2}(1-2\nu_m)\right]\sin 2\theta\right\}$$

from Eqn. A.36d,

$$u_\ell = \left(\frac{1+\nu_m}{E_m}\right)(a)\left\{\left[\left(\frac{P_o}{2}\right)(1+K)(1-2\nu_m) - \frac{L}{a^2}\right] - \left[\left(\frac{P_o}{2}\right)(1-K) - \frac{2J}{a^4} - \frac{4N}{a^2}(1-\nu_m)\right]\cos 2\theta\right\}$$

from Eqn. A.36c,

$$\mathfrak{T}_{r\theta} = \left[\left(\frac{P_o}{2}\right)(1-K) - \frac{6J}{a^4} - \frac{2N}{a^2}\right]\sin 2\theta$$

from Eqn. A.43b,

$$\frac{a}{E_\ell^* A} = (1-2\nu_m)\,C\left(\frac{1+\nu_m}{E_m}\right)$$

Substituting these expressions into Eqn. A.41a, performing the indicated differentiations, and rearranging terms we find

$$N = \left[\frac{(1 - 2\nu_m)C - 2}{2(1 - 2\nu_m)C + 8\nu_m}\right]\left(\frac{P_o}{2}\right)(1 - K) - \left[\frac{6(1 - 2\nu_m)C + 12}{2(1 - 2\nu_m)C + 8\nu_m}\right]\left(\frac{J}{a^2}\right) \quad (A1.1)$$

From Eqn. A.41b we have

$$\frac{\partial v_\ell}{\partial \theta} + u_\ell + \frac{E_\ell^* I}{E_\ell^* A a^2}\left[\frac{\partial^4 u_\ell}{\partial \theta^4} + 2\frac{\partial^2 u_\ell}{\partial \theta^2} + u_\ell\right] = \frac{a^2}{E_\ell^* A} P_r \quad (A.41b)$$

The expressions for v_ℓ, u_ℓ, and $a/E_\ell^* A$ are given above. From Eqns. A.43 we have

$$\frac{E_\ell^* I}{E_\ell^* A a^2} = \left(\frac{E_\ell^* I}{a^3}\right)\left(\frac{a}{E_\ell^* A}\right) = \left[\frac{1}{6F}\left(\frac{E_m}{1 + \nu_m}\right)\right]\left[(1 - 2\nu_m)\, C\, \left(\frac{1 + \nu_m}{E_m}\right)\right] = \frac{(1 - 2\nu_m)C}{6F}$$

From BC3 and Eqn. A.36a we have

$$P_r = \left[\left(\frac{P_o}{2}\right)(1 + K) + \frac{L}{a^2}\right] - \left[\left(\frac{P_o}{2}\right)(1 - K) + \frac{6J}{a^4} + \frac{4N}{a^2}\right]\cos 2\theta$$

After substituting all of these expressions into Eqn. A.41b, performing the required differentiations, and rearranging terms we obtain an equation of the form

$$X = Y \cos 2\theta$$

where X and Y are constants (i.e.,do not contain r or θ). In order for this equality to hold for all values of θ we must have X = Y = 0.

From the requirement that X = 0 we find the first expression for a stress function constant. This expression is

$$L = -\left(\frac{P_o}{2}\right)(1 + K)a^2 L_n \qquad \text{(A1.2a)}$$

where,

$$L_n = \frac{(1 - 2\nu_m)(C - 1) - (1 - 2\nu_m)\dfrac{(1 - 2\nu_m)C}{6F}}{1 + (1 - 2\nu_m)C + \dfrac{(1 - 2\nu_m)C}{6F}}$$

Note that by substituting in the expressions for C and F (Eqns. A.42) we find that

$$\frac{(1 - 2\nu_m)C}{6F} = \left(\frac{1}{12}\right)\left(\frac{t}{a}\right)^2$$

For the "thin liner" solutions we have assumed that (t/a) < 0.10. Thus

$$\left[\frac{(1 - 2\nu_m)C}{6F}\right]_{max} < 0.00083.$$

Because this term will always have a very small value, setting it equal to zero here will not significantly alter the solution. Thus we have

$$L_n = \frac{(1 - 2\nu_m)(C - 1)}{1 + (1 - 2\nu_m)C} \qquad \text{(A1.2b)}$$

From the requirement that Y = 0 we have

$$\left(\frac{P_o}{2}\right)(1 - K)\left[2F - 3(1 - 2\nu_m)C + 2(1 - 2\nu_m)CF\right] +$$

$$+ \left(\frac{J}{a^4}\right)\left[12F + 6(1 - 2\nu_m)C + 12(1 - 2\nu_m)CF\right] +$$

$$+ \left(\frac{N}{a^2}\right)\left[8\nu_m F + 12(1 - \nu_m)(1 - 2\nu_m)C + 8(1 - 2\nu_m)CF\right] = 0$$

Substituting the expression for N as a function of J (Eqn. A1.1) into this equation and collecting terms we find that

$$J = -\tfrac{1}{2}\left(\frac{P_o}{2}\right)(1 - K)a^4 J_n \qquad \text{(A1.3a)}$$

where,

$$J_n = \frac{\left[(1 - 2\nu_m)(1 - C)\right]F - \tfrac{1}{2}(1 - 2\nu_m)^2 C + 2}{\left[(3 - 2\nu_m) + (1 - 2\nu_m)C\right]F + \tfrac{1}{2}(5 - 6\nu_m)(1 - 2\nu_m)C + (6 - 8\nu_m)} \qquad \text{(A1.3b)}$$

Substituting Eqns. A1.3a and b back into Eqn. A1.1 and collecting terms we find

$$N = -\left(\frac{P_o}{2}\right)(1 - K)a^2 N_n \qquad \text{(A1.4a)}$$

where,

$$N_n = \frac{\left[1 + (1 - 2\nu_m)C\right]F - \tfrac{1}{2}(1 - 2\nu_m)C - 2}{\left[(3 - 2\nu_m) + (1 - 2\nu_m)C\right]F + \tfrac{1}{2}(5 - 6\nu_m)(1 - 2\nu_m)C + (6 - 8\nu_m)} \qquad \text{(A1.4b)}$$

Now that expressions have been obtained for the three nonzero stress function constants, the final equations for ground mass stresses and displacements are obtained by direct substitution of Eqns. A1.2a, 3a, and 4a into Eqns. A.36. The boundary conditions BC3 and BC4 then yield the equations for the external pressures acting on the liner. Similarily, BC1 and BC2 allow determination of the final equations for liner displacements. The final equation for liner bending moments is obtained by substituting the resulting expression for u_ℓ into Eqn. A.40b. Then the equations for liner thrust and shear forces can be obtained from Eqns. A.39b and d, respectively.

All of the final equations for Solution No. 1 are presented in Section B.1 of Appendix B.

A.3.6 SOLUTION NO. 2 : OVERPRESSURE LOADING - FULL SLIPPAGE CONDITION

The additional boundary conditions that apply for this problem require that at r = a,

$$u_m = u_\ell \qquad \text{(BC1)}$$

$$\sigma_{rm} = P_r \qquad \text{(BC2)}$$

$$\tau_{r\theta m} = \mathcal{T}_{r\theta} = 0 \qquad \text{(BC3)}$$

Thus, from BC3 and Eqn. A.36c we have that

$$N = \left(\frac{P_o a^2}{4}\right)(1 - K) - \frac{3J}{a^2} \qquad \text{(A2.1)}$$

From BC3 and Eqn. A.41a we have

$$\frac{\partial^2 v_\ell}{\partial \theta^2} + \frac{\partial u_\ell}{\partial \theta} = 0$$

Integrating this equation with respect to θ twice we find that

$$v_\ell = -\int u_\ell \, d\theta + f_1(r)\theta + f_2(r)$$

From BC1 we have that for $r = a$, u_ℓ is given by Eqn. A.36d. Substituting this expression for u_ℓ into the above equation for v_ℓ, performing the indicated integration, and invoking the requirement that $v_\ell = 0$ for $\theta = n\pi/2$ (where $n = 0, 1, 2, 3, \ldots\ldots$) we find that*

$$f_1(r) = \left(\frac{1 + \nu_m}{E_m}\right)(a)\left[(1 - 2\nu_m)\left(\frac{P_o}{2}\right)(1 + K) - \frac{L}{a^2}\right]$$

$$f_2(r) = 0$$

Thus, the above equation for v_ℓ can be rewritten as follows:

$$v_\ell + \int u_\ell \, d\theta = \left\{\left(\frac{1 + \nu_m}{E_m}\right)(a)\left[(1 - 2\nu_m)\left(\frac{P_o}{2}\right)(1 + K) - \frac{L}{a^2}\right]\right\}(\theta)$$

Taking the partial derivative with respect to θ of each term in this equation we find that

$$\frac{\partial v_\ell}{\partial \theta} + u_\ell = \left(\frac{1 + \nu_m}{E_m}\right)(a)\left[(1 - 2\nu_m)\left(\frac{P_o}{2}\right)(1 + K) - \frac{L}{a^2}\right]$$

---

*The resulting expression for v_ℓ is

$$v_\ell = \left(\frac{1 + \nu_m}{E_m}\right)\left(\frac{a}{2}\right)\left[\left(\frac{P_o}{2}\right)(1 - K) - \frac{2J}{a^4} - \frac{4N}{a^2}(1 - \nu_m)\right]\sin 2\theta$$

Substituting this result into Eqn. A.41b we have

$$\left(\frac{1+\nu_m}{E_m}\right)(a)\left[(1-2\nu_m)\left(\frac{P_o}{2}\right)(1+K)-\frac{L}{a^2}\right]+\frac{E_\ell^* I}{E_\ell^* A a^2}\left[\frac{\partial^4 u_\ell}{\partial\theta^4}+2\frac{\partial^2 u_\ell}{\partial\theta^2}+u_\ell\right]=$$

$$=\frac{a^2}{E_\ell^* A}P_r$$

The following equations are obtained from the boundary conditions and from Eqn. A.36d,

$$u_\ell=\left(\frac{1+\nu_m}{E_m}\right)(a)\left[\left(\frac{P_o}{2}\right)(1+K)(1-2\nu_m)-\frac{L}{a^2}\right]-$$

$$-\left[\left(\frac{P_o}{2}\right)(1-K)-\frac{2J}{a^4}-\frac{4N}{a^2}(1-\nu_m)\right]\cos 2\theta$$

from Eqn. A.36a,

$$P_r=\left[\left(\frac{P_o}{2}\right)(1+K)+\frac{L}{a^2}\right]-\left[\left(\frac{P_o}{2}\right)(1-K)+\frac{6J}{a^4}+\frac{4N}{a^2}\right]\cos 2\theta$$

from Eqn. A.43b,

$$\frac{a}{E_\ell^* A}=(1-2\nu_m)\,C\left(\frac{1+\nu_m}{E_m}\right)$$

from Eqns. A.43a and b,

$$\frac{E_\ell^* I}{E_\ell^* A a^2}=\frac{(1-2\nu_m)C}{6F}$$

After substituting all of these equations into the above equation, taking the required derivatives, and rearranging terms we obtain an equation of the form

$$X = Y \cos 2\theta$$

where X and Y are constants (i.e., do not contain r or θ). In order for this equality to hold for all values of θ we must have X = Y = 0.

From the requirement that X = 0 we obtain the same result as in the derivation of the first solution (See page 342 , Section A.3.5). That is, that

$$L = -\left(\frac{P_o}{2}\right)(1 + K)a^2 L_f \qquad \text{(A2.2a)}$$

where,

$$L_f = L_n = \frac{(1 - 2\nu_m)(C - 1)}{1 + (1 - 2\nu_m)C} \qquad \text{A2.2b)}$$

From the requirement that Y = 0 we find

$$\left(\frac{P_o}{2}\right)(1 - K)[3 - 2F] - \frac{J}{a^4}[6 + 12F] - \frac{N}{a^2}[12(1 - \nu_m) + 8F] = 0$$

Substituting the expression for N as a function of J (Eqn. A2.1) into this equation and collecting terms we find that

$$J = \tfrac{1}{2}\left(\frac{P_o}{2}\right)(1 - K)a^4 J_f \qquad \text{(A2.3a)}$$

where,

$$J_f = \frac{2F + (1 - 2\nu_m)}{2F + (5 - 6\nu_m)} \qquad \text{(A2.3b)}$$

Substituting Eqns. A2.3 back into Eqn. A2.1 and collecting terms we find

$$N = -\left(\frac{P_o}{2}\right)(1 - K)a^2 N_f \qquad \text{(A2.4a)}$$

where,

$$N_f = \frac{2F - 1}{2F + (5 - 6\nu_m)} \qquad \text{(A2.4b)}$$

Now that expressions have been obtained for the three nonzero stress function constants, the final equations for ground mass stresses and displacements are obtained by direct substitution of Eqns. A2.2a, 3a, and 4a into Eqns. A.36. The boundary conditions BC2 and BC3 then yield the equations for the external pressures acting on the liner. Similarily, BC1 allows determination of the final equation for the liner radial displacements. The equation for liner tangential displacements is obtained by substituting Eqns. A2.3a and 4a into the equation for v_ℓ given at the bottom of page 345. Substitution of the final equation for u_ℓ into Eqn. A.40b yields the equation for liner bending moments. Then the equations for liner thrust and shear forces can be obtained from Eqns. A.39b and d, respectively.

All of the equations for Solution No. 2 are presented in Section B.2 of Appendix B.

A.3.7 SOLUTION NO. 3 : EXCAVATION LOADING - NO SLIPPAGE CONDITION

The additional boundary conditions that apply for this problem require that at r = a,

$$u_m = u_\ell \qquad \text{(BC1)}$$

$$v_m = v_\ell \qquad \text{(BC2)}$$

$$\sigma_{rm} = P_r \qquad \text{(BC3)}$$

$$\tau_{r\theta m} = \mathfrak{T}_{r\theta} \qquad \text{(BC4)}$$

From Eqn. A.41a we have

$$\frac{\partial^2 v_\ell}{\partial \theta^2} + \frac{\partial u_\ell}{\partial \theta} = -\frac{a^2}{E_\ell^* A}\,\mathfrak{T}_{r\theta} \qquad \text{(A.41a)}$$

We get the following from the boundary conditions and

from Eqn. A.38e,

$$v_\ell = \left(\frac{1+\nu_m}{E_m}\right)(a)\left\{\left[\frac{2J}{a^4} - \frac{2N}{a^2}(1-2\nu_m)\right]\sin 2\theta\right\}$$

from Eqn. A.38d,

$$u_\ell = \left(\frac{1+\nu_m}{E_m}\right)(a)\left\{\left[-\frac{L}{a^2}\right] + \left[\frac{2J}{a^4} + \frac{4N}{a^2}(1-\nu_m)\right]\cos 2\theta\right\}$$

from Eqn. A.38c,

$$\mathfrak{T}_{r\theta} = \left[\left(\frac{\gamma H}{2}\right)(1-K_o) - \frac{6J}{a^4} - \frac{2N}{a^2}\right]\sin 2\theta$$

from Eqn. A.43b,

$$\frac{a}{E^* A} = (1-2\nu_m)\,C\left(\frac{1+\nu_m}{E_m}\right)$$

Substituting these expressions into Eqn. A.41a and collecting terms we find

$$N = \left[\frac{(1-2\nu_m)C}{2(1-2\nu_m)C + 8\nu_m}\right]\left(\frac{\gamma H}{2}\right)(1-K_o) - \left[\frac{6(1-2\nu_m)C + 12}{2(1-2\nu_m)C + 8\nu_m}\right]\left(\frac{J}{a^2}\right) \qquad \text{(A3.1)}$$

From Eqn. A.41b we have

$$\frac{\partial v_\ell}{\partial \theta} + u_\ell + \frac{E_\ell^* I}{E_\ell^* A a^2}\left[\frac{\partial^4 u_\ell}{\partial \theta^4} + 2\frac{\partial^2 u_\ell}{\partial \theta^2} + u_\ell\right] = \frac{a^2}{E_\ell^* A} P_r \qquad \text{(A.41b)}$$

The expressions for v_ℓ, u_ℓ, and $a/E_\ell^* A$ are given above. From Eqns. A.43 we have

$$\frac{E_\ell^* I}{E_\ell^* A a^2} = \frac{(1 - 2\nu_m)C}{6F}$$

From BC3 and Eqn. A.38a we have

$$P_r = \left[\left(\frac{\gamma H}{2}\right)(1 + K_o) + \frac{L}{a^2}\right] - \left[\left(\frac{\gamma H}{2}\right)(1 - K_o) + \frac{6J}{a^4} + \frac{4N}{a^2}\right]\cos 2\theta$$

After substituting all of these expressions into Eqn. A.41b, taking the required derivations, and rearranging terms we obtain an equation of the form

$$X = Y \cos 2\theta$$

where X and Y are constants (i.e., do not contain r or θ). In order for this equality to hold for all values of θ we must have $X = Y = 0$.

From the requirement that $X = 0$ we find that

$$L = -\left(\frac{\gamma H}{2}\right)(1 + K_o) a^2 L_n^* \qquad \text{(A3.2a)}$$

where,

$$L_n^* = \frac{(1 - 2\nu_m)C}{1 + (1 - 2\nu_m)C + \dfrac{(1 - 2\nu_m)C}{6F}}$$

As was done in the previous derivations we set

$$\frac{(1 - 2\nu_m)C}{6F} = 0$$

to obtain

$$L_n^* = \frac{(1 - 2\nu_m)C}{1 + (1 - 2\nu_m)C} \tag{A3.2b}$$

From the requirement that Y = 0 we find

$$\left(\frac{\gamma H}{2}\right)(1 + K_o)\left[(1 - 2\nu_m)CF\right] +$$

$$+ \frac{J}{a^4}\left[6F + 3(1 - 2\nu_m)C + 6(1 - 2\nu_m)CF\right] +$$

$$+ \frac{N}{a^2}\left[4\nu_m F + 6(1 - \nu_m)(1 - 2\nu_m)C + 4(1 - 2\nu_m)CF\right] = 0$$

Substituting the expression for N in terms of J (Eqn. A3.1) into this equation and collecting terms we find that

$$J = -\tfrac{1}{2}\left(\frac{\gamma H}{2}\right)(1 - K_o)a^4 J_n^* \tag{A3.3a}$$

where,

$$J_n^* = \frac{\left[2\nu_m + (1 - 2\nu_m)C\right]F + (1 - \nu_m)(1 - 2\nu_m)C}{\left[(3 - 2\nu_m) + (1 - 2\nu_m)C\right]F + \tfrac{1}{2}(5 - 6\nu_m)(1 - 2\nu_m)C + (6 - 8\nu_m)} \tag{A3.3b}$$

Substituting Eqns. A3.3a and b back into Eqn. A3.1 and collecting terms we find the expression for N,

$$N = -\tfrac{1}{2}\left(\frac{\gamma H}{2}\right)(1 - K_o)a^2 N_n^* \qquad \text{(A3.4a)}$$

where,

$$N_n^* = \frac{\left[3 + 2(1 - 2\nu_m)C\right]F + \tfrac{1}{2}(1 - 2\nu_m)C}{\left[(3 - 2\nu_m) + (1 - 2\nu_m)C\right]F + \tfrac{1}{2}(5 - 6\nu_m)(1 - 2\nu_m)C + (6 - 8\nu_m)} \qquad \text{(A3.4b)}$$

Now that expressions have been obtained for the three nonzero stress function constants, the final equations for ground mass stresses and displacements are obtained by direct subatitution of Eqns. A3.2a, 3a, and 4a into Eqns. A.38. The boundary conditions BC3 and BC4 then yield the equations for the external pressures acting on the liner. Similarily, BC1 and BC2 allow determination of the final equations for liner displacements. The final equation for liner bending moments is obtained by substituting the resulting expression for u_ℓ into Eqn.A.40b. then the equations for liner thrust and shear forces can be obtained from Eqns. A.39b and d, respectively.

All of the final equations for Solution No. 3 are presented in Section B.3 of Appendix B.

A.3.8 SOLUTION NO. 4 : EXCAVATION LOADING - FULL SLIPPAGE CONDITION

The additional boundary conditions that apply for this problem require that at r = a,

$$u_m = u_\ell \qquad \text{(BC1)}$$

$$\sigma_{rm} = P_r \qquad \text{(BC2)}$$

$$\tau_{r\theta m} = \mathfrak{T}_{r\theta} = 0 \qquad \text{(BC3)}$$

From BC3 and Eqn. A.38c we find that

$$N = \left(\frac{\gamma Ha^2}{4}\right)(1 - K_o) - \frac{3J}{a^2} \qquad (A4.1)$$

From Eqn. A.41a and BC3 we have

$$\frac{\partial^2 v_\ell}{\partial \theta^2} + \frac{\partial u_\ell}{\partial \theta} = 0$$

Integrating this equation with respect to θ twice we find

$$v_\ell = - \int u_\ell d\theta + f_1(r)\theta + f_2(r)$$

From BC1 we have that for r = a, u_ℓ is given by Eqn. A.38d. Substituting this expression for u_ℓ into the above equation for v_ℓ, performing the indicated integration, and invoking the requirement that $v_\ell = 0$ for $\theta = n\pi/2$ (where n = 0, 1, 2, 3, ...) we find that*

$$f_1(r) = - \left(\frac{1 + \nu_m}{E_m}\right)(a)\left[\frac{L}{a^2}\right]$$

$$f_2(r) = 0$$

thus, the above equation for v_ℓ can be rewritten as follows:

$$v_\ell + \int u_\ell d\theta = - \left\{\left(\frac{1 + \nu_m}{E_m}\right)(a)\left[\frac{L}{a^2}\right]\right\}\theta$$

---

*The resulting expression for v_ℓ is

$$v_\ell = - \left(\frac{1 + \nu_m}{E_m}\right)\left(\frac{a}{2}\right)\left[\frac{2J}{a^4} + \frac{4N}{a^2}(1 - \nu_m)\right]\sin 2\theta$$

Taking the partial derivative with respect to θ of each term in this equation we find that

$$\frac{\partial v_\ell}{\partial \theta} + u_\ell = -\left(\frac{1+\nu_m}{E_m}\right)(a)\left[\frac{L}{a^2}\right]$$

Substituting this result into Eqn. A.41b we have

$$-\left(\frac{1+\nu_m}{E_m}\right)(a)\left[\frac{L}{a^2}\right] + \frac{E_\ell^* I}{E_\ell^* A a^2}\left[\frac{\partial^4 u_\ell}{\partial\theta^4} + 2\frac{\partial^2 u_\ell}{\partial\theta^2} + u_\ell\right] = \frac{a^2}{E_\ell^* A} P_r$$

The following equations are obtained from the boundary conditions and from Eqn. A.38d,

$$u_\ell = \left(\frac{1+\nu_m}{E_m}\right)(a)\left\{\left[-\frac{L}{a^2}\right] + \left[\frac{2J}{a^4} + \frac{4N}{a^2}(1-\nu_m)\right]\cos 2\theta\right\}$$

from Eqn. A.38a,

$$P_r = \left[\left(\frac{\gamma H}{2}\right)(1+K_o) + \frac{L}{a^2}\right] - \left[\left(\frac{\gamma H}{2}\right)(1-K_o) + \frac{6J}{a^4} + \frac{4N}{a^2}\right]\cos 2\theta$$

from Eqn. A.43b,

$$\frac{a}{E_\ell^* A} = (1-2\nu_m)\, C \left(\frac{1+\nu_m}{E_m}\right)$$

from Eqns. A.43a and b,

$$\frac{E_\ell^* I}{E_\ell^* A a^2} = \frac{(1-2\nu_m)C}{6F}$$

After substituting all of these expressions into the above equation, taking the required derivatives, and rearranging terms we obtain an equation

of the form

$$X = Y \cos 2\theta$$

where X and Y are constants (i.e., do not contain r or θ). In order for this equality to hold for all values of θ we must have X = Y = 0.

From the requirement that X = 0 we obtain the same result as in the derivation of the third solution. That is, that

$$L = -(\frac{\gamma H}{2})(1 + K_o)a^2 L_f^* \qquad \text{(A4.2a)}$$

where,

$$L_f^* = L_n^* = \frac{(1 - 2\nu_m)C}{1 + (1 - 2\nu_m)C} \qquad \text{(a4.2b)}$$

(See page 351 , Section A.3.7)

From the requirement that Y = 0 we find

$$(\frac{\gamma H}{2})(1 - K_o)[F] + \frac{J}{a^4}[3 + 6F] + \frac{N}{a^2}[4F + 6(1 - \nu_m)] = 0$$

Substituting the expression for N in terms of J (Eqn. A4.1) into this equation and collecting terms we find

$$J = (\frac{\gamma H}{2})(1 - K_o)a^4 J_f^* \qquad \text{(A4.3a)}$$

where,

$$J_f^* = \frac{F + (1 - \nu_m)}{2F + (5 - 6\nu_m)} \qquad \text{(A4.3b)}$$

Substituting Eqns. A4.3a and b back into Eqn. A4.1 we find the expression

for N.

$$N = -\tfrac{1}{2}\left(\frac{\gamma H}{2}\right)(1 - K_o)a^2 N_f^* \qquad \text{(A4.4a)}$$

where,

$$N_f^* = \frac{4F + 1}{2F + (5 - 6\nu_m)} \qquad \text{(A4.4b)}$$

Now that expressions have been obtained for the three nonzero stress function constants, the final equations for ground mass stresses and displacements are obtained by direct substitution of Eqns. A4.2a, 3a, and 4a into Eqns. A.38. The boundary conditions BC2 and BC3 then yield the equations for the external pressures acting on the liner. Similarily, BC1 allows determination of the final equation for the liner radial displacements. The equation for liner tangential displacements is obtained by substituting Eqns. A4.3a and 4a into the equation for v_ℓ given at the bottom of page 353. Substitution of the final equation for u_ℓ into Eqn. A.40b yields the equation for liner bending moments. Then the equations for liner thrust and shear forces can be obtained from Eqns. A.39b and d, respectively.

All of the final equations for Solution No. 4 are presented in Section B.4 of Appendix B.

A.4 SOLUTIONS FOR A THICK LINER

A.4.1 GENERAL COMMENTS

The "thick liner" solutions are obtained by combining the generalized stress and displacement equations for the ground mass (Section A.3.2) and the corresponding equations for the liner (Section A.4.3) in accordance with the appropriate boundary conditions. Both sets of equations are obtained from Eqn. A.32 and A.34.

The positive sign conventions and the relevant geometrical quantities adopted for these solutions are illustrated in Fig. A.5.

A.4.2 EQUATIONS FOR STRESSES AND DISPLACEMENTS IN THE SURROUNDING GROUND MASS IN TERMS OF STRESS FUNCTION CONSTANTS

The equations for stresses and displacements in the elastic ground mass surrounding the tunnel were derived in Section A.3.2. The resulting Eqns. A.36 (page 335) apply in the case of overpressure loading, while for excavation loading Eqns. A.38 (page 336) must be used.

A.4.3 EQUATIONS FOR STRESSES AND DISPLACEMENTS IN THE LINER IN TERMS OF STRESS FUNCTION CONSTANTS

The general equations for liner stresses and displacements are obtained from Eqns. A.32 and A.34 by invoking the following two conditions:

1) $r = r_\ell$, where $R_i \leq r \leq R_o$

2) $v_\ell = 0$ for $\theta = \frac{n\pi}{2}$ $\quad (n = 0, 1, 2, 3, \ldots\ldots)$

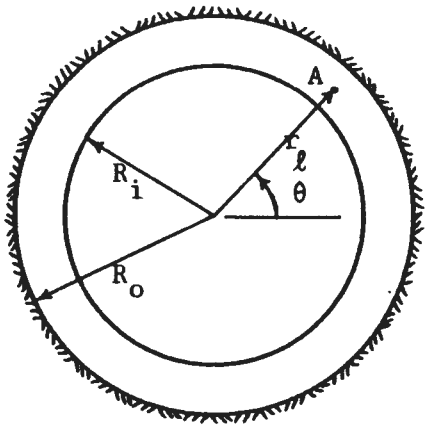

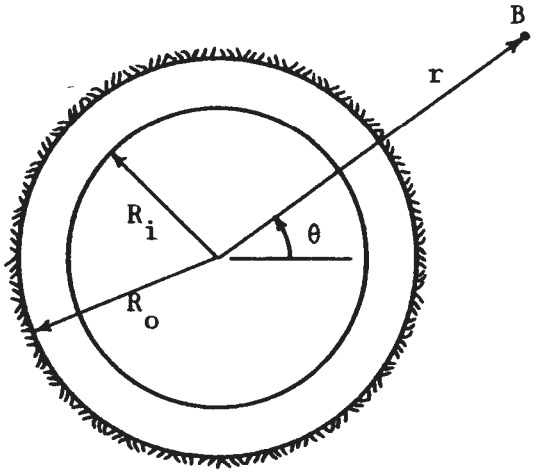

At point A:

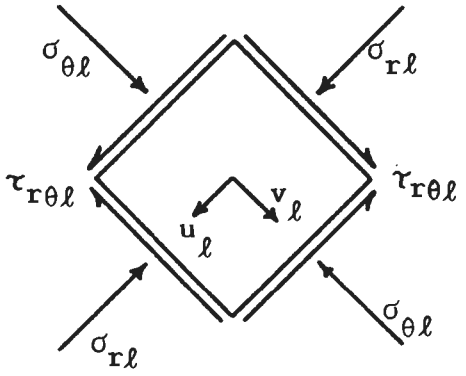

At point B:

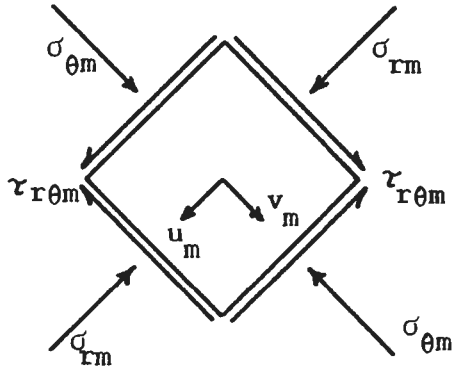

FIGURE A.5 POSITIVE SIGN CONVENTIONS - "THICK LINER" SOLUTIONS

Only the second of these requirements allows determination of values for the constants of integration. After substitution of $\theta = n\pi/2$ in Eqn. A.34b and equating the result to zero for n = 0 and 1 we have

$$A_1 = 0$$

$$A_2 = \text{unknown} = Q$$

$$A_3 = \text{unknown} = S$$

$$B_1 = \text{unknown} = W$$

$$B_2 = \text{unknown} = X$$

$$B_3 = \text{unknown} = Y$$

$$B_4 = \text{unknown} = Z$$

$$A_o = 0$$

$$B_o = 0$$

$$C_o = 0$$

Substituting these values for the constants back into Eqns. A.32 and A.34, along with $r = r_\ell$, we obtain the general equations for liner stresses and displacements.

$$\sigma_{r\ell} = \left[2Q + \frac{S}{r_\ell^2}\right] - \left[2W + \frac{6X}{r_\ell^4} + \frac{4Y}{r_\ell^2}\right]\cos 2\theta \qquad \text{(A.44a)}$$

$$\sigma_{\theta\ell} = \left[2Q - \frac{S}{r_\ell^2}\right] + \left[2W + \frac{6X}{r_\ell^4} + 12Zr_\ell^2\right]\cos 2\theta \qquad \text{(A.44b)}$$

$$\tau_{r\theta\ell} = \left[2W - \frac{6X}{r_\ell^4} - \frac{2Y}{r_\ell^2} + 6Zr_\ell^2\right]\sin 2\theta \qquad \text{(A.44c)}$$

$$u_\ell = \left(\frac{1+\nu_\ell}{E_\ell}\right)(r_\ell)\left[2(1-2\nu_\ell)Q - \frac{S}{r_\ell^2}\right] -$$

$$- \left[2W - \frac{2X}{r_\ell^4} - \frac{4Y}{r_\ell^2}(1-\nu_\ell) + 4\nu_\ell Z r_\ell^2\right]\cos 2\theta \qquad \text{(A.44d)}$$

$$v_\ell = \left(\frac{1+\nu_\ell}{E_\ell}\right)(r_\ell)\left[2W + \frac{2X}{r_\ell^4} - \frac{2Y}{r_\ell^2}(1-2\nu_\ell) + 2(3-2\nu_\ell)Z r_\ell^2\right]\sin 2\theta \qquad \text{(A.44e)}$$

A.4.4 COMMENTS ON METHOD OF DERIVATION

Solutions for the thick liner problems are obtained from Eqns. A.36 or A.38, Eqns. A.44, and the appropriate boundary conditions. In each derivation these equations and conditions are used to obtain nine equations in nine unknowns (the constants of integration remaining in the equations already given). Each derivation then follows the procedure outlined below.

The nine equations can be seperated into three groups, as follows:

1) Three equations in the three unknowns L, Q, and S. These equations can be solved by direct substitution.

2) Four equations in the four unknowns J, N, X, and Y. These equations are too complex to be easily solved by direct substitution; thus, use is made of Cramer's Rule (See, for example, Kreyszig, 1967).

3) The remaining two equations give the unknowns W and Z as functions of X and Y. Thus, once X and Y have been found W and Z are obtained by direct substitution.

The use of Cramer's Rule requires the solution of a number of determinants. Because such solutions involve rather lengthy calculations, the procedure is briefly described here rather than given for each derivation in the sections that follow.

For four unknowns the four simultaneous equations can be written as follows:

$$\begin{aligned} a_{11}X + a_{12}Y + a_{13}J + a_{14}N &= b_1 \\ a_{21}X + a_{22}Y + a_{23}J + a_{24}N &= b_2 \\ a_{31}X + a_{32}Y + a_{33}J + a_{34}N &= b_3 \\ a_{41}X + a_{42}Y + a_{43}J + a_{44}N &= b_4 \end{aligned} \qquad \text{(A.45)}$$

The four unknowns are then given by

$$X = \frac{D_1}{D}$$

$$Y = \frac{D_2}{D}$$

$$J = \frac{D_3}{D}$$

$$N = \frac{D_4}{D}$$

where,

$$D = \begin{vmatrix} a_{11} & a_{12} & a_{13} & a_{14} \\ a_{21} & a_{22} & a_{23} & a_{24} \\ a_{31} & a_{32} & a_{33} & a_{34} \\ a_{41} & a_{42} & a_{43} & a_{44} \end{vmatrix}$$

and,

$$D_1 = \begin{vmatrix} b_1 & a_{12} & a_{13} & a_{14} \\ b_2 & a_{22} & a_{23} & a_{24} \\ b_3 & a_{32} & a_{33} & a_{34} \\ b_4 & a_{42} & a_{43} & a_{44} \end{vmatrix}$$

Similarily, D_2 is obtained by replacing the second column of D by b_1 through b_4, D_3 by replacing the third column and D_4 by replacing the fourth column.

A.4.5 SOLUTION NO. 5 : OVERPRESSURE LOADING - NO SLIPPAGE CONDITION

The additional boundary conditions that apply for this problem requires that

at $r_\ell = R_i$,

$$\sigma_{r\ell} = 0 \qquad \text{(BC1)}$$

$$\tau_{r\theta\ell} = 0 \qquad \text{(BC2)}$$

at $r_\ell = R_o = r$,

$$\sigma_{r\ell} = \sigma_{rm} \qquad \text{(BC3)}$$

$$\tau_{r\theta\ell} = \tau_{r\theta m} \qquad \text{(BC4)}$$

$$u_\ell = u_m \qquad \text{(BC5)}$$

$$v_\ell = v_m \qquad \text{(BC6)}$$

From BC1 and Eqn. A.44a we obtain two equations (because $\sigma_{r\ell} = 0$ for all values of $\cos 2\theta$) which yield

$$S = -2QR_i^2 \qquad \text{(A5.1)}$$

$$W = -\frac{3X}{R_i^4} - \frac{2Y}{R_i^2} \qquad (A5.2)$$

From BC2 and Eqn. A.44c we find that

$$Z = \frac{X}{R_i^6} + \frac{Y}{3R_i^4} - \frac{W}{3R_i^2}$$

Substituting the expression for W (Eqn. A5.2) into this equation we obtain

$$Z = \frac{2X}{R_i^6} + \frac{Y}{R_i^4} \qquad (A5.3)$$

From BC3 and Eqns. A.44a and A.36a we find that

$$2Q + \frac{S}{R_o^2} = (\frac{P_o}{2})(1 + K) + \frac{L}{R_o^2}$$

and,

$$2W + \frac{6X}{R_o^4} + \frac{4Y}{R_o^2} = (\frac{P_o}{2})(1 - K) + \frac{6J}{R_o^4} + \frac{4N}{R_o^2}$$

Substituting the expression for S (Eqn. A5.1) into the first of these equations and rearranging terms we find that

$$L = -(\frac{P_o}{2})(1 + K)R_o^2 + 2Q\alpha_1 R_i^2 \qquad (A5.4a)$$

where,

$$\alpha_1 = [(\frac{R_o}{R_i})^2 - 1] \qquad (A5.4b)$$

Substituting the expression for W (Eqn. A5.2) into the second of the

above equalities and rearranging terms we obtain

$$\left(\frac{3\alpha_2}{R_o^4}\right)X + \left(\frac{2\alpha_1}{R_o^2}\right)Y + \left(\frac{3}{R_o}\right)J + \left(\frac{2}{R_o^2}\right)N = -\left(\frac{P_o}{4}\right)(1 - K) \qquad \text{(A5.5a)}$$

where,

$$\alpha_2 = \left[\left(\frac{R_o}{R_i}\right)^4 - 1\right] \qquad \text{(A5.5b)}$$

From BC4 and Eqns. A.44c and A.36c we obtain the following equation:

$$2W - \frac{6X}{R_o^4} - \frac{2Y}{R_o^2} + 6ZR_o^2 = \left(\frac{P_o}{2}\right)(1 - K) - \frac{6J}{R_o^4} - \frac{2N}{R_o^2}$$

Substituting the expressions for Z (Eqn. A5.3) and W (Eqn. A5.2) into this equation and rearranging terms we obtain

$$\left(\frac{3\alpha_3}{R_o^4}\right)X + \left(\frac{\alpha_4}{R_o^2}\right)Y + \left(\frac{3}{R_o^4}\right)J + \left(\frac{1}{R_o^2}\right)N = \left(\frac{P_o}{4}\right)(1 - K) \qquad \text{(A5.6a)}$$

where,

$$\alpha_3 = \left[2\left(\frac{R_o}{R_i}\right)^6 - \left(\frac{R_o}{R_i}\right)^4 - 1\right] \qquad \text{(A5.6b)}$$

$$\alpha_4 = \left[3\left(\frac{R_o}{R_i}\right)^4 - 2\left(\frac{R_o}{R_i}\right)^2 - 1\right] \qquad \text{(A5.6c)}$$

From BC5 and Eqns. A.44d and A.36d we obtain the following two equations.

$$\left(\frac{R_o}{2G_\ell}\right)\left[2(1 - 2\nu_\ell)Q - \frac{S}{R_o^2}\right] = \left(\frac{R_o}{2G_m}\right)\left[\left(\frac{P_o}{2}\right)(1 + K)(1 - 2\nu_m) - \frac{L}{R_o^2}\right]$$

$$\left(\frac{R_o}{2G_\ell}\right)\left[2W - \frac{2X}{R_o^4} - \frac{4Y}{R_o^2}(1 - \nu_\ell) + 4\nu_\ell ZR_o^2\right] =$$

$$= \left(\frac{R_o}{2G_m}\right)\left[\left(\frac{P_o}{2}\right)(1 - K) - \frac{2J}{R_o^4} - \frac{4N}{R_o^2}(1 - \nu_m)\right]$$

Note that the following substitutions have been made

$$\left(\frac{1 + \nu_\ell}{E_\ell}\right) = \frac{1}{2G_\ell} \quad \text{and} \quad \left(\frac{1 + \nu_m}{E_m}\right) = \frac{1}{2G_m}$$

where G is the shear modulus (or modulus of rigidity) which is given by

$$G = \frac{E}{2(1 + \nu)}$$

Substituting the expression for S (Eqn. A5.1) into the first of the above equalities and rearranging terms we find

$$Q = \left(\frac{G_\ell}{G_m}\right)\left(\frac{R_o}{R_i}\right)^2\left(\frac{1}{2\alpha_5}\right)\left[\left(\frac{P_o}{2}\right)(1 + K)(1 - 2\nu_m) - \frac{L}{R_o^2}\right] \tag{A5.7a}$$

where,

$$\alpha_5 = \left[(1 - 2\nu_\ell)\left(\frac{R_o}{R_i}\right)^2 + 1\right] \tag{A5.7b}$$

Substituting the expressions for W (Eqn. A5.2) and Z(Eqn. A5.3) into the second of the above equations and rearranging terms we obtain

$$\left(\frac{G_m}{G_\ell}\right)\left(\frac{\alpha_6}{R_o^4}\right)X + \left(\frac{G_m}{G_\ell}\right)\left(\frac{2\alpha_7}{R_o^2}\right)Y + \left(\frac{1}{R_o^4}\right)J + \left[\frac{2(1 - \nu_m)}{R_o^2}\right]N = \left(\frac{P_o}{4}\right)(1 - K) \tag{A5.8a}$$

where,

$$\alpha_6 = \left[4\nu_\ell\left(\frac{R_o}{R_i}\right)^6 - 3\left(\frac{R_o}{R_i}\right)^4 - 1\right] \tag{A5.8b}$$

$$\alpha_7 = \left[\nu_\ell \left(\frac{R_o}{R_i}\right)^4 - \left(\frac{R_o}{R_i}\right)^2 - (1 - \nu_\ell)\right] \qquad \text{(A5.8c)}$$

From BC6 and Eqns. A.44e and A.36e we have that

$$\left(\frac{R_o}{2G_\ell}\right)\left[2W + \frac{2X}{R_o^4} - \frac{2Y}{R_o^2}(1 - 2\nu_\ell) + 2(3 - 2\nu_\ell)ZR_o^2\right] =$$

$$= \left(\frac{R_o}{2G_m}\right)\left[\left(\frac{P_o}{2}\right)(1 - K) + \frac{2J}{R_o^4} - \frac{2N}{R_o^2}(1 - 2\nu_m)\right]$$

Substituting the expressions for W (Eqn. A5.2) and Z (Eqn. A5.3) into this equation and rearranging terms we find

$$\left(\frac{G_m}{G_\ell}\right)\left(\frac{\alpha_8}{R_o^4}\right)X + \left(\frac{G_m}{G_\ell}\right)\left(\frac{\alpha_9}{R_o^2}\right)Y - \left(\frac{1}{R_o^4}\right)J + \left[\frac{(1 - 2\nu_m)}{R_o^2}\right]N = \left(\frac{P_o}{4}\right)(1 - K) \qquad \text{(A5.9a)}$$

where,

$$\alpha_8 = \left[2(3 - 2\nu_\ell)\left(\frac{R_o}{R_i}\right)^6 - 3\left(\frac{R_o}{R_i}\right)^4 + 1\right] \qquad \text{(A5.9a)}$$

$$\alpha_9 = \left[(3 - 2\nu_\ell)\left(\frac{R_o}{R_i}\right)^4 - 2\left(\frac{R_o}{R_i}\right)^2 - (1 - 2\nu_\ell)\right] \qquad \text{(A5.9c)}$$

Substitution of Eqn. A5.4a into Eqn. A5.7a yields the expression for the constant Q.

$$Q = \left(\frac{P_o}{2}\right)(1 + K)\left(\frac{R_o}{R_i}\right)^2(1 - \nu_m)\left(\frac{G_\ell}{G_m}\right)Q_n \qquad \text{(A5.10a)}$$

where,

$$Q_n = \frac{1}{\left(\frac{G_\ell}{G_m}\right)b_1 + b_2} \qquad \text{(A5.10b)}$$

and

$$b_1 = \alpha_1 = \left[\left(\frac{R_o}{R_i}\right)^2 - 1\right] \tag{A5.10c}$$

$$b_2 = \alpha_5 = \left[(1 - 2\nu_\ell)\left(\frac{R_o}{R_i}\right)^2 + 1\right] \tag{A5.10d}$$

Substitution of Eqns. A5.10a and b into Eqn. A5.4a yields the expression for the constant L.

$$L = \left(\frac{P_o}{2}\right)(1 + K)R_o^2 L_n \tag{A5.11a}$$

where,

$$L_n = \frac{(1 - 2\nu_m)\left(\frac{G_\ell}{G_m}\right)b_1 - b_2}{\left(\frac{G_\ell}{G_m}\right)b_1 + b_2} \tag{A5.11b}$$

Substitution of Eqns. A5.10a and b into Eqn. A5.1 yields the expression for the constant S.

$$S = -P_o(1 + K)(1 - \nu_m)\left(\frac{G_\ell}{G_m}\right)R_o^2 S_n \tag{A5.12a}$$

where,

$$S_n = Q_n = \frac{1}{\left(\frac{G_\ell}{G_m}\right)b_1 + b_2} \tag{A5.12b}$$

Equations A5.5a, 6a, 8a, and 9a can be solved for X, Y, J, and N by using Cramer's Rule (See Section A4.4). From these equations we have that

$$a_{11} = \frac{3\alpha_2}{R_o^4} \quad ; \quad a_{12} = \frac{2\alpha_1}{R_o^2} \quad ; \quad a_{13} = \frac{3}{R_o^4} \quad ; \quad a_{14} = \frac{2}{R_o^2}$$

$$a_{21} = \frac{3\alpha_3}{R_o^4} \quad ; \quad a_{22} = \frac{\alpha_4}{R_o^2} \quad ; \quad a_{23} = \frac{3}{R_o^4} \quad ; \quad a_{24} = \frac{1}{R_o^2}$$

$$a_{31} = \left(\frac{G_m}{G_\ell}\right)\left(\frac{\alpha_6}{R_o^4}\right) \quad ; \quad a_{32} = \left(\frac{G_m}{G_\ell}\right)\left(\frac{2\alpha_7}{R_o^2}\right) \quad ; \quad a_{33} = \frac{1}{R_o^4} \quad ; \quad a_{34} = \frac{2(1-\nu_m)}{R_o^2}$$

$$a_{41} = \left(\frac{G_m}{G_\ell}\right)\left(\frac{\alpha_8}{R_o^4}\right) \quad ; \quad a_{42} = \left(\frac{G_m}{G_\ell}\right)\left(\frac{\alpha_9}{R_o^2}\right) \quad ; \quad a_{43} = -\frac{1}{R_o^4} \quad ; \quad a_{44} = \frac{(1-2\nu_m)}{R_o^2}$$

and, $$-b_1 = b_2 = b_3 = b_4 = \left(\frac{P_o}{4}\right)(1-K)$$

Solving for each of the required determinants we obtain the following results.

$$D = -3\left(\frac{G_m}{G_\ell}\right)^2 (R_o^{-12})\{(3-4\nu_m)\left(\frac{G_\ell}{G_m}\right)^2 b_3 + 2\left(\frac{G_\ell}{G_m}\right)[b_4 - 2\nu_m b_5] + b_6\} \quad \text{(A5.13a)}$$

where,

$$b_3 = \left[\left(\frac{R_o}{R_i}\right)^2 - 1\right]^4 \quad \text{(A5.13b)}$$

$$b_4 = \left[(5-6\nu_\ell)\left(\frac{R_o}{R_i}\right)^6 + (5-2\nu_\ell)\left(\frac{R_o}{R_i}\right)^4 - (1-2\nu_\ell)\left(\frac{R_o}{R_i}\right)^2 + \right.$$

$$\left. + (3-2\nu_\ell)\right]\left[\left(\frac{R_o}{R_i}\right)^2 - 1\right] \quad \text{(A5.13c)}$$

$$b_5 = \left[(3 - 4\nu_\ell)\left(\frac{R_o}{R_i}\right)^6 + 3\left(\frac{R_o}{R_i}\right)^4 - 3\left(\frac{R_o}{R_i}\right)^2 + 1\right]\left[\left(\frac{R_o}{R_i}\right)^2 - 1\right] \quad \text{(A5.13d)}$$

$$b_6 = \left[(3 - 4\nu_\ell)\left(\frac{R_o}{R_i}\right)^8 + 4(3 - 6\nu_\ell + 4\nu_\ell^2)\left(\frac{R_o}{R_i}\right)^6 - 6\left(\frac{R_o}{R_i}\right)^4 + \right.$$

$$\left. + 4\left(\frac{R_o}{R_i}\right)^2 + (3 - 4\nu_\ell)\right] \quad \text{(A5.13e)}$$

$$D_1 = -3P_o(1 - K)(1 - \nu_m)\left(\frac{G_m}{G_\ell}\right)(R_o^{-8})\left\{\left(\frac{G_\ell}{G_m}\right)b_7 + b_8\right\} \quad \text{(A5.14a)}$$

where,

$$b_7 = \left[\left(\frac{R_o}{R_i}\right)^4 - 1\right] \quad \text{(A5.14b)}$$

$$b_8 = -\left[(3 - 4\nu_\ell)\left(\frac{R_o}{R_i}\right)^4 + 1\right] \quad \text{(A5.14c)}$$

$$D_2 = 6P_o(1 - K)(1 - \nu_m)\left(\frac{G_m}{G_\ell}\right)(R_o^{-10})\left\{\left(\frac{G_\ell}{G_m}\right)b_9 + b_{10}\right\} \quad \text{(A5.15a)}$$

where,

$$b_9 = \left[\left(\frac{R_o}{R_i}\right)^6 - 1\right] \quad \text{(A5.15b)}$$

$$b_{10} = \left[(3 - 4\nu_\ell)\left(\frac{R_o}{R_i}\right)^6 + 1\right] \quad \text{(A5.15c)}$$

$$D_3 = \left(\frac{3}{2}\right)\left(\frac{P_o}{2}\right)(1 - K)\left(\frac{G_m}{G_\ell}\right)^2(R_o^{-8})\left\{\left(\frac{G_\ell}{G_m}\right)^2 b_3 + 2\left(\frac{G_\ell}{G_m}\right)\left[b_{11} - 8\nu_m b_{12}\right] - b_6\right\} \quad \text{(A5.16a)}$$

where,

$$b_{11} = \left[(1 - 2\nu_\ell)\left(\frac{R_o}{R_i}\right)^8 + 4(2 - \nu_\ell)\left(\frac{R_o}{R_i}\right)^6 - 2(7 - 4\nu_\ell)\left(\frac{R_o}{R_i}\right)^4 + \right.$$

$$\left. + 4\left(\frac{R_o}{R_i}\right)^2 + (1 - 2\nu_\ell)\right] \quad \text{(A5.16b)}$$

$$b_{12} = (1 - \nu_\ell)\left[\left(\frac{R_o}{R_i}\right)^6 - \left(\frac{R_o}{R_i}\right)^4\right] \tag{A5.16c}$$

$$D_4 = -3\left(\frac{P_o}{2}\right)(1 - K)\left(\frac{G_m}{G_\ell}\right)^2 (R_o^{-10})\left\{\left(\frac{G_\ell}{G_m}\right)^2 b_3 + 2\left(\frac{G_\ell}{G_m}\right) b_{13} - b_6\right\} \tag{A5.17a}$$

where,

$$b_{13} = \left[(1 - 2\nu_\ell)\left(\frac{R_o}{R_i}\right)^8 + 4\nu_\ell\left(\frac{R_o}{R_i}\right)^6 - 6\left(\frac{R_o}{R_i}\right)^4 + 4\left(\frac{R_o}{R_i}\right)^2 + (1 - 2\nu_\ell)\right] \tag{A5.17b}$$

From these expressions for the determinants we can now obtain the expressions for the four constants X, Y, J, and N.

$$X = \frac{D_1}{D} = P_o(1 - K)(1 - \nu_m)\left(\frac{G_\ell}{G_m}\right) R_o^4 X_n \tag{A5.18a}$$

where,

$$X_n = \frac{\left(\frac{G_\ell}{G_m}\right) b_7 + b_8}{(3 - 4\nu_m)\left(\frac{G_\ell}{G_m}\right)^2 b_3 + 2\left(\frac{G_\ell}{G_m}\right)\left[b_4 - 2\nu_m b_5\right] + b_6} \tag{A5.18b}$$

$$Y = \frac{D_2}{D} = -2P_o(1 - K)(1 - \nu_m)\left(\frac{G_\ell}{G_m}\right) R_o^2 Y_n \tag{A5.19a}$$

where,

$$Y_n = \frac{\left(\frac{G_\ell}{G_m}\right) b_9 + b_{10}}{(3 - 4\nu_m)\left(\frac{G_\ell}{G_m}\right)^2 b_3 + 2\left(\frac{G_\ell}{G_m}\right)\left[b_4 - 2\nu_m b_5\right] + b_6} \tag{A5.19b}$$

$$J = \frac{D_3}{D} = -\tfrac{1}{2}\left(\frac{P_o}{2}\right)(1 - K)R_o^4 J_n \tag{A5.20a}$$

where,

$$J_n = \frac{\left(\frac{G_\ell}{G_m}\right)^2 b_3 + 2\left(\frac{G_\ell}{G_m}\right)\left[b_{11} - 8\nu_m b_{12}\right] - b_6}{(3 - 4\nu_m)\left(\frac{G_\ell}{G_m}\right)^2 b_3 + 2\left(\frac{G_\ell}{G_m}\right)\left[b_4 - 2\nu_m b_5\right] + b_6} \tag{A5.20b}$$

$$N = \frac{D_4}{D} = \left(\frac{P_o}{2}\right)(1 - K)R_o^2 N_n \tag{A5.21a}$$

where,

$$N_n = \frac{\left(\frac{G_\ell}{G_m}\right)^2 b_3 + 2\left(\frac{G_\ell}{G_m}\right) b_{13} - b_6}{(3 - 4\nu_m)\left(\frac{G_\ell}{G_m}\right)^2 b_3 + 2\left(\frac{G_\ell}{G_m}\right)\left[b_4 - 2\nu_m b_5\right] + b_6} \tag{A5.21b}$$

Substitution of the expression for X (Eqns. A5.18) and Y (Eqns. A5.19) into Eqns. A5.2 and A5.3 yields the expressions for the constants W and Z.

$$W = P_o(1 - K)(1 - \nu_m)\left(\frac{G_\ell}{G_m}\right) W_n \tag{A5.22a}$$

where,

$$W_n = \frac{\left(\frac{G_\ell}{G_m}\right) b_{14} + b_{15}}{(3 - 4\nu_m)\left(\frac{G_\ell}{G_m}\right)^2 b_3 + 2\left(\frac{G_\ell}{G_m}\right)\left[b_4 - 2\nu_m b_5\right] + b_6} \tag{A5.22b}$$

and,

$$b_{14} = \left[\left(\frac{R_o}{R_i}\right)^8 + 3\left(\frac{R_o}{R_i}\right)^4 - 4\left(\frac{R_o}{R_i}\right)^2\right] \tag{A5.22c}$$

$$b_{15} = \left[(3 - 4\nu_\ell)\left(\frac{R_o}{R_i}\right)^8 - 3\left(\frac{R_o}{R_i}\right)^4 + 4\left(\frac{R_o}{R_i}\right)^2\right] \qquad \text{(A5.22d)}$$

$$Z = -2P_o(1 - K)(1 - \nu_m)\left(\frac{G_\ell}{G_m}\right)\left(\frac{Z_n}{R_i^2}\right) \qquad \text{(A5.23a)}$$

where,

$$Z_n = \frac{\left[\left(\frac{G_\ell}{G_m}\right) - 1\right]b_{16}}{(3 - 4\nu_m)\left(\frac{G_\ell}{G_m}\right)^2 b_3 + 2\left(\frac{G_\ell}{G_m}\right)\left[b_4 - 2\nu_m b_5\right] + b_6} \qquad \text{(A5.23b)}$$

and,

$$b_{16} = \left[\left(\frac{R_o}{R_i}\right)^4 - \left(\frac{R_o}{R_i}\right)^2\right] \qquad \text{(A5.23c)}$$

Now that expressions have been obtained for the nine unknown constants, these expressions can be substituted back into Eqns. A.36 and A.44 to obtain the final equations for liner and ground mass stresses and displacements. These equations are given in Section B.5 of Appendix B.

A.4.6 SOLUTION NO. 6 : OVERPRESSURE LOADING - FULL SLIPPAGE CONDITION

The additional boundary conditions that apply for this problem require that

$$\text{at } r_\ell = R_i, \qquad \sigma_{r\ell} = 0 \qquad \text{(BC1)}$$

$$\tau_{r\theta\ell} = 0 \qquad \text{(BC2)}$$

$$\text{at } r_\ell = R_o = r, \qquad \sigma_{r\ell} = \sigma_{rm} \qquad \text{(BC3)}$$

$$u_\ell = u_m \qquad \text{(BC4)}$$

$$\tau_{r\theta\ell} = 0 \qquad \text{(BC5)}$$

$$\tau_{r\theta m} = 0 \qquad \text{(BC6)}$$

From BC1 and Eqn. A.44a we obtain two equations which yield

$$S = -2QR_i^2 \qquad \text{(A6.1)}$$

$$W = -\frac{3X}{R_i^4} - \frac{2Y}{R_i^2} \qquad \text{(A6.2)}$$

From BC2 and Eqn. A.44c we find that

$$Z = \frac{X}{R_i^6} + \frac{Y}{3R_i^4} - \frac{W}{3R_i^2}$$

Substituting the expression for W (Eqn. A.6.2) into this equation we obtain

$$Z = \frac{2X}{R_i^6} + \frac{Y}{R_i^4} \qquad \text{(A6.3)}$$

From BC3 and Eqns. A.44a and A.36a we find that

$$2Q + \frac{S}{R_o^2} = (\frac{P_o}{2})(1 + K) + \frac{L}{R_o^2}$$

and,

$$2W + \frac{6X}{R_o^4} + \frac{4Y}{R_o^2} = (\frac{P_o}{2})(1 - K) + \frac{6J}{R_o^4} + \frac{4N}{R_o^2}$$

Substituting the expression for S (Eqn. A6.1) into the first of these equations and rearranging terms we find that

$$L = -(\frac{P_o}{2})(1 + K)R_o^2 + 2Q\beta_1 R_i^2 \qquad (A6.4a)$$

where,

$$\beta_1 = [(\frac{R_o}{R_i})^2 - 1] \qquad (A6.4b)$$

Substituting the expression for W (Eqn. A6.2) into the second of the above equations and rearranging terms we obtain

$$(\frac{3\beta_2}{R_o^4})X + (\frac{2\beta_1}{R_o^2})Y + (\frac{3}{R_o^4})J + (\frac{2}{R_o^2})N = -(\frac{P_o}{4})(1 - K) \qquad (A6.5a)$$

where,

$$\beta_2 = [(\frac{R_o}{R_i})^4 - 1] \qquad (A6.5b)$$

From BC4 and Eqns. A.44d and A.36d we obtain the following two equalities (See p. 365)

$$(\frac{R_o}{2G_\ell})[2(1 - 2\nu_\ell)Q - \frac{S}{R_o^2}] = (\frac{R_o}{2G_m})[(\frac{P_o}{2})(1 + K)(1 - 2\nu_m) - \frac{L}{R_o^2}]$$

$$(\frac{R_o}{2G_\ell})[2W - \frac{2X}{R_o^4} - \frac{4Y}{R_o^2}(1 - \nu_\ell) + 4\nu_\ell ZR_o^2] =$$

$$= (\frac{R_o}{2G_m})[(\frac{P_o}{2})(1 - K) - \frac{2J}{R_o^4} - \frac{4N}{R_o^2}(1 - \nu_m)]$$

Substituting the expression for S (Eqn. A6.1) into the first of these equalities and rearranging terms we find

$$Q = \left(\frac{G_\ell}{G_m}\right)\left(\frac{R_o}{R_i}\right)^2\left(\frac{1}{2\beta_3}\right)\left[\left(\frac{P_o}{2}\right)(1 + K)(1 - 2\nu_m) - \frac{L}{R_o^2}\right] \qquad \text{(A6.6a)}$$

where,

$$\beta_3 = \left[(1 - 2\nu_\ell)\left(\frac{R_o}{R_i}\right)^2 + 1\right] \qquad \text{(A6.6b)}$$

Substituting the expression for W (Eqn. A6.2) and Z (Eqn. A6.3) into the second of the above equalities and rearranging terms we obtain

$$\left(\frac{G_m}{G_\ell}\right)\left(\frac{\beta_4}{R_o^4}\right)X + \left(\frac{G_m}{G_\ell}\right)\left(\frac{2\beta_5}{R_o^2}\right)Y + \left(\frac{1}{R_o^4}\right)J + \left[\frac{2(1 - \nu_m)}{R_o^2}\right]N = \left(\frac{P_o}{4}\right)(1 - K) \qquad \text{(A6.7a)}$$

where,

$$\beta_4 = \left[4\nu_\ell\left(\frac{R_o}{R_i}\right)^6 - 3\left(\frac{R_o}{R_i}\right)^4 - 1\right] \qquad \text{(A6.7b)}$$

$$\beta_5 = \left[\nu_\ell\left(\frac{R_o}{R_i}\right)^4 - \left(\frac{R_o}{R_i}\right)^2 - (1 - \nu_\ell)\right] \qquad \text{(A6.7c)}$$

From BC5 and Eqn. A.44c we have

$$W - \frac{3X}{R_o^4} - \frac{Y}{R_o^2} + 3ZR_o^2 = 0$$

Substituting the expressions for W (Eqn. A6.2) and Z (Eqn. A6.3) into this equation and collecting terms we obtain

$$\left(\frac{3\beta_6}{R_o^4}\right)X + \left(\frac{\beta_7}{R_o^2}\right)Y = 0 \qquad \text{(A6.8a)}$$

where,

$$\beta_6 = \left[2\left(\frac{R_o}{R_i}\right)^6 - \left(\frac{R_o}{R_i}\right)^4 - 1\right] \tag{A6.8b}$$

$$\beta_7 = \left[3\left(\frac{R_o}{R_i}\right)^4 - 2\left(\frac{R_o}{R_i}\right)^2 - 1\right] \tag{A6.8c}$$

From BC6 and Eqn. A.36c we have

$$\left(\frac{3}{R_o^4}\right)J + \left(\frac{1}{R_o^2}\right)N = \left(\frac{P_o}{4}\right)(1 - k) \tag{A6.9}$$

Substitution of Eqn. A6.4a into Eqn. A6.6a yields the expression for the constant Q.

$$Q = \left(\frac{P_o}{2}\right)(1 + K)\left(\frac{R_o}{R_i}\right)^2(1 - \nu_m)\left(\frac{G_\ell}{G_m}\right)Q_f \tag{A6.10a}$$

where,

$$Q_f = \frac{1}{\left(\frac{G_\ell}{G_m}\right)d_1 + d_2} \tag{A6.10b}$$

and,

$$d_1 = \beta_1 = \left[\left(\frac{R_o}{R_i}\right)^2 - 1\right] \tag{A6.10c}$$

$$d_2 = \beta_3 = \left[(1 - 2\nu_\ell)\left(\frac{R_o}{R_i}\right)^2 + 1\right] \tag{A6.10d}$$

Substitution of Eqns. A6.10a and b into Eqn. A6.4a yields the expression for the constant L.

$$L = \left(\frac{P_o}{2}\right)(1 + K)R_o^2 L_f \tag{A6.11a}$$

where,

$$L_f = \frac{(1 - 2\nu_m)(\frac{G_\ell}{G_m})d_1 - d_2}{(\frac{G_\ell}{G_m})d_1 + d_2} \qquad \text{(A6.11b)}$$

Substitution of Eqns. A6.10a and b into Eqn. A6.1 yields the expression for the constant S.

$$S = -P_o(1 + K)(1 - \nu_m)(\frac{G_\ell}{G_m})R_o^2 S_f \qquad \text{(A6.12a)}$$

where,

$$S_f = Q_f = \frac{1}{(\frac{G_\ell}{G_m})d_1 + d_2} \qquad \text{(A6.12b)}$$

Equations A6.5a, 7a, 8a, and 9 can be solved for X, Y, J, and N by using Cramer's Rule (See Section A.4.4). Where,

$$a_{11} = \frac{3\beta_2}{R_o^4} \quad ; \quad a_{12} = \frac{2\beta_1}{R_o^2} \quad ; \quad a_{13} = \frac{3}{R_o^4} \quad ; \quad a_{14} = \frac{2}{R_o^2}$$

$$a_{21} = (\frac{G_m}{G_\ell})(\frac{\beta_4}{R_o^4}) \quad ; \quad a_{22} = (\frac{G_m}{G_\ell})(\frac{2\beta_5}{R_o^2}) \quad ; \quad a_{23} = \frac{1}{R_o^4} \quad ; \quad a_{24} = \frac{2(1 - \nu_m)}{R_o^2}$$

$$a_{31} = \frac{3\beta_6}{R_o^4} \quad ; \quad a_{32} = \frac{\beta_7}{R_o^2} \quad ; \quad a_{33} = 0 \quad ; \quad a_{34} = 0$$

$$a_{41} = 0 \quad ; \quad a_{42} = 0 \quad ; \quad a_{43} = \frac{3}{R_o^4} \quad ; \quad a_{44} = \frac{1}{R_o^2}$$

and,

$$-b_1 = b_2 = b_4 = \left(\frac{P_o}{4}\right)(1 - K) \; ; \quad b_3 = 0$$

Solving for each of the required determinants we obtain the following results.

$$D = -3d_1\left(\frac{G_m}{G_\ell}\right)(R_o^{-12})\{(5 - 6\nu_m)\left(\frac{G_\ell}{G_m}\right)d_3 + d_4\} \tag{A6.13a}$$

where,

$$d_3 = \left[\left(\frac{R_o}{R_i}\right)^2 - 1\right]^3 \tag{A6.13b}$$

$$d_4 = \left[(3 - 2\nu_\ell)\left(\frac{R_o}{R_i}\right)^6 + 3(5 - 6\nu_\ell)\left(\frac{R_o}{R_i}\right)^4 + 3(3 - 2\nu_\ell)\left(\frac{R_o}{R_i}\right)^2 + (5 - 6\nu_\ell)\right] \tag{A6.13c}$$

$$D_1 = -3d_1P_o(1 - K)(1 - \nu_m)(R_o^{-8})\{d_5\} \tag{A6.14a}$$

where,

$$d_5 = \left[3\left(\frac{R_o}{R_i}\right)^2 + 1\right] \tag{A6.14b}$$

$$D_2 = 9d_1P_o(1 - K)(1 - \nu_m)(R_o^{-10})\{d_6\} \tag{A6.15a}$$

where,

$$d_6 = \left[2\left(\frac{R_o}{R_i}\right)^4 + \left(\frac{R_o}{R_i}\right)^2 + 1\right] \tag{A6.15b}$$

$$D_3 = -(\frac{3}{2})d_1(\frac{P_o}{2})(1 - K)(\frac{G_m}{G_\ell})(R_o^{-8})\{(1 - 2\nu_m)(\frac{G_\ell}{G_m})d_3 + d_4\} \quad (A6.16)$$

and,

$$D_4 = -3d_1(\frac{P_o}{2})(1 - K)(\frac{G_m}{G_\ell})(R_o^{-10})\{(\frac{G_\ell}{G_m})d_3 - d_4\} \quad (A6.17)$$

From these expressions for the determinants we can now obtain the expressions for the four constants X, Y, J, and N.

$$X = \frac{D_1}{D} = P_o(1 - K)(1 - \nu_m)(\frac{G_\ell}{G_m})R_o^4 X_f \quad (A6.18a)$$

where,

$$X_f = \frac{d_5}{(5 - 6\nu_m)(\frac{G_\ell}{G_m})d_3 + d_4} \quad (A6.18b)$$

$$Y = \frac{D_2}{D} = -3P_o(1 - K)(1 - \nu_m)(\frac{G_\ell}{G_m})R_o^2 Y_f \quad (A6.19a)$$

where,

$$Y_f = \frac{d_6}{(5 - 6\nu_m)(\frac{G_\ell}{G_m})d_3 + d_4} \quad (A6.19b)$$

$$J = \frac{D_3}{D} = \tfrac{1}{2}(\frac{P_o}{2})(1 - K)R_o^4 J_f \quad (A6.20a)$$

where,

$$J_f = \frac{(1 - 2\nu_m)(\frac{G_\ell}{G_m})d_3 + d_4}{(5 - 6\nu_m)(\frac{G_\ell}{G_m})d_3 + d_4} \quad (A6.20b)$$

$$N = \frac{D_4}{D} = \left(\frac{P_o}{2}\right)(1 - K)R_o^2 N_f \tag{A6.21a}$$

where,

$$N_f = \frac{\left(\frac{G}{G_m}\right)d_3 - d_4}{(5 - 6\nu_m)\left(\frac{G}{G_m}\right)d_3 + d_4} \tag{A6.21b}$$

Substitution of the expressions for X (Eqns. A6.18) and Y (Eqns. A6.19) into Eqns. A6.2 and A6.3 yields the expressions for the constants W and Z.

$$W = 3P_o(1 - K)(1 - \nu_m)\left(\frac{G}{G_m}\right)W_f \tag{A6.22a}$$

where,

$$W_f = \frac{d_7}{(5 - 6\nu_m)\left(\frac{G}{G_m}\right)d_3 + d_4} \tag{A6.22b}$$

and,

$$d_7 = \left[\left(\frac{R_o}{R_i}\right)^6 + \left(\frac{R_o}{R_i}\right)^4 + 2\left(\frac{R_o}{R_i}\right)^2\right] \tag{A6.22c}$$

$$Z = -P_o(1 - K)(1 - \nu_m)\left(\frac{G}{G_m}\right)\left(\frac{Z_f}{R_i^2}\right) \tag{A6.23a}$$

where,

$$Z_f = \frac{d_8}{(5 - 6\nu_m)\left(\frac{G}{G_m}\right)d_3 + d_4} \tag{A6.23b}$$

and,

$$d_8 = \left[\left(\frac{R_o}{R_i}\right)^4 + 3\left(\frac{R_o}{R_i}\right)^2\right] \tag{A6.23c}$$

Now that expressions have been obtained for the nine unknown constants, these expressions can be substituted back into Eqns. A.36 and A.44 to obtain the final equations for liner and ground mass stresses and displacements. These equations are given in Section B.6 of Appendix B.

A.4.7 SOLUTION NO. 7 : EXCAVATION LOADING - NO SLIPPAGE CONDITION

The additional boundary conditions that apply for this problem require that

$$\text{at } r_\ell = R_i, \qquad \sigma_{r\ell} = 0 \qquad \text{(BC1)}$$

$$\tau_{r\theta\ell} = 0 \qquad \text{(BC2)}$$

$$\text{at } r_\ell = R_o = r, \qquad \sigma_{r\ell} = \sigma_{rm} \qquad \text{(BC3)}$$

$$\tau_{r\theta\ell} = \tau_{r\theta m} \qquad \text{(BC4)}$$

$$u_\ell = u_m \qquad \text{(BC5)}$$

$$v_\ell = v_m \qquad \text{(BC6)}$$

From BC1 and Eqn. A.44a we obtain two equations which yield

$$S = -2QR_i^2 \qquad \text{(A7.1)}$$

$$W = -\frac{3X}{R_i^4} - \frac{2Y}{R_i^2} \qquad \text{(A7.2)}$$

From BC2 and Eqn. A.44c we find

$$Z = \frac{X}{R_i^6} + \frac{Y}{3R_i^4} - \frac{W}{3R_i^2}$$

Substituting the expression for W (Eqn. A7.2) into this equation we obtain

$$Z = \frac{2X}{R_i^6} + \frac{Y}{R_i^4} \tag{A7.3}$$

From BC3 and Eqns. A.44a and A.38a we find that

$$2Q + \frac{S}{R_o^2} = (\frac{\gamma H}{2})(1 + K_o) + \frac{L}{R_o^2}$$

and,

$$2W + \frac{6X}{R_o^4} + \frac{4Y}{R_o^2} = (\frac{\gamma H}{2})(1 - K_o) + \frac{6J}{R_o^4} + \frac{4N}{R_o^2}$$

Substituting the expression for S (Eqn. A7.1) into the first of these equalities and rearranging terms we find that

$$L = -(\frac{\gamma H}{2})(1 + K_o)R_o^2 + 2Q\delta_1 R_i^2 \tag{A7.4a}$$

where,

$$\delta_1 = [(\frac{R_o}{R_i})^2 - 1] \tag{A7.4b}$$

Substituting the expression for W (Eqn. A7.2) into the second of the above equalities and rearranging terms we obtain

$$(\frac{3\delta_2}{R_o^4})X + (\frac{2\delta_1}{R_o^2})Y + (\frac{3}{R_o^4})J + (\frac{2}{R_o^2})N = -(\frac{\gamma H}{4})(1 - K_o) \tag{A7.5a}$$

where,

$$\delta_2 = \left[\left(\frac{R_o}{R_i}\right)^4 - 1\right] \qquad \text{(A7.5b)}$$

From BC4 and Eqns. A.44c and A.38c we obtain the following equation:

$$2W - \frac{6X}{R_o^4} - \frac{2Y}{R_o^2} + 6ZR_o^2 = \left(\frac{\gamma H}{2}\right)(1 - K_o) - \frac{6J}{R_o^4} - \frac{2N}{R_o^2}$$

Substituting the expressions for W (Eqn. A7.2) and Z (Eqn. A7.3) into this equation and rearranging terms we obtain

$$\left(\frac{3\delta_3}{R_o^4}\right)X + \left(\frac{\delta_4}{R_o^2}\right)Y + \left(\frac{3}{R_o^4}\right)J + \left(\frac{1}{R_o^2}\right)N = \left(\frac{\gamma H}{4}\right)(1 - K_o) \qquad \text{(A7.6a)}$$

where,

$$\delta_3 = \left[2\left(\frac{R_o}{R_i}\right)^6 - \left(\frac{R_o}{R_i}\right)^4 - 1\right] \qquad \text{(A7.6b)}$$

$$\delta_4 = \left[3\left(\frac{R_o}{R_i}\right)^4 - 2\left(\frac{R_o}{R_i}\right)^2 - 1\right] \qquad \text{(A7.6c)}$$

From BC5 and Eqns. A.44d and A.38d we obtain the following two equations (See p. 365).

$$\left(\frac{R_o}{2G_\ell}\right)\left[2(1 - 2\nu_\ell)Q - \frac{S}{R_o^2}\right] = \left(\frac{R_o}{2G_m}\right)\left[-\frac{L}{R_o^2}\right]$$

and,

$$-\left(\frac{R_o}{2G_\ell}\right)\left[2W - \frac{2X}{R_o^4} - (1 - \nu_\ell)\frac{4Y}{R_o^2} + 4\ ZR_o^2\right] = \left(\frac{R_o}{2G_m}\right)\left[\frac{2J}{R_o^4} + (1 - \nu_m)\frac{4N}{R_o^2}\right]$$

Substituting the expression for S (Eqn. A7.1) into the first of these equalities and rearranging terms we find

$$Q = -\left(\frac{G_\ell}{G_m}\right)\left(\frac{R_o}{R_i}\right)^2\left(\frac{1}{2\delta_5}\right)\left[\frac{L}{R_o^2}\right] \tag{A7.7a}$$

where,

$$\delta_5 = \left[(1 - 2\nu_\ell)\left(\frac{R_o}{R_i}\right)^2 + 1\right] \tag{A7.7b}$$

Substituting the expressions for W (Eqn. A7.2) and Z (Eqn. A7.3) into the second of the above equalities and rearranging terms we obtain

$$\left(\frac{G_m}{G_\ell}\right)\left(\frac{\delta_6}{R_o^4}\right)X + \left(\frac{G_m}{G_\ell}\right)\left(\frac{2\delta_7}{R_o^2}\right)Y + \left(\frac{1}{R_o^4}\right)J + \left[\frac{2(1 - \nu_m)}{R_o^2}\right]N = 0 \tag{A7.8a}$$

where,

$$\delta_6 = \left[4\nu_\ell\left(\frac{R_o}{R_i}\right)^6 - 3\left(\frac{R_o}{R_i}\right)^4 - 1\right] \tag{A7.8b}$$

$$\delta_7 = \left[\nu_\ell\left(\frac{R_o}{R_i}\right)^4 - \left(\frac{R_o}{R_i}\right)^2 - (1 - \nu_\ell)\right] \tag{A7.8c}$$

From BC6 and Eqns. A.44e and A.38e we have

$$\left(\frac{R_o}{2G_\ell}\right)\left[2W + \frac{2X}{R_o^4} - (1 - 2\nu_\ell)\frac{2Y}{R_o^2} + 2(3 - 2\nu_\ell)ZR_o^2\right] =$$

$$= \left(\frac{R_o}{2G_m}\right)\left[\frac{2J}{R_o^4} - (1 - 2\nu_m)\frac{2N}{R_o^2}\right]$$

Substituting the expressions for W (Eqn. A7.2) and Z (Eqn. A7.3) into this equation we obtain

$$\left(\frac{G_m}{G_\ell}\right)\left(\frac{\delta_8}{R_o^4}\right)X + \left(\frac{G_m}{G_\ell}\right)\left(\frac{\delta_9}{R_o^2}\right)Y - \left(\frac{1}{R_o^4}\right)J + \left[\frac{(1 - 2\nu_m)}{R_o^2}\right]N = 0 \qquad \text{(A7.9a)}$$

where,

$$\delta_8 = \left[2(3 - 2\nu_\ell)\left(\frac{R_o}{R_i}\right)^6 - 3\left(\frac{R_o}{R_i}\right)^4 + 1\right] \qquad \text{(A7.9b)}$$

$$\delta_9 = \left[(3 - 2\nu_\ell)\left(\frac{R_o}{R_i}\right)^4 - 2\left(\frac{R_o}{R_i}\right)^2 - (1 - 2\nu_\ell)\right] \qquad \text{(A7.9c)}$$

Substituting Eqn. A7.4a into Eqn. A7.7a we find the expression for the constant Q.

$$Q = \tfrac{1}{2}\left(\frac{\gamma H}{2}\right)(1 + K_o)\left(\frac{G_\ell}{G_m}\right)\left(\frac{R_o}{R_i}\right)^2 Q_n^* \qquad \text{(A7.10a)}$$

where,

$$Q_n^* = \frac{1}{\left(\frac{G_\ell}{G_m}\right)b_1^* + b_2^*} \qquad \text{(A7.10b)}$$

and,

$$b_1^* = \delta_1 = \left[\left(\frac{R_o}{R_i}\right)^2 - 1\right] \qquad \text{(A7.10c)}$$

$$b_2^* = \delta_5 = \left[(1 - 2\nu_\ell)\left(\frac{R_o}{R_i}\right)^2 + 1\right] \qquad \text{(A7.10d)}$$

Substituting Eqns. A7.10a and b into Eqn. A7.4a we obtain the expression for the constant L.

$$L = -\left(\frac{\gamma H}{2}\right)(1 + K_o)R_o^2 L_n^* \qquad \text{(A7.11a)}$$

where,

$$L_n^* = \frac{b_2^*}{(\frac{G_\ell}{G_m})b_1^* + b_2^*} \qquad \text{(A7.11b)}$$

Substituting Eqns. A7.10a and b into Eqn. A7.1 we obtain the expression for the constant S.

$$S = -(\frac{\gamma H}{2})(1 + K_o)(\frac{G_\ell}{G_m})R_o^2 S_n^* \qquad \text{(A7.12a)}$$

where,

$$S_n^* = Q_n^* = \frac{1}{(\frac{G_\ell}{G_m})b_1^* + b_2^*} \qquad \text{(A7.12b)}$$

Equations A7.5a, 6a, 8a, and 9a can be solved for the constants X, Y, J, and N by using Cramer's Rule (See Section A.4.4). Where,

$$a_{11} = \frac{3\delta_2}{R_o^4} \quad ; \quad a_{12} = \frac{2\delta_1}{R_o^2} \quad ; \quad a_{13} = \frac{3}{R_o^4} \quad ; \quad a_{14} = \frac{2}{R_o^2}$$

$$a_{21} = \frac{3\delta_3}{R_o^4} \quad ; \quad a_{22} = \frac{\delta_4}{R_o^2} \quad ; \quad a_{23} = \frac{3}{R_o^4} \quad ; \quad a_{24} = \frac{1}{R_o^2}$$

$$a_{31} = (\frac{G_m}{G_\ell})(\frac{\delta_6}{R_o^4}) \quad ; \quad a_{32} = (\frac{G_m}{G_\ell})(\frac{2\delta_7}{R_o^2}) \quad ; \quad a_{33} = \frac{1}{R_o^4} \quad ; \quad a_{34} = \frac{2(1 - \nu_m)}{R_o^2}$$

$$a_{41} = (\frac{G_m}{G_\ell})(\frac{\delta_8}{R_o^4}) \quad ; \quad a_{42} = (\frac{G_m}{G_\ell})(\frac{\delta_9}{R_o^2}) \quad ; \quad a_{43} = -\frac{1}{R_o^4} \quad ; \quad a_{44} = \frac{(1 - 2\nu_m)}{R_o^2}$$

and,

$$-b_1 = b_2 = \left(\frac{\gamma H}{4}\right)(1 - K_o) \quad ; \quad b_3 = b_4 = 0$$

Solving for each of the required determinants we obtain the following results.

$$D = -3\left(\frac{G_m}{G_\ell}\right)^2 (R_o^{-12}) \{(3 - 4\nu_m)\left(\frac{G_\ell}{G_m}\right)^2 b_3^* + 2\left(\frac{G_\ell}{G_m}\right)[b_4^* - 2\nu_m b_5^*] + b_6^*\} \quad \text{(A7.13a)}$$

where,

$$b_3^* = \left[\left(\frac{R_o}{R_i}\right)^2 - 1\right]^4 \quad \text{(A7.13b)}$$

$$b_4^* = \left[(5 - 6\nu_\ell)\left(\frac{R_o}{R_i}\right)^6 + (5 - 2\nu_\ell)\left(\frac{R_o}{R_i}\right)^4 - (1 - 2\nu_\ell)\left(\frac{R_o}{R_i}\right)^2 + (3 - 2\nu_\ell)\right]\left[\left(\frac{R_o}{R_i}\right)^2 - 1\right] \quad \text{(A7.13c)}$$

$$b_5^* = \left[(3 - 4\nu_\ell)\left(\frac{R_o}{R_i}\right)^6 + 3\left(\frac{R_o}{R_i}\right)^4 - 3\left(\frac{R_o}{R_i}\right)^2 + 1\right]\left[\left(\frac{R_o}{R_i}\right)^2 - 1\right] \quad \text{(A7.13d)}$$

$$b_6^* = \left[(3 - 4\nu_\ell)\left(\frac{R_o}{R_i}\right)^8 + 4(3 - 6\nu_\ell + 4\nu_\ell^2)\left(\frac{R_o}{R_i}\right)^6 - 6\left(\frac{R_o}{R_i}\right)^4 + 4\left(\frac{R_o}{R_i}\right)^2 + (3 - 4\nu_\ell)\right] \quad \text{(A7.13e)}$$

$$D_1 = -\left(\frac{3}{2}\right)\left(\frac{\gamma H}{2}\right)(1 - K_o)(3 - 4\nu_m)\left(\frac{G_m}{G_\ell}\right)(R_o^{-8})\{\left(\frac{G_\ell}{G_m}\right) b_7^* + b_8^*\} \quad \text{(A7.14a)}$$

where,

$$b_7^* = \left[\left(\frac{R_o}{R_i}\right)^4 - 1\right] \quad \text{(A7.14b)}$$

$$b_8^* = \left[(3 - 4\nu_\ell)\left(\frac{R_o}{R_i}\right)^4 + 1\right] \quad \text{(A7.14c)}$$

$$D_2 = 3\left(\frac{\gamma H}{2}\right)(1 - K_o)(3 - 4\nu_m)\left(\frac{G_m}{G_\ell}\right)(R_o^{-10})\left\{\left(\frac{G_\ell}{G_m}\right)b_9^* + b_{10}^*\right\} \quad \text{(A7.15a)}$$

where,

$$b_9^* = \left[\left(\frac{R_o}{R_i}\right)^6 - 1\right] \quad \text{(A7.15b)}$$

$$b_{10}^* = \left[(3 - 4\nu_\ell)\left(\frac{R_o}{R_i}\right)^6 + 1\right] \quad \text{(A7.15c)}$$

$$D_3 = -\left(\frac{3}{2}\right)\left(\frac{\gamma H}{2}\right)(1 - K_o)\left(\frac{G_m}{G_\ell}\right)^2(R_o^{-8})\left\{\left(\frac{G_\ell}{G_m}\right)\left[b_{11}^* + 16\nu_m b_{12}^*\right] + b_6^*\right\} \quad \text{(A7.16a)}$$

where,

$$b_{11}^* = \left[\left(\frac{R_o}{R_i}\right)^6 - (11 - 8\nu_\ell)\left(\frac{R_o}{R_i}\right)^4 + (7 - 4\nu_\ell)\left(\frac{R_o}{R_i}\right)^2 + \right.$$
$$\left. + (3 - 4\nu_\ell)\right]\left[\left(\frac{R_o}{R_i}\right)^2 - 1\right] \quad \text{(A7.16b)}$$

$$b_{12}^* = (1 - \nu_\ell)\left[\left(\frac{R_o}{R_i}\right)^6 - \left(\frac{R_o}{R_i}\right)^4\right] \quad \text{(A7.16c)}$$

$$D_4 = 3\left(\frac{\gamma H}{2}\right)(1 - K_o)\left(\frac{G_m}{G_\ell}\right)^2(R_o^{-10})\left\{\left(\frac{G_\ell}{G_m}\right)b_{13}^* + b_6^*\right\} \quad \text{(A7.17a)}$$

where,

$$b_{13}^* = \left[\left(\frac{R_o}{R_i}\right)^6 + (1 - 4\nu_\ell)\left(\frac{R_o}{R_i}\right)^4 + (7 - 4\nu_\ell)\left(\frac{R_o}{R_i}\right)^2 + \right.$$
$$\left. + (3 - 4\nu_\ell)\right]\left[\left(\frac{R_o}{R_i}\right)^2 - 1\right] \quad \text{(A7.17b)}$$

From these expressions for the determinants we can now obtain the expressions for the four constants X, Y, J, and N.

$$X = \frac{D_1}{D} = \tfrac{1}{2}\left(\frac{\gamma H}{2}\right)(1 - K_o)(3 - 4\nu_m)\left(\frac{G_\ell}{G_m}\right)R_o^4 X_n^* \tag{A7.18a}$$

where,

$$X_n^* = \frac{\left(\frac{G_\ell}{G_m}\right)b_7^* + b_8^*}{(3 - 4\nu_m)\left(\frac{G_\ell}{G_m}\right)^2 b_3^* + 2\left(\frac{G_\ell}{G_m}\right)\left[b_4^* - 2\nu_m b_5^*\right] + b_6^*} \tag{A7.18b}$$

$$Y = \frac{D_2}{D} = -\left(\frac{\gamma H}{2}\right)(1 - K_o)(3 - 4\nu_m)\left(\frac{G_\ell}{G_m}\right)R_o^2 Y_n^* \tag{A7.19a}$$

where,

$$Y_n^* = \frac{\left(\frac{G_\ell}{G_m}\right)b_9^* + b_{10}^*}{(3 - 4\nu_m)\left(\frac{G_\ell}{G_m}\right)^2 b_3^* + 2\left(\frac{G_\ell}{G_m}\right)\left[b_4^* - 2\nu_m b_5^*\right] + b_6^*} \tag{A7.19b}$$

$$J = \frac{D_3}{D} = \tfrac{1}{2}\left(\frac{\gamma H}{2}\right)(1 - K_o)R_o^4 J_n^* \tag{A7.20a}$$

where,

$$J_n^* = \frac{\left(\frac{G_\ell}{G_m}\right)\left[b_{11}^* + 16\ {}_m b_{12}^*\right] + b_6^*}{(3 - 4\nu_m)\left(\frac{G_\ell}{G_m}\right)^2 b_3^* + 2\left(\frac{G_\ell}{G_m}\right)\left[b_4^* - 2\nu_m b_5^*\right] + b_6^*} \tag{A7.20b}$$

$$N = \frac{D_4}{D} = -\left(\frac{\gamma H}{2}\right)(1 - K_o)R_o^2 N_n^* \tag{A7.21a}$$

where,

$$N_n^* = \frac{\left(\frac{G_\ell}{G_m}\right)b_{13}^* + b_6^*}{(3 - 4\nu_m)\left(\frac{G_\ell}{G_m}\right)^2 b_3^* + 2\left(\frac{G_\ell}{G_m}\right)\left[b_4^* - 2\nu_m b_5^*\right] + b_6^*} \tag{A7.21b}$$

Substitution of the expressions for X (Eqns. A7.18) and Y (Eqns. A7.19) into Eqns. A7.2 and A7.3 yields the expressions for the constants W and Z.

$$W = \tfrac{1}{2}\left(\frac{\gamma H}{2}\right)(1 - K_o)(3 - 4\nu_m)\left(\frac{G_\ell}{G_m}\right)W_n^* \tag{A7.22a}$$

where,

$$W_n^* = \frac{\left(\frac{G_\ell}{G_m}\right)b_{14}^* + b_{15}^*}{(3 - 4\nu_m)\left(\frac{G_\ell}{G_m}\right)^2 b_3^* + 2\left(\frac{G_\ell}{G_m}\right)\left[b_4^* - 2\nu_m b_5^*\right] + b_6^*} \tag{A7.22b}$$

and,

$$b_{14}^* = \left[\left(\frac{R_o}{R_i}\right)^8 + 3\left(\frac{R_o}{R_i}\right)^4 - 4\left(\frac{R_o}{R_i}\right)^2\right] \tag{A7.22c}$$

$$b_{15}^* = \left[(3 - 4\nu_\ell)\left(\frac{R_o}{R_i}\right)^8 - 3\left(\frac{R_o}{R_i}\right)^4 + 4\left(\frac{R_o}{R_i}\right)^2\right] \tag{A7.22d}$$

$$Z = -\left(\frac{\gamma H}{2}\right)(1 - K_o)(3 - 4\nu_m)\left(\frac{G_\ell}{G_m}\right)\left(\frac{Z_n^*}{R_i^2}\right) \tag{A7.23a}$$

where,

$$Z_n^* = \frac{\left[\left(\frac{G_\ell}{G_m}\right) - 1\right]b_{16}^*}{(3 - 4\nu_m)\left(\frac{G_\ell}{G_m}\right)^2 b_3^* + 2\left(\frac{G_\ell}{G_m}\right)\left[b_4^* - 2\nu_m b_5^*\right] + b_6^*} \tag{A7.23b}$$

and,

$$b_{16}^* = \left[\left(\frac{R_o}{R_i}\right)^4 - \left(\frac{R_o}{R_i}\right)^2\right] \tag{A7.23c}$$

Now that expressions have been obtained for the nine unknown constants, these expressions can be substituted back into Eqns. A.44 and A.38 to obtain

the final equations for the liner and ground mass stresses and displacements. These equations are given in Section B.7 of Appendix B.

A.4.8 SOLUTION NO. 8 : EXCAVATION LOADING - FULL SLIPPAGE CONDITION

The additional boundary conditions that apply for this problem require that

$$\text{at } r_\ell = R_i, \qquad \sigma_{r\ell} = 0 \qquad \text{(BC1)}$$

$$\tau_{r\theta\ell} = 0 \qquad \text{(BC2)}$$

$$\text{at } r_\ell = R_o = r, \qquad \sigma_{r\ell} = \sigma_{rm} \qquad \text{(BC3)}$$

$$u_\ell = u_m \qquad \text{(BC4)}$$

$$\tau_{r\theta\ell} = 0 \qquad \text{(BC5)}$$

$$\tau_{r\theta m} = 0 \qquad \text{(BC6)}$$

From BC1 and Eqn. A.44a we obtain two equations which yield

$$S = -2QR_i^2 \qquad \text{(A8.1)}$$

$$W = -\frac{3X}{R_i^4} - \frac{2Y}{R_i^2} \qquad \text{(A8.2)}$$

From BC2 and Eqn. A.44c we find that

$$Z = \frac{X}{R_i^6} + \frac{Y}{3R_i^4} - \frac{W}{3R_i^2}$$

Substituting the expression for W (Eqn. A8.2) into this equation we obtain

$$Z = \frac{2X}{R_i^6} + \frac{Y}{R_i^4} \tag{A8.3}$$

From BC3 and Eqns. A.44a and A.38a we find that

$$2Q + \frac{S}{R_o^2} = (\frac{\gamma H}{2})(1 + K_o) + \frac{L}{R_o^2}$$

and,

$$2W + \frac{6X}{R_o^4} + \frac{4Y}{R_o^2} = (\frac{\gamma H}{2})(1 - K_o) + \frac{6J}{R_o^4} + \frac{4N}{R_o^2}$$

Substituting the expression for S (Eqn. A8.1) into the first of these equalities and rearranging terms we find

$$L = -(\frac{\gamma H}{2})(1 + K_o)R_o^2 + 2Q\lambda_1 R_i^2 \tag{A8.4a}$$

where,

$$\lambda_1 = [(\frac{R_o}{R_i})^2 - 1] \tag{A8.4b}$$

Substituting the expression for W (Eqn. A8.2) into the second of the above equalities and rearranging terms we obtain

$$(\frac{3\lambda_2}{R_o^4})X + (\frac{2\lambda_1}{R_o^2})Y + (\frac{3}{R_o^4})J + (\frac{2}{R_o^2})N = -(\frac{\gamma H}{2})(1 - K_o) \tag{A8.5a}$$

where,

$$\lambda_2 = [(\frac{R_o}{R_i})^4 - 1] \tag{A8.5b}$$

From BC4 and Eqns. A.44d and A.38d we obtain the following two

equalities (See p. 365).

$$\left(\frac{R_o}{2G_\ell}\right)\left[2(1-2\nu_\ell)Q - \frac{S}{R_o^2}\right] = \left(\frac{R_o}{2G_m}\right)\left[-\frac{L}{R_o^2}\right]$$

$$-\left(\frac{R_o}{2G_\ell}\right)\left[2W - \frac{2X}{R_o^4} - (1-\nu_\ell)\frac{4Y}{R_o^2} + 4\nu_\ell ZR_o^2\right] =$$

$$= \left(\frac{R_o}{2G_m}\right)\left[\frac{2J}{R_o^4} + (1-\nu_m)\frac{4N}{R_o^2}\right]$$

Substituting the expression for S (Eqn. A8.1) into the first of these equalities and rearranging terms we find

$$Q = -\left(\frac{G_\ell}{G_m}\right)\left(\frac{R_o}{R_i}\right)^2\left(\frac{1}{2\lambda_3}\right)\left[\frac{L}{R_o^2}\right] \tag{A8.6a}$$

where,

$$\lambda_3 = \left[(1-2\nu_\ell)\left(\frac{R_o}{R_i}\right)^2 + 1\right] \tag{A8.6b}$$

Substituting the expressions for W (Eqn. A8.2) and Z (Eqn. A8.3) into the second of the above equalities and rearranging terms we obtain

$$\left(\frac{G_m}{G_\ell}\right)\left(\frac{\lambda_4}{R_o^4}\right)X + \left(\frac{G_m}{G_\ell}\right)\left(\frac{2\lambda_5}{R_o^2}\right)Y + \left(\frac{1}{R_o^4}\right)J + \left[\frac{2(1-\nu_m)}{R_o^2}\right]N = 0 \tag{A8.7a}$$

where,

$$\lambda_4 = \left[4\nu_\ell\left(\frac{R_o}{R_i}\right)^6 - 3\left(\frac{R_o}{R_i}\right)^4 - 1\right] \tag{A8.7b}$$

$$\lambda_5 = \left[\nu_\ell\left(\frac{R_o}{R_i}\right)^4 - \left(\frac{R_o}{R_i}\right)^2 - (1-\nu_\ell)\right] \tag{A8.7c}$$

From BC5 and Eqn. A.44c we have

$$W - \frac{3X}{R_o^4} - \frac{Y}{R_o^2} + 3ZR_o^2 = 0$$

Substituting the expressions for W (Eqn. A8.2) and Z (Eqn. A8.3) into this equation and collecting terms we obtain

$$(\frac{3\lambda_6}{R_o^4})X + (\frac{\lambda_7}{R_o^2})Y = 0 \qquad \text{(A8.8a)}$$

where,

$$\lambda_6 = [2(\frac{R_o}{R_i})^6 - (\frac{R_o}{R_i})^4 - 1] \qquad \text{(A8.8b)}$$

$$\lambda_7 = [3(\frac{R_o}{R_i})^4 - 2(\frac{R_o}{R_i})^2 - 1] \qquad \text{(A8.8c)}$$

From BC6 and Eqn. A.38c we have

$$(\frac{3}{R_o^4})J + (\frac{1}{R_o^2})N = (\frac{\gamma H}{4})(1 - K_o) \qquad \text{(A8.9)}$$

Substitution of Eqn. A8.4a into Eqn. A8.6a yields the expression for the constant Q.

$$Q = \tfrac{1}{2}(\frac{\gamma H}{2})(1 + K_o)(\frac{R_o}{R_i})^2(\frac{G_\ell}{G_m})Q_f^* \qquad \text{(A8.10a)}$$

where,

$$Q_f^* = \frac{1}{(\frac{G_\ell}{G_m})d_1^* + d_2^*} \qquad \text{(A8.10b)}$$

and,

$$d_1^* = \lambda_1 = \left[\left(\frac{R_o}{R_i}\right)^2 - 1\right] \tag{A8.10c}$$

$$d_2^* = \lambda_3 = \left[(1 - 2\nu_\ell)\left(\frac{R_o}{R_i}\right)^2 + 1\right] \tag{A8.10d}$$

Substitution of Eqns. A8.10a and b into Eqn. A8.4a yields the expression for the constant L.

$$L = -\left(\frac{\gamma H}{2}\right)(1 + K_o)R_o^2 L_f^* \tag{A8.11a}$$

where,

$$L_f^* = \frac{d_2^*}{\left(\frac{G_\ell}{G_m}\right)d_1^* + d_2^*} \tag{A8.11b}$$

Substitution of Eqns. A8.10a and b into Eqn. A8.1 yields the expression for the constant S.

$$S = -\left(\frac{\gamma H}{2}\right)(1 + K_o)\left(\frac{G_\ell}{G_m}\right)R_o^2 S_f^* \tag{A8.12a}$$

where,

$$S_f^* = Q_f^* = \frac{1}{\left(\frac{G_\ell}{G_m}\right)d_1^* + d_2^*} \tag{A8.12b}$$

Equations A8.5a, 7a, 8a, and 9 can be solved for the constants X, Y, J, and N by using Cramer's Rule (See Section A.4.4). Where,

$$a_{11} = \frac{3\lambda_2}{R_o^4} \quad ; \quad a_{12} = \frac{2\lambda_1}{R_o^2} \quad ; \quad a_{13} = \frac{3}{R_o^4} \quad ; \quad a_{14} = \frac{2}{R_o^2}$$

$$a_{21} = \left(\frac{G_m}{G_\ell}\right)\left(\frac{\lambda_4}{R_o^4}\right) \quad ; \quad a_{22} = \left(\frac{G_m}{G_\ell}\right)\left(\frac{2\lambda_5}{R_o^2}\right) \quad ; \quad a_{23} = \frac{1}{R_o^4} \quad ; \quad a_{24} = \frac{2(1 - \nu_m)}{R_o^2}$$

$$a_{31} = \frac{3\lambda_6}{R_o^4} \quad ; \quad a_{32} = \frac{\lambda_7}{R_o^2} \quad ; \quad a_{33} = 0 \quad ; \quad a_{34} = 0$$

$$a_{41} = 0 \quad ; \quad a_{42} = 0 \quad ; \quad a_{43} = \frac{3}{R_o^4} \quad ; \quad a_{44} = \frac{1}{R_o^2}$$

and,

$$-b_1 = b_4 = \left(\frac{\gamma H}{4}\right)(1 - K_o) \quad ; \quad b_2 = b_3 = 0$$

Solving for each of the required determinants we obtain the following results.

$$D = -3d_1^*\left(\frac{G_m}{G_\ell}\right)(R_o^{-12})\left\{(5 - 6\nu_m)\left(\frac{G_\ell}{G_m}\right)d_3^* + d_4^*\right\} \tag{A8.13a}$$

where,

$$d_3^* = \left[\left(\frac{R_o}{R_i}\right)^2 - 1\right]^3 \tag{A8.13b}$$

$$d_4^* = \left[(3 - 2\nu_\ell)\left(\frac{R_o}{R_i}\right)^6 + 3(5 - 6\nu_\ell)\left(\frac{R_o}{R_i}\right)^4 + 3(3 - 2\nu_\ell)\left(\frac{R_o}{R_i}\right)^2 + (5 - 6\nu_\ell)\right] \tag{A8.13c}$$

$$D_1 = -\left(\frac{3}{2}\right)d_1^*\left(\frac{\gamma H}{2}\right)(1 - K_o)(3 - 4\nu_m)(R_o^{-8})\{d_5^*\} \tag{A8.14a}$$

where,

$$d_5^* = \left[3\left(\frac{R_o}{R_i}\right)^2 + 1\right] \tag{A8.14b}$$

$$D_2 = \left(\frac{9}{2}\right)d_1^*\left(\frac{\gamma H}{2}\right)(1 - K_o)(3 - 4\nu_m)(R_o^{-10})\{d_6^*\} \tag{A8.15a}$$

where,

$$d_6^* = \left[2\left(\frac{R_o}{R_i}\right)^4 + \left(\frac{R_o}{R_i}\right)^2 + 1\right] \tag{A8.15b}$$

$$D_3 = -\left(\frac{3}{2}\right)d_1^*\left(\frac{\gamma H}{2}\right)(1 - K_o)\left(\frac{G_m}{G_\ell}\right)(R_o^{-8})\{2(1 - \nu_m)\left(\frac{G_\ell}{G_m}\right)d_3^* + d_4^*\} \tag{A8.16}$$

and,

$$D_4 = \left(\frac{3}{2}\right)d_1^*\left(\frac{\gamma H}{2}\right)(1 - K_o)\left(\frac{G_m}{G_\ell}\right)(R_o^{-10})\{\left(\frac{G_\ell}{G_m}\right)d_3^* + 2d_4^*\} \tag{A8.17}$$

From these expressions for the determinants we can now obtain the expressions for the four constants X, Y, J, and N.

$$X = \frac{D_1}{D} = \tfrac{1}{2}\left(\frac{\gamma H}{2}\right)(1 - K_o)(3 - 4\nu_m)\left(\frac{G_\ell}{G_m}\right)R_o^4 X_f^* \tag{A8.18a}$$

where,

$$X_f^* = \frac{d_5^*}{(5 - 6\nu_m)\left(\frac{G_\ell}{G_m}\right)d_3^* + d_4^*} \tag{A8.18b}$$

$$Y = \frac{D_2}{D} = -\left(\frac{3}{2}\right)\left(\frac{\gamma H}{2}\right)(1 - K_o)(3 - 4\nu_m)\left(\frac{G_\ell}{G_m}\right)R_o^2 Y_f^* \tag{A8.19a}$$

where,

$$Y_f^* = \frac{d_6^*}{(5 - 6\nu_m)(\frac{G_\ell}{G_m})d_3^* + d_4^*} \tag{A8.19b}$$

$$J = \frac{D_3}{D} = \tfrac{1}{2}(\frac{\gamma H}{2})(1 - K_o)R_o^4 J_f^* \tag{A8.20a}$$

where,

$$J_f^* = \frac{2(1 - \nu_m)(\frac{G_\ell}{G_m})d_3^* + d_4^*}{(5 - 6\nu_m)(\frac{G_\ell}{G_m})d_3^* + d_4^*} \tag{A8.20b}$$

$$N = \frac{D_4}{D} = -\tfrac{1}{2}(\frac{\gamma H}{2})(1 - K_o)R_o^2 N_f^* \tag{A8.21a}$$

where,

$$N_f^* = \frac{(\frac{G_\ell}{G_m})d_3^* + d_4^*}{(5 - 6\nu_m)(\frac{G_\ell}{G_m})d_3^* + d_4^*} \tag{A8.21b}$$

Substitution of the expressions for X (Eqns. A8.18) and Y (Eqns. A8.19) into Eqns. A8.2 and A8.3 yields the expressions for the constants W and Z.

$$W = (\frac{3}{2})(\frac{\gamma H}{2})(1 - K_o)(3 - 4\nu_m)(\frac{G_\ell}{G_m})W_f^* \tag{A8.22a}$$

where,

$$W_f^* = \frac{d_7^*}{(5 - 6\nu_m)(\frac{G_\ell}{G_m})d_3^* + d_4^*} \tag{A8.22b}$$

and,

$$d_7^* = \left[\left(\frac{R_o}{R_i}\right)^6 + \left(\frac{R_o}{R_i}\right)^4 + 2\left(\frac{R_o}{R_i}\right)^2\right] \tag{A8.22c}$$

$$Z = -\tfrac{1}{2}\left(\frac{\gamma H}{2}\right)(1 - K_o)(3 - 4\nu_m)\left(\frac{G_\ell}{G_m}\right)\left(\frac{Z_f^*}{R_i^2}\right) \tag{A8.23a}$$

where,

$$Z_f^* = \frac{d_8^*}{(5 - 6\nu_m)\left(\frac{G_\ell}{G_m}\right)d_3^* + d_4^*} \tag{A8.23b}$$

and,

$$d_8^* = \left[\left(\frac{R_o}{R_i}\right)^4 + 3\left(\frac{R_o}{R_i}\right)^2\right] \tag{A8.23c}$$

Now that expressions have been obtained for the nine unknown constants, these expressions can be substituted back into Eqns. A.44 and A.38 to obtain the final equations for the liner and ground mass stresses and displacements. These equations are given in Section B.8 of Appendix B.

APPENDIX B

FINAL EQUATIONS OF THE ANALYTICAL SOLUTIONS FOR GROUND-LINER INTERACTION

B.1 SOLUTION NO. 1 : OVERPRESSURE LOADING - NO SLIPPAGE CONDITION - THIN LINER

B.1.1 EXTERNAL PRESSURES ACTING ON LINER

$$P_r = \left(\frac{P_o}{2}\right)\{(1 + K)[1 - L_n] - (1 - K)[1 - 3J_n - 4N_n]\cos 2\theta\}$$

$$\mp_{r\theta} = \left(\frac{P_o}{2}\right)\{(1 - K)[1 + 3J_n + 2N_n]\sin 2\theta\}$$

B.1.2 LINER DISPLACEMENTS

$$u_\ell = \left(\frac{P_o a}{2}\right)\left(\frac{1 + \nu_m}{E_m}\right)\{(1 + K)[(1 - 2\nu_m)C][1 - L_n] - (1 - K)(F)[1 - J_n - 2N_n]\cos 2\theta\}$$

$$v_\ell = \left(\frac{P_o a}{2}\right)\left(\frac{1 + \nu_m}{E_m}\right)\{(1 - K)[1 - J_n + 2(1 - 2\nu_m)N_n]\sin 2\theta\}$$

B.1.3 LINER THRUST, SHEAR, AND MOMENTS

$$T = \left(\frac{P_o a}{2}\right)\{(1 + K)[1 - L_n] + (1 - K)[1 + J_n]\cos 2\theta\}$$

$$V = -\left(\frac{P_o a}{2}\right)\{(1 - K)[1 - J_n - 2N_n]\sin 2\theta\}$$

$$M = \left(\frac{P_o a^2}{2}\right)\left\{(1 + K)\left[\frac{(1 - 2\nu_m)C}{6F}\right]\left[1 - L_n\right] + \right.$$

$$\left. + \tfrac{1}{2}(1 - K)\left[1 - J_n - 2N_n\right]\cos 2\theta \right\}$$

B.1.4 GROUND MASS STRESSES AND DISPLACEMENTS

$$\sigma_{rm} = \left(\frac{P_o}{2}\right)\left\{(1 + K)\left[1 - L_n\left(\frac{a}{r}\right)^2\right] - \right.$$

$$\left. - (1 - K)\left[1 - 3J_n\left(\frac{a}{r}\right)^4 - 4N_n\left(\frac{a}{r}\right)^2\right]\cos 2\theta\right\}$$

$$\sigma_{\theta m} = \left(\frac{P_o}{2}\right)\left\{(1 + K)\left[1 + L_n\left(\frac{a}{r}\right)^2\right] + (1 - K)\left[1 - 3J_n\left(\frac{a}{r}\right)^4\right]\cos 2\theta\right\}$$

$$\tau_{r\theta m} = \left(\frac{P_o}{2}\right)\left\{(1 - K)\left[1 + 3J_n\left(\frac{a}{r}\right)^4 + 2N_n\left(\frac{a}{r}\right)^2\right]\sin 2\theta\right\}$$

$$u_m = \left(\frac{P_o r}{2}\right)\left(\frac{1 + \nu_m}{E_m}\right)\left\{(1 + K)\left[(1 - 2\nu_m) + L_n\left(\frac{a}{r}\right)^2\right] - \right.$$

$$\left. - (1 - K)\left[1 + J_n\left(\frac{a}{r}\right)^4 + 4(1 - \nu_m)N_n\left(\frac{a}{r}\right)^2\right]\cos 2\theta\right\}$$

$$v_m = \left(\frac{P_o r}{2}\right)\left(\frac{1 + \nu_m}{E_m}\right)\left\{(1 - K)\left[1 - J_n\left(\frac{a}{r}\right)^4 + 2(1 - 2\nu_m)N_n\left(\frac{a}{r}\right)^2\right]\sin 2\theta\right\}$$

B.1.5 CONSTANTS

$$L_n = \frac{(1 - 2\nu_m)(C - 1)}{1 + (1 - 2\nu_m)C}$$

$$J_n = \frac{\left[(1 - 2\nu_m)(1 - C)\right]F - \tfrac{1}{2}(1 - 2\nu_m)^2 C + 2}{\left[(3 - 2\nu_m) + (1 - 2\nu_m)C\right]F + \tfrac{1}{2}(5 - 6\nu_m)(1 - 2\nu_m)C + (6 - 8\nu_m)}$$

$$N_n = \frac{\left[1 + (1 - 2\nu_m)C\right]F - \frac{1}{2}(1 - 2\nu_m)C - 2}{\left[(3 - 2\nu_m) + (1 - 2\nu_m)C\right]F + \frac{1}{2}(5 - 6\nu_m)(1 - 2\nu_m)C + (6 - 8\nu_m)}$$

Expressions for C and F are given on page 338 in Appendix A. Positive sign conventions are illustrated in Fig. A.4, Appendix A.

B.2 SOLUTION NO. 2 : OVERPRESSURE LOADING - FULL SLIPPAGE CONDITION - THIN LINER

B.2.1 EXTERNAL PRESSURES ACTING ON LINER

$$P_r = \left(\frac{P_o}{2}\right)\{(1 + K)[1 - L_f] - 3(1 - K)[1 - J_f]\cos 2\theta\}$$

$$T_{r\theta} = 0$$

B.2.2 LINER DISPLACEMENTS

$$u_\ell = \left(\frac{P_o a}{2}\right)\left(\frac{1 + \nu_m}{E_m}\right)\{(1 + K)[(1 - 2\nu_m)C][1 - L_f] - (1 - K)(2F)[1 - J_f]\cos 2\theta\}$$

$$v_\ell = \left(\frac{P_o a}{2}\right)\left(\frac{1 + \nu_m}{E_m}\right)\{(1 - K)(F)[1 - J_f]\sin 2\theta\}$$

B.2.3 LINER THRUST, SHEAR, AND MOMENTS

$$T = \left(\frac{P_o a}{2}\right)\{(1 + K)[1 - L_f] + (1 - K)[1 - J_f]\cos 2\theta\}$$

$$V = -(P_o a)\{(1 - K)[1 - J_f]\sin 2\theta\}$$

$$M = \left(\frac{P_o a^2}{2}\right)\{(1 + K)\left[\frac{(1 - 2\nu_m)C}{6F}\right][1 - L_f] + (1 - K)[1 - J_f]\cos 2\theta\}$$

B.2.4 GROUND MASS STRESSES AND DISPLACEMENTS

$$\sigma_{rm} = (\frac{P_o}{2})\{(1 + K)[1 - L_f(\frac{a}{r})^2] - (1 - K)[1 + 3J_f(\frac{a}{r})^4 - 4N_f(\frac{a}{r})^2]\cos 2\theta\}$$

$$\sigma_{\theta m} = (\frac{P_o}{2})\{(1 + K)[1 + L_f(\frac{a}{r})^2] + (1 - K)[1 + 3J_f(\frac{a}{r})^4]\cos 2\theta\}$$

$$\tau_{r\theta m} = (\frac{P_o}{2})\{(1 - K)[1 - 3J_f(\frac{a}{r})^4 + 2N_f(\frac{a}{r})^2]\sin 2\theta\}$$

$$u_m = (\frac{P_o r}{2})(\frac{1 + \nu_m}{E_m})\{(1 + K)[(1 - 2\nu_m) + L_f(\frac{a}{r})^2] - (1 - K)[1 - J_f(\frac{a}{r})^4 + 4(1 - \nu_m)N_f(\frac{a}{r})^2]\cos 2\theta\}$$

$$v_m = (\frac{P_o r}{2})(\frac{1 + \nu_m}{E_m})\{(1 - K)[1 + J_f(\frac{a}{r})^4 + 2(1 - 2\nu_m)N_f(\frac{a}{r})^2]\sin 2\theta\}$$

B.2.5 CONSTANTS

$$L_f = \frac{(1 - 2\nu_m)(C - 1)}{1 + (1 - 2\nu_m)C}$$

$$J_f = \frac{2F + (1 - 2\nu_m)}{2F + (5 - 6\nu_m)}$$

$$N_f = \frac{2F - 1}{2F + (5 - 6\nu_m)}$$

Expressions for C and F are given on page 338 in Appendix A. Positive sign conventions are illustrated in Fig. A.4 of Appendix A.

B.3 SOLUTION NO. 3 : EXCAVATION LOADING - NO SLIPPAGE CONDITION - THIN LINER

B.3.1 EXTERNAL PRESSURES ACTING ON LINER

$$P_r = \left(\frac{\gamma H}{2}\right)\{(1 + K_o)[1 - L_n^*] - (1 - K_o)[1 + 3J_n^* - 2N_n^*]\cos 2\theta\}$$

$$T_{r\theta} = \left(\frac{\gamma H}{2}\right)\{(1 - K_o)[1 - 3J_n^* + N_n^*]\sin 2\theta\}$$

B.3.2 LINER DISPLACEMENTS

$$u_\ell = \left(\frac{\gamma Ha}{2}\right)\left(\frac{1 + \nu_m}{E_m}\right)\{(1 + K_o)[L_n^*] - (1 - K_o)(F)[1 + J_n^* - N_n^*]\cos 2\theta\}$$

$$v_\ell = -\left(\frac{\gamma Ha}{2}\right)\left(\frac{1 + \nu_m}{E_m}\right)\{(1 - K_o)[J_n^* + (1 - 2\nu_m)N_n^*]\sin 2\theta\}$$

B.3.3 LINER THRUST, SHEAR, AND MOMENTS

$$T = \left(\frac{\gamma Ha}{2}\right)\{(1 + K_o)[1 - L_n^*] + (1 - K_o)[1 - J_n^*]\cos 2\theta\}$$

$$V = -\left(\frac{\gamma Ha}{2}\right)\{(1 - K_o)[1 + J_n^* - N_n^*]\sin 2\theta\}$$

$$M = \left(\frac{\gamma Ha^2}{2}\right)\{(1 + K_o)\left[\frac{L_n^*}{6F}\right] + \tfrac{1}{2}(1 - K_o)[1 + J_n^* - N_n^*]\cos 2\theta\}$$

B.3.4 GROUND MASS STRESSES AND DISPLACEMENTS

$$\sigma_{rm} = \left(\frac{\gamma H}{2}\right)\{(1 + K_o)\left[1 - L_n^*\left(\frac{a}{r}\right)^2\right] -$$

$$- (1 - K_o)\left[1 + 3J_n^*\left(\frac{a}{r}\right)^4 - 2N_n^*\left(\frac{a}{r}\right)^2\right]\cos 2\theta\}$$

$$\sigma_m = \left(\frac{\gamma H}{2}\right)\left\{(1 + K_o)\left[1 + L_n^*\left(\frac{a}{r}\right)^2\right] + (1 - K_o)\left[1 + 3J_n^*\left(\frac{a}{r}\right)^4\right]\cos 2\theta\right\}$$

$$\tau_{r\theta m} = \left(\frac{\gamma H}{2}\right)\left\{(1 - K_o)\left[1 - 3J_n^*\left(\frac{a}{r}\right)^4 + N_n^*\left(\frac{a}{r}\right)^2\right]\sin 2\theta\right\}$$

$$u_m = \left(\frac{\gamma H r}{2}\right)\left(\frac{1 + \nu_m}{E_m}\right)\left\{(1 + K_o)\left[L_n^*\left(\frac{a}{r}\right)^2\right] + \right.$$

$$\left. + (1 - K_o)\left[J_n^*\left(\frac{a}{r}\right)^4 - 2(1 - \nu_m)N_n^*\left(\frac{a}{r}\right)^2\right]\cos 2\theta\right\}$$

$$v_m = \left(\frac{\gamma H r}{2}\right)\left(\frac{1 + \nu_m}{E_m}\right)\left\{(1 - K_o)\left[J_n^*\left(\frac{a}{r}\right)^4 + (1 - 2\nu_m)N_n^*\left(\frac{a}{r}\right)^2\right]\sin 2\theta\right\}$$

B.3.5 CONSTANTS

$$L_n^* = \frac{(1 - 2\nu_m)C}{1 + (1 - 2\nu_m)C}$$

$$J_n^* = \frac{\left[2\nu_m + (1 - 2\nu_m)C\right]F + (1 - \nu_m)(1 - 2\nu_m)C}{\left[(3 - 2\nu_m) + (1 - 2\nu_m)C\right]F + \frac{1}{2}(5 - 6\nu_m)(1 - 2\nu_m)C + (6 - 8\nu_m)}$$

$$N_n^* = \frac{\left[3 + 2(1 - 2\nu_m)C\right]F + \frac{1}{2}(1 - 2\nu_m)C}{\left[(3 - 2\nu_m) + (1 - 2\nu_m)C\right]F + \frac{1}{2}(5 - 6\nu_m)(1 - 2\nu_m)C + (6 - 8\nu_m)}$$

Expressions for C and F are given on page 338 in Appendix A. Positive sign conventions are illustrated in Fig. A.4 of Appendix A.

B.4 SOLUTION NO. 4 : EXCAVATION LOADING - FULL SLIPPAGE CONDITION - THIN LINER

B.4.1 EXTERNAL PRESSURES ACTING ON LINER

$$P_r = \left(\frac{\gamma H}{2}\right)\{(1 + K_o)\left[1 - L_f^*\right] - 3(1 - K_o)\left[1 - 2J_f^*\right]\cos 2\theta\}$$

$$T_{r\theta} = 0$$

B.4.2 LINER DISPLACEMENTS

$$u_\ell = \left(\frac{\gamma Ha}{2}\right)\left(\frac{1 + \nu_m}{E_m}\right)\{(1 + K_o)\left[L_f^*\right] - (1 - K_o)(2F)\left[1 - 2J_f^*\right]\cos 2\theta\}$$

$$v_\ell = \left(\frac{\gamma Ha}{2}\right)\left(\frac{1 + \nu_m}{E_m}\right)\{(1 - K_o)(F)\left[1 - 2J_f^*\right]\sin 2\theta\}$$

B.4.3 LINER THRUST, SHEAR, AND MOMENTS

$$T = \left(\frac{\gamma Ha}{2}\right)\{(1 + K_o)\left[1 - L_f^*\right] + (1 - K_o)\left[1 - 2J_f^*\right]\cos 2\theta\}$$

$$V = -\left(\frac{\gamma Ha}{2}\right)\{(1 - K_o)\left[1 - 2J_f^*\right]\sin 2\theta\}$$

$$M = \left(\frac{\gamma Ha^2}{2}\right)\{(1 + K_o)\left[\frac{L_f^*}{6F}\right] + (1 - K_o)\left[1 - 2J_f^*\right]\cos 2\theta\}$$

B.4.4 GROUND MASS STRESSES AND DISPLACEMENTS

$$\sigma_{rm} = \left(\frac{\gamma H}{2}\right)\{(1 + K_o)\left[1 - L_f^*\left(\frac{a}{r}\right)^2\right] -$$

$$- (1 - K_o)\left[1 + 6J_f^*\left(\frac{a}{r}\right)^4 - 2N_f^*\left(\frac{a}{r}\right)^2\right]\cos 2\theta\}$$

$$\sigma_{\theta m} = \left(\frac{\gamma H}{2}\right)\left\{(1 + K_o)\left[1 + L_f^*\left(\frac{a}{r}\right)^2\right] + (1 - K_o)\left[1 + 6J_f^*\left(\frac{a}{r}\right)^4\right]\cos 2\theta\right\}$$

$$\tau_{r\theta m} = \left(\frac{\gamma H}{2}\right)\left\{(1 - K_o)\left[1 - 6J_f^*\left(\frac{a}{r}\right)^4 + N_f^*\left(\frac{a}{r}\right)^2\right]\sin 2\theta\right\}$$

$$u_m = \left(\frac{\gamma H r}{2}\right)\left(\frac{1 + \nu_m}{E_m}\right)\left\{(1 + K_o)\left[L_f^*\left(\frac{a}{r}\right)^2\right] + \right.$$

$$\left. + (1 - K_o)\left[2J_f^*\left(\frac{a}{r}\right)^4 - 2(1 - \nu_m)N_f^*\left(\frac{a}{r}\right)^2\right]\cos 2\theta\right\}$$

$$v_m = \left(\frac{\gamma H r}{2}\right)\left(\frac{1 + \nu_m}{E_m}\right)\left\{(1 - K_o)\left[2J_f^*\left(\frac{a}{r}\right)^4 + (1 - 2\nu_m)N_f^*\left(\frac{a}{r}\right)^2\right]\sin 2\theta\right\}$$

B.4.5 CONSTANTS

$$L_f^* = \frac{(1 - 2\nu_m)C}{1 + (1 - 2\nu_m)C}$$

$$J_f^* = \frac{F + (1 - \nu_m)}{2F + (5 - 6\nu_m)}$$

$$N_f^* = \frac{4F + 1}{2F + (5 - 6\nu_m)}$$

Expressions for C and F are given on page 338 in Appendix A. Positive sign conventions are illustrated in Fig. A.4 of Appendix A.

B.5 SOLUTION NO. 5 : OVERPRESSURE LOADING - NO SLIPPAGE CONDITION - THICK LINER

B.5.1 LINER STRESSES AND DISPLACEMENTS

$$\sigma_{r\ell} = P_o\left(\frac{G_\ell}{G_m}\right)(1-\nu_m)\left\{(1+K)S_n\left[\left(\frac{R_o}{R_i}\right)^2 - \left(\frac{R_o}{r_\ell}\right)^2\right] - 2(1-K)\left[W_n + 3X_n\left(\frac{R_o}{r_\ell}\right)^4 - 4Y_n\left(\frac{R_o}{r_\ell}\right)^2\right]\cos 2\theta\right\}$$

$$\sigma_{\theta\ell} = P_o\left(\frac{G_\ell}{G_m}\right)(1-\nu_m)\left\{(1+K)S_n\left[\left(\frac{R_o}{R_i}\right)^2 + \left(\frac{R_o}{r_\ell}\right)^2\right] + 2(1-K)\left[W_n + 3X_n\left(\frac{R_o}{r_\ell}\right)^4 - 12Z_n\left(\frac{r_\ell}{R_i}\right)^2\right]\cos 2\theta\right\}$$

$$\tau_{r\theta\ell} = P_o\left(\frac{G_\ell}{G_m}\right)(1-\nu_m)\left\{2(1-K)\left[W_n - 3X_n\left(\frac{R_o}{r_\ell}\right)^4 + 2Y_n\left(\frac{R_o}{r_\ell}\right)^2 - 6Z_n\left(\frac{r_\ell}{R_i}\right)^2\right]\sin 2\theta\right\}$$

$$u_\ell = \left(\frac{P_o r_\ell}{2G_m}\right)(1-\nu_m)\left\{(1+K)S_n\left[(1-2\nu_\ell)\left(\frac{R_o}{R_i}\right)^2 + \left(\frac{R_o}{r_\ell}\right)^2\right] - 2(1-K)\left[W_n - X_n\left(\frac{R_o}{r_\ell}\right)^4 + 4(1-\nu_\ell)Y_n\left(\frac{R_o}{r_\ell}\right)^2 - 4\nu_\ell Z_n\left(\frac{r_\ell}{R_i}\right)^2\right]\cos 2\theta\right\}$$

$$v_\ell = \left(\frac{P_o r_\ell}{2G_m}\right)(1-\nu_m)\left\{2(1-K)\left[W_n + X_n\left(\frac{R_o}{r_\ell}\right)^4 + 2(1-2\nu_\ell)Y_n\left(\frac{R_o}{r_\ell}\right)^2 - 2(3-2\nu_\ell)Z_n\left(\frac{r_\ell}{R_i}\right)^2\right]\sin 2\theta\right\}$$

B.5.2 GROUND MASS STRESSES AND DISPLACEMENTS

$$\sigma_{rm} = \left(\frac{P_o}{2}\right)\left\{(1+K)\left[1 + L_n\left(\frac{R_o}{r}\right)^2\right] - (1-K)\left[1 - 3J_n\left(\frac{R_o}{r}\right)^4 + 4N_n\left(\frac{R_o}{r}\right)^2\right]\cos 2\theta\right\}$$

$$\sigma_{\theta m} = \left(\frac{P_o}{2}\right)\left\{(1 + K)\left[1 - L_n\left(\frac{R_o}{r}\right)^2\right] + (1 - K)\left[1 - 3J_n\left(\frac{R_o}{r}\right)^4\right]\cos 2\theta\right\}$$

$$\tau_{r\theta m} = \left(\frac{P_o}{2}\right)\left\{(1 - K)\left[1 + 3J_n\left(\frac{R_o}{r}\right)^4 - 2N_n\left(\frac{R_o}{r}\right)^2\right]\sin 2\theta\right\}$$

$$u_m = \left(\frac{P_o r}{4G_m}\right)\left\{(1 + K)\left[(1 - 2\nu_m) - L_n\left(\frac{R_o}{r}\right)^2\right] - \right.$$

$$\left. - (1 - K)\left[1 + J_n\left(\frac{R_o}{r}\right)^4 - 4(1 - \nu_m)N_n\left(\frac{R_o}{r}\right)^2\right]\cos 2\theta\right\}$$

$$v_m = \left(\frac{P_o r}{4G_m}\right)\left\{(1 - K)\left[1 - J_n\left(\frac{R_o}{r}\right)^4 - 2(1 - 2\nu_m)N_n\left(\frac{R_o}{r}\right)^2\right]\sin 2\theta\right\}$$

B.5.3 CONSTANTS

$$L_n = \frac{(1 - 2\nu_m)\left(\frac{G_\ell}{G_m}\right)b_1 - b_2}{\left(\frac{G_\ell}{G_m}\right)b_1 + b_2}$$

$$J_n = \frac{\left(\frac{G_\ell}{G_m}\right)^2 b_3 + 2\left(\frac{G_\ell}{G_m}\right)\left[b_{11} - 8\nu_m b_{12}\right] - b_6}{(3 - 4\nu_m)\left(\frac{G_\ell}{G_m}\right)^2 b_3 + 2\left(\frac{G_\ell}{G_m}\right)\left[b_4 - 2\nu_m b_5\right] + b_6}$$

$$N_n = \frac{\left(\frac{G_\ell}{G_m}\right)^2 b_3 + 2\left(\frac{G_\ell}{G_m}\right)b_{13} - b_6}{(3 - 4\nu_m)\left(\frac{G_\ell}{G_m}\right)^2 b_3 + 2\left(\frac{G_\ell}{G_m}\right)\left[b_4 - 2\nu_m b_5\right] + b_6}$$

$$S_n = \frac{1}{\left(\frac{G_\ell}{G_m}\right) b_1 + b_2}$$

$$W_n = \frac{\left(\frac{G_\ell}{G_m}\right) b_{14} + b_{15}}{(3 - 4\nu_m)\left(\frac{G_\ell}{G_m}\right)^2 b_3 + 2\left(\frac{G_\ell}{G_m}\right)\left[b_4 - 2\nu_m b_5\right] + b_6}$$

$$X_n = \frac{\left(\frac{G_\ell}{G_m}\right) b_7 + b_8}{(3 - 4\nu_m)\left(\frac{G_\ell}{G_m}\right)^2 b_3 + 2\left(\frac{G_\ell}{G_m}\right)\left[b_4 - 2\nu_m b_5\right] + b_6}$$

$$Y_n = \frac{\left(\frac{G_\ell}{G_m}\right) b_9 + b_{10}}{(3 - 4\nu_m)\left(\frac{G_\ell}{G_m}\right)^2 b_3 + 2\left(\frac{G_\ell}{G_m}\right)\left[b_4 - 2\nu_m b_5\right] + b_6}$$

$$Z_n = \frac{\left[\left(\frac{G_\ell}{G_m}\right) - 1\right] b_{16}}{(3 - 4\nu_m)\left(\frac{G_\ell}{G_m}\right)^2 b_3 + 2\left(\frac{G_\ell}{G_m}\right)\left[b_4 - 2\nu_m b_5\right] + b_6}$$

$$b_1 = \left[\left(\frac{R_o}{R_i}\right)^2 - 1\right]$$

$$b_2 = \left[(1 - 2\nu_\ell)\left(\frac{R_o}{R_i}\right)^2 + 1\right]$$

$$b_3 = \left[\left(\frac{R_o}{R_i}\right)^2 - 1\right]^4$$

$$b_4 = \left[(5 - 6\nu_\ell)\left(\frac{R_o}{R_i}\right)^6 + (5 - 2\nu_\ell)\left(\frac{R_o}{R_i}\right)^4 - (1 + 2\nu_\ell)\left(\frac{R_o}{R_i}\right)^2 + \right.$$
$$\left. + (3 - 2\nu_\ell)\right]\left[\left(\frac{R_o}{R_i}\right)^2 - 1\right]$$

$$b_5 = \left[(3 - 4\nu_\ell)\left(\frac{R_o}{R_i}\right)^6 + 3\left(\frac{R_o}{R_i}\right)^4 - 3\left(\frac{R_o}{R_i}\right)^2 + 1\right]\left[\left(\frac{R_o}{R_i}\right)^2 - 1\right]$$

$$b_6 = \left[(3 - 4\nu_\ell)\left(\frac{R_o}{R_i}\right)^8 + 4(3 - 6\nu_\ell + 4\nu_\ell^2)\left(\frac{R_o}{R_i}\right)^6 - 6\left(\frac{R_o}{R_i}\right)^4 + \right.$$
$$\left. + 4\left(\frac{R_o}{R_i}\right)^2 + (3 - 4\nu_\ell)\right]$$

$$b_7 = \left[\left(\frac{R_o}{R_i}\right)^4 - 1\right]$$

$$b_8 = \left[(3 - 4\nu_\ell)\left(\frac{R_o}{R_i}\right)^4 + 1\right]$$

$$b_9 = \left[\left(\frac{R_o}{R_i}\right)^6 - 1\right]$$

$$b_{10} = \left[(3 - 4\nu_\ell)\left(\frac{R_o}{R_i}\right)^6 + 1\right]$$

$$b_{11} = \left[(1 - 2\nu_\ell)\left(\frac{R_o}{R_i}\right)^8 + 4(2 - \nu_\ell)\left(\frac{R_o}{R_i}\right)^6 - 2(7 - 4\nu_\ell)\left(\frac{R_o}{R_i}\right)^4 + \right.$$
$$\left. + 4\left(\frac{R_o}{R_i}\right)^2 + (1 - 2\nu_\ell)\right]$$

$$b_{12} = (1 - \nu_\ell)\left[\left(\frac{R_o}{R_i}\right)^6 - \left(\frac{R_o}{R_i}\right)^4\right]$$

$$b_{13} = \left[(1 - 2\nu_\ell)\left(\frac{R_o}{R_i}\right)^8 + 4\nu_\ell\left(\frac{R_o}{R_i}\right)^6 - 6\left(\frac{R_o}{R_i}\right)^4 + 4\left(\frac{R_o}{R_i}\right)^2 + (1 - 2\nu_\ell)\right]$$

$$b_{14} = \left[\left(\frac{R_o}{R_i}\right)^8 + 3\left(\frac{R_o}{R_i}\right)^4 - 4\left(\frac{R_o}{R_i}\right)^2\right]$$

$$b_{15} = \left[(3 - 4\nu_\ell)\left(\frac{R_o}{R_i}\right)^8 - 3\left(\frac{R_o}{R_i}\right)^4 + 4\left(\frac{R_o}{R_i}\right)^2\right]$$

$$b_{16} = \left[\left(\frac{R_o}{R_i}\right)^4 - \left(\frac{R_o}{R_i}\right)^2\right]$$

Positive sign conventions are illustrated in Fig. A.5 of Appendix A

B.6 SOLUTION NO. 6 : OVERPRESSURE LOADING - FULL SLIPPAGE CONDITION - THICK LINER

B.6.1 LINER STRESSES AND DISPLACEMENTS

$$\sigma_{r\ell} = P_o\left(\frac{G_\ell}{G_m}\right)(1-\nu_m)\{(1+K)S_f\left[\left(\frac{R_o}{R_i}\right)^2 - \left(\frac{R_o}{r_\ell}\right)^2\right] - 6(1-K)\left[W_f + X_f\left(\frac{R_o}{r_\ell}\right)^4 - 2Y_f\left(\frac{R_o}{r_\ell}\right)^2\right]\cos 2\theta\}$$

$$\sigma_{\theta\ell} = P_o\left(\frac{G_\ell}{G_m}\right)(1-\nu_m)\{(1+K)S_f\left[\left(\frac{R_o}{R_i}\right)^2 + \left(\frac{R_o}{r_\ell}\right)^2\right] + 6(1-K)\left[W_f + X_f\left(\frac{R_o}{r_\ell}\right)^4 - 2Z_f\left(\frac{r_\ell}{R_i}\right)^2\right]\cos 2\theta\}$$

$$\tau_{r\theta\ell} = P_o\left(\frac{G_\ell}{G_m}\right)(1-\nu_m)\{6(1-K)\left[W_f - X_f\left(\frac{R_o}{r_\ell}\right)^4 + Y_f\left(\frac{R_o}{r_\ell}\right)^2 - Z_f\left(\frac{r_\ell}{R_i}\right)^2\right]\sin 2\theta\}$$

$$u_\ell = \left(\frac{P_o r_\ell}{2G_m}\right)(1-\nu_m)\{(1+K)S_f\left[(1-2\nu_\ell)\left(\frac{R_o}{R_i}\right)^2 + \left(\frac{R_o}{r_\ell}\right)^2\right] - 2(1-K)\left[3W_f - X_f\left(\frac{R_o}{r_\ell}\right)^4 + 6(1-\nu_\ell)Y_f\left(\frac{R_o}{r_\ell}\right)^2 - 2\nu_\ell Z_f\left(\frac{r_\ell}{R_i}\right)^2\right]\cos 2\theta\}$$

$$v_\ell = \left(\frac{P_o r_\ell}{2G_m}\right)(1 - \nu_m)\{2(1 - K)\left[3W_f + X_f\left(\frac{R_o}{r_\ell}\right)^4 + 3(1 - 2\nu_\ell)Y_f\left(\frac{R_o}{r_\ell}\right)^2 - \right.$$
$$\left. - (3 - 2\nu_\ell)Z_f\left(\frac{r_\ell}{R_i}\right)^2\right]\sin 2\theta\}$$

B.6.2 GROUND MASS STRESSES AND DISPLACEMENTS

$$\sigma_{rm} = \left(\frac{P_o}{2}\right)\{(1 + K)\left[1 + L_f\left(\frac{R_o}{r}\right)^2\right] - (1 - K)\left[1 + 3J_f\left(\frac{R_o}{r}\right)^4 + \right.$$
$$\left. + 4N_f\left(\frac{R_o}{r}\right)^2\right]\cos 2\theta\}$$

$$\sigma_{\theta m} = \left(\frac{P_o}{2}\right)\{(1 + K)\left[1 - L_f\left(\frac{R_o}{r}\right)^2\right] + (1 - K)\left[1 + 3J_f\left(\frac{R_o}{r}\right)^4\right]\cos 2\theta\}$$

$$\tau_{r\theta m} = \left(\frac{P_o}{2}\right)\{(1 - K)\left[1 - 3J_f\left(\frac{R_o}{r}\right)^4 - 2N_f\left(\frac{R_o}{r}\right)^2\right]\sin 2\theta\}$$

$$u_m = \left(\frac{P_o r}{4G_m}\right)\{(1 + K)\left[(1 - 2\nu_m) - L_f\left(\frac{R_o}{r}\right)^2\right] -$$
$$- (1 - K)\left[1 - J_f\left(\frac{R_o}{r}\right)^4 - 4(1 - \nu_m)N_f\left(\frac{R_o}{r}\right)^2\right]\cos 2\theta\}$$

$$v_m = \left(\frac{P_o r}{4G_m}\right)\{(1 - K)\left[1 + J_f\left(\frac{R_o}{r}\right)^4 - 2(1 - 2\nu_m)N_f\left(\frac{R_o}{r}\right)^2\right]\sin 2\theta\}$$

B.6.3 CONSTANTS

$$L_f = \frac{(1 - 2\nu_m)(\frac{G_\ell}{G_m})d_1 - d_2}{(\frac{G_\ell}{G_m})d_1 + d_2}$$

$$J_f = \frac{(1 - 2\nu_m)(\frac{G_\ell}{G_m})d_3 + d_4}{(5 - 6\nu_m)(\frac{G_\ell}{G_m})d_3 + d_4}$$

$$N_f = \frac{(\frac{G_\ell}{G_m})d_3 - d_4}{(5 - 6\nu_m)(\frac{G_\ell}{G_m})d_3 + d_4}$$

$$S_f = \frac{1}{(\frac{G_\ell}{G_m})d_1 + d_2}$$

$$W_f = \frac{d_7}{(5 - 6\nu_m)(\frac{G_\ell}{G_m})d_3 + d_4}$$

$$X_f = \frac{d_5}{(5 - 6\nu_m)(\frac{G_\ell}{G_m})d_3 + d_4}$$

$$Y_f = \frac{d_6}{(5 - 6\nu_m)(\frac{G_\ell}{G_m})d_3 + d_4}$$

$$Z_f = \frac{d_8}{(5 - 6\nu_m)(\frac{G_\ell}{G_m})d_3 + d_4}$$

$$d_1 = \left[(\frac{R_o}{R_i})^2 - 1\right]$$

$$d_2 = \left[(1 - 2\nu_\ell)(\frac{R_o}{R_i})^2 + 1\right]$$

$$d_3 = \left[(\frac{R_o}{R_i})^2 - 1\right]^3$$

$$d_4 = \left[(3 - 2\nu_\ell)(\frac{R_o}{R_i})^6 + 3(5 - 6\nu_\ell)(\frac{R_o}{R_i})^4 + 3(3 - 2\nu_\ell)(\frac{R_o}{R_i})^2 + (5 - 6\nu_\ell)\right]$$

$$d_5 = \left[3(\frac{R_o}{R_i})^2 + 1\right]$$

$$d_6 = \left[2(\frac{R_o}{R_i})^4 + (\frac{R_o}{R_i})^2 + 1\right]$$

$$d_7 = \left[(\frac{R_o}{R_i})^6 + (\frac{R_o}{R_i})^4 + 2(\frac{R_o}{R_i})^2\right]$$

$$d_8 = \left[(\frac{R_o}{R_i})^4 + 3(\frac{R_o}{R_i})^2\right]$$

Positive sign conventions are illustrated in Fig. A.5 of Appendix A.

B.7 SOLUTION NO. 7 : EXCAVATION LOADING — NO SLIPPAGE CONDITION — THICK LINER

B.7.1 LINER STRESSES AND DISPLACEMENTS

$$\sigma_{r\ell} = \left(\frac{\gamma H}{2}\right)\left(\frac{G_\ell}{G_m}\right)\left\{(1 + K_o)S_n^*\left[\left(\frac{R_o}{R_i}\right)^2 - \left(\frac{R_o}{r_\ell}\right)^2\right] - \right.$$

$$\left. - (3 - 4\nu_m)(1 - K_o)\left[W_n^* + 3X_n^*\left(\frac{R_o}{r_\ell}\right)^4 - 4Y_n^*\left(\frac{R_o}{r_\ell}\right)^2\right]\cos 2\theta\right\}$$

$$\sigma_{\theta\ell} = \left(\frac{\gamma H}{2}\right)\left(\frac{G_\ell}{G_m}\right)\left\{(1 + K_o)S_n^*\left[\left(\frac{R_o}{R_i}\right)^2 + \left(\frac{R_o}{r_\ell}\right)^2\right] + \right.$$

$$\left. + (3 - 4\nu_m)(1 - K_o)\left[W_n^* + 3X_n^*\left(\frac{R_o}{r_\ell}\right)^4 - 12Z_n^*\left(\frac{r_\ell}{R_i}\right)^2\right]\cos 2\theta\right\}$$

$$\tau_{r\theta\ell} = \left(\frac{\gamma H}{2}\right)\left(\frac{G_\ell}{G_m}\right)\left\{(3 - 4\nu_m)(1 - K_o)\left[W_n^* - 3X_n^*\left(\frac{R_o}{r_\ell}\right)^4 + 2Y_n^*\left(\frac{R_o}{r_\ell}\right)^2 - \right.\right.$$

$$\left.\left. - 6Z_n^*\left(\frac{r_\ell}{R_i}\right)^2\right]\sin 2\theta\right\}$$

$$u_\ell = \left(\frac{\gamma H r_\ell}{4G_m}\right)\left\{(1 + K_o)S_n^*\left[(1 - 2\nu_\ell)\left(\frac{R_o}{R_i}\right)^2 + \left(\frac{R_o}{r_\ell}\right)^2\right] - \right.$$

$$- (3 - 4\nu_m)(1 - K_o)\left[W_n^* - X_n^*\left(\frac{R_o}{r_\ell}\right)^4 + 4(1 - \nu_\ell)Y_n^*\left(\frac{R_o}{r_\ell}\right)^2 - \right.$$

$$\left. \left. - 4\nu_\ell Z_n^*\left(\frac{r_\ell}{R_i}\right)^2\right]\cos 2\theta\right\}$$

$$v_\ell = \left(\frac{\gamma H r_\ell}{4G_m}\right)\{(3 - 4\nu_m)(1 - K_o)\left[W_n^* + X_n^*\left(\frac{R_o}{r_\ell}\right)^4 + 2(1 - 2\nu_\ell)Y_n^*\left(\frac{R_o}{r_\ell}\right)^2 - \right.$$

$$\left. - 2(3 - 2\nu_\ell)Z_n^*\left(\frac{r_\ell}{R_i}\right)^2\right]\sin 2\theta\}$$

B.7.2 GROUND MASS STRESSES AND DISPLACEMENTS

$$\sigma_{rm} = \left(\frac{\gamma H}{2}\right)\{(1 + K_o)\left[1 - L_n^*\left(\frac{R_o}{r}\right)^2\right] -$$

$$- (1 - K_o)\left[1 + 3J_n^*\left(\frac{R_o}{r}\right)^4 - 4N_n^*\left(\frac{R_o}{r}\right)^2\right]\cos 2\theta\}$$

$$\sigma_{\theta m} = \left(\frac{\gamma H}{2}\right)\{(1 + K_o)\left[1 + L_n^*\left(\frac{R_o}{r}\right)^2\right] + (1 - K_o)\left[1 + 3J_n^*\left(\frac{R_o}{r}\right)^4\right]\cos 2\theta\}$$

$$\tau_{r\theta m} = \left(\frac{\gamma H}{2}\right)\{(1 - K_o)\left[1 - 3J_n^*\left(\frac{R_o}{r}\right)^4 + 2N_n^*\left(\frac{R_o}{r}\right)^2\right]\sin 2\theta\}$$

$$u_m = \left(\frac{\gamma H r}{4G_m}\right)\{(1 + K_o)\left[L_n^*\left(\frac{R_o}{r}\right)^2\right] + (1 - K_o)\left[J_n^*\left(\frac{R_o}{r}\right)^4 - \right.$$

$$\left. - 4(1 - \nu_m)N_n^*\left(\frac{R_o}{r}\right)^2\right]\cos 2\theta\}$$

$$v_m = \left(\frac{\gamma H r}{4G_m}\right)\{(1 - K_o)\left[J_n^*\left(\frac{R_o}{r}\right)^4 + 2(1 - 2\nu_m)N_n^*\left(\frac{R_o}{r}\right)^2\right]\sin 2\theta\}$$

B.7.3 CONSTANTS

$$L_n^* = \frac{b_2^*}{\left(\frac{G_\ell}{G_m}\right) b_1^* + b_2^*}$$

$$J_n^* = \frac{\left(\frac{G_\ell}{G_m}\right)\left[b_{11}^* + 16\nu_m b_{12}^*\right] + b_6^*}{(3 - 4\nu_m)\left(\frac{G_\ell}{G_m}\right)^2 b_3^* + 2\left(\frac{G_\ell}{G_m}\right)\left[b_4^* - 2\nu_m b_5^*\right] + b_6^*}$$

$$N_n^* = \frac{\left(\frac{G_\ell}{G_m}\right) b_{13}^* + b_6^*}{(3 - 4\nu_m)\left(\frac{G_\ell}{G_m}\right)^2 b_3^* + 2\left(\frac{G_\ell}{G_m}\right)\left[b_4^* - 2\nu_m b_5^*\right] + b_6^*}$$

$$S_n^* = \frac{1}{\left(\frac{G_\ell}{G_m}\right) b_1^* + b_2^*}$$

$$W_n^* = \frac{\left(\frac{G_\ell}{G_m}\right) b_{14}^* + b_{15}^*}{(3 - 4\nu_m)\left(\frac{G_\ell}{G_m}\right)^2 b_3^* + 2\left(\frac{G_\ell}{G_m}\right)\left[b_4^* - 2\nu_m b_5^*\right] + b_6^*}$$

$$X_n^* = \frac{\left(\frac{G_\ell}{G_m}\right) b_7^* + b_8^*}{(3 - 4\nu_m)\left(\frac{G_\ell}{G_m}\right)^2 b_3^* + 2\left(\frac{G_\ell}{G_m}\right)\left[b_4^* - 2\nu_m b_5^*\right] + b_6^*}$$

$$Y_n^* = \frac{\left(\frac{G_\ell}{G_m}\right) b_9^* + b_{10}^*}{(3 - 4\nu_m)\left(\frac{G_\ell}{G_m}\right)^2 b_3^* + 2\left(\frac{G_\ell}{G_m}\right)\left[b_4^* - 2\nu_m b_5^*\right] + b_6^*}$$

$$z_n^* = \frac{[(\frac{G_\ell}{G_m}) - 1]b_{16}^*}{(3 - 4\nu_m)(\frac{G_\ell}{G_m})^2 b_3^* + 2(\frac{G_\ell}{G_m})[b_4^* - 2\nu_m b_5^*] + b_6^*}$$

$$b_1^* = [(\frac{R_o}{R_i})^2 - 1]$$

$$b_2^* = [(1 - 2\nu_\ell)(\frac{R_o}{R_i})^2 + 1]$$

$$b_3^* = [(\frac{R_o}{R_i})^2 - 1]^4$$

$$b_4^* = [(5 - 6\nu_\ell)(\frac{R_o}{R_i})^6 + (5 - 2\nu_\ell)(\frac{R_o}{R_i})^4 - (1 + 2\nu_\ell)(\frac{R_o}{R_i})^2 + (3 - 2\nu_\ell)][(\frac{R_o}{R_i})^2 - 1]$$

$$b_5^* = [(3 - 4\nu_\ell)(\frac{R_o}{R_i})^6 + 3(\frac{R_o}{R_i})^4 - 3(\frac{R_o}{R_i})^2 + 1][(\frac{R_o}{R_i})^2 - 1]$$

$$b_6^* = [(3 - 4\nu_\ell)(\frac{R_o}{R_i})^8 + 4(3 - 6\nu_\ell + 4\nu_\ell^2)(\frac{R_o}{R_i})^6 - 6(\frac{R_o}{R_i})^4 + 4(\frac{R_o}{R_i})^2 + (3 - 4\nu_\ell)]$$

$$b_7^* = [(\frac{R_o}{R_i})^4 - 1]$$

$$b_8^* = [(3 - 4\nu_\ell)(\frac{R_o}{R_i})^4 + 1]$$

$$b_9^* = [(\frac{R_o}{R_i})^6 - 1]$$

$$b_{10}^* = [(3 - 4\nu_\ell)(\frac{R_o}{R_i})^6 + 1]$$

$$b_{11}^* = [(\frac{R_o}{R_i})^6 - (11 - 8\nu_\ell)(\frac{R_o}{R_i})^4 + (7 - 4\nu_\ell)(\frac{R_o}{R_i})^2 + (3 - 4\nu_\ell)][(\frac{R_o}{R_i})^2 - 1]$$

$$b_{12}^* = (1 - \nu_\ell)[(\frac{R_o}{R_i})^6 - (\frac{R_o}{R_i})^4]$$

$$b_{13}^* = [(\frac{R_o}{R_i})^6 + (1 - 4\nu_\ell)(\frac{R_o}{R_i})^4 + (7 - 4\nu_\ell)(\frac{R_o}{R_i})^2 + (3 - 4\nu_\ell)][(\frac{R_o}{R_i})^2 - 1]$$

$$b_{14}^* = [(\frac{R_o}{R_i})^8 + 3(\frac{R_o}{R_i})^4 - 4(\frac{R_o}{R_i})^2]$$

$$b_{15}^* = [(3 - 4\nu_\ell)(\frac{R_o}{R_i})^8 - 3(\frac{R_o}{R_i})^4 + 4(\frac{R_o}{R_i})^2]$$

$$b_{16}^* = [(\frac{R_o}{R_i})^4 - (\frac{R_o}{R_i})^2]$$

Positive sign conventions are illustrated in Fig. A.5 of Appendix A.

B.8 SOLUTION NO. 8 : EXCAVATION LOADING — FULL SLIPPAGE CONDITION — THICK LINER

B.8.1 LINER STRESSES AND DISPLACEMENTS

$$\sigma_{r\ell} = \left(\frac{\gamma H}{2}\right)\left(\frac{G_\ell}{G_m}\right)\{(1 + K_o)S_f^*\left[\left(\frac{R_o}{R_i}\right)^2 - \left(\frac{R_o}{r_\ell}\right)^2\right] - 3(3 - 4\nu_m)(1 - K_o)\left[W_f^* + X_f^*\left(\frac{R_o}{r_\ell}\right)^4 - 2Y_f^*\left(\frac{R_o}{r_\ell}\right)^2\right]\cos 2\theta\}$$

$$\sigma_{\theta\ell} = \left(\frac{\gamma H}{2}\right)\left(\frac{G_\ell}{G_m}\right)\{(1 + K_o)S_f^*\left[\left(\frac{R_o}{R_i}\right)^2 + \left(\frac{R_o}{r_\ell}\right)^2\right] + 3(3 - 4\nu_m)(1 - K_o)\left[W_f^* + X_f^*\left(\frac{R_o}{r_\ell}\right)^4 - 2Z_f^*\left(\frac{r_\ell}{R_i}\right)^2\right]\cos 2\theta\}$$

$$\tau_{r\theta\ell} = \left(\frac{\gamma H}{2}\right)\left(\frac{G_\ell}{G_m}\right)\{3(3 - 4\nu_m)(1 - K_o)\left[W_f^* - X_f^*\left(\frac{R_o}{r_\ell}\right)^4 + Y_f^*\left(\frac{R_o}{r_\ell}\right)^2 - Z_f^*\left(\frac{r_\ell}{R_i}\right)^2\right]\sin 2\theta\}$$

$$u_\ell = \left(\frac{\gamma H r_\ell}{4G_m}\right)\{(1 + K_o)S_f^*\left[(1 - 2\nu_\ell)\left(\frac{R_o}{R_i}\right)^2 + \left(\frac{R_o}{r_\ell}\right)^2\right] - (3 - 4\nu_m)(1 - K_o)\left[3W_f^* - X_f^*\left(\frac{R_o}{r_\ell}\right)^4 + 6(1 - \nu_\ell)Y_f^*\left(\frac{R_o}{r_\ell}\right)^2 - 2\nu_\ell Z_f^*\left(\frac{r_\ell}{R_i}\right)^2\right]\cos 2\theta\}$$

$$v_\ell = \left(\frac{\gamma H r_\ell}{4G_m}\right)\{(3 - 4\nu_m)(1 - K_o)\left[3W_f^* + X_f^*\left(\frac{R_o}{r_\ell}\right)^4 + \right.$$

$$\left. + 3(1 - 2\nu_\ell)Y_f^*\left(\frac{R_o}{r_\ell}\right)^2 - (3 - 2\nu_\ell)Z_f^*\left(\frac{r_\ell}{R_o}\right)^2\right]\sin 2\theta\}$$

B.8.2 GROUND MASS STRESSES AND DISPLACEMENTS

$$\sigma_{rm} = \left(\frac{\gamma H}{2}\right)\{(1 + K_o)\left[1 - L_f^*\left(\frac{R_o}{r}\right)^2\right] - (1 - K_o)\left[1 + 3J_f^*\left(\frac{R_o}{r}\right)^4 - \right.$$

$$\left. - 2N_f^*\left(\frac{R_o}{r}\right)^2\right]\cos 2\theta\}$$

$$\sigma_{\theta m} = \left(\frac{\gamma H}{2}\right)\{(1 + K_o)\left[1 + L_f^*\left(\frac{R_o}{r}\right)^2\right] + (1 - K_o)\left[1 + 3J_f^*\left(\frac{R_o}{r}\right)^4\right]\cos 2\theta\}$$

$$\tau_{r\theta m} = \left(\frac{\gamma H}{2}\right)\{(1 - K_o)\left[1 - 3J_f^*\left(\frac{R_o}{r}\right)^4 + N_f^*\left(\frac{R_o}{r}\right)^2\right]\sin 2\theta\}$$

$$u_m = \left(\frac{\gamma H r}{4G_m}\right)\{(1 + K_o)\left[L_f^*\left(\frac{R_o}{r}\right)^2\right] + (1 - K_o)\left[J_f^*\left(\frac{R_o}{r}\right)^4 - \right.$$

$$\left. - 2(1 - \nu_m)N_f^*\left(\frac{R_o}{r}\right)^2\right]\cos 2\theta\}$$

$$v_m = \left(\frac{\gamma H r}{4G_m}\right)\{(1 - K_o)\left[J_f^*\left(\frac{R_o}{r}\right)^4 + (1 - 2\nu_m)N_f^*\left(\frac{R_o}{r}\right)^2\right]\sin 2\theta\}$$

B.8.3 CONSTANTS

$$L_f^* = \frac{d_2^*}{\left(\frac{G_\ell}{G_m}\right) d_1^* + d_2^*}$$

$$J_f^* = \frac{2(1 - \nu_m)\left(\frac{G_\ell}{G_m}\right) d_3^* + d_4^*}{(5 - 6\nu_m)\left(\frac{G_\ell}{G_m}\right) d_3^* + d_4^*}$$

$$N_f^* = \frac{\left(\frac{G_\ell}{G_m}\right) d_3^* + 2d_4^*}{(5 - 6\nu_m)\left(\frac{G_\ell}{G_m}\right) d_3^* + d_4^*}$$

$$S_f^* = \frac{1}{\left(\frac{G_\ell}{G_m}\right) d_1^* + d_2^*}$$

$$W_f^* = \frac{d_7^*}{(5 - 6\nu_m)\left(\frac{G_\ell}{G_m}\right) d_3^* + d_4^*}$$

$$X_f^* = \frac{d_5^*}{(5 - 6\nu_m)\left(\frac{G_\ell}{G_m}\right) d_3^* + d_4^*}$$

$$Y_f^* = \frac{d_6^*}{(5 - 6\nu_m)\left(\frac{G_\ell}{G_m}\right) d_3^* + d_4^*}$$

$$Z_f^* = \frac{d_8^*}{(5 - 6\nu_m)(\frac{G_\ell}{G_m})d_3^* + d_4^*}$$

$$d_1^* = \left[(\frac{R_o}{R_i})^2 - 1\right]$$

$$d_2^* = \left[(1 - 2\nu_\ell)(\frac{R_o}{R_i})^2 + 1\right]$$

$$d_3^* = \left[(\frac{R_o}{R_i})^2 - 1\right]^3$$

$$d_4^* = \left[(3 - 2\nu_\ell)(\frac{R_o}{R_i})^6 + 3(5 - 6\nu_\ell)(\frac{R_o}{R_i})^4 + 3(3 - 2\nu_\ell)(\frac{R_o}{R_i})^2 + (5 - 6\nu_\ell)\right]$$

$$d_5^* = \left[3(\frac{R_o}{R_i})^2 + 1\right]$$

$$d_6^* = \left[2(\frac{R_o}{R_i})^4 + (\frac{R_o}{R_i})^2 + 1\right]$$

$$d_7^* = \left[(\frac{R_o}{R_i})^6 + (\frac{R_o}{R_i})^4 + 2(\frac{R_o}{R_i})^2\right]$$

$$d_8^* = \left[(\frac{R_o}{R_i})^4 + 3(\frac{R_o}{R_i})^2\right]$$

Positive sign conventions are illustrated in Fig. A.5 of Appendix A.

☆U.S. GOVERNMENT PRINTING OFFICE: 1978-281-568/302